



UNIVERSIDAD NACIONAL AUTÓNOMA DE MÉXICO

PROGRAMA DE DOCTORADO EN CIENCIAS BIOMÉDICAS

FACULTAD DE MEDICINA

Estudio del sistema vasopresinérgico hipotalámico como puente entre la homeostasis y las funciones cognitivas y emocionales

TESIS

QUE PARA OPTAR POR EL GRADO DE:

Doctor en Ciencias Biomédicas

Presenta

**M.C. Vito Salvador Rogelio Hernández
Melchor**

Directora de Tesis:

Dra. en C. Limei Zhang

Facultad de Medicina

Ciudad Universitaria, México D. F

Junio de 2015



Universidad Nacional
Autónoma de México

Dirección General de Bibliotecas de la UNAM

Biblioteca Central



UNAM – Dirección General de Bibliotecas
Tesis Digitales
Restricciones de uso

DERECHOS RESERVADOS ©
PROHIBIDA SU REPRODUCCIÓN TOTAL O PARCIAL

Todo el material contenido en esta tesis esta protegido por la Ley Federal del Derecho de Autor (LFDA) de los Estados Unidos Mexicanos (México).

El uso de imágenes, fragmentos de videos, y demás material que sea objeto de protección de los derechos de autor, será exclusivamente para fines educativos e informativos y deberá citar la fuente donde la obtuvo mencionando el autor o autores. Cualquier uso distinto como el lucro, reproducción, edición o modificación, será perseguido y sancionado por el respectivo titular de los Derechos de Autor.



Universidad Nacional
Autónoma de México



UNAM – Dirección General de Bibliotecas
Tesis Digitales
Restricciones de uso

DERECHOS RESERVADOS ©
PROHIBIDA SU REPRODUCCIÓN TOTAL O PARCIAL

Todo el material contenido en esta tesis esta protegido por la Ley Federal del Derecho de Autor (LFDA) de los Estados Unidos Mexicanos (México).

El uso de imágenes, fragmentos de videos, y demás material que sea objeto de protección de los derechos de autor, será exclusivamente para fines educativos e informativos y deberá citar la fuente donde la obtuvo mencionando el autor o autores. Cualquier uso distinto como el lucro, reproducción, edición o modificación, será perseguido y sancionado por el respectivo titular de los Derechos de Autor.

El presente trabajo fue realizado en el Laboratorio de Neurociencias de Sistemas del Departamento de Fisiología de la Facultad de Medicina de la UNAM, campus Ciudad Universitaria, bajo la tutoría de la **Dra. en C. (Fisiológicas) Limei Zhang Ji** y el comité tutorial integrado por el **Dr. Jean Louis Charli Casalonga**, el **Dr. Rafael Ángel Barrio Paredes** y el **Dr. Oscar Prospero García**. Durante los estudios de doctorado, el autor de la tesis obtuvo generosos apoyos del programa de **Doctorado en Ciencias Biomédicas, UNAM**, y de los donativos de DGAPA-UNAM (PAPIIT): IN128111 y IN216214 y CONACyT 179716 y 127777. El autor contó con una beca de CONACyT para estudios de posgrado

Miembros del Jurado:

Presidente:	Dr. Stefan Mihailescu
Secretaria:	Dra. Limei Zhang
Vocal:	Dr. Daniel Martínez Fong
Vocal:	Dr. Miguel Ángel Morales
Vocal:	Prof. Dr. John A. Russell

Quiero agradecer a todas aquellas personas que de una u otra manera han hecho posible concluir esta tesis.

De manera especial:

A Limei, que más que una directora de tesis se ha convertido en una gran amiga, con quien he tenido la dicha de compartir este interesante camino.

A mis co-tutores, Jean Louis Charli, Rafael Barrio y Oscar Prospero que hicieron aportaciones fundamentales al contenido de esta tesis.

A los miembros del jurado, quienes hicieron comentarios pertinentes y enriquecedores para la elaboración de esta tesis.

Al laboratorio del Dr. Enrique Pedernera y a Maria José Gómora por el apoyo durante todos estos años con el uso de su microscopio confocal.

Al Dr. Enrique Pinzón que nos facilitó todos los animales utilizados en mis estudios, en inmejorables condiciones.

Al Dr. David García por facilitarnos las condiciones de trabajo para los experimentos de electrofisiología *in-vivo*.

A la Facultad de Medicina que me ha formado desde los inicios de mi vida académica.

Al posgrado en Ciencias Biomédicas, por el gran apoyo que me brindó en mi formación académica.

A CONACyT por el apoyo económico brindado que me permitió dedicarme de tiempo completo a este proyecto.

A todos los que compartieron conmigo ideas y trabajaron codo a codo conmigo durante estos años en el laboratorio, gracias Alicia Nava, Claudine Irlés, Erika Vázquez, Felipe Estrada, Fermín Barrio, Fernando Jáuregui, Freya Chay, Hernán Barrio, Ileana Hernández, Itzel Nissen, Javier González, Marianita Márquez, Mauricio Medina, Pablo Hofmann.

Índice

	Página
1. Resumen/ <i>Abstract in English</i>	1
2. Introducción	4
2.1 El sistema vasopresinérgico	5
2.2 El sistema de respuesta al estrés	13
3. Planteamiento del Problema	20
4. Hipótesis	22
5. Objetivos	24
6. Métodos	28
6.1 Animales	29
6.2 Inserción de bombas de liberación prolongada de hormonas tiroideas	29
6.3 Apareamiento y selección de grupos control y HM	30
6.4 Inmunohistoquímica para Fos y AVP en ratas sometidas a hipertiroidismo materno	30
6.5 Medición de concentraciones plasmáticas de vasopresina (para animales sometidos a hipertiroidismo materno y separación materna)	32
6.6 Protocolo de separación materna (3hSM)	33
6.7 Inmunohistoquímica para determinar el volumen de los núcleos AVP+ hipotalámicos en animales sometidos a separación materna	33
6.8 Medición del volumen de los núcleos	

hipotalámicos vasopresinérgicos en animales sometidos a separación materna	34
6.9 Reconstrucción tridimensional representativa del PVN	35
6.10 Evaluación de la activación de neuronas vasopresinérgicas en el PVN y SON al día P10 tras una exposición aguda a 3hSM	35
6.11 Inmunohistoquímica para análisis por microscopía de luz de densidad de fibras vasopresinérgicas y trayectorias hacia hipocampo	36
6.12 Análisis de densidad de fibras vasopresinérgicas en hipocampo	38
6.13 Aplicación de trazadores retrógrados en hipocampo ventral y dorsal	39
6.14 Registro extracelular y marcaje juxtacelular de neuronas aisladas en PVN	40
6.15 Procesamiento anatómico y reconstrucción de las células marcadas	40
6.16 Laberinto elevado en cruz (EPM) - evaluación de ansiedad no condicionada	41
6.17 Prueba de conflicto de Vogel (VCT) - evaluación de ansiedad condicionada	42
6.18 Evaluación del aprendizaje espacial: MWM (Morris Water Maze)	43
6.19 Exposición al gato vivo y puntuación conductual	44
6.20 Inmunohistoquímica contra c-Fos después de	

exposición al predador	45
6.21 Análisis estadístico	46
7. Resultados	47
<i>Sección I: La estructura y función del sistema vasopresinérgico hipotalámico neurosecretory puede modificarse por estresores perinatales</i>	49
7.1 Efectos del hipertiroidismo prenatal sobre el desarrollo del sistema vasopresinérgico	50
7.2 Efectos de la separación materna sobre el desarrollo del sistema vasopresinérgico	55
<i>Sección II: El sistema vasopresinérgico hipotalámico magnocelular tiene proyecciones intracerebrales mas extensas de lo anteriormente reportado</i>	60
7.3 Las neuronas magnocelulares neurosecretoras (MNN's) del hipotálamo inervan el hipocampo dorsal y ventral	61
7.4 Las neuronas vasopresinérgicas magnocelulares neurosecretoras (MNN's) del núcleo paraventricular inervan regiones intra y extra hipotalámicas a través de múltiples procesos tipo axónicos o colaterales axónicas	80
<i>Sección III La modulación a la alta o a la baja del sistema vasopresinérgico produce deterioro en conductas emocionales y cognitivas</i>	86
7.5 Las Ratas HM presentan “ansiedad condicionada”	

si son sometidas a un estresor osmótico	87
8. Discusión general	96
9. Tabla de abreviaturas	103
10. Bibliografía	107
11. Apéndice: Productos científicos derivados de mis estudios	
del doctorado	118
11.1 Publicaciones derivadas directamente de esta tesis	119

- **Hernández V. S.**, Vázquez-Juárez E., Márquez M. M., Jáurequi-Huerta F., Barrio R. A. and Zhang L. Intracerebral axonal projections of individual vasopressinergic magnocellular neurons of rat hypothalamus. *Frontiers in Neuroanatomy*. (en revision)
 (pags. 120 - 146)

- Zhang L., **Hernández V. S.**, Synaptic innervation to rat hippocampus by vasopressin-immuno-positive fibres from the hypothalamic supraoptic and paraventricular nuclei. *Neuroscience*. 2013 Jan 3;228:139-62
 (pags. 147 - 171)

- **Hernández V. S.**, Ruíz-Velazco S., Zhang L. Differential effects of osmotic and SSR149415 challenges in maternally separated and control rats: the role of vasopressin on spatial learning. *Neurosci Lett*. 2012 Oct 24;528(2).
 (pags. 172 - 177)

- Zhang L.*, **Hernández V. S.***, Liu B., Medina M. P., Nava-Kopp A. T., Irles C., Morales M. Hypothalamic vasopressin system regulation by maternal separation: its impact on anxiety in rats. *Neuroscience*. 2012 Jul 26;215:135-48.
 (*Primer autor compartido) (pags. 178 - 192)

- Zhang L., Medina M. P., **Hernández V. S.**, Estrada F. S., Vega-González A. Vasopressinergic network abnormalities potentiate conditioned anxious state of rats subjected to maternal hyperthyroidism. *Neuroscience*. 2010, 168:416-28 (pags. 193 - 206)
- Zhang L., **Hernández V. S.**, Medina-Pizarro M., Valle-Leija P., Vega-González A., Morales T. Maternal hyperthyroidism in rats impairs stress coping of adult offspring. *J. Neurosci. Res*, 2008, 86:1306 – 1315. (publicado en periodo propedeúutico para estudios del doctorado) (pags. 207 - 217)

11.2 Otras publicaciones científicas durante mis estudios

doctorales

218

- **Hernández V. S.**, Luquín S., Jáuregui-Huerta F., Corona-Morales A. A., Medina M. P., Ruíz-Velasco S., Zhang L. Dopamine receptor dysregulation in hippocampus of aged rats underlies chronic pulsatile L-Dopa treatment induced cognitive and emotional alterations. *Neuropharmacology* 2014, Jul 82:88-100 (pags. 219 - 232)
- Zhang L., **Hernández V. S.**, Estrada F. S., Luján R. Hippocampal CA field neurogenesis after pilocarpine insult: The hippocampal fissure as a neurogenic niche. *J Chem Neuroanat*. 2014 Mar; 56:45-57 (pags. 233 - 246)
- Estrada F. S., **Hernandez V. S.**, López-Hernández E., Corona-Morales A. A., Solís H., Escobar A., Zhang L. Glial activation in

a pilocarpine rat model for epileptogenesis: A morphometric and quantitative analysis. *Neurosci Lett*. 2012 Apr 11; 514(1):51-6
(pags. 247 - 253)

- Estrada F. S., **Hernandez V. S.**, Medina M. P., Corona-Morales A. A., Gonzalez-Perez O., Vega-Gonzalez A., Zhang L. Astrogliosis is temporally correlated with enhanced neurogenesis in adult rat hippocampus following a glucoprivic insult. *Neurosci Lett*, 2009 Aug 14;459(3):109-14
(pags. 254 - 260)

11.3 Presentaciones en congresos nacionales e internacionales

(pags. 261-308)

- **Hernandez V.S.**, Vazquez-Juarez E, Chay F, Zhang L. Anatomical and electrophysiological characterization of vasopressinergic innervation in rat lateral habenula. Neurobiology of stress workshop, 2014, Cincinnati, USA.
- Vazquez-Juarez E, **Hernandez V.S.**, Zhang L. Multi-axonal feature of hypothalamic PVN magnocellular vasopressinergic neurons revealed by in vivo juxtacellular recording: its rhythmic changes under osmotic stress and implications on predator fear processing. Neurobiology of stress workshop, 2014, Cincinnati, USA
- **Hernandez V.S.**, Chay F, Vazquez-Juarez E, Zhang L. Origin, distribution, synaptic targets and electrophysiological actions of vasopressin innervation in rat lateral habenula: its role in behavioural despair. FENS, 2014, Milan Italy
- **V. S. Hernandez**, F. Chay, C. Irlles, L. Zhang. Vasopressin modulates lateral habenula network activity via both V1a and V1b receptors: Dual electrophysiological mechanisms revealed

by *in vitro* whole-cell patch clamp recording. Society for Neuroscience annual meeting, Washington, USA, 2014

- L. Zhang, E Vazquez-Juarez, **V. S. Hernandez**. Límbic Region projections of vasopressin containing magnocellular neurosecretory neurons revealed by *in vivo* juxtacellular recording and anatomical analysis: its rhythmic changes under osmotic stress and implications on predator fear processing. Society for Neuroscience annual meeting, Washington, USA, 2014
- E Vazquez-Juarez, F Jauregui-Huerta, **V. S. Hernandez**, L. Zhang. Hypertonicity increases arousal and anxiety following predator exposure: The direct and indirect modulation of hypothalamic vasopressin containing magnocellular neurosecretory neurons on Fos expression in limbic regions in rat. Society for Neuroscience annual meeting, Washington, USA, 2014
- **Hernandez, V.S.**, Zhang, L. Role of vasopressinergic innervation of habenula in the selection of stress coping strategies in rat. Society for Neuroscience annual meeting, San Diego, USA, 2013
- **Hernandez V.S.** & Zhang L. The vasopressinergic V1b receptor antagonist SSR149415 exerts a differential effect on spatial learning in normal and maternally separated rat. 8th FENS forum of Neuroscience. Barcelona, Spain. 2012
- Zhang L., **Hernandez V.S.**, NavaKopp A.T. & Irls C. Maternal separation upregulates hypothalamic vasopressin expression in rat early postnatal and young adult stages: impacts on conditioned anxious state. 8th FENS forum of Neuroscience. Barcelona, Spain. 2012
- **Hernandez V.S.**, Zhang, L. Vasopressin containing fibers distribution and synaptic innervation in the medial and central amygdala: an immunohistochemical study using light and electron microscopy. Society for Neuroscience annual meeting, New Orleans, USA, October 2012

- **Hernandez, V.S.**, Zhang, L. Effects of chronic levodopa treatment on hippocampal dopamine receptors and spatial learning: a comparative study in young and aged intact rats. I congreso FALAN - LV Congreso Internacional 2012 Cancún, Quintana Roo, México. Noviembre, 2012
- **Hernandez V.S** , Zhang L. Efecto dual del antagonista vasopresinergico v1b ssr-149415 sobre el aprendizaje espacial en ratas normales y con separación materna, en condiciones basales y ante un estrés osmótico agudo LIV congreso Nacional de Ciencias Fisiológicas, Leon, Guanajuato, Mexico (sept 2011).
- Zhang L, **Hernandez V.S.** Innervacion vasopresinergica al hipocampo de ratas normales y sometidas a separación materna neonatal: origen, distribucion y blancos sinápticos. LIV congreso Nacional de Ciencias Fisiológicas, Leon, Guanajuato, Mexico (sept 2011).
- **V. S. Hernandez**, I. Nissen, L. Zhang. Dual effect of AVP V1b antagonist SSR-149415 on spatial learning in normal and maternal separated rats under basal and mild stress conditions. Society for Neuroscience annual meeting, Washington DC, Nov. 2011
- **V. S. Hernandez**, M. P. Medina, I. Nissen, E. Pinzón, A. Vega-Gonzalez, L. Zhang. Neonatal maternal separation on developing hypothalamic vasopressinergic system of rats: A quantitative topographic analysis. Society for Neuroscience annual meeting, San Diego, Nov. 2010
- **V. S. Hernandez**, M. P. Medina, F. S. Estrada, A. Vega-Gonzalez, C. Mendez, L. Zhang. Evidences of an altered vasopressinergic system in hypothalamic PVN and SON of maternal hyperthyroid rat offspring. Society for Neuroscience annual meeting, Chicago, Oct 2009.
- F. S. Estrada, H. S. Gonzalez, **V. S. Hernandez**, A. Vega-Gonzalez, A. De La Peña, J. M. Fernandez-G, L. Zhang.

Anxiogenesis and impaired spatial memory induced by ovariectomy are reverted by a 17beta-aminoestrogen (prolame): a behavioral study in young female rats. Society for Neuroscience annual meeting, Chicago, Oct 2009.

- **V. S. Hernandez**, F. S. Estrada, A. Vega-Gonzalez, L. Zhang. Immunohistochemical characterization of catecholaminergic innervation during development in amygdala and hippocampus of maternal hyperthyroid rat offspring. Society for Neuroscience annual meeting, Washington DC, Nov 2008
- F. S. Estrada, A. Corona-Morales, **V. S Hernández**, M. P. Medina, A. Vega-Gonzalez, L. Zhang. A temporal correlation between cell proliferation and astrocytic reactivity in the adult rat hippocampus induced by a single 2-Deoxy-D-glucose application. Society for Neuroscience annual meeting, Washington DC, Nov 2008
- Zhang L., Medina-Pizarro M., **Hernandez V. S.** & Vega-Gonzalez A. Vasopressinergic innervations to locus coeruleus in normal and maternal hyperthyroid rats: its role in triggering anxiety-like behaviour during stress coping. 6th FENS forum of Neuroscience. Geneva, Switzerland. 2008
- **V. S. Hernandez**, A. Vega-Gonzalez, L. Zhang. Maternal hyperthyroidism enhances basal exploratory activity and increases TH immunoreactivity in the amygdala of adult rat offspring. 37th Annual Meeting, Society for Neuroscience, San Diego, 2007
- L. Zhang, **V. S. Hernandez**, A. Vega-Gonzalez, A. A. Corona-Morales. Chronic pulsatile L-DOPA application alters emotionality and cognitive functions: a study in intact aged rat. 37th Annual Meeting, Society for Neuroscience, San Diego, 2007.
- Estrada F.S., **V. S. Hernandez**, A. Vega-Gonzalez, L. Zhang; Effects of chronic application of beta-1 adrenergic antagonist

metoprolol on spatial learning and c-Fos expression. 37th Annual Meeting, Society for Neuroscience, San Diego, 2007

- **Hernandez V.S.**, Medina M.P., Valle-Leija P. Vega-Gonzalez A., Morales T. and Zhang L. Enhanced basal exploratory activity, anti-nociceptive behaviour and increased TH and CRF immunoreactivity in amygdala of adult rats subjected to maternal hyperthyroidism. IBRO world congress of neuroscience Melbourne, Australia 2007
- Zhang L., **Hernandez V.S.**, Medina M.P., Valle-Leija P., Hofmann P.G. Vega-Gonzalez A. and Morales T. Maternal hyperthyroidism in rats impairs stress coping of adult offspring. . IBRO world congress of neuroscience Melbourne, Australia. 2007
- Medina M.P., **Hernandez V.S.**, Valle-Leija P., Vega-Gonzalez A. and Zhang L. Morphological analysis of hippocampal projections neurons in different postnatal stages of rats subjected to maternal hyperthyroidism. IBRO world congress of neuroscience Melbourne, Australia. 2007
- **Hernandez VS**, Medina MP, Guadarrama L, Galindo L, Vega-Gonzalez A, Luquin-de-Anda S, Garcia-Estrada J, Zhang L. Adult anxiety-like behavior, cognitive deficiency and neocortical pyramidal cell structural changes in rats subjected to transient neonatal hyperthyroidism. 36th Annual Meeting, Society for Neuroscience, Atlanta., 2006
- Medina MP, **Hernandez VS**, Guadarrama L, Galindo CA, Vega-Gonzalez A, Solis H, Zhang L. Stress differentially affects transcription factor c-Fos expression and SGZ neurogenesis in adult rats subjected to transient neonatal hyperthyroidism. 36th Annual Meeting, Society for Neuroscience, Atlanta, 2006.

1. Resumen

La arginina-vasopresina (AVP) se sintetiza en el hipotálamo y es principalmente secretada por la neurohipófisis hacia el torrente circulatorio. Sus funciones periféricas principales son la regulación de la homeostasis hidroelectrolítica corporal y la presión arterial. La AVP pertenece al grupo de señalizadores llamados neuromoduladores peptídicos que, según nuestro entendimiento actual, coordinan las actividades neurales para optimizar el procesamiento de información a través de modular funciones de diferentes áreas cerebrales, tales como comportamiento social, la cognición y la emocionalidad. Por otro lado, los últimos años han participado de un auge en las investigaciones que ligan eventos estresantes durante la vida temprana con alteraciones en el neurodesarrollo normal. Muchos modelos de estrés perinatal han evaluado la participación del clásico eje de respuesta al estrés (hipotálamo-pituitaria-adrenal). Sin embargo, las evidencias recientes sugieren que el sistema vasopresinérgico podría tener un papel preponderante en la respuesta al estrés durante el periodo perinatal. Cabe señalar que durante el desarrollo temprano, el sistema vasopresinérgico tiene un papel importante en la morfogénesis de sus órganos diana. Durante la transición de la vida fetal a extrauterina, éste ayuda a mantener el equilibrio hidroelectrolítico y un adecuado flujo sanguíneo a órganos vitales. Al nacimiento el sistema vasopresinérgico aún es inmaduro y continuará desarrollándose hasta la pubertad.

Dada la asociación anatomofuncional y neuroquímica entre el sistema vasopresinérgico hipotalámico y el enfrentamiento al estrés, tanto en la edad temprana como en la edad adulta, la presente tesis pretende profundizar en el conocimiento de la neuroanatomía funcional del sistema vasopresinérgico neurosecretor y sus cambios dinámicos, cuando el organismo se somete a situaciones adversas durante el desarrollo y en la adultez. El objetivo es aportar información sobre la influencia del estrés en la edad temprana al sistema vasopresinérgico y una descripción detallada enfocada sobre la conectómica de este sistema y su consecuencia en el comportamiento. Para ello, empleamos técnicas electrofisiológicas (registros *in vivo* e *in vitro*), marcajes yuxtacelulares, reconstrucciones anatómicas, métodos inmunohistoquímicos y anatómicos, en combinación con modelos de estrés perinatal, hipertiroidismo prenatal y separación materna neonatal, y pruebas conductuales para evaluar la emocionalidad y cognición.

Los resultados de esta tesis consisten en una serie de trabajos científicos publicados o en vía de ser publicados. Todos los trabajos fueron realizados por nuestro grupo de investigación con una importante participación mía durante el periodo que comprende de mis estudios doctorales.

Dentro de estos resultados, se resaltan los siguientes: 1) los sujetos sometidos a estrés perinatal exhiben un alto nivel de ansiedad sólo cuando los sujetos experimentales se encuentran con el sistema vasopresinérgico regulado a la alta ("ansiedad condicionada"); 2) la separación materna neonatal potencia el sistema vasopresinérgico incrementando el mRNA de AVP en el hipotálamo tanto en el periodo neonatal como en la adultez, resultando un mayor volumen de los núcleos paraventricular y supraóptico; la liberación de ligando durante un reto osmótico también se ve incrementado significativamente; 3) la hipertonicidad

y la administración de antagonista específico del receptor V1b (SSR149415) modifica diferencialmente el desempeño de los sujetos estresados y control, en el laberinto acuático de Morris; 4) las fibras vasopresinérgicas provenientes de los núcleos magnocelulares del hipotálamo inervan extensivamente la subregión CA2 del hipocampo tanto ventral como dorsal estableciendo sinapsis con neuronas piramidales e interneuronas. Por último, el uso de la técnica de registro extracelular y marcaje yuxtacelular con neurobiotina, en combinación con análisis anatómico e inmunohistoquímico *post hoc*, nos han permitido visualizar una gran porción axónica de las neuronas vasopresinérgicas neurosecretoras magnocelulares (*MNN's*, por sus siglas en inglés para homogeneizar la terminología con las publicaciones) que antes no se habían podido visualizar. La característica de poseer colaterales axónicos que proyectan hacia una extensa área intracerebral ya no es un fenómeno esporádico sino común, dejando un desafiante tema de investigación para el futuro cercano que es el descubrir sus significados fisiológicos.

La relación entre estos resultados experimentales y sus implicaciones para nuestro entendimiento sobre la modulación de las regiones cerebrales sub-corticales a las funciones corticales, sobre todo para los trastornos emocionales y sociales se discute al final de esta tesis, así como las virtudes y limitaciones de estos experimentos. La tesis concluye con algunos comentarios sobre trabajos a futuro y sobre la relevancia del estudio de las neurohormonas (vasopresina y oxitocina) para la salud y el bienestar del ser humano.

Resumen en Inglés:

Abstract

Vasopressin (AVP) is synthesized in the hypothalamus and is mainly secreted by the posterior pituitary into the bloodstream. Its main peripheral functions are the regulation of body fluid and electrolyte homeostasis and blood pressure. The AVP is in a group of signaling peptides called neuromodulators that, according to our current understanding, coordinate activities to optimize neural information processing and modulate behaviors, such as social behavior, cognition and emotionality. On the other hand, in recent years there has been a boom in research linking stressful events during early life with alterations in the normal neural development. Many models have been developed to assess the impact of perinatal stress on the classic stress response axis (hypothalamic-pituitary-adrenal). However, recent evidence suggests that the vasopressinergic system could have a major role in the stress response during the perinatal period. It is worth mentioning that during early development, the vasopressinergic system has an important role in morphogenesis of its target organs. During the transition from fetal to extra uterine life, it helps maintain fluid balance and adequate blood flow to vital organs. At birth, the vasopressinergic system is still immature and continues to develop until puberty.

Given the anatomical and neurochemical association between the hypothalamic vasopressinergic system and stress coping mechanisms, both during early life and adulthood,

this thesis aims to broaden the knowledge of the functional vasopressinergic neuroanatomy of the neurosecretory system and its dynamic changes when the body is subjected to adverse conditions, during development and in adulthood. The goal is to provide information on the influence of early life stress on the vasopressinergic system and a detailed description focused on this system's connectomics and its consequences on behavior. To do this, we applied electrophysiological techniques (in vivo and in vitro recordings), juxtacellular labeling, anatomical reconstruction, immunohistochemical and anatomical methods, combined with perinatal stress models, prenatal hyperthyroidism, neonatal maternal separation and behavioral tests to assess emotionality and cognition.

The results of this thesis consist of a number of scientific papers published or in the process of being published. All articles were conducted by our research group, in which I contributed importantly, during the period covered by my doctoral studies.

Within these results, the following results may be highlighted: 1) the experimental subjects that underwent perinatal stress exhibit a high level of anxiety, only when their vasopressinergic system was up-regulated ("conditioned anxiety"); 2) neonatal maternal separation enhanced AVP mRNA expression in the hypothalamus in both the neonatal period and during adulthood, resulting in a greater volume of the paraventricular and supraoptic nuclei; the release of ligand after an osmotic challenge also increased significantly; 3) hypertonicity and management of specific V1b receptor antagonist (SSR149415) modified the performances of stressed and control subjects in the Morris water maze differentially; 4) vasopressinergic fibers from the magnocellular nuclei of the hypothalamus extensively innervate the CA2 subregion of both ventral and dorsal hippocampus establishing synapses with both interneurons and pyramidal neurons. Finally, extracellular recording techniques and juxtacellular neurobiotin labelling, combined with post hoc anatomical and immunohistochemical analysis has allowed us to visualize a greater portion of vasopressinergic magnocellular neurosecretory neurons (MNN's) axon collaterals that previously were not visible had not been able to be seen. Possessing axon collaterals projecting to extensive intracerebral areas is no longer a sporadic but common phenomenon. This opens a new challenging research topic, i.e., to discover the functional implications of these MNNs intracerebral collaterals.

The relationship between the experimental results and their implications for our understanding of sub-cortical modulation to cortical functions, especially for emotional and social disorders is discussed at the end of this thesis, as well as the strengths and limitations of these experiments. The thesis concludes with some comments on the future works and the relevance of neurohormones (vasopressin and oxytocin) on health and welfare of human beings.

2.Introducción

2.1 El sistema vasopresinérgico

La arginina-vasopresina (AVP) también llamada hormona antidiurética (ADH), fue caracterizada desde 1895 por Oliver y Shaefer, quienes demostraron que extractos de hipófisis alteraban la presión arterial (Oliver and Schafer, 1895). En 1925 a través de los trabajos pioneros de Starling y Verney se describió el principal efecto de la vasopresina, su efecto antidiurético, (Starling and Verney, 1925). Para 1951, el grupo de du Vigneaud logró su purificación (Selye, 1936) y la caracterizó como un nona-péptido (Cys-Tyr-Phe-Gln-Asn-Cys-Pro-Arg-GlyNH₂) que consiste de un anillo de 6 aminoácidos con un puente disulfuro uniendo la cisteína 1 y 6, y una cola de 3 aminoácidos (Figura 2-1) (Vigneaud et al., 1953). Los estudios de Gottschalk y Mylle mostraron que el efecto antidiurético de la vasopresina se ejercía principalmente aumentando la permeabilidad de los túbulos colectores distales del riñón (Gottschalk and Mylle, 1959).

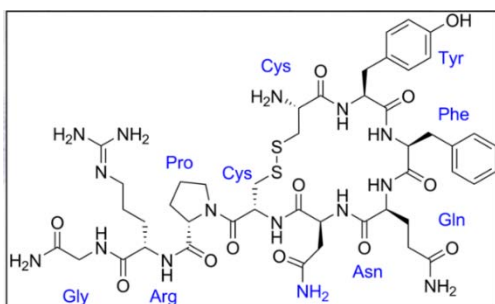


Figura 2-1 Estructura química de la arginina vasopresina véase la arginina presente en la octava posición (imagen tomada de Wikipedia: <http://en.wikipedia.org/wiki/Vasopressin>).

El sistema vasopresinérgico participa en numerosas funciones *e.g.* regulación del equilibrio hidro-electrolítico (Ludwig et al., 1994, Robertson et al., 1976); regulación de la presión arterial (Dunn et al., 1973); coagulación sanguínea (Haslam and Rosson, 1972); metabolismo energético (Hems et al., 1975); liberación de corticotropina (Scott and Dinan, 1998); procesos de memoria (Dietrich and Allen, 1997), emocionalidad (Landgraf et al., 1995) comportamiento social (Bielsky and Young, 2004) y ritmos circadianos (Castel et al., 1990). La importancia de éste sistema es enfatizada por su filogenia, se han caracterizado especies de invertebrados que poseen péptidos pertenecientes a la superfamilia de vasopresina/oxitocina, sugiriendo su origen hace aproximadamente 700 millones de años (Acher et al., 1995).

El gen de la vasopresina al igual que el de la oxitocina, de la cual difiere tan solo en dos aminoácidos (Ile por Phe en la posición 3 y Leu por Arg en la posición 8), está localizado en el cromosoma 20 en el humano y en el cromosoma 3 en la rata (Khegay, 1996). La vasopresina es sintetizada como parte de un pre-pro-péptido que contiene además neurofisisina II, y un glicopéptido asociado a vasopresina (Schmale et al., 1983, Land et al., 1982). Para el caso del sistema hipotálamo neurohipofiseal, la vasopresina se sintetiza en los somas de neuronas magnocelulares neurosecretoras (MNN's) de los núcleos paraventricular (PVN) y supraóptico (SON) hipotalámicos (Figura 2-2). Posteriormente, este péptido es transportado anterógradamente por los axones de las células MNN's hasta el lóbulo posterior de la hipófisis o neurohipófisis donde es liberado de las terminales axónicas ante un aumento de la osmolaridad plasmática o por pérdida de volumen sanguíneo (Dunn et al., 1973) contribuyendo al control periférico del equilibrio hidroelectrolítico, del metabolismo hepático de glucosa y del sistema cardiovascular (Hatton, 1990). Es de notar que la hormona es sintetizada inicialmente como un precursor inactivo y es durante el transporte axonal que se forma la molécula biológicamente activa (Zimmerman and Robinson, 1976, Sachs and Takabatake, 1964), además, se desconocen las funciones del glicopéptido asociado a vasopresina y de la neurofisisina II, que son co-liberados con la vasopresina en la neurohipófisis.

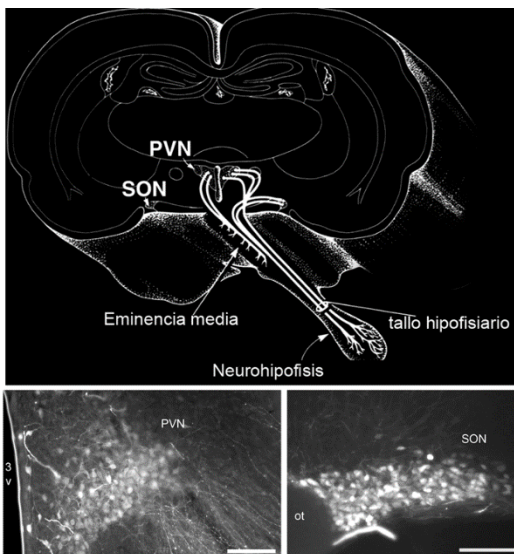
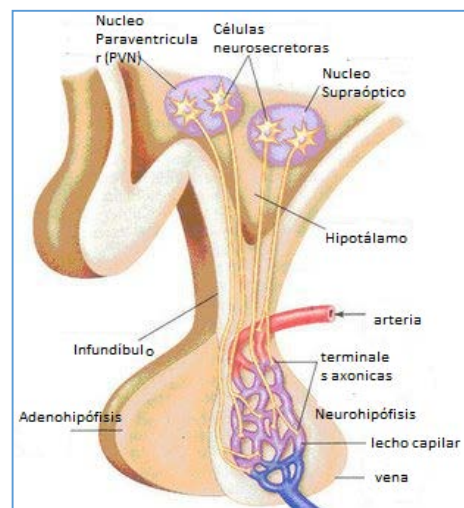


Figura 2-2 El núcleo paraventricular y supraóptico del hipotálamo son los principales sitios de producción de vasopresina y forman el inicio del sistema hipotálamo neurohipofiseal. Panel superior: Esquema que muestra la localización de los núcleos PVN y SON así como el tracto hipotálamo neurohipofiseal dirigiéndose a la eminencia media - tallo hipofisiario y terminando en la neurohipófisis. En el esquema están representados axones que terminan en la eminencia media, donde liberan su contenido hacia la circulación porta-hipofisiaria. Paneles inferiores: Fotomicrografías de reacciones contra AVP en núcleo paraventricular (izquierda) y supraóptico (derecha). Barras de escala: 200 μ m.

La hipófisis fue descrita desde los tiempos de Galeno (AD 129-216), quien proponía que su principal papel era el de drenar la flema del cerebro hacia la nasofaringe (Kaplan, 2007), la palabra pituitaria deriva del latín *pituita* que significa flema. Para 1838, Rathke, describió el desarrollo de la hipófisis, como formada a partir de la fusión de una invaginación de la cavidad bucal primitiva y una evaginación de la base del cerebro, la estructura interna de la hipófisis refleja este origen, la parte anterior que deriva de la bolsa de Rathke está compuesta de células secretoras, mientras que la parte posterior de la hipófisis (neurohipófisis) se compone de axones que provienen del hipotálamo (Laycock, 2010) (Figura 2-3).

Figura 2-3 El sistema hipotalámico neurohipofiseal: Neuronas vasopresinérgicas del núcleo paraventricular y núcleo supraóptico envían axones a la parte posterior de la hipófisis, donde liberan su contenido a la circulación para ejercer sus efectos antidiuréticos y vasopresores. Modificado de www.vetbook.org/wiki/cat/index.php/Diabetes_insididus.



La primera observación de fibras nerviosas en el lóbulo posterior de la hipófisis fue hecha por Ecker en 1853 y posteriormente fue confirmada por otros investigadores, entre ellos Santiago Ramón y Cajal, que en 1894, describió un núcleo situado detrás del quiasma óptico como fuente de estas fibras (Harris and Donovan, 1966). Una característica importante de estos axones es que son de gran diámetro y que presentan varicosidades o ensanchamientos llamados cuerpos de Herring, en honor a quien en 1908 los describió como gotas de coloide en el lóbulo neural (Herring, 1908). Además de las neuronas magnocelulares, las neuronas parvocelulares cuyos somas se ubican principalmente en la parte medial del núcleo paraventricular, envían terminales axónicas a la eminencia media, donde la vasopresina liberada entra al sistema porta hipofisario y es transportada a la hipófisis anterior (adenohipófisis), donde puede modular la actividad de los corticotropos (Figura 2-2).

Además de las proyecciones de las neuronas vasopresinérgicas hipotalámicas hacia la hipófisis, proyecciones axonales vasopresinérgicas con origen en el núcleo paraventricular y supraóptico se dirigen al cerebro posterior y a la médula espinal, donde probablemente controlan funciones autonómicas tales como tensión arterial y frecuencia cardíaca (Sawchenko and Swanson, 1982). El núcleo supraquiasmático, que también tiene una población de pequeñas células vasopresinérgicas, envía axones hacia áreas alrededor del tercer ventrículo, probablemente regulando funciones circadianas (Hoorneman and Buijs, 1982). El núcleo del lecho de la *estría terminalis* (BNST) y la amígdala medial también contienen células que sintetizan vasopresina y se ha mostrado que proyectan a estructuras del cerebro anterior, tales como el septum lateral y núcleo de la habénula lateral y a estructuras del cerebro medio tales como núcleo rafe dorsal y *locus coeruleus* (De Vries and Buijs, 1983, Caffè et al., 1987, Caffè and van Leeuwen, 1983). Es de notar que aunque se han identificado con relativa claridad las regiones intracerebrales que expresan receptores de vasopresina o fibras que contienen vasopresina, ha sido muy discutido el origen de éstas.

Las neuronas vasopresinérgicas se originan en el neuroepitelio del tercer ventrículo entre el día embrionario 13 (E13) y E15 y migran al núcleo supraóptico y paraventricular (E17-19); durante la migración y una vez establecidas en estos núcleos, las neuronas empiezan a producir vasopresina ante estímulos osmóticos. A finales de la etapa fetal y los primeros días de vida extrauterina, el número de neuronas que expresan vasopresina y la concentración de vasopresina continúa aumentando hasta la pubertad (Figura 2-4).

Figura 2-4 El contenido cerebral de vasopresina aumenta considerablemente después del nacimiento. Modificado de Ugrumov, 2002 (Ugrumov 2002)



Durante el desarrollo temprano, la vasopresina contribuye a la regulación de la proliferación y la morfogénesis de las células y órganos diana (cerebro, hipófisis, riñones e hígado), alrededor del nacimiento contribuye al establecimiento de un nuevo equilibrio en los fluidos corporales y la adaptación del feto en el periodo de parto. Después del nacimiento, la vasopresina, induce una redistribución del flujo sanguíneo a través del sistema cardiovascular con el fin de aumentar el volumen de sangre en los órganos vitales y en los responsables de la reacción al estrés (el cerebro, la glándula pituitaria, el corazón, las glándulas suprarrenales), mientras que reduce el flujo sanguíneo en otros órganos periféricos. Después del nacimiento el papel fisiológico de la vasopresina se extiende a la regulación del sistema cardiovascular, la reabsorción del agua en los riñones y la glucogenólisis en el hígado (Ugrumov, 2002). Las fibras extra-hipotalámicas vasopresinérgicas aparecen por vez primera el día fetal 17 (Buijs et al., 1980). Una vía ventral directa hacia el bulbo olfatorio comienza a desarrollarse el día 18 del feto, fibras AVP-positivas son también demostrables en otras áreas extra-hipotalámicas, por ejemplo en la amígdala y en el cuerpo calloso, y con frecuencia se ven procesos penetrando en la capa de células endimarias del tercer ventrículo. Para el día postnatal 2 se pueden observar fibras en el hipocampo ventral y en la parte ventral del tallo cerebral, para el día postnatal 10 fibras provenientes del núcleo supraquiasmático alcanzan el núcleo habenuar y el septum lateral (Ugrumov, 2002).

Los efectos de la vasopresina dependen de la unión con sus receptores, de los cuales se han caracterizado tres tipos. Periféricamente, el receptor V1a se distribuye principalmente en los vasos sanguíneos, corazón, hígado, riñones y plaquetas, el receptor V1b se expresa principalmente en los corticotropos de la hipófisis anterior (Laycock, 2010), ambos receptores están acoplados a proteínas Gq/11 que se asocian a la activación de la cascada de inositol trifosfato (IP3) y la movilización de calcio intracelular. El receptor V2 se ubica principalmente en las células principales de los túbulos renales distales y se halla acoplado a la activación de la fosfolipasa C (PLC) y a la producción de AMP cíclico (cAMP) (Barberis et al., 1998). A nivel del sistema nervioso central, la vasopresina ejerce sus efectos a través de la activación de receptores V1a y V1b, los receptores V1a se distribuyen ampliamente en todo el cerebro (Szot et al., 1994) mientras que la expresión de los receptores V1b se ha demostrado en el hipotálamo, la amígdala, el cerebelo, los órganos circunventriculares, el

hipocampo, el cuerpo estriado, la corteza, el tálamo, el bulbo olfatorio, y el cerebelo (Hernando et al., 2001, Young et al., 2006).

La vasopresina puede ser considerada una hormona de estrés i.e. es liberada en respuesta a situaciones que comprometen la homeostasis del organismo y sus principales efectos son aumentar la reabsorción renal de agua y aumentar el tono del músculo liso vascular para aumentar la tensión arterial, principalmente en respuesta a pérdidas de volumen sanguíneo o a un aumento de osmolaridad plasmática (Figura 2-5).

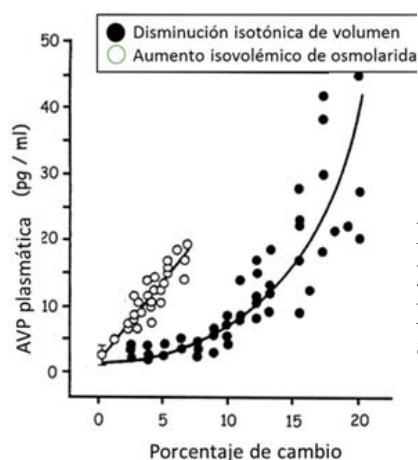


Figura 2-5 Efecto del cambio de osmolaridad plasmática y de volumen sanguíneo sobre la concentración plasmática de vasopresina. Modificado de Dunn, F.L. et al. 1973

Además de los efectos clásicos sobre la homeostasis hidroelectrolítica y la función cardiovascular, se han demostrado otros efectos de esta hormona ante situaciones de estrés físico o emocional, tales como aumentar la glucemia estimulando la glucólisis (Hems et al., 1975) y estimulando la actividad del ciclo de Krebs (Patel, 1986); induce hemostasia favoreciendo la agregación plaquetaria (Haslam and Rosson, 1972) y estimulando la liberación del factor de von Willebrand (Nussey et al., 1986) y la síntesis de factor VIII (Mannucci et al., 1977); además sinergiza con el factor liberador de corticotropina (CRF) para la estimulación de los corticotropos. En condiciones normales el efecto de CRF es predominante, en respuesta ante la mayoría de los estímulos estresantes, sin embargo, en algunas situaciones tales como estrés crónico (Chowdrey et al., 1995) o en el periodo perinatal (Zelena et al., 2008, Ducsay et al., 2009), es el sistema vasopresinérgico quien juega el papel primordial de control sobre el eje hipotálamo-pituitaria-adrenal (HPA).

Más aun, también se han descrito acciones sobre el sistema nervioso central. Los trabajos pioneros que mostraban un efecto de la vasopresina sobre la conducta fueron realizados por el grupo de De Wied, el cuál demostró que la remoción del lóbulo posterior de la hipófisis evitaba que las ratas pudieran ser condicionadas en una prueba de evitación, y que los extractos de pituitaria o la vasopresina restauraban la conducta de evitación (De Wied, 1965, De Wied, 1971). A partir de entonces una plétora de estudios han evaluado los efectos de la vasopresina en la modulación de conductas de agresión, sexuales (Hari Dass and Vyas, 2014), afiliativas (Caldwell et al., 2008), de memoria (Hernandez et al., 2012), reconocimiento social (Wacker and Ludwig, 2012), ritmos circadianos, emocionalidad y respuesta al estrés crónico (Albeck et al., 1997) y agudo (Landgraf et al., 1988, Ueta et al., 2011).

El papel de la vasopresina como promotor de un estado de ansiedad no es ampliamente aceptado, aunque existen evidencias funcionales para asignar un papel a la vasopresina en la modulación de los estados de ansiedad, entre las cuales encontramos que con la exposición al estrés hay un aumento en la síntesis y la liberación de vasopresina en el hipotálamo, núcleo central de la amígdala y el septum entre otros (Aguilera and Rabadan-Diehl, 2000, Albeck et al., 1997, Chen and Herbert, 1995, Ebner et al., 2002, Makino et al., 2002, Wotjak et al., 1998, Zhang et al., 2008). Más aún, las ratas Brattleboro, que genéticamente no expresan vasopresina, tienen niveles bajos de ansiedad (Williams et al., 1985), farmacológicamente, antagonistas no selectivos V1a/V1b han mostrado propiedades ansiolíticas (Liebsch et al., 1996), y el nuevo antagonista selectivo del receptor V1b, SR149415, provocó un aumento selectivo y significativo de respuestas castigadas en la prueba de ansiedad de Vogel (VCT) indicando un efecto ansiolítico (Griebel et al., 2002). Por último, la aplicación en septum del oligonucleótido anti sentido del receptor V1a suprime el comportamiento ansioso en ratas (Landgraf et al., 1995).

En relación a los efectos de la vasopresina sobre el aprendizaje y la memoria, los trabajos iniciales de De Wied mostraban que la inyección de vasopresina sistémicamente mejoraba el desempeño de las ratas en un protocolo de evitación pasiva (De Wied, 1965), efecto confirmado con la inyección de vasopresina directamente al hipocampo ventral (Ibragimov et al., 1989), múltiples líneas de investigación indican que la vasopresina y sus

metabolitos pueden modular procesos de memoria y aprendizaje dependientes del hipocampo. Por ejemplo, Egashira y colaboradores demuestran que ratones KO para el receptor V1a muestran déficit en una prueba de aprendizaje espacial dependiente de hipocampo (Egashira et al., 2009), Engelmann demuestra que la inyección de vasopresina por microdiálisis en el septum interfiere con la adquisición de aprendizaje en la prueba de aprendizaje espacial del laberinto acuático de Morris (MWM) (Engelmann et al., 1992), otros estudios electrofisiológicos han mostrado la facilitación de potenciales postsinápticos excitatorios en el giro dentado (Chen et al., 1993) así como un aumento prolongado de la excitabilidad de neuronas en el hipocampo ventral ((Chen et al., 1993, Chepkova et al., 2001, Urban, 1998). El sistema septo-hipocampal recibe una importante inervación vasopresinérgica (Alescio-Lautier et al., 2000, Buijs, 1978) y se considera que en esta estructura las acciones de la vasopresina están mediadas por receptores V1a acoplados a proteínas Gq y a la activación de PLC, que se expresan ampliamente en CA1, CA2, CA3 y giro dentado (Barberis and Tribollet, 1996, Bielsky et al., 2005, Raggenbass, 2001, Szot et al., 1994).

Los receptores V1b también están acoplados a la activación de PLC, pero su distribución es más específica (Hernando et al., 2001, Lolait et al., 1995a, Stemmelin et al., 2005). Young realizó un estudio de hibridación *in-situ* utilizando ribosondas marcadas, con alta sensibilidad contra el receptor V1b y encontró que en ratones, los receptores V1b sólo se expresan prominentemente en neuronas piramidales de CA2 de hipocampo (Young et al., 2006), la función de dichos receptores V1b aún no ha sido esclarecida. En contraste con la gran cantidad de estudios sobre los efectos conductuales y electrofisiológicos de la administración de vasopresina en el hipocampo, o los detallados estudios sobre la expresión de subtipos de receptores en hipocampo, poco se conoce sobre el origen de las fibras que inervan el hipocampo, la distribución de esta inervación dentro de las regiones hipocampales o el tipo de sinapsis que forman.

2.2 El sistema de respuesta al estrés

La habilidad que tenga un organismo de responder a amenazas internas o externas es crítica para su sobrevivencia. A la serie de respuestas fisiológicas que se ponen en marcha para restaurar el equilibrio cuando el organismo es expuesto a estímulos que lo alejan de la homeostasis se le define como estrés (Selye, 1936). El término estresor se refiere a cualquier estímulo, real o percibido que induce una respuesta de estrés. Generalmente un aumento significativo en la concentración de “hormonas de estrés” (i.e. adrenalina, noradrenalina, glucocorticoides) es un indicador de una respuesta al estrés. Es importante notar que hay múltiples sistemas que están encargados de orquestrar dicha respuesta al estrés y que éstos tendrán una mayor o menor participación dependiendo del tipo, severidad y temporalidad del estresor.

El sistema autónomo está encargado de la regulación de muchas funciones a través de sus conexiones recíprocas con prácticamente todos los órganos del cuerpo. La parte central de este sistema se ubica principalmente a nivel de la médula espinal y tallo cerebral y se divide en sistema simpático y parasimpático, los cuales preparan al cuerpo para un estado de escape/lucha o de reposo/síntesis respectivamente. Por ejemplo, ante una amenaza la rama simpática promoverá el incremento en la frecuencia y fuerza de contracción del corazón, aumento de flujo sanguíneo a músculos esqueléticos, disminución del peristaltismo intestinal, y aumento de la glucemia. El sistema nervioso simpático inerva la porción medular de las glándulas suprarrenales, y la activación de este sistema simpato-adrenal lleva a la liberación de catecolaminas (adrenalina y noradrenalina), lo que induce una respuesta adaptativa rápida ante el estresor (Figura 2-6), al mismo tiempo que se ponen en marcha otros sistemas que sostendrán esta respuesta por más tiempo si es necesario (Boron and Boulpaep, 2009).

El eje HPA es clave en la respuesta sostenida al estrés. Los componentes clave de éste sistema se encuentran en el hipotálamo, una región filogenéticamente antigua del cerebro en la que neuronas localizadas en el núcleo paraventricular del hipotálamo (PVN) integran información recibida de diferentes partes del cerebro sobre la naturaleza de diversos estresores y liberan el factor liberador de corticotropina (CRF). El CRF es transportado

hacia la pituitaria anterior donde activa células que secretan hormona adrenocorticotropa (ACTH) a la circulación periférica, la ACTH tiene receptores en células que se hallan en la corteza de las glándulas adrenales, las cuales son capaces de sintetizar glucocorticoides (principalmente cortisol en humanos y corticosterona en ratas) (Figura 2-6). Los glucocorticoides secretados tienen efectos pleiotrópicos, con un curso temporal diferido y más duradero. Entre sus efectos destacan la alteración del metabolismo energético, la degradación proteica, efectos cardiovasculares y efectos sobre la conducta (Boron and Boulpaep, 2009). Se considera clásicamente que ante prácticamente cualquier estresor respondemos con una activación estereotípica del eje HPA, con liberación de CRF → ACTH → glucocorticoides.

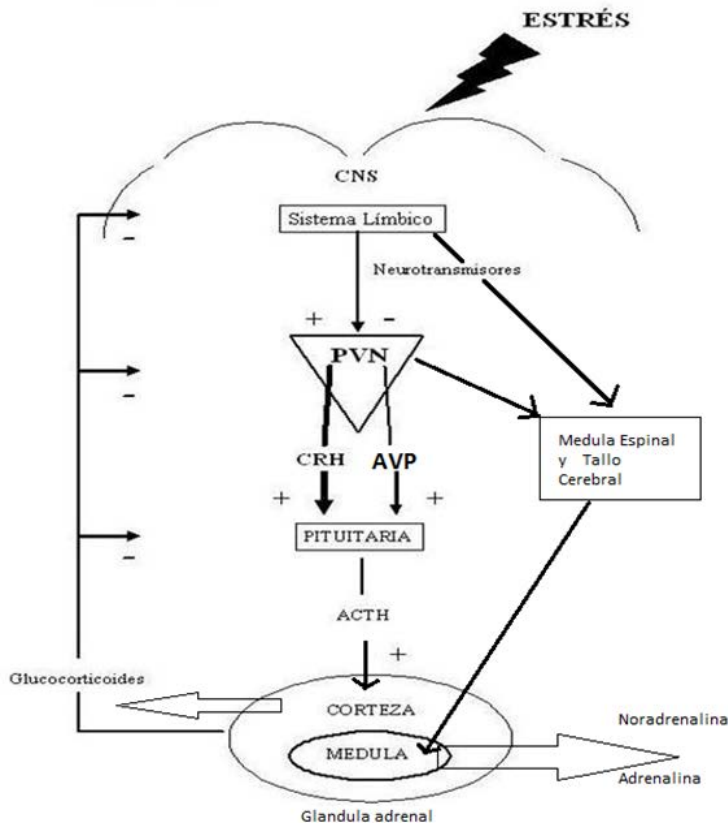


Figura 2-6 El sistema de respuesta al estrés puede actuar de una forma rápida a través del sistema simpato-adrenal y la consiguiente liberación de catecolaminas por la médula adrenal, o más lenta y prolongadamente por medio de la activación del sistema HPA y la consiguiente liberación de glucocorticoides. Ante algunos estresores, la hormona vasopresina juega un papel relevante como sinergista de CRF o como protagonista en la respuesta al estrés. Sistemas de retroalimentación negativa contribuyen a terminar la respuesta cuando se alcanza la homeostasis, fallas en dichos sistemas son deletéreos para el individuo.

Se ha demostrado que en algunos casos el sistema vasopresinérgico neurohipofiseal también participa en la respuesta al estrés. En condiciones normales la vasopresina, sintetizada por neuronas vasopresinérgicas MNN's, sinergiza con el CRF para activar a los corticotropos de la hipófisis (Aguilera and Rabadan-Diehl, 2000, Antoni, 1993). En casos de pérdida de volumen sanguíneo o de aumento de la osmolaridad plasmática, se recluta preferentemente al sistema vasopresinérgico (Dunn et al., 1973). Otros casos en que se ha sugerido que la vasopresina tiene un papel preponderante son en la etapa neonatal (Dent et al., 2000, Makara et al., 2008), y en casos de estrés crónico (Zelena et al., 2008, Ducsay et al., 2009, Chowdrey et al., 1995).

La respuesta individual al estrés está determinada por la configuración genética del individuo y la influencia del ambiente a las que ha estado sujeto. Cada vez es más claro que el estrés durante el desarrollo temprano es un factor importante en la programación de distintos aspectos de la fisiología del individuo. Durante la vida fetal estresores tales como carencias nutricionales (Creasy, 1991), ingesta de alcohol (Faden et al., 1997) y tabaquismo (Tuthill et al., 1999) pueden alterar el desarrollo normal del feto y tener como consecuencia nacimientos pre término, bajo peso al nacer o abortos. Por otro lado, condiciones adversas durante la etapa fetal se han asociado a enfermedades durante la vida adulta, por ejemplo, la privación de comida durante la gestación incrementa el riesgo de padecer diabetes, obesidad y enfermedades cardiovasculares durante la vida adulta (Barker and Osmond, 1986, Ravelli et al., 1998) y el uso de fármacos (talidomida) se ha asociado a defectos en la formación de las extremidades (McCredie and Willert, 1999). Por último, la alteración del ambiente fetal puede tener efectos sobre el desarrollo del cerebro y dichos efectos pueden perdurar hasta la vida adulta, en forma de alteraciones morfo-funcionales.

Experiencias negativas durante la vida temprana como abuso, abandono, o trauma severo han sido iterativamente asociadas a una mayor propensión a sufrir trastornos emocionales como depresión y ansiedad (Heim et al., 2004, Zhang et al., 2008, Zhang et al., 2010), esquizofrenia, (Howes et al., 2004, van Os and Selten, 1998) deterioro cognitivo (Hernandez et al., 2012, LeWinn et al., 2009, Richards and Wadsworth, 2004) y abuso de sustancias adictivas (Faden et al., 1997, Kalinichev et al., 2003). Sin embargo, no todos los individuos que experimentan situaciones adversas durante las primeras etapas de la vida

desarrollan psicopatologías. Cada vez es más claro que la interacción entre el ambiente y el genoma determinará en qué punto en el *continuum* del espectro resiliencia-vulnerabilidad se ubicará el individuo (Figura 2-7).

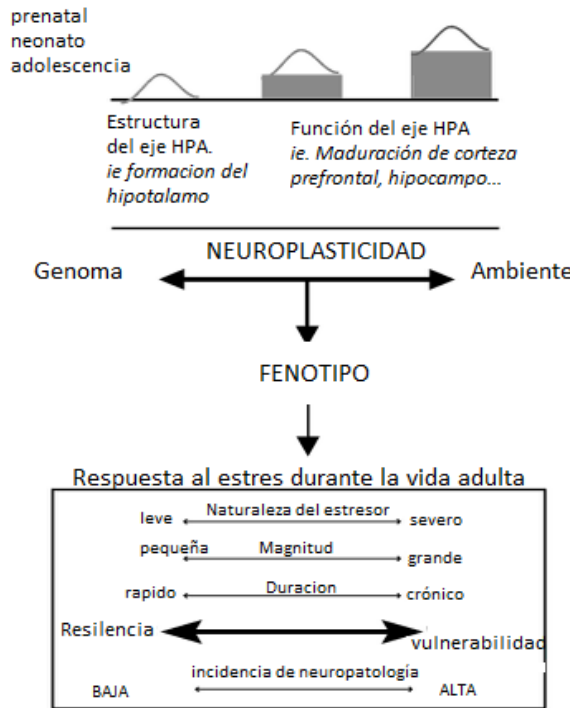


Figura 2-7. La respuesta al estrés durante la vida adulta es altamente variable entre individuos, y depende de factores tales como la naturaleza del estresor (intensidad, duración, predictibilidad, tipo, etc). La eficiencia de los individuos para enfrentarse al estrés los coloca en algún punto del espectro de resiliencia-vulnerabilidad, siendo los más vulnerables aquellos individuos que ante un estrés tienen más posibilidades de desarrollar respuestas mal adaptativas o psicopatologías. El lugar que ocupa un individuo dentro de este espectro está determinado por la influencia modeladora que el ambiente tuvo sobre su genoma (neuroplasticidad). Existen etapas críticas en la formación de los circuitos de respuesta al estrés (líneas curvas) donde hay una mayor neuroplasticidad, durante estas etapas sensibles el ambiente puede alterar importante y perdurablemente el desarrollo de estos sistemas. Estas etapas ocurren sobre la base de etapas que previamente fueron críticas en el desarrollo de dichos sistemas. Modificado de Wright, L. 2012. (Wright and Perrot, 2012)

Durante todo el desarrollo, pero en mayor grado durante el desarrollo prenatal, infancia y adolescencia, el sistema nervioso se remodela a través de distintos procesos específicos de tipos celulares, regiones cerebrales y ventanas temporales (diferenciación celular, proliferación y migración neuronal, formación de sinapsis, mielinización, apoptosis) (Rice and Barone, 2000). Es durante estos procesos que la experiencia puede modelar el neurodesarrollo, a este fenómeno se le llama neuro-plasticidad. Los pronunciados efectos organizacionales del estrés perinatal pueden deberse a la aumentada plasticidad durante estas etapas. La teoría del origen de la enfermedad y salud en el desarrollo, propuesta por Barker en 1986 plantea que la adaptación temprana del organismo a las condiciones ambientales prevalentes modela la estructura y función de los órganos (Barker and Osmond, 1986). Es de esperarse que los circuitos neuronales inmaduros que procesan la respuesta ante un estresor funcionen de forma diferente durante estas etapas tempranas, los estresores coincidentes con el desarrollo ontogénico de dichos circuitos tendrán mayor posibilidad de alterar su desarrollo

normal (Fumagalli et al., 2007). La identificación de los sustratos neurobiológicos que son afectados por los estresores perinatales puede ayudar a esclarecer cómo es que la experiencia puede “programar” nuestra personalidad y conducta y contribuir a identificar blancos para el tratamiento de trastornos psiquiátricos.

Con el fin de poder investigar bajo un ambiente controlado el efecto de distintos tipos de estresores durante ventanas particulares del desarrollo, se han desarrollado numerosos modelos animales. En la mayoría de los modelos de estrés prenatal hembras gestantes se exponen a diversos estresores físicos, psicológicos u hormonales y se estudian los cambios estructurales y conductuales a corto y largo plazo. Diversos paradigmas han sido usados tales como inmovilización (Maccari et al., 1995), estrés crónico variable (Koenig et al., 2005), exposición a privación de sueño, choques eléctricos, inmersión en agua fría, entre otros. (Weinstock, 2001).

En el caso del estrés durante la etapa fetal, se considera que la información ambiental es traducida por la madre al feto a través de mensajes hormonales. Se han realizado estudios donde se modifica el ambiente hormonal del feto y se observa que aún pequeñas variaciones en las concentraciones hormonales ejercen poderosos efectos sobre el neurodesarrollo, en particular las hormonas gonadales, los corticosteroides y las hormonas tiroideas han sido ampliamente estudiadas y han mostrado tener una gran influencia sobre el desarrollo del sistema nervioso (Collaer and Hines, 1995, Sikich and Todd, 1988, Weinstock, 2001, Abduljabbar and Afifi, 2012, Burrow, 1993, Zhang et al., 2008)

En relación a los estresores post-natales, en roedores durante las dos primeras semanas de vida extrauterina, las concentraciones basales de glucocorticoides son bajas y estímulos nociceptivos o la administración de ACTH inducen sólo una tenue respuesta del eje HPA, a este periodo se le ha llamado periodo hipo-responsivo al estrés (Sapolsky and Meaney, 1986, Levine, 1994, Lupien et al., 2009, Schapiro et al., 1962). Algunos de los estímulos que han sido exitosos en activar la respuesta al estrés durante este periodo y propiciar cambios perdurables se mencionan a continuación.

Manipulación temprana: es uno de los primeros paradigmas descritos que manipulan la interacción entre la madre y las crías (Levine, 1957). Este modelo consiste en separar y

manipular a las crías durante periodos de aproximadamente 15 minutos diarios durante las primeras dos semanas de vida. Esta breve manipulación induce una respuesta neuroendocrina en las crías y una mayor atención por parte de las madres al ser reincorporadas a su camada. Generalmente se observa que al llegar a la edad adulta, estas ratas muestran menos conductas tipo ansiedad (Durand 1998).

Separación materna repetida: este protocolo consiste en separar a las crías de sus madres por periodos que oscilan entre una y ocho horas al día y entre una y tres semanas. Dentro de este paradigma hay variaciones en relación al tiempo de separación, el periodo durante el cual son separadas las crías, si las crías se separan individualmente o la camada entera, la temperatura y la humedad durante la separación (Heinrichs and Koob, 2006). Las consecuencias en conductas emocionales y cognitivas durante la vida adulta son aun materia de debate.

Separación materna por 24 horas: este paradigma consiste en un único episodio de 24 horas de separación de la madre. Este modelo ha sido usado ampliamente en el estudio de la función neuroendocrina durante el desarrollo temprano (Dent et al., 2000, Dent et al., 2001, Ladd et al., 1996, Liebl et al., 2009, Sutanto et al., 1996), aunque ha sido poco usado para estudiar los efectos a largo plazo sobre las conductas emocionales y cognitivas.

Variaciones naturales en el cuidado materno: este modelo se basa en la selección de madres que expresan pocas conductas maternas y madres que expresan conductas maternas excesivas, en general se ha visto que las crías de madres con pocas conductas maternas expresan un fenotipo más ansioso que las que fueron criadas por madres protectoras (Caldji et al., 1998, Landgraf and Wigger, 2002, Liu et al., 1997).

Empobrecimiento del material para nido: este modelo ha sido recientemente establecido por el grupo de Baram (Brunson et al., 2005, Ivy et al., 2008, Rice et al., 2008). Las madres son provistas de poco material para hacer su nido, lo que ocasiona cambios en las conductas maternas y un cuidado maternal fragmentado. Este modelo propicia un fenotipo de ansiedad y déficits cognitivos.

Glucocorticoides postnatales: este modelo se basa en la aplicación postnatal de dosis grandes de glucocorticoides y se ha observado que modela muchos de los efectos que se observan a largo plazo en niños prematuros tratados con glucocorticoides, tales como: déficits cognitivos, motores y alteraciones neuroendocrinas (Felszeghy et al., 1993, Feng et al., 2015). La aplicación exógena de glucocorticoides durante la etapa neonatal induce aumento en conductas de ansiedad y depresión en ratas adultas.

Siendo el hipotálamo una región particularmente vulnerable a diversos estresores perinatales (Zhang et al., 2008, Aisa et al., 2007, Anisman et al., 1998, Tsuda et al., 2011, Orelan et al., 2010, Veenema and Neumann, 2009, Murgatroyd et al., 2009, Korosi and Baram, 2009), numerosos estudios han evaluado el sistema HPA (CRF→ACTH→CORT), sin embargo son pocos los estudios que han evaluado las consecuencias de estresores perinatales sobre el desarrollo del sistema vasopresinérgico (Desbonnet et al., 2008, Murgatroyd et al., 2009, Orelan et al., 2010, Tsuda et al., 2011, Veenema and Neumann, 2009, Aisa et al., 2007, Zhang et al., 2012, Zhang et al., 2010).

Tradicionalmente se considera que en el eje HPA la liberación de CRF y AVP del PVN estimula la secreción de ACTH desde la pituitaria y esto a su vez provoca la liberación de glucocorticoides adrenales. Además de la gran cantidad de reportes que describen la secreción de CRF-ACTH-glucocorticoides y las anormalidades en sus receptores observadas en roedores sometidos a separación materna (Fumagalli et al., 2007, Kalinichev et al., 2002, Korosi and Baram, 2009, Kuhn and Schanberg, 1998), se ha reportado que la maduración normal del sistema de AVP desde el periodo perinatal hasta la etapa adulta puede verse afectada por la separación materna. Sin embargo no existe un acuerdo respecto al efecto que ésta tiene sobre los niveles de AVP, ya que en el hipotálamo se han reportado como incrementados (Murgatroyd et al., 2009, Veenema and Neumann, 2009), reducidos (Desbonnet et al., 2008) o sin cambios (Orelan et al., 2010). Actualmente no existe información acerca de los posibles mecanismos fisiológicos detrás de estas modificaciones del sistema vasopresinérgico.

3. Planteamiento del Problema

Se ha reportado abundante evidencia indicando que estresores durante la vida temprana pueden ejercer efectos de re-organización en el sistema nervioso central de los organismos. La mayoría de estos trabajos coinciden en afirmar que la reactividad al estrés durante la vida adulta aumenta a través de modificar el eje de respuesta al estrés (eje hipotálamo-pituitaria-adrenal, HPA). Durante el periodo perinatal, el sistema vasopresinérgico participa importantemente en las adaptaciones homeostáticas para la transición desde la vida fetal hasta la vida extrauterina, por lo que es posible suponer que este sistema también modula el desarrollo del eje HPA.

Aunque existen en la literatura algunos reportes sobre los efectos epigenéticos del estrés perinatal sobre el sistema vasopresinérgico, no es claro si los estresores perinatales pueden alterar la organización anatómico-funcional del sistema vasopresinérgico neurohipofiseal (i.e. el sistema que incluyen las neuronas vasopresinérgicas neurosecretoras magnocelulares, *MNN's*). Si lo hacen, sería importante identificar las conexiones funcionales alteradas, y los efectos de la activación de dichas conexiones sobre la actividad neural de regiones innervadas por neuronas *MNN's* y sobre las conductas asociadas a dichas regiones.

4. Hipótesis

- La activación temprana del sistema vasopresinérgico hipotálamo - neurohipofiseal por estresores durante el periodo perinatal genera modificaciones perdurables en su estructura y función.
- Las neuronas hipotálamicas vasopresinérgicas magnocelulares neurosecretoras (MNN's) proyectan a diversas estructuras corticales involucradas en conductas emocionales y cognitivas.
- La modulación a la alta del sistema vasopresinérgico neurohipofiseal de los individuos que se han sometido a estrés temprano, con el sistema vasopresinérgico re-organizado, generará cambios en los patrones de activación de las regiones inervadas por MNN's y modificará el comportamiento en que dichas regiones participan.

5. Objetivos

Objetivo general:

Nuestro objetivo general es evaluar el efecto del estrés perinatal sobre el desarrollo del sistema vasopresinérgico neurohipofiseal y describir la conectividad funcional de la red neural vasopresinérgica intracerebral intacta. Concretamente, es obtener el *conectoma* vasopresinérgico en ratas control y sometidas a estrés durante el desarrollo temprano. Pondremos el énfasis en la regulación del eje hipotálamo-pituitario-adrenal (HPA) y la modulación de la cognición y emocionalidad.

Objetivo específicos:

1. Determinar si la exposición a estresores perinatales (hipertiroidismo materno y separación materna) alteran el desarrollo normal del sistema vasopresinérgico hipotalámico neurohipofiseal (HNS).
 - 1.1. Determinar por ELISA si el hipertiroidismo prenatal modifica las concentraciones séricas de AVP en condiciones basales o ante un reto osmótico.
 - 1.2. Determinar por medio de la expresión de Fos (producto del gen de expresión temprana *c-fos*) si el hipertiroidismo prenatal modifica el patrón de activación de neuronas MNNs ante un reto osmótico, o estímulos ansiogénicos.
 - 1.3. Determinar por inmunohistoquímica si el hipertiroidismo prenatal modifica la expresión de vasopresina en el sistema hipotálamo neurohipofiseal.
 - 1.4. Determinar por ELISA si la separación materna modifica las concentraciones séricas de AVP en condiciones basales o ante un reto osmótico.

- 1.5. Determinar por medio de la expresión de Fos, si los episodios de separación materna pueden activar al sistema vasopresinérgico desde etapas tempranas del desarrollo.
- 1.6. Determinar por hibridación *in-situ* e inmunohistoquímica si la separación materna induce modificaciones en la expresión del mRNA y el péptido de vasopresina en los núcleos PVN y SON del hipotálamo.
2. Determinar los patrones de innervación intracerebral de neuronas vasopresinérgicas magnocelulares neurosecretoras (MNN's).
 - 2.1. Determinar por inmunohistoquímica la densidad y el patrón de innervación vasopresinérgica en hipocampo.
 - 2.2. Identificar el fenotipo inmunohistoquímico de los blancos postsinápticos de los axones AVP+ en hipocampo.
 - 2.3. Determinar por medio de trazadores neurales, si los núcleos PVN y SON del hipotálamo participan en la innervación vasopresinérgica del hipocampo.
 - 2.4. Caracterizar por medio de inmunohistoquímica y trazado auxiliado por computadora el trayecto que toman los axones de proyección central de neuronas MNNs vasopresinérgicas que se dirigen hacia hipocampo.
 - 2.5. Caracterizar por medio de marcaje yuxtacelular, las vías de proyección intracerebral de axones de neuronas MNN's vasopresinérgicas y sus blancos regionales.
3. Determinar las consecuencias de la activación del sistema HNS sobre conductas emocionales y cognitivas que sean moduladas por áreas inervadas por neuronas MNN's.

- 3.1. Evaluar la conducta de ansiedad condicionada (bajo estrés osmótico, en prueba de Vogel Conflict Test) y no condicionada (condiciones basales, en prueba de EPM) de animales que fueron sometidos a hipertiroidismo materno.
- 3.2. Evaluar el aprendizaje espacial por medio de la prueba de Morris water maze (MWM) en ratas que fueron sometidas a separación materna (sistema AVP modificado) en condiciones de modulación a la alta (estrés osmótico agudo) o modulación a la baja (antagonista de receptor vasopresinérgico).
- 3.3. Evaluar el efecto de la activación del sistema vasopresinérgico (inyección de solución hipertónica), sobre las conductas pasivas o activas de enfrentamiento a un estrés por predador.
- 3.4. Determinar si las áreas cerebrales que reciben innervación AVP por neuronas MNNs, modifican su patrón de activación (inmunohistoquímica anti Fos) inducido por el predador, cuando el animal es sometido a un estrés osmótico.

6. Métodos

6.1 Animales

Se usaron ratas Wistar del bioterio de la Facultad de Medicina de la UNAM, todos los procedimientos fueron hechos con base en los principios presentados en las Guías para el Cuidado y Uso de Mamíferos en Investigación en Neurociencias y Conductual, editada por el *National Research Council* (National Research Council, 2003), los animales fueron alojados en un cuarto con adecuada ventilación y temperatura controlada entre 20 y 24 °C, con agua y comida *ad libitum*, y un ciclo de luz/oscuridad de 12/12 horas, salvo que sea especificado de otra forma. En caso de cirugías donde los animales se recuperasen, éstos se mantuvieron con temperatura controlada y se les administró un analgésico mientras se recuperaban de la anestesia, posteriormente se dejaron una semana en cajas individuales durante la recuperación y posteriormente se regresaron a las condiciones iniciales. En caso de registros yuxtacelulares, los animales se mantuvieron profundamente anestesiados hasta su sacrificio.

6.2 Inserción de bombas de liberación prolongada de hormonas tiroideas

Ratas hembras en el día postnatal 90 (P90) fueron sometidas a cirugía para la inserción de una bomba osmótica Alzet (modelo 2ML4, tasa de bombeo de 2.5 µl/h, durante 28 días, DURECT Corporation), las bombas se implantaron de forma subcutánea en la región inter-escapular, bajo anestesia general (pentobarbital, 50 mg/kg *i.p.* Barbital, Holland de México, SA de C. V). Las bombas Alzet fueron llenadas con solución salina o con una solución de L-tiroxina (T4, Sigma-Aldrich Inc. T2501, St. Louis, MO, EE.UU), calculada para liberar 15 µg/día por kg de peso. Con esta dosis la concentración plasmática de T4 libre en la rata fue de aproximadamente 2.26 ± 0.14 ng/dl (n=4), mientras que las ratas controles tenían aproximadamente 1.34 ± 0.11 ng/dl (n=4), estos niveles se consideran un hipertiroidismo leve (Evans et al., 2002, Varas et al., 2001). Las mediciones de las concentraciones plasmáticas de vasopresina fueron hechas con un inmunoensayo de quimioluminiscencia (CMIA,

ARCHITECT®, Abbott Laboratories, Abbott Park, IL, USA) a partir de muestras tomadas de ratas en el día 10 de gestación, las ratas fueron anestesiadas profundamente y se sacrificaron antes de que despertaran.

6.3 Apareamiento y selección de grupos control y HM

Después de dos días de recuperación de la cirugía, las ratas hembras se aparearon con machos normales durante tres días consecutivos. Las hembras fueron alojadas individualmente durante el período gestacional. Las crías nacieron entre 19 y 21 días después de los 3 días de apareamiento y los tamaños de las camadas fueron de 11.8 ± 0.82 (media \pm SEM) ratas sometidas a hipertiroidismo materno (HM) contra 11.6 ± 0.66 para los controles. Las madres fueron alojadas con su camada durante el período de lactancia evitando manipularlas salvo para el cambio de cama y la administración de alimento y agua. Las bombas osmóticas fueron extirpadas de las ratas 1 día después del parto (P1), bajo anestesia local (0.2 ml de lidocaína al 1%). Después de la extracción la piel se suturó y fueron devueltas a sus jaulas. Las suturas se retiraron después de 4 días. Todos estos procedimientos duraron como máximo 20 min. No observamos anomalía alguna respecto a la atención materna entre las ratas con HM y las ratas controles. En P30, se separaron las ratas en cajas de 4 animales cada una, evitando poner más de un individuo de la misma camada en cada caja, los experimentos se realizaron con ratas provenientes de distintas camadas. La actividad locomotora, el peso corporal, la glucemia y el nivel de T4 en suero fueron evaluados en el día P90 y no se hallaron diferencias significativas entre HM y controles. Los experimentos conductuales se llevaron a cabo entre P90 y P100.

6.4 Inmunohistoquímica para Fos y AVP en ratas sometidas a hipertiroidismo materno

Los sujetos de experimentación para este experimento fueron perfundidos 90 min después de 6 horas de privación de agua (WD6h) y posterior a la prueba de conflicto de Vogel (PVCT). Se realizó un doble marcaje inmunofluorescente, se eligieron dos rebanadas alternas entre Bregma -1.6 y -1.8 mm de acuerdo al atlas de Paxinos (Paxinos and Watson, 2007) de cada

rata, que contuvieran la región magnocelular principal del núcleo paraventricular (PVN_{lm}), la zona dorsal del PVN (PVN_{mpd}, principal región de expresión del mRNA para CRF (Viau and Sawchenko, 2002)) y al núcleo supraóptico (SON); este criterio se aplicó para hacer comparaciones válidas entre los datos obtenidos. Las rebanadas se bloquearon en suero normal de caballo (NHS) al 20%, en buffer de Tris (TB, 0.05 M, pH 7.4), más solución salina (0.9%), más Tritón X -100 al 0.3% (TBST) por una hora, a temperatura ambiente. Posteriormente se hizo la reacción inmune con los siguientes anticuerpos: conejo anti-AVP (cortesía de Buijs RM, 1:1000) y cobayo anti-CRF (T-5007, 1:2000, Península Laboratories, Torrence, CA, USA); para el marcaje de Fos se usó conejo anti-Fos (SC52, 1:1000, Santa Cruz Biotechnology, Santa Cruz, CA, USA) y cobayo anti-AVP (T-5048, 1:2000, Peninsula Laboratories). Las rebanadas se incubaron toda la noche a 4 °C con agitación suave; se lavaron adecuadamente y posteriormente se incubaron con Alexa Fluor 488 burro anti-conejo IgG (1:1000, Molecular Probes Inc., Eugene, OR, USA) y Cy3 conjugado burro anti-cobayo (1:1000, Jackson ImmunoResearch Laboratories Inc., Baltimore, PA, USA) como anticuerpos secundarios, toda la noche a 4 °C. Al terminar la reacción inmune las rebanadas se enjuagaron y se montaron con Vectashield (Vector Laboratories Inc., Burlingame, CA, USA) y se analizaron por microscopía de epifluorescencia.

Para la cuantificación de neuronas Fos/AVP doble marcadas y para la cuantificación de Fos total, se contó el número de neuronas AVP+ y Fos+/AVP+ en el PVN_{lm} y en el SON, por rebanada, se calculó el porcentaje de neuronas doble marcadas en relación al número total de neuronas AVP+, para la cuantificación de la activación total de Fos se contaron todos los núcleos Fos+ dentro de la región magnocelular inmunoreactiva (PVN_{lm} y SON AVP+). Para PVN_{mpd}, se hizo el conteo con la ayuda de un tubo de dibujo: se colocó un cuadrado dibujado de 0.04 mm² en el campo visual del tubo, coincidiendo con la zona PVN_{mpd} de tal manera que los núcleos Fos+ pudieran ser vistos y contados claramente.

La meta de la segunda serie de experimentos fue la de evaluar el contenido de AVP en el sistema hipotálamo-neurohipofiseal (HNS) antes de la aplicación del estresor. Se hizo una IHC contra AVP a 4 ratas en condiciones basales, utilizando los anticuerpos cobayo anti-AVP (T-5048, 1:2000, Peninsula Laboratories) y Alexa Fluor 488 burro anti-cobayo (1:1000, Molecular Probes). Se midió la densidad óptica asociada al tracto hipotálamo-

neurohipofiseal (HNT) en el área hipotalámica anterior (AHA-zona dorsal y ventral) de cada grupo, pareando rebanadas coronales antero-posteriormente (n=10) del hipotálamo anterior (Bregma -1.08 a -1.86 mm). Los campos (zona dorsal y ventral, correspondientes al HNT) con un área de 0.22 mm² se eligieron con el objetivo 40X y se fotografiaron, usando una cámara digital. Las fotografías digitales se analizaron utilizando Fovea Pro 4.0 (Reindeer Graphics, Asheville, NC, USA). Se cuantificaron los cuerpos de Herring (varicosidades axonales en el HNT); se ha sugerido que los cuerpos de Herring funcionan como amortiguadores para la producción masiva de AVP, formada por la síntesis intermitente de este péptido (Yukitake et al., 1977).

6.5 Medición de concentraciones plasmáticas de vasopresina (para animales sometidos a hipertiroidismo materno y separación materna)

Para determinar los niveles plasmáticos de vasopresina (AVP) durante la privación de agua (WD) y posterior a la prueba de VCT se obtuvieron muestras de sangre de la cola de las ratas en 6 puntos temporales diferentes: basal, antes de comenzar la WD, a las 6h de WD (WD6h), a las 12 h de WD (WH12h), a las 24 h de WD (WD24h), a las 48 de WD (WD48h) e inmediatamente después de la prueba de VCT (PVCT), para esto se inmovilizó a las ratas usando un tubo de restricción. Para minimizar el efecto estresante de este procedimiento las ratas fueron puestas en el mismo tubo (estándar para ratas (Heinrichs and Koob, 2006)) durante 30 min, los 3 días anteriores al inicio de la prueba. Se muestrearon 4 ratas por punto temporal (2 machos de la misma camada proveyeron una muestra de sangre en el mismo punto temporal, en total, 24 ratas por cada grupo) y cada rata proveyó sólo una muestra de sangre; esto con la intención de medir la liberación de AVP en respuesta a la WD como único estresor osmótico, y evitando que el estrés de la pérdida de sangre ocasionara una mayor liberación de AVP. Se tuvo especial cuidado en no utilizar ratas de la misma camada en el mismo punto temporal.

En cada punto temporal se recolectaron 500 µl de sangre en micro-tubos enfriados, con 0.5 mg de EDTA en las paredes (se agregaron 50 µl de solución de EDTA 10 mg/ml a

un tubo, este fue agitado y posteriormente refrigerado). Los tubos con muestras fueron inmediatamente centrifugados a 16 000 rpm, a 4 °C, por 15 min; el plasma sobrenadante (200 µl por tubo) fue recolectado en otro tubo y almacenado a -70 °C hasta realizar la prueba de ELISA. Se utilizó el kit de ELISA Arg8-Vasopressin EIA (cat. 900-017, Assay Designs Inc., Ann Arbor, MI 48108, EUA), se siguieron las recomendaciones del fabricante y cada muestra se analizó por duplicado. Los coeficientes de variación (CV: desviación estándar/promedio) para la variabilidad intra- e inter-ensayo fueron de 11.28% y 9.9%, respectivamente, este parámetro se obtuvo calculando el CV de 3 curvas estándar de los 3 kits utilizados.

6.6 Protocolo de separación materna (3hSM)

El protocolo de separación materna por 3 horas diarias (3hSM), se realizó de acuerdo a lo descrito por Veenema (Veenema et al., 2006). Ratas Wistar adultas, hembras y machos obtenidos del bioterio local, se aparearon durante dos días. Durante la última semana de gestación, las hembras se colocaron cada una en una caja estándar de plexiglás y se mantuvieron en condiciones estándar con ciclos 12h: 12h de luz-oscuridad (luz encendida a las 18 horas), temperatura de $22 \pm 2^\circ \text{C}$, comida y agua *ad libitum*. En el día siguiente al parto, P2, cada camada fue ajustada para tener 7 a 8 crías, siendo machos 5 a 6 de cada una. Durante el período P2 al P15 las crías fueron separadas diariamente de la madre entre las 900 horas y las 1200 horas. Las crías fueron removidas de la cama manualmente, las manos del manipulador previamente cubiertas por aserrín del nido. Posteriormente se colocaron individualmente en una caja pequeña llena con material de su propio nido, se colocaron en una incubadora húmeda mantenida a $29 \pm 1^\circ \text{C}$. Después de 3 horas las crías fueron devueltas a la caja correspondiente junto a su madre y camada. Como grupo control se usaron camadas criadas en el bioterio (AFR).

6.7 Inmunohistoquímica para determinar el volumen de los núcleos AVP+ hipotalámicos en animales sometidos a separación materna

Perfusión, fijación e inmunohistoquímica. Ocho ratas en el día P75 fueron profundamente anestesiadas con pentobarbital sódico (Sedalpharma, México, 63 mg/kg i.p.) y perfundidas vía aorta ascendente con solución salina 0.9% seguida por 15 minutos de fijador frío (compuesto de paraformaldehído 4% en buffer de fosfato de sodio 0.1 M (PB, pH 7.4), más 15 % v/v de ácido pícrico saturado). Los cerebros fueron removidos, bloqueados y lavados con PB. Con el fin de favorecer la inmunoreacción, inmediatamente después de la perfusión se obtuvieron, con la ayuda de un vibratomo, secciones coronales de 70µm del hipotálamo desde Bregma -0.24mm a -2.64mm (Paxinos and Watson, 2007). Se seleccionaron secciones alternadas y se bloquearon con buffer de Tris + NaCl 0.9% y Tritón 100x al 0.3% (TBST) más 20% de suero normal de cerdo (NSS) por una hora, a temperatura ambiente. Posteriormente se incubaron con conejo anti-AVP (T-4563, 1:2000, Peninsula Laboratories, San Carlos, CA, 94070) en TBST + 1% NSS a 4 °C, durante dos noches. Después de este lapso, las rebanadas se lavaron y se incubaron en anticuerpo secundario cerdo anti-conejo IgG conjugado con peroxidasa de rábano (P021702, 1:100, Dako, Alemania) en TBST + 1%NSS toda la noche, a 4 °C. La inmunoreacción fue revelada con 3.3'-diaminobencidina (DAB, Electron Microscopy Sciences Hatfield, PA, 19440) al 0.05% y H₂O₂, 0.01% como sustratos. Las secciones fueron montadas en cubreobjetos cubiertos de gelatina y dejadas a secar por un día. Posteriormente fueron deshidratadas pasándolas por etanol 100% durante 5 minutos, y xileno 2 veces por 5 minutos, por último fueron montadas con medio de montaje Permout (Fischer Scientific).

6.8 Medición del volumen de los núcleos hipotalámicos vasopresinérgicos en animales sometidos a separación materna

Las rebanadas reveladas por inmunohistoquímica fueron observadas, analizadas y fotografiadas digitalmente en campo claro usando un microscopio Nikon Eclipse 50i con un objetivo 4X y una cámara digital Nikon DS. Los núcleos AVP positivos en la región hipotalámica fueron clasificados como SON o PVN de acuerdo a Paxinos y Watson (Paxinos and Watson, 2007). El grupo de neuronas AVP+ de cada región fue delimitado usando Adobe

Photoshop y el área en mm^2 fue calculado con el *plug-in* Fovea Pro 4.0 (Reindeer Graphics, Asheville, NC, USA). Los volúmenes de cada núcleo/región fueron determinados integrando todas las áreas dentro de cada región, multiplicando por 0.07 mm (el grosor de cada rebanada), por dos (ya que se tomaron rebanadas alternadas) y por una constante de reducción (k). La reducción lineal del tejido después de la reacción de inmunohistoquímica fue determinada midiendo el diámetro del cerebro fresco en el quiasma óptico inmediatamente después de la perfusión (L_f) y del ancho de la sección coronal deshidratada en las mismas coordenadas, después del montaje permanente (L_d). Por lo tanto, $k=L_f/L_d$.

6.9 Reconstrucción tridimensional representativa del PVN.

Para poder visualizar la dirección del crecimiento del PVN, se hizo una reconstrucción tridimensional basada en las coordenadas anatómicas determinadas en microfotografías digitales. Se eligió un par de series de rebanadas post-inmunoreacción. Las neuronas AVP+ dentro del PVN fueron marcadas usando ImageJ (NIH, MD, USA) en microfotografías secuenciales. Las neuronas parvocelulares y magnocelulares fueron diferenciadas de acuerdo a sus ejes longitudinales, considerándose magnocelulares aquellas con ejes longitudinales mayores a $20 \mu\text{m}$, (Armstrong, 2004). Para cada una de las neuronas marcadas se obtuvieron sus coordenadas x, y, z de la siguiente manera: las coordenadas correspondientes a la ubicación bidimensional (x, y) se obtuvieron de ImageJ, (NIH, MD, USA) y la coordenada z correspondía a la posición secuencial de la rebanada. La gráfica tridimensional fue dibujada usando un programa escrito en Python (Python Software Foundation).

6.10 Evaluación de la activación de neuronas vasopresinérgicas en el PVN y SON al día P10, tras una exposición aguda a 3hSM

Para determinar el efecto de una sola exposición a 3hSM en la activación neuronal de los núcleos magnocelulares vasopresinérgicos en la región hipotalámica, se perfundieron ratas de camadas AFR y MS en el día P10. Se evaluaron dos condiciones: (1) perfusión y fijación en condiciones basales (2) perfusión y fijación 90 minutos después de un episodio de 3hSM.

Se usaron en total 20 crías de 10 camadas, cinco AFR y cinco MS. Las ratas fueron profundamente anestesiadas con una sobredosis de pentobarbital sódico (63 mg/kg, Sedalparma, México) y perfundidas con 10 ml de solución salina 0.9% seguida de 20 ml de fijador frío, compuesto de paraformaldehído 4% en buffer de fosfato de sodio 0.1 M (PB, pH 7.4), ácido pícrico saturado 15% v/v y glutaraldehído 0.05%. Posteriormente se extrajo el cerebro, se realizaron cortes coronales de 70 micras que contuvieran la región hipotalámica y se realizó sobre estas secciones una reacción de inmunofluorescencia AVP/Fos. Los anticuerpos primarios usados fueron: cobayo anti-AVP (T-5048, 1:2000, Peninsula Laboratories) y conejo anti-Fos (SC52, 1:1000, Santa Cruz Biotechnology, Santa Cruz, CA), incubados toda la noche a 4 °C con agitación leve. Después de varios lavados las secciones fueron incubadas con los anticuerpos secundarios: Alexa Fluor 488 burro anti-conejo IgG (1:1000, Molecular Probes Inc. Eugene, OR) y Cy3-burro anti-cobayo IgG (1:1000, Jackson Immuno Research Laboratories, Inc., Baltimore, PA), en TBST más 1% de suero normal de caballo (NHS) a 4 °C, toda la noche. Posteriormente, las secciones se lavaron y montaron con Vectashield (Vector Laboratories, Inc., Burlingame, CA) y se analizaron por microscopía de epifluorescencia, usando un microscopio Nikon 50i con un filtro de emisión pasa-altos N-2B. Se escogieron campos al azar en las regiones PVN y SON con el objetivo de 40x, correspondientes a áreas de 0.22 mm² y se tomaron microfotografías con una cámara digital. Se contó el número total de neuronas AVP+ y el número de neuronas Fos+/AVP+ de los núcleos PVN y SON (en tres secciones coincidentes por rata, n=15). Se calculó el porcentaje de las neuronas con doble marcaje respecto al total de neuronas AVP+.

6.11 Inmunohistoquímica para análisis por microscopía de luz de densidad de fibras vasopresinérgicas y trayectorias hacia hipocampo.

Para estos experimentos se utilizaron 10 ratas, observaciones previas del laboratorio habían mostrado que existen variaciones individuales importantes en la inmunoreactividad anti vasopresina, probablemente debido a una regulación circadiana o a las demandas fisiológicas que experimenta el individuo al momento de la perfusión. Con esto en mente, inyectamos

intraperitonealmente una solución hipertónica de NaCl 900 mMol, con un volumen del 2% del peso corporal y restringimos el acceso a los bebederos de agua durante 2 horas después de la inyección, posteriormente se les permitió a las ratas beber ad-libitum por las dos horas previas a la perfusión, esto con el fin de poner en marcha los mecanismos de síntesis de vasopresina (Robertson et al., 1976, Summy-Long et al., 1978), evitando la liberación de vasopresina en las dos horas previas a la perfusión, es de notar que se ha reportado que el estrés osmótico produce un aumento en la expresión hipotalámica de Fos que es un inductor transcripcional temprano del gen de la vasopresina (Yoshida, 2008). Tomando estas medidas hallamos una mayor y más homogénea inmunoreactividad de vasopresina.

Para la perfusión se anestesió profundamente a las ratas con una sobredosis de pentobarbital sódico (Sedalpharma, Mexico), se perfundieron con solución salina al 0.9% por vía trans-aórtica y posteriormente 400 ml de fijador a 4 °C: (4% paraformaldehído (PFA) en buffer de fosfatos (PB 0.1M, pH 7.4), más 15% v/v de ácido pícrico saturado). Los cerebros fueron inmediatamente removidos del cráneo, lavados varias veces en PB y posteriormente fueron seccionados a 70 µm con un vibra tomo Leica VT1000.

Se realizaron cortes en 4 planos: 3 coronal, 3 sagital; 2 septo temporal (plano 45° entre coronal y sagital) y 2 semi horizontal (30 grados respecto a plano horizontal). Se realizó la inmunohistoquímica de dos series de rebanadas alternas. En la serie uno (reacción de inmunoperoxidasa), las rebanadas se bloquearon con suero normal de cerdo al 20% en TBST, (Buffer de Tris 0.05 M, pH 7.4, NaCl 0.9% y 0.3% tritón) por una hora. En la serie 2 (inmunofluorescencia) se bloquearon en TBST + 20% suero normal de caballo, por una hora a temperatura ambiente. Posteriormente las rebanadas se incubaron con los siguientes anticuerpos: conejo anti-AVP, conejillo de indias anti-mGluR1α y ratón anti-parvalbúmina en TBST más 1% del suero del animal de origen del anticuerpo secundario, durante dos noches a 4° C. Para la reacción de inmunoperoxidasa, las secciones se lavaron tres veces con TBST y se incubaron con anticuerpo cerdo anti-conejo conjugado con peroxidasa de rábano (HRP) (P021702, 1: 100, Dako, Dinamarca) en TBST más 1% de suero normal de cerdo a 4° C toda la noche. La reacción fue revelada usando 3, 3'-diaminobencidina (DAB, 0.05%) y peróxido de hidrógeno 0.01% como sustratos. Las secciones se montaron en gelatina, se clarificaron con alcohol y xileno y se montaron permanentemente con Permout. Para las

reacciones de inmunofluorescencia se usaron los siguientes anticuerpos secundarios: Cy3-burro anti-conejo, Alexa-488 burro anti-ratón y DyLight-649 burro anti-conejillo de indias (dilución 1:1000 en TBST mas 1% suero normal de burro) por dos horas a temperatura ambiente. Las secciones fueron montadas con Vectashield (Vector Laboratories, CA, USA) y analizadas con un microscopio de epifluorescencia (Nikon eclipse 50I) y por microscopía confocal (Leica TCS-SP5).

6.12 Análisis de densidad de fibras vasopresinérgicas en hipocampo

La observación de la densidad de fibras vasopresinérgicas en distintas subregiones de hipocampo y amígdala se realizó bajo microscopía de luz, las regiones se definieron en base al atlas de Paxinos y Watson (Paxinos and Watson, 2007). Para evaluar la distribución y densidad de las fibras de vasopresina se tomaron fotos con el objetivo 20X en diferentes subcampos del hipocampo. A, partir de estas fotos se realizaron proyecciones planares de cinco microfotografías en diferentes planos focales, posteriormente, en estas microfotografías, se trazó la longitud de los axones por medio del programa Neuron J. La suma de las longitudes de los axones se obtuvo usando el mismo programa. La longitud máxima hallada (2460 μm) fue a nivel de CA1 stratum oriens (str. or.) en la sección sagital 5.72 mm (Tabla 1) y fue asignada como la longitud máxima (100%, ++++). El mismo procedimiento de trazado y cálculo de la longitud fue realizado en las proyecciones planares para cada una de las regiones de hipocampo, longitudes entre el 100% y el 76% fueron asignadas como (++++) de 75% a 51% fueron calificadas como (+++); de 50% a 26% (++) y menos de 26% (+), cuando no había fibras observadas en esa región se calificó como (-) y cuando no fue aplicable realizar el análisis en dicha sección (NA) . Los esquemas de la distribución de densidad de fibras vasopresinérgicas fueron realizados sobre microfotografías digitales con ayuda de observación microscópica. El mapeo tridimensional (1:1) de los axones vasopresinérgicos fue realizado usando 38 secciones alternativas de 70 μm cada una, por medio de una estación de trabajo NeuroLucida la cual incluye un microscopio Nikon OptiHot 2, el software NeuroLucida versión 9.14 y NeuroLucida Explorer versión 9.14.

6.13 Aplicación de trazadores retrógrados en hipocampo ventral y dorsal

Se utilizó un método modificado de trazador retrógrado con Fluoro-Gold (Schmued, 1986, 1989, 1990, Morales y Wang, 2002, Yamaguchi, 2011). Usamos 16 ratas Wistar macho de 300 g (10 para hipocampo ventral y 6 para hipocampo dorsal). Se realizó anestesia con xilazina (20 mg/ml) y ketamina (100 mg/ml) mezcladas 1:1 y administradas intramuscularmente con una dosis de 1 ml/kg. Las ratas fueron colocadas en un aparato estereotáxico y se procedió a la aplicación de Fluoro-Gold (FG), disuelto al 1% en un buffer de cacodilato de sodio al 0.1 M en hipocampo ventral (vHi, sitio A: Bregma -5.2 mm, lateral 5.4 mm y dorsoventral 6.3 mm, sitio B: Bregma -4.4 mm, lateral 4.6 mm y dorsoventral 7.6 mm) o en hipocampo dorsal (dHi, sitio C: Bregma -2.2 mm, lateral 2 mm y dorsoventral 3.4 mm). Las coordenadas de los sitios B y C fueron determinadas después del análisis de densidad axónica en las subregiones de hipocampo, utilizando los sitios con mayor densidad de fibras, el sitio A se escogió antes de hacer este análisis. Otro punto a notar es que utilizamos una bomba de iontoforesis (Value Kation SCI vab-500) para aplicar el FG a través de una micro pipeta de vidrio (WPI 1.65/1.1 mm, OD/ID) con una punta de aproximadamente 40 μm y aplicando una corriente de 0.1 μA y un ciclo de trabajo de 50%, con una duración del pulso de 5 s durante 20 min. La pipeta se dejó en el sitio por 15 min adicionales para evitar el reflujo del trazador. Tras la cirugía se aplicó un analgésico y un antibiótico intraperitonealmente por tres días; tres a cuatro semanas después se perfundió a las ratas como se describió anteriormente y se realizó una inmunohistoquímica en rebanadas coronales y sagitales de 70 μm con un anticuerpo conejo anti-vasopresina y un anticuerpo secundaria Cy5 burro anti-conejo. Las observaciones de estas muestras se hicieron bajo microscopía de epifluorescencia y confocal; para observación confocal del FG se utilizó un láser de argón de 452 nm.

6.14 Marcaje yuxtacelular de neuronas vasopresinérgicas magnocelulares neurosecretoras en el PVN

Los procedimientos de registro yuxtacelular y marcaje de neuronas in vivo se basaron en los métodos descritos en la referencia ((Pinault, 1996, Tukker et al., 2007)). Las ratas fueron anestesiadas con uretano (1,3 g / kg, vía intraperitoneal), con dosis suplementarias de xilazina (30 mg / kg) según sea necesario. La temperatura corporal se mantuvo a 36 °C con la ayuda de un dispositivo de calefacción. Una vez anestesiados, los animales se colocaron en un marco estereotáxico y se realizó una craneotomía alrededor de las coordenadas -1,7 mm posterior del bregma y 0,4 mm lateral. Un electrodo de vidrio de resistencia (8-10 M Ω) lleno de 1% neurobiotina en NaCl 0.15 M se colocó verticalmente en las coordenadas previamente estandarizadas: PVN (1.7 mm posterior y 0.4 mm derecha / izquierda, ~ 6,9 mm de profundidad todas con referencia a bregma). Después de la obtención del registro electrofisiológico (datos no mostrados aquí), La célula fue marcada iontoforéticamente con neurobiotina utilizando el método de marcaje yuxtacelular (Pinault, 2004) Un tren de pulsos de corriente de 1-10 nA, a 2,5 Hz, con un ciclo de trabajo del 50%, fueron administrados a través del electrodo de registro. La corriente fue aumentada gradualmente para inducir y mantener el “entrainement” de la actividad de la neurona, i.e. un mayor número de picos en la fase positiva de la corriente las células fueron moduladas entre 2 a 10 min.

6.15 Procesamiento anatómico y reconstrucción de las células marcadas.

Aproximadamente cinco horas después del marcaje los animales fueron perfundidos transcardialmente con solución salina seguida por 15 min de solución fijadora de paraformaldehído al 4%, 15% v/v ácido pícrico saturado, y 0.05% de glutaraldehído en PB 0,1 M. Secciones coronales (70 micras) se almacenaron en serie en pozos de cultivo de tejidos en 0.1PB con 0,05% NaN₃. Cuatro a seis secciones cerca del trayecto del electrodo se incubaron con estreptavidina-conjugada a Alexa Fluor 488 (1: 1000; Invitrogen) en TBST durante 1 h a temperatura ambiente (RT). Después las secciones se montaron en portaobjetos

con Vectashield (Vector Laboratories, Burlingame, CA). Secciones de los casos marcados con éxito que contenían los cuerpos celulares fueron bloqueadas con 10% de suero normal de burro (NDS) y posteriormente se incubaron durante la noche con suero de conejo anti-AVP (1: 500; Peninsula Laboratories) y cobaya anti transportador vesicular de glutamato (VGLUT2-GP-Af810, Frontier Instituto Co., LTD, Ishikari, Japón).

Para la reconstrucción, las secciones fueron procesadas adicionalmente con complejo avidina-biotina peroxidasa (kit Vectastain ABC Elite, Vector Laboratories Burlingame, CA) para revelar la neurobiotina con diaminobencidina (DAB, 0,05%; SIGMA, St. Louis, MO). Las secciones se secaron al aire y se cubrieron con medio de montaje Permount (Electron Ciencias Microscopía, Hatfield, PA). Cinco células magnocelulares neurosecretoras (MNN's) marcadas yuxtacelularmente dentro del núcleo paraventricular (EV40, VH52, EV16, MM15 y VH25) fueron seleccionadas para la reconstrucción (proyección 2D) bajo el microscopio de luz con un tubo de dibujo.

Para MM15, usamos un microscopio confocal para realizar una reconstrucción 3D que permite ilustrar la presencia de el tracto hipotálamo-neurohipófisis y de colaterales axónicas de proyección. Los criterios de inclusión fueron que las células tenían que ser positivas a AVP, que se encontrasen dentro de la PVNlmd y que poseyeran axones que se unieran al tracto de Greving (tracto hipotálamo neurohipofiseal) (Armstrong, 2004).

6.16 Laberinto elevado en cruz (EPM) - evaluación de ansiedad no condicionada

Se utilizó el EPM para analizar el estado de ansiedad agudo no condicionado, una semana antes de la prueba de VCT. El laberinto consistió en una plataforma en forma de cruz, elevada 50 cm del piso, hecha de madera, con dos brazos cerrados (50x10x40 cm) y dos brazos abiertos (50x10 cm) con un borde sobresaliente de 0.5 cm de la orilla para evitar que la rata cayera, sin comprometer los parámetros elementales de esta prueba, los brazos se encuentran conectados por un cuadro central de 10x10 cm. La prueba se hizo bajo luz roja tenue y fue monitoreada por un circuito cerrado de televisión. Antes de cada prueba se limpió el laberinto con agua y detergente.

Antes del EPM se puso a las ratas en una caja de campo abierto estándar (40x40x40 cm, de madera (Pierce and Kalivas, 2007)) durante 5 min en los tres días previos y el mismo día de la prueba; esto para aumentar la probabilidad de entradas a los brazos abiertos, aumentando la sensibilidad de la prueba (Walf and Frye, 2007). La prueba se realizó en la etapa temprana del periodo de actividad de las ratas y consistió en depositar a la rata en el cuadro central del laberinto viendo hacia un brazo abierto y después se dejó que explorase libremente durante 5 minutos. Tanto el porcentaje de tiempo transcurrido en los brazos abiertos como de entradas a ellos, en proporción al número total de entradas (entrada a brazos cerrados más entradas a brazos abiertos) fueron tomados como una medida inversamente proporcional al estado de ansiedad no condicionada (exploración vs. evitación).

6.17 Prueba de conflicto de Vogel (VCT) - evaluación de ansiedad condicionada

La prueba de VCT (File et al., 2004) se usó para estudiar el estado de ansiedad aguda condicionada, esta prueba involucra dos pasos básicamente: privación de agua (WD) durante 48 h + privación de alimento durante las últimas 24, y la prueba de conflicto *per se*. Las ratas normalmente toleran WD durante 72 h, con una pérdida de peso dentro de un rango aceptable (alrededor del 11%), sin pérdida aparente de vigor (Rowland, 2007). Al terminar el periodo de WD las ratas fueron expuestas a una corriente eléctrica leve e intermitente, aplicada a través de una botella de agua; este procedimiento incorpora un elemento de conflicto donde el sujeto experimenta sentimientos opuestos y concomitantes de deseo (gratificación al tomar agua) y de miedo (evitación de un estímulo potencialmente dañino). Un indicador de un estado de ansiedad condicionada es cuando el miedo predomina en esta prueba siendo que no existe un peligro real (Millan and Brocco, 2003). Determinamos el número de descargas recibidas como nuestro parámetro operacional para medir ansiedad condicionada, de acuerdo con File. (File et al., 2004).

Antes de la prueba de VCT se habituó a los animales a la cámara descrita a continuación, metiéndolos diariamente 30 min, sin aplicación de corriente, durante 4 días consecutivos. La cámara del conflicto consistió de una caja de plexiglás translúcida (20 cm

x 30 cm x 20 cm), con piso metálico y tapa, una botella de agua con bebedero de acero inoxidable, un generador de corriente constante, un indicador para contar el número de descargas eléctricas y una cámara de video. Para la prueba se utilizó una solución de dextrosa al 10%, los cables para las descargas fueron colocados en el bebedero y en el piso de la caja. Antes de la prueba se probaron con un set diferente de ratas, diferentes corrientes (de 0.1 a 0.3 mA, a intervalos de 0.05 mA) para determinar el amperaje óptimo y se determinó que a 0.15 mA las ratas podían beber de la solución con molestia mínima.

Al concluir las 48 h de WD, la prueba de conflicto se realizó en otro cuarto y fue grabada por una cámara sensible a la baja intensidad de luz; la prueba se realizó durante el periodo de oscuridad del ciclo de iluminación artificial. Para iniciar la prueba se introdujo a cada animal a la cámara de conflicto y durante los primeros 25 s de la prueba se le dejó beber de la solución sin aplicar ninguna corriente, posteriormente se dieron descargas de 0.15 mA con un ciclo de trabajo del 50% con una duración de 5 s, entre el piso laminado y el bebedero metálico durante 5 min. Las ratas recibirían un toque sólo cuando coincidiera el intervalo de descarga con que estuvieran en contacto con el bebedero; se contó el número de toques tolerados.

6.18 Evaluación del aprendizaje espacial: MWM (Morris Water Maze)

Al día P90 (peso 350 ± 10 g), 12 ratas Ctrl y 12 SM se designaron a 4 tratamientos: (a) isotónico (tratamiento 1, T1): las ratas recibieron sólo una inyección *i.p.* de solución salina al 0.9%, el 2% de su peso corporal, 1 h previa al MWM; (b) hipertónico (T2): las ratas recibieron una inyección *i.p.* de 900 mM NaCl, 2% de su peso corporal, 1 h previa al MWM; (c) SSR149415 (T3): las ratas recibieron una inyección de SSR149415 (Axon 1114, Axon Med Chem, Amsterdam, Netherlands, diluido en DMSO y posteriormente en salina 0.9%, 1:20) *i.p.* al 2% de su peso corporal, 1 h y 30 min previo al MWM; (d) hipertónico + SSR149415 (T4): las ratas recibieron la combinación de los tratamientos T3 y T4. Las botellas de agua fueron removidas al momento de la primera inyección hasta 10 minutos antes del MWM.

Se utilizó la prueba de MWM (Zhang et al., 2008): una alberca circular de color negro (diámetro 156 cm) llena con 30 cm de agua a 25 °C con pistas visuales distantes. Una plataforma circular con un diámetro de 12 cm se hallaba sumergido 1 cm por debajo de la superficie. Las ratas se habituaron previamente a esta prueba sin la presencia de la plataforma, una semana antes del MWM. El día de la prueba se permitió a las ratas nadar por 60 s para encontrar la plataforma de escape; si los sujetos no encontraban la plataforma en el tiempo permitido eran guiados a ella, una vez en la plataforma se les permitía observar su localización durante 10 s, cada rata realizó ocho ensayos en el mismo día, con un intervalo inter ensayo de 5 min. El tiempo para hallar la plataforma fue evaluado.

6.19 Exposición al gato vivo y puntuación conductual

Se realizó la prueba de comportamiento durante el período de actividad temprana de las ratas (oscuridad). Los sujetos experimentales (N = 60), alojados cuatro por jaula, se dividieron en tres grupos: el grupo control, el grupo con solución salina isotónica (inyección *i.p.* de vehículo) el grupo de solución hipertónica (inyección *i.p.* de 900 mm de NaCl, 2% de peso corporal). Las inyecciones se realizaron 30 min antes de la prueba bajo anestesia transitoria por la inhalación de vapor de sevoflurano (Sevorane, Abad, México) para reducir las molestias causadas por la manipulación durante las inyecciones. Las ratas se recuperaron de este procedimiento después de 1 a 3 min.

Para la prueba conductual, cada rata se colocó individualmente en una jaula de rejilla (28,5 × 21 × 30 cm), por lo que la rata podrían trepar. La jaula se colocó dentro de una cámara de plástico transparente ventilada más grande (60 × 80 × 40 cm), donde luego se introdujo un gato macho adulto. El gato era domesticado y estaba castrado (una mascota llamado Balam), de alrededor de 5 kg de peso corporal Balam se mantuvo tranquilo / inmóvil durante la mayor parte del experimento. Una ventaja de esta disposición es que las ratas fueron expuestas a estímulos fisiológicamente relevantes el olor, la apariencia de un depredador vivo y dichos estímulos eran relativamente constante para todos los sujetos experimentales. Cada rata permaneció en la cámara antes descrita durante un único periodo de 10 min. Una vez que el tiempo se completó, las ratas fueron devueltas a sus jaulas.

Los comportamientos relevantes se cuantificaron fuera de línea, dando una de las seis puntuaciones cada cinco segundos: 1) "congelamiento" se le asignó a la conducta de la inmovilidad más de 2 seg con piloerección; 2) "Escalada": cuando las ratas subieron la jaula de malla interna utilizando las extremidades tratando de escapar por la puerta superior; 3) "erguirse", cuando las ratas estaban olfateando con rotaciones cortas la cabeza; 4) "Desplazamiento", cuando las ratas estaban caminando, trotando o corriendo; 5) "Orientación": cuando los cuatro miembros de las ratas estaban inmóviles pero presentaban movimientos de extensión de la cabeza; 6) "Grooming": cuando las ratas se acicalaban con sus patas delanteras. Los comportamientos activos de escape se asignaron a las conductas 2, 3 y 4. El resto fue considerado como conductas pasivas de enfrentamiento al estrés.

Las diferencias entre grupos fueron analizadas por medio de la prueba ANOVA de 1 vía, y la prueba post-Hoc de Bonferroni utilizando el software Graphpad Prism.

6.20 Inmunohistoquímica contra c-Fos después de exposición al predador

Noventa minutos posteriores al periodo de exposición al depredador, 5 ratas de cada grupo fueron profundamente anestesiadas con una sobredosis de pentobarbital y transcárdialmente perfundidas con 0,9% de solución salina seguida por 15 min de fijador frío que contiene 4% de paraformaldehído y el 15% (v / v) de ácido pícrico saturado en PB.

Se obtuvieron secciones de 50 micras con un vibratomo (Leica VT 1000 vibratome). Para la inmunotinción, conjuntos de uno de cada cuatro secciones de Bregma -0,48 a -4,08 mm fueron bloqueadas con 10% de suero normal de burro (Vector Laboratories, Burlingame, CA) en solución salina tamponada con Tris con 0,3% Triton X-100 (TBST) durante 1 hora a temperatura ambiente (RT) y luego fueron reaccionadas con anticuerpo de conejo anti-Fos (1: 1000, SC52 Santa Cruz Biotechnology, Santa Cruz, CA) en TBST + 1% NGS a 4 °C durante la noche. Posteriormente, las secciones se enjuagaron tres veces por 10 min con TBST y luego se incubaron durante 2 h a TA con anticuerpo secundario anti conejo hecho en cabra y biotinilado (1: 200; Vector Labs, Burlingame, CA). Por último, las secciones se incubaron en complejo (kit Elite ABC, Vector Labs) avidina-biotina-peroxidasa durante 1 h

a temperatura ambiente. La peroxidasa se detectó usando DAB 0,05% como cromógeno. Las secciones fueron lavadas y montadas permanentemente con medio de montaje Permout (Electron Microscopy Ciencias, Hatfield, PA).

Las siguientes regiones del cerebro se evaluaron: hipotálamo, tálamo, amígdala y habenula lateral. El análisis cuantitativo se realizó con ImageJ software (NIH) (<http://rsb.info.nih.gov/ij/macros/>). Los datos se expresaron como el promedio del número de núcleos positivos c-Fos por 0,02 mm². Los resultados cuantitativos se expresaron como media \pm error estándar de la media (SEM). Se realizaron las pruebas de diferencias por el análisis de t-test, utilizando GraphPad Prism Software®. (GraphPad Software, San Diego, CA). Las diferencias se consideraron estadísticamente significativas a $P < 0,05$ (“*”: $P < 0,05$, “**”: $p < 0,01$ y “***”: $P < 0.001$).

6.21 Análisis estadístico

Los resultados se expresaron como promedio \pm error estándar de la media (SEM). Se evaluaron diferencias a través de pruebas T de student , y ANOVAS de una dos y tres vias dependiendo del experimento y posterior evaluación por pruebas post-hoc de Bonferroni. Para la mayoría de los cálculos Se utilizó el programa Prism (GraphPad), para la prueba de ANOVA de tres vias realizada en análisis de datos de MWM, se usó el programa Stata11 y se consideraron diferencias significativas valores de: * $p < 0.05$; ** $p < 0.01$; *** $p < 0.001$.

7. Resultados

Los resultados de esta tesis doctoral se dividen en 3 secciones. En la primera, "*La estructura y función del sistema vasopresinérgico hipotalámico neurosecretor puede modificarse por estresores perinatales*", se reportan datos que indican que los paradigmas de estrés prenatal y postnatal, i.e. hipertiroidismo materno y separación materna, respectivamente, alteran la ontogenia del sistema vasopresinérgico neurohipofiseal y generan cambios perdurables en la estructura y función de dicho sistema.

En la segunda sección, "*El sistema vasopresinérgico hipotalámico magnocelular tiene proyecciones intracerebrales más extensas de lo anteriormente reportado*", nos dimos a la tarea de caracterizar las proyecciones intracerebrales de neuronas magnocelulares neurosecretoras neurohipofisiarias (MNN's) vasopresinérgicas.

En la última sección, "*La modulación a la alta o a la baja del sistema vasopresinérgico produce deterioro en conductas emocionales y cognitivas*", usamos varias pruebas conductuales y herramientas farmacológicas para determinar si la activación del sistema vasopresinérgico neurosecretor aberrante podía traer consecuencias para el comportamiento en la edad adulta, que servirán como sustratos de algunos trastornos emocionales y cognitivos.

Sección I:

La estructura y función del sistema vasopresinérgico hipotalámico neurosecretor puede modificarse por estresores perinatales

- a) Hipertiroidismo Materno
- b) Separación Materna

7.1 Efectos del hipertiroidismo prenatal, sobre el desarrollo del sistema vasopresinérgico.

En un trabajo previo (Zhang et al., 2008), demostramos que en ratas, la exposición prenatal a un exceso de hormonas tiroideas (hipertiroidismo materno prenatal, HM), genera deterioro en el aprendizaje espacial y conductas tipo depresivas durante la vida adulta, cuando las ratas son sometidas a un protocolo de estrés sub-crónico.

Los resultados que a continuación presentaré fueron publicados en el artículo "*Vasopressinergic network abnormalities potentiate conditioned anxious state of rats subjected to maternal hyperthyroidism*". Aquí reportamos que ratas sometidas a HM presentan durante la edad adulta un cambio más rápido en la concentración de vasopresina plasmática cuando los animales son sometidos a privación de agua, una mayor activación de las neuronas vasopresinérgicas magnocelulares hipotalámicas (medido con la proteína c-Fos) ante un estrés osmótico y una mayor inmunoreactividad contra la proteína vasopresina en el tracto hipotálamo-neurohipofiseal.

7.1.1 El HM, no afecta la actividad locomotora, el peso corporal o las concentraciones de hormonas tiroideas.

En los días postnatales 30 y 90, tomamos animales de camadas diferentes y medimos la actividad locomotora, las concentraciones séricas de hormonas tiroideas, el peso corporal y la glucemia. No hallamos diferencias entre los animales HM y los controles

7.1.2 Las ratas sometidas a HM presentan un rápido aumento en las concentraciones plasmáticas de AVP ante un estímulo osmótico.

Las mediciones de vasopresina plasmática se realizaron en un lote de animales que posteriormente fue evaluado en una prueba de ansiedad condicionada (Vogel Conflict Test, VCT), los resultados de dicha prueba se pueden hallar en la última sección de los resultados: "*La modulación a la alta o a la baja del sistema vasopresinérgico produce deterioro en*

conductas emocionales y cognitivas". Tanto la osmolaridad como la concentración de AVP plasmáticas alcanzan su máximo entre las 12 y las 16 h de privación de agua (water deprivation, WD), después de eso ambos parámetros fisiológicos permanecen relativamente estables (Rowland, 2007). Como se puede observar (Figura 7-1), la cantidad de AVP circulante medida alcanzó su máximo durante las primeras 12 horas. En ambos grupos, el valor basal de AVP era alrededor de 4.8 pg/ml (control: 4.94 ± 0.26 pg/ml; HM: 4.74 ± 0.27 pg/ml), sin embargo en el grupo control el punto WD6h cambió poco respecto al basal (5.55 ± 0.19 pg/ml), mientras que las concentraciones plasmáticas de AVP en los animales HM ya se encontraban elevadas a las 6 hrs (14.79 ± 0.71 pg/mL). Después de alcanzar el máximo las concentraciones se mantuvieron sin cambios. Inmediatamente después del VCT las concentraciones de AVP aumentaron en el grupo HM respecto al control (Figura 7-1, ver puntos temporales 6h y PVCT).

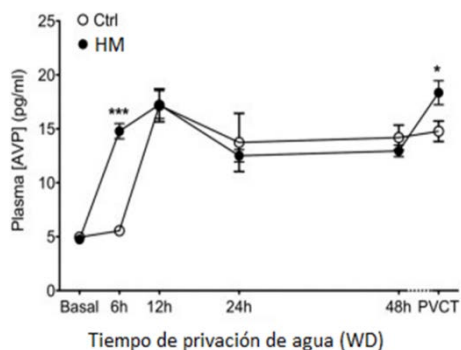


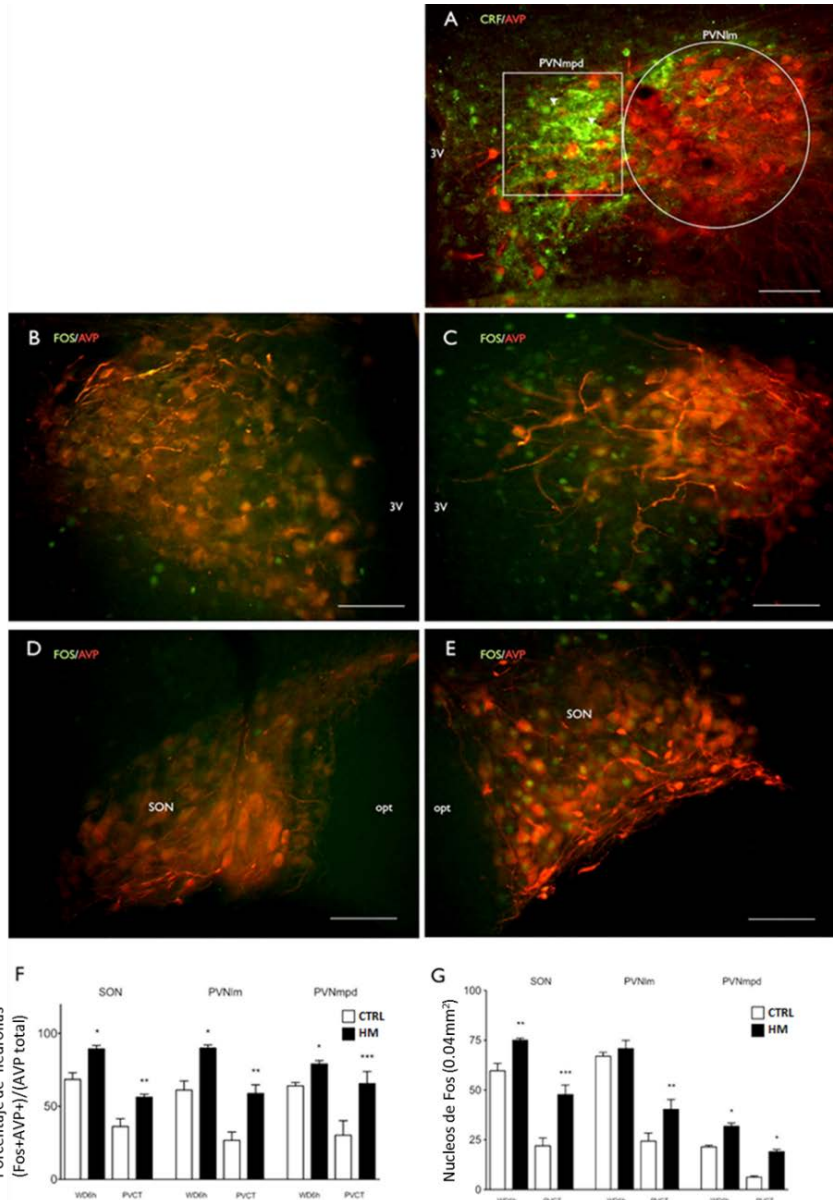
Figura 7-1 Los animales HM muestran una cinética alterada en la curva de concentración de vasopresina en plasma durante la privación de agua y posterior a la prueba de conflicto de Vogel (PVCT). Promedio \pm SEM ($n = 4$ para cada punto de tiempo). *** $P < 0,001$, * $P < 0,05$. Modificado de (Zhang et al., 2010)

7.1.3 La privación de agua y la prueba de VCT induce una mayor activación de neuronas AVP+ en animales HM.

Para evaluar la inducción de Fos en el SON, PVN_{lm} y el PVN_{mpd}, los sujetos experimentales se perfundieron 90 min después del punto temporal donde la concentración plasmática de AVP mostró diferencias significativas. Se observó un incremento significativo en el número de neuronas AVP+ que expresaban Fos en los animales HM (Figura 7-2). En las 3 regiones anatómicas analizadas se observó una mayor diferencia en el punto PVCT.

Figura 7-1. Expresión de Fos aumentada en sujetos HM respecto a control 90 min posterior a 6hWD y PVCT.

Se evaluó la expresión de Fos a los puntos de tiempo WD6h (6 h de privación de agua) y PVCT (posterior a la prueba VCT, PVCT). (A) Microfotografía que muestra la expresión de CRF (verde) / AVP (rojo) en PVN, correspondiente a los sitios donde los núcleos Fos+ fueron contados. Círculo: PVNlm (parte magnocelular del PVN); cuadrado: PVNmpd (parte parvocelular de PVN). Las puntas de flecha indican axones AVP en el PVNmpd. (B, C) fotografías de PVN en control y HM respectivamente, (D, E) Fotografías de SON en control y HM respectivamente. (F) Diagrama de barras que muestra los porcentajes de neuronas vasopresinérgicas activadas (AVP+Fos+) respecto a todas las células AVP+. (G) Conteo de los núcleos Fos+ en las tres regiones anatómicas para WD6h y PVCT. 3V, tercer ventrículo; opt, tracto óptico. Escala = 100 micras. (n = 6), promedio ± SEM, * P < 0,05, ** P < 0,01, *** P < 0,001. Microfotografías A-E realizadas en punto PVCT. Modificado de (Zhang et al., 2008).



7.1.4 El hipertiroidismo materno induce un almacenamiento anormal de AVP bajo condiciones basales

Se observó por inmunofluorescencia un incremento en la expresión de AVP (aumento en la densidad óptica) en el tracto hipotálamo-neurohipofiseal (HNT) tanto en su parte ventral como dorsal (Figura 7-3). Este aumento en la inmunoreactividad puede deberse a un número aumentado de axones, o un contenido mayor de AVP dentro de las fibras, o ambos.

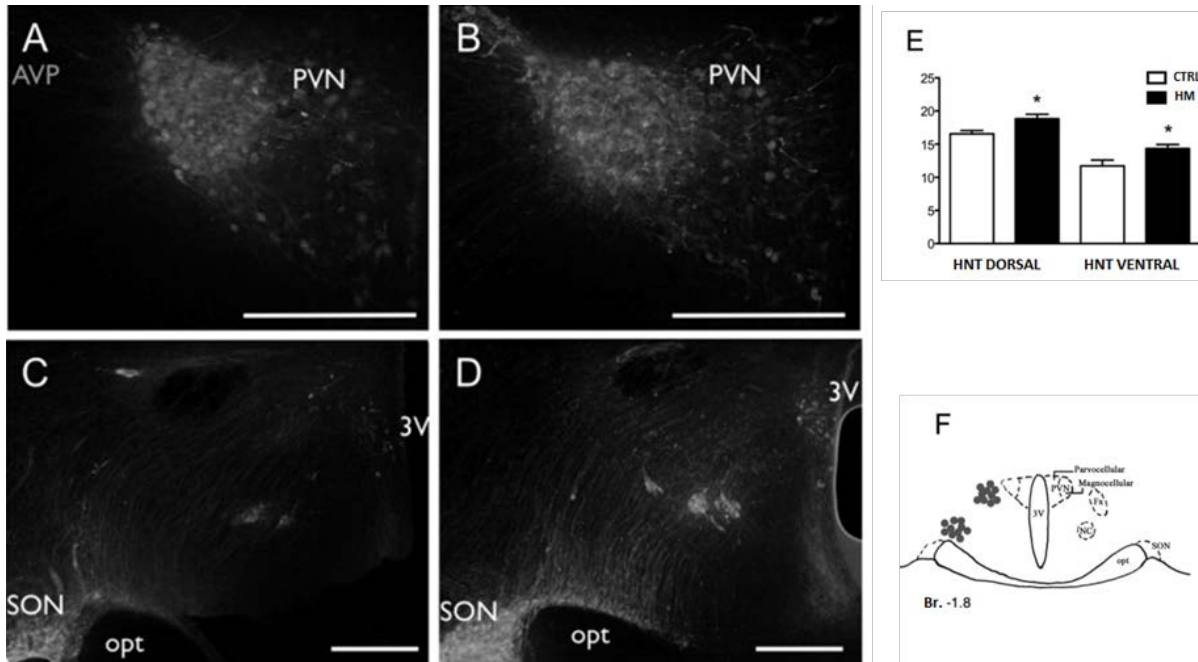


Figura 7-3 Aumento en la inmunoreactividad de AVP en el tracto hipotálamo-neurohipofiseal (HNT) de sujetos HM en condiciones basales. Las fotomicrografías muestran el marcaje de inmunofluorescencia para AVP en el PVN, (A) y (B), y el HNT (C) y (D), de ratas control y HM reaspectivamente. (E) Diagrama de barras que muestra el análisis de densidad óptica (OD) de inmunoreactividad anti AVP. El grupo HM muestra un aumento significativo tanto en la parte dorsal como ventral del tracto HNT. (F) Representación esquemática del tracto HNT donde se realizaron las mediciones de la densidad óptica (círculos grises) 3V, tercer ventrículo; PVN, núcleo paraventricular; opt, tracto óptico, SON, núcleo supraóptico; Fx, fornix, NC, núcleo circularis. Escala = 200 micras. * $P < 0,05$. Modificado de (Zhang et al., 2010)

También el número de cuerpos de Herring, contados en un área de 0.22 mm² dentro del tracto HNS, fue mayor en los animales que fueron sometidos a HM. (7.2 +/- 0.73) que los controles (1.2 +/- 0.2) Figura 7-4. Estos cuerpos de Herring miden de 1-4 micras y contienen una gran cantidad de vesículas de núcleo denso, se consideran sitios de almacén de péptidos.

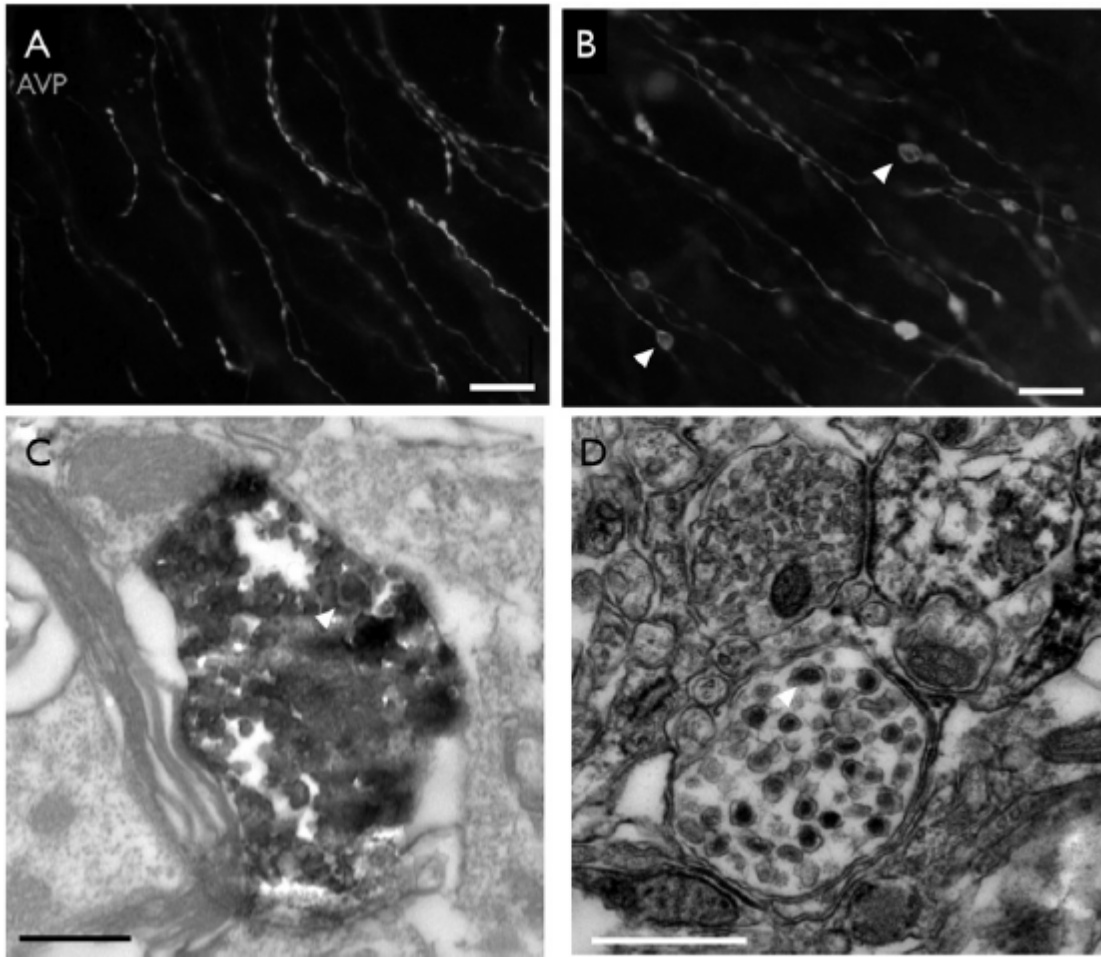


Figura 7.4 Abundantes cuerpos de Herring se ven en condiciones basales en los sujetos que fueron sometidos a HM. (A y B) fotomicrografía en el tracto HNS que muestra axones AVP+ con varicosidades (cuerpos de Herring) en un sujeto control y HM, respectivamente. (C) Fotomicrografías de un cuerpo de Herring inmuno-marcado contra AVP. (D) cuerpo de Herring sin inmunotinción, solo contrastado con plomo para evidenciar las vesículas de núcleo denso típicas de péptidos. Barra de escala 0.5μm

7.2 Efectos de la separación materna sobre el desarrollo del sistema vasopresinérgico.

En esta segunda parte, reportamos los efectos que un estrés postnatal (separación materna durante las dos primeras semanas de vida), produce en la morfogénesis del sistema vasopresinérgico hipotalámico. En resumen las ratas que fueron así estresadas, presentan durante la vida adulta un mayor y más rápido aumento en las concentraciones de vasopresina plasmática ante un estrés osmótico, una mayor cantidad de mRNA de vasopresina y un mayor volumen ocupado por neuronas vasopresinérgicas en los núcleos paraventricular y supraóptico. En este mismo estudio reportamos que dichas alteraciones anatómicas se observan desde los últimos días del protocolo de separación materna y proponemos que son consecuencia de la activación homeostática del sistema vasopresinérgico durante los episodios de separación materna. Los resultados de este trabajo fueron publicados en el artículo “*Hypothalamic vasopressin system regulation by maternal separation: its impact on anxiety in rats*”.

7.2.1 Un episodio de agudo de separación materna es capaz de activar a las neuronas vasopresinérgicas hipotalámicas magnocelulares.

La exposición aguda a un episodio de 3 horas de separación materna (3hSM) incrementó significativamente la producción de la proteína Fos, producto del gen de expresión temprana c-fos, (un marcador genérico de activación neuronal) tanto en SON ($F_{(3,36)}= 154.3, p < 0.001$) como en PVN ($F_{(3, 36)}=179.6, p<0.0001$) en animales AFR y SM al día P10. Como se esperaba, se observaron pocos núcleos Fos+ en la población AVP+ en PVN y SON en condiciones basales (Tabla 1, y Figura 7-5 A, B). Sin embargo, después de 3hSM, la mayoría de esta población neuronal expresó Fos (Tabla 1, y Figura 7-5 A', B'). La ANOVA no mostró diferencias entre los grupos AFR y 3hSM después de las dos condiciones experimentales.

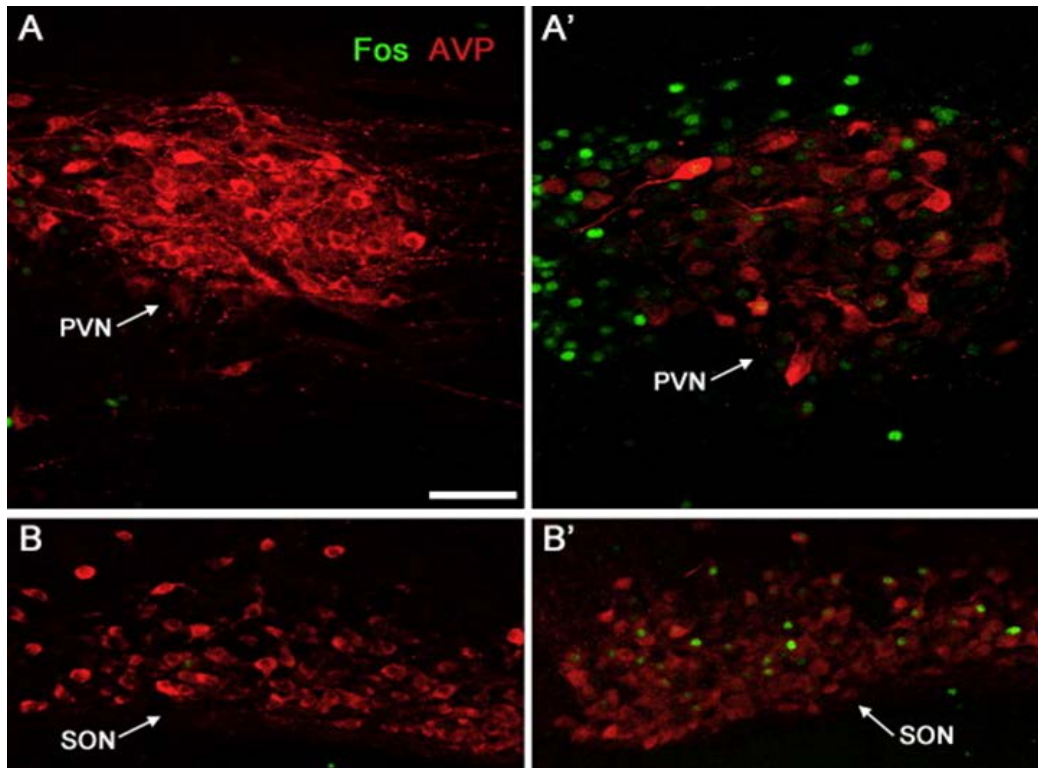


Figura 7.5 Activación de neuronas AVP+ por el protocolo de separación materna. Expresión de Fos (verde) en la neuronas AVP+ (rojo) de PVN y SON. (A, B) En condiciones basales y (A', B') después de un episodio único de 3hSM en P10. Barra de escala = 100 micras. . Modificado de (Zhang et al., 2012)

Porcentaje de neuronas Fos+/AVP+ respecto al número total de neuronas AVP+ en PVN y SON en P10				
Región	Grupo	Basal (%)	3hSM (%)	
PVN	AFR	12.6 ± 0.40	56.83 ± 2.46	p < 0.001
	SM	15.49 ± 1.28	63.7 ± 2.87	p < 0.001
		ns	ns	
SON	AFR	9.87 ± 2.27	58.08 ± 2.85	p < 0.001
	SM	5.02 ± 0.89	63.71 ± 2.87	p < 0.001
		ns	ns	

Tabla 1 Activación neuronas por un episodio de separación materna. ns: no significativo estadísticamente; AFR: animal control criado en el bioterio (animal facility reared); SM: Animales sometidos a separación materna por 3h diarias; Basal: En el día de la perfusión no se realizó separación de la madre; 3hMS: se llevó a cabo el procedimiento de separación materna por 3 horas previo a la perfusión. Los valores representan el promedio +/- el error estándar de los porcentajes de neuronas Fos + / AVP + respecto al total de neuronas AVP+ en el PVN y SON. Modificado de (Zhang et al., 2010)

7.2.2 La separación materna induce un aumento en la expresión del mRNA de AVP y en el volumen ocupado por neuronas AVP+ en el PVN, SON y SCN.

Encontramos un aumento en los niveles de expresión del mRNA de vasopresina al final del protocolo de 2 semanas de separación materna y este aumento persistía en la edad adulta, (Figura 7-6) y figuras 2 y 3 del artículo (Zhang et al., 2012). (Resultados obtenidos por las doctoras Limei Zhang y Claudine Irles, en el laboratorio de la doctora Maricela Morales del Instituto Nacional de Salud de los Estados Unidos).

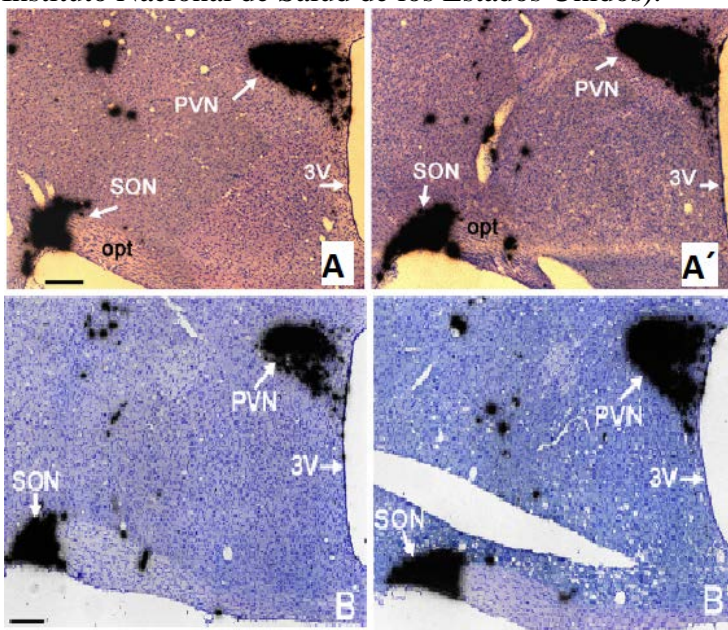


Figura 7-6 La separación materna (MS), induce una mayor expresión de mRNA de vasopresina en el núcleo paraventricular (PVN) y supraóptico (SON), desde el día postnatal 10 (A y A') y perdura hasta edad adulta (B y B'). A' y B': muestran una mayor expresión de mRNA de AVP en los núcleos PVN y SON en animales sometidos a separación materna respecto a los animales controles (A y B).

Para evaluar si a nivel traduccional también se observaba dicho efecto, se realizaron inmunohistoquímicas contra AVP. Los resultados mostraron un aumento significativo en el volumen ocupado por neuronas inmunoreactivas para AVP en el núcleo PVN y SON de ratas SM evaluadas en P75 (Figura 7.7 A y A'). El volumen promedio de AVP-SON fue de $0.2086 \text{ mm}^3 \pm 0.0064$ en el grupo SM, contra $0.1671 \text{ mm}^3 \pm 0.0055 \text{ mm}^3$ en el grupo AFR ($t=4.883$, $df=14$, $p < 0.001$). Respecto a AVP-PVN, el volumen ocupado en los animales SM fue $0.0853 \text{ mm}^3 \pm 0.0062 \text{ mm}^3$ contra $0.0588 \text{ mm}^3 \pm 0.038 \text{ mm}^3$ en los animales AFR

(Figura 7.7 D; $t=4.75$, $df = 14$, $p < 0.001$). En el caso del PVN, el aumento en el volumen que ocupan las células AVP, fue en los tres ejes (Figura 7.7 B, B' y C, C').

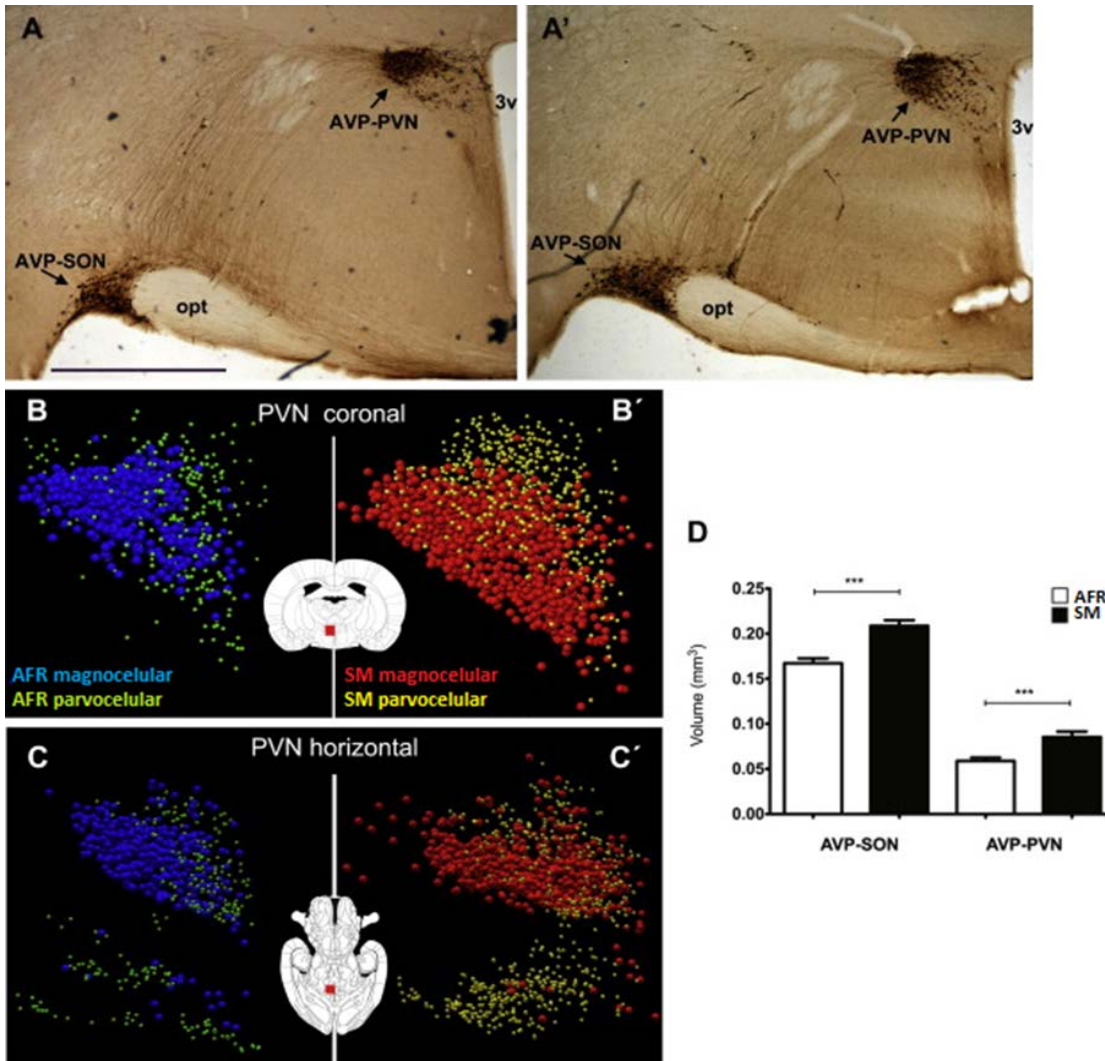


Figura 7-7 Efectos de MS3h sobre la extensión ocupada por neuronas AVP + dentro del PVN y SON, en PND75. (A y A') fotomicrografías representativas que muestran la tinción inmunohistoquímica para vasopresina en secciones coronales donde se observa el incremento en las áreas ocupadas por las neuronas de vasopresina en paraventricular (PVN) y supraóptico (SON) en los animales SM respecto a los AFR. (B, B', C, C') reconstrucciones 3D de PVN en vistas coronales (B y B') y horizontales (C y C') las neuronas magnocelular AVP + se muestran en azul para AFR, y en rojo para SM y las neuronas parvocelulares en verde para AFR y en amarillo para SM. (D) Histograma que muestra el promedio \pm SEM de las mediciones del volumen ocupado por AVP en regiones SON y PVN. 3v: tercer ventrículo; opt, tracto óptico. *** $P < 0,001$. Escala = 1 mm. Modificado de (Zhang et al., 2012).

7.2.3 La separación materna modifica la dinámica de cambio en las concentraciones plasmáticas de AVP en respuesta a un estrés osmótico

La concentración de AVP en plasma se midió en ambos grupos durante el periodo de privación de agua requerido para la prueba de VCT (Figura 7-8). El grupo SM a las 12 horas de WD mostró un incremento significativo (16.14 ± 1.15 pg/ml) comparado contra el grupo AFR (12.23 ± 1.12 pg/ml) ($p < 0.05$). La ANOVA de dos vías indicó un efecto significativo del tiempo ($F_{4, 72} = 46.7, p < 0.0001$) y del grupo ($F_{1, 72} = 14.35, p = 0.0013$).

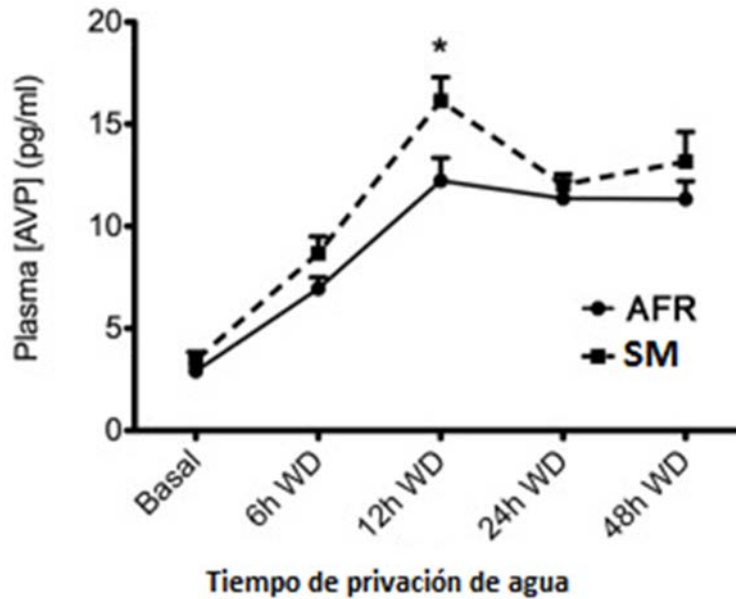


Figura 7-8 Curva de evolución de las concentraciones plasmáticas de AVP en función de la privación de agua (WD (promedio \pm SEM)). * $P < 0,05$. Modificado de (Zhang et al., 2012).

Sección II:

El sistema vasopresinérgico hipotalámico magnocelular tiene proyecciones intracerebrales más extensas de lo anteriormente reportado.

7.3 Las neuronas magnocelulares neurosecretoras (MNN's) del hipotálamo inervan el hipocampo dorsal y ventral.

En los resultados que a continuación expongo, caracterizamos la distribución y densidad de la innervación vasopresinérgica en el hipocampo, una estructura a la que se han asignado funciones cognitivas (principalmente hipocampo dorsal) y funciones emocionales (principalmente hipocampo ventral). Para tal fin, utilizamos técnicas de inmunohistoquímica, reconstrucción anatómica auxiliada por computadora (NeuroLucida) y trazadores neurales para identificar el origen de dicha innervación, concluimos que neuronas magnocelulares vasopresinérgicas hipotalámicas son una fuente importante de innervación hacia el hipocampo dorsal y ventral y demostramos contactos sinápticos entre axones AVP+ y dendritas de interneuronas en hipocampo.

7.3.1 Las fibras vasopresinérgicas (AVP) en hipocampo (Hi) tienen una densidad de innervación heterogénea.

Los resultados de la IHC mostraron una alta densidad de fibras AVP en *stratum oriens* (str. or.) de hipocampo ventral CA1, CA2 y CA3 (Figura 7-9 A-C). Para la cuantificación (Tabla 1), se calculó la densidad de diferentes regiones del hipocampo con el programa NeuronJ. La región con máxima densidad midió 2460 μm y se tomó como referencia (100%, +++++, figura 7.9 C). Regiones en el cuartil superior se consideraron como con innervación densa (++++), en el cuartil superior como densidad moderada (+++), en el tercer cuartil como diseminada (++) y en el cuartil inferior como innervación escasa (+). Como se observa en la Tabla 1 los campos conteniendo innervaciones densas o moderadas incluyeron CA2, vHi (str. or. y str. rad.); CA1, vHi (str. or.); CA3, vHi (str. or. y str. rad.). El hipocampo dorsal mostró mucha menor innervación, localizada principalmente en la parte rostral (Figura 7.9 D-F). Esquemas representativos de la innervación AVP en vHi y dHi se muestran en la figura 7.10.

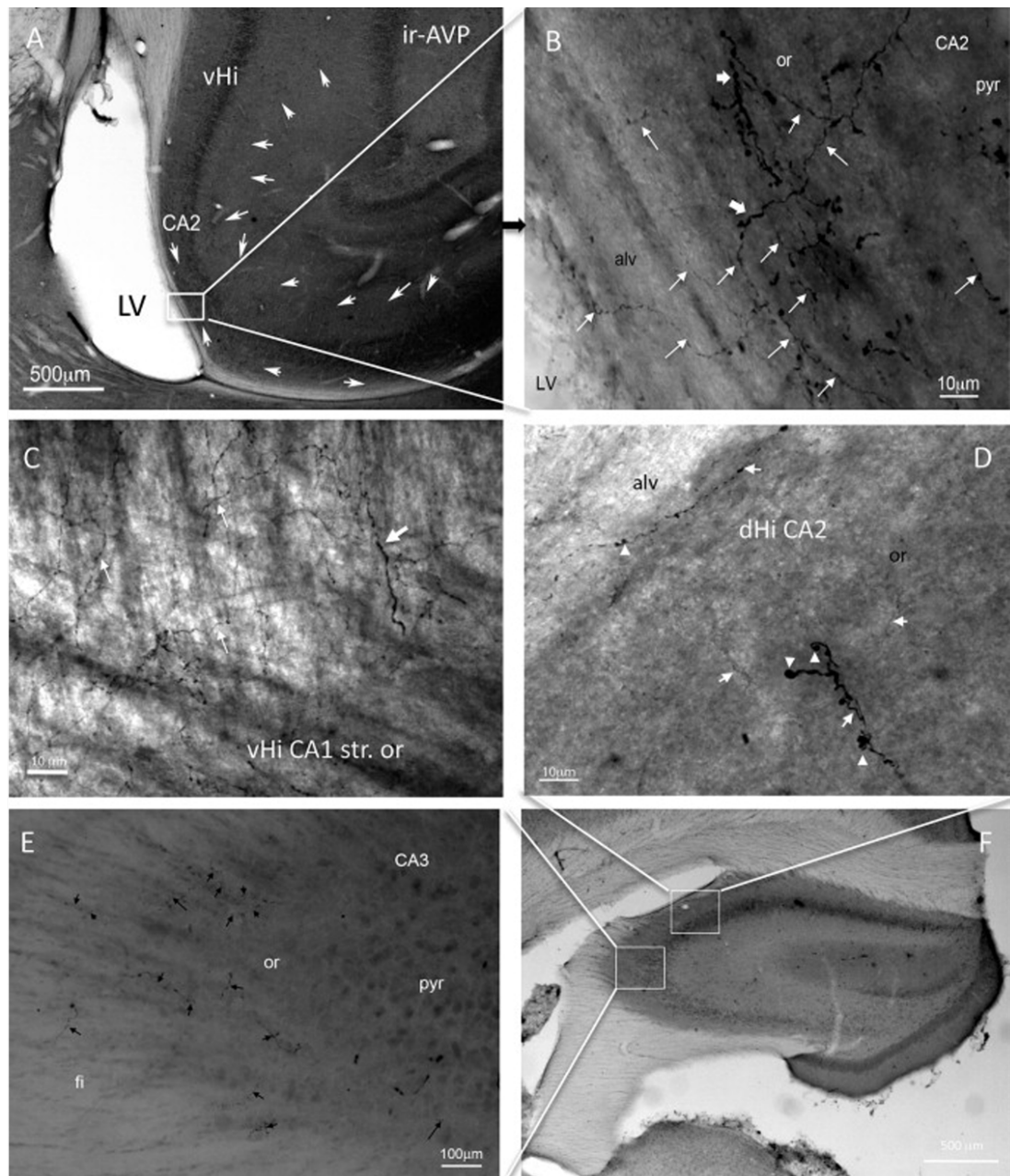


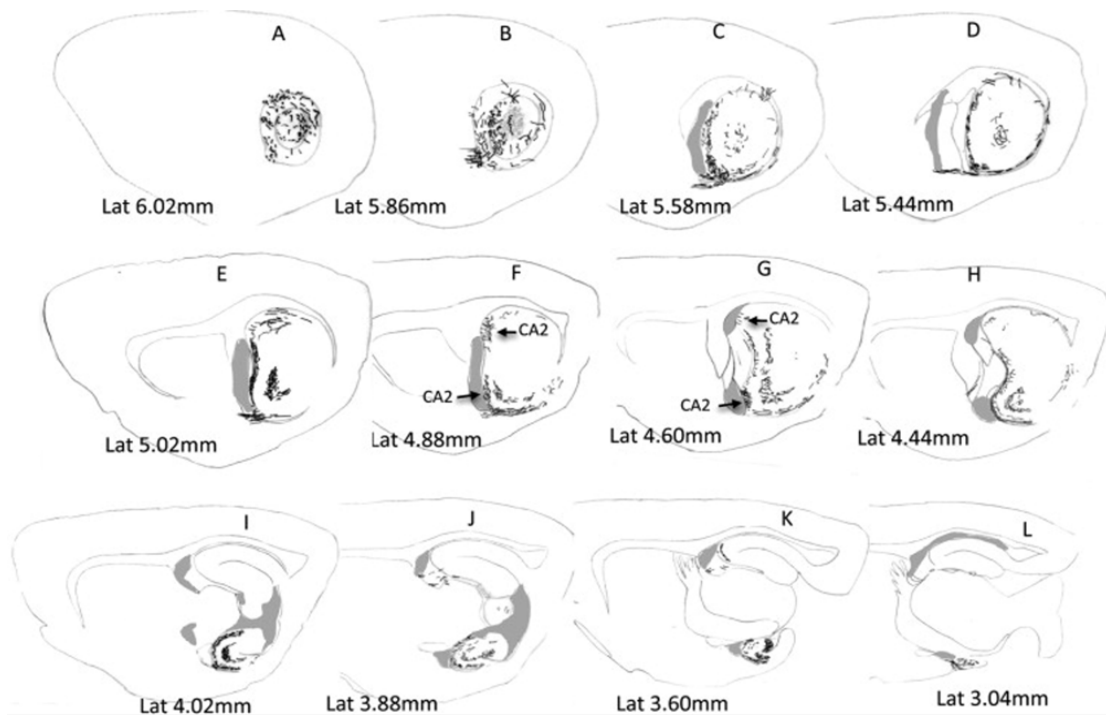
Figura 7-9. Visualización por inmunohistoquímica de la expresión de vasopresina en el hipocampo ventral (vHi; A-C) e hipocampo dorsal (dHi: D-F). Se pueden observar dos tipos de fibras AVP+. Las fibras tipo A (Fibras gruesas señaladas con flecha gruesa) y las tipo B (fibras delgadas señaladas con flechas delgadas). Las puntas de flecha indican terminales axónicas gigantes que no se observan comúnmente. pyr: stratum piramidale; or: stratum oriens; fi: fimbria; alv: alveus; LV: ventrículo lateral. Modificado de (Zhang and Hernandez, 2013).

Table 2. AVP axonal projection to HI subfields: distribution analysis based on IHC using "NeuronJ" for ImageJ

	CA1				CA2				CA3				DG				VS		
	or	pyr	rad	lm	or	lm	pyr	rad	lm	or	lm	pyr	rad	lm	mod	gr	po		
<i>vhi</i>																			
Laterol (mm)																			
6.02	++	+	n.a.	n.a.	n.a.	n.a.	n.a.	n.a.	n.a.	n.a.	n.a.	n.a.	n.a.	n.a.	n.a.	n.a.	n.a.	+	
5.86	+++	+	n.a.	n.a.	++	+	+	+	+	+	+	+	+	+	n.a.	n.a.	n.a.	+	
5.72	++++*	+	+	n.a.	++	+	+	+	+	+	+	+	+	+	n.a.	n.a.	n.a.	+	
5.58	++++	+	+	++	+++	+	+	+	+	+	+	+	+	+	n.a.	n.a.	n.a.	+	
5.44	++++	+	+	++	+++	+	+	+	+	+	+	+	+	+	n.a.	n.a.	n.a.	+	
5.30	++++	+	+	++	+++	+	+	+	+	+	+	+	+	+	n.a.	n.a.	n.a.	+	
5.16	++	+	-	+	++	+	+	+	+	+	+	+	+	+	n.a.	n.a.	n.a.	+	
5.02	+	-	+	++	+++	+	+	+	+	+	+	+	+	+	-	-	-	+	
4.88	+++	+	+	++	+++	+	+	+	+	+	+	+	+	+	-	-	-	+	
4.74	+++	+	+	++	+++	+	+	+	+	+	+	+	+	+	-	-	-	+	
4.60	+++	+	+	++	+++	+	+	+	+	+	+	+	+	+	-	-	-	+	
4.44	+++	+	+	++	+++	+	+	+	+	+	+	+	+	+	-	-	-	+	
4.30	+++	+	+	++	+++	+	+	+	+	+	+	+	+	+	-	-	-	+	
4.16	++	+	+	++	+++	+	+	+	+	+	+	+	+	+	-	-	-	+	
4.02	++	+	+	++	+++	+	+	+	+	+	+	+	+	+	-	-	-	+	
3.88	++	+	+	++	+++	+	+	+	+	+	+	+	+	+	-	-	-	+	
3.74	++	+	+	++	+++	+	+	+	+	+	+	+	+	+	-	-	-	+	
3.60	++	+	+	++	+++	+	+	+	+	+	+	+	+	+	-	-	-	+	
3.46	+	+	+	++	n.a.	n.a.	n.a.	n.a.	n.a.	n.a.	n.a.	n.a.	n.a.	n.a.	+	+	+	+	
3.32	+	+	+	++	n.a.	n.a.	n.a.	n.a.	n.a.	n.a.	n.a.	n.a.	n.a.	n.a.	+	+	+	+	
3.18	n.a.	n.a.	n.a.	n.a.	n.a.	n.a.	n.a.	n.a.	n.a.	n.a.	n.a.	n.a.	n.a.	n.a.	+	+	+	+	
3.02	n.a.	n.a.	n.a.	n.a.	n.a.	n.a.	n.a.	n.a.	n.a.	n.a.	n.a.	n.a.	n.a.	n.a.	+	+	+	n.a.	
<i>dhi</i>																			
Bregma (mm)																			
-1.72	n.a.	n.a.	n.a.	n.a.	n.a.	n.a.	n.a.	n.a.	n.a.	n.a.	n.a.	n.a.	n.a.	n.a.	n.a.	n.a.	n.a.	n.a.	n.a.
-1.92	n.a.	n.a.	n.a.	n.a.	n.a.	n.a.	n.a.	n.a.	n.a.	n.a.	n.a.	n.a.	n.a.	n.a.	n.a.	n.a.	n.a.	n.a.	n.a.
-2.16	-	-	-	-	+	-	-	-	-	-	-	-	-	-	-	-	-	-	-
-2.40	-	-	-	-	+	-	-	-	-	-	-	-	-	-	-	-	-	-	-
-2.64	-	-	-	-	-	-	-	-	-	-	-	-	-	-	-	-	-	-	-
-2.80	-	-	-	-	+	-	-	-	-	-	-	-	-	-	-	-	-	-	-
-3.12	-	-	-	-	-	-	-	-	-	-	-	-	-	-	-	-	-	-	-
-3.36	-	-	-	-	-	-	-	-	-	-	-	-	-	-	-	-	-	-	-
-3.60	-	-	-	-	-	-	-	-	-	-	-	-	-	-	-	-	-	-	-

stratum oriens; pyr: stratum pyramidalis; rad: stratum radiatum; luc: stratum lacunosum-moleculare; lm: stratum lacidum; lm: stratum lacidum; mod: molecular layer of the dentate gyrus; gr: granular cell layer; po: polymorphic layer; vhi: ventral hippocampus in sagittal sections; dhi: dorsal hippocampus in coronal sections.
 * Axon length was maximal in CA1 in the sagittal section at Lat: 5.72 mm (shaded box); this length of 2460 μ m was assigned as "100%". For each subfield, a summed axon length of 100–76% was assigned as "+++", 76–51% as "++", 50–26% as "+", <26% as "n.a.". "n.a." indicates that the subfield is not applicable in the analyzed section.

Tabla 1 Distribución de la innervación vasopresinergica en hipocampo dorsal y ventral



7.3.2 Dos diferentes tipos de axones AVP+ hacen sinapsis en hipocampo.

Se observaron dos tipos de fibras AVP+ bajo microscopía de luz, de acuerdo a su diámetro, tamaño y varicosidades. Las fibras gruesas (tipo A) presentaban diámetros grandes y varicosidades frecuentes (Figura 7-9 y Figura 7-11 flechas gruesas), mientras que las fibras delgadas (tipo B) presentaban diámetros pequeños y varicosidades escasas (Figura 7, y Figura 7-11 flechas delgadas). Sin embargo, algunas fibras mostraron un diámetro axonal intermedio y varicosidades grandes y frecuentes (Figura 7-11 B, cabezas de flecha).

Bajo el análisis de microscopía electrónica las varicosidades contenían tanto vesículas claras pequeñas como vesículas grandes granuladas (vesículas de núcleo denso, dcv) en una frecuencia muy variable, ambos tipos de terminales hacían sinapsis con neuronas hipocampales. Fue menos frecuente la presencia de sinapsis de varicosidades grandes que

pequeñas. Respecto al tipo de sinapsis, la mayoría (72%, n=18) fueron simétricas (Gray tipo II). De acuerdo con características estructurales de los blancos postsinápticos, pudimos observar que axones de diámetro grueso formaban sinapsis asimétricas (Gray tipo I, generalmente excitatorias) sobre tallos dendríticos de neuronas piramidales (Figura 7-11C) y que axones AVP+ de diámetro delgado formaban sinapsis simétricas (generalmente inhibitorias) sobre procesos de interneuronas (Figura 7-11 D). Para más detalle ver figura 3, de (Zhang and Hernandez, 2013).

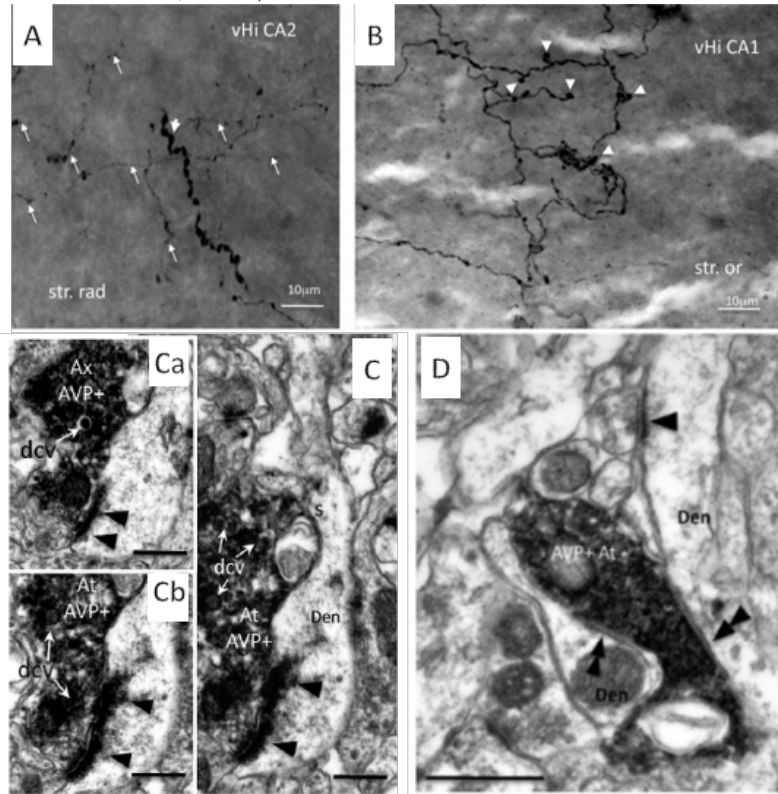


Figura 7-11. Tipos de fibras y sinapsis en hipocampo ventral. Se observan dos tipos de fibras AVP+ y sus terminales, en microscopía de luz (A) un axón con varicosidades de diámetro grueso (flecha gruesa) entre otros axones con botones pequeños (flechas delgadas), en stratum radiatum de CA2 ventral. (B) una red de fibras axónicas en CA1 de hipocampo ventral. (C) sinapsis asimétrica de una terminación de un axón de diámetro grueso sobre un tallo dendrítico con abundantes espinas que reciben otras sinapsis tipo I, no marcadas con vasopresina (característica indicativa de que es un proceso proveniente de una neurona piramidal), observese la gran cantidad de vesículas de núcleo denso “DCV” generalmente asociadas a vesículas que contienen péptidos, y algunas vesículas redondeadas pequeñas, generalmente asociadas a vesículas de glutamato. (D) Algunas terminaciones provenientes de axones con diámetro delgado hacen sinapsis simétricas sobre tallos dendríticos sin espinas adyacentes a sinápsis asimétricas, características sugerentes de una identidad de interneurona (Modificado de Zhang and Hernandez 2013). Fotomicrografías provenientes de artículo (Zhang and Hernandez, 2013), y realizadas por la doctora Limei Zhang en el laboratorio del Dr. Peter Somogyi, en MRC, Oxford.

7.3.3 Interneuronas mGluR1 α en *stratum oriens* de hipocampo son posible blanco de axones AVP+.

Encontramos en *stratum oriens* una fuerte correlación entre axones AVP+ y segmentos dendríticos expresando mGluR1 α (Figura 7-12 A-D) y una correlación débil con segmentos dendríticos y cuerpos parvalbumina+ (Figura 7-12 E-F).

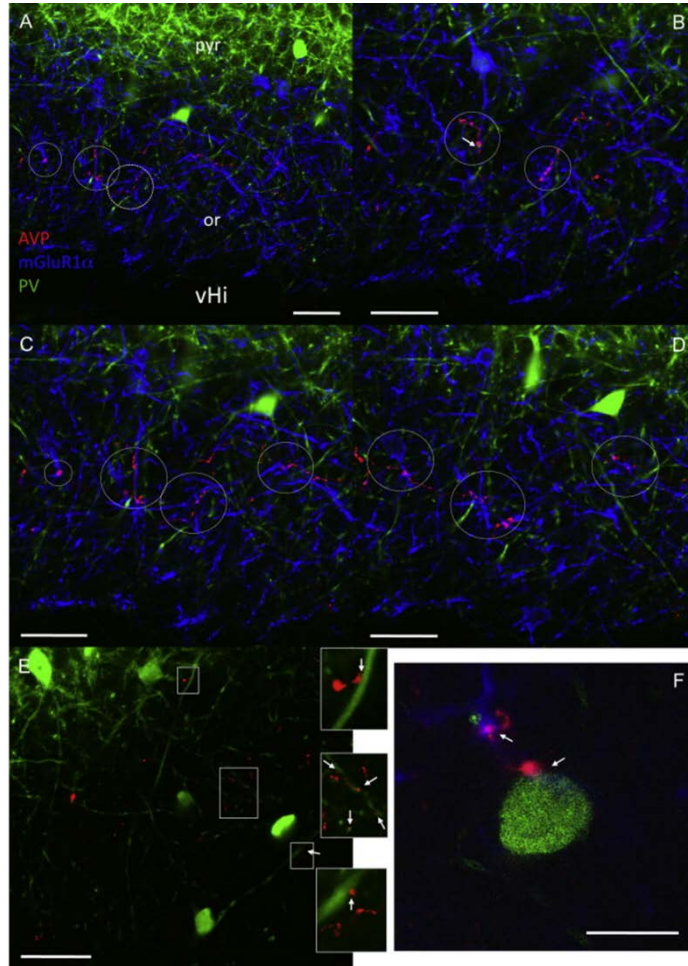


Figura 7-12. Algunas interneuronas mGluR1 α + en hipocampo son posibles blancos de axones AVP. Imágenes confocales tomadas en *stratum oriens* (or) de hipocampo ventral. Mostrando inmunoreactividad para AVP (rojo), mGluR α (azul) y parvalbumina (PV, verde). Nótese la fuerte relación entre los axones AVP+ y segmentos dendríticos que expresan mGluR α (círculos A-D). También se muestra una relación de contacto débil (flechas) con somas (F) y segmentos dendríticos (E, flechas) que expresan PV. El grueso de la sección óptica fue de 3 μ m. Escala para A-E: 50 μ m y F: 15 μ m (Zhang and Hernandez, 2013).

7.3.4 Los núcleos hipotalámicos PVN y SON participan en la innervación vasopresinérgica del hipocampo.

En este experimento se utilizaron 16 ratas, la tabla 3 muestra una descripción de los resultados obtenidos, las categorías excelente, buena, débil, fallido o dañado se refieren a la intensidad y tamaño del marcado, a la localización o al grado de daño en el tejido adyacente. Las ratas fueron perfundidas después de 3 semanas de la aplicación de FG. 5 de 10 intentos en el vHi (hipotálamo ventral) y 4 de 6 en el dHi /hipotálamo dorsal) fueron caracterizados como excelentes/buenos indicando diámetros menores a 350 μm y localizados con precisión en las regiones de más alta innervación vasopresinérgica.

Tabla 3. Descripción de los sitios de inyección de fluorogold y núcleos marcados retrógradamente. Modificado de (Hernandez and Zhang, 2012)

ID de sujeto y número de días hasta la perfusión	Coordenadas (mm): (Bregma; lateral; dorso-vHi)	Región blanco y calidad del marcaje	Análisis semicuantitativo de los núcleos marcados retrógradamente*			
			PVN	SON	SCN	BNST
vHi-1: 14	-5.20; 5.40; 6.00	vHi CA2: bueno	-	-	-	STIA: +
vHi-2: 35	-5.20; 5.40; 6.00	vHi CA2: debil	-	+	-	STIA: +
vHi-3: 21	-5.20; 5.40; 6.00	vHi CA2: dañado	+	+	-	STIA: +
vHi-4: 14	-4.40; 4.60; 7.60	vHi CA2/3: bueno	++	++	-	STIA: +
vHi-5: 21	-4.40; 4.60; 7.60	vHi CA2/3: dañado	n. e.	n. e.	n. e.	n. e.
vHi-6: 22	-4.40; 4.60; 7.60	vHi CA2/3: dos sitios marcados	n. e.	n. e.	n. e.	n. e.
vHi-7: 22	-4.40; 4.60; 7.60	vHi CA2/3: dañado	n. e.	n. e.	n. e.	n. e.
vHi-8: 28	-4.40; 3.80; 8.00	vHi CA2/3: excelente	++	+++	-	STIA: +
vHi-9: 18	-4.40; 4.60; 7.60	vHi CA2/3: excelente	++	+++	-	STIA: +
vHi-10: 18	-4.40; 4.60; 7.60	vHi CA2/3: excelente	++	+++	-	STIA: +
dHi-1: 21	-2.20; 2.00; 3.40	dHi CA2/3: excelente	++	++	-	STIA: +
dHi-2: 14	-2.20; 2.00; 3.40	dHi CA2/3: bueno	++	++	-	STIA: +
dHi-3: 21	-2.20; 2.00; 3.40	dHi CA2/3: excelente	+++	++	-	STIA: +
dHi-4: 21	-2.20; 2.00; 3.40	dHi CA2/3: fallido	n. e.	n. e.	n. e.	n. e.
dHi-5: 21	-2.20; 2.00; 3.40	dHi CA2/3: fallido	n. e.	n. e.	n. e.	n. e.
dHi-6: 28	-2.20; 2.00; 3.40	dHi CA2/3: excelente	+++	+++	-	STIA: +

n.e.: no evaluada; STIA: stria terminalis división intra-amigdaloides; vHi: hipocampo ventral; dHi hipocampo dorsal

* numero de células fluorogold+/AVP+ por 0.2mm² : 1-5 (+); 6-10 (++); >10 (+++)

** Los calificativos: excelente, bueno, debil o fallido, se refieren a la precisión de la inyección y el calificativo dañado se refiere a el grado de daño en el tejido circundante al sitio de inyección, todos los parámetros fueron evaluados 3 semanas después de la inyección de fluorogold.

La inyección en hipocampo ventral CA2, previo al análisis de la densidad de innervación AVP+ en hipocampo resultó en muy pocas células débilmente marcadas en el hipotálamo (Tabla 3); sin embargo, se observaron células FG/AVP+ en la división intra-amigdalina del núcleo del lecho de la *stria terminalis* (STIA), estos intentos sirvieron como control negativo para nuestra interpretación de los datos. Después del análisis de la densidad de la innervación AVP+ (Tabla 1), modificamos el sitio de inyección para dirigir nuestros intentos al máximo sitio de innervación vasopresinérgica en vHi CA2 (Bregma -4.4 mm, lateral 4.6 mm y

dorsoventral 7.6 mm). La inyección precisa en las ratas vHi8, vHi9 y vHi10 resultó en un número importante de neuronas AVP+ con marcaje FG en el SON y el PVN (Figura 7-13). El marcaje FG se acumuló principalmente en gránulos parecidos a lisosomas (Figura 7-13 F, I e insertos), lo que se ha reportado como una característica prominente del marcaje a largo plazo con FG (Persson and Havton, 2009, Schmued and Fallon, 1986, Wessendorf, 1991). Para controlar la posibilidad de una señal de FG por captura desde la sangre o LCR, examinamos cuidadosamente los órganos subfornical y los plexos coroideos. No detectamos señales en estos sitios en ninguna de las 3 ratas examinadas (Figura 7-14 e insertos). En STIA, una cantidad moderada de células FG fueron halladas, de las cuales unas cuantas mostraron doble marcaje con AVP (Figura 7-14 A-D).

Respecto a la inyección en dHi, utilizamos como blanco la porción más rostral de CA2 (Bregma -2.2 mm, lateral 2 mm y dorsoventral 3.4 mm) donde se encontró la mayor cantidad de inervación vasopresinérgica (Tabla 2 y Figura 7-9). En la Figura 7-15, paneles A y B, se muestran los sitios de aplicación de FG en el sujeto vHi1, perfundido 28 días después de la inyección de FG, nótese que las neuronas piramidales acumularon FG en el citoplasma y en gránulos tipo lisosoma (Figura 7-15 B e inserto) y algunas de las neuronas piramidales CA3 contralaterales fueron marcadas (Figura 7-15 C). Patrones de marcaje débiles en el SON (Figura 7-15 D-F) y PVN (Figura 7-15-I) se observaron con el microscopio confocal, los gránulos tipo lisosoma se muestran con (*) en los injertos del panel F e I.

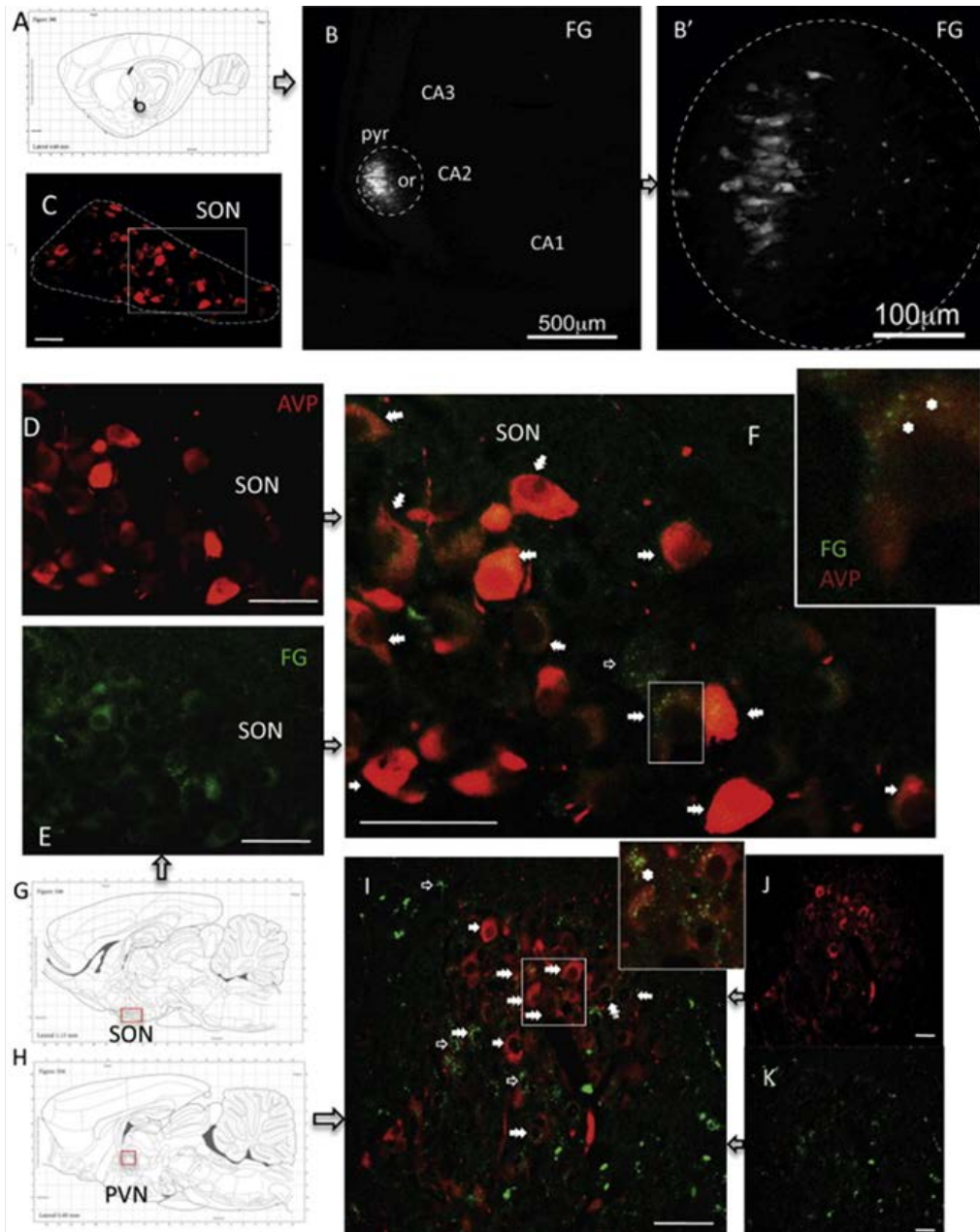


Figura 7-13 Demostración por medio del trazador retrógrado fluorogold de las aferencias hacia el hipocampo ventral (vHi) provenientes del SON y PVN del hipotálamo. (A) representación esquemática del sitio de inyección en vHi, indicado por un círculo. (B, B') sitios de inyección de FG en vHi CA2. Nótese el pequeño diámetro. (C-G) imágenes confocales que muestran cuerpos celulares retrógradamente marcados en SON. Nótese el injerto de (F), la acumulación de FG (puntos verdes) en estructuras parecidas a lisosomas (*). (H-J). También se observaron células retrógradamente marcadas en PVN. (Flechas sólidas indican marcaje con AVP, flechas huecas indican marcaje con FG y flechas dobles indican células doblemente marcadas. Escala 50 μ m Modificado de (Zhang and Hernandez 2013).

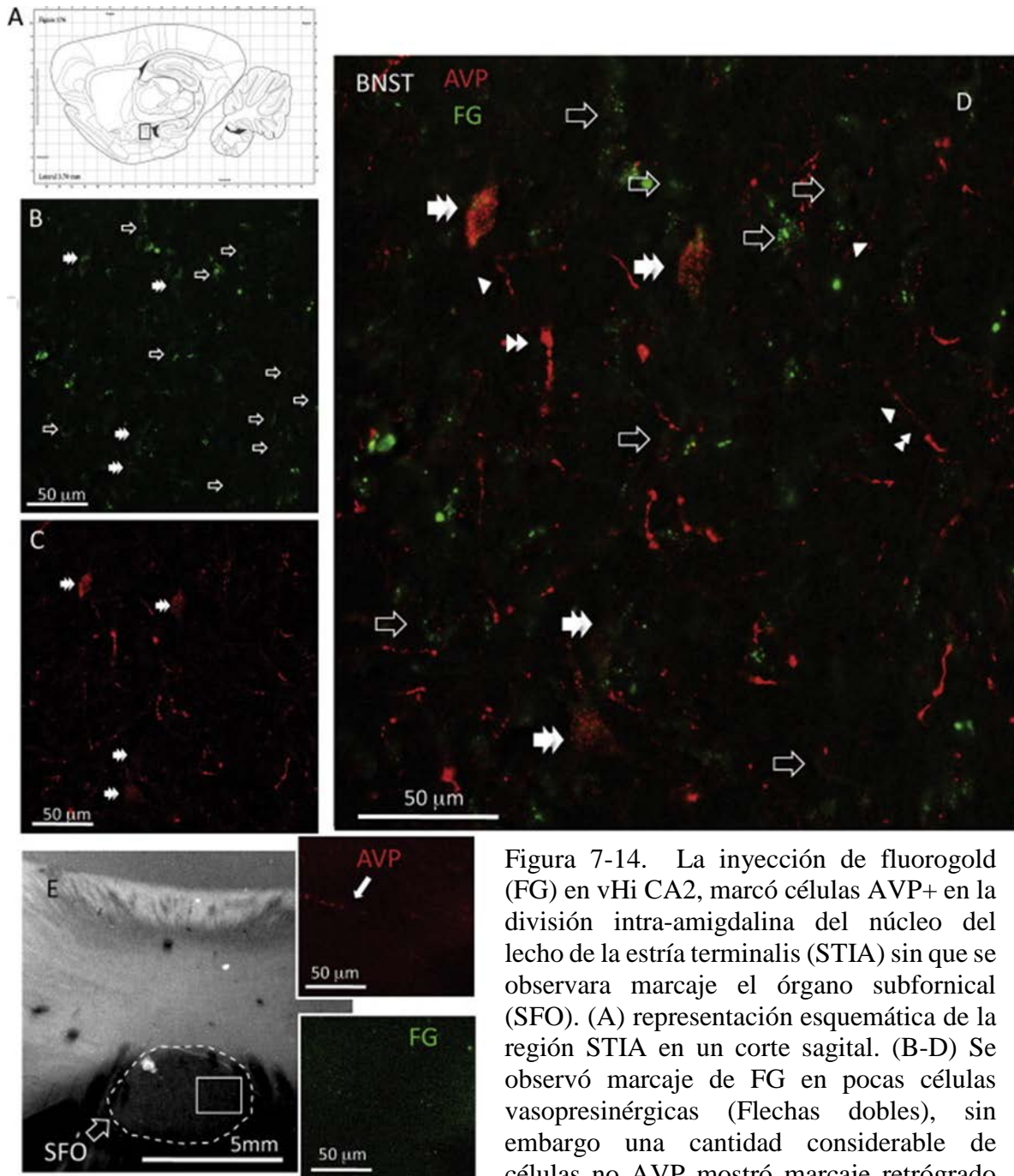


Figura 7-14. La inyección de fluorogold (FG) en vHi CA2, marcó células AVP+ en la división intra-amigdalina del núcleo del lecho de la estría terminalis (STIA) sin que se observara marcaje el órgano subfornical (SFO). (A) representación esquemática de la región STIA en un corte sagital. (B-D) Se observó marcaje de FG en pocas células vasopresinérgicas (Flechas dobles), sin embargo una cantidad considerable de células no AVP mostró marcaje retrógrado con FG. Nótese que en la región se observan fibras AVP gruesas tipo A (doble punta de flecha) y fibras delgadas Tipo B puntas de flecha). (E e injertos) El SFO, no mostró marcaje retrógrado con FG. Modificado de (Zhang and Hernandez, 2013).

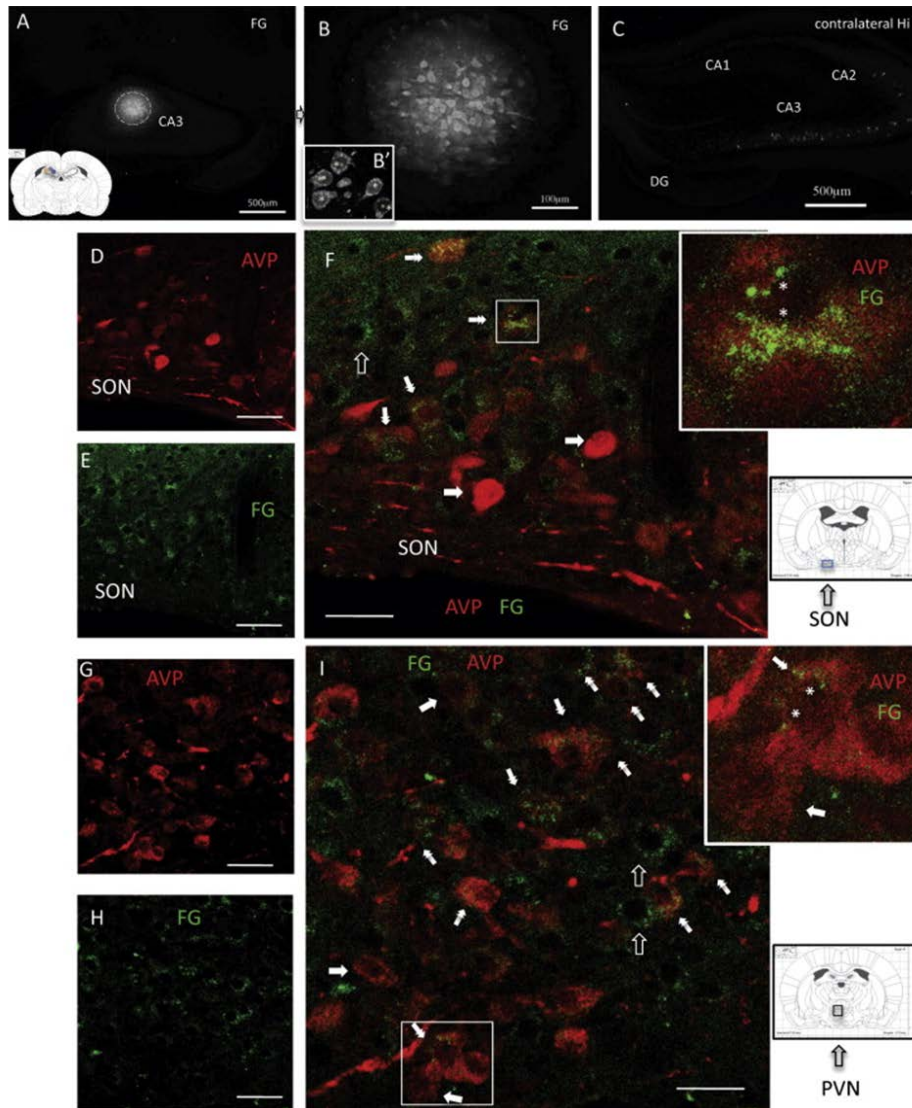


Figura 7-15. El hipocampo dorsal (dHi), recibe aferencias vasopresinérgicas desde el SON y el PVN del hipotálamo. (A) se observa el sitio de inyección en dHi con un diámetro < 350 µm. El injerto muestra un esquema de los sitios de inyección (círculos de colores). (B) magnificación de sitio de inyección. Injerto B, muestra que después de 28 días el FG se acumula en gránulos tipo lisosomal (*). (C) imagen de hipocampo contralateral al sitio de inyección, se ven neuronas piramidales en CA2 y CA3 marcadas retrógradamente. (D — F) Se muestran cuerpos celulares retrógradamente marcados en SON nótese en el inserto de F, la acumulación de fluorogold en gránulos tipo lisomas (*). (G — I) Cuerpos celulares retrógradamente marcados en PVN. El inserto en I muestra la acumulación de FG en gránulos tipo lisomas (*) y también se observa una neurona AVP+ no marcada con FG, (flecha). Flechas sólidas indican marcaje AVP+ solamente; Flechas huecas indican marcaje con FG solamente; flechas dobles indican doble marcaje. Escala 50 µm para D – I Modificado de (Zhang and Hernandez, 2013).

7.3.5 Los axones AVP+ viajan desde el SON y PVN hacia hipocampo a través de tres trayectorias principales.

A través de una estación de trabajo de NeuroLucida se realizó una reconstrucción 3D “1 a 1” a partir de 38 secciones alternadas. Es de notarse que las fibras tipo A y B, su continuidad y sus patrones de ramificación (rectos con pocas ramificaciones contra tortuosos con muchas ramificaciones) se podían distinguir y documentar claramente (Figura 7-16). Los resultados de este análisis aunados a los esquemas de las proyecciones hechos bajo observación con microscopía de luz mostraron 3 vías conectando al sistema magnocelular hipotalámico vasopresinérgico con el hipocampo.

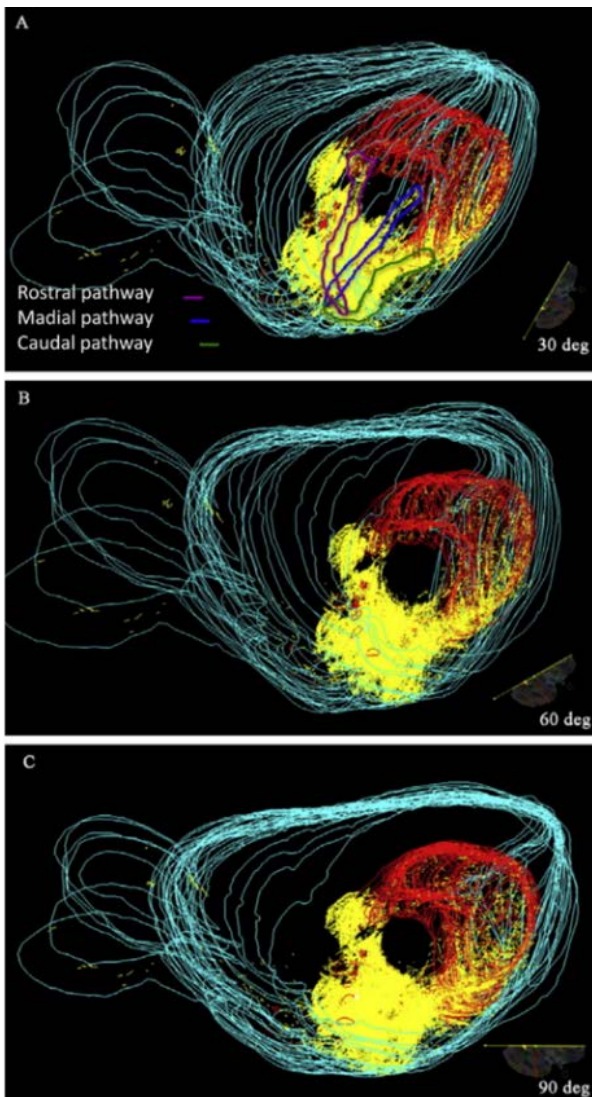
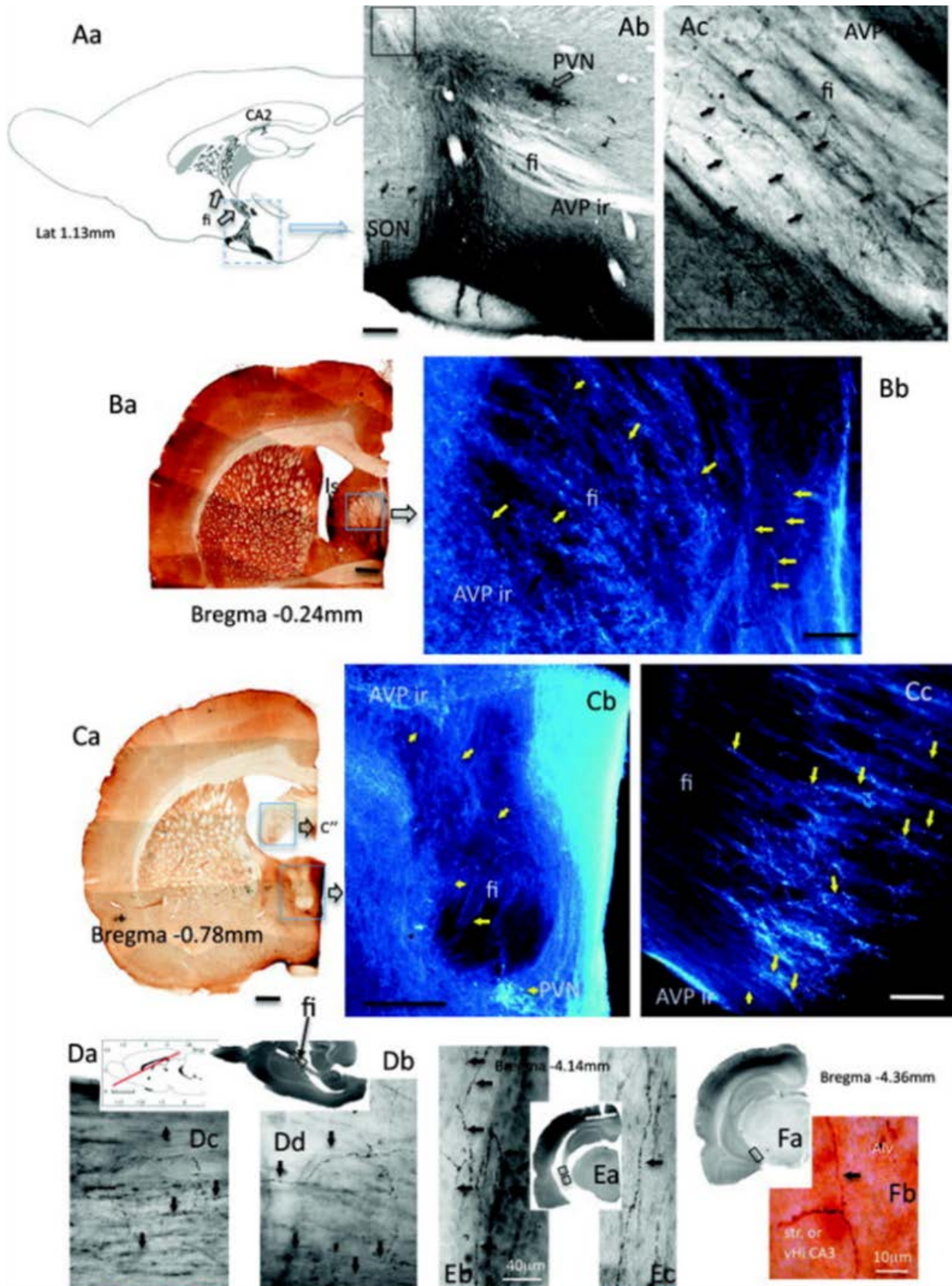


Figura 7-16. Mapeo computarizado 3D de la innervación vasopresinérgica realizado en NeuroLucida. La reconstrucción fue hecha en secciones sagitales desde stratum oriens de CA1 ventral hasta el núcleo PVN. Se definen 3 rutas de axones hacia el hipocampo. Vía rostral (color morado, hipotálamo-septum-fimbria-dHi-vHi); la vía media (color azul, hipotálamo-capsula interna-fimbria-dHi) y la vía caudal (color verde, hipotálamo-amígdala cortico_medial-vHi e hipotálamo-amígdala cortico_lateral). Las líneas rojas delimitan el hipocampo, las líneas amarillas delimitan los axones vasopresinérgicos. (A) rotación de 30° a partir de vista frontal (B) rotación de 60° respecto a vista frontal, (C) vista lateral Modificado de (Zhang and Hernandez, 2013).

Vía rostral-fimbria-fornix

Esta vía provee el mayor conducto para las aferencias subcorticales al hipocampo y las conexiones eferentes (Daitz and Powell, 1954, Powell et al., 1957). Esta vía vasopresinérgica hacia hipocampo había sido sugerida previamente (Buijs, 1978). Después del análisis anatómico exhaustivo fue evidente que tanto del PVN como del SON, fibras AVP+ seguían el fornix dorso rostralmente (Figura 7-17 Aa, Ab, Ac) hasta el hipocampo dorsal. Desde ahí, parte de las fibras proyectaban dorsalmente, alcanzando las porciones rostrales de CA3 y CA2 vía el alveus (Figura 7-9 B, D). El resto de las fibras continuaba dentro de la fimbria hacia el hipocampo ventral (Figura 7-17 D, E). Se pueden observar abundantes fibras AVP+ dentro de la fimbria, en Bregma -0.24 mm (Figura 7-17 Ba, Bb) y -0.78 mm (Figura 7-17 Ca, Cb, Cc). En las secciones semi-horizontales también se observan estas fibras dentro de la fimbria (Figura 7-17 Da-Dd). A nivel de la fimbria ventral también se observaron abundantes fibras AVP rectas (Figura 7-17 Eb, Ec y Figura 7-19 Ea); era frecuente hallar fibras AVP+ dentro del alveus que hacían giros de 90° para introducirse al str. or. (Figura 7-17 Fa, Fb).

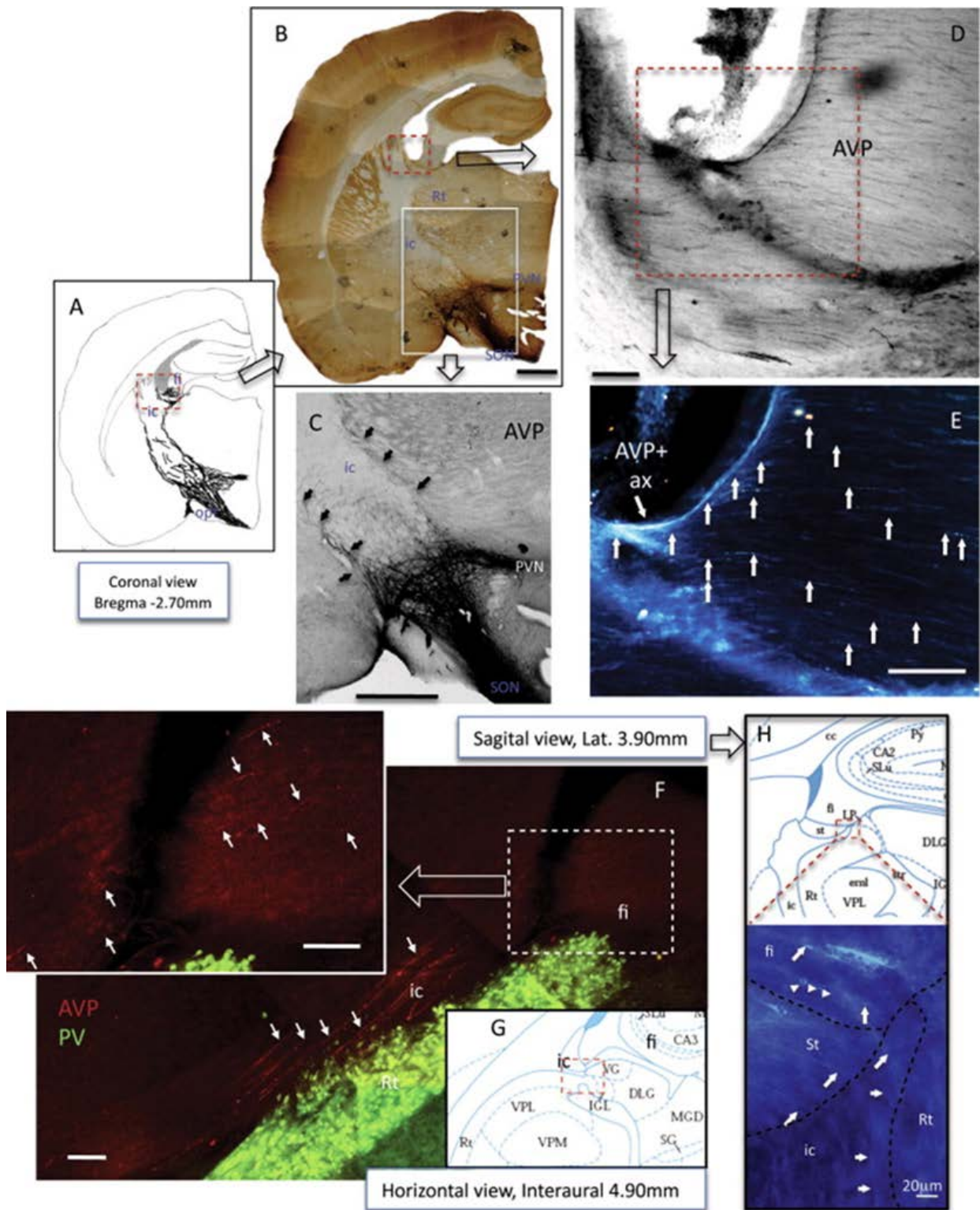
Figura 7-17 Características relevantes de la vía rostral (hipotálamo-septum-fimbria-dHi-vHi), (Aa) diagrama que ejemplifica que las fibras AVP+ de PVN y SON siguen el sistema de fibras de fornix dorso-rostralmente hasta el hipocampo dorsal (dHi) e inervan la parte de CA2. (Ab) Fibras AVP+ de SON y PVN proyectando dorso-rostralmente y uniéndose a fimbria-fornix, se pueden observar fibras AVP+ en la superficie de la sustancia blanca de fimbria (fi) (Ac, flechas negras). (Paneles B y C) secciones coronales en bregma -0.24 mm y -0.78 mm respectivamente muestran abundantes fibras AVP+ adentro de fimbria (flechas amarillas). (Paneles D) Se observan abundantes fibras como se ven en secciones semihorizontales. (Paneles E) se muestran abundantes fibras en Fimbria-Alveus ventral corriendo en dirección paralela a este sistema de fibras (flechas). (Paneles F) algunas fibras que viajan paralelas a sistema de Fimbria dan vueltas ortogonales e inervan stratum oriens. Las fotos azules son fotos en negativo para aumentar la visualización de las fibras. Escala: Ab, Ba, Ca, Cb: 500 µm; Ac, Bb, Cc: 100 µm. Modificado de (Zhang and Hernandez, 2013). Ver figura en la siguiente página.



Vía medial-cápsula interna-fimbria.

Una considerable cantidad de axones AVP de las divisiones magnocelulares de SON y PVN siguieron una ruta latero-postero-dorsal (Figura 7-18 A, B) dentro de la cápsula interna (IC). Estos axones se podían observar claramente en la superficie de la materia blanca de la IC (Figura 7-18 C). Las fibras continuaban caudalmente y se veían claramente en la frontera entre IC y el núcleo reticular talámico (Figura 7-18 F, vista horizontal). En la región de la fimbria, alrededor de las coordenadas Bregma -2.7 mm, lateral 3.9 mm y dorsoventral 4.9 mm (Figura 7-18 De, H) se observaron abundantes fibras AVP.

Figura 7-18 Características relevantes de la vía medial (hipotálamo-cápsula interna-fimbria-dHi). (A, B) Esquema y microfotografía de bajo aumento, mostrando que una cantidad importante de axones de SON y PVN, proyectan latero-caudal y dorsalmente para unirse a la cápsula interna (ic). (C) Fibras AVP+ (flechas) en la superficie de la ic. (D, E) se observa un haz denso de fibras AVP+ en la frontera entre ic y fimbria (rectángulo punteado en D), algunas de estas fibras entran a fimbria y cambian su trayectoria dirigiéndose hacia la línea media. La figura en E es una imagen en negativo para mostrar con mayor claridad las fibras AVP+ (flechas blancas). (F-G) corte horizontal para observar la región de unión entre ic y fimbria. (G) esquema que muestra la región analizada, (F) se observan claramente fibras AVP+ (flechas) viajando en dirección caudal-dorsal y lateral, paralelamente a la ic, y adyacentes a núcleo reticular talámico (Rt), en la fimbria adyacente (F, inserto), se observan fibras AVP+ (flechas que continúan en la misma dirección. (H) Se muestra la misma región en un corte sagital. Escala 500 mm para B y C; 100 mm para D — F e inserto Modificado de(Zhang and Hernandez, 2013). **Ver figura en la siguiente página.**



Vía caudal-cortico-amigdalina.

Proyecciones vasopresinérgicas con origen en el SON hacia amígdala e hipocampo ventral se revelaron a través de un detallado análisis anatómico realizado en secciones seriales. Los trazos en (Figura 7-19 A-G) hechos bajo microscopía de luz y los resultados del mapeo con Neurolucida (Figura 7-16) mostraron que una considerable cantidad de fibras AVP del SON proyectaban caudalmente hacia la neurohipófisis a través de la eminencia media y el tallo infundibular. Observamos que un número importante de fibras continuaban caudo-lateralmente, pasaban a través del área tuberomamilar y supramamilar, entraban a la amígdala cortico medial (CoMeA) y después se dirigieron dorsalmente a el área de transición amígdalo-hipocampal. Algunas de ellas entrando al hipocampo ventral (Figura 7-19 A-G), región delimitada por una línea azul punteada. Algunas de estas fibras giraron ortogonalmente para entrar a la corteza amígdalo-hipocampal (Figura 7-19 Da), estos axones parecían continuar en el vHi, principalmente en el str. or. De CA1 y CA2, donde se encontró una densa inervación vasopresinérgica (Tabla 1 y Figura 7-9 A y B).

También se encontraron proyecciones AVP+ caudolaterales del SON y PVN hacia vHi vía amígdala lateral, éstas entraban a la región vHi a través de la cápsula externa-alveus. Esta vía puede ser vista claramente en una sección semihorizontal (Figura 7-18, grupo H). Otra característica importante de esta vía se muestra en la Figura 7-20 He: 2 tipos de axones morfológicamente distintos pueden ser distinguidos, unos rectos y paralelos parecen proyectar a la cápsula externa y alveus de CA1 y CA2 ventral (flechas amarillas) y los axones tortuosos con ramificaciones locales (flechas negras pequeñas), que parecen inervar densamente el BNST, y la amígdala central y baso lateral (Figura 7-18 He). Los axones rectos, después de entrar al alveus de CA1 en vHi, se ramifican localmente o continúan en la materia blanca hacia CA1-subiculum o hacia CA2 (Figura 7-19 Hc. Hd).

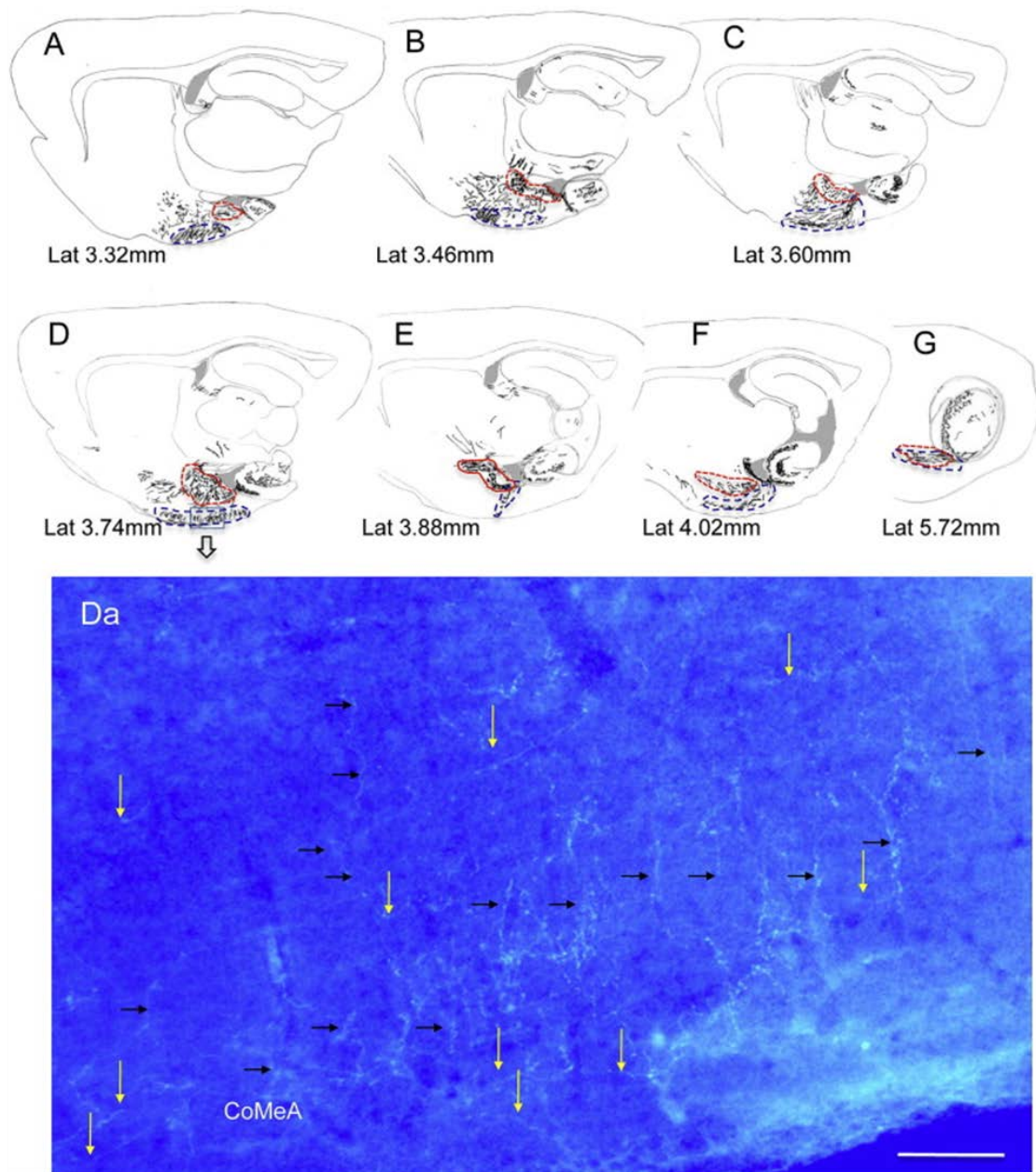


Figura 7-19. Características relevantes de la vía caudal (hipotálamo-CoMeA-vHi e hipotálamo-BLA-vHi). (A — G) Esquemas de secciones sagitales seleccionadas para mostrar el origen en SON de axones vasopresinérgicos que proyectan hacia la amígdala corticomedial (CoMeA) e hipocampo ventral (vHi). Se observaron dos tipos de fibras: fibras tortuosas que principalmente viajaban en amígdala medial (trazos rojos), y fibras con trayectorias rectas en CoMeA (trazos punteados azules). Algunas de estas fibras rectas hacían vueltas ortogonales y se ramificaban localmente en la superficie de la corteza amígdalo-hipocampal (Panel D, Da, flechas amarillas indican fibras que hacen vueltas ortogonales y fibras negras fibras que continúan trayecto recto hacia hipocampo). Escala 50 μ m. Modificado de (Zhang and Hernandez, 2013).

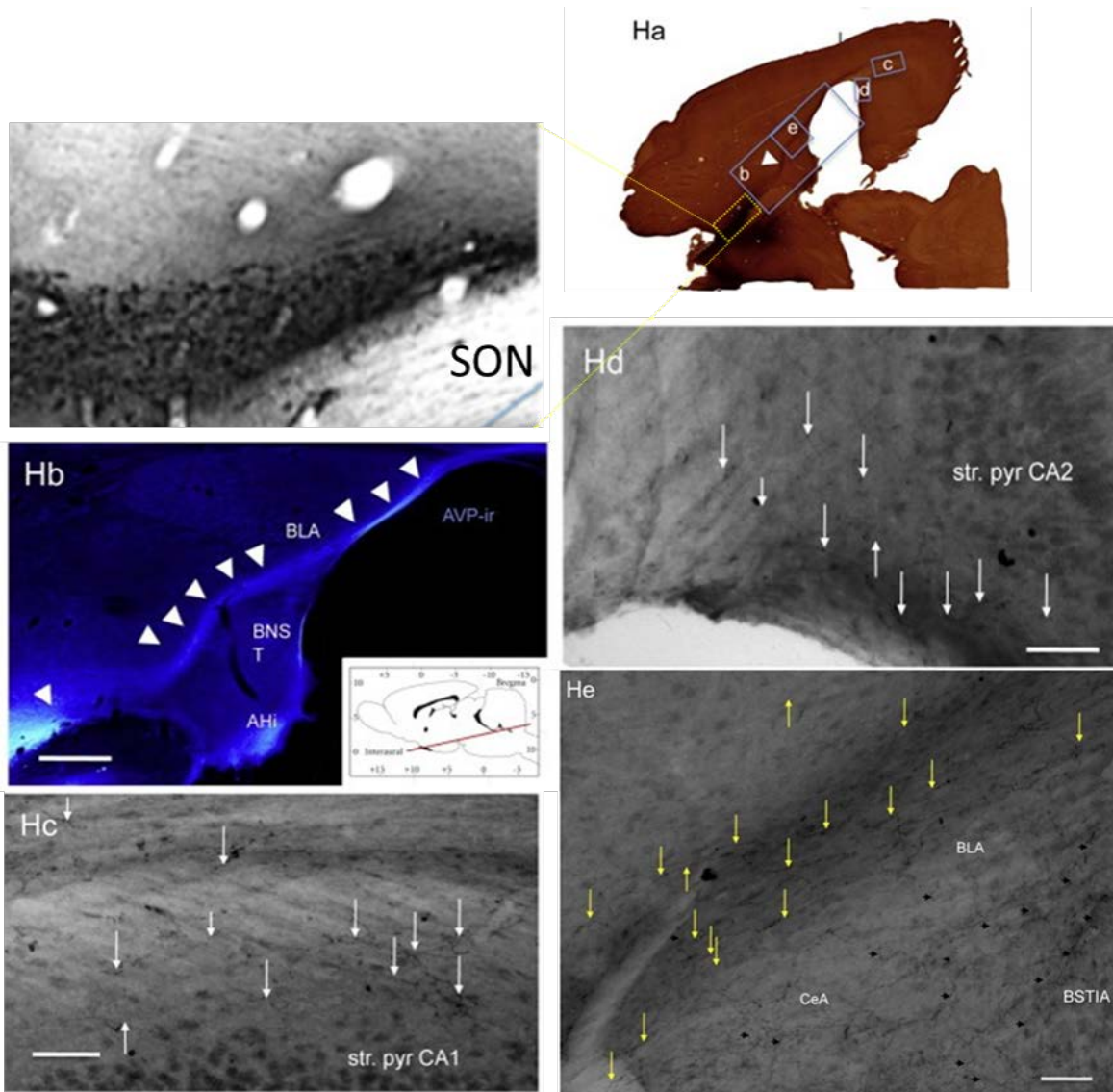


Figura 7-20. Algunas fibras AVP de SON y PVN proyectan a vHi por una vía caudo-lateral a través de la amígdala baso-lateral (BLA), entrando a el hipocampo vía capsula externa-alveus (puntas de flecha en Ha y Hb). (Hc — He) la flechas blancas indican fibras de vasopresina dentro de hipocampo, las flechas amarillas indican fibras rectas proyectando hacia hipocampo a través de BLA; las flechas blancas indican fibras tortuosas y con muchas ramificaciones en amígdala central y medial y en núcleo STIA. Ahi: zona de transición amígdalo hipocampal; BNST, núcleo del lecho de la stría terminalis. Escala: Hc, Hd y He: 50 μ m; Hb 500 μ m. Modificado de (Zhang and Hernandez, 2013).

7.4 Las neuronas vasopresinérgicas magnocelulares neurosecretoras (MNN's) del núcleo paraventricular inervan regiones intra y extra hipotalámicas a través de múltiples procesos tipo axónicos o colaterales axónicas.

Los resultados sobre la innervación vasopresinérgica a hipocampo sugieren que la innervación intracerebral a partir de neuronas magnocelulares hipotalámicas que expresan vasopresina es más extensa que lo que se pensaba anteriormente. Para investigar con más detalle la conectividad de las neuronas vasopresinérgicas magnocelulares usamos la técnica de marcaje yuxtacelular en neuronas vasopresinérgicas magnocelulares que se encontrasen dentro del núcleo paraventricular del hipotálamo, posteriormente realizamos procesamientos inmnohistoquímicos para identificar el fenotipo de la neurona marcada y por último revelamos la neurona con diaminobenzidina (DAB) para la reconstrucción de sus neuritas. Nuestros resultados muestran que además de la clásica proyección hacia neurohipófisis, las neuronas magnocelulares vasopresinérgicas hipotalámicas poseen múltiples colaterales axónicas y procesos “tipo axonales” caracterizados como glutamatérgicos que inervan regiones intra y extra hipotalámicas, tales como el área preóptica medial, el núcleo supraquiasmático, la amígdala y la habénula y se integran a sistemas de conducción intracerebral como el fórnix, la cápsula interna y la *stria medularis*.

7.4.1 La técnica de marcaje yuxtacelular, permitió identificar con detalle las características morfológicas de MNN's previamente identificadas.

La técnica de registro extracelular con marcaje yuxtacelular (Pinault, 1996) es un método poderoso para identificar las características morfo-funcionales de células identificadas y aisladas electrofisiológicamente. Permite obviar algunas de las dificultades inherentes a los estudios clásicos de conectómica. Esta técnica permite llenar iontoforéticamente con

neurobiotina una célula que previamente fue registrada. Después de un tiempo, la neurobiotina difunde por los procesos axónicos y dendríticos de la célula y es factible hacer una reconstrucción de esta, identificar sus blancos regionales y celulares y caracterizar la identidad inmunohistoquímica de la célula registrada.

En este estudio, cinco células (Figura 7-21) yuxtacelularmente marcadas que se encontraron en el núcleo paraventricular al ser visualizadas por fluorescencia (marcaje con estreptavidina fluorescente), fueron procesadas para identificar vGlut2 (marcador de células glutamatérgicas). Posteriormente fueron procesadas para revelado permanente con DAB y fueron reconstruidas (proyección 2D de la morfología tridimensional), por medio de un tubo de dibujo acoplado al microscopio de luz. Por sus características morfológicas los axones o sus colaterales fueron clasificados como tales y marcados de color rojo si se unían al tracto de Greving o surgían de un axón que se unía al tracto de Greving, si expresaban vGlut2, si eran proyecciones a distancias largas (extra hipotalámicas) o si ramificaban dentro del hipotálamo extensivamente (terminales axónicas) con varicosidades que parecían “racimos de perlas”. (Armstrong, 2004). Las dendritas fueron representadas de color negro. Para ser incluidas en este estudio como neuronas vasopresinérgicas neurosecretoras neurohipofiseales (MNN's), las células debían cumplir los siguientes criterios: 1) que fueran reveladas como AVP+ y 2) que mandaran un axón al tracto de Greving (via hipotálamo-neurohipofiseal).

Tomando en cuenta los criterios mencionados, observamos que las MNN's, pueden poseer más de un axón primario, originado bien del soma o de una dendrita principal. La célula “EV40”, Figura 7-21 A) muestra claramente dicha característica. En esta célula se observaron tres dendritas principales, dos mediales, una lateral. Dos axones principales se originan del mismo sitio de la dendrita lateral (flechas roja y azul). El axón dorsal se incorpora al tracto hipotálamo neurohipofiseal, y una de sus colaterales se dirige ventral y posteriormente, uniéndose al tracto óptico, algunas terminales se hallaron en amígdala central y medial. El axón ventral se dividió en dos, una rama se dirige hacia el tercer ventrículo mientras que la otra se dirige lateralmente y entra al fornix.

Las neuronas “EV16” y “VH52” (Figura 7-21 B y C), fueron registradas en la parte medial del PVN_{lm}. Ambas células presentan dendritas mediales que ramifican extensamente y

dendritas laterales de donde emergen los axones principales y procesos en forma de “racimos de perlas”, (recuadro 2 en “VH52” y proceso tipo axónico que se dirige ventro-medialmente (1) en “E16”), que han sido descritos como terminaciones axónicas (Armstrong, 2004). En los paneles 3 a 6, se observan procesos axónicos dentro o en proximidad de vías importantes de conducción (i.e. fornix, cápsula interna, *stria medularis*). “EV16” presenta una dendrita dorsal y una ventral, la dendrita ventral se ramifica extensamente en dirección medial, la dendrita dorsal se divide en una parte medial que se ramifica de la misma manera, y una rama lateral que da origen al axón principal, este axón se dirige al tracto hipotálamo neurohipofiseal y en el trayecto emite proximalmente una colateral (número 2 en panel B) que se integra a la *stria medularis*, donde deja de observarse, pero se puede ver un proceso axónico emergiendo de este tracto a nivel de habenula. Otra colateral axónica distal (número 3, en panel B), se dirige a fornix donde deja de verse.

La neurona “MM15” (Figura 7-21 D) fue registrada en la parte posterior del núcleo paraventricular, sin embargo era AVP+, en este caso también observamos tres procesos dendríticos, (uno medial y dos laterales). Los procesos laterales no se bifurcan tan extensivamente y el proceso medial da origen a 4 axones (asteriscos dentro de recuadro), dos de ellos se dirigen hacia la eminencia media y dos de ellos dan una vuelta abrupta y se dirigen dorsalmente, estos procesos axónicos resultaron positivos para vGLUT2.

La quinta neurona “VH25” (Figura 7-21 E), se hallaba en la frontera medial del PVNIm, en este caso dos dendritas emergen del polo dorsal y una del polo ventral, esta última da origen al axón principal que se dirige a eminencia media, y a un proceso tipo axónico en forma de “racimos de perlas”.

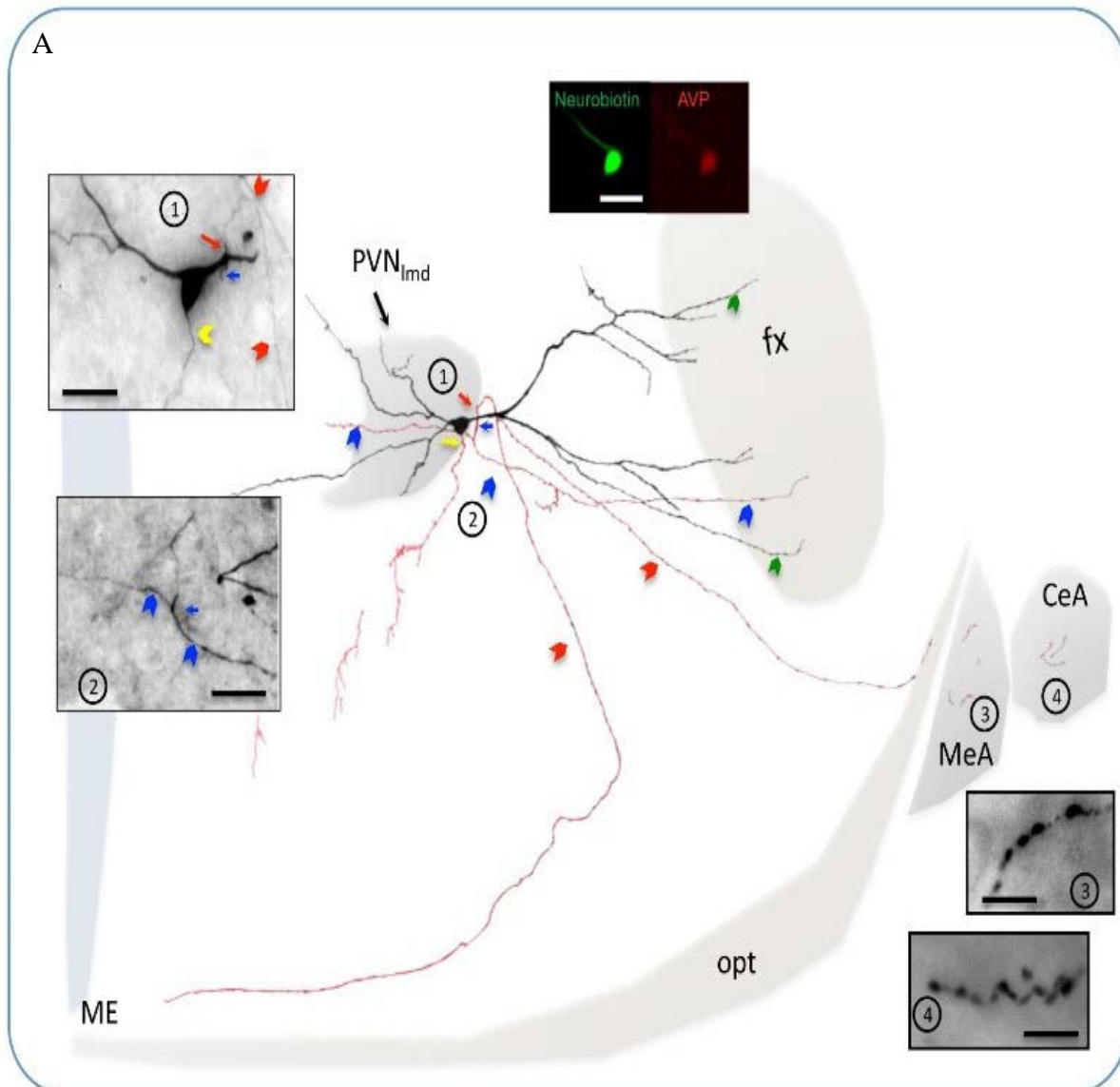


Figura 7-21. Proyecciones 2D de neuronas vasopresinérgicas magnocelulares marcadas yuxtacelularmente con neurobiotina. Todas las neuronas aquí representadas proyectaban a tracto de Greving y fueron positivas a vasopresina. Las reconstrucciones muestran los axones en rojo y las dendritas en negro. (A) “EV40”, registrada en parte lateral del PVN_{Imd}, presenta dos dendritas mediales y una dendrita que se ramifica en dirección lateral. Dos axones primarios emergen de la dendrita lateral a la misma altura (flechas rojas y azul en reconstrucción y fotomicrografías seriales 1 y 2). Insets 3 y 4 muestran procesos axónicos hallados en amígdala medial y central. Algunos otros procesos axónicos (punta de flecha azul) y dendríticos (punta de flecha verde) se vieron ingresando al fornix. Barra de escala 50 micras. Datos no publicados, enviados a *Frontiers in Neuroanatomy*.

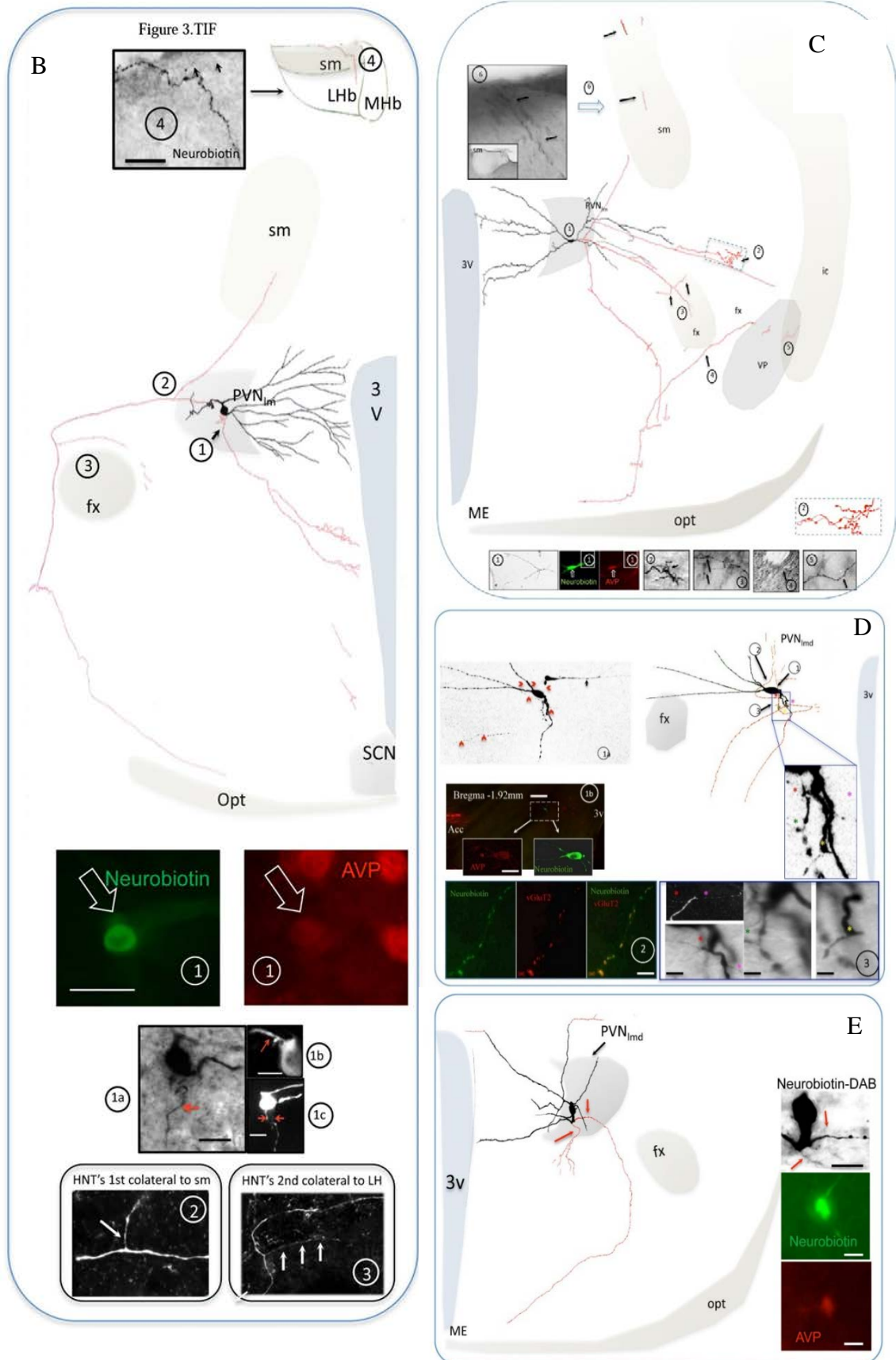


Figura 7-21. Proyecciones 2D de neuronas vasopresinérgicas magnocelulares marcadas yuxtacelularmente con neurobiotina. (B) “E16” muestra dos dendritas, dorsal y ventral. La dendrita ventral ramifica extensamente en dirección medial, la dendrita dorsal se divide en rama medial que ramifica medialmente y rama lateral que da lugar al axón. El axón se dirige lateralmente, inmediatamente después de salir de PVN emite una colateral dorsal que se integra a *stria medularis* donde se pierde temporalmente y se hallan procesos saliendo de sm a nivel de habenula. El axón principal continúa hacia eminencia media y en su paso por arriba de fornix emite una colateral que se pierde en la frontera de fornix. Esta neurona posee procesos tipo axónicos que forman un “racimo de perlas”, terminaciones axónicas se hallaron en el área preoptica medial (MPO) y en núcleo supraquiasmático (SCN). (C) “VH52” También registrada en la parte medial del PVN, se observa el mismo patrón de dendritas ramificando medialmente y axón que emerge de dendrita lateral, presenta un claro ejemplo de axón en “racimo de perlas” y se observan varias colaterales axónicas ingresando o en proximidad de vías importantes de conducción, i.e.: fornix (fx), cápsula interna (ic), *stria medularis* (sm) ver fotomicrografías 3-6. (D) “MM15” fue localizada en parte postero-lateral de PVN, en este caso las dendritas se dirigieron lateral y dorsalmente. A partir de la dendrita ventral emergen cuatro axones, dos de ellos se dirigen ventralmente hacia eminencia media y dos giran abruptamente en dirección dorsal, estos axones son positivos a vGlut2. (E) “VH25” ubicada en parte medial del núcleo, presenta dendritas emergiendo de un polo dorsal y uno ventral, no presenta ramificaciones extensas. De la dendrita ventral emerge el axón principal que se dirige a eminencia media y un proceso tipo axonal en forma de “racimo de perlas”. Datos no publicados, enviados a *Frontiers in Neuroanatomy*.

Sección III

La modulación a la alta o a la baja del sistema vasopresinérgico produce deterioro en conductas emocionales y cognitivas.

7.5.1 Las Ratas HM presentan “ansiedad condicionada” si son sometidas a un estresor osmótico.

Se evaluó el estado de ansiedad condicionada y no condicionada con dos pruebas conductuales bien consolidadas: el laberinto elevado en cruz (EPM) y la prueba de conflicto de Vogel (VCT) (Figura 7-22). El EPM compara el comportamiento de exploración contra el de evitación situando a la rata en un ambiente no condicionado, donde los brazos cerrados ofrecen seguridad y los brazos abiertos y elevados denotan novedad pero también riesgo. Menor tiempo en los brazos abiertos y un número reducido de entradas a ellos implican un estado de mayor ansiedad no condicionada. Los animales HM no mostraron diferencias significativas en estos parámetros, comparados con los control (Figura 7-22 A).

Posteriormente las ratas se sometieron a WD durante 48 h como estresor osmótico y tras esto se les colocó en la caja de prueba del VCT donde debían decidir entre tomar del bebedero y posiblemente recibir un toque eléctrico, o mantenerse apartadas de él. El grupo HM mostró una reducción en el número de toques recibidos durante los 5 min que duró la prueba (11.2 ± 1.68 , promedio \pm SEM) en comparación a los controles (37.5 ± 1.5) (Figura 7-22 B). La administración de diazepam 30 min antes de la prueba aumentó efectivamente la cantidad de toques tolerados, tanto en el grupo HM (240.6 ± 47.17) como en el control (258.2 ± 48.6) sin diferencia significativa entre ellos.

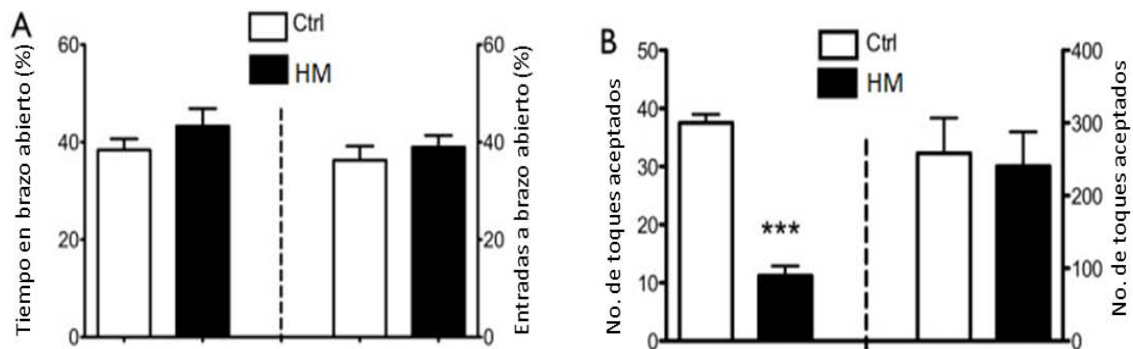


Figura 7-22. Pruebas para evaluar conductas tipo ansiedad. El grupo HM mostró una conducta de ansiedad diferencial respecto al control en las pruebas de ansiedad no condicionada y ansiedad condicionada. (A) prueba del laberinto en cruz elevado realizado antes de la privación de agua (WD) para evaluar la conducta de ansiedad no-condicionada. El histograma de la izquierda muestra el porcentaje de tiempo (s) que la rata pasó en el brazo abierto, el histograma de la derecha, el porcentaje de entradas al brazo abierto en relación al número total de entradas a brazos abiertos y cerrados. (B) Prueba de conflicto Vogel (VCT), después de 48 h de WD para evaluar el estado de ansiedad condicionada, que se refleja en el número de toques aceptados durante el lapso de la prueba (5 min). Panel izquierdo: sin ansiolítico, las ratas HM mostraron una disminución significativa en el número de descargas recibidas durante la prueba. (n = 8). Panel derecho: con la administración de diazepam i.p., 2,5 mg / kg de peso corporal, 30 minutos antes de la prueba, los toques recibidos tanto por HM y los sujetos control se incrementaron en gran medida y la diferencia observada entre los grupos desapareció. (n = 8), promedio \pm SEM, *** P <0.001. Modificado de (Zhang et al., 2010).

7.5.1 Déficit en el aprendizaje espacial cuando se modula a la alta o a la baja el sistema vasopresinérgico.

En este estudio, se comparó el desempeño de las ratas que sufrieron separación materna (SM, poseen un sistema vasopresinérgico potenciado) y ratas controles (sistema vasopresinérgico normal). Evaluamos a ambos grupos bajo cuatro condiciones 1) sin ningún tipo de estímulo 2) bajo un estado agudo de activación del sistema vasopresinérgico (inyección de solución hipertónica de NaCl); 3) bloqueando la transmisión vasopresinérgica via un antagonista del receptor V1b (receptor con una distribución muy localizada en hipocampo); 4) con los estímulos 2 y 3 simultáneamente.

No se observaron diferencias significativas en el aprendizaje espacial entre los grupos Ctrl y SM cuando se administró solución isotónica (T1, Figura 7-23 Panel A). Bajo el tratamiento hipertónico (T2) el grupo SM mostró latencias de escape significativamente aumentadas respecto al grupo control en los ensayos II, III VII y VIII (Figura 7-23 panel B). También se observó diferencia cuando se comparó el grupo SM hipertónico con el grupo SM isotónico en los ensayos III, VII y VIII (Figura 7-23 F, línea azul (T2) vs. línea negra (T1) y Tabla 2, panel de la derecha, intersección de T2 y T1 para los ensayos III, VII y VIII). El tratamiento hipertónico T2 no tuvo efectos significativos en el grupo control (Figura 7-23 E, línea azul (T2) vs. línea negra (T1) y Tabla 2, panel de la izquierda, intersección de T2 y T1). En el grupo control (Figura 7-23E), el antagonista del receptor V1b, SSR149415 (T3), produjo diferencias significativas en el desempeño en esta prueba cuando se comparó con el tratamiento isotónico (T1) en los ensayos II, III, IV, V, VI y VII (Figura 7-23E, línea roja (T3) vs. línea negra (T1) y Tabla 2, panel de la izquierda, intersección de T3 y T1 para dichos ensayos), mientras que en los animales SM, el SSR149415 (T3) sólo produjo diferencia significativa respecto al control contra el tratamiento isotónico (T1) (Figura 7-23 F, línea roja (T3) vs. línea negra (T1)). También se observaron diferencias significativas en los ensayos III, IV y V cuando se compararon Ctrl y SM tratados con SSR149415 (Figura 7-23 C). Sorprendentemente, una mejoría inicial en el desempeño durante la prueba se observó en el ensayo II, tanto en animales Ctrl como SM tratados con SSR149415 (Figura 7-23 E y F, líneas rojas (T3) contra líneas negras (T1)). Cuando se aplicó el tratamiento combinado (T4) los efectos deletéreos sobre el aprendizaje espacial del SSR149415 y de la solución

hipertónica se cancelaron y no se observó diferencia en el desempeño comparado con el isotónico, tanto en el grupo Ctrl como en el SM (Figura 7-23 E y F, línea verde (T4) vs. línea negra (T1)).

Grupo AFR					Grupo SM				
Ensayo I	T1	T2	T3	T4	Ensayo I	T1	T2	T3	T4
T1					T1				
T2					T2				
T3					T3				
T4					T4				
Ensayo III	T1	T2	T3	T4	Ensayo III	T1	T2	T3	T4
T1					T1				
T2		###			T2				
T3	***	***			T3	**	***		
T4	*		*		T4		*	**	
Ensayo III	T1	T2	T3	T4	Ensayo III	T1	T2	T3	T4
T1					T1				
T2		##			T2	***			
T3	***	***	###		T3		***		
T4			***		T4		***		
Ensayo IV	T1	T2	T3	T4	Ensayo IV	T1	T2	T3	T4
T1					T1				
T2					T2				
T3	***	***	###		T3		*		
T4			***		T4		**		
Ensayo V	T1	T2	T3	T4	Ensayo V	T1	T2	T3	T4
T1					T1				
T2					T2				
T3	***	***	###		T3				
T4			***	##	T4				
Ensayo VI	T1	T2	T3	T4	Ensayo VI	T1	T2	T3	T4
T1					T1				
T2					T2				
T3	*	*			T3				
T4			***	##	T4				
Ensayo VII	T1	T2	T3	T4	Ensayo VII	T1	T2	T3	T4
T1					T1				
T2		##			T2	***			
T3	**				T3				
T4			**	###	T4		**		
Ensayo VIII	T1	T2	T3	T4	Ensayo VIII	T1	T2	T3	T4
T1					T1				
T2		###			T2	***			
T3					T3		**		
T4					T4		***		

Tabla 4. Tabla de valores de significancia para la comparación entre los distintos tratamientos en el MWM: El panel izquierdo muestra diferencias estadísticamente significativas entre los tratamientos para los diferentes ensayos en el grupo de AFR. *, **, *** Representan 0.05, 0.01 y 0.001 diferencias significativas. #, # #, # # #, representan diferencias significativas de 0.05, 0.01, 0.001 entre los grupos SM y AFR para diferentes tratamientos y pruebas. El panel derecho muestra diferencias estadísticamente significativas entre los tratamientos para los diferentes ensayos en el grupo de MS. T1: Tratamiento isotónico; T2: Tratamiento hipertónico; T3: Tratamiento SSR149415; T4 Tratamiento hipertónico + tratamiento SSR149415. AFR: criados en el bioterio, SM: sometidos a protocolo de separación materna.

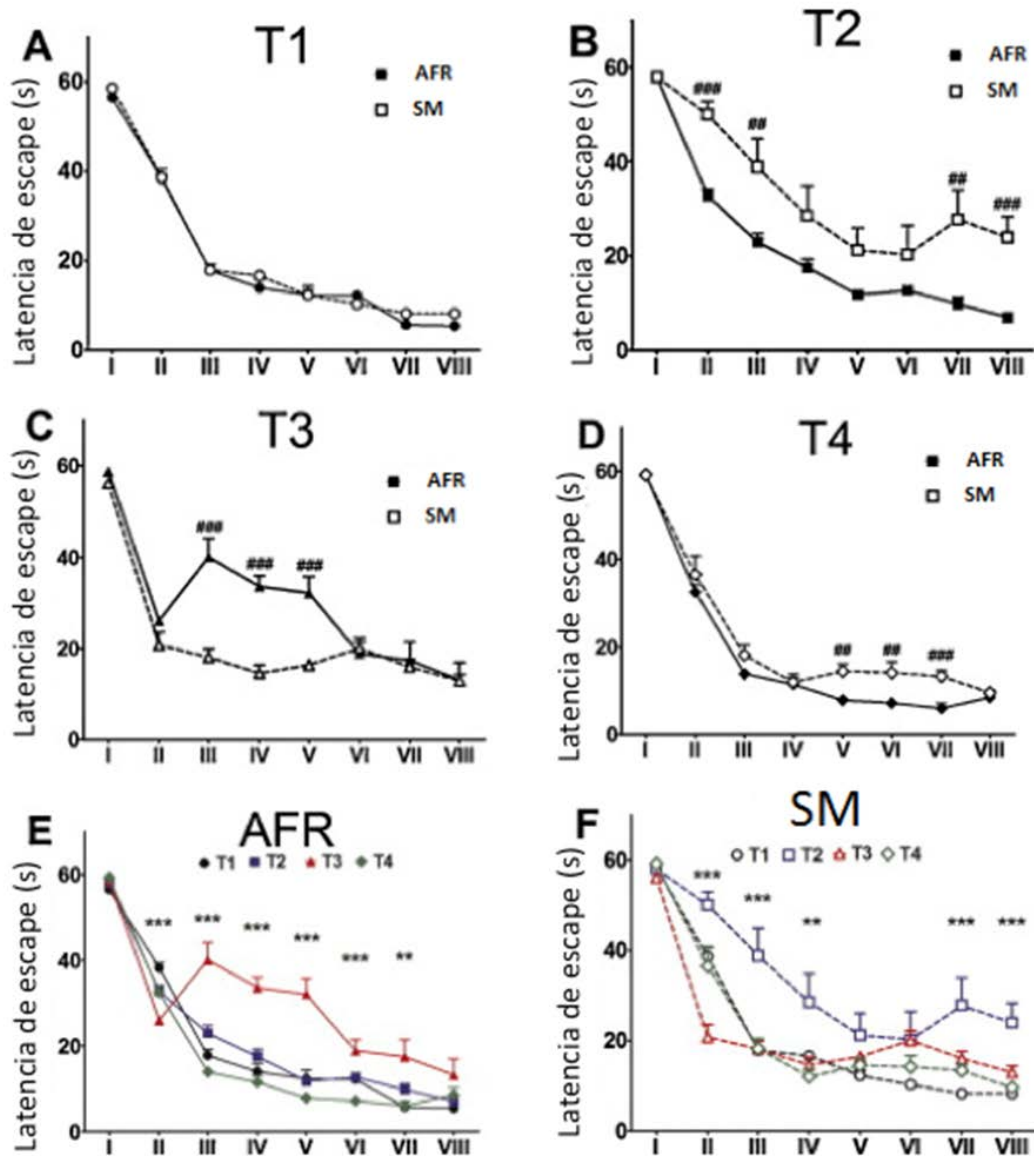


Figura 7-23. Desempeño en la prueba de aprendizaje espacial de MWM. Las pruebas se realizaron en ratas macho adultas en P90, tanto en ratas criadas en el bioterio (AFR) y ratas expuestas a separación materna neonatal (SM), después de recibir 4 tratamientos diferentes: (A) Solución isotónica (T1), (B) Solución hipertónica (T2), (C) SSR149415 (T3), (D) solución hipertónica + SSR149415 (T4). Panel E y F comparan los efectos de cada uno de los tratamientos dentro de los grupos AFR (E) y SM (F). Las comparaciones estadísticas detalladas se muestran en la Tabla 6.1. Los datos muestran el promedio \pm SEM ($n = 12$) del tiempo de latencia de escape a través de 8 ensayos realizados el mismo día. *, **, *** Representan diferencias significativas de 0.05, 0.01 y 0.001 entre los tratamientos para los diferentes ensayos y los diferentes grupos (SM y AFR). #, ##, ### Representan diferencias significativas de 0.05, 0.01, 0.001 entre los grupos, para los diferentes tratamientos y pruebas. Ver Tabla 1 para obtener mayor información sobre las diferencias significativa. Modificado de (Hernandez et al., 2012).

7.5.2 La activación del sistema vasopresinérgico, disminuye las conductas pasivas (congelamiento) y aumenta las conductas activas (escape) en respuesta a un estrés por predador.

Para evaluar las posibles implicaciones funcionales de las proyecciones intracerebrales vasopresinérgicas de las MNN's, diseñamos un experimento conductual donde activamos el sistema vasopresinérgico magnocelular (inyección sistémica de solución salina hipertónica, 30 minutos antes de iniciar el experimento). La figura 7-24 muestra un decremento en las conductas pasivas de escape (15 ± 2.8) en animales inyectados con solución hipertónica vs (32.85 ± 5.34) en controles y (32.25 ± 5.3) en animales inyectados con solución isotónica. Por el contrario las conductas activas de escape, aumentaron en el grupo hipertónico (44.05 ± 3.06) vs control (27.85 ± 3.2) y vehículo (23.1 ± 2.26).

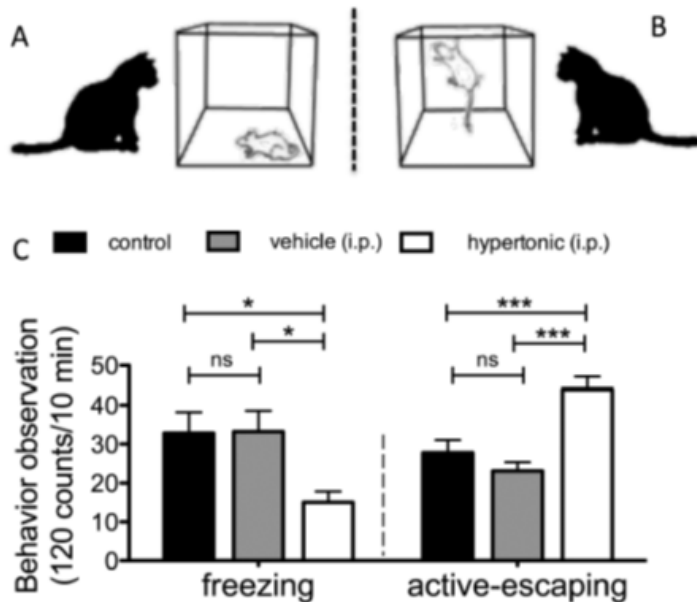


Figura 7-24. Aumento en las conductas activas de escape inducido por estrés osmótico. (A y B) representan típicas conductas pasivas (congelamiento) y activas (escalar) de escape ante un predador. (C) lado izquierdo muestra que el estrés osmótico genera una disminución en conductas pasivas de enfrentamiento al estrés aunado a un aumento en las conductas activas de escape (lado derecho).

7.5.3 El estrés osmótico modifica el patrón de activación neural inducido por el gato en estructuras inervadas por axones de la MNN's.

Tras 90 minutos de haber sido enfrentadas al predador, las ratas fueron sacrificadas para evaluar la expresión de Fos en regiones inervadas por axones de MNN's. Observamos que el gato induce un aumento en el número de núcleos de Fos en el hipotálamo (PVN, Pa, PALM), en amígdala y en habenula lateral. Sin embargo, los patrones de expresión inducidos por el predador se modificaron con la inyección de solución hipertónica (letras con apostrofe en la Figura 7-25). La solución hipertónica indujo un aumento en el número de núcleos de Fos en el núcleo supraquiasmático dorsal (SCNd), el núcleo supraóptico (SON, B y B'), el paraventricular lateral magnocelular (PVNlm, A'), la parte medial magnocelular del PVN (PVNmm, C y C'), el área preóptica medial (MPO), la parte central medial de amígdala (Sea, F y F') y la habenula lateral, parte medial (LHbm, . D y D'). Se observaron reducciones significativas en la amígdala medial (MeA) y baso lateral (BLA, F y F') y en la parte lateral de habenula lateral (LHbl, D y D'). No observamos cambios en la parte ventral del supraquiasmático (SCNv, B y B'), y la región parvocelular del paraventricular (PVNmpd, A y A'). En el tálamo la expresión de Fos se hizo más densa y organizada. La Figura 7-25 G indica la activación inducida por estrés osmótico en células vasopresinérgicas magnocelulares de PVNlm. El histograma en la figura 7-25 H y la tabla 4 comparan cuantitativamente la expresión de Fos en grupos vehículo e hipertónico. Datos no publicados, enviados a *Frontiers in Neuroanatomy*.

Tabla 4. Número de células Fos+ en un áreas de 0.02 mm².

Region Cat	Vehicle + Cat	Hypertonic +
Hypothalamus		
1. Suprachiasmatic nucleus, ventral part (SCN _v) ns	75.6 ± 7.4	90.8 ± 12.4
2. Suprachiasmatic nucleus, dorsal part (SCN _d) ***	1.2 ± 0.3	127.2 ± 6.4
3. Paraventricular lateral magnocellular (PVN _{lm}) ***	4.6 ± 1.1	189.8 ± 14.6
4. Paraventricular medial parvocellular (PVN _{mp}) ns	217.2 ± 26.9	166.8 ± 13.1
5. Paraventricular medial magnocellular (PVN _{mm}) ***	26.8 ± 3.6	122.5 ± 9.1
6. Supraoptic nucleus (SON) ***	28.5 ± 2.9	126.4 ± 12.6
7. Medial preoptic area (MPO) **	27.5 ± 4.8	67.5 ± 6.5
Amygdala		
1. Medial amygdala (MeA) ***	89.4 ± 8	32. ± 5.6
2. Central amygdala medial (CeA _m) ***	18.2 ± 1.3	48.2 ± 3.3
3. Basolateral amygdala (BLA) **	8.5 ± 0.7	2.8 ± 0.5
Epithalamus		
1. Lateral habenula medial part (LHb _m) *	25.5 ± 4	14.8 ± 2.7
2. Lateral habenula lateral part (LHb _l) ***	13.2 ± 1.6	4.4 ± 0.5

*, ** and *** for $P < 0.05$, $P < 0.01$ and $P < 0.001$, significance levels

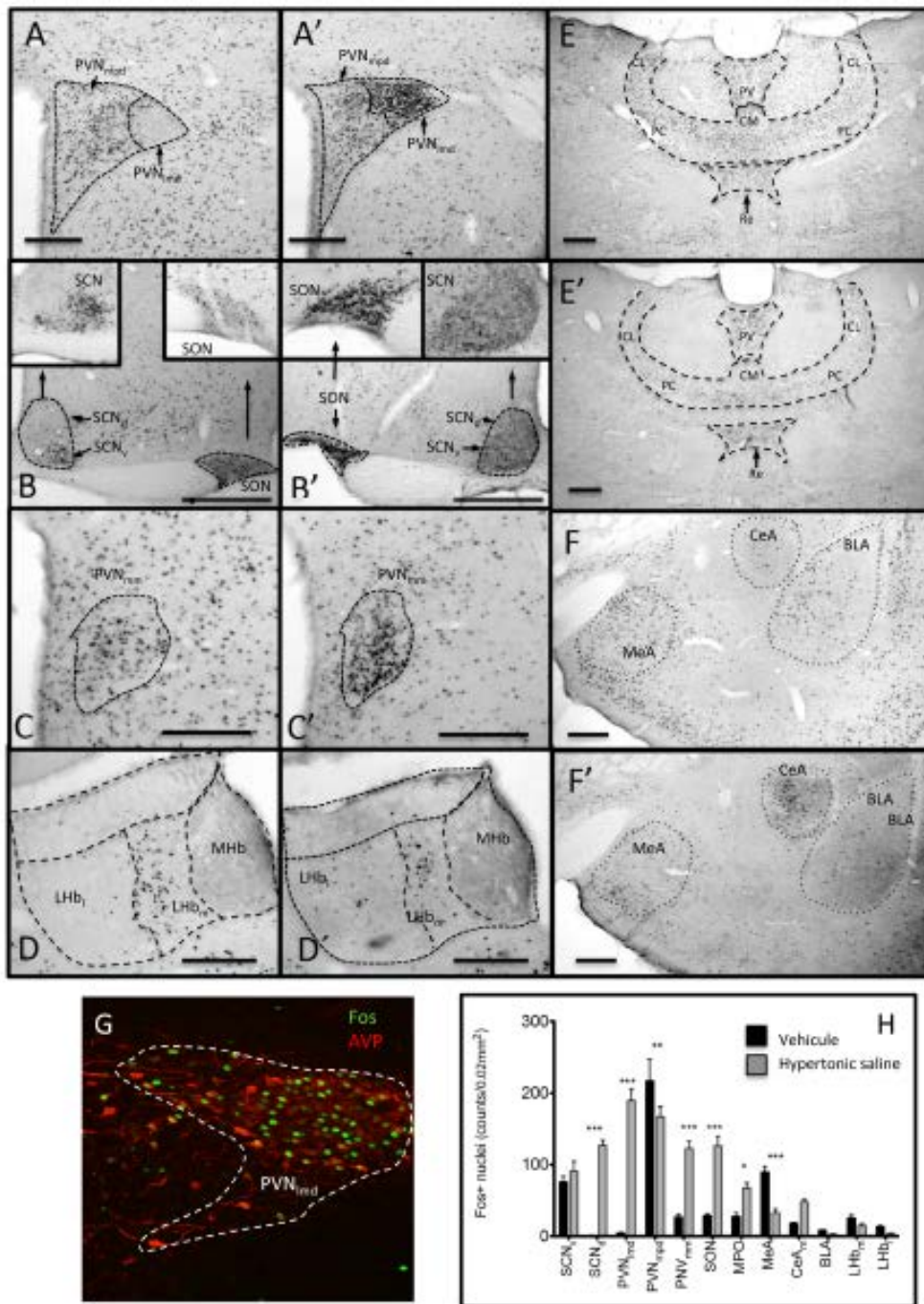


Figura 7-25. El estrés osmótico modifica el patrón de expresión de Fos inducido por predador. A-F: fotomicrografías que comparan la expresión de Fos en animales vehículo (letras no marcadas) vs animales con inyección de sol hipertónica (letras con apostrofe). (G) muestra la expresión de Fos (verde) en MNN's vasopresinérgicas (rojo) después de 90 minutos de una inyección hipertónica *i.p.*. (H) muestra un histograma comparando la expresión de Fos en las áreas mostradas por las microfotografías. *, ** y *** representan $P < 0.05$, $P < 0.01$ y $P < 0.001$, respectivamente. Datos no publicados, enviados a *Frontiers in Neuroanatomy*.

8. Discusión general

El término de homeostasis fue propuesto por Walter Cannon en su libro “The wisdom of the body”(Cannon, 1932), dicho termino fue derivado de los vocablos griegos *homeo* = similar y *stasis* = estabilidad y se le define como la capacidad de un sistema para regular su medio ambiente interno con el fin de mantener una condición estable. El mantener la homeostasis es fundamental para la sobrevivencia del individuo y de la especie, por lo que múltiples y complejos sistemas han evolucionado para reaccionar adecuadamente ante cambios en el ambiente interno y externo. Dichos cambios van desde ajustes en el medio interno hasta respuestas conductuales. Se considera clásicamente que el hipotálamo, una estructura filogenéticamente antigua es un nodo importante en la integración de estas respuestas homeostáticas. Dentro del hipotálamo los núcleos paraventricular y supraóptico contienen una importante población de neuronas vasopresinérgicas magnocelulares neurosecretoras (MNN's), estas neuronas responden a la disminución de la presión arterial o al aumento de la osmolaridad plasmática secretando vasopresina a la circulación sistémica por medio de axones que envían hacia la neurohipófisis. El efecto de la vasopresina sobre sus órganos blancos es una reabsorción de agua por el riñón y una contracción en el músculo liso de los vasos sanguíneos.

Es comúnmente aceptado que durante la vida adulta, el sistema HPA controla fundamentalmente la respuesta al estrés, sin embargo, durante la vida perinatal el sistema vasopresinérgico tiene un papel clave en mantener la homeostasis ante diversas clases de estresores (Makara et al., 2008, Zhang et al., 2012, Zhang et al., 2010, Zelena et al., 2008). Por ejemplo se ha demostrado que estresores que durante el periodo neonatal de hiporesponsividad al estrés son capaces de inducir una activación del eje HPA en ratas normales, no logran inducir una elevación de ACTH en ratas Brattelboro (KO natural para vasopresina), aunque sí responden con una elevación de corticosterona (CORT). Esto podría sugerir que la vasopresina es la responsable de la liberación de CORT y que las neuronas CRF aún no han madurado. Sin embargo en un estudio reciente se encontró un fenómeno bifásico en relación a la elevación de CORT como consecuencia de la separación materna: en P3 los animales MS mostraron una mayor elevación de CORT respecto a los AFR, sin embargo en P12 el grupo MS mostró una elevación menor que los AFR (Lajud et al., 2012). Los datos anteriores dan pie a proponer que la hiper-activación del sistema AVP durante la separación materna en la etapa postnatal temprana, representa un mecanismo homeostático para mantener el

balance del eje HPA hiper-activado y esto pueda contribuir al llamado “periodo hiporresponsivo al estrés” (Sapolsky and Meaney, 1986). El sistema vasopresinérgico hipotalámico durante esta etapa se encuentra en un importante proceso de maduración-remodelación, con distintos procesos ocurriendo simultáneamente (Antoni, 1993, Buijs et al., 1980, De Vries and Panzica, 2006, Ugrumov, 2002), lo que confiere gran plasticidad a este sistema para ser modificado por diversas influencias ambientales.

En la primera sección de esta tesis reportamos un aumento en la reactividad del sistema vasopresinérgico neurohipofiseal ante un estrés osmótico (i.e. más rápida y mayor liberación de vasopresina a la sangre), mayor número de neuronas vasopresinérgicas MNN's activadas ante un estrés osmótico, numerosos cuerpos de Herring (sitio de almacenamiento de la hormona, mayor expresión de mRNA de AVP y mayor volumen ocupado por neuronas AVP+. Estos resultados obtenidos en dos paradigmas de estrés perinatal (HM y SM), sugieren que el delicado ambiente endócrino prenatal puede sufrir modificaciones por diversas clases de estresores, de forma inmediata como mecanismo homeostático, pero a largo plazo pueden producir cambios perdurables en la estructura y función del sistema vasopresinérgico, dichos cambios pueden ser silentes en condiciones basales pero que se pueden evidenciar al tener que hacer frente a situaciones estresantes que requieran el reclutamiento de dicho sistema.

Se considera tradicionalmente que las proyecciones del sistema vasopresinérgico hipotalámico neurosecretor son exclusivas hacia la neurohipófisis, donde participan en la regulación hidroelectrolítica y de la presión arterial. Y que las proyecciones centrales vasopresinérgicas provienen de otros núcleos que expresan vasopresina (neuronas parvocelulares del núcleo paraventricular, núcleo supraquiasmático, amígdala, BNST, bulbo olfatorio). Sin embargo los resultados obtenidos, que demostraban que las ratas con un sistema vasopresinérgico magnocelular potenciado presentaban un deterioro en la respuesta al estrés (alteraciones cognitivas y emocionales) cuando dicho sistema era potenciado, sugería que el rol del sistema magnocelular vasopresinérgico no se limitaba a sus funciones periféricas. Algunos estudios previos habían sugerido por medio de métodos bioquímicos (Landgraf et al., 1988), inmunohistoquímicos (Buijs, 1978, Sofroniew and Glasmann, 1981)) y electrofisiológicos ((Inyushkin et al., 2009) la presencia de proyecciones intracerebrales

provenientes de estos núcleos magnocelulares, sin embargo dicha hipótesis no había sido aceptada dado que no eran métodos conclusivos. Nuevas técnicas para revelar la conectividad intracerebral se han desarrollado, y con esto en mente revisamos la hipótesis de que existían proyecciones intracerebrales desde los núcleos hipotalámicos magnocelulares hacia regiones centrales involucradas en el control de funciones cognitivas y emocionales y que la activación del sistema hipotalámico vasopresinérgico magnocelular tendría consecuencias en la activación neuronal de dichas regiones y en las conductas que a estas regiones estuvieren asociadas.

Los trabajos en la sección 2 de resultados describen los datos obtenidos al analizar las proyecciones intracerebrales de las neuronas magnocelulares del sistema vasopresinérgico hipotalámico. Por medio del uso de trazadores neurales, reconstrucción asistida por computadora y registro yuxtacelular in vivo con marcaje de neurona única, describimos una extensa red de proyecciones intracerebrales del sistema vasopresinérgico. Reportamos una determinación detallada del patrón de inervación en hipocampo y definimos la presencia de sinapsis en dichas regiones, así como la identidad celular de algunos blancos de axones vasopresinérgicos en el hipocampo, estos resultados contribuyen a explicar los mecanismos mediante los cuales la innervación proveniente de neuronas AVP+ magnocelulares de hipotálamo puede modificar la función de hipocampo y conductas asociadas tales como el aprendizaje espacial (Fanselow and Dong, 2010) o conductas de ansiedad (Adhikari et al., 2010).

Para confirmar inequívocamente el origen de la innervación intracerebral a partir de neuronas vasopresinérgicas neurosecretoras utilizamos el método de marcaje yuxtacelular, que ha demostrado ser un método poderoso para identificar con certeza la morfología de las proyecciones neuronales, sus blancos regionales y celulares así como el fenotipo inmunohistoquímico de las neuronas registradas. Aunado a esto, permite registrar la actividad electrofisiológica de la neurona registrada y el potencial local de campo del sitio donde se realiza el registro, permitiendo una correlación entre estructura y función. Con este método, para nuestra sorpresa, hallamos que algunas neuronas neurosecretoras vasopresinérgicas poseen más de un axón o colaterales axónicas que pueden surgir desde el axón que se dirige a la neurohipófisis o desde otros axones. Estos axones o colaterales inervan

estructuras intrahipotalámicas (área preóptica, núcleo supraquiasmático, área hipotalámica lateral) o se integran a vías de conducción (fimbria-fornix, *stria medularis*, cápsula interna) para inervar otras regiones intracerebrales (habénula, pálido ventral). Los resultados de este trabajo intentan proveer algunas respuestas en un antiguo debate sobre si las neuronas magnocelulares vasopresinérgicas neurosecretoras pueden tener proyecciones centrales, los resultados presentados indican que en efecto el sistema vasopresinérgico neurohipofiseal tiene una inervación intracerebral más extensa de lo que anteriormente se había propuesto.

En la última sección evaluamos los efectos que la modulación “aguda” del sistema vasopresinérgico (estrés osmótico o antagonistas de receptor vasopresinérgico) tiene sobre conductas en donde participan áreas que hemos demostrado son innervadas por neuronas vasopresinérgicas MNN’s, y evaluamos si la potenciación “crónica” del sistema vasopresinérgico magnocelular en animales sometidos a estrés perinatal, confiere susceptibilidad para desarrollar alteraciones en la motricidad y la cognición. Los resultados muestran que aunque bajo condiciones basales existe un sistema vasopresinérgico potenciado, no existen cambios conductuales evidentes, sin embargo cuando estos individuos son sometidos a condiciones que requieran la participación de dicho sistema, *e.g.* condiciones de privación de agua o administración de una solución hiperosmótica, se puede evidenciar una serie de alteraciones en parámetros conductuales.

Para evaluar las conductas de ansiedad, usamos dos pruebas conductuales: El laberinto en cruz elevado (EPM) y la prueba de conflicto de Vogel (VCT). La diferencia entre estas dos pruebas es que el EPM evalúa el conflicto “no condicionado”, que la rata presenta ante la tendencia a explorar lugares nuevos y la aversión a lugares abiertos mientras que la segunda (VCT) evalúa las conductas de “ansiedad condicionada”, en un estado de privación de agua por 24 horas. En ninguno de los dos modelos de estrés perinatal observamos que las ratas presentasen conductas de ansiedad no condicionada durante la edad adulta, lo cual apoya los datos obtenidos por (Lajud et al., 2012). La prueba de conflicto de Vogel, tiene como característica la activación del HNS y el aumento de la liberación de AVP y en este caso observamos que los animales HM y MS presentan conductas de ansiedad. Es lógico suponer que el aumento en ansiedad visto en esta prueba sea debido a la liberación de vasopresina intracerebral, estos datos van en concordancia a estudios previos que sugieren

efectos ansiogénicos/ansiolíticos de agonistas/antagonistas vasopresinérgicos cuando estos son administrados intracerebralmente(Landgraf et al., 1995, Mak et al., 2012) y una mayor liberación de vasopresina cuando las ratas presentan conductas tipo ansiedad (Landgraf and Wigger, 2002, Veenema et al., 2006, Zhang et al., 2012, Zhang et al., 2010).

En una prueba de aprendizaje espacial, observamos que la modulación aguda a la alta (estrés osmótico) o a la baja (antagonista vasopresinérgico) del sistema vasopresinérgico, produce un efecto diferencial en animales controles y MS. Deterioro en el aprendizaje espacial de animales MS (con un sistema vasopresinérgico potenciado) si se someten a activación aguda del sistema vasopresinérgico y en animales controles si se modula de forma aguda a la baja el sistema vasopresinérgico por medio de un antagonista del receptor V1b de vasopresina (expresado importantemente en hipocampo). Este es el primer estudio que demuestra que los animales que fueron sometidos a separación materna, presentan deterioro en aprendizaje espacial. El hipocampo es importante en procesos de aprendizaje y memoria, y desde los trabajos pioneros de deWied (Dewied et al., 1958), se ha propuesto que la vasopresina puede modular la función del hipocampo, posteriormente se han realizado estudios de electrofisiología que muestran que la AVP produce LTP en rebadadas de hipocampo (Chepkova et al., 1995) y la administración de vasopresina en el septum por microdialisis, produce deterioro en el aprendizaje espacial(Engelmann et al., 1992). Se ha reportado que los receptores V1b de vasopresina se hallan expresados importantemente en el hipocampo (Hernando et al., 2001, Lolait et al., 1995b, Young et al., 2006). Los estudios sobre el papel de estos receptores sobre el aprendizaje espacial son contradictorios, Egashira reporta que ratones KO para V1b no muestran déficits en una prueba de aprendizaje espacial, (Egashira et al., 2009), mientras Murgatroyd reporta que ratones que presentan déficits de aprendizaje espacial en el MWM, mejoran su curva de aprendizaje cuando son tratados con el antagonista V1b (SSR149415), (Murgatroyd et al., 2009).

Por último en la última serie de experimentos realizados en ratas sin estrés perinatal, observamos que la activación in-vivo de las neuronas magnocelulares neurosecretoras vasopresinérgicas, por medio de un estrés osmótico, produce una significativa reducción en las conductas pasivas de escape y un aumento en las conductas activas de escape ante un predador. Esta modificación conductual se asocia a la activación de regiones cerebrales que

reciben innervación de neuronas magnocelulares neurosecretoras. Los resultados anteriores sugieren que la hiperactivación del sistema vasopresinérgico que fue potenciado durante la etapa perinatal como un mecanismo de mantener la homeostasis, durante la edad adulta al ser reclutado puede sentar la base de neuropatologías.

Consideraciones Finales

En la presente tesis hemos demostrado que dos estresores perinatales tienen la capacidad de modificar el desarrollo del sistema vasopresinérgico. Probablemente estas alteraciones perdurables tengan su génesis en los intentos homeostáticos del sistema vasopresinérgico en desarrollo ante cambios en el ambiente interno o externo. En la edad adulta, cuando el sistema vasopresinérgico ha culminado su maduración, estos mecanismos inicialmente adaptativos pueden sentar las bases para la expresión de psicopatología durante la edad adulta. Hemos caracterizado la conectividad intracerebral de este sistema vasopresinérgico y hemos hallado que las MNN's además de la vía hipotálamo-neurohipofiseal clásica, generan una red de conexiones intracerebrales mucho más extensa de lo anteriormente propuesta, mediante la cual puede modular funciones cognitivas y emocionales

Estos resultados abren una serie de posibilidades de exploración sobre cómo el sistema vasopresinérgico magnocelular hipotalámico puede modular sus regiones blanco, será importante determinar cuál es el efecto de la liberación de vasopresina en los sitios diana, identificar los blancos celulares de estos axones, evaluar si existe alguna coherencia entre el potencial local de campo registrado en hipotálamo y en las regiones blanco tales como hipocampo o amígdala, y si esto es cierto verificar cómo se modulan estas conexiones funcionales por medio de estímulos que regulen a la alta o a la baja al sistema vasopresinérgico.

9. Tabla de abreviaturas

3hSM	Episodio de separación materna por 3 horas
ACTH	Hormona adrenocorticotropina, (adrenocorticotropic hormone)
ADH	Hormona antidiurética, (antidiuretic hormone)
AFR	Ratas controles criadas en el bioterio, (animal facility reared)
AHA	Área hipotalámica anterior
AT	Terminal axónica, (axón terminal)
AVP	Arginina vasopresina
BNST	Núcleo del lecho de la <i>estria terminalis</i> (bed nuclei of the <i>stria terminalis</i>)
cAMP	AMP cíclico (cyclic adenosine monophosphate)
CCTV	Cámara de circuito cerrado (Closed circuit television)
CeA	Núcleo central de la amígdala
CORT	Corticosterona
CRF	Factor liberador de corticotropina, (corticotropin releasing factor)
Crtl	Control
CV	Coefficiente de variación
DAB	3,3'-diaminobencidina
DEPC	Dietilpirocarbonato
Ei	Día embrionario <i>i</i>
ELISA	Enzyme linked immuno-sorbent assay
EPM	Elevated Plus Maze
EPSP	Potenciales post-sinápticos excitatorios, (Excitatory post-synaptic potencial)
FG	Fluoro-Gold
FST	Prueba de nado forzado, (Forced swimming test)
GD	Giro dentado
HM	Hipertiroidismo materno
HNS	Sistema hipotálamo-neurohipofiseal (Hypothalamic-neurohypophyseal system)
HNT	Tracto hipotálamo-neurohipofiseal (Hypothalamic-neurohypophyseal tract)
HPA	Hipotálamo-pituitaria-adrenal
HT	Hormonas tiroideas

IC	Cápsula interna (Internal capsule)
IHC	Inmunohistoquímica (Immunohistochemistry)
IP3	Inositol trifosfato
ISH	Hibridación <i>in-situ</i> , (<i>in-situ</i> hybridation)
LTP	Long term potentiation
LTVP	Potenciación vasopresinérgica de largo plazo, (Long term vasopressinergic potentiation)
mRNA	ARN mensajero
MWM	Laberinto acuático de Morris, (Morris water maze)
MS	Separación materna
NGS	Suero normal de cabra, (normal goat serum)
NIH	Instituto Nacional de Salud de Estados Unidos, (National Institute of Health)
NSS	Suero normal de cerdo, (Normal swine serum)
PB	Buffer de fosfato de sodio, (phosphate buffer)
PFA	Paraformaldehído
Pi	Día postnatal <i>i</i>
PLC	Fosfolipasa C, (Phospholipase C)
PVN	Núcleo paraventricular, (paraventricular nucleus)
PVN mpd	División medial parvocelular del PVN, (PVN medial parvocelular division)
PVNIm	División lateral magnocelular del PVN, (PVN lateral magnocelular division)
RFST	Prueba de nado forzado repetido, (Repeated forced swimming test)
SCMS	Estrés leve sub-crónico moderado, (Sub-chronic mild stress)
SCN	Núcleo supraquiasmático, (Suprachiasmatic nucleus)
SEM	Error estándar del promedio, (Standard error of mean)
SON	núcleo supraóptico, (Supraoptic nucleus)
STIA	<i>stria terminalis</i>
str. or	<i>stratum oriens</i>
T3	Triyodotironina
T4	L- tiroxina
TB	Buffer de Tris
TBS	Buffer de Tris + NaCl 0.9%
TBST	Buffer de Tris + NaCl 0.9% y Tritón 100x al 0.3%

TDHA	Trastorno de déficit de atención e hiperactividad
TST	Prueba de suspensión del rabo, (Tail suspension test)
VCT	Prueba de conflicto de Vogel, (Vogel conflict test)
WD	Privación de agua, (Water deprivation)

10. Bibliografía

- ABDULJABBAR, M. A. & AFIFI, A. M. 2012. Congenital hypothyroidism. *J Pediatr Endocrinol Metab*, 25, 13-29.
- ACHER, R., CHAUVET, J. & CHAUVET, M. T. 1995. Man and the chimaera. Selective versus neutral oxytocin evolution. *Adv Exp Med Biol*, 395, 615-27.
- ADHIKARI, A., TOPIWALA, M. A. & GORDON, J. A. 2010. Synchronized activity between the ventral hippocampus and the medial prefrontal cortex during anxiety. *Neuron*, 65, 257-69.
- AGUILERA, G. & RABADAN-DIEHL, C. 2000. Vasopressinergic regulation of the hypothalamic-pituitary-adrenal axis: implications for stress adaptation. *Regul Pept*, 96, 23-9.
- AISA, B., TORDERA, R., LASHERAS, B., DEL RÍO, J. & RAMÍREZ, M. J. 2007. Cognitive impairment associated to HPA axis hyperactivity after maternal separation in rats. *Psychoneuroendocrinology*, 32, 256-66.
- ALBECK, D. S., MCKITTRICK, C. R., BLANCHARD, D. C., BLANCHARD, R. J., NIKULINA, J., MCEWEN, B. S. & SAKAI, R. R. 1997. Chronic social stress alters levels of corticotropin-releasing factor and arginine vasopressin mRNA in rat brain. *J Neurosci*, 17, 4895-903.
- ALESCIO-LAUTIER, B., PABAN, V. & SOUMIREU-MOURAT, B. 2000. Neuromodulation of memory in the hippocampus by vasopressin. *Eur J Pharmacol*, 405, 63-72.
- ANISMAN, H., ZAHARIA, M. D., MEANEY, M. J. & MERALI, Z. 1998. Do early-life events permanently alter behavioral and hormonal responses to stressors? *International journal of developmental neuroscience : the official journal of the International Society for Developmental Neuroscience*, 16, 149-64.
- ANTONI, F. A. 1993. Vasopressinergic control of pituitary adrenocorticotropin secretion comes of age. *Front Neuroendocrinol*, 14, 76-122.
- ARMSTRONG, W. 2004. Hypothalamic supraoptic and paraventricular nuclei. In: PAXINOS, G. (ed.) *The rat nervous system*. Elsevier.
- BARBERIS, C., MOUILLAC, B. & DURROUX, T. 1998. Structural bases of vasopressin/oxytocin receptor function. *J Endocrinol*, 156, 223-9.
- BARBERIS, C. & TRIBOLLET, E. 1996. Vasopressin and oxytocin receptors in the central nervous system. *Crit Rev Neurobiol*, 10, 119-54.
- BARKER, D. J. & OSMOND, C. 1986. Infant mortality, childhood nutrition, and ischaemic heart disease in England and Wales. *Lancet*, 1, 1077-81.
- BIELSKY, I. F., HU, S. B., REN, X., TERWILLIGER, E. F. & YOUNG, L. J. 2005. The V1a vasopressin receptor is necessary and sufficient for normal social recognition: a gene replacement study. *Neuron*, 47, 503-13.
- BIELSKY, I. F. & YOUNG, L. J. 2004. Oxytocin, vasopressin, and social recognition in mammals. *Peptides*, 25, 1565-74.
- BORON, W. F. & BOULPAEP, E. L. 2009. *Medical physiology : a cellular and molecular approach*, Philadelphia, PA, Saunders/Elsevier.
- BRUNSON, K. L., KRAMAR, E., LIN, B., CHEN, Y., COLGIN, L. L., YANAGIHARA, T. K., LYNCH, G. & BARAM, T. Z. 2005. Mechanisms of late-onset cognitive decline after early-life stress. *J Neurosci*, 25, 9328-38.
- BUIJS, R. M. 1978. Intra- and extrahypothalamic vasopressin and oxytocin pathways in the rat. Pathways to the limbic system, medulla oblongata and spinal cord. *Cell Tissue Res*, 192, 423-35.

- BUIJS, R. M., VELIS, D. N. & SWAAB, D. F. 1980. Ontogeny of vasopressin and oxytocin in the fetal rat: early vasopressinergic innervation of the fetal brain. *Peptides*, 1, 315-24.
- BURROW, G. N. 1993. Thyroid function and hyperfunction during gestation. *Endocr Rev*, 14, 194-202.
- CAFFE, A. R. & VAN LEEUWEN, F. W. 1983. Vasopressin-immunoreactive cells in the dorsomedial hypothalamic region, medial amygdaloid nucleus and locus coeruleus of the rat. *Cell Tissue Res*, 233, 23-33.
- CAFFE, A. R., VAN LEEUWEN, F. W. & LUITEN, P. G. 1987. Vasopressin cells in the medial amygdala of the rat project to the lateral septum and ventral hippocampus. *J Comp Neurol*, 261, 237-52.
- CALDJJI, C., TANNENBAUM, B., SHARMA, S., FRANCIS, D., PLOTSKY, P. M. & MEANEY, M. J. 1998. Maternal care during infancy regulates the development of neural systems mediating the expression of fearfulness in the rat. *Proc Natl Acad Sci U S A*, 95, 5335-40.
- CALDWELL, H. K., LEE, H. J., MACBETH, A. H. & YOUNG, W. S., 3RD 2008. Vasopressin: behavioral roles of an "original" neuropeptide. *Prog Neurobiol*, 84, 1-24.
- CANNON, W. B. 1932. *The wisdom of the body*, New York, W.W. Norton & Company, Inc.
- CASTEL, M., FEINSTEIN, N., COHEN, S. & HARARI, N. 1990. Vasopressinergic innervation of the mouse suprachiasmatic nucleus: an immuno-electron microscopic analysis. *J Comp Neurol*, 298, 172-87.
- COLLAER, M. L. & HINES, M. 1995. Human behavioral sex differences: a role for gonadal hormones during early development? *Psychol Bull*, 118, 55-107.
- CREASY, R. K. 1991. Lifestyle influences on prematurity. *J Dev Physiol*, 15, 15-20.
- CHEN, C., DIAZ BRINTON, R. D., SHORS, T. J. & THOMPSON, R. F. 1993. Vasopressin induction of long-lasting potentiation of synaptic transmission in the dentate gyrus. *Hippocampus*, 3, 193-203.
- CHEN, X. & HERBERT, J. 1995. Alterations in sensitivity to intracerebral vasopressin and the effects of a V1a receptor antagonist on cellular, autonomic and endocrine responses to repeated stress. *Neuroscience*, 64, 687-97.
- CHEPKOVA, A. N., FRENCH, P., DE WIED, D., ONTSKUL, A. H., RAMAKERS, G. M., SKREBITSKI, V. G., GISPEN, W. H. & URBAN, I. J. 1995. Long-lasting enhancement of synaptic excitability of CA1/subiculum neurons of the rat ventral hippocampus by vasopressin and vasopressin(4-8). *Brain Res*, 701, 255-66.
- CHEPKOVA, A. N., KAPAI, N. A. & SKREBITSKII, V. G. 2001. Arginine vasopressin fragment AVP(4-9) facilitates induction of long-term potentiation in the hippocampus. *Bull Exp Biol Med*, 131, 136-8.
- CHOWDREY, H. S., LARSEN, P. J., HARBUZ, M. S., JESSOP, D. S. & LIGHTMAN, S. L. 1995. Evidence for Arginine-Vasopressin as the Primary Activator of the Hypothalamopituitary-Adrenal Axis during Chronic Inflammatory Stress. *British Journal of Pharmacology*, 114, P65-P65.
- DAITZ, H. M. & POWELL, T. P. 1954. Studies of the connexions of the fornix system. *J Neurol Neurosurg Psychiatry*, 17, 75-82.
- DE VRIES, G. J. & BUIJS, R. M. 1983. The origin of the vasopressinergic and oxytocinergic innervation of the rat brain with special reference to the lateral septum. *Brain Res*, 273, 307-17.

- DE VRIES, G. J. & PANZICA, G. C. 2006. Sexual differentiation of central vasopressin and vasotocin systems in vertebrates: different mechanisms, similar endpoints. *Neuroscience*, 138, 947-55.
- DE WIED, D. 1965. The Influence of the Posterior and Intermediate Lobe of the Pituitary and Pituitary Peptides on the Maintenance of a Conditioned Avoidance Response in Rats. *Int J Neuropharmacol*, 4, 157-67.
- DE WIED, D. 1971. Long term effect of vasopressin on the maintenance of a conditioned avoidance response in rats. *Nature*, 232, 58-60.
- DENT, G. W., OKIMOTO, D. K., SMITH, M. A. & LEVINE, S. 2000. Stress-induced alterations in corticotropin-releasing hormone and vasopressin gene expression in the paraventricular nucleus during ontogeny. *Neuroendocrinology*, 71, 333-42.
- DENT, G. W., SMITH, M. A. & LEVINE, S. 2001. Stress-induced alterations in locus coeruleus gene expression during ontogeny. *Brain Res Dev Brain Res*, 127, 23-30.
- DESBONNET, L., GARRETT, L., DALY, E., MCDERMOTT, K. W. & DINAN, T. G. 2008. Sexually dimorphic effects of maternal separation stress on corticotrophin-releasing factor and vasopressin systems in the adult rat brain. *Int J Dev Neurosci*, 26, 259-68.
- DEWIED, D., BOUMAN, P. R. & SMELIK, P. G. 1958. The effect of a lipide extract from the posterior hypothalamus and of pitressin on the release of ACTH from the pituitary gland. *Endocrinology*, 62, 605-13.
- DIETRICH, A. & ALLEN, J. D. 1997. Vasopressin and memory. I. The vasopressin analogue AVP4-9 enhances working memory as well as reference memory in the radial arm maze. *Behav Brain Res*, 87, 195-200.
- DUCSAY, C. A., MLYNARCZYK, M., KAUSHAL, K. M., HYATT, K., HANSON, K. & MYERS, D. A. 2009. Long-term hypoxia enhances ACTH response to arginine vasopressin but not corticotropin-releasing hormone in the near-term ovine fetus. *Am J Physiol Regul Integr Comp Physiol*, 297, R892-9.
- DUNN, F. L., BRENNAN, T. J., NELSON, A. E. & ROBERTSON, G. L. 1973. The role of blood osmolality and volume in regulating vasopressin secretion in the rat. *J Clin Invest*, 52, 3212-9.
- EBNER, K., WOTJAK, C. T., LANDGRAF, R. & ENGELMANN, M. 2002. Forced swimming triggers vasopressin release within the amygdala to modulate stress-coping strategies in rats. *Eur J Neurosci*, 15, 384-8.
- EGASHIRA, N., MISHIMA, K., IWASAKI, K., OISHI, R. & FUJIWARA, M. 2009. New Topics in Vasopressin Receptors and Approach to Novel Drugs: Role of the Vasopressin Receptor in Psychological and Cognitive Functions. *Journal of Pharmacological Sciences*, 109, 44-49.
- ENGELMANN, M., BURES, J. & LANDGRAF, R. 1992. Vasopressin administration via microdialysis into the septum interferes with the acquisition of spatial memory in rats. *Neurosci Lett*, 142, 69-72.
- EVANS, I. M., PICKARD, M. R., SINHA, A. K., LEONARD, A. J., SAMPSON, D. C. & EKINS, R. P. 2002. Influence of maternal hyperthyroidism in the rat on the expression of neuronal and astrocytic cytoskeletal proteins in fetal brain. *J Endocrinol*, 175, 597-604.
- FADEN, V. B., GRAUBARD, B. I. & DUFOUR, M. 1997. The relationship of drinking and birth outcome in a US national sample of expectant mothers. *Paediatr Perinat Epidemiol*, 11, 167-80.

- FANSELOW, M. S. & DONG, H. W. 2010. Are the dorsal and ventral hippocampus functionally distinct structures? *Neuron*, 65, 7-19.
- FELSZEGHY, K., SASVARI, M. & NYAKAS, C. 1993. Behavioral depression: opposite effects of neonatal dexamethasone and ACTH-(4-9) analogue (ORG 2766) treatments in the rat. *Horm Behav*, 27, 380-96.
- FENG, Y., KUMAR, P., WANG, J. & BHATT, A. J. 2015. Dexamethasone but not the equivalent doses of hydrocortisone induces neurotoxicity in neonatal rat brain. *Pediatr Res*.
- FILE, S. E., LIPPA, A. S., BEER, B. & LIPPA, M. T. 2004. Animal tests of anxiety. *Curr Protoc Neurosci*, Chapter 8, Unit 8 3.
- FUMAGALLI, F., MOLTENI, R., RACAGNI, G. & RIVA, M. A. 2007. Stress during development: Impact on neuroplasticity and relevance to psychopathology. *Prog Neurobiol*, 81, 197-217.
- GOTTSCHALK, C. W. & MYLLE, M. 1959. Micropuncture Study of the Mammalian Urinary Concentrating Mechanism - Evidence for the Countercurrent Hypothesis. *American Journal of Physiology*, 196, 927-936.
- GRIEBEL, G., SIMIAND, J., SERRADEIL-LE GAL, C., WAGNON, J., PASCAL, M., SCATTON, B., MAFFRAND, J. P. & SOUBRIE, P. 2002. Anxiolytic- and antidepressant-like effects of the non-peptide vasopressin V1b receptor antagonist, SSR149415, suggest an innovative approach for the treatment of stress-related disorders. *Proc Natl Acad Sci U S A*, 99, 6370-5.
- HARI DASS, S. A. & VYAS, A. 2014. Copulation or sensory cues from the female augment Fos expression in arginine vasopressin neurons of the posterodorsal medial amygdala of male rats. *Front Zool*, 11, 42.
- HARRIS, G. W. & DONOVAN, B. T. 1966. *The Pituitary Gland*, University of California Press.
- HASLAM, R. J. & ROSSON, G. M. 1972. Aggregation of Human Blood-Platelets by Vasopressin. *American Journal of Physiology*, 223, 958-&.
- HATTON, G. I. 1990. Emerging concepts of structure-function dynamics in adult brain: the hypothalamo-neurohypophysial system. *Prog Neurobiol*, 34, 437-504.
- HEIM, C., PLOTSKY, P. M. & NEMEROFF, C. B. 2004. Importance of studying the contributions of early adverse experience to neurobiological findings in depression. *Neuropsychopharmacology*, 29, 641-8.
- HEINRICHS, S. C. & KOOB, G. F. 2006. Application of experimental stressors in laboratory rodents. *Curr Protoc Neurosci*, Chapter 8, Unit8 4.
- HEMS, D. A., WHITTON, P. D. & MA, G. Y. 1975. Metabolic actions of vasopressin, glucagon and adrenalin in the intact rat. *Biochim Biophys Acta*, 411, 155-64.
- HERNANDEZ, V. S., RUIZ-VELAZCO, S. & ZHANG, L. 2012. Differential effects of osmotic and SSR149415 challenges in maternally separated and control rats: the role of vasopressin on spatial learning. *Neurosci Lett*, 528, 143-7.
- HERNANDO, F., SCHOOTS, O., LOLAIT, S. J. & BURBACH, J. P. 2001. Immunohistochemical localization of the vasopressin V1b receptor in the rat brain and pituitary gland: anatomical support for its involvement in the central effects of vasopressin. *Endocrinology*, 142, 1659-68.
- HERRING, P. T. 1908. A contribution to the comparative physiology of the pituitary body. *Quarterly Journal of Experimental Physiology*, 1, 261-U14.

- HOORNEMAN, E. M. & BUIJS, R. M. 1982. Vasopressin fiber pathways in the rat brain following suprachiasmatic nucleus lesioning. *Brain Res*, 243, 235-41.
- HOWES, O. D., MCDONALD, C., CANNON, M., ARSENEAULT, L., BOYDELL, J. & MURRAY, R. M. 2004. Pathways to schizophrenia: the impact of environmental factors. *Int J Neuropsychopharmacol*, 7 Suppl 1, S7-S13.
- IBRAGIMOV, R., BAIRAMOVA, F. M. & DADASHEV, F. G. 1989. [The effect of oxytocin and vasopressin on individual behavior and EEG-correlates of narcotic dependent rats in the "open field" test]. *Fiziol Zh SSSR Im I M Sechenova*, 75, 441-6.
- INYUSHKIN, A. N., ORLANS, H. O. & DYBALL, R. E. 2009. Secretory cells of the supraoptic nucleus have central as well as neurohypophysial projections. *J Anat*, 215, 425-34.
- IVY, A. S., BRUNSON, K. L., SANDMAN, C. & BARAM, T. Z. 2008. Dysfunctional nurturing behavior in rat dams with limited access to nesting material: a clinically relevant model for early-life stress. *Neuroscience*, 154, 1132-42.
- KALINICHEV, M., EASTERLING, K. W. & HOLTZMAN, S. G. 2003. Long-lasting changes in morphine-induced locomotor sensitization and tolerance in Long-Evans mother rats as a result of periodic postpartum separation from the litter: a novel model of increased vulnerability to drug abuse? *Neuropsychopharmacology*, 28, 317-28.
- KALINICHEV, M., EASTERLING, K. W., PLOTSKY, P. M. & HOLTZMAN, S. G. 2002. Long-lasting changes in stress-induced corticosterone response and anxiety-like behaviors as a consequence of neonatal maternal separation in Long-Evans rats. *Pharmacol Biochem Behav*, 73, 131-40.
- KAPLAN, S. A. 2007. The pituitary gland: a brief history. *Pituitary*, 10, 323-5.
- KHEGAY, II 1996. Localization of the vasopressin gene to rat chromosome 3. *Mamm Genome*, 7, 867.
- KOENIG, J. I., ELMER, G. I., SHEPARD, P. D., LEE, P. R., MAYO, C., JOY, B., HERCHER, E. & BRADY, D. L. 2005. Prenatal exposure to a repeated variable stress paradigm elicits behavioral and neuroendocrinological changes in the adult offspring: potential relevance to schizophrenia. *Behav Brain Res*, 156, 251-61.
- KOROSI, A. & BARAM, T. Z. 2009. The pathways from mother's love to baby's future. *Front Behav Neurosci*, 3, 27.
- KUHN, C. M. & SCHANBERG, S. M. 1998. Responses to maternal separation: mechanisms and mediators. *Int J Dev Neurosci*, 16, 261-70.
- LADD, C. O., OWENS, M. J. & NEMEROFF, C. B. 1996. Persistent changes in corticotropin-releasing factor neuronal systems induced by maternal deprivation. *Endocrinology*, 137, 1212-8.
- LAJUD, N., ROQUE, A., CAJERO, M., GUTIERREZ-OSPINA, G. & TORNER, L. 2012. Periodic maternal separation decreases hippocampal neurogenesis without affecting basal corticosterone during the stress hyporesponsive period, but alters HPA axis and coping behavior in adulthood. *Psychoneuroendocrinology*, 37, 410-20.
- LAND, H., SCHUTZ, G., SCHMALE, H. & RICHTER, D. 1982. Nucleotide sequence of cloned cDNA encoding bovine arginine vasopressin-neurophysin II precursor. *Nature*, 295, 299-303.
- LANDGRAF, R., GERSTBERGER, R., MONTKOWSKI, A., PROBST, J. C., WOTJAK, C. T., HOLSBOER, F. & ENGELMANN, M. 1995. V1 vasopressin receptor antisense oligodeoxynucleotide into septum reduces vasopressin binding, social discrimination abilities, and anxiety-related behavior in rats. *J Neurosci*, 15, 4250-8.

- LANDGRAF, R., NEUMANN, I. & SCHWARZBERG, H. 1988. Central and peripheral release of vasopressin and oxytocin in the conscious rat after osmotic stimulation. *Brain Res*, 457, 219-25.
- LANDGRAF, R. & WIGGER, A. 2002. High vs low anxiety-related behavior rats: an animal model of extremes in trait anxiety. *Behav Genet*, 32, 301-14.
- LAYCOCK, J. F. 2010. Introduction to vasopressin. *Perspectives on vasopressin*. London: Imperial College Press.
- LEVINE, S. 1957. Infantile experience and resistance to physiological stress. *Science*, 126, 405.
- LEVINE, S. 1994. The ontogeny of the hypothalamic-pituitary-adrenal axis. The influence of maternal factors. *Ann N Y Acad Sci*, 746, 275-88; discussion 289-93.
- LEWINN, K. Z., STROUD, L. R., MOLNAR, B. E., WARE, J. H., KOENEN, K. C. & BUKA, S. L. 2009. Elevated maternal cortisol levels during pregnancy are associated with reduced childhood IQ. *Int J Epidemiol*, 38, 1700-10.
- LIEBL, C., PANHUYSEN, M., PUTZ, B., TRUMBACH, D., WURST, W., DEUSSING, J. M., MULLER, M. B. & SCHMIDT, M. V. 2009. Gene expression profiling following maternal deprivation: involvement of the brain Renin-Angiotensin system. *Front Mol Neurosci*, 2, 1.
- LIEBSCH, G., WOTJAK, C. T., LANDGRAF, R. & ENGELMANN, M. 1996. Septal vasopressin modulates anxiety-related behaviour in rats. *Neurosci Lett*, 217, 101-4.
- LIU, D., DIORIO, J., TANNENBAUM, B., CALDJI, C., FRANCIS, D., FREEDMAN, A., SHARMA, S., PEARSON, D., PLOTSKY, P. M. & MEANEY, M. J. 1997. Maternal care, hippocampal glucocorticoid receptors, and hypothalamic-pituitary-adrenal responses to stress. *Science*, 277, 1659-62.
- LOLAIT, S. J., O'CARROLL, A. M. & BROWNSTEIN, M. J. 1995a. Molecular biology of vasopressin receptors. *Ann N Y Acad Sci*, 771, 273-92.
- LOLAIT, S. J., O'CARROLL, A. M., MAHAN, L. C., FELDER, C. C., BUTTON, D. C., YOUNG, W. S., 3RD, MEZEY, E. & BROWNSTEIN, M. J. 1995b. Extrahypothalamic expression of the rat V1b vasopressin receptor gene. *Proc Natl Acad Sci U S A*, 92, 6783-7.
- LUDWIG, M., HORN, T., CALLAHAN, M. F., GROSCHE, A., MORRIS, M. & LANDGRAF, R. 1994. Osmotic stimulation of the supraoptic nucleus: central and peripheral vasopressin release and blood pressure. *Am J Physiol*, 266, E351-6.
- LUPIEN, S. J., MCEWEN, B. S., GUNNAR, M. R. & HEIM, C. 2009. Effects of stress throughout the lifespan on the brain, behaviour and cognition. *Nat Rev Neurosci*, 10, 434-45.
- MACCARI, S., PIAZZA, P. V., KABBAJ, M., BARBAZANGES, A., SIMON, H. & LE MOAL, M. 1995. Adoption reverses the long-term impairment in glucocorticoid feedback induced by prenatal stress. *J Neurosci*, 15, 110-6.
- MAK, P., BROUSSARD, C., VACY, K. & BROADBEAR, J. H. 2012. Modulation of anxiety behavior in the elevated plus maze using peptidic oxytocin and vasopressin receptor ligands in the rat. *J Psychopharmacol*, 26, 532-42.
- MAKARA, G. B., DOMOKOS, A., MERGL, Z., CSABAI, K., BARNA, I. & ZELENA, D. 2008. Gender-specific regulation of the hypothalamo-pituitary-adrenal axis and the role of vasopressin during the neonatal period. *Ann N Y Acad Sci*, 1148, 439-45.

- MAKINO, S., HASHIMOTO, K. & GOLD, P. W. 2002. Multiple feedback mechanisms activating corticotropin-releasing hormone system in the brain during stress. *Pharmacol Biochem Behav*, 73, 147-58.
- MANNUCCI, P. M., RUGGERI, Z. M., PARETI, F. I. & CAPITANIO, A. 1977. 1-Deamino-8-d-arginine vasopressin: a new pharmacological approach to the management of haemophilia and von Willebrands' diseases. *Lancet*, 1, 869-72.
- MCCREDIE, J. & WILLERT, H. G. 1999. Longitudinal limb deficiencies and the sclerotomes. An analysis of 378 dysmelic malformations induced by thalidomide. *J Bone Joint Surg Br*, 81, 9-23.
- MILLAN, M. J. & BROCCO, M. 2003. The Vogel conflict test: procedural aspects, gamma-aminobutyric acid, glutamate and monoamines. *Eur J Pharmacol*, 463, 67-96.
- MURGATROYD, C., PATCHEV, A. V., WU, Y., MICALÉ, V., BOCKMÜHL, Y., FISCHER, D., HOLSBOER, F., WOTJAK, C. T., ALMEIDA, O. F. X. & SPENGLER, D. 2009. Dynamic DNA methylation programs persistent adverse effects of early-life stress. *Nature neuroscience*, 12, 1559-66.
- NATIONAL RESEARCH COUNCIL 2003. Guidelines for the Care and Use of Mammals in Neuroscience and Behavioral Research.
- NUSSEY, S. S., BEVAN, D. H., ANG, V. T. & JENKINS, J. S. 1986. Effects of arginine vasopressin (AVP) infusions on circulating concentrations of platelet AVP, factor VIII: C and von Willebrand factor. *Thromb Haemost*, 55, 34-6.
- OLIVER, G. & SCHAFER, E. A. 1895. On the Physiological Action of Extracts of Pituitary Body and certain other Glandular Organs: Preliminary Communication. *J Physiol*, 18, 277-9.
- ORELAND, S., GUSTAFSSON-ERICSON, L. & NYLANDER, I. 2010. Short- and long-term consequences of different early environmental conditions on central immunoreactive oxytocin and arginine vasopressin levels in male rats. *Neuropeptides*, 44, 391-8.
- PATEL, T. B. 1986. Hormonal regulation of the tricarboxylic acid cycle in the isolated perfused rat liver. *Eur J Biochem*, 159, 15-22.
- PAXINOS, G. & WATSON, C. 2007. *The Rat Brain in Stereotaxic Coordinates*, San Diego, California. USA, Academic Press.
- PERSSON, S. & HAVTON, L. A. 2009. Retrogradely transported fluorogold accumulates in lysosomes of neurons and is detectable ultrastructurally using post-embedding immuno-gold methods. *J Neurosci Methods*, 184, 42-7.
- PIERCE, R. C. & KALIVAS, P. W. 2007. Locomotor behavior. *Curr Protoc Neurosci*, Chapter 8, Unit 8 1.
- PINAULT, D. 1996. A novel single-cell staining procedure performed in vivo under electrophysiological control: Morpho-functional features of juxtacellularly labeled thalamic cells and other central neurons with biocytin or Neurobiotin. *Journal of Neuroscience Methods*, 65, 113-136.
- POWELL, T. P., GUILLERY, R. W. & COWAN, W. M. 1957. A quantitative study of the fornixmamillo-thalamic system. *J Anat*, 91, 419-37.
- RAGGENBASS, M. 2001. Vasopressin- and oxytocin-induced activity in the central nervous system: electrophysiological studies using in-vitro systems. *Prog Neurobiol*, 64, 307-26.

- RAVELLI, A. C., VAN DER MEULEN, J. H., MICHELS, R. P., OSMOND, C., BARKER, D. J., HALES, C. N. & BLEKER, O. P. 1998. Glucose tolerance in adults after prenatal exposure to famine. *Lancet*, 351, 173-7.
- RICE, C. J., SANDMAN, C. A., LENJAVI, M. R. & BARAM, T. Z. 2008. A novel mouse model for acute and long-lasting consequences of early life stress. *Endocrinology*, 149, 4892-900.
- RICE, D. & BARONE, S., JR. 2000. Critical periods of vulnerability for the developing nervous system: evidence from humans and animal models. *Environ Health Perspect*, 108 Suppl 3, 511-33.
- RICHARDS, M. & WADSWORTH, M. E. 2004. Long term effects of early adversity on cognitive function. *Arch Dis Child*, 89, 922-7.
- ROBERTSON, G. L., SHELTON, R. L. & ATHAR, S. 1976. The osmoregulation of vasopressin. *Kidney Int*, 10, 25-37.
- ROWLAND, N. E. 2007. Food or fluid restriction in common laboratory animals: balancing welfare considerations with scientific inquiry. *Comp Med*, 57, 149-60.
- SACHS, H. & TAKABATAKE, Y. 1964. Evidence for a Precursor in Vasopressin Biosynthesis. *Endocrinology*, 75, 943-8.
- SAPOLSKY, R. M. & MEANEY, M. J. 1986. Maturation of the adrenocortical stress response: neuroendocrine control mechanisms and the stress hyporesponsive period. *Brain Res*, 396, 64-76.
- SAWCHENKO, P. E. & SWANSON, L. W. 1982. Immunohistochemical identification of neurons in the paraventricular nucleus of the hypothalamus that project to the medulla or to the spinal cord in the rat. *J Comp Neurol*, 205, 260-72.
- SCOTT, L. V. & DINAN, T. G. 1998. Vasopressin and the regulation of hypothalamic-pituitary-adrenal axis function: implications for the pathophysiology of depression. *Life Sci*, 62, 1985-98.
- SCHAPIRO, S., GELLER, E. & EIDUSON, S. 1962. Neonatal adrenal cortical response to stress and vasopressin. *Proc Soc Exp Biol Med*, 109, 937-41.
- SCHMALE, H., HEINSOHN, S. & RICHTER, D. 1983. Structural organization of the rat gene for the arginine vasopressin-neurophysin precursor. *EMBO J*, 2, 763-7.
- SCHMUED, L. C. & FALLON, J. H. 1986. Fluoro-Gold: a new fluorescent retrograde axonal tracer with numerous unique properties. *Brain Res*, 377, 147-54.
- SELYE, H. 1936. A syndrome produced by diverse nocuous agents. *Nature*, 138, 32.
- SIKICH, L. & TODD, R. D. 1988. Are the neurodevelopmental effects of gonadal hormones related to sex differences in psychiatric illnesses? *Psychiatr Dev*, 6, 277-309.
- SOFRONIEW, M. V. & GLASMANN, W. 1981. Golgi-like immunoperoxidase staining of hypothalamic magnocellular neurons that contain vasopressin, oxytocin or neurophysin in the rat. *Neuroscience*, 6, 619-43.
- STARLING, E. H. & VERNEY, E. B. 1925. The secretion of urine as studied on the isolated kidney. *Proceedings of the Royal Society of London Series B-Containing Papers of a Biological Character*, 97, 321-363.
- STEMMELIN, J., LUKOVIC, L., SALOME, N. & GRIEBEL, G. 2005. Evidence that the lateral septum is involved in the antidepressant-like effects of the vasopressin V1b receptor antagonist, SSR149415. *Neuropsychopharmacology*, 30, 35-42.
- SUMMY-LONG, J. Y., KEIL, L. C. & SEVERS, W. B. 1978. Identification of vasopressin in the subfornical organ region: effects of dehydration. *Brain Res*, 140, 241-50.

- SUTANTO, W., ROSENFELD, P., DE KLOET, E. R. & LEVINE, S. 1996. Long-term effects of neonatal maternal deprivation and ACTH on hippocampal mineralocorticoid and glucocorticoid receptors. *Brain Res Dev Brain Res*, 92, 156-63.
- SZOT, P., BALE, T. L. & DORSA, D. M. 1994. Distribution of messenger RNA for the vasopressin V1a receptor in the CNS of male and female rats. *Brain Res Mol Brain Res*, 24, 1-10.
- TSUDA, M. C., YAMAGUCHI, N. & OGAWA, S. 2011. Early life stress disrupts peripubertal development of aggression in male mice. *Neuroreport*, 22, 259-63.
- TUKKER, J. J., FUENTEALBA, P., HARTWICH, K., SOMOGYI, P. & KLAUSBERGER, T. 2007. Cell type-specific tuning of hippocampal interneuron firing during gamma oscillations in vivo. *J Neurosci*, 27, 8184-9.
- TUTHILL, D. P., STEWART, J. H., COLES, E. C., ANDREWS, J. & CARTLIDGE, P. H. 1999. Maternal cigarette smoking and pregnancy outcome. *Paediatr Perinat Epidemiol*, 13, 245-53.
- UETA, Y., DAYANITHI, G. & FUJIHARA, H. 2011. Hypothalamic vasopressin response to stress and various physiological stimuli: visualization in transgenic animal models. *Horm Behav*, 59, 221-6.
- UGRUMOV, M. V. 2002. Magnocellular vasopressin system in ontogenesis: development and regulation. *Microsc Res Tech*, 56, 164-71.
- URBAN, I. J. 1998. Effects of vasopressin and related peptides on neurons of the rat lateral septum and ventral hippocampus. *Prog Brain Res*, 119, 285-310.
- VAN OS, J. & SELTEN, J. P. 1998. Prenatal exposure to maternal stress and subsequent schizophrenia. The May 1940 invasion of The Netherlands. *Br J Psychiatry*, 172, 324-6.
- VARAS, S. M., JAHN, G. A. & GIMENEZ, M. S. 2001. Hyperthyroidism affects lipid metabolism in lactating and suckling rats. *Lipids*, 36, 801-6.
- VEENEMA, A. H., BLUME, A., NIEDERLE, D., BUWALDA, B. & NEUMANN, I. D. 2006. Effects of early life stress on adult male aggression and hypothalamic vasopressin and serotonin. *Eur J Neurosci*, 24, 1711-20.
- VEENEMA, A. H. & NEUMANN, I. D. 2009. Maternal separation enhances offensive play-fighting, basal corticosterone and hypothalamic vasopressin mRNA expression in juvenile male rats. *Psychoneuroendocrinology*, 34, 463-7.
- VIAU, V. & SAWCHENKO, P. E. 2002. Hypophysiotropic neurons of the paraventricular nucleus respond in spatially, temporally, and phenotypically differentiated manners to acute vs. repeated restraint stress: rapid publication. *J Comp Neurol*, 445, 293-307.
- VIGNEAUD, V. D., LAWLER, H. C. & POPENOE, E. A. 1953. ENZYMATIC CLEAVAGE OF GLYCINAMIDE FROM VASOPRESSIN AND A PROPOSED STRUCTURE FOR THIS PRESSOR-ANTIDIURETIC HORMONE OF THE POSTERIOR PITUITARY. *Journal of the American Chemical Society*, 75, 4880-4881.
- WACKER, D. W. & LUDWIG, M. 2012. Vasopressin, oxytocin, and social odor recognition. *Horm Behav*, 61, 259-65.
- WALF, A. A. & FRYE, C. A. 2007. The use of the elevated plus maze as an assay of anxiety-related behavior in rodents. *Nat Protoc*, 2, 322-8.
- WEINSTOCK, M. 2001. Alterations induced by gestational stress in brain morphology and behaviour of the offspring. *Prog Neurobiol*, 65, 427-51.

- WESSENDORF, M. W. 1991. Fluoro-Gold: composition, and mechanism of uptake. *Brain Res*, 553, 135-48.
- WILLIAMS, A. R., CAREY, R. J. & MILLER, M. 1985. Altered emotionality of the vasopressin-deficient Brattleboro rat. *Peptides*, 6 Suppl 1, 69-76.
- WOTJAK, C. T., GANSTER, J., KOHL, G., HOLSBOER, F., LANDGRAF, R. & ENGELMANN, M. 1998. Dissociated central and peripheral release of vasopressin, but not oxytocin, in response to repeated swim stress: new insights into the secretory capacities of peptidergic neurons. *Neuroscience*, 85, 1209-22.
- YOSHIDA, M. 2008. Gene regulation system of vasopressin and corticotropin-releasing hormone. *Gene Regul Syst Bio*, 2, 71-88.
- YOUNG, W. S., LI, J., WERSINGER, S. R. & PALKOVITS, M. 2006. The vasopressin 1b receptor is prominent in the hippocampal area CA2 where it is unaffected by restraint stress or adrenalectomy. *Neuroscience*, 143, 1031-9.
- YUKITAKE, Y., TANIGUCHI, Y. & KUROSUMI, K. 1977. Ultrastructural studies on the secretory cycle of the neurosecretory cells and the formation of Herring bodies in the paraventricular nucleus of the rat. *Cell Tissue Res*, 177, 1-8.
- ZELENA, D., DOMOKOS, A., BARNA, I., MERGL, Z., HALLER, J. & MAKARA, G. B. 2008. Control of the hypothalamo-pituitary-adrenal axis in the neonatal period: adrenocorticotropin and corticosterone stress responses dissociate in vasopressin-deficient brattleboro rats. *Endocrinology*, 149, 2576-83.
- ZHANG, L. & HERNANDEZ, V. S. 2013. Synaptic innervation to rat hippocampus by vasopressin-immuno-positive fibres from the hypothalamic supraoptic and paraventricular nuclei. *Neuroscience*, 228, 139-62.
- ZHANG, L., HERNANDEZ, V. S., LIU, B., MEDINA, M. P., NAVA-KOPP, A. T., IRLLES, C. & MORALES, M. 2012. Hypothalamic vasopressin system regulation by maternal separation: its impact on anxiety in rats. *Neuroscience*, 215, 135-48.
- ZHANG, L., HERNANDEZ, V. S., MEDINA-PIZARRO, M., VALLE-LEIJA, P., VEGA-GONZALEZ, A. & MORALES, T. 2008. Maternal hyperthyroidism in rats impairs stress coping of adult offspring. *J Neurosci Res*, 86, 1306-15.
- ZHANG, L., MEDINA, M. P., HERNANDEZ, V. S., ESTRADA, F. S. & VEGA-GONZALEZ, A. 2010. Vasopressinergic network abnormalities potentiate conditioned anxious state of rats subjected to maternal hyperthyroidism. *Neuroscience*, 168, 416-28.
- ZIMMERMAN, E. A. & ROBINSON, A. G. 1976. Hypothalamic neurons secreting vasopressin and neurophysin. *Kidney Int*, 10, 12-24.

11. Apéndice: Productos científicos derivados de mis estudios de doctorado

11.1 Publicaciones derivadas directamente de esta tesis

Intracerebral axonal projections of individual vasopressinergic magnocellular neurons of rat hypothalamus

Hernández V. S., Vázquez-Juárez E., Márquez M. M., Jáurequi-Huerta F., Barrio R. A. and Zhang L.

(Under review, Frontiers in Neuroanatomy)

My contributions in:

- Conception of the study: +++
- Performance of the experiments:
 - o In vivo extracellular recording and juxtacelular labelling: +++
 - o Tissue processing of juxtacellulary filled neurons: +++
 - o Reconstruction of juxtacellulary filled neurons: +
 - o Evaluation of behavioral test: ++
 - o c-Fos Immunohistochemistry: ++
- Statistical analysis: +++
- Discussion of the results: ++
- Preparation of the paper: ++

(+): Average contribution; (++): Important contribution; (+++): Main contribution

Intracerebral axonal projections of individual vasopressinergic magnocellular neurons of rat hypothalamus

Vito Salvador Hernandez, Erika Vazquez-Juarez, Mariana M Marquez, Fernando Jauregui_Huerta, Rafael A Barrio and Limei Zhang

Journal Name:	Frontiers in Neuroanatomy
ISSN:	1662-5129
Article type:	Original Research Article
First received on:	12 May 2015
Frontiers website link:	www.frontiersin.org

1 **Intracerebral axonal projections of individual**
2 **vasopressinergic magnocellular neurons of rat hypothalamus**

3
4 *Running title: Multi-axonic AVP neurosecretory neurons*

5
6
7 Vito S. Hernández^{a§}, Erika Vazquez-Juárez^{a§}, Mariana M. Márquez^a, Fernando
8 Jáurequi-Huerta^b, Rafael A. Barrio^c and Limei Zhang^{a*}

9
10
11 ^aDepartamento de Fisiología, Facultad de Medicina, Universidad Nacional Autónoma
12 de México, México D. F., México

13 ^bDepartamento de Neurociencias, Centro Universitario de Ciencias de la Salud,
14 Universidad de Guadalajara, Guadalajara, México

15 ^cInstituto de Física, Universidad Nacional Autónoma de México, México D. F., México

16 [§]Authors contributed equally to this work.

17
18
19
20
21
22
23
24
25
26
27
28
29
30
31 *Correspondence:

32 Limei Zhang, M.D., Ph.D.

33 Departamento de Fisiología,

34 Facultad de Medicina, UNAM,

35 Av. Universidad 3000,

36 Col. Universidad Nacional Autónoma de México,

37 México, 04510, D. F. MEXICO.

38 Phone and Fax: +52-55-56232348

39 limei@unam.mx

40
41
42
43
44
45
46
47
48
49
50
51
52
53
54
55
56
57
58
59
60
61
62
63
64
65
66
67
68

Abstract

Conventional neuroanatomical, immunohistochemical and *in vitro* recording and labeling methods may fail to detect long range intracerebral-projecting axons of vasopressinergic (AVP) magnocellular neurosecretory neurons (MNNs) of the hypothalamic paraventricular nucleus (PVN). Here, by using *in vivo* extracellular recording and juxtacellular labeling, we show that MNNs possess multi-axon-like processes and axonal collaterals branching very near to the somata, projecting intracerebrally to areas including the medial and lateral preoptical area, suprachiasmatic nucleus, lateral habenula, medial and central amygdala and to the conducting systems such as *stria medullaris*, the fornix and the internal capsule. Axon-collaterals were detected to express vesicular glutamate transporter 2. Furthermore, *in vivo* activation of AVP-MNNs by hypertonic saline administration produced significant reduction of freezing behavior and an increase in active escaping, measured as climbing, rearing and displacement, during live cat exposure. Modified Fos expression patterns during fear processing in hypothalamus, amygdala, thalamus and LHb were also observed. Our data demonstrated that AVP-MNNs possessed multiple axon-like processes and the long-range intracerebral projection is a more common feature of the MNNs, than an “occasional” phenomenon as previously thought. The magnocellular AVP-glutamatergic non-canonical pathways found here may constitute a part of the central motivational circuit activated under multifaceted stress coping.

Key words: Paraventricular nucleus (PVN), juxtacellular labeling, vasopressin, extra-hypothalamic projections, axon collaterals, magnocellular neurosecretory system.

69 Arginine-vasopressin (AVP) containing cells located in the lateral division of the
70 paraventricular nucleus of the hypothalamus have large somata (diameters around 20-35
71 μm , named *magnocellular*) and are commonly known to project to the neurolobe of the
72 hypophysis releasing the nonapeptide vasopressin, which is critical for cardiovascular
73 functions and hydro-electrolytic homeostasis (Bargmann and Scharrer, 1951). They are
74 traditionally referred to as vasopressinergic magnocellular neurosecretory neurons
75 (AVP-MNNs).

76 Osmotic stimulation, such as dehydration or acute salt loading, produces a rapid
77 activation of AVP-MNNs. Under salt loading, MNNs respond with an increased firing
78 rate and often are continuously activated (tonic firing patterning) in the initial phase of
79 stimulation (Brimble and Dyball, 1976).

80 There is growing evidence supporting the role of AVP as a molecule involved in
81 the modulation of behavior, such as social interactions, anxiety, aggression and fear
82 (Debiec, 2005;Caldwell et al., 2008). It is generally accepted that the AVP-containing
83 parvocellular neurons of the hypothalamic paraventricular nucleus (PVN) are the main
84 players for both the corticotropin-releasing hormone synergetic action on
85 adenohipophyseal corticotropin secretion and the intracerebral projections, together
86 with AVP containing neurons from the bed nucleus of *stria terminalis* (BNST) and
87 from the medial amygdala (MeA) (Caffe and van Leeuwen, 1983;Buijs et al., 1991).

88 It has been established that the magnocellular axons emanate from the AVP-
89 MNNs, either from the soma or a primary dendrite (Armstrong et al., 1980;van den Pol,
90 1982;Hatton et al., 1985;Rho and Swanson, 1989) and course in a wide arc, passing
91 over or beneath the fornix before turning medially above the supraoptic nucleus to join
92 the tract of Greving (Laqueur, 1954) before reaching the internal medial eminence
93 (MEI) and then the neural lobe. AVP-MNN axons from magnocellular neurons have
94 been seen to occasionally branch (van den Pol, 1982;Hatton et al., 1985;Ray and
95 Choudhury, 1990), but the final destination and synaptic relationship of collaterals
96 remain to be determined (Armstrong, 2004).

97
98 Besides the finding of dendritic release of AVP in their vicinity influencing the
99 local neuronal activities through paracrine mechanisms (Pow and Morris, 1989;Son et
100 al., 2013), recent investigations using both *in vivo* and *in vitro* electrophysiological
101 recording (Inyushkin et al., 2009), anatomical analysis and fluorogold retrograde tracing
102 (Hernandez and Zhang, 2012;Zhang and Hernandez, 2013), have suggested that the
103 AVP-MNNs have important intracerebral axonal projections establishing synaptic
104 innervations in some limbic regions, such as hippocampus (Zhang and Hernandez,
105 2013) and amygdala (Hernandez and Zhang, 2012). Activation of the AVP-MNNs
106 modifies significantly the conditioned anxiety state (Zhang et al., 2012) and the spatial
107 learning (Hernandez et al., 2012).

108 The conventional neuroanatomical, immunohistochemical and *in vitro*
109 electrophysiology methods may fail to detect the complete dendritic arborization and
110 the presence of long-range intracerebral-projecting axons of AVP-MNNs in the PVN.
111 The difficulties include the large cell size for any kind of brain slide-based methods; the
112 high cellular density and the intermingled populations of both AVP parvo- and magno-
113 cells; the chemical structural changes of the peptide from propressophysin to
114 vasopressin during the intra-axonal transport, which decrease the labeling with a single
115 antibody (Zhang and Hernandez, 2013); and also the uneven axonal distribution of the
116 dense core vesicles, making it confusing when following the thin axons under light and
117 electron microscopy (Zhang and Hernandez, 2013). In contrast, the *in vivo* extracellular
118 recording with juxtacellular labeling technique (Deschenes et al., 1994;Pinault, 1994;
119 1996), combined with a *post hoc* anatomo-immunohistological analysis, is able to
120 overcome these difficulties and enabled us to investigate the overall MNN morphology
121 and its long-range intracerebral projections.

122 Hence, the aim of this work is to reinforce our previous observation of the
123 intracerebral vasopressinergic innervation by AVP-MNNs, using *in vivo* juxtacellular
124 single neuron labeling method, to accurately identify the intracerebral projections of
125 these neurons from PVN and to evaluate the functional implications of the activation
126 of the AVP-MNNs. To this end, we used osmotic stressor to activate the AVP-MNNs
127 and cat exposure as an ethologically and physiologically relevant natural stimulus, to
128 evaluate passive vs. active stress coping and the c-Fos expression in the regions where
129 the axon-collaterals from juxtacellularly labeled AVP-MNNs were found.

130 2. Materials and methods

131 2.1 Animals

132
133 Experiments were conducted in adult male Wistar rats (250 – 300 g) provided by the
134 local animal facility and housed at 20 – 24° C on a 12h dark/light cycle (lights-on at
135 19:00 h) with tap water and standard rat chow pellets available *ad libitum*. The local
136 bioethical and research committees approved all procedures involving experimental
137 animals (approval ID CIEFM-086-2013).

138

139 2.2 *In vivo* extracellular recording and juxtacellular labeling

140

141 The procedures for *in vivo* extracellular recording and juxtacellular labeling were based
142 on the methods described in references (Leng, 1991;Pinault, 1996;Tukker et al., 2013).
143 Anesthesia was induced with 4% isoflurane in oxygen, followed by urethane injection
144 (1.3 g / kg, *i.p.*, Sigma-Aldrich), with supplemental doses of xylazine (30 mg/kg) as
145 necessary. Body temperature was maintained at 36 °C with a heating pad. Once
146 anesthetized, animals were placed into a stereotaxic frame and craniotomy was
147 performed around the coordinates: -1.7 mm posterior from Bregma and 0.4 mm lateral.
148 A long-taper glass electrode (8-15 M Ω) filled with 1% neurobiotin (Vector

149 Laboratories), in 0.15 M NaCl was vertically placed at previously standardized
150 hypothalamic PVN coordinates (1.7 mm posterior and 0.4 mm right/left from Bregma,
151 6.9 mm deep) and referenced against a wire implanted subcutaneously in the neck.

152

153 Neuronal activity was detected, amplified and filtered using differential
154 amplifiers ELC-01MX, DPA-2FL and BF-48DGX (npi electronics, GmbH, Tamm,
155 Germany). Signals were filtered in a 300-3000 Hz bandwidth.

156

157 All the five AVP-MNNs reported here were labeled under hypertonicity
158 condition (900mM NaCl solution, 2% b. w., i.p.) to facilitate the location of AVP-
159 MNNs *in vivo*. This procedure was set to increase the experiment effectiveness. There
160 are several factors in basal conditions that hamper the experimental effectiveness,
161 amongst which we could mention 1) the small size of PVN; 2) the individual coordinate
162 differences; 3) the high presence of pulsatile blood vessels (3.3 times) and longer lumen
163 perimeters (3.6 times) than in control regions of ventrolateral hypothalamus (van den
164 Pol, 1982)); 4) the very low spontaneous firing rates (<0.1Hz) of AVP-MNNs under
165 basal condition in urethane anesthetized rat.

166

167 After recordings, the cell was iontophoretically labeled with neurobiotin using
168 juxtacellular-labeling method (Pinault, 1994). Current pulses of 1–10 nA, at 2.5 Hz,
169 with a 50% duty cycle, were delivered through the recording electrode. The current was
170 gradually increased to induce and maintain entrainment of the activity of the neuron,
171 yielding a higher number of spikes on the current "on" periods. Cells were entrained
172 between 2 and 10 min.

173

174 2.3 Tissue processing and reconstruction of juxtacellular labeled neurons

175 Two to five hours after labeling, animals were transcardially perfused with saline
176 followed by 15 min of fixative solution containing 4% paraformaldehyde, 15% v/v
177 saturated picric acid, and 0.05% glutaraldehyde in 0.1M PB. Each recorded cell was
178 coded with the electrophysiologist's initials followed by the sequential number of
179 experiments for internal control.

180

181 Coronal sections (70 μ m) were stored serially in tissue culture wells in 0.1PB
182 containing 0.05% NaN₃. Four to six sections near the electrode tract were incubated
183 with streptavidin-conjugated Alexa Fluor 488 (1:1000; Invitrogen) in TBST (Tris-
184 buffered saline with 0.3% Triton X-100) for 1 h at room temperature (RT). After
185 rinsing, sections were mounted on slides in VectaShield (Vector Laboratories,
186 Burlingame, CA). Sections from successfully labeled cases containing the somata were
187 blocked with 10% normal donkey serum (NDS) and later incubated overnight with
188 rabbit anti-AVP (1:500; Peninsula Laboratories) and guinea-pig anti-vesicular
189 glutamate transporter (vGluT2-GP-Af810, Frontier Institute Co., LTD, Ishikari, Japan).
190 For reconstruction, sections were further processed using avidine-biotin peroxidase
191 complex (Vectastain ABC Elite kit, Vector Laboratories Burlingame, CA) to reveal

192 neurobiotin with diaminobenzidine (DAB, 0.05%; SIGMA, St.Louis, MO). Mounted
193 sections were air-dried and coverslipped with Permount mounting medium (Electron
194 Microscopy Sciences, Hatfield, PA).

195

196 Five neurobiotin-labeled AVP immunopositive MNNs (EV40, VH52, EV16,
197 MM15, VH25, corresponding the Fig. 1-5) were selected for reconstruction under light
198 microscope with a drawing tube. For MM15, a 3D confocal microscope reconstruction
199 of the soma section (70 μ m of thickness) was provided (supplemental information) to
200 illustrate the presence of both the hypothalamic-neurohypophyseal tract –joining axons
201 and the intracerebral projecting collaterals. The selection criteria include that the cells
202 had to be tested positive to AVP; to be located inside the PVN_{lmd} and to possess the
203 main axons joining the tract of Greving (Armstrong, 2004).

204

205 2.4 Live cat exposure and behavioral scoring

206

207 The behavior test was performed during the early activity period of the rats (dark
208 period). Experimental subjects (N=60), housed four per cage, were divided into three
209 groups: the undisturbed control group was housed as described before; the isotonic
210 saline (vehicle) injected groups and the salt challenged group (900mM of NaCl, 2% of
211 b.w.). The injections were made 30 min before the test under transient anesthesia by
212 inhaling sevoflurane vapor (Sevorane, Abbot, Mexico) to reduce the nuisance caused by
213 the manipulation during the injections. Rats recovered from this procedure after 1 to 3
214 min.

215

216 Each rat was placed individually in a grid cage (28.5 \times 21 \times 30 cm), so the rat
217 could climb. The cage was placed inside a larger ventilated clear plastic chamber (60 \times
218 80 \times 40 cm), where a male adult cat was then introduced. The cat was tamed and
219 castrated (a pet named *Balam*), about 5 kg of b.w. Balam mostly stayed quiet/immobile
220 during the experiment. One advantage of this arrangement is that the rats were exposed
221 to physiologically relevant stimuli - a live predator's odor, appearance and breathing
222 sounds, which were relatively constant for all the experimental subjects. Each rat
223 remained in the above-described chamber for a single period of 10 min. Once the time
224 of exposure was completed, they were returned to their home cage.

225

226 Relevant behaviors were quantified offline by giving one of the six scores every
227 five seconds: 1) "Freezing" was assigned to the behavior of immobility more than 2 sec
228 with piloerection; 2) "Climbing": when rats climbed the internal mesh cage using limbs
229 trying to escape from the top door; 3) "Rearing", when rats were rearing still, sniffing
230 with short head rotations; 4) "Displacement", when the rats were walking, trotting or
231 running; 5) "Orientation": when the four limbs of the rats were still with head extension,
232 rotation; 6) "Grooming": when rats groomed themselves (nose, head, face, eyes and
233 body) with their paws, using very short movements. "Active Escaping" measured in the
234 study included the behaviors 2, 3 and 4.

235 Groups were tested for differences by performing one-way-ANOVA followed
236 by Bonferroni test. Differences were considered statistically significant at a value
237 $p < 0.05$.

238

239

240 2.5 c-Fos immunohistochemistry and analysis

241 Ninety minutes post- predator exposure period, 5 rats from each group were deeply
242 anesthetized with an overdose of pentobarbital and transcardially perfused with 0.9%
243 saline followed by 15 min with cold fixative containing 4% paraformaldehyde and 15%
244 (v/v) saturated picric acid in PB 0.1 M. Brains were removed and 50 μ m coronal
245 sections were obtained (Leica VT 1000 vibratome). For immunostaining, sets of one out
246 of every four sections from Bregma -0.48 to -4.08 mm were blocked with 10% normal
247 donkey serum (Vector Laboratories, Burlingame, CA) in Tris-buffered saline with 0.3%
248 Triton X-100 (TBST) for 1h at room temperature (RT) and then immunoreacted with
249 rabbit anti-Fos primary antibody (1:1000, SC52 Santa Cruz Biotechnology, Santa Cruz,
250 CA) in TBST + 1% NGS at 4 °C overnight. Afterwards, sections were rinsed three times
251 for 10 min with TBST and then incubated for 2 h at RT with biotinylated goat anti-
252 rabbit secondary antibody (1:200; Vector Labs, Burlingame, CA). Finally, sections were
253 incubated in avidin-biotin-peroxidase complex (Elite ABC kit, Vector Labs) for 1 h at
254 RT. Peroxidase was detected using DAB 0.05% as a chromogen. Sections were rinsed
255 and permanently mounted with Permout mounting medium (Electron Microscopy
256 Sciences, Hatfield, PA).

257

258 The following brain regions were assessed: hypothalamus, thalamus, amygdala
259 and lateral habenular regions. The quantitative analysis was performed with ImageJ
260 software (NIH) (<http://rsb.info.nih.gov/ij/macros/>). Data were expressed as the mean
261 number of positive c-Fos nuclei per 0.02 mm². Quantitative results were expressed as
262 mean \pm standard error of mean (SEM). Groups were tested for differences by *t*-test
263 analysis, using GraphPad Prism software® (GraphPad Software, San Diego, CA).
264 Differences were considered statistically significant at $P < 0.05$ ("*": $P < 0.05$, "***": $P <$
265 0.01 and "****": $P < 0.001$).

266

3. Results

267 3.1. Multi-axonal feature of AVP-MNNs

268

269 Five juxtacellularly labeled cells with complete somata-dendritic arborizations
270 and large portion of axonal process were located in the lateral magnocellular division of
271 the paraventricular nucleus of the hypothalamus (PVN_{lmd}) (Figs. 1-5). It is worth noting
272 that the projections that entered to myelinated structures were mostly invisible except
273 the ones located in the surface. Besides, the time between labeling and
274 perfusion/fixation was a crucial factor for juxtacellular labeling success: while shorter
275 time (2-5 hrs.) makes a strong somato-dendritic labeling, the longer time helps the
276 filling of long-range axons, but the risk that neurobiotine is metabolized increased

277 which has showed individual differences. All of five cells were tested positive to AVP
278 and possessed medial eminence internal part (MEI) projecting axons joining the
279 hypothalamic-neurohypophysial tract (HNT, *i.e.* tract of Greving). Hence they were
280 classified as AVP-MNNs. Other labeled neurons, either lacking the AVP expressing or
281 the main axons joining the HNT, were excluded in this report.

282 After immunohistochemical reaction for AVP and vGluT2, the serial sections
283 were reacted with avidin-biotin peroxidase complex to convert to permanent samples
284 and the whole cell morphology was reconstructed. The soma and dendrites were
285 represented with black drawing and axonal segments were represented with red
286 processes. The “main axons” were judged by the classical description of beaded
287 neurosecretory axons, which emit laterally from either soma or a primary dendrite and
288 course in a wide arc, passing over or beneath the fornix before turning medially above
289 the supraoptic nucleus and optical tract, toward the MEI (Armstrong, 2004). The “axon-
290 collaterals” were assigned to the branches arisen from the main axons and the “axon-
291 like” processes were judged by either expressing vesicular glutamate transporter 2
292 (vGluT2) and/or being long distance projection and/or branched extensively (axon
293 terminals) with constantly thin *strings of pearls* shaped swellings (Armstrong, 2004).

294
295
296
297

Fig. 1 near here

298 According to the criteria above mentioned, some labeled AVP-MNNs clearly
299 possessed more than one primary axons originated from soma or proximal dendrites.
300 The cell showed in the Fig. 1, "EV40", internal code, is a clear example. This cell was
301 located in the lateral part of the PVN_{lmd}. Its somatic long axis was perpendicular to the
302 3v. The cell had 3 primary dendrites, two directed medially and one laterally. The main
303 axons originated at the same point of the lateral primary dendrite, proximal to the soma,
304 giving two primary (parents) axons (red and blue arrows, both in the drawing and the
305 photomicrographs of two adjacent sections, 1 and 2). The top branch turned ventrally to
306 project to the MEI (red arrowhead). A collateral was emitted from the parent axon
307 proximally and projected to the border of the optical tract. Labeled axon traces were
308 found inside the medial and central amygdala. The ventral primary axonal segment
309 (blue arrow) was split into two branches of axon-collaterals (indicated with blue
310 arrowheads) directed either medially or laterally. The lateral branch entered the fornix
311 (fx). Additionally, several beaded processes originated from the dendritic processes also
312 entered the fornix (green arrowheads). This kind of processes were described in an early
313 study and were considered as axonal processes (Sofroniew and Glasmann, 1981).

314 AVP-MNNs in the Fig. 2 and Fig. 3 ("VH52" and EV16), were located in the
315 central region of PVN_{lmd}, with large dendritic arborization mainly directed toward the
316 3v. Its main axon arose from the proximal portion of the lateral primary dendrite,
317 making several collaterals. Note that in Fig.1 B (neuron VH52), number (2), a particular
318 structure was observed: axon with several small branches and classical image of *strings-*

319 *of-pearls* in a small region in the lateral preoptical area. The panels (3), (4), (5) and (6)
320 of this panel show the presence of labeled axon segments in or near the conducting
321 systems, fornix (fx), internal capsule (ic) and stria medullaris (sm). Next cell, EV16,
322 gave rise initially to two short and thick primary dendrites, which branched proximally.
323 The bottom dendrite branched extensively till the fifth order of branches - all directed
324 medially reaching the wall of the 3v. The top dendrite emitted two secondary branches,
325 the medial and the lateral ones. The medial branch was similar to the bottom group. The
326 lateral portion curled up proximally near the soma but gave rise the main axon (panel
327 1b, arrow). The main axon coursed laterally till the fornix (fx), turned ventrally and then
328 medial posteriorly toward the MEI. Two main collaterals were observed. Number (2)
329 indicates the first branch position. This tracer containing process coursed dorsally and
330 reached the border of the stria medullaris (sm). The continuation was lost from sight
331 temporarily in the myelinated conducting structure but appeared again in the surface of
332 sm and entered the epithalamic region, the lateral habenula (LHb) (4). The second
333 branch arose from the parent axon (3), coursed medially and was lost in the border of
334 the fornix.

335
336 -----
337 Fig. 2 and 3 near here
338 -----
339

341 3.2. Axon-like processes emanated from soma or proximal dendrites expressed vGluT2

342
343 The 4th cell (internally coded "MM15") we present here is an AVP containing
344 MNN located in the posterolateral border of the PVN_{lmd} (Fig. 4). It emitted 3 primary
345 dendrites. In contrast to the 3 previous cells, this cell's main dendritic arborizations
346 were directed laterally and ventrally. Four axonal processes arose from the proximal
347 dendritic loci belonging to the same primary dendrite (colored asterisks). Two of them
348 projected ventrally toward IME. The other two axon-like processes bended dorsally.
349 Those thin axon-like processes were tested positive to vGluT2 (Fig. 2, (2)).

350 -----
351 Fig. 4 near here
352 -----
353

354 The 5th cell, internally coded as "VH25" (Fig. 5), was located in the medial
355 border of the PVN_{lmd} with the long somatic axis in parallel to the third ventricle (3v).
356 The primary dendrites emanated from the dorsal and ventral poles and directed toward
357 the 3v. There were few branching points. The main axon emanated from the proximal
358 thick portion of the ventral dendrite (Fig. 5, top red arrow) and coursed toward the MEI.
359 A second axon-like process emanated from the same point of the main axon, with
360 *string-of-pearls* appearance and branches like axon terminals in the ventral medial
361 hypothalamus (Fig. 5 blue arrow).

362 Those axon-like processes were also seen in EV40 (Fig. 1) and EV16 (Fig. 3). In
363 the first cell (Fig.1), an axon-like process (indicated with an yellow arrow) emanated
364 from soma and coursed ventrally with *strings-of-pearls* swellings and branched in
365 ventral hypothalamus. In the third cell (Fig. 3), two axon-like beaded processes, with
366 the classical image of *strings-of-pearls* (1a and 1c) were likely arisen from soma and
367 coursed ventral medially. Tracers containing axonal segments were found in medial
368 preoptical area and suprachiasmatic nucleus (SCN).

369 -----
370 Fig. 5 near here
371 -----

372

373 3.3 Hypertonic challenge decreased the freezing behavior and increased the active
374 escaping upon live predator exposure.

375
376 To evaluate the possible functional implications of those intracerebrally projecting
377 axons/axonic collaterals from the AVP-MNNs on fear processing, we chose salt loading
378 as a physiological stimulus to strongly activate the magnocellular vasopressin system
379 and a live cat exposure scheme to assess the behavior.

380
381 As shown in the Fig. 6, two types of relevant behaviors, freezing and
382 active escaping symbolized in the panels A and B,) were counted in this test. The 30
383 min previous salt loading induced a significant effect on freezing ($F(2,57) = 5.01, p <$
384 0.01) and active escaping behavior ($F(2,57) 14.65, p < 0.0001$). Post hoc comparisons
385 using Bonferroni test showed a significant reduction in freezing counts of hypertonic
386 (15 ± 2.85 SEM) with respect to control (32.85 ± 5.34) and vehicle groups ($32.25 \pm$
387 5.33) (Fig. 3, C left panel). Active escaping behavior showed an increase in the salt
388 loading group (44.05 ± 3.06) compared to control (27.85 ± 3.2) and vehicle groups
389 (23.1 ± 2.26) (Fig. 6C, right panel).

390
391 -----
392 Fig. 6 near here
393 -----

394 3.4 Fos expression patterns induced by cat exposure in several limbic regions were
395 modified by salt loading.

396
397 Rats exposed to the cat displayed increased Fos activity in hypothalamic
398 paraventricular nuclei (Pa, PaMP and PaLM), amygdala and lateral habenula (LHb)
399 compared with basal state (data not shown here). However, expression patterns induced
400 by the predator exposure differed between vehicle (Fig. 7, undecorated letters) and
401 hypertonic (primed letters) groups. The hypertonic injection significantly increased the
402 c-Fos expressing nuclei in the dorsal part of suprachiasmatic nucleus (SCN_d) and the

403 supraoptic nucleus (SON), (Fig. 3B and B'), the lateral magnocellular (PVN_{lm}, Fig 7A
404 and A') and medial magnocellular (PVN_{mm}, 7C and C') parts of the paraventricular
405 nucleus, the medial preoptic area (MPO), the medial part of central amygdala (CeA_m,
406 Fig. 7F and F') and the medial part of lateral habenula (LHb_m, Fig. 7. D and D').
407 Significant reductions were observed in medial (MeA) and basolateral (BLA) amygdala
408 (Fig. 7F and F') and in the lateral part of lateral habenula (LHb_l, Fig. 7D and D').
409 Finally, the ventral part of suprachiasmatic nucleus (SCN_v, Fig. 7B and B'), and the
410 parvocellular part of paraventricular nucleus (PVN_{mpd}, Fig. 7A and A') showed no
411 modification after hypertonic salt injection. In the thalamus the expression changed
412 from diffuse to a more localized pattern. Fig. 7G shows Fos expression in the
413 vasopressinergic neurons in the magnocellular part of the PVN after hypertonic *i.p*
414 injection. Fig. 7H and Table 1 compare the c-Fos expression elicited by cat exposure in
415 control and hypertonic groups.

416
417 -----
418 Fig. 7 and Tab. 1 near here
419 -----
420

421 4. Discussion

422
423 We have used juxtacellular recording methods to successfully visualize individual
424 neurons in very deep subcortical regions – five vasopressin containing MNNs in the
425 hypothalamic paraventricular nucleus were presented here with complete somato-
426 dendritic morphology and their intracerebral long-range projections were demonstrated.
427 Furthermore, multi-axon features of these AVP-MNNs were revealed by single neuron-
428 tracing and intracerebral downstream regions were identified by localizing labeled
429 axon/axon terminals. These regions include: medial and lateral preoptical area,
430 suprachiasmatic nucleus, lateral habenula, medial and central amygdala and to the
431 conducting systems such as stria medullaris, the fornix and the internal capsule. Axon-
432 like processes, which branched locally were detected to express vGluT2. Moreover, in
433 vivo activation of AVP-MNNs by hypertonic saline administration produced significant
434 reduction of freezing behavior and an increase in active escaping, measured as
435 climbing, rearing and displacement, during live cat exposure. Modified Fos expression
436 patterns during fear processing in hypothalamus, amygdala, thalamus and LHB were
437 also observed.

438
439 4.1 New contributions to the morphology and efferent paths of magnocellular
440 paraventricular AVP containing neurons.

441
442 There have been some excellent studies on the morphology of the magnocellular
443 neurosecretory neurons (MNNs) using immunohistochemical and Golgi-like
444 immunoperoxidase staining methods (Sofroniew and Glasmann, 1981;van den Pol,
445 1982;Armstrong, 2004). However, the quasi-two-dimension nature of the previous
446 method (i.e., labeling and reactions on brain slices, as thick as 150µm) impaired

447 crucially the overall visualization of individual magnocellular neurosecretory neurons.
448 This is particularly true regarding the efferent pathways of the MNNs. Traditionally it
449 has been described that the axons of paraventricular MNNs egress laterally from either
450 the soma or a primary dendrite (Armstrong et al., 1980;van den Pol, 1982;Hatton et al.,
451 1985;Rho and Swanson, 1989) to join the tract of Greving before reaching the MEI and
452 the neural lobe (Armstrong, 2004). It was thought that the PVN AVP-MNNs axons
453 from magnocellular neurons only occasionally branch (van den Pol, 1982;Hatton et al.,
454 1985;Ray and Choudhury, 1990), let alone the final destination and synaptic
455 relationship of collaterals.

456 Juxtacellular neuronal labeling technique has proven to be a powerful method
457 for the identification of single neuron projection targets (Pinault, 1996). It provides
458 precise information of anatomical location, morphology and neurochemical phenotype,
459 of the neuron labeled (Toney and Daws, 2006) and long range axon projections. Herein,
460 we report that, at least, some of these AVP containing magnocellular neurosecretory
461 neurons AVP-MNNs possessed multi-axonal projections or axons collaterals branching
462 very near the soma projecting to preoptical and anterior hypothalamic areas, SCN,
463 thalamus and, especially, a long range projection was detected entering the stria
464 medularis fiber-system innervating lateral habenula (LHb).

465
466 It is worth clarifying that the categorization of “axon” or “axon-like” processes
467 used in this study was based on anatomical and immunohistochemical criteria published
468 in the literature (Sofroniew and Glasmann, 1981;van den Pol, 1982;Armstrong, 2004)
469 Ultrastructural features, such as the presence of axon-initial segment, remain to be
470 determined.

471
472 4.2 Activation of vasopressinergic hypothalamic-neurohypophysial system (HNS)
473 modified the stress coping strategies during fear processing: differential neural
474 activation (Fos expression) in the brain regions with direct projections from AVP-
475 MNNs

476
477 We examined the functional implications of the selective activation of the AVP-MNNs
478 during predator exposure using behavioral measurement and c-Fos expression
479 assessment. We report here that the selective activation of HNS plays an important role
480 on promoting motivational behavior, i.e. active escaping, and reducing the passive stress
481 coping, i.e. freezing behavior. This observation was correlated with differential Fos
482 activation patterns in the amygdala, dorsal centro-medial thalamic nucleus and the
483 lateral habenula, a limbic regions possessed extensive AVP projections. Our data
484 findings clearly indicate a regulatory role of HNS for motivational behavior toward
485 survival, during stress coping.

486
487 **Acknowledgements**

488
489 This work was supported by grants PAPIIT-UNAM 216214 (LZ) and CONACYT
490 grants 127777, 238744 (LZ), 79641 and 176916 (RB), 221092 (FJH). We would like to

491 thank Prof. Harold Gainer for kind donation of mouse anti-AVP antibodies; Prof.
492 Enrique Pedernera and Ms. Maria José Gómora for providing the confocal imaging
493 facility and Mr. Angel Fermín Barrio-Zhang for the drawing of experimental design
494 EVJ, VSH would like to thank the DGAPA-UNAM for postdoctoral fellowship and
495 CONACYT for PhD student scholarship, respectively. A part of this work was
496 completed while LZ was visiting NIDA/NIH, Dr. Marisela Morales' Lab, supported by
497 a CONACYT fellowship for short research stay. This work forms part of the thesis of
498 VSH to obtain the degree of Doctor en Ciencias Biomédicas from Programa de
499 Doctorado en Ciencias Biomédicas of the Universidad Nacional Autónoma de México.
500 The authors report no conflicts of interest.

501

502 **References**

503

504 Armstrong, W. (2004). "Hypothalamic supraoptic and paraventricular nuclei," in
505 *The Rat Nervous System*, ed. G. Paxinos. 3rd ed (Amsterdam: Elsevier),
506 369-388.

507 Armstrong, W.E., Warach, S., Hatton, G.I., and McNeill, T.H. (1980). Subnuclei
508 in the rat hypothalamic paraventricular nucleus: a cytoarchitectural,
509 horseradish peroxidase and immunocytochemical analysis.
510 *Neuroscience* 5, 1931-1958.

511 Bargmann, W., and Scharrer, E. (1951). The site of origin of the hormones of
512 the posterior pituitary. *Am Sci* 39, 255-259.

513 Brimble, M.J., and Dyball, R.E. (1976). Contrasting pattern changes in the firing
514 of vasopressin and oxytocin secreting neurones during osmotic
515 stimulation [proceedings]. *J Physiol* 263, 189P-190P.

516 Buijs, R.M., Hermes, M.L., Kalsbeek, A., Woude, T., and Van Heerikhuizen, J.J.
517 (Year). "Vasopressin distribution, origin and functions in the central
518 nervous system", in: *Colloque INSERM/John Libbey Eurotext Ltd.*

519 Caffé, A.R., and Van Leeuwen, F.W. (1983). Vasopressin-immunoreactive cells
520 in the dorsomedial hypothalamic region, medial amygdaloid nucleus and
521 locus coeruleus of the rat. *Cell Tissue Res* 233, 23-33.

522 Caldwell, H.K., Lee, H.J., Macbeth, A.H., and Young, W.S., 3rd (2008).
523 Vasopressin: behavioral roles of an "original" neuropeptide. *Prog*
524 *Neurobiol* 84, 1-24. doi: 10.1016/j.pneurobio.2007.10.007.

525 Debiec, J. (2005). Peptides of love and fear: vasopressin and oxytocin
526 modulate the integration of information in the amygdala. *Bioessays* 27,
527 869-873. doi: 10.1002/bies.20301.

528 Deschenes, M., Bourassa, J., and Pinault, D. (1994). Corticothalamic
529 projections from layer V cells in rat are collaterals of long-range
530 corticofugal axons. *Brain Res* 664, 215-219.

- 531 Hatton, G.I., Cobbett, P., and Salm, A.K. (1985). Extranuclear axon collaterals
532 of paraventricular neurons in the rat hypothalamus: intracellular staining,
533 immunocytochemistry and electrophysiology. *Brain Res Bull* 14, 123-132.
- 534 Hernandez, V.S., Ruiz-Velazco, S., and Zhang, L. (2012). Differential effects of
535 osmotic and SSR149415 challenges in maternally separated and control
536 rats: the role of vasopressin on spatial learning. *Neurosci Lett* 528, 143-
537 147. doi: 10.1016/j.neulet.2012.09.002.
- 538 Hernandez, V.S., and Zhang, L. (Year). "Vasopressin containing fibers
539 distribution and synaptic innervation in the medial and central amygdala:
540 an immunohistochemical study using light and electron microscopy", in:
541 *Neuroscience: Society for Neuroscience*).
- 542 Inyushkin, A.N., Orlans, H.O., and Dyball, R.E. (2009). Secretory cells of the
543 supraoptic nucleus have central as well as neurohypophysial projections.
544 *J Anat* 215, 425-434. doi: 10.1111/j.1469-7580.2009.01121.x.
- 545 Laqueur, G.L. (1954). Neurosecretory pathways between the hypothalamic
546 paraventricular nucleus and the neurohypophysis. *J Comp Neurol* 101,
547 543-563.
- 548 Leng, G.a.D., R. E. J. (1991). "Functional identification of magnocellular
549 neuroendocrine neurons," in *Neuroendocrine Research Methods*, ed. B.
550 Greenstein. Harwood Academics Publishers GmbH, 769–791.
- 551 Pinault, D. (1994). Golgi-like labeling of a single neuron recorded extracellularly.
552 *Neurosci Lett* 170, 255-260.
- 553 Pinault, D. (1996). A novel single-cell staining procedure performed in vivo
554 under electrophysiological control: morpho-functional features of
555 juxtacellularly labeled thalamic cells and other central neurons with
556 biocytin or Neurobiotin. *J Neurosci Methods* 65, 113-136.
- 557 Pow, D.V., and Morris, J.F. (1989). Dendrites of hypothalamic magnocellular
558 neurons release neurohypophysial peptides by exocytosis. *Neuroscience*
559 32, 435-439.
- 560 Ray, P.K., and Choudhury, S.R. (1990). Vasopressinergic axon collaterals and
561 axon terminals in the magnocellular neurosecretory nuclei of the rat
562 hypothalamus. *Acta Anat (Basel)* 137, 37-44.
- 563 Rho, J.H., and Swanson, L.W. (1989). A morphometric analysis of functionally
564 defined subpopulations of neurons in the paraventricular nucleus of the
565 rat with observations on the effects of colchicine. *J Neurosci* 9, 1375-
566 1388.
- 567 Sofroniew, M.V., and Glasmann, W. (1981). Golgi-like immunoperoxidase
568 staining of hypothalamic magnocellular neurons that contain
569 vasopressin, oxytocin or neurophysin in the rat. *Neuroscience* 6, 619-
570 643.

- 571 Son, S.J., Filosa, J.A., Potapenko, E.S., Biancardi, V.C., Zheng, H., Patel, K.P.,
572 Tobin, V.A., Ludwig, M., and Stern, J.E. (2013). Dendritic peptide release
573 mediates interpopulation crosstalk between neurosecretory and
574 preautonomic networks. *Neuron* 78, 1036-1049. doi:
575 10.1016/j.neuron.2013.04.025.
- 576 Toney, G.M., and Daws, L.C. (2006). Juxtacellular labeling and chemical
577 phenotyping of extracellularly recorded neurons in vivo. *Methods Mol*
578 *Biol* 337, 127-137. doi: 10.1385/1-59745-095-2:127.
- 579 Tukker, J.J., Lasztocki, B., Katona, L., Roberts, J.D., Pissadaki, E.K., Dalezios,
580 Y., Marton, L., Zhang, L., Klausberger, T., and Somogyi, P. (2013).
581 Distinct dendritic arborization and in vivo firing patterns of parvalbumin-
582 expressing basket cells in the hippocampal area CA3. *J Neurosci* 33,
583 6809-6825. doi: 10.1523/JNEUROSCI.5052-12.2013.
- 584 Van Den Pol, A.N. (1982). The magnocellular and parvocellular paraventricular
585 nucleus of rat: intrinsic organization. *J Comp Neurol* 206, 317-345. doi:
586 10.1002/cne.902060402.
- 587 Zhang, L., and Hernandez, V.S. (2013). Synaptic innervation to rat
588 hippocampus by vasopressin-immuno-positive fibres from the
589 hypothalamic supraoptic and paraventricular nuclei. *Neuroscience* 228,
590 139-162. doi: 10.1016/j.neuroscience.2012.10.010.
- 591 Zhang, L., Hernandez, V.S., Liu, B., Medina, M.P., Nava-Kopp, A.T., Irlles, C.,
592 and Morales, M. (2012). Hypothalamic vasopressin system regulation by
593 maternal separation: its impact on anxiety in rats. *Neuroscience* 215,
594 135-148. doi: 10.1016/j.neuroscience.2012.03.046.
595
596

596

597

Figure legends

598

599 Fig. 1. Anatomical characterization of individual vasopressinergic magnocellular
600 neurosecretory neurons (AVP-MNNs) of rat hypothalamic paraventricular nucleus. All
601 of five cells were tested positive to AVP and possessed medial eminence internal part
602 (MEI) projecting axons joining the hypothalamic-neurohypophysial tract (HNT, *i.e.*
603 tract of Greving). Hence they were classified as AVP-MNNs. Camera-lucida drawing of
604 a labeled cell, "EV40": somato-dendritic position (black) and axonal characteristics
605 (red). EV40 was located in the lateral part of the PVN_{lmd}. Its somatic long axis was
606 perpendicular to the 3v. The cell had 3 primary dendrites, two directed medially and one
607 laterally. The main axons originated at the same point of the lateral primary dendrite,
608 proximal to soma, giving two primary (parents) axons (red and blue arrows, both in the
609 drawing and in the photomicrographs of two adjacent sections, 1 and 2). The top branch
610 turned ventrally to project to the MEI (red arrowhead). A collateral was emitted from
611 the parent axon proximally projecting to the border of optical tract. Labeled axon traces
612 were found inside the medial and central amygdala. The primary axonal segment
613 branched ventrally (blue arrow) was split into two branches of axon-collaterals
614 (indicated with blue arrowheads) directed either medially or laterally. The lateral
615 branch entered the fornix (fx). Additionally, several beaded processes originated from
616 the dendritic processes also entered the fornix (green arrowheads). Scale bars 50µm.
617 Neuronal nuclei were symbolized with gray shadows and conducting systems (*i.e.*
618 optical tract, opt, *stria medullaris* st, fornix, fx, internal capsule, ic) were symbolized
619 with light beige shadows.

620

621

622 Fig. 2: VH52, a AVP+ (1) MMN located in the medial portion of PVN_{lmd} with large
623 dendritic arborization. (2) Axon with several small branches and classical image of
624 strings of pearls in a small region in the lateral preoptical area. (3), (4), (5) and (6),
625 presence of labeled axon segments in or near the conducting systems, fornix (fx),
626 internal capsule (ic) and *stria medullaris* (sm). Neuronal nuclei were symbolized with
627 gray shadows and conducting systems (*i.e.* optical tract, opt, *stria medullaris* st, fornix,
628 fx, internal capsule, ic) were symbolized with light beige shadows.

629

630

631 Fig. 3: EV16: 1, immunofluorescence photomicrographs showing the expression of
632 AVP. It gave rise initially to two short thick primary dendrites, which branched
633 proximally. The bottom dendrite branched extensively till the fifth order of branches, all
634 directed medially reaching the wall of the third ventricle (3v). The top dendrite gave rise
635 two secondary branches, the medial and the lateral ones. The medial branch was similar
636 to the bottom group. The lateral portion curled up proximally near the soma but gave
637 rise the main axon (panel 1b, arrow). The main axon coursed laterally till the fornix
638 (fx), turned ventrally and then medial posteriorly toward the internal medial eminence.
639 Two main collaterals were observed. Number (2) indicates the first branch position
640 (panel 2). This tracer containing process coursed dorsally and reached the boarder of the
641 *stria medullaris* (sm). The continuation was lost temporarily in the myelinated
642 conducting structure but appeared again in the surface of sm and inside the epithalamic
643 region, the lateral habenula (4). The second branch arised dorsally to the fx, coursed
644 medially and lost in the boarder of this myelinated structure. Another two axon-like
645 beaded processes, with the classical image of strings of string-pearls (1a and 1c) were

646 likely arisen from soma and coursed rostro-ventral-medially. Tracers containing axonal
647 segments were found in medial preoptical area and suprachiasmatic nucleus (SCN).
648 Scale bars 50µm. Neuronal nuclei were symbolized with gray shadows and conducting
649 systems (*i.e.* optical tract, opt, *stria medullaris* st, fornix, fx, internal capsule, ic) were
650 symbolized with light beige shadows.

651

652

653 Fig. 4: MM15: AVP containing MNN located the posterolateral boarder of the PVN_{lmd}.
654 It emitted 3 primary dendrites. In contrast to the 3 previous cells, this cell's main
655 dendritic arbolizations were directed laterally and ventrally. Four axonal processes arose
656 from the proximal dendritic loci belonging to the same primary dendrite (colored
657 asterisks). Two of them projected ventrally toward IME. The other two axon-like
658 processes bended dorsally. Those thin axon-like processes were tested positive to
659 vGluT2 (2). Scale bars: for panel 1b, 500 µm; for panels 2's, 10µm; for panels 3's,
660 20µm. Neuronal nuclei were symbolized with gray shadows and conducting systems
661 (*i.e.* optical tract, opt, *stria medullaris* st, fornix, fx, internal capsule, ic) were
662 symbolized with light beige shadows.

663

664

665 Fig. 5 "VH25" was located in the medial border of the PVN_{lmd} with the long somatic
666 axis in parallel to the third ventricle (3v). The primary dendrites emanated from the
667 dorsal and ventral poles and directed toward the 3v. There were few branching points.
668 The main axon emanated from the proximal thick portion of the ventral dendrite (top
669 red arrow) and coursed toward the MEI. A second axon-like process emanated from the
670 same point of the main axon, with *string-of-pearls* appearance and branches like axon
671 terminals in the ventral medial hypothalamus (blue arrow). Scale bars, 50µm
672 Neuronal nuclei were symbolized with gray shadows and conducting systems (*i.e.*
673 optical tract, opt, *stria medullaris* st, fornix, fx, internal capsule, ic) were symbolized
674 with light beige shadows.

675

676 Figure 6. Salt loading modulated the behavioral response during predator exposure. A
677 and B symbolize the passive behavior "freezing" and active behavior, such as climbing.
678 C. Histogram showed a significant reduction of freezing behavior under osmotic stress,
679 whereas active behavior "rearing", "climbing" and "displacemente" showed a
680 significant increase. (* P<0.05, *** P<0.001, n=20).

681

682 Figure 7. Representative sections immunostained for c-Fos nuclei in response to
683 predator exposition in control and hypertonic group (primed letters). Lateral
684 magnocellular (PaLM) and medial parvocellular (PaMP) paraventricular nucleus (A and
685 A'); supraoptic (SON) and suprachiasmatic (SCN) nucleus (B and B'); paraventricular
686 anterior (Pa) nucleus (C and C'); medial part of the lateral habenula (mLHb) (D and D');
687 paraventricular anterior (PVA), central medial (CM) and antero-dorsal (AD) thalamic
688 nuclei (E and E'); basolateral (BLA), central (CeA) and medial (MeA) amigdalar nuclei
689 (F and F'). Scale Bars: 500 µm.

690

691

692

692
 693
 694
 695
 696
 697
 698
 699
 700
 701
 702
 703
 704
 705
 706
 707
 708
 709
 710
 711
 712
 713
 714
 715
 716
 717
 718
 719
 720
 721
 722
 723
 724
 725
 726
 727
 728
 729
 730
 731
 732

Table 1. Number of Fos-positive cells counted within a 0.02 mm² area (mean +/- S.E.M.)

Region Cat		Vehicle + Cat	Hypertonic +
Hypothalamus			
1.	Suprachiasmatic nucleus, ventral part (SCN _v) ns	75.6 ± 7.4	90.8 ± 12.4
2.	Suprachiasmatic nucleus, dorsal part (SCN _d) ***	1.2 ± 0.3	127.2 ± 6.4
3.	Paraventricular lateral magnocellular (PVN _{lm}) ***	4.6 ± 1.1	189.8 ± 14.6
4.	Paraventricular medial parvocellular (PVN _{mp}) ns	217.2 ± 26.9	166.8 ± 13.1
5.	Paraventricular medial magnocellular (PVN _{mm}) ***	26.8 ± 3.6	122.5 ± 9.1
6.	Supraoptic nucleus (SON) ***	28.5 ± 2.9	126.4 ± 12.6
7.	Medial preoptic area (MPO) **	27.5 ± 4.8	67.5 ± 6.5
Amygdala			
1.	Medial amygdala (MeA) ***	89.4 ± 8	32. ± 5.6
2.	Central amygdala medial (CeA _m) ***	18.2 ± 1.3	48.2 ± 3.3
3.	Basolateral amygdala (BLA) **	8.5 ± 0.7	2.8 ± 0.5
Epithalamus			
1.	Lateral habenula medial part (LHb _m) *	25.5 ± 4	14.8 ± 2.7
2.	Lateral habenula lateral part (LHb) ***	13.2 ± 1.6	4.4 ± 0.5

*, ** and *** for $P < 0.05$, $P < 0.01$ and $P < 0.001$, significance levels

Figure 1.TIF

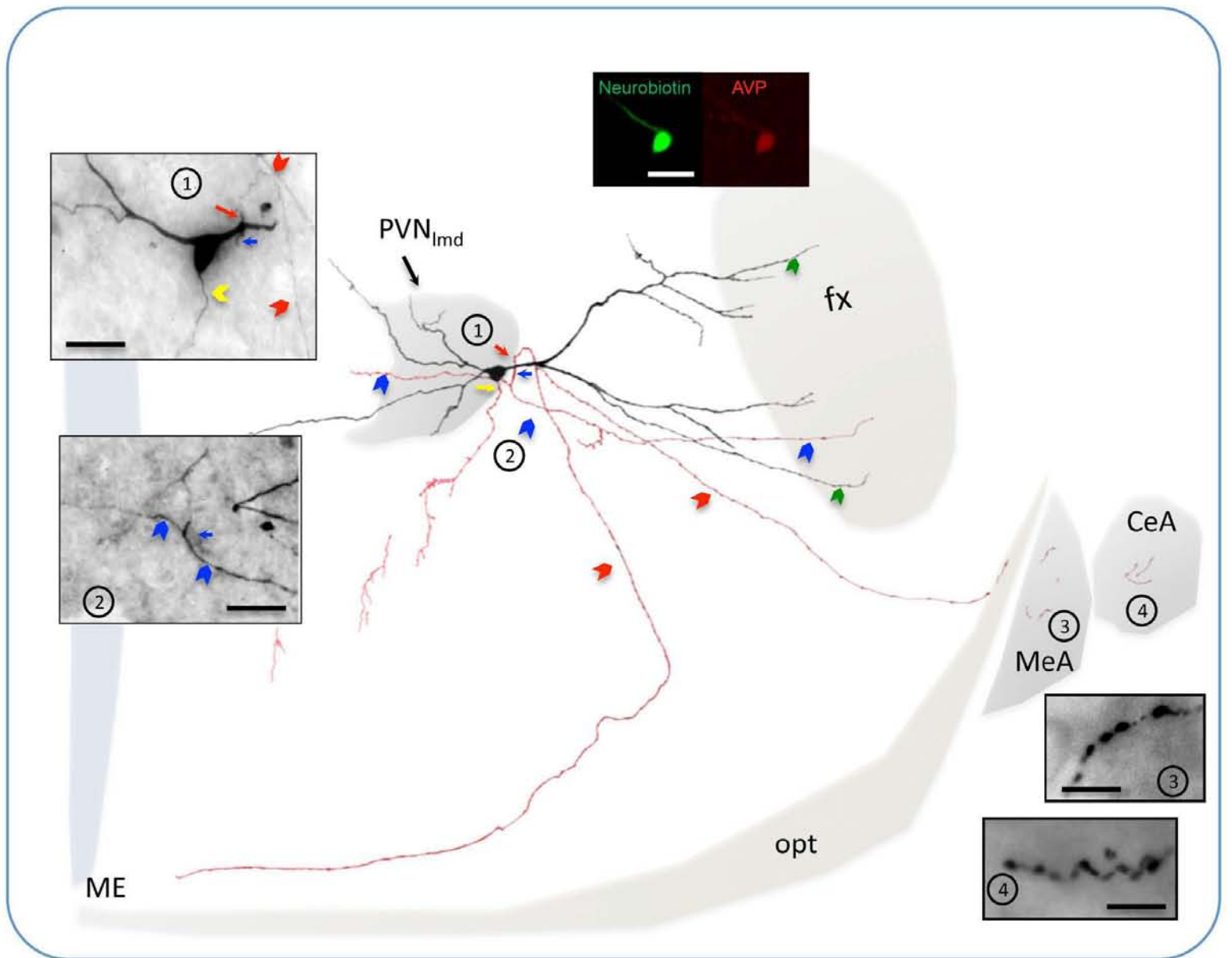


Figure 2.TIF

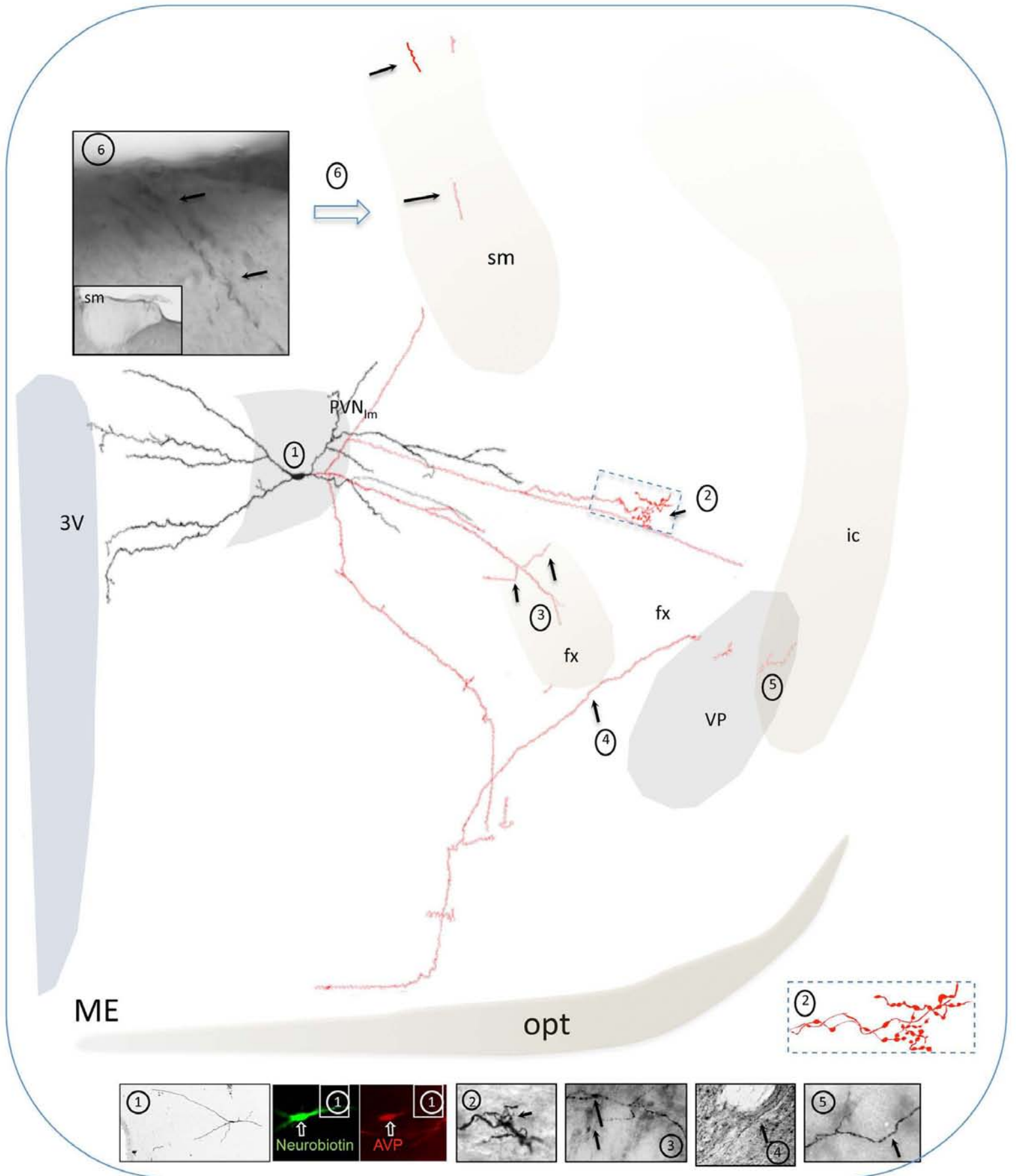


Figure 3.TIF

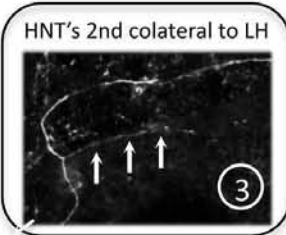
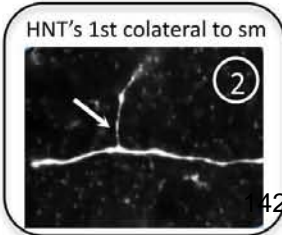
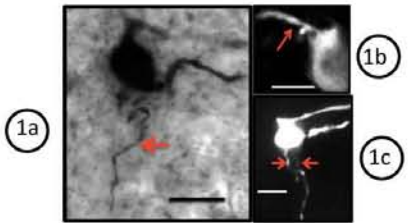
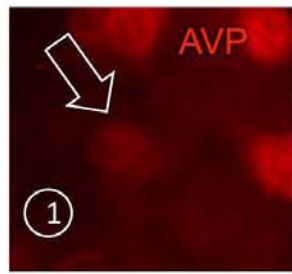
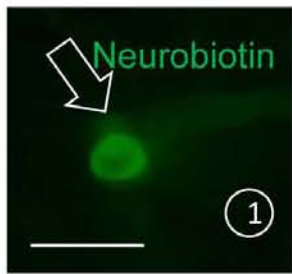
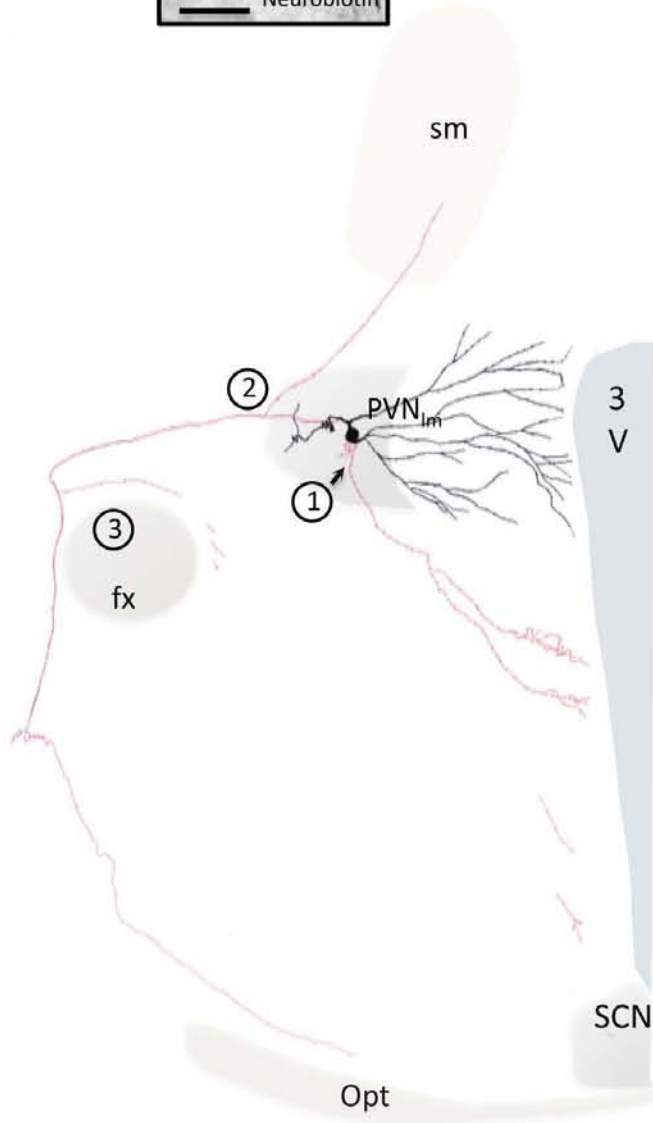
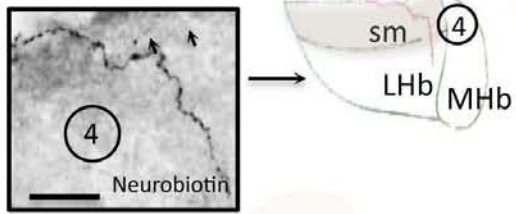


Figure 4.TIF

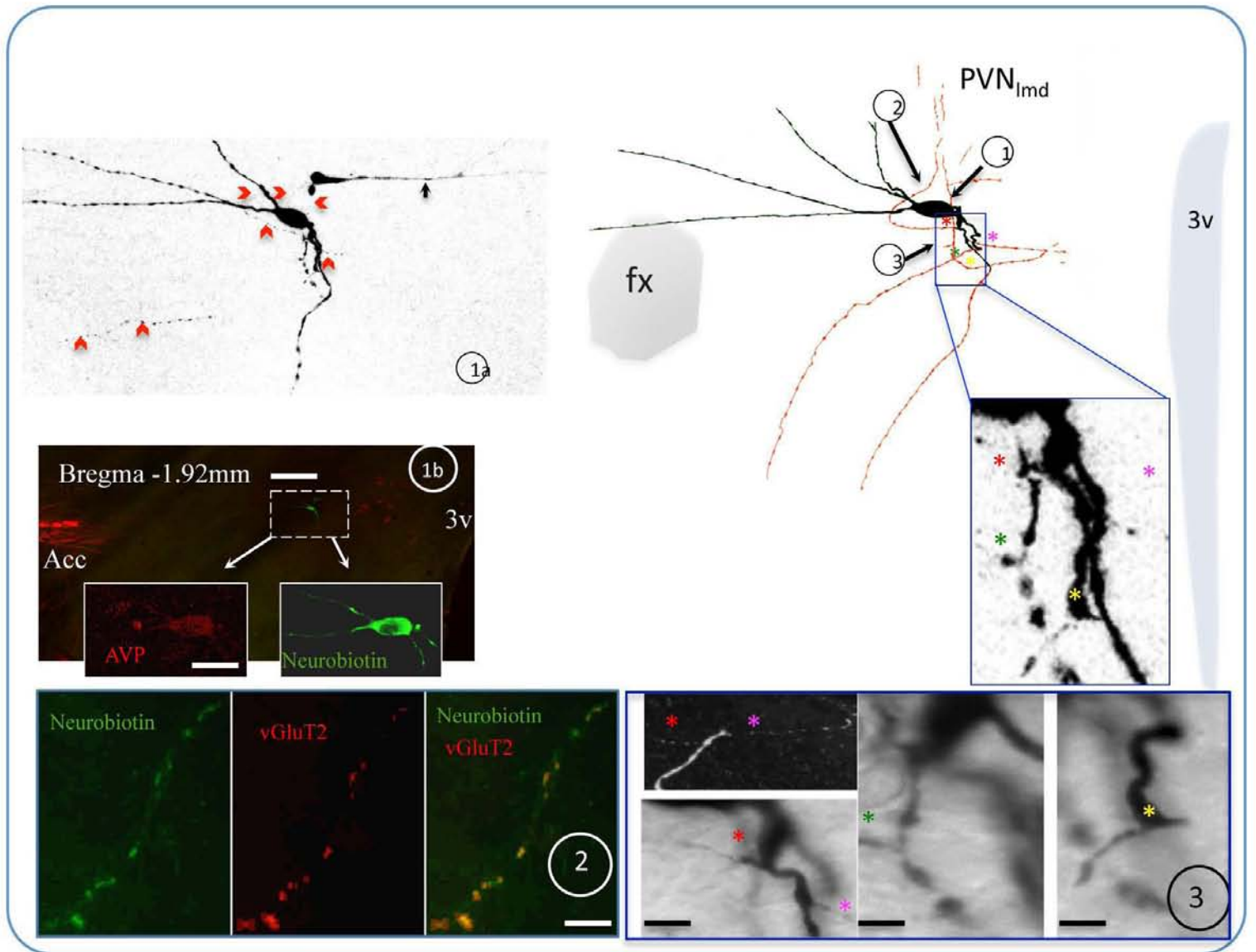


Figure 5.TIF

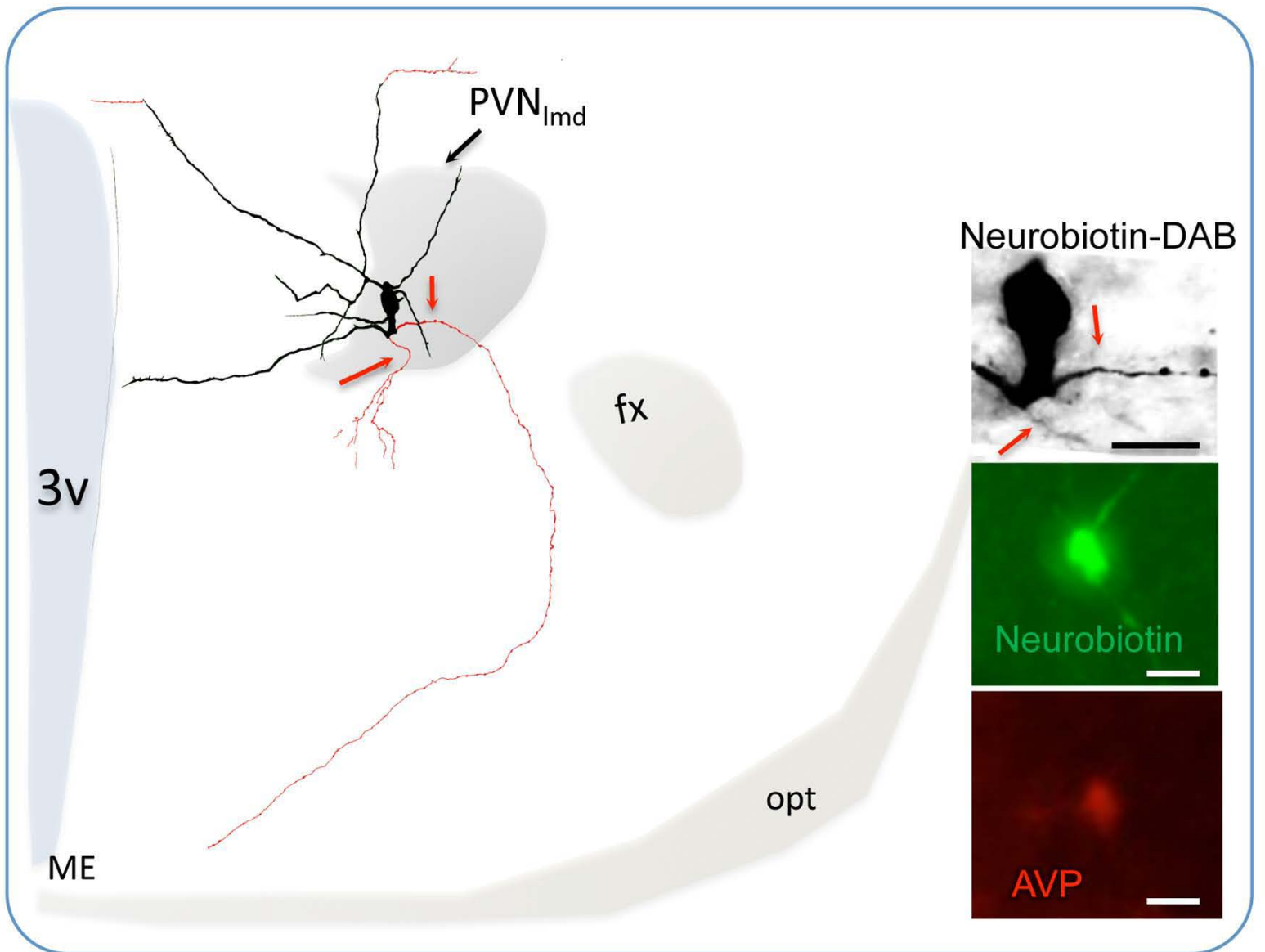


Figure 6.TIF

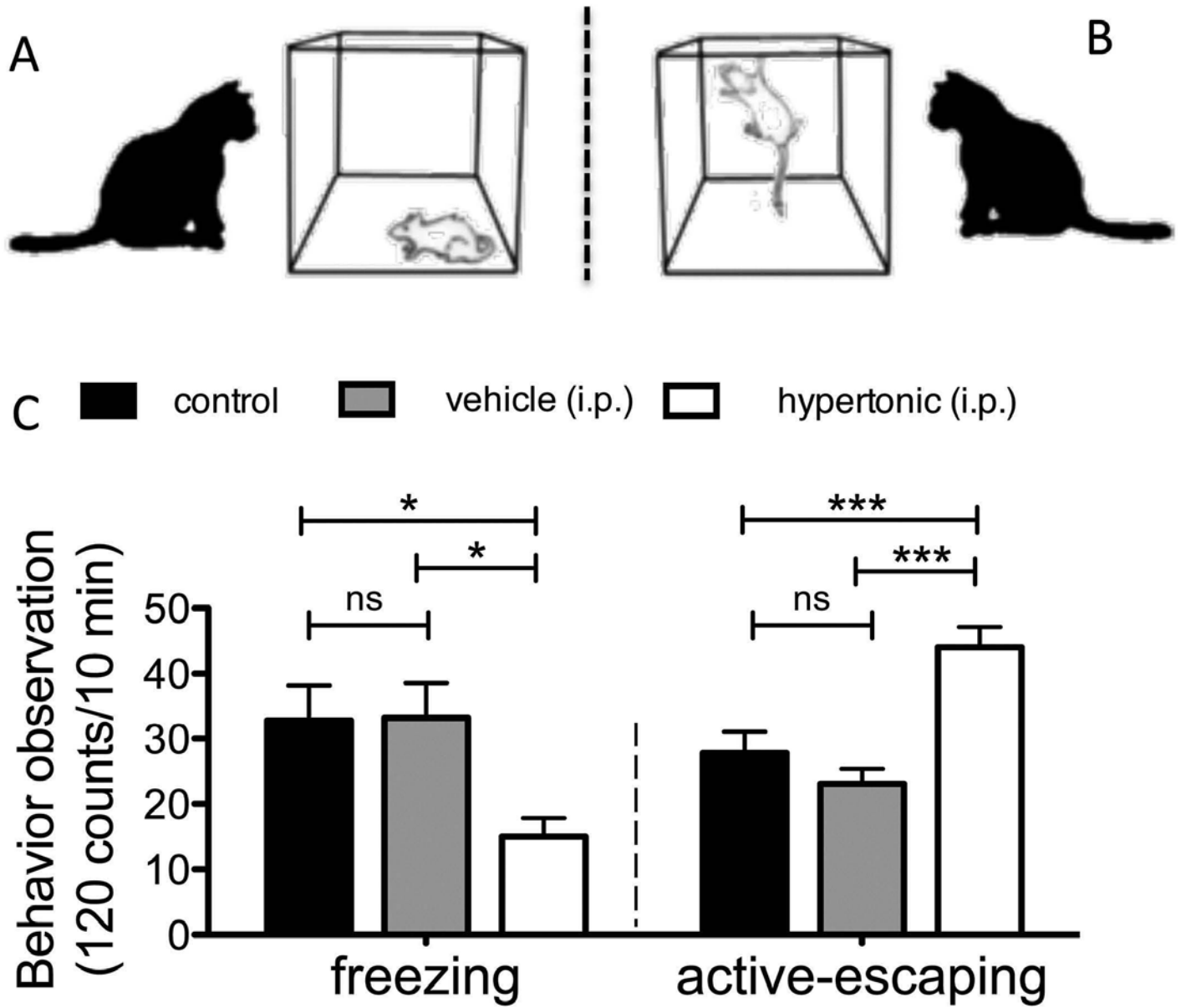
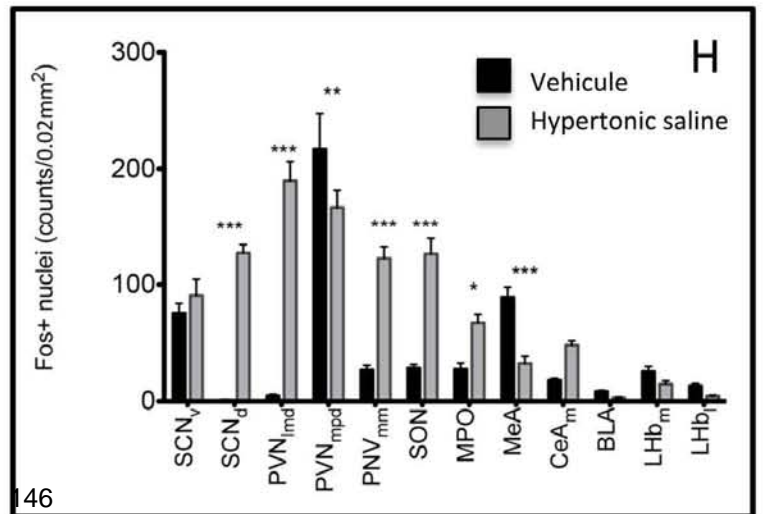
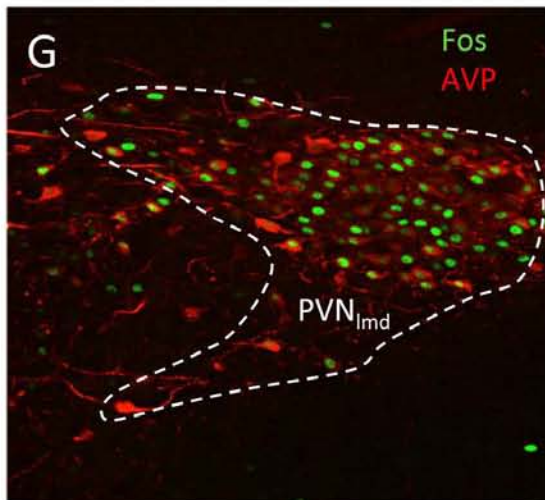
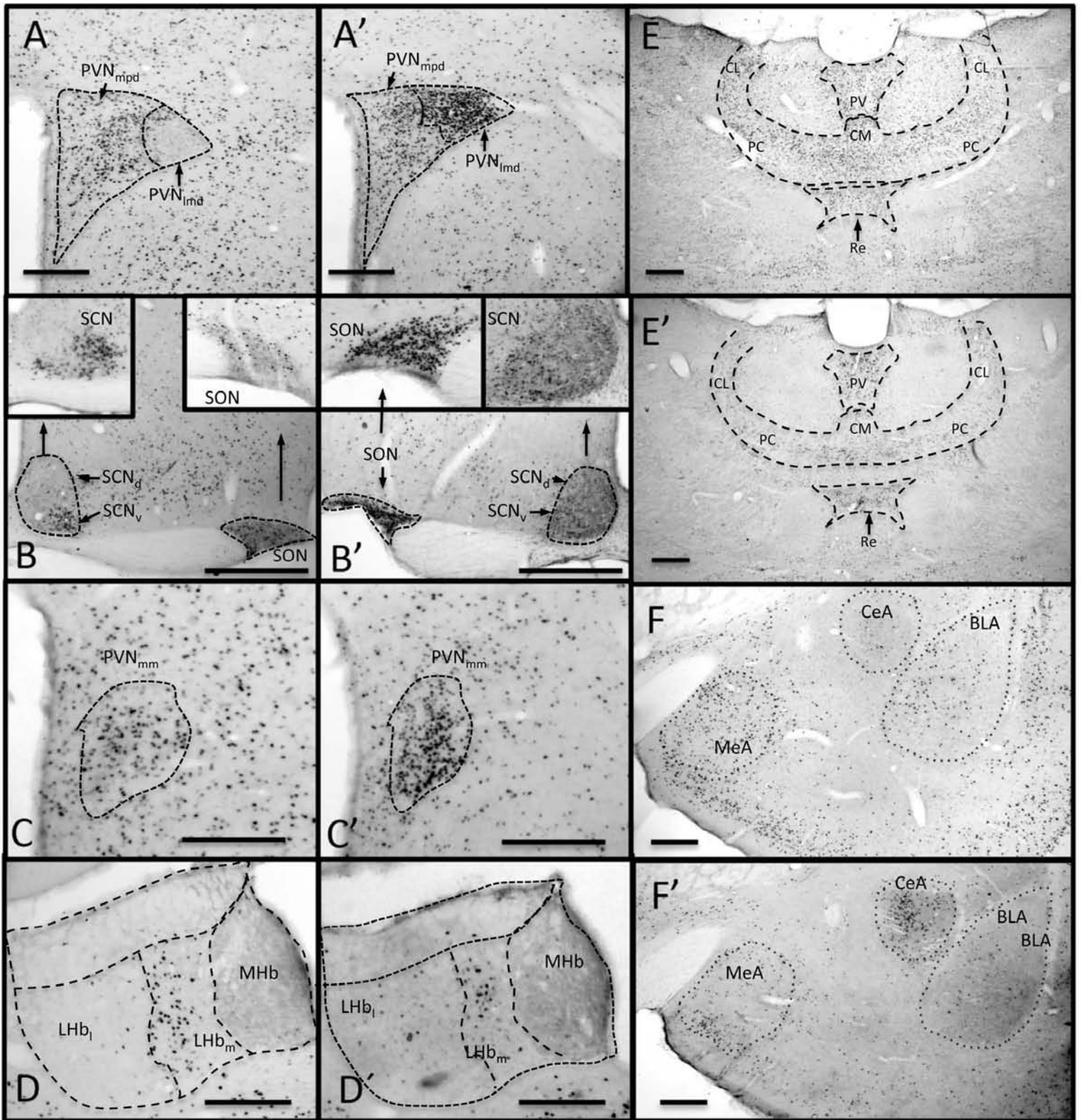


Figure 7.TIF



Synaptic innervation to rat hippocampus by vasopressin-immuno-positive fibres from the hypothalamic supraoptic and paraventricular nuclei

Zhang L. and Hernández V. S.

Neuroscience. 2013, 228: 139-62

My contributions in:

- Conception of the study: ++
- Performance of the experiments:
 - o Immunohistochemistry: +++
 - o AVP fibre density analysis: +++
 - o Electron microscopy: -
 - o Fluorogold retrograde tracing experiments: +++
 - o 3D reconstruction via neurolucida: +
- Discussion of the results: +++
- Preparation of the paper: ++

(-): No contribution; (+): Average contribution; (++): Important contribution; (+++); Main contribution

SYNAPTIC INNERVATION TO RAT HIPPOCAMPUS BY VASOPRESSIN-IMMUNO-POSITIVE FIBRES FROM THE HYPOTHALAMIC SUPRAOPTIC AND PARAVENTRICULAR NUCLEI

L. ZHANG * AND V. S. HERNÁNDEZ

Departamento de Fisiología, Facultad de Medicina, Universidad Nacional Autónoma de México, Mexico City 04510, Mexico

Abstract—The neuropeptide arginine vasopressin (AVP) exerts a modulatory role on hippocampal excitability through vasopressin V_{1A} and V_{1B} receptors. However, the origin and mode of termination of the AVP innervation of the hippocampus remain unknown. We have used light and electron microscopy to trace the origin, distribution and synaptic relationships of AVP-immuno-positive fibres and nerve terminals in the rat hippocampus. Immuno-positive fibres were present in all areas (CA1–3, dentate gyrus) of the whole septo-temporal extent of the hippocampus; they had the highest density in the CA2 region, strongly increasing in density towards the ventral hippocampus. Two types of fibres were identified, both establishing synaptic junctions. Type A had large varicosities packed with immuno-positive large-granulated peptidergic vesicles and few small clear vesicles forming type I synaptic junctions with pyramidal neuron dendrites, dendritic spines and with axonal spines. Type B had smaller varicosities containing mostly small clear vesicles and only a few large-granulated vesicles and established type II synaptic junctions mainly with interneuron dendrites. The AVP-positive axons in stratum oriens appeared to follow and contact metabotropic glutamate receptor 1α (mGluR1 α)-immuno-positive interneuron dendrites. Fluoro-Gold injection into the hippocampus revealed retrogradely labelled AVP-positive somata in hypothalamic supraoptic and paraventricular nuclei. Hypothalamo-hippocampal AVP-positive axons entered the hippocampus mostly through a ventral route, also innervating the amygdala and to a lesser extent through the dorsal

fimbria fornix, in continuation of the septal AVP innervation. Thus, it appears the AVP-containing neurons of the magnocellular hypothalamic nuclei serve as important sources for hippocampal AVP innervation, although the AVP-expressing neurons located in amygdala and bed nucleus of the stria terminalis reported previously may also contribute. © 2012 IBRO. Published by Elsevier Ltd. All rights reserved.

Key words: arginine vasopressin (AVP), Fluoro-Gold, electron microscopy, Neurolucida, anatomical tracing.

INTRODUCTION

Vasopressin (VP), also referred to as antidiuretic hormone (ADH), is a neuropeptide originated in several brain regions but preferentially in the supraoptic (SON) and paraventricular (PVN) nuclei (Buijs, 1978; Hou-Yu et al., 1986). As a hormone, VP regulates water-electrolyte metabolism, hepatic glucose metabolism, and cardiovascular function (Hatton, 1990). In the central nervous system (CNS), VP exerts influences on behaviours and cognitive function (Goodson, 2008). For instance, arginine vasopressin (AVP) plays a prominent role in the regulation of aggression, affiliation and certain aspects of pair bonding, as well as social recognition (for a review, see Caldwell et al., 2008). AVP system abnormalities have also been reported to be linked to stress over-responsiveness, anxiety, and depressive states (Wigger et al., 2004; Zhang et al., 2010). In peripheral cells, VP binds to three distinct receptors: (i) vasopressin V_{1A} receptors that trigger phospholipase- $C\beta$ (PLC β) activation and calcium mobilization, and are present in smooth muscle, liver and platelets; (ii) vasopressin V_{1B} receptors that are also coupled to PLC β and are found in the anterior pituitary; (iii) vasopressin V_2 receptors, that are coupled to adenylyl cyclase, and are present in the kidney (Barberis et al., 1998; Schoneberg et al., 1998; Thibonnier et al., 1998; Birnbaumer, 2000). In the CNS, V_{1A} is the prevalent receptor with a wide distribution whereas V_{1B} receptors are expressed in only a few brain regions (Lolait et al., 1995; Hernando et al., 2001; Stemmelin et al., 2005).

The hippocampus has been reported to be a highly sensitive site for the effects of VP on learning and memory. Behavioural studies show that VP injections into the ventral hippocampus improve memory when tested in a passive avoidance paradigm (Ibragimov,

*Corresponding author. Address: Departamento de Fisiología, Facultad de Medicina, UNAM, Av. Universidad 3000, Col. Universidad Nacional Autónoma de México, México 04510, D.F., Mexico. Tel/fax: +52-55-56232348.

E-mail address: limei@unam.mx (L. Zhang).

Abbreviations: ADH, antidiuretic hormone; AIS, axon initial segment; AVP, arginine vasopressin; BLA, baso-lateral amygdala; BNST, bed nucleus of stria terminalis; CNS, central nervous system; CoMeA, cortico-medial amygdala; DAB, 3,3'-diaminobenzidine; dcv, dense-core vesicle; dHi, dorsal hippocampus; EPSP, excitatory postsynaptic potential; FG, Fluoro-Gold; fi, fimbria; fx, fornix; HRP, horseradish peroxidase; ic, internal capsule; IR, immunoreaction; ir, immunoreactive; LTVP, long-term vasopressin potentiation; mGluR1 α , metabotropic glutamate receptor 1α ; NHS, normal horse serum; NSS, normal swine serum; PB, phosphate buffer 0.1 M; PLC β , phospholipase- $C\beta$; PVN, paraventricular nucleus; SCN, supraoptic nucleus; SON, supraoptic nucleus; STIA, stria terminalis, intra-amygdaloid division; TBS, Tris (0.05 M)-buffered saline; TBST, Tris (0.05 M)-buffered saline plus 0.3% of Triton X-100; vHi, ventral hippocampus; VP, vasopressin; VS, ventral subiculum; WD, water deprivation.

1989). Ex-vivo electrophysiological studies showed that nanomolar concentrations of [Arg⁸]-vasopressin (AVP) induced a prolonged increase in the amplitude and slope of the evoked population response in the presence of 1.5 mM calcium (Chen et al., 1993). This AVP-induced potentiation of the excitatory postsynaptic potential (EPSP) persisted following removal of AVP from the perfusion medium. The AVP-induced sustained increase of EPSP is known as long-term vasopressin potentiation (LTVP) (Chen et al., 1993). A pronounced effect of VP and its metabolite AVP (4–8) was found to elicit a long-lasting enhancement of hippocampal excitability, mostly in neurons within the ventral hippocampus (Chen et al., 1993; Urban, 1998; Chepkova et al., 2001; Dubrovsky et al., 2003). In the hippocampus V_{1A} receptors are present in the dentate gyrus as well as the CA1, CA2 and CA3 fields (Sztot et al., 1994; Barberis and Tribollet, 1996; Raggenbass, 2001; Bielsky et al., 2005). In contrast, V_{1B} receptor expression is restricted to the CA2 field (Young et al., 2006).

In contrast to the detailed information of AVP on hippocampus excitability and its receptor distributions, much less is known about the neuronal sources of hippocampal VP innervation, its fibre-distribution across subfields and targets. Earlier anatomical studies suggested that both VP- and oxytocin-containing fibres originated from the hypothalamic PVN (Buijs, 1978, 1980). This view was indirectly supported by microdialysis studies (Landgraf et al., 1988; Landgraf and Neumann, 2004). However, due to the lack of evidence from anterograde- and retrograde-tracing studies performed in the following years, this hypothesis was gradually abandoned and replaced by the hypothesis that VP cells from the bed nucleus of stria terminalis (BNST) and medial amygdala served as the main sources of the hippocampal VP innervation in rats (De Vries and Buijs, 1983; Sofroniew, 1985; Caffè et al., 1987; van Wimersma-Greidanus et al., 2000).

In this study, we re-examined the sources of AVP innervation into the hippocampus by retrograde tract-tracing analysis and investigated the pattern of distribution of AVP fibres throughout different hippocampal subfields, types of synapses formed by AVP axons, and the nature of postsynaptic targets.

EXPERIMENTAL PROCEDURES

Chemicals

Chemicals were obtained from Sigma–Aldrich, St. Louis, MO, USA, if not indicated otherwise. Sources of primary antibodies and their dilutions are depicted in Table 1.

Animals

Experiments were carried out according to the principles set out in the National Institute of Health Guide for the Care and Use of Laboratory Animals (NIH Publications No. 80-23), revised 1996. All animal procedures were approved by the local bioethical and research committees, with the approval ID 138-2009. All efforts were made to reduce the number of animals used.

Adult male Wistar rats ($N = 26$, 250–310 g) were obtained from the local animal facility. Animals were housed 3 per cage under controlled temperature (22 °C) and illumination (12 h), with water and food *ad libitum*. After surgery, animals were kept warm until fully recovered from anaesthesia and then kept individually under the above-mentioned conditions for 1 week and then returned to the original housing conditions.

Fixation of animals by vascular perfusion and immunohistochemistry (IHC) for light microscopy AVP fibre density and pathways to hippocampus analysis

Ten rats were used in this study. Four hours before the perfusion, the rats received an i.p. 900 mM hypertonic saline injection. The rats were restrained from drinking water for the first 2 h and then they were allowed to drink *ad libitum*. It is worth mentioning that according to our observation, the nonapeptide AVP immunoreactivity is variable among individuals under the animal's basal conditions, which might be related to the individual oscillatory state and physiological demands at the time of the perfusion. The salt induction was intended to up-regulate the hypothalamic osmotic-sensitive magnocellular AVP systems (Verney, 1947; Robertson et al., 1976; Summy-Long et al., 1978), but not to stimulate its release by allowing the rat to drink *ad libitum* during the last 2 h before the perfusion-fixation. With this measure a more homogenous AVP immunoreaction (IR) was achieved among the subjects for the AVP-immuno-positive fibre-density analysis. It is worth mentioning that the osmotic stimuli increase Fos proteins mRNAs, which mediate the rapid transcriptional induction of the vasopressin gene (Yoshida, 2008).

Rats were deeply anaesthetized with an overdose of sodium pentobarbital (63 mg/kg, Sedalpharma, Mexico) and perfused transaortically with 0.9% saline followed by cold fixative containing 4% of paraformaldehyde in 0.1 M sodium phosphate buffer (PB, pH 7.4) plus 15% v/v saturated picric acid for 15 min. Brains were immediately removed, blocked, then thoroughly rinsed with PB. Brains were sectioned soon after perfusion using a Leica VT 1000S vibratome, at 70 μm thickness in the following four planes: sagittal ($n = 3$), coronal ($n = 3$), semihorizontal (30° to the horizontal plane, $n = 2$) and septo-temporal (between coronal and sagittal planes, 45° to both planes, $n = 2$). Freshly-cut freely-floating alternate sections from different cutting planes were blocked with 20% normal swine serum (NSS, for immunoperoxidase reaction) or 20% normal horse serum (NHS, for immunofluorescence reaction) in Tris-buffered (0.05 M, pH 7.4) saline (0.9%) plus 0.3% of Triton X-100 (TBST) for 1 h at room temperature and incubated with the following primary antibodies: rabbit anti-AVP antibodies, guinea pig anti-metabotropic glutamate receptor 1α (mGluR1α) and mouse anti-parvalbumin (Table 1) in TBST plus 1% NSS or 1% NHS (for corresponding reactions) over two nights at 4 °C with gentle shaking. For immunoperoxidase reaction, sections were rinsed and incubated with swine anti-rabbit IgG conjugated with horseradish peroxidase (HRP) (P021702, 1:100, Dako, Denmark) in TBST + 1% NSS overnight at 4 °C. This IR was developed using 3,3'-diaminobenzidine (DAB, 0.05%, Electron Microscopy Sciences, Fort Washington, PA, USA) and hydrogen peroxide (H₂O₂, 0.01%) as the substrate. Sections were then mounted in gelatine solution (0.5 g gelatine, 0.05 g chromic potassium sulfate in 200 ml of dH₂O) and air-dried overnight. After passing briefly through 100% ethanol and xylene, the slides were coverslipped with permanent synthetic mounting medium Permount. For immunofluorescence reactions the following secondary antibodies were used: Cy3-donkey anti-rabbit IgG, Alexa Fluor 488 donkey anti-mouse IgG (1:1000, Molecular Probes Inc., Eugene, USA) and donkey anti-guinea pig IgG DyLight 649 (1:1000, Jackson ImmunoResearch Laboratories,

Table 1. Primary antibodies used and their dilutions for light microscopy (LM) and electron microscopy (EM) studies

Antibody to	Host	Dilution	Source	Address
[Arg ⁸]-vasopressin	Rabbit	1:5000 (LM, EM)	PenLabs/Bachem Cat. T4563	a
[Arg ⁸]-vasopressin	Rabbit	1:2000 (LM)	Prof. R.M. Buijs	b
mGluR1 α (metabotropic glutamate receptor 1 α)	Guinea pig	1:1000 (LM)	Prof. M. Watanabe, Frontier Institute Co., Ltd. Af66001	c
Parvalbumin	Mouse	1:5000 (LM)	Swant, Cat. 235	d

^a San Carlos, CA 94070, USA.

^b Instituto de Investigaciones Biomédicas, UNAM, Mexico.

^c 1-777-12, Shinko-nishi, Ishikari, Hokkaido, Japan.

^d CH-1723 Marly 1, Switzerland.

PA, USA). Sections were mounted with Vectashield (Vector Laboratories Inc., Burlingame, CA, USA) and analyzed with epifluorescence (Nikon ECLIPSE 50i) and confocal microscopy (Leica TCS-SP5).

Image acquisition and hippocampal AVP fibre density analysis

Observations were made under light microscopy. Anatomical nomenclature, especially on hippocampal subfields, and regional delineation were according to Paxinos and Watson (2007). For distribution density analysis, digital pictures were taken with a 20 \times objective in the corresponding subfields. Measurements were made on planar projections of microphotograph stacks of five focal planes each. Tracing was performed manually on the computer monitor using the NeuronJ plug-in for ImageJ (NIH, Bethesda, USA) and the sum of the axon lengths was obtained using the same program. Axon length of CA1 stratum oriens (str. or.) from the sagittal section at 5.72 mm lateral was 2460 μ m in one planar projection of the region and was assigned as the maximum length "100%". Summed axon lengths from 100% to 76% were assigned as "+++" and consequently: "+++": 75–51%, "++": 50–26%; "+": <26%; "–" indicated that no fibres were observed in the subfield and "n.a." indicated that the term was not applicable in the analysed section. Charting was made on whole section digital photomicrographs under microscopic observation. Three-dimensional (3D) "one-to-one" mapping of AVP axons was made using 38 alternative 70 μ m-thick sagittal sections with a Neurolucida workstation which includes: light microscope Nikon Optiphot-2, (Nikon Corporation, Tokyo, Japan), software Neurolucida software v. 9.14 for tracing and Neurolucida Explorer v. 9.14 for visualization (MicroBrightField Biosciences, VT, USA).

Fixation of animals by vascular perfusion and electron microscopic immunocytochemistry

Rats were deeply anaesthetized with an overdose of sodium pentobarbital and then perfused first with 0.9% saline followed by a fixative containing 4% paraformaldehyde, 15% v/v saturated picric acid and 0.05% glutaraldehyde in 0.1 M sodium phosphate buffer (PB, pH 7.4) for 15 min. Horizontal sections of 70- μ m thickness containing ventral hippocampus were cryoprotected with 10% and 20% sucrose with gentle shaking, followed by freeze–thawing in liquid nitrogen and room temperature phosphate buffer (PB 0.1 M). Non-specific antibody binding was blocked with 20% NSS in TBS for 1 h. The sections were incubated with rabbit anti-AVP (Table 1) in TBS plus 1% NSS for 48 h at 4 °C with gentle shaking. Sections were then rinsed and proceeded to the secondary antibody incubation with swine anti-rabbit IgG conjugated with HRP (P021702, 1:100, Dako, Denmark) in TBS containing 1% NSS, overnight at 4 °C. Peroxidase enzyme reaction was

carried out using the chromogen 3,3'-diaminobenzidine (DAB, 0.05%, Electron Microscopy Sciences) and hydrogen peroxide (H₂O₂, 0.01%) as the substrate. The reaction end product in some sections was intensified with nickel. Sections were then post-fixed with 1% osmium tetroxide in 0.1 MPB for 1 h and dehydrated through a series of graded alcohols (including 45 min of incubation in 1% uranyl acetate in 70% ethanol), then transferred to propylene oxide, followed by Durcupan ACM epoxy resin (Electron Microscopy Sciences). Sections were flat embedded on glass microscope slides, and the resin was polymerized at 60 °C for 2 days. Areas containing AVP-immuno-labelled axons were re-embedded in capsules in Durcupan resin. Ultrathin sections (~70 nm) were cut with an ultramicrotome using a diamond knife. Sections were collected onto Piloform-coated single slot grids and examined with a Philips CM100 transmission electron microscope. Digital electron micrographs were obtained with a digital micrograph 3.4 camera (Gatan Inc., Pleasanton, CA, USA) and scaled with ImageJ (Image Processing and analysis in Java, Bethesda, NIH, USA) and Adobe Photoshop. Axon terminal diameters were calculated using ImageJ on the EM photomicrographs where the synapses were best represented, measuring the widest segment of the secant line perpendicular to the axon long axis, between the two endpoints where the secant intersects with the plasmatic membrane.

Fluoro-Gold (FG) retrograde tracing from ventral (vHi) and dorsal (dHi) hippocampus

The FG retrograde injection method was modified from previously published methods (Schmued and Fallon, 1986; Schmued et al., 1989; Schmued and Heimer, 1990; Morales and Wang, 2002; Yamaguchi et al., 2011). Sixteen 300–330 g Wistar male rats (10 for vHi and 6 for dHi) were anesthetized with xylazine (Procin, Mexico) (20 mg/ml) and ketamine (Inoketam, Virbac, Mexico) (100 mg/ml) mixed in a 1:1 volume ratio and administered intramuscularly a dose of 1 ml/kg body weight. Deeply anesthetized rats were fixed in a stereotaxic apparatus and the retrograde tracer Fluoro-Gold (FG, Fluorochrome, LLC, Denver, Colorado 80218, USA), dissolved 1% in 0.1 M cacodylate buffer (pH 7.5), was delivered in the vHi (site A: Bregma –5.2 mm, lateral 5.40 mm and dorso-ventral 6.00 mm; site B: Bregma –4.40 mm, lateral 4.60 mm and dorso-ventral 7.60 mm) or dHi (site C: Bregma –2.20 mm, lateral 2.00 mm, dorso/ventral 3.40 mm). The coordinates of sites B and C were determined according to the AVP axon-density analysis where regions with highest fibre density (showed in the "Results" section) were chosen for injection sites, while the site A was chosen without specific reason. The FG was delivered iontophoretically using an iontophoresis pump (Value Kation Sci VAB-500) through a stereotaxically positioned glass micropipette (WPI 1.65 mm OD/1.1 mm ID, PG52165-4) with an inner tip diameter of around 40 μ m, by applying a 0.1 μ A current with a 5-s pulse-duration for a 50% duty cycle during 20 min. The micropipette was left in place for

an additional 10 min after each injection, to prevent backflow of tracer up the injection track. After completing the surgery rats received 0.4 mg/kg i.p. ketorolac (Apotex, Mexico) and 50 mg/kg i.p. ceftriaxone (Kendric, Mexico) daily per 3 consecutive days as analgesic/anti-inflammatory and antibiotic agents. Three to four weeks after the FG injections, the rats were perfused as previously described. Coronal and sagittal sections of 70 μm were obtained with a Leica VT1000S vibratome and AVP IHC was made with rabbit anti-AVP antibody (Table 1) as described above and Cy5-AffiniPure Donkey Anti-Rabbit IgG (1:1000, Jackson ImmunoResearch Laboratories, PA, USA) as secondary antibody. Observations were made under light (Nikon ECLIPSE 50i with B-2A long-pass emission filter) and confocal microscopy (LSM 710, DUO, Carl Zeiss, from Instituto Nacional de Cancerología, Mexico). For confocal observation, the FG at the target regions was excited with a 452-nm Argon filter (Zeiss).

RESULTS

AVP projection to hippocampus (Hi): heterogeneous distributions through Hi subfields

By means of IHC, we revealed high-density AVP fibres in the stratum oriens (str. or.) of ventral CA1, CA2 and CA3 fields (Fig. 1, panels A–C) that was far denser than previously reported (Buijs, 1978, 1980). Using the “NeuronJ” program, the summed fibre-lengths in different hippocampal regions were measured (Table 2) and calculated taking as reference the region in Fig. 1C, determined as 2460 μm (“100%”). The upper quartile was denoted as “dense innervation, + + + +”, the second upper quartile was denoted as “moderate innervation, + + +”, the third quartile was denoted as “scattered innervation, + +” and the lowest quartile was denoted as “sparse innervation, +”. As summarized in Table 2, subfields containing dense and moderate VP innervation included: ventral CA2, str. or. and stratum radiatum (str. rad.); ventral CA1, str. or.; ventral CA3, str. or. and str. rad. The AVP fibres innervated sparse but significantly the rostral portion of dorsal hippocampus (Fig. 1, panels D–F) mainly in the CA2–3 region. Representative tracings of the AVP innervation distribution through the ventral and lateral portion of dorsal hippocampus are shown in Fig. 2.

Synaptic junctions of AVP-immuno-positive axons in the hippocampus

Two types of AVP-positive fibres were recognized under the light microscope according to the diameter, size and spatial frequency of their varicosities. Thick fibres (type A) had large diameters and frequent varicosities (Figs. 1C and 3A, thick arrows), whereas the thin ones (type B) had small diameters and spatially sparse varicosities (Fig. 1C and 3A thin arrows). However, some fibres having large and frequent varicosities (Fig. 3B) showed an intermediate axonal diameter and huge axon terminal swellings not commonly seen (Fig. 3B, arrowheads). When analysed under the electron microscope (EM), the labelled varicosities contained both small clear as well as large-granulated vesicles (dense-core vesicles, dcv) at highly variable ratios. In some varicosities small clear vesicles, both

elongated and round ones, were predominant with few AVP+ dcv (Fig. 3C), whereas others contained mostly large-diameter-granulated vesicles (Fig. 3D). Both types of axon terminals made synaptic junctions with hippocampal neurons (Fig. 3E, F). Large varicosities established synaptic junctions less frequently than the small ones. Due to the changing of the diameter of the axon and the presence of the peroxidase reaction end-product that might obscure synapses, it was not possible to provide quantitative data on synapse frequency. The synapses found in hippocampus were either Gray type I (“asymmetric”) or Gray type II (“symmetric”). The type I synapses comprised 28% ($n = 7$) of a total of 25 synaptic junctions established by AVP-positive boutons. For instance, one type I synapse made by an AVP-labelled axon terminal was on a dendritic shaft in ventral CA1, str. or. (Fig. 3G). This terminal had a diameter of 1.5 μm and was densely packed with large-granulated vesicles together with the small, clear and round vesicles (Fig. 3G, Ga, Gb), which are generally associated with glutamatergic synaptic junctions (Peters et al., 1991). The postsynaptic target was a spiny dendritic shaft with several spines seen receiving unlabelled type I small synapses. These features indicated that the dendrite originated from a pyramidal neuron in ventral CA1 (Fig. 3G). Another type I synapse was on a dendritic spine (Fig. 3H and inset from a serial section) and was followed in serial sections (Fig. 3I) where the same spine connected to a dendritic shaft. This AVP axon terminal had a diameter of about 1.3 μm and contained many large-granulated vesicles. Another postsynaptic structure in the str. pyr. of the ventral CA3 (Fig. 3, panels J–L) originated from an axon initial segment (AIS) and was identified as an axonal spine (Kosaka, 1980). It contained a high density of intracellular organelles and received a type I synapse from a large AVP+ axon terminal. In one of the subsequent serial sections, a type II unlabelled synapse was found on the AIS (Fig. 3L). The latter feature and the presence of the spine suggested that this AIS originated from a CA3 pyramidal neuron (Kosaka, 1980). Some AVP-positive axon terminals made type II synapses onto dendritic shafts, which also received unlabelled type I synapse (Fig. 3M, N). This feature indicated that the postsynaptic dendrites originated from interneurons (Takacs et al., 2012). It is worth noting that the axon terminals found to make type II synapses were of diameters around 0.5 μm . These axon terminals had abundant small clear vesicles, both round and elongated (Fig. 3N), which are generally associated with inhibitory (GABAergic) synaptic junctions (Peters et al., 1991).

AVP projection to hippocampus: mGluR1 α expressing interneurons were among the possible targets for AVP axons

When looking for the identity of the interneurons, we found a strong-contacting relationship between AVP axons and mGluR1 α -expressing dendritic segments (Fig. 4A–D) and a weak-contacting relationship with parvalbumin-expressing soma and dendritic segments (Fig. 4E, F). The AVP-positive axons in stratum oriens

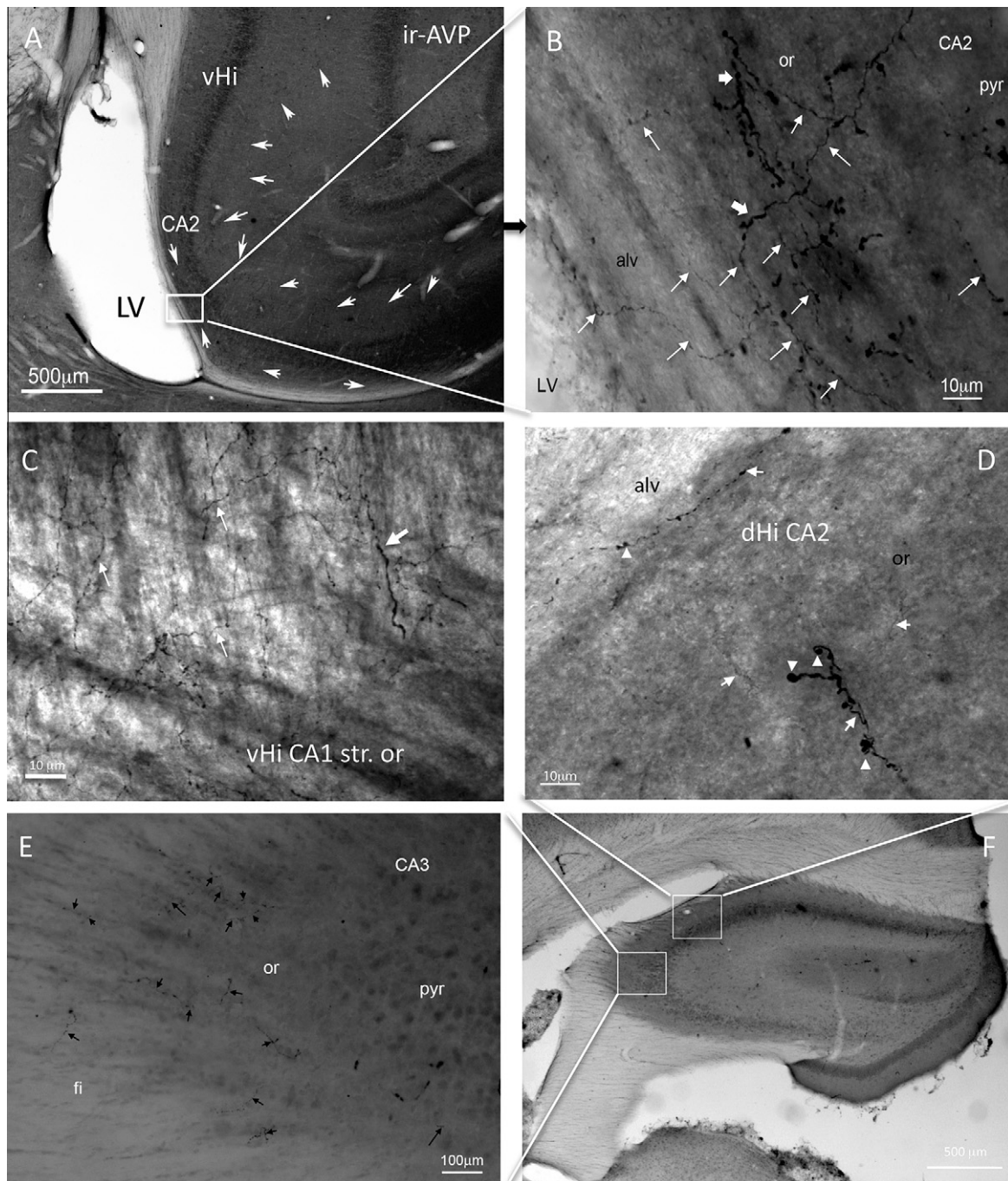


Fig. 1. Immunohistochemical visualization of the AVP innervation in ventral (vHi: A–C) and dorsal hippocampus (dHi: D–F). Two types of AVP fibres can be seen: the thick ones (type A, indicated with thick arrow) and the thin ones (type B, indicated with the thin arrows). Arrow heads indicate huge axon terminal swellings not commonly seen. pyr: stratum pyramidale; or: stratum oriens; fi: fimbria; alv: alveus; LV, lateral ventricle.

appeared to follow and contact mGluR1 α -immunopositive interneuron dendrites, but did not have a strong association with parvalbumin-positive dendrites.

Hippocampus received vasopressinergic input from SON and PVN of the hypothalamus revealed by Fluoro-Gold (FG) neurotracing

Table 3 shows a survey and anatomical description of the results from all 16 rats studied in this experiment. The

quality descriptions “excellent”, “good”, “weak”, “missed” or “damaged” referred to the resulting labelling location, strength, sizes and grade of damage in the surrounding tissue after about 3 weeks post-FG application. Five out of ten attempts in the vHi and four out of six attempts in the dHi were “excellent/good” which meant that the FG-labelled sites had a diameter of less than 350 μ m and were precisely targeted to the regions with high vasopressinergic innervations revealed by anatomical analysis (Table 2). Furthermore, in the

Table 2. AVP axonal projection to Hi subfields: distribution analysis based on IHC using “NeuronJ” for ImageJ

	CA1				CA2				CA3				DG			VS
	or	pyr	rad	lm	or	pyr	rad	lm	or	pyr	luc-rad	lm	mol	gr	po	
<i>vHi</i>																
Lateral (mm)																
6.02	++	+	n.a.	n.a.	n.a.	n.a.	n.a.	n.a.	n.a.	n.a.	n.a.	n.a.	n.a.	n.a.	n.a.	+
5.86	+++	+	n.a.	n.a.	+++	+	+	n.a.	n.a.	n.a.	n.a.	n.a.	n.a.	n.a.	n.a.	+
5.72	++++*	+	+	n.a.	+++	+	n.a.	n.a.	n.a.	n.a.	n.a.	n.a.	n.a.	n.a.	n.a.	+
5.58	++++	+	+	++	++++	+	++	+	n.a.	n.a.	n.a.	n.a.	n.a.	n.a.	n.a.	++
5.44	+++	+	+	++	++++	+	+	+	n.a.	n.a.	n.a.	n.a.	n.a.	n.a.	n.a.	++
5.30	+++	+	+	++	+++	+	++	+	n.a.	n.a.	n.a.	n.a.	n.a.	n.a.	n.a.	+
5.16	++	+	–	–	+++	+	+	+	+	++	++	–	–	n.a.	n.a.	+
5.02	+	–	+	+	++	+	++	+	+++	+	+++	+++	–	–	–	+
4.88	+++	+	++	++	++++	+	+++	+	+++	+	+++	+	–	–	–	+
4.74	++	+	++	++	++++	+	++	+	++	+	+++	–	–	–	–	+++
4.60	+++	+	++	++	++++	+	+++	+	+++	+	+++	++	–	–	–	++
4.44	+++	+	++	++	+++	+	+++	+	+++	–	+++	+++	–	–	–	++
4.30	+++	–	++	+	++	–	+++	+	++	+	++	+	–	–	+	+
4.16	++	+	++	++	++	–	+++	+	+	–	++	+	–	+	+	+
4.02	++	–	++	+	+++	+	++++	+	++	–	++	+	–	–	–	+
3.88	++	+	++	+	++	–	++	+	+	–	+++	+	–	+	+	+
3.74	++	–	++	++	+++	+	+++	++	+	–	++	+	+	+	+	+
3.60	+++	+	++	+	++	–	++	++	++	–	++	–	++	++	++	+
3.46	+	+	++	++	n.a.	n.a.	n.a.	n.a.	+	–	++	+	+	+	+	+
3.32	+	–	+	+	n.a.	n.a.	n.a.	n.a.	+	–	+	+	+	+	+	+
3.18	n.a.	n.a.	n.a.	n.a.	n.a.	n.a.	n.a.	n.a.	+	+	+	+	+	+	+	+
3.02	n.a.	n.a.	n.a.	n.a.	n.a.	n.a.	n.a.	n.a.	++	n.a.	+	+	+	+	+	n.a.
<i>dHi</i>																
Bregma (mm)																
–1.72	n.a.	n.a.	n.a.	n.a.	n.a.	n.a.	n.a.	n.a.	+	n.a.	n.a.	n.a.	–	–	n.a.	n.a.
–1.92	n.a.	n.a.	n.a.	n.a.	n.a.	n.a.	–	n.a.	+	n.a.	n.a.	n.a.	+	–	–	–
–2.16	–	–	–	–	+	–	–	–	–	–	–	–	+	–	–	–
–2.40	+	–	–	–	+	+	–	–	–	–	–	–	–	–	–	–
–2.64	–	–	–	–	–	–	–	–	–	–	–	–	–	–	–	–
–2.90	–	–	–	–	+	+	–	–	–	–	–	–	–	–	–	–
–3.12	–	–	–	–	–	–	–	–	–	–	–	–	–	–	–	–
–3.36	–	–	–	–	–	–	–	–	–	–	–	–	–	–	–	–
–3.60	–	–	–	–	–	–	–	–	–	–	–	–	–	–	–	–

stratum oriens; pyr: stratum pyramidale; rad: stratum radiatum; luc: stratum lucidum, lm: stratum lacunosum-moleculare, mol: molecular layer of the dentate gyrus; gr: granular cell layer; po: polymorphic layer. vHi: ventral hippocampus in sagittal sections. dHi: dorsal hippocampus in coronal sections.

* Axon length was maximal in CA1 in the sagittal section at Lat. 5.72 mm (shaded box); this length of 2460 μm was assigned as “100%”. For each subfield, a summed axon length of 100–76% was assigned as “++++”; “+++”: 75–51%; “++”: 50–26%; “+”: <26%; “–” indicates that no fibre was observed in the subfield and “n.a.” indicates that the subfield is not applicable in the analyzed section.

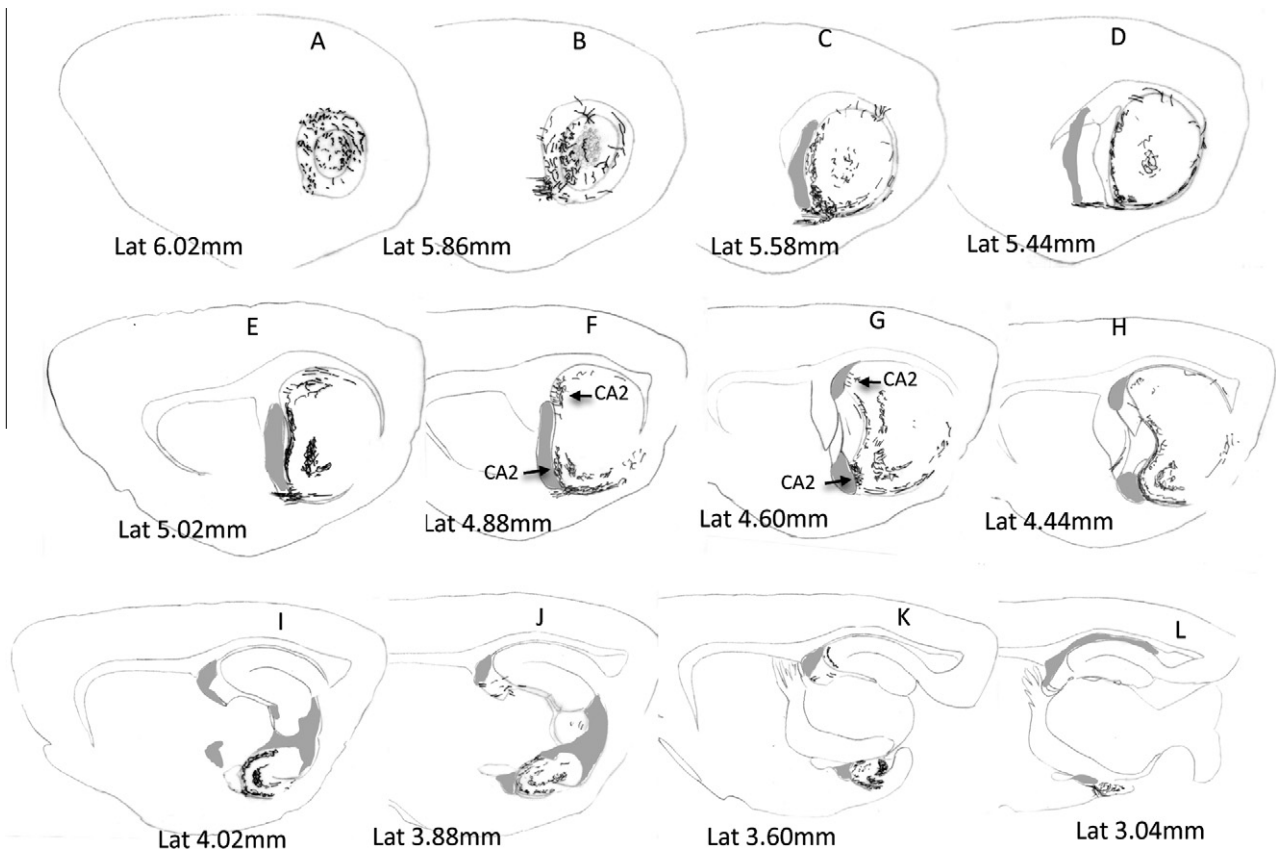


Fig. 2. Chartings of sagittal sections at 12 mediolateral levels with line drawings representing AVP fibre distribution through the entire ventral hippocampus. The lateral portion of the dorsal hippocampus is also included. Shaded areas denote ventricles.

“good” and “excellent” subjects, the labelling was clearly visible for as long as 28 days.

For vHi, the iontophoretic FG injection was initially targeted to the lateral segment of the CA2 (Bregma -5.20 mm, lat. 5.40 mm and dorso-ventral 6.00 mm) without prior knowledge of the AVP fibre density in this region. Injections in this segment of the CA2 resulted in very few weakly labelled cells in the hypothalamus (Table 3). However, scattered labelled FG/AVP+ cells were seen in the bed nucleus of the stria terminalis, intraamygdaloid division (STIA) 14 days after the injection. These attempts served as our “negative control” for our data interpretation. Once information of the detailed AVP fibre distribution became available (Table 2), we changed the injection location to ventral CA2 (str. or. – str. pyr., Bregma -4.40 mm, lat. 4.60 mm and dorso-ventral 7.60 mm) where the densest AVP innervations were observed. The precise localized injection into 3 rats (“vHi-8”, “vHi-9” and vHi10”; Table 3) resulted in a number of AVP+ neurons displaying FG-labelling within the SON and PVN magnocellular division (Fig. 5). The FG labelling was mainly accumulated in the perikarya of lysosome-like granules (Fig. 5, panels F, I and insets), which is a prominent characteristic reported for long-term weak FG labelling (Schmued and Fallon, 1986; Wessendorf, 1991; Persson and Havton, 2009). To discard the possibility of an unspecific FG signal due to leak into

blood vessels or cerebro-spinal fluid, the choroid plexus and the subfornical organ (SFO) were carefully examined. FG signal was not detected in the SFO nor the choroid plexus of the three examined rats (Fig. 6, panel E and inserts). In the STIA, a moderate amount of FG labelled cells were found, a few of which were double labelled with AVP/FG (Fig. 6, panels A–D). It is worth mentioning that the AVP-IR in this region is generally weak and variable.

For dHi, the injection site was the foremost rostral part of CA2 and CA3 (Bregma -2.20 mm antero-posterior, 2.00 mm lateral and 3.40 mm dorso-ventral) where, according to the AVP fibre distribution analysis (Table 2), most of AVP innervations in dHi were found (Fig. 1D–F). Fig. 7, panels A and B showed the FG application site of the subject “dHi1” (Table 3), which was perfused 28 days after the FG injection. Note that the labelled region, CA2–3 str. or. – str. pyr. was relatively small and precise. The labelled pyramidal neurons accumulated FG in both cytoplasm and in the perikarya lysosome-like granules mentioned above (Fig. 7B and its inset) and some of the contra-lateral CA3 pyramidal neurons were labelled (Fig. 7C). Panels D–I (Fig. 7) showed the weak FG labelling patterns in hypothalamus SON (D–F) and PVN (G–I) seen with confocal microscope, the perikarya lysosome-like granules labelling was indicated by * in the insets of panel F and panel I.

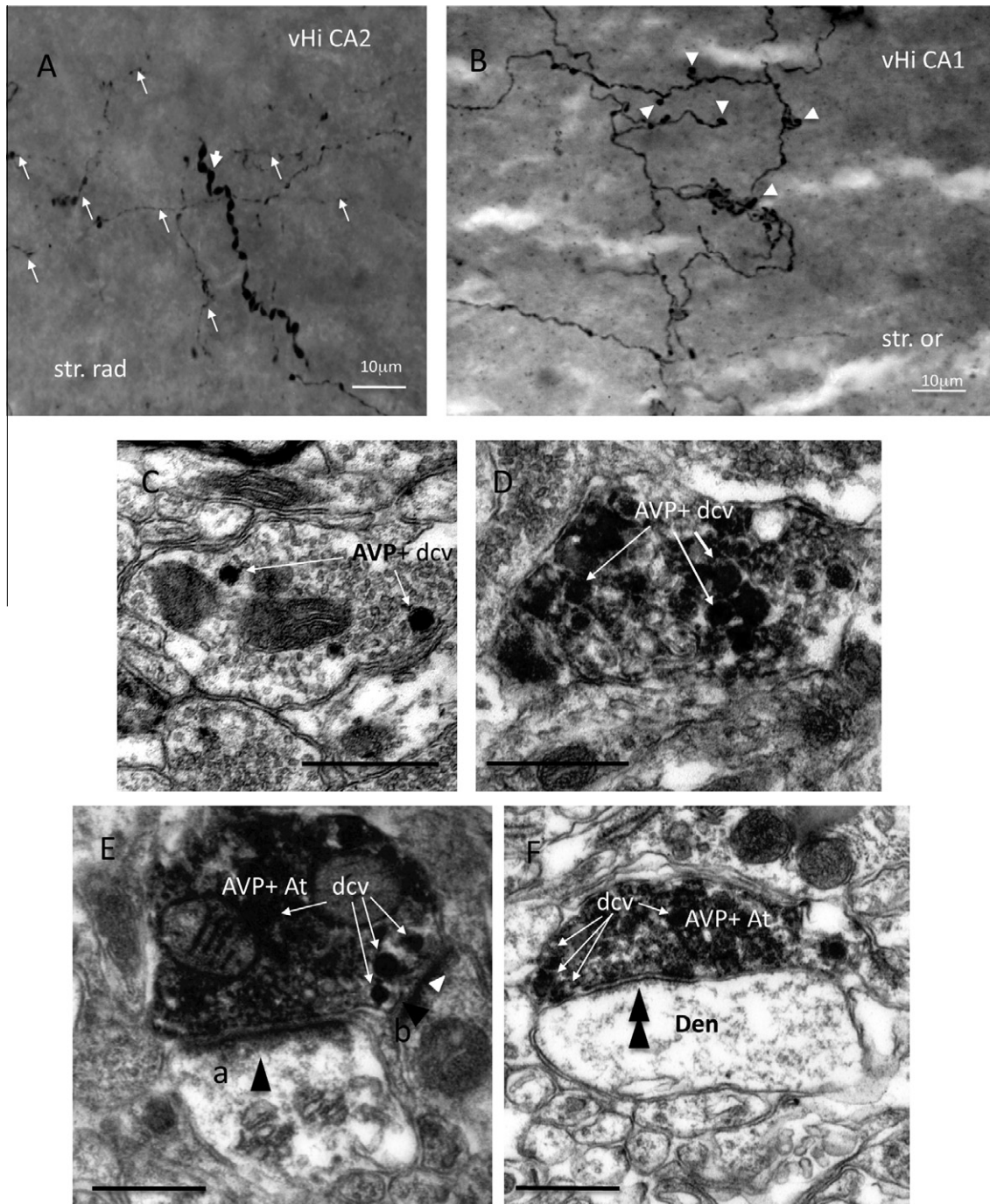


Fig. 3. Two types of AVP immunoperoxidase labelled fibres and their terminals as shown by light (A, B) or electron (C–N) microscopy. (A) An axon with large diameter varicosities (thick arrow) amongst thin axons with sparse boutons (thin arrows) in stratum radiatum (str. rad.) of the ventral CA2. (B) AVP+ axonal network in str. oriens (str. or.) of the ventral CA1. Note large swellings (arrowheads). (C) Example of a thin axon terminal containing few large AVP+ dense-core vesicles (dcv, arrows) along with small clear both round and elongated vesicles. (D) Varicosities of the thick axons contained mainly the large-granulated vesicles (dcv). (E) Type I synapses (black arrowhead) made by an AVP+ bouton with a dendritic spine (a) and an axon-spine (b). White arrowhead indicates the electron-opaque membrane undercoating – an EM characteristic of axon initial segments (AIS). Note the proximity of three large-granulated vesicles to the presynaptic membrane in the active zone of synapse b. (F) Type II synapse (double arrowheads) made by an AVP+ bouton with a dendritic shaft (den). (G) A postsynaptic dendritic shaft receives a labelled type I synapse and emits several spines (s), one of them receives an unlabelled type I small synapse (arrowhead). (H and inset) Serial sections of a type I synapse on a dendritic spine (s) connected to a dendrite (l). (J and inset, K, L) Serial sections of an AVP+ axon (Ax) forming a type I synapse with a large spine (Ax-s) originating from an AIS in the ventral CA3. The electron-opaque membrane undercoating of the AIS is indicated by white arrowhead. The axonal spine contains membranous intracellular organelles (J, K), and receives a type II synapse from an unlabelled terminal (L, double arrowhead). (M, N) AVP+ boutons making type II synapses (double arrowheads) onto dendrite shafts (den), which also receive type I synapses (arrowheads) from unlabelled boutons, suggesting that they originate from interneurons. At: axon terminal, s: spine; Ax: axon; den: dendrite; dcv: dense-core vesicle. Scale bars for A and B: 10 μ m, C–N: 0.5 μ m.

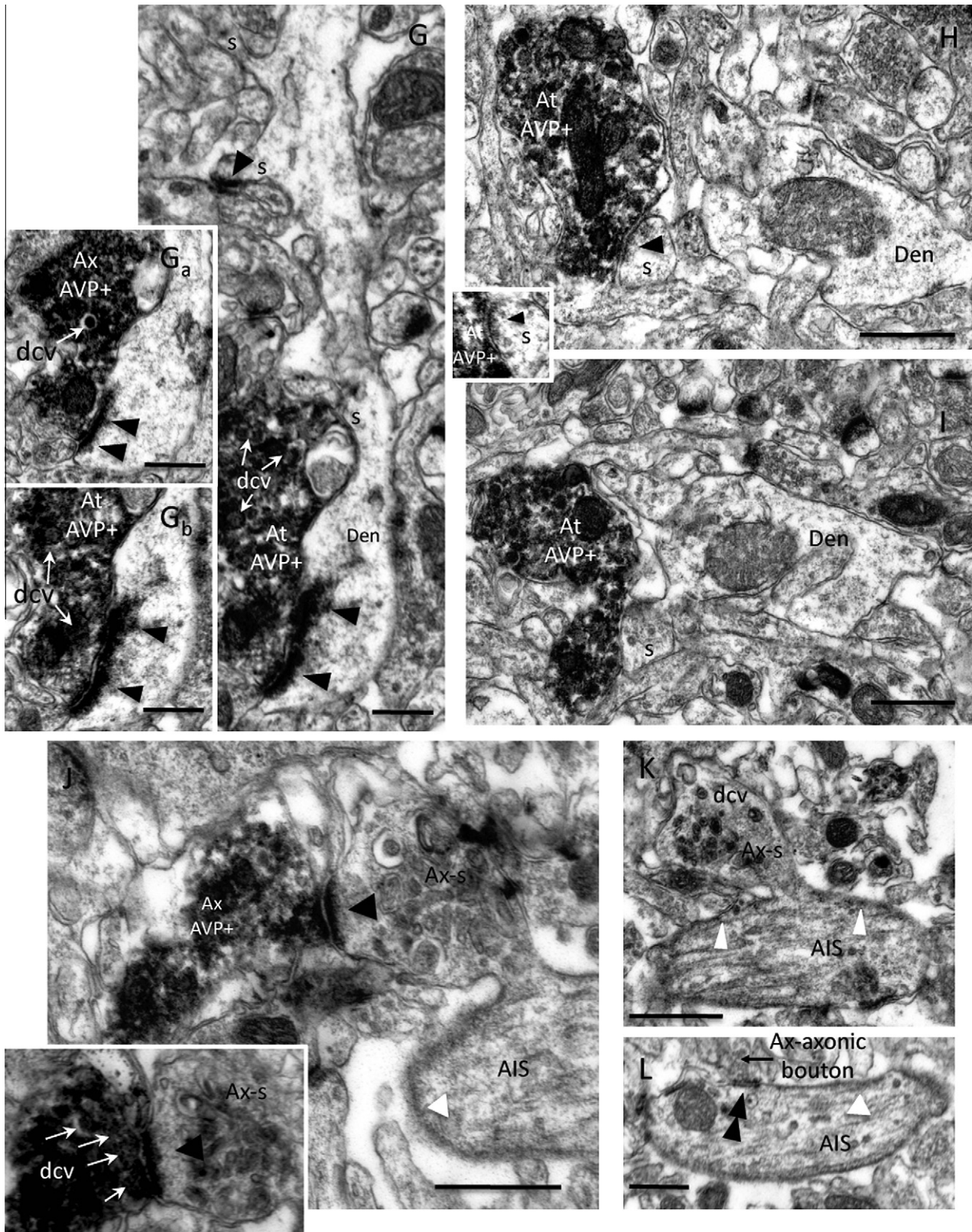


Fig. 3. (continued)

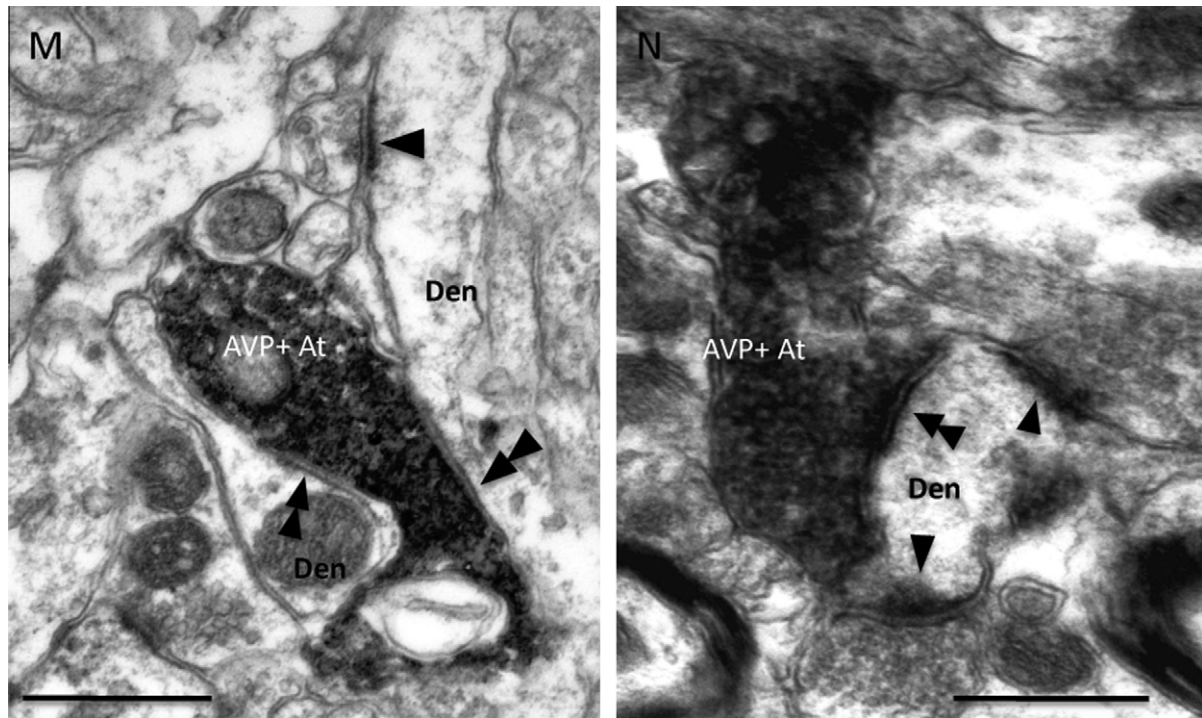


Fig. 3. (continued)

Neurolucida 3D mapping and visualization coupled with an anatomical study suggested three main pathways from SON and PVN to hippocampus

Using computer-aided light microscopy (Neurolucida workstation), a 3D “one-to-one” reconstruction was done under a light microscope using objectives from 4× to 20×, from 38 alternative serial sections. It is worth noting that the type A and B fibres, their continuity and the branching patterns (straight/low branching vs. winding highly branching) could be clearly distinguished and documented (Fig. 8). Using this method, together with line drawings under LM made from the seven sets of serial sections (sagittal plane: 2; septo-temporal plane: 2; coronal plane: 2; semi-horizontal plane: 1) three pathways connecting hypothalamic magnocellular AVP nuclei and the hippocampus can be clearly seen.

The rostral route of AVP fibres from hypothalamic magnocellular neurons projecting to hippocampus was mainly through the fimbria–fornix fibre system. The fimbria–fornix fibre system provides the major conduit for hippocampus–subcortical afferent and efferent connections (Daitz and Powell, 1954; Powell et al., 1957). It was suggested that the PVN vasopressin fibres projected to hippocampus through this fibre system (Buijs, 1978). After analysing the anatomical study results, it became evident that from both PVN and SON, AVP-containing fibres followed the fornix dorso-rostrally (Fig. 9Aa, Ab, Ac) into the dorsal hippocampus. From there, part of the fibres projected dorsally reaching the rostral portions of the CA3 and CA2, via the alveus (Fig. 1, panels B, D). The remaining fibres continued inside the fimbria descending to ventral hippocampus

(Fig. 9, groups D, E). At Bregma AP -0.24 mm (Fig. 9Ba, Bb) and -0.78 mm (Fig. 9Ca, Cb, Cc) abundant AVP fibres could be clearly observed inside the fimbria. The panels Fig. 9Dc and Dd showed the AVP fibres inside the fimbria in semi-horizontal sections (Fig. 9Da, Db). Fig. 9Eb and Ec showed the abundant straight AVP fibres inside the ventral fimbria (Fig. 11Ea). It was not rare to observe that the straight AVP fibres inside the alveus made orthogonal turns to go inside the str. or. (Fig. 9Fa, Fb).

The medial route of AVP fibres from hypothalamic magnocells projected to hippocampus via the internal capsule (ic) to join the fimbria. A considerable amount of AVP axons from both SON and PVN magnocellular neurons travelled latero-postero-dorsally (Fig. 10A, B) into the ic. The AVP axons can be clearly seen on the surface of the white matter ic (Fig. 10C). The fibres continued caudally and could be clearly seen on the border between the ic and the reticular thalamic nucleus in a straight and parallel fashion (Fig. 10F, horizontal view). In the adjacent fimbria (Fig. 10F and inset), AVP fibres with the same orientation and straight and parallel fashion could be observed. In the region of the fimbria around the coordinates: Bregma AP -2.70 mm to -3.10 mm, 3.90 mm lateral and interaural 4.90 mm, both in the coronal view (Fig. 10D, E) and sagittal view (Fig. 10H), abundant AVP fibres were observed.

The caudal route of AVP fibres from hypothalamic magnocellular neurons projecting to ventral hippocampus via cortico-medial-amygdala and lateral amygdala. AVP projections originated in SON projecting towards the

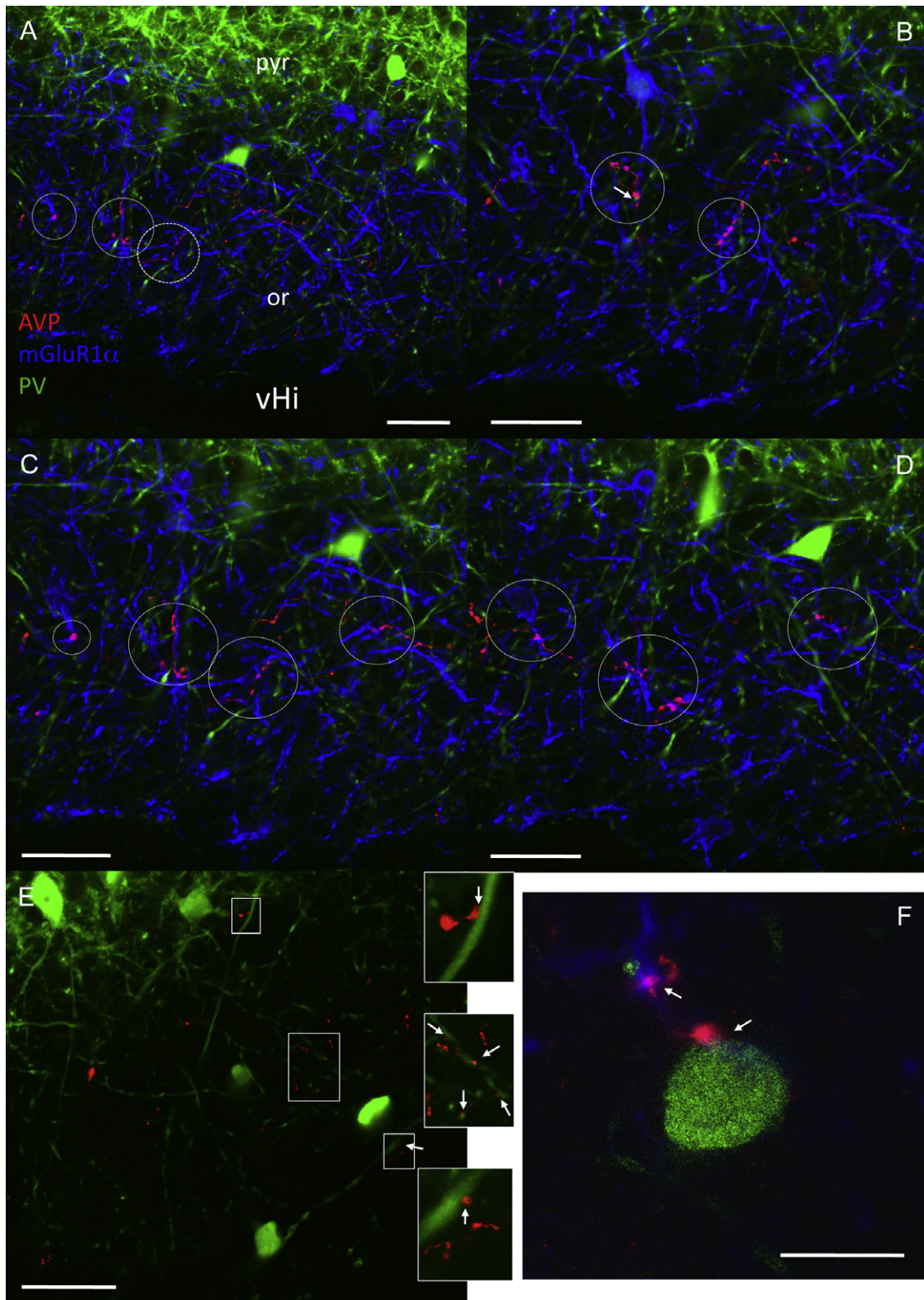


Fig. 4. Confocal images of immunohistochemical labelling of AVP (red), mGluR1 α (blue) and parvalbumin (PV, green) taken in stratum oriens (or) of the ventral hippocampus (vHi). Note that there was a strong-contacting relationship between AVP axons and mGluR1 α expressing dendritic segments (A–D, circles). Also a weak-contacting relationship (arrows) with PV expressing somata (F) and dendritic segments (E, arrows) was observed. The scanning thickness was 3 μ m. Scale bars for A–E: 50 μ m and F: 15 μ m.

Table 3. Fluorogold retrograde labelled subjects: survey and anatomical description

Subject ID and surgery to perfusion interval (days)	Stereotaxic coords. relative to Bregma: anteroposterior; lateral; dorso-ventral (mm)	Iontophoretically labelled hippocampal subfield and quality**	Retrograde labelled AVP nuclei: semi-quantitative analysis*			
			PVN	SON	SCN	BNST
vHi-1: 14	−5.20; 5.40; 6.00	Ventral CA2: good	−	−	−	STIA: +
vHi-2: 35	−5.20; 5.40; 6.00	Ventral CA2: weak	−	+	−	STIA: +
vHi-3: 21	−5.20; 5.40; 6.00	Ventral CA2: damaged	+	+	−	STIA: +
vHi-4: 14	−4.40; 4.60; 7.60	Ventral CA2/3: good	++	++	−	STIA: +
vHi-5: 21	−4.40; 4.60; 7.60	Ventral CA2/3: damaged	n. e.	n. e.	n. e.	n. e.
vHi-6: 22	−4.40; 4.60; 7.60	Ventral CA2/3: 2 labelled sites	n. e.	n. e.	n. e.	n. e.
vHi-7: 22	−4.40; 4.60; 7.60	Ventral CA2/3: damaged	n. e.	n. e.	n. e.	n. e.
vHi-8: 28	−4.40; 3.80; 8.00	Ventral CA2/3: excellent	++	+++	−	STIA: +
vHi-9: 18	−4.40; 4.60; 7.60	Ventral CA2/3: excellent	++	+++	−	STIA: +
vHi-10: 18	−4.40; 4.60; 7.60	Ventral CA2/3: excellent	++	+++	−	STIA: +
dHi-1: 21	−2.20; 2.00; 3.40	Dorsal CA2/3: excellent	++	++	−	STIA: +
dHi-2: 14	−2.20; 2.00; 3.40	Dorsal CA2/3: good	++	++	−	STIA: +
dHi-3: 21	−2.20; 2.00; 3.40	Dorsal CA2/3: excellent	+++	++	−	STIA: +
dHi-4: 21	−2.20; 2.00; 3.40	Dorsal CA2/3: missed	n. e.	n. e.	n. e.	n. e.
dHi-5: 21	−2.20; 2.00; 3.40	Dorsal CA2/3: missed	n. e.	n. e.	n. e.	n. e.
dHi-6: 28	−2.20; 2.00; 3.40	Dorsal CA2/3: excellent	+++	+++	−	STIA: +

n.e., not evaluated; STIA, stria terminalis intra-amygdaloid division; vHi, ventral hippocampus; dHi, dorsal hippocampus.

* Fluorogold + AVP + cell number per 0.2 mm²: +, 1–5; ++, 6–10; +++, > 10.

** The qualitative descriptions “excellent”, “good”, “weak” refer to the strength of labelling, “missed” refers to the precision of targeting, and “damaged” refers to the grade of damage in the tissue surrounding the labelling site, all evaluated at around 3 weeks post-FG application.

amygdala and ventral hippocampus were revealed by detailed anatomical analysis. Serial section line-drawings (Fig. 11A–G) under light microscopy and using Neurolucida 3D mapping (Fig. 8) showed that a considerable amount of the AVP fibres from SON projected caudally towards the neurohypophysis through the medial eminence and infundibular stem. We observed that quite a few fibres continued caudo-laterally, passing through the tuberomammillary and supramammillary areas, entering the cortico-medial amygdala (CoMeA) and then turning dorsally to the amygdalo-hippocampal transition area – some of them entered the ventral hippocampus (Fig. 11A–G, delineated region by a blue-dashed line). Some of these fibres made almost orthogonal turns to enter the amygdalo-hippocampal cortex (Fig. 11D, Da) and these axons seemed to continue in the vHi, mainly in the str. or. of CA1 and CA2 where heavy innervation was found (Table 2 and Fig. 3A, B). The AVP projections from hypothalamic SON and PVN to vHi were also found projecting caudo-laterally via the lateral amygdala division and entered the vHi region through external capsule-alveus. This pathway could be clearly seen in a semi-horizontal section (Fig. 10, group H). Another important feature of this pathway was shown in Fig. 11He: Two morphologically different axons could be clearly distinguished, the ones which were straight and parallel, seemed to project to the external capsule and alveus of ventral CA1 and CA2 (yellow arrows), and the winding, locally branched ones (black small arrows). The latter ones innervate densely the BNST, central and basolateral amygdala (Fig. 10He). The straight axons, after entering the alveus of CA1 of vHi, branched locally or continued in the white matter to CA1-subiculum or to the CA2 directions (Fig. 11Hc, Hd).

DISCUSSION

In the present study we have provided the first comprehensive description of AVP-ir fibre-distributions across the whole septo-temporal extent of the hippocampus of the Wistar rat. We presented the first evidence on (1) AVP-ir fibre synapses onto hippocampal neurons and their postsynaptic targets, namely, pyramidal neurons and interneurons. Dendrites and somata of interneurons expressing mGluR1 α and parvalbumin located in the str. oriens (or.) of CA1–2 in the ventral hippocampus were identified as possible targets; (2) the hypothalamic magnocellular AVP neurons from SON and PVN projected to both dHi and vHi. Moreover, according to the anatomical study, three suggested pathways of vasopressin innervation from the hypothalamus to the hippocampus were described.

Although effects of AVP on the hippocampus excitability and its receptor distribution had been extensively reported, the hippocampal AVP innervations with respect to their subfield-fibre-distribution, synaptic formation and targets remained unknown. Early investigation had shown AVP innervations of the rat hippocampus (Buijs, 1978; Caffé et al., 1987; Rood and De Vries, 2011), and a recent study in mice found that the main innervation sites were vHi, while the dHi was devoid of AVP-ir fibres (Rood and De Vries, 2011). In this study, we reported a denser innervation pattern by the AVP-immuno-positive fibres than previously reported. Several methodological factors could render our AVP-IR more sensitive than other studies. As mentioned above, we used two antisera against AVP raised in rabbits (see Table 1). The first antibody was obtained using glutaraldehyde-treated AVP as the antigen (Buijs et al., 1989) and the second one used synthetic AVP as the antigen. In our previous

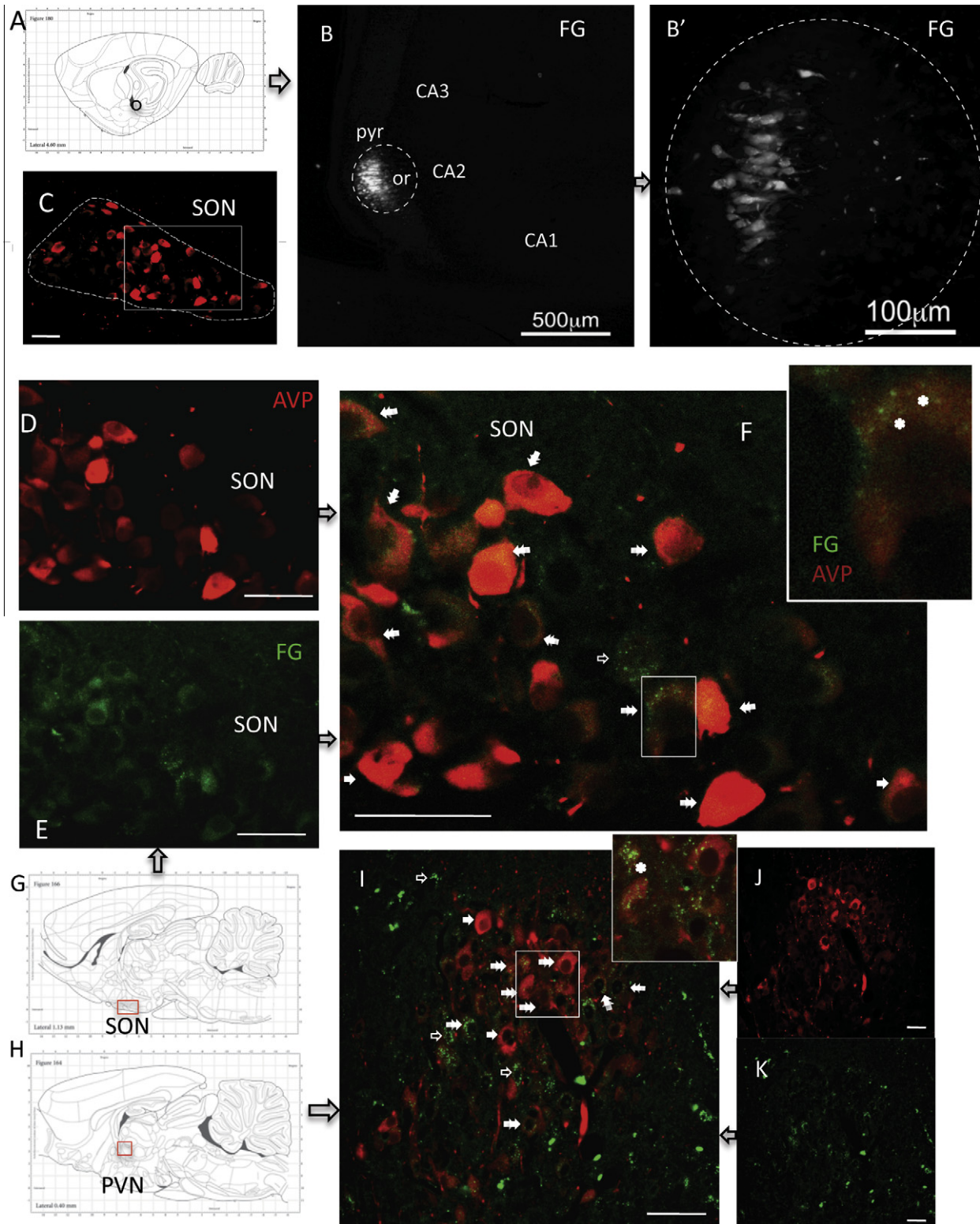


Fig. 5. Ventral hippocampus (vHi) received vasopressinergic input from SON and PVN of the hypothalamus revealed by Fluoro-Gold (FG) neurotracing. Panel A showed a schematic representation with circle indicating the injection site, which was determined according to the AVP fibre-distribution analysis. (B, B') Fluoro-Gold (FG) injection sites in the vHi CA2. Note that the injection site had a diameter of $< 350 \mu\text{m}$. Panels C–G illustrate retrogradely labelled cell bodies in SON. (C, D) Confocal images of AVP-ir in SON. (E) Confocal image of FG in SON. (F) Overlay of (D) and (E). Note that in the inset of (F) the accumulation of FG was in lysosome-like granules (*). Panels H–J illustrate retrogradely labelled cell bodies in PVN. Green, FG. Red, AVP-ir. Solid arrows indicate AVP labelling. Hollow arrows indicate cells labelled with FG only and double arrows indicate double labelling. Scale bars: $50 \mu\text{m}$ if not indicated otherwise.

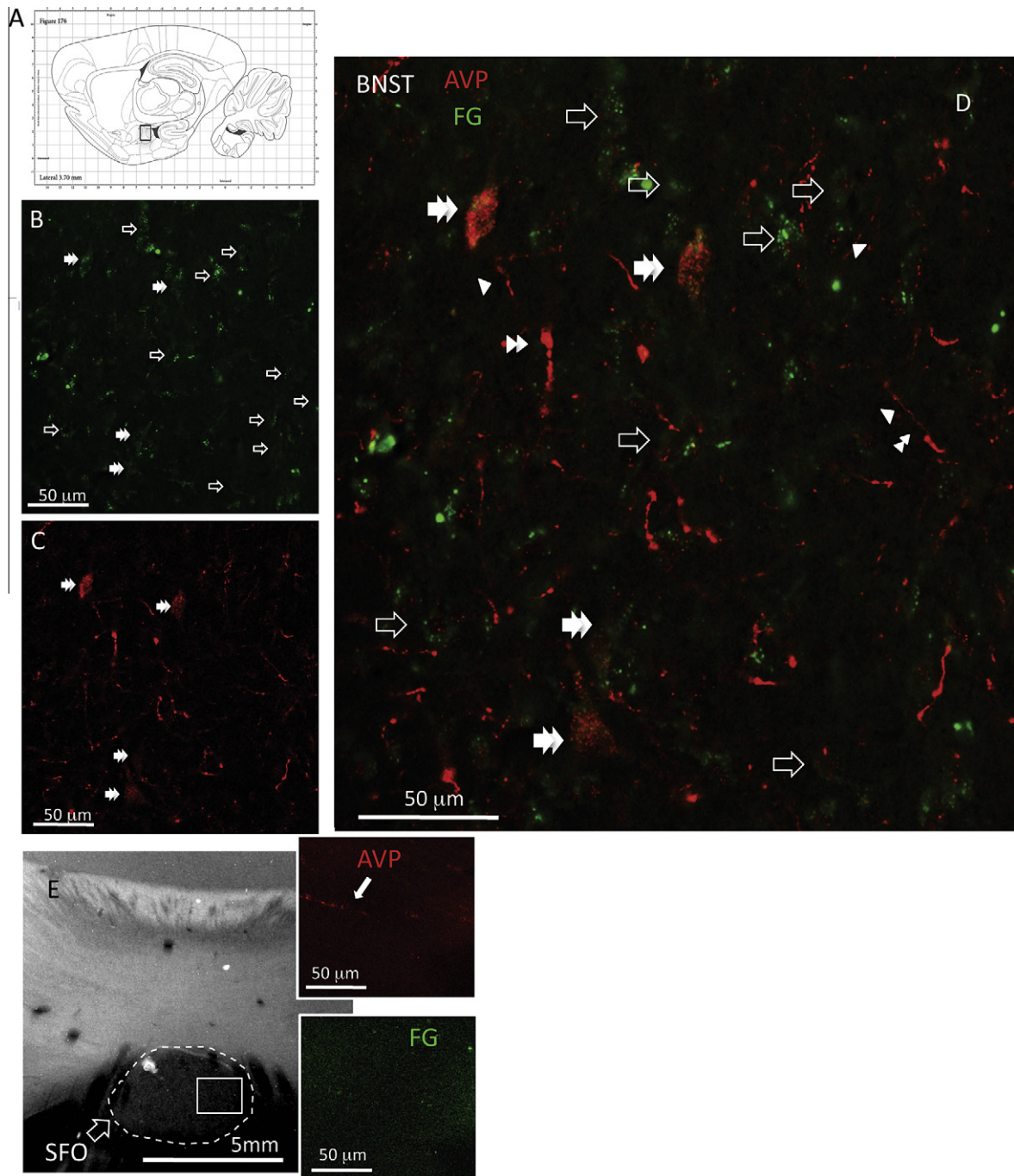


Fig. 6. Fluoro-Gold (FG) injection in vHi CA2 resulted in FG/AVP double labelling in the bed nucleus of stria terminalis intraamygdaloid division (STIA) and no labelling in subfornical organ (SFO). (A) Schematic representation of STIA in a sagittal section. (B–D) Four AVP-containing neurons in the region were labelled with FG (double arrows). Note that both type A (double arrowhead) and type B (arrowheads) AVP-immunopositive fibres were present in this region. Panel E and its inset (confocal photomicrographs) illustrate the no-FG labelling in the SFO, used as negative control in this experiment. Green, FG. Red, AVP-ir. Solid arrows indicate AVP labelling. Hollow arrows indicate cells labelled with FG only.

experiments, different labelling patterns by those two antibodies against AVP-containing neuron's soma, dendrites and axons were observed. These differences in labelling between the two antibodies might be due to AVP's structural changes, occurring during the synthesis and transport from the soma to the terminals, and/or caused by the fixation process. Hence the antiserum we used for AVP-IR for the anatomical studies (except

for EM study) was a mixture of those two antibodies. The AVP-IR was markedly enhanced, especially in the hippocampal subfields. Another important issue is the quick processing after perfusion. Our experience indicates that AVP-IR depends strongly on the histological procedures (for details, see Zhang et al., 2012).

So far, synapses made by axon terminals containing AVP immunoreactivity have been described only in rat

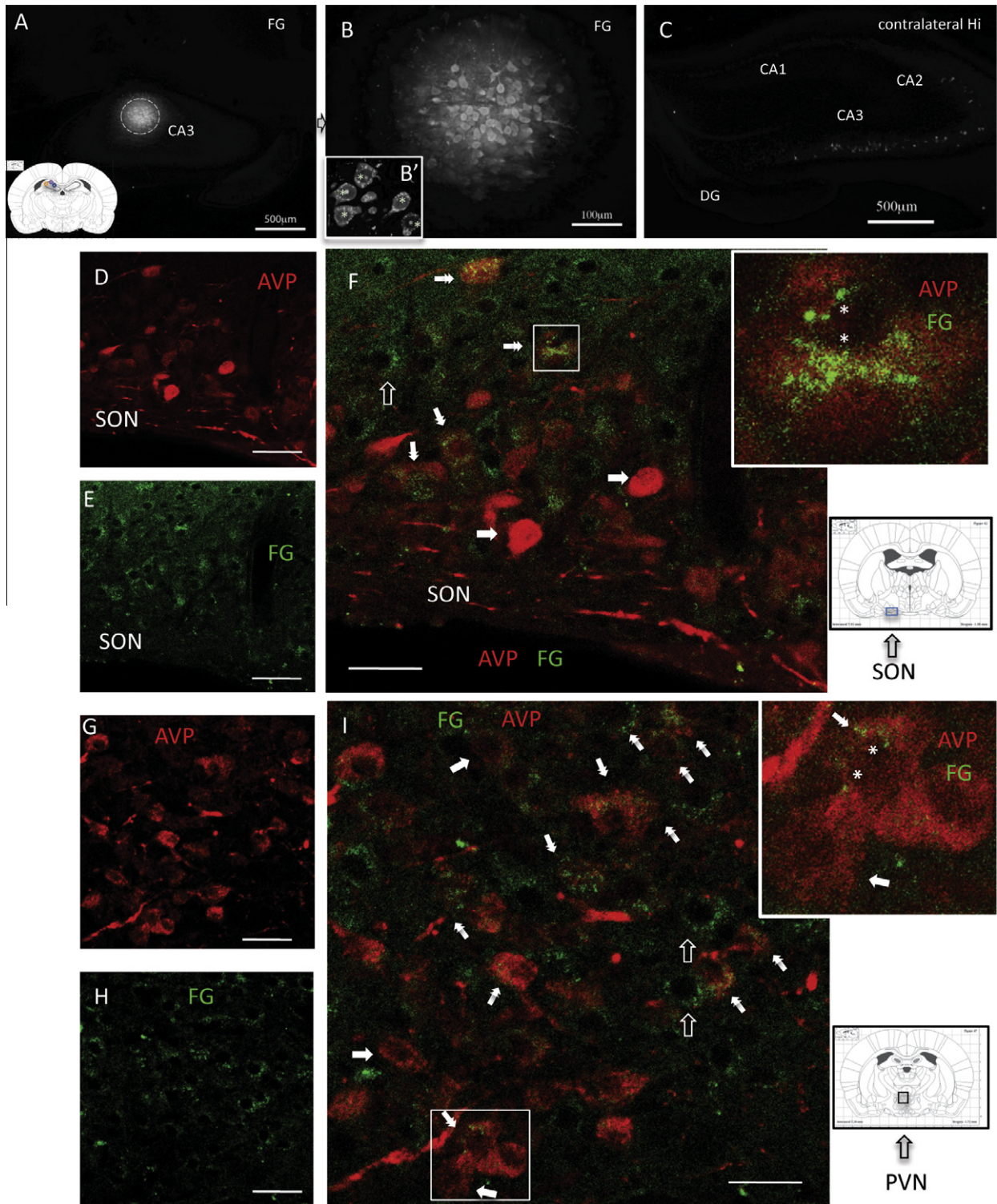


Fig. 7. Dorsal hippocampus (dHi) received vasopressinergic input from SON and PVN of the hypothalamus revealed by Fluoro-Gold (FG) neurotracing. Panel A illustrates the dHi injection site (rostral CA2–3, diameter <math>< 350 \mu\text{m}</math>). Inset showed a schematic representation with circles indicating the injection sites, which were determined according to the AVP fibre-distribution analysis. Panel B illustrates the site with higher magnification. Inset of (B), confocal photomicrograph shows that after 28 days the labelled pyramidal neurons accumulated FG in lysosome-like granules in the perikarya (*). Panel C illustrates some of the contra-lateral CA3 pyramidal neurons were labelled with FG. Panels D–F illustrate retrogradely labelled cell bodies in SON. (D) Confocal image of AVP-ir in SON. (E) Confocal image of FG in SON. (F) Overlay of (D) and (E). Note in the inset of F the accumulation of FG in lysosome-like granules (*). Panels G–I illustrate retrogradely labelled cell bodies in PVN. Green, FG. Red, AVP-ir. The inset of (I) shows the accumulation of FG in lysosome-like granules (*) and a magnocellular neuron which is not labelled by FG (single solid arrow). Solid arrows indicate AVP labelling. Hollow arrows indicate cells labelled with FG only and double arrows indicate double labelling. Scale bars: 50 μm if not indicated otherwise.

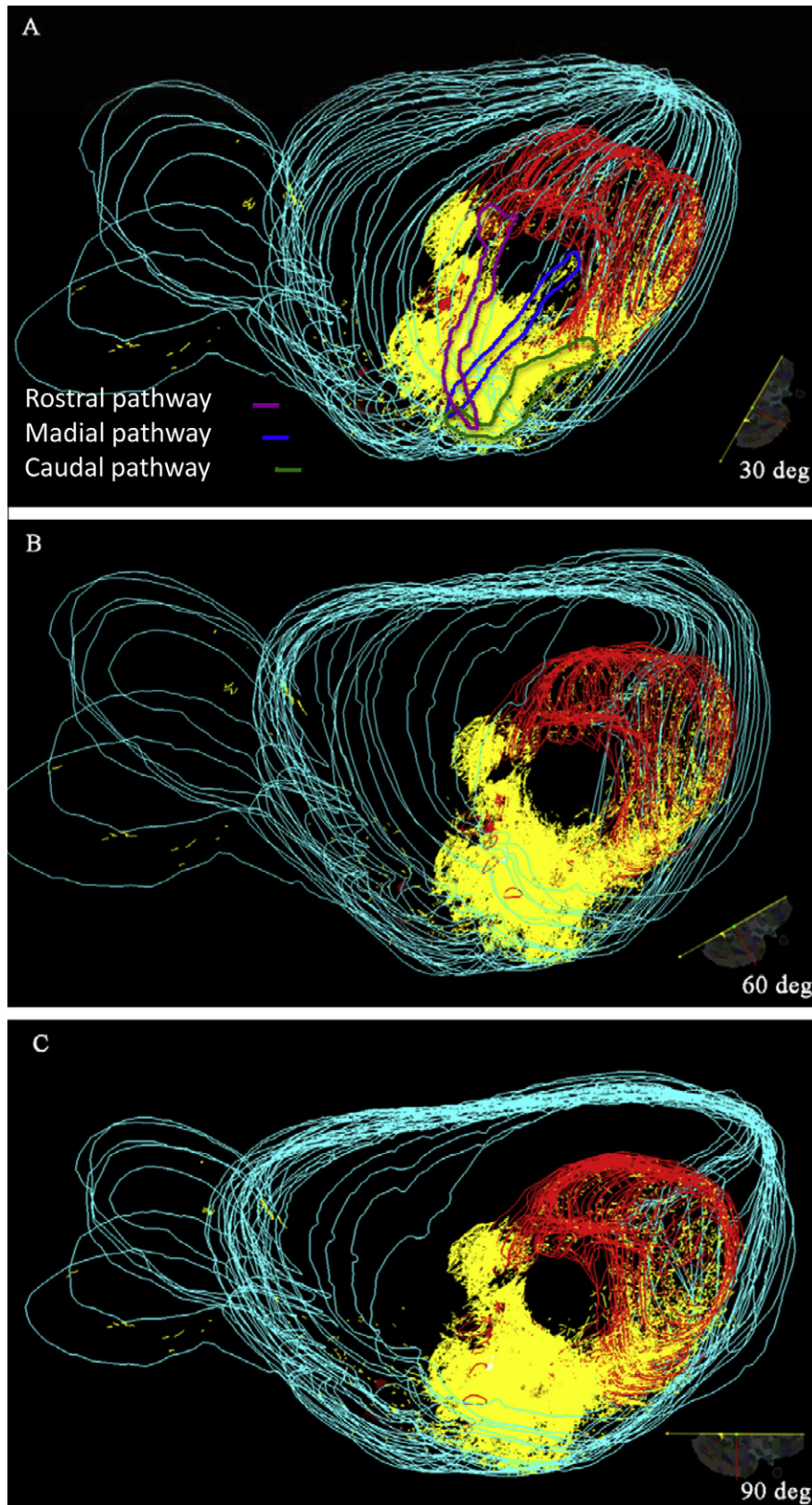


Fig. 8. Computerized 3D “one-to-one” mapping of AVP-ir fibres in sagittal sections (hypothalamic PVN and SON as the medial border, extending to stratum oriens of ventral CA1 as the lateral border). Three pathways are delineated as follows (see the Results section for detailed descriptions): the rostral pathway (purple outline, “Hyp-sepfi-dHi path”); the medial pathway (blue outline, “Hyp-ic-fimria path”); and the caudal pathway (green outline: “Hyp-amyg-vHi path”). Bright red lines delineate the hippocampus; yellow lines denote the AVP-ir fibres and the turquoise lines are the outlines of the sagittal sections. (A) 30° rotation from the front view. (B) 60° rotation from the front view. (C) Lateral view from lateral edge.

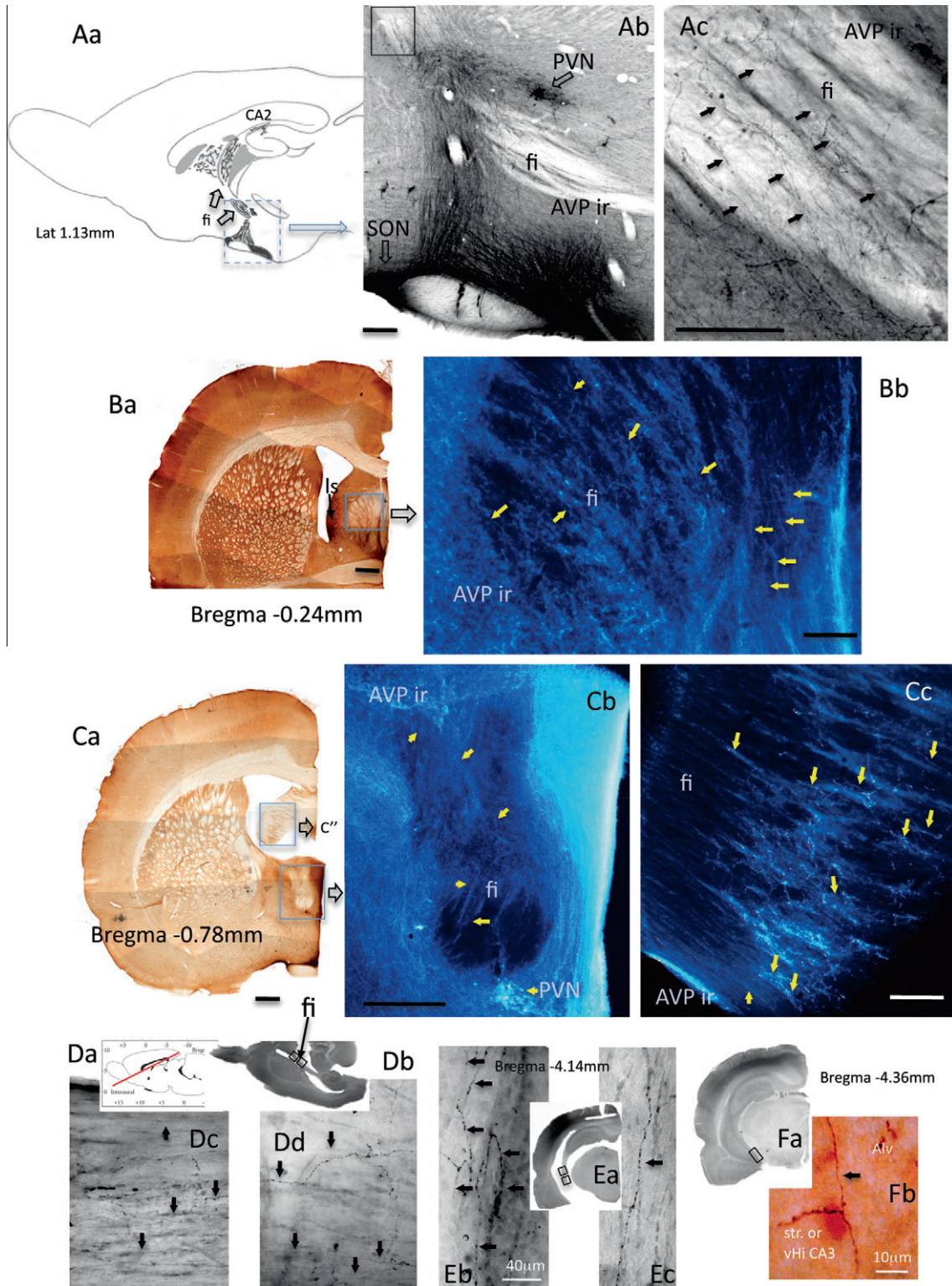


Fig. 9. Relevant anatomical features of the rostral pathway: hypothalamo-septo-fimbria-dHi-vHi. (Aa) Tracing showing that AVP-containing fibres from PVN and SON followed the fornix fibre-system dorso-rostrally into the dorsal hippocampus (dHi) where the CA2 received AVP + fibres. (Ab) AVP-immuno-positive fibres from SON and PVN projecting dorso-rostrally joining the fornix–fimbria fibre-system (fi). (Ac) AVP-immuno-positive fibres can be clearly seen on the surface of fi. Panels B (Bregma –0.24 mm) and C (Bregma –0.78 mm) show abundant AVP fibres observed inside the fimbria (fi) at different coronal levels. Panels D show the AVP fibres inside the fi in semi-horizontal section (insets). Panels E show the abundant straight AVP fibres inside the ventral fimbria–alveus. It was not rare to observe the straight AVP fibres inside the alveus (Alv) making orthogonal turn to go inside the str. or. (panels F). Arrows indicate the straight AVP fibres in parallel to the fornix–fimbria–alveus fibre-systems. Is, lateral septum. The blue pictures are negative digital pictures to enhance the fibre-visualization. Scale bars for Ab, Ba, Ca, Cb: 500 µm; for Ac, Bb and Cc: 100 µm; others were indicated in the figures.

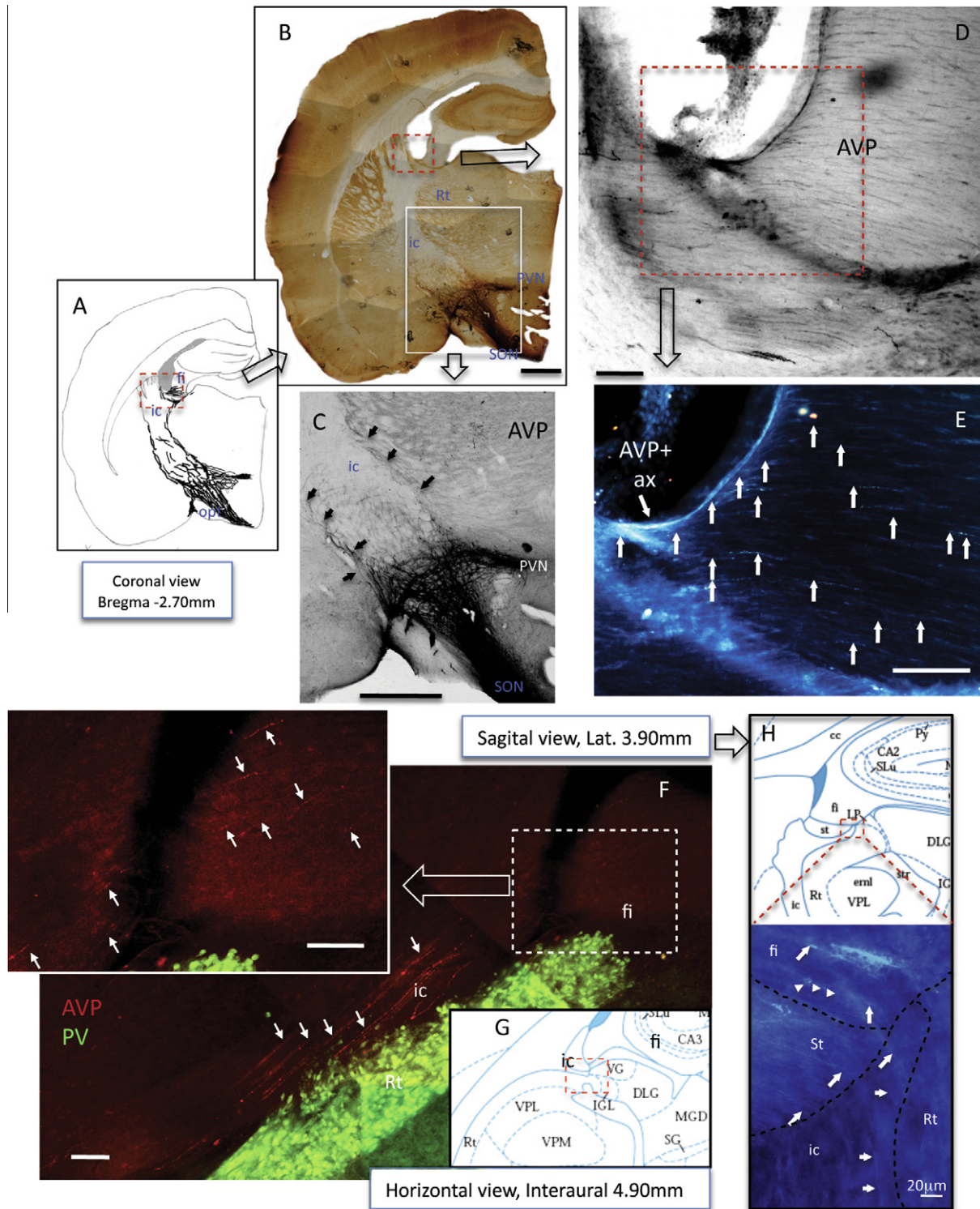


Fig. 10. Relevant anatomical features of the medial pathway. Hypothalamo-ic-fimbria pathway is depicted in coronal, horizontal and sagittal sections. (A, B) Drawing and low-power photomicrograph showing that considerable amount of AVP-immuno-positive fibres from both SON and PVN magnocellular nuclei project latero-postero-dorsally into the internal capsule (ic). (C) AVP-immuno-positive fibres (arrows) on the surface of ic. (D, E) A dense bundle of AVP+ fibres was observed in the lateral boarder of fimbria contacting the ic (around the relative coordinates of Bregma -2.70 mm to -3.10 mm; lateral 3.90 mm, and interaural 4.90 mm). Once entering the fimbria, the fibres travelled in a radial fashion medially (E: Negative digital photo to enhance the fibre visualization inside the fimbria). (F, G) Horizontal view of the above location, the fibres originating from SON and PVN travelled caudo-dorso-laterally and can be clearly seen on the border between of the reticular thalamic nucleus (Rt, parvalbumin immunofluorescence reaction in green) and ic in a *straight* and *parallel* fashion (arrows). In the adjacent fimbria (F, inset), AVP fibres (arrows) continued in the same direction and fashion. Panel H is the same location with a sagittal view. Solid arrows indicate AVP axons; fi, fimbria; ic, internal capsule; st, stria terminalis; rt, reticulo-thalamic nucleus. Scale bars: B and C: $500\ \mu\text{m}$; and for D, E, F and inset: $100\ \mu\text{m}$.

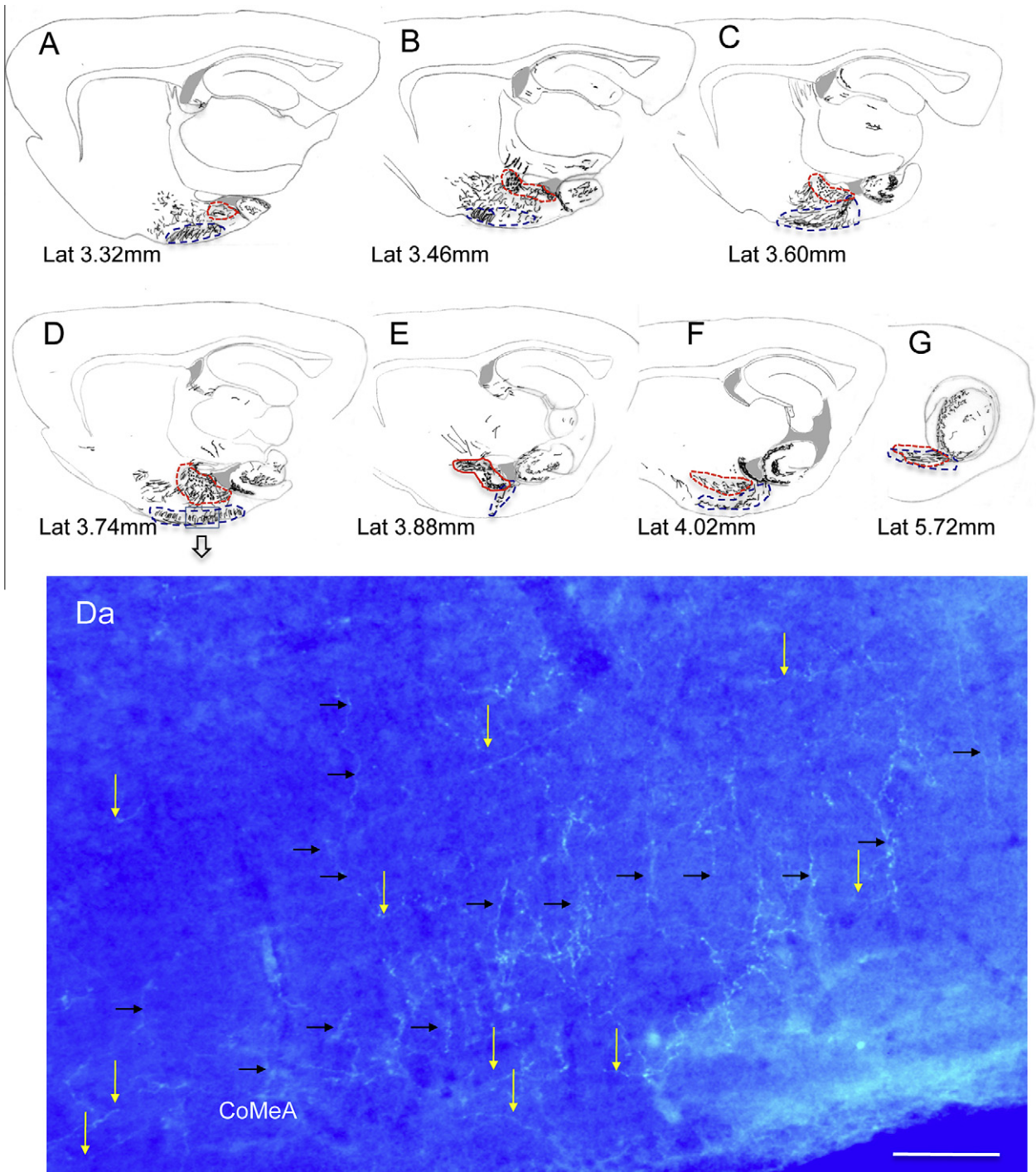


Fig. 11. Relevant anatomical features of the caudal pathway. The caudal route of AVP fibres from hypothalamic magnocellular neurons projected to ventral hippocampus was via cortico-medial-amygdala and lateral amygdala. (A–G) Chartings of selective sagittal sections showing AVP projections originated in SON, towards cortico-medial amygdala (CoMeA) and ventral hippocampus. The outlines showed a coarse separation of two different types of fibres observed under light microscope: the straight fibres seen in cortico-medial amygdala (CoMeA, blue) and the winding, highly branched fibres in medial amygdala (red). Some of these fibres in the blue outlined route made almost orthogonal turns to enter the amygdalo-hippocampal cortex (panels D and Da). The yellow arrows indicate the parallel straight fibres and the black arrows indicate the vertical fibres to the cortical surface. The group H: the AVP projections from hypothalamic SON and PVN to ventral hippocampus (vHi) were also found projecting in a caudo-lateral fashion via the lateral amygdala division and entered the vHi region through external capsule-alveus (indicated by arrowheads in Ha and Hb). For panels Hc and Hd, arrows indicate vasopressin-immuno-positive fibres in three fashions: the white ones indicate the fibres inside hippocampus, the yellow ones indicate the straight fibres projecting to hippocampus through basolateral (BLA) amygdala and the black ones indicate the winding and highly branched ones in the central and medial amygdala and in the bed nucleus of stria terminalis intraamygdaloid division (BSTIA). AHi, amygdalo-hippocampal transition zone; BNST, bed nucleus of stria terminalis. Scale bars: Da, Hc, Hd and He 50 μ m; Hb: 500 μ m.

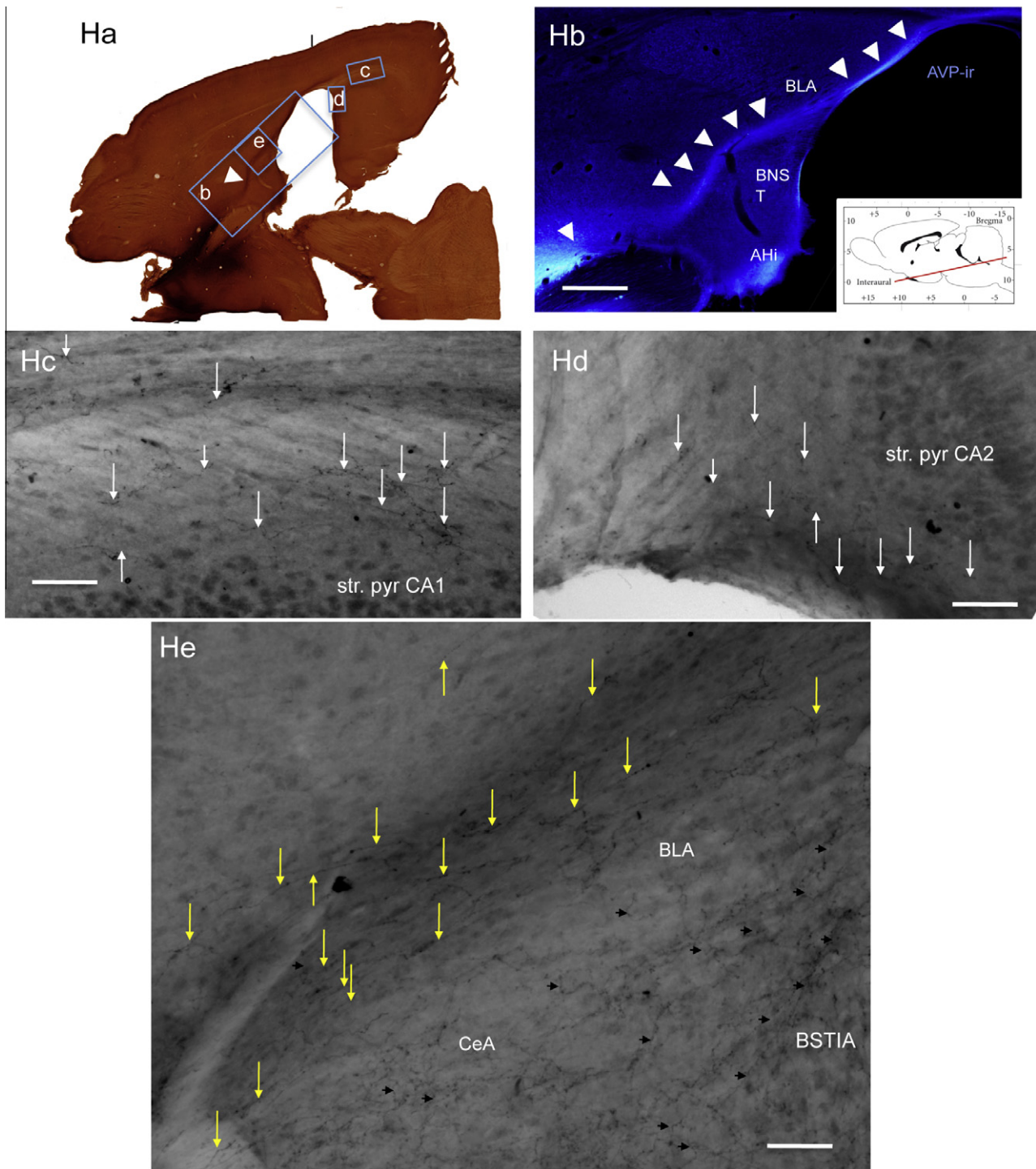


Fig. 11. (continued)

lateral septum, medial amygdala and thalamic lateral habenular nucleus (Buijs and Swaab, 1979; Rood and De Vries, 2011) and mouse suprachiasmatic nuclei (Castel et al., 1990; Rood and De Vries, 2011). The results from our study demonstrated that, in the first place, both types, the thick axons (type A) with a high ratio between dense-core vesicles and small clear vesicles and the thin axons (type B) with a low ratio of this parameter, were able to establish conventional

synaptic connections. The large axon terminals establishing synaptic contact were less frequent than the small ones according to our observational experience throughout the EM study as we mentioned in the Results section. This observation points to the possibility of the “terminal fields” extrasynaptic release of AVP, as recently suggested in other study (Rood and De Vries, 2011). However, pyramidal neuron’s dendrites, dendritic spines and axonic spines (these last

ones were from the vHi CA3 subfield) were among the type I synaptic targets. The presynaptic AVP+ terminals innervating the previous elements were large and the content of dcv was high (Fig. 3G–K). Glutamatergic neurons form prominent cell populations in the SON and PVN (Ziegler et al., 2002) and neurosecretory nonapeptide/glutamate co-release has been demonstrated (Ziegler et al., 2002; Hrabovszky et al., 2007). This experimental evidence corroborates our observation and altogether suggests that the hypothalamic magnocellular AVP-containing neurons may be the source of this excitatory innervation of ventral hippocampal CA2–3 pyramidal neurons.

The AVP axons establish type II synapses on the interneuron dendrites. Although the precise identities of the postsynaptic interneurons remained unclear, according to the IR features observed by confocal microscopy and the location, the “O-LM”, “interneuron specific type I–III” and “enkephalin-expressing” interneurons are amongst the candidates targeted by AVP+ axons (Somogyi, 2010). The thin diameter and the high content of small clear vesicles of type B fibres seen under EM, suggest that the soma locations of these axons should be elsewhere other than the hypothalamic magnocellular nuclei. The currently accepted source of vasopressinergic projection to hippocampus, i.e. the parvocellular AVP-containing neurons located in the BNST and medial amygdala in rats (Sofroniew, 1985; Caffé et al., 1987; van Wimersma-Greidanus et al., 2000) could be the sources.

The present study describes for the first time the hypothalamic source of AVP innervation in the hippocampus using Fluoro-Gold neurotracing, immunohistochemical and neuroanatomical methods coupled with computerized reconstruction. Fluoro-Gold injection into the hippocampus revealed retrograde labelled AVP-positive cells in hypothalamic supraoptic and paraventricular nuclei. There are several technical issues concerning this observation that we considered important to discuss here. The *iontophoretic* application of FG in the disclosed regions with highest AVP innervation contributed essentially to the success of this part of the experiment. The region issue was corroborated by the fact that our first attempt to label the ventral-lateral CA2, str. lacunosum moleculare coordinates yielded almost no FG labelling in hypothalamic magnocellular nuclei (Table 2, subjects “vHi1”, “vHi2”, “vHi3”). Concerning the possibility of indirect capture of FG by the PVN and SON magnocellular neurons from the cerebral-spinal fluid or from the bloodstream, we consider that it is highly improbable in our case, using the protocol we described. It has been demonstrated that Fluoro-Gold injected in high concentrations in the lateral ventricle produces a diffuse labelling around the ventricles; however it was reported that there was no retrograde transport of the tracer from the circumventricular organs (Schmued and Fallon, 1986). When 50 μm of a 5% Fluoro-Gold solution (or similar dose) was injected i.v., labelling in PVN and SON neurons was reported (Ambalavanar and Morris, 1989). In our case, however,

the Fluoro-Gold was delivered iontophoretically through a glass micropipette with an aperture of around 40 μm , filled with 1% of Fluoro-Gold solution, applied in CA2 region. In the accurate labelled cases, the labelling regions had a diameter <350 μm . Hence, it is very unlikely that a significant amount of this substance could reach the general circulation and during a very short period, before being eliminated, retrogradely label a significant amount of the magnocellular neurons in the SON and PVN, still observable 28 days later. This possibility is also discarded by the observation of no labelling in the subfornical organ (SFO), a brain region that lacks a brain–blood-barrier (Fig. 6E). Another important technical factor is the usage of cacodylate buffer (Yamaguchi et al., 2011). Sodium cacodylate is an organic arsenic compound that is metabolized to produce inorganic, trivalent arsenate *in vivo*. Because arsenate is a phosphate analogue, it can enter cells via phosphate transport systems and interfere with the cell metabolism through uncoupling oxidative phosphorylation from energy production. It also interferes with glycolysis by forming 1-arseno-3-phosphoglycerate instead of 1,3-bisphosphoglycerate (see Sigma product information sheet) (Sigma–Aldrich, 2012). After analyzing the possible VP-pathways, we realized that if hypothalamic magnocellular neurons project to hippocampus, the projection length from the soma to the targets could be as long as 10 mm. Hence, we considered that there was a need for longer time-intervals between retrograde tracer FG injection and perfusion, i.e. 3–4 weeks. In this case, a general slowdown of cellular metabolic rate, which had taken up the FG, would help to find the labelling after such long intervals. The results showed that when the iontophoretic injection was made precisely into the densest regions of AVP innervations, a number of AVP-containing neurons of hypothalamic SON and PVN were labelled with the characteristic weak long-term perikarya lysosome labelling (Schmued and Fallon, 1986; Wessendorf, 1991; Persson and Havton, 2009).

There have been a small number of reports dealing specifically with the extrinsic inputs and outputs of the hippocampus CA2 region (Amaral and Lavenex, 2007). However, it has been demonstrated that CA2 field received particularly prominent innervation from the posterior hypothalamus, in particular from the supramammillary area and tuberomammillary nucleus (Magloczky et al., 1994; Amaral and Lavenex, 2007). In a recent study, the group led by W.S. Young had demonstrated a vasopressinergic projection from the PVN to the mouse hippocampal CA2 using various adeno-associated viruses that express fluorescent proteins (personal communication) that is in agreement with our observations.

Through the detailed anatomical study of the serial sections cut in four different planes (i.e. sagittal, coronal, septo-temporal and horizontal) and 3D NeuroLucida visualization, we could conclude intuitively that the most significant route for hypothalamic AVP projection to the hippocampus was the caudal one. AVP fibres from SON mainly projected caudally to neurohypophysis through

the medial eminence and infundibular stem. This has been one of the best-described neurosecretory pathways (Hou-Yu et al., 1986). However, we have observed that quite a few fibres continued caudo-laterally, passing through the tuberomammillary and supramammillary areas entering the CoMeA and then turned dorsally to the amygdalo-hippocampal transition area, some of them entered the ventral hippocampus (Figs. 10 and 11). Haglund et al. (1984) made anterograde transport studies with the lectin phaseolus vulgaris leucoagglutinin (PHA-L) and concluded that fibres from the supramammillary nucleus innervate all parts of the hippocampal formation. However, Lee et al. (1988) later demonstrated that PHA-L could also be retrogradely transported. Hence, the possibility that AVP passing axons in the supra- and tuberomammillary areas could also take up the PHA-L and the possibility of a bi-directional transport of this tracer cannot be excluded. Furthermore, Inyushkin et al. (2009), using *in vivo* electrophysiological recording, demonstrated a clear dual projection system, neurohypophyseal and central, from the AVP-immuno-positive magnocellular neurons of the SON and suggested the existence of projections from these neurons in the SON that are much more widespread and longer than had previously been suspected. On the other hand, a substantial amount of AVP fibres from magnocellular PVN and SON, projected caudo-laterally to medial amygdala (MeA) and bed nucleus of stria terminalis, intra-amygdaloid division (BSTIA) – region where scattered AVP-ir parvocellular neurons, were also observed in our study (data not shown) and FG/AVP retrogradely labelled cells were presented (Fig. 6). However, in this region both thick and thin axons were clearly observed (Fig. 6D) and a great amount of AVP-ir fibres converged under the lateral ventricle to project caudally to ventral hippocampus (Fig. 11A–G, dashed red line delineated zone). Since the region of MeA and BNST also served as a key intermediate region where the AVP fibres from the hypothalamus passed through, the previous lesion and tracer studies (De Vries and Buijs, 1983; Caffè et al., 1987) suggesting that the BNST and MeA were the sources of hippocampal AVP fibres cannot exclude the hypothalamic origin.

FUNCTIONAL IMPLICATIONS

Our results concerning the hypothalamic AVP-containing magnocellular neurons projecting to the hippocampus are consistent with experimental evidence of a significant increase of AVP in the perfusate at both 30 and 60 min after a hypertonic stressor observed by Landgraf et al. (1988) and behaviour results from our studies (Hernandez et al., 2012) in which i.p. administration of 900 mM saline (2% of body weight, b.w.) is able to impair the Morris water-maze performance 2 h later in young adult male rats with a potentiated hypothalamic vasopressinergic system, due to neonatal maternal separation (Hernandez et al., 2012; Zhang et al., 2012). Administration of an AVP V_{1B} receptor-selective antagonist, SSR149515, restored the impaired learning (Hernandez et al., 2012). These data

indicate a close functional relationship between the hypothalamic magnocellular vasopressin system and the hippocampus.

CONCLUSION

Altogether, the present data highlight for the first time distinctive features that make the vasopressin fibres a unique subcortical peptidergic innervation to the hippocampus: (1) the AVP fibres extensively innervate the ventral hippocampus and sparsely but significantly innervate the rostral portion of the dorsal hippocampus, mainly in the CA2 region; (2) the AVP axons in the hippocampus establish conventional synapses with the hippocampal neurons: the large axon terminals with a high content of large-granulated vesicles establish type I synapses on ventral CA2–3 pyramidal neuron dendrites, dendritic spines and axon spines whereas the small axon terminals with a high content of small clear vesicles establish type II synapses onto interneuron dendrites; (3) the AVP axons in stratum oriens maintain a strong-contacting relationship with mGluR1 α -expressing interneuron dendrites; (4) FG retrograde tracing revealed an important AVP projection from the hypothalamic SON and PVN to the hippocampus. Thus, it appears that an important source of hypothalamic VP in the hippocampus are the magnocellular hypothalamic nuclei, but the AVP-expressing neurons located in the amygdala and the BNST reported previously may also contribute.

The synaptic innervation of the hippocampus by the magnocellular hypothalamic nuclei indicates that in addition to exerting a modulatory role through V_{1A} and V_{1B} G protein-coupled receptors, these fibres may have an additional fast synaptic action, possibly through co-transmission via ionotropic receptors. Like other subcortical modulatory pathways to the hippocampus the magnocellular nuclei may act partly via direct action on principal cells and partly via modulating GABAergic action of select populations of interneurons.

Acknowledgements—This study was supported by grants: CONACYT: 79641, 127777 and PAPIIT-UNAM: IN218111. A part of this work was done while L.Z. was on sabbatical leave at the MRC Anatomical Neuropharmacology Unit, Oxford University supported by fellowships from UNAM and CONACYT Mexico. We are thankful to R.M. Buijs for his gift of an antibody against AVP and for his helpful discussions; to M. Morales, H.L. Wang for suggestions on Fluoro-Gold retrograde tracing; to P. Somogyi for advice and comments on an earlier version of the manuscript; to D. Roberts, K. Detzner, J.D. Swinny (MRC, Oxford), H. González, M.P. Medina, M. Tapia, M.J. Gómora and E. Pinzon (UNAM, Mexico City) and A. López (IN-CAN, Mexico City) for excellent technical assistance, to M. Morales, J. Tukker and R. Lujan for critical reading of the manuscript and to A.T. Nava-Kopp (UNAM) and Christel Kopp (Univ. Ottawa) for language editing.

REFERENCES

- Amaral D, Lavenex P (2007) Hippocampal neuroanatomy. In: Andersen P. et al., eds. The hippocampus book. Oxford, New York: Oxford University Press. p. 37–114.

- Ambalavanar R, Morris R (1989) Fluoro-Gold injected either subcutaneously or intravascularly results in extensive retrograde labelling of CNS neurones having axons terminating outside the blood–brain barrier. *Brain Res* 505:171–175.
- Barberis C, Mouillac B, Durroux T (1998) Structural bases of vasopressin/oxytocin receptor function. *J Endocrinol* 156:223–229.
- Barberis C, Tribollet E (1996) Vasopressin and oxytocin receptors in the central nervous system. *Crit Rev Neurobiol* 10:119–154.
- Bielsky IF, Hu SB, Ren X, Terwilliger EF, Young LJ (2005) The V1a vasopressin receptor is necessary and sufficient for normal social recognition: a gene replacement study. *Neuron* 47:503–513.
- Birnbaumer M (2000) Vasopressin receptors. *Trends Endocrinol Metab* 11:406–410.
- Buijs RM (1978) Intra- and extrahypothalamic vasopressin and oxytocin pathways in the rat. Pathways to the limbic system, medulla oblongata and spinal cord. *Cell Tissue Res* 192:423–435.
- Buijs RM (1980). Vasopressin and oxytocin innervation of the rat brain: a light- and electronmicroscopical study, vol. Doctor in Medical Science. Amsterdam: Universiteit van Amsterdam. p. 133.
- Buijs RM, Swaab DF (1979) Immuno-electron microscopical demonstration of vasopressin and oxytocin synapses in the limbic system of the rat. *Cell Tissue Res* 204:355–365.
- Buijs RM, PCW, Van Heerikhuizen JJ, Sluiter AA, Van de Sluis PJ, Ramkema M, Van der Woude TP, Van der Beek E (1989) Antibodies to small transmitter molecules and peptides: production and application of antibodies to dopamine, serotonin, GABA, vasopressin, vasoactive intestinal peptide, neuropeptide Y, somatostatin and substance P. *Biomedical Research* 10:213–221.
- Caffe AR, van Leeuwen FW, Luiten PG (1987) Vasopressin cells in the medial amygdala of the rat project to the lateral septum and ventral hippocampus. *J Comp Neurol* 261:237–252.
- Caldwell HK, Lee HJ, Macbeth AH, Young 3rd WS (2008) Vasopressin: behavioral roles of an “original” neuropeptide. *Prog Neurobiol* 84:1–24.
- Castel M, Feinstein N, Cohen S, Harari N (1990) Vasopressinergic innervation of the mouse suprachiasmatic nucleus: an immunoelectron microscopic analysis. *J Comp Neurol* 298:172–187.
- Chen C, Diaz Brinton RD, Shors TJ, Thompson RF (1993) Vasopressin induction of long-lasting potentiation of synaptic transmission in the dentate gyrus. *Hippocampus* 3:193–203.
- Chepkova AN, Kapai NA, Skrebitskii VG (2001) Arginine vasopressin fragment AVP(4–9) facilitates induction of long-term potentiation in the hippocampus. *Bull Exp Biol Med* 131:136–138.
- Daitz HM, Powell TP (1954) Studies of the connexions of the fornix system. *J Neurol Neurosurg Psychiatry* 17:75–82.
- De Vries GJ, Buijs RM (1983) The origin of the vasopressinergic and oxytocinergic innervation of the rat brain with special reference to the lateral septum. *Brain Res* 273:307–317.
- Dubrovsky B, Tatarinov A, Gijsbers K, Harris J, Tsiodras A (2003) Effects of arginine-vasopressin (AVP) on long-term potentiation in intact anesthetized rats. *Brain Res Bull* 59:467–472.
- Goodson JL (2008) Nonapeptides and the evolutionary patterning of sociality. In: Neumann IDLR, editor. *Advances in vasopressin and oxytocin: from genes to behaviour to disease*. Amsterdam: Elsevier. p. 3–15.
- Haglund L, Swanson LW, Kohler C (1984) The projection of the supramammillary nucleus to the hippocampal formation: an immunohistochemical and anterograde transport study with the lectin PHA-L in the rat. *J Comp Neurol* 229:171–185.
- Hatton GI (1990) Emerging concepts of structure-function dynamics in adult brain: the hypothalamo-neurohypophysial system. *Prog Neurobiol* 34:437–504.
- Hernandez VS, Ruiz-Velazco S, Zhang L (2012) Differential effects of osmotic and SSR149415 challenges in maternally separated and control rats: the role of vasopressin on spatial learning. *Neurosci Lett* 528:143–147.
- Hernando F, Schoots O, Lolait SJ, Burbach JP (2001) Immunohistochemical localization of the vasopressin V1b receptor in the rat brain and pituitary gland: anatomical support for its involvement in the central effects of vasopressin. *Endocrinology* 142:1659–1668.
- Hou-Yu A, Lamme AT, Zimmerman EA, Silverman AJ (1986) Comparative distribution of vasopressin and oxytocin neurons in the rat brain using a double-label procedure. *Neuroendocrinology* 44:235–246.
- Hrabovszky E, Deli L, Turi GF, Kallo I, Liposits Z (2007) Glutamatergic innervation of the hypothalamic median eminence and posterior pituitary of the rat. *Neuroscience* 144:1383–1392.
- Ibragimov R (1989) The effect of neurohypophysial peptides on the formation of conditioned active avoidance behavior. *Fiziol Zh SSSR Im I M Sechenova* 75:8–12.
- Inyushkin AN, Orlans HO, Dyball RE (2009) Secretory cells of the supraoptic nucleus have central as well as neurohypophysial projections. *J Anat* 215:425–434.
- Kosaka T (1980) The axon initial segment as a synaptic site: ultrastructure and synaptology of the initial segment of the pyramidal cell in the rat hippocampus (CA3 region). *J Neurocytol* 9:861–882.
- Landgraf R, Neumann I, Schwarzberg H (1988) Central and peripheral release of vasopressin and oxytocin in the conscious rat after osmotic stimulation. *Brain Res* 457:219–225.
- Landgraf R, Neumann ID (2004) Vasopressin and oxytocin release within the brain: a dynamic concept of multiple and variable modes of neuropeptide communication. *Front Neuroendocrinol* 25:150–176.
- Lee CL, McFarland DJ, Wolpaw JR (1988) Retrograde transport of the lectin *Phaseolus vulgaris* leucoagglutinin (PHA-L) by rat spinal motoneurons. *Neurosci Lett* 86:133–138.
- Lolait SJ, O’Carroll AM, Mahan LC, Felder CC, Button DC, Young 3rd WS, Mezey E, Brownstein MJ (1995) Extrahypophysial expression of the rat V1b vasopressin receptor gene. *Proc Natl Acad Sci USA* 92:6783–6787.
- Magloczky Z, Acsady L, Freund TF (1994) Principal cells are the postsynaptic targets of supramammillary afferents in the hippocampus of the rat. *Hippocampus* 4:322–334.
- Morales M, Wang SD (2002) Differential composition of 5-hydroxytryptamine3 receptors synthesized in the rat CNS and peripheral nervous system. *J Neurosci* 22:6732–6741.
- Paxinos G, Watson C (2007) *The rat brain in stereotaxic coordinates*. San Diego, CA, USA: Academic Press.
- Persson S, Havton LA (2009) Retrogradely transported fluorogold accumulates in lysosomes of neurons and is detectable ultrastructurally using post-embedding immuno-gold methods. *J Neurosci Methods* 184:42–47.
- Peters A, Palay SL, Webster Hd (1991) *The fine structure of the nervous system: neurons and their supporting cells*. New York: Oxford University Press. pp. 138–211.
- Powell TP, Guillery RW, Cowan WM (1957) A quantitative study of the fornixmamillo-thalamic system. *J Anat* 91:419–437.
- Raggenbass M (2001) Vasopressin- and oxytocin-induced activity in the central nervous system: electrophysiological studies using in-vitro systems. *Prog Neurobiol* 64:307–326.
- Robertson GL, Shelton RL, Athar S (1976) The osmoregulation of vasopressin. *Kidney Int* 10:25–37.
- Rood BD, De Vries GJ (2011) Vasopressin innervation of the mouse (*Mus musculus*) brain and spinal cord. *J Comp Neurol* 519:2434–2474.
- Schmued LC, Fallon JH (1986) Fluoro-Gold: a new fluorescent retrograde axonal tracer with numerous unique properties. *Brain Res* 377:147–154.
- Schmued LC, Heimer L (1990) Iontophoretic injection of fluoro-gold and other fluorescent tracers. *J Histochem Cytochem* 38:721–723.
- Schmued LC, Kyriakidis K, Fallon JH, Ribak CE (1989) Neurons containing retrogradely transported Fluoro-Gold exhibit a variety of lysosomal profiles: a combined brightfield, fluorescence, and electron microscopic study. *J Neurocytol* 18:333–343.
- Schoneberg T, Kostenis E, Liu J, Gudermann T, Wess J (1998) Molecular aspects of vasopressin receptor function. *Adv Exp Med Biol* 449:347–358.

- Sigma–Aldrich (2012) Sodium cacodylate trihydrate, vol. 20, Saint Louis, Missouri.
- Sofroniew MV (1985) Vasopressin- and neurophysin-immunoreactive neurons in the septal region, medial amygdala and locus coeruleus in colchicine-treated rats. *Neuroscience* 15:347–358.
- Somogyi P (2010) Hippocampus: intrinsic organization. In: Shepherd GM, Grillner Sten, editors. *Handbook of brain microcircuits*. Oxford: Oxford University Press. p. 148–164.
- Stemmelin J, Lukovic L, Salome N, Griebel G (2005) Evidence that the lateral septum is involved in the antidepressant-like effects of the vasopressin V1b receptor antagonist, SSR149415. *Neuropsychopharmacology* 30:35–42.
- Summy-Long JY, Keil LC, Severs WB (1978) Identification of vasopressin in the subfornical organ region: effects of dehydration. *Brain Res* 140:241–250.
- Szot P, Bale TL, Dorsa DM (1994) Distribution of messenger RNA for the vasopressin V1a receptor in the CNS of male and female rats. *Brain Res Mol Brain Res* 24:1–10.
- Takacs VT, Klausberger T, Somogyi P, Freund TF, Gulyas AI (2012) Extrinsic and local glutamatergic inputs of the rat hippocampal CA1 area differentially innervate pyramidal cells and interneurons. *Hippocampus* 22:1379–1391.
- Thibonnier M, Berti-Mattera LN, Dulin N, Conarty DM, Mattera R (1998) Signal transduction pathways of the human V1-vascular, V2-renal, V3-pituitary vasopressin and oxytocin receptors. *Prog Brain Res* 119:147–161.
- Urban IJ (1998) Effects of vasopressin and related peptides on neurons of the rat lateral septum and ventral hippocampus. *Prog Brain Res* 119:285–310.
- van Wimersma-Greidanus TB, Croiset G, de Wied d (2000) Neuroendocrine regulation of learning and memory. In: Conn PM, Freeman ME, eds. *Neuroendocrinology in physiology and medicine* Totowa, New Jersey: Humana Press. p. 353–370.
- Verney EB (1947) The antidiuretic hormone and the factors which determine its release. *Proc R Soc Lond B Biol Sci* 135:25–106.
- Wessendorf MW (1991) Fluoro-Gold: composition, and mechanism of uptake. *Brain Res* 553:135–148.
- Wigger A, Sanchez MM, Mathys KC, Ebner K, Frank E, Liu D, Kresse A, Neumann ID, Holsboer F, Plotsky PM, Landgraf R (2004) Alterations in central neuropeptide expression, release, and receptor binding in rats bred for high anxiety: critical role of vasopressin. *Neuropsychopharmacology* 29:1–14.
- Yamaguchi T, Wang HL, Li X, Ng TH, Morales M (2011) Mesocorticolimbic glutamatergic pathway. *J Neurosci* 31: 8476–8490.
- Yoshida M (2008) Gene regulation system of vasopressin and corticotropin-releasing hormone. *Gene Regulat Syst Biol* 2:71–88.
- Young WS, Li J, Wersinger SR, Palkovits M (2006) The vasopressin 1b receptor is prominent in the hippocampal area CA2 where it is unaffected by restraint stress or adrenalectomy. *Neuroscience* 143:1031–1039.
- Zhang L, Hernandez VS, Liu B, Medina MP, Nava-Kopp AT, Irls C, Morales M (2012) Hypothalamic vasopressin system regulation by maternal separation: its impact on anxiety in rats. *Neuroscience* 215:135–148.
- Zhang L, Medina MP, Hernandez VS, Estrada FS, Vega-Gonzalez A (2010) Vasopressinergic network abnormalities potentiate conditioned anxious state of rats subjected to maternal hyperthyroidism. *Neuroscience* 168:416–428.
- Ziegler DR, Cullinan WE, Herman JP (2002) Distribution of vesicular glutamate transporter mRNA in rat hypothalamus. *J Comp Neurol* 448:217–229.

(Accepted 5 October 2012)
(Available online 17 October 2012)

Differential effects of osmotic and SSR149415 challenges in maternally separated and control rats: the role of vasopressin on spatial learning

Hernández V. S., Ruíz-Velazco S., Zhang L.

Neurosci Lett. 2012, 528: 143-47

My contributions in:

- Conception of the study: +++
- Performance of the experiments:
 - o Maternal separation protocol: +++
 - o Spatial learning assessment: +++
- Statistical analysis: -
- Discussion of the results: +++
- Preparation of the paper: +++

(-): No contribution; (+++); Main contribution



Differential effects of osmotic and SSR149415 challenges in maternally separated and control rats: The role of vasopressin on spatial learning

Vito S. Hernandez^a, Silvia Ruíz-Velazco^b, Limei Zhang^{a,*}

^a Departamento de Fisiología, Facultad de Medicina, Universidad Nacional Autónoma de México, México 04510, D.F., Mexico

^b Instituto de Investigaciones en Matemáticas Aplicadas y Sistemas, Universidad Nacional Autónoma de México, México 04510, D.F., Mexico

HIGHLIGHTS

- ▶ Maternal separation (MS) up-regulates the hypothalamic vasopressin (VP) system.
- ▶ i.p hypertonic saline or SSR149415 was used to up or down regulate the VP system.
- ▶ The Morris water maze (MWM), was used to test learning, after the i.p. injections.
- ▶ MS rats had impairment after hypertonic saline, and control rats after V1b antagonism.
- ▶ This data support a role for VP in learning, dependent on the individual background.

ARTICLE INFO

Article history:

Received 18 May 2012

Received in revised form 13 August 2012

Accepted 4 September 2012

Keywords:

Vasopressin
Spatial-learning
Maternal separation
SSR149415
V1b
Osmotic challenge
Morris Water Maze

ABSTRACT

Maternal separation (MS) has been demonstrated to up-regulate the hypothalamic vasopressin (VP) system. Intracerebrally released VP has been demonstrated to affect several types of animal behaviour, such as active/passive avoidance, social recognition, and learning and memory. However, the role of VP in spatial learning remains unclear. In the present study, we investigated the effects of an osmotic challenge and a V1b receptor-specific (V1bR) antagonist, SSR149415, on spatial learning of maternally separated and animal facility reared (AFR) adult male Wistar rats. The osmotic challenge was applied by injecting a hypertonic saline solution, 1 h before the Morris water maze test (MWM). V1bR antagonist SSR149415 (5 mg/kg) was injected i.p. twice (1 h and 30 min) previous to the MWM. A combined treatment with both osmotic challenge and the SSR149415 was applied to the third group whereas rats for basal condition were injected with isotonic saline. Under basal condition no differences between AFR and MS groups were observed. MS rats showed severe impairment during the MWM after the osmotic challenge, but not after the administration of SSR149415. For AFR rats, the opposite phenomenon was observed. The joint application of SSR149415 and osmotic challenge restored the spatial learning ability for both groups. The differential impairment produced by osmotic stress-induced up-regulation and SSR149415 induced V1bR blockage in MS and control rats suggested that VP involvement in spatial learning depends on the individual intrinsic ligand-receptor functional state.

© 2012 Elsevier Ireland Ltd. All rights reserved.

1. Introduction

The neuropeptide vasopressin (VP) is synthesized primarily in the paraventricular and supraoptic nuclei of the hypothalamus, secreted from the neural lobe of the pituitary into the circulation, and serves various hormonal actions on peripheral tissues: regulation of water–electrolyte balance, hepatic glucose metabolism, and cardiovascular functions [1,19]. VP secretion is regulated principally by blood osmolality and volume [14]. VP neurons also project

intracerebrally to several brain regions, particularly to limbic brain areas including the septo-hippocampal system [2,6]. It has been shown that VP and its metabolites can modulate the hippocampal theta rhythm [27] and facilitate memory processes [10,11] in intact animals. Ex vivo electrophysiological studies showed that nanomolar concentration of [Arg⁸]-vasopressin (AVP) induced a prolonged increase in the amplitude and slope of the evoked population response in the presence of 1.5 mM calcium [8]. This AVP induced potentiation of the excitatory postsynaptic potential (EPSP) persisted following removal of AVP from the perfusion medium. The AVP induced sustained increase of EPSP is known as long-term vasopressin potentiation (LTVP) [8].

VP exerts its effects through three subtypes of receptors: V1a and V1b receptors are associated with phosphoinositol turnover, while the V2 receptor activates adenylate cyclase [19]. In the brain,

* Corresponding author at: Departamento de Fisiología, Facultad de Medicina, Universidad Nacional Autónoma de México, México 04510, D.F., Mexico.
Tel.: +52 55 56232348; fax: +52 55 56232348.

E-mail address: limei@unam.mx (L. Zhang).

VP exerts its effects mainly by binding to V1a and V1b receptors. While V1a are widely distributed in the CNS [4,5,22,26], V1b receptors are much more specifically distributed [17,20,25]. Young et al. performed *in situ* hybridization histochemistry using a highly specific vasopressin V1b receptor riboprobe and found that in mice, vasopressin V1b receptors were prominently expressed in hippocampal pyramidal neurons located in the CA2 field [29]. Interestingly the short-term effects of VP mentioned before were blocked by a V1a receptor antagonist whereas the long-term facilitatory effects remained despite this antagonism [27]. Moreover, Engelmann et al., administered either vasopressin or a V1a receptor antagonist via microdialysis into the rat septum, and found a lack of effect of the antagonist, but an impairment in the Morris water maze (MWM) performance of rat treated with exogenous vasopressin [16]. This evidence implied a possible role played by the V1b receptors. However, some studies showed that V1b receptor-knockout mice had no impairment on spatial learning performance [7,15], although VP system differences between rats and mice have been reported [23].

In the present study, we hypothesized that VP could exert a fine-tuning effect of spatial learning through the V1b receptor in rat and these effects could be uncovered with up- or down-regulation of the VP system in rats.

In order to demonstrate this hypothesis, we used male adult rats reared in two neonatal conditions: animal facility reared (AFR) and neonatal maternal separation (MS). These latter ones were demonstrated to have a persistent potentiated vasopressinergic system [21,28,30]. MS increase significantly the expression of AVP mRNA and peptide in the hypothalamus and produced a faster and higher release of vasopressin to plasma when MS rats are subjected to water deprivation [30]. By using salt load which is well known to up-regulate the VP release [14] and to increase its intracerebral release [18], and a recently characterized non-peptide vasopressinergic V1b receptor antagonist SSR149415 [24] to down-regulate the VP transmission, we examined VP modulatory effects on spatial learning in both animal facility reared (AFR) and MS male rats. The results of this study show that spatial learning in MS animals is vulnerable to an osmotic challenge, while AFR animals show disrupted learning only in presence of a high dose of vasopressinergic V1b antagonist SSR149415, compared with the literature [24].

2. Materials and methods

2.1. Animals and treatment

Wistar rats from the local animal facility were used in this study. All animal procedures were approved by the local bioethical and research committees in accordance with the principles exposed in the Handbook for the Use of Animals in Neuroscience Research (Society for Neuroscience, Washington DC, 1991). Rats were housed four per cage, maintained on an inverted 12 h light schedule in a room with controlled temperature between 20°C and 24°C with ventilation and given access to standard rat chow and water *ad libitum*.

Maternal separation (3 h daily, MS3h) procedure was described elsewhere [30]. Briefly, female and male adult rats were mated for two days. During the last week of gestation, female rats were single-housed in standard rat Plexiglas cages and maintained under standard laboratory conditions. On the day after parturition, postnatal day (PND) 2, each litter was culled to 7–8 pups, in which 5–6 were males. During the period from PND2–PND16, the pups were separated daily from their dams between 0900 h and 1200 h, placed into an incubator at 29°C ± 1°C. After this period rats were returned to their home cages. After ending the maternal separation protocol, animals were left undisturbed until the weaning at PND28, when

male and female rats were separated. Four littermates were put in one cage and each one was assigned to one of the four different treatment groups. Animals were then left undisturbed until PND90 when spatial learning assessment was performed during their activity period. Animal facility reared (AFR) rats were treated in the same conditions as above mentioned except that these animals were left undisturbed in their cages during the period when MS3h rats were separated from their dam. All the cages were cleaned twice a week with minimum disturbance to the rats.

Ninety-six young adult male rats (PND90, body weight 350 ± 10 g) from 12 AFR and 12 MS3h litters, were designated to 4 treatment groups: (A) isotonic (treatment 1, T1): rats received only a 2% b.w., i.p. injection of NaCl 0.9% 1 h previous to the MWM; (B) hypertonic (T2): rats received a 2% b.w., i.p. injection of 900 mM NaCl 1 h previous to the test; (C) SSR149415 (T3): rats received a 5 mg/kg i.p. injection of SSR149415 (Axon 1114, Axon Medchem BV Amsterdam, Netherland, diluted in dimethyl sulfoxide (DMSO) first and then diluted in 0.9% saline, 1:20 respectively), twice at 1 h and 30 min time-points before the MWM test; (D) hypertonic + SSR149415 (T4): rats received combined “hypertonic” and “SSR149415” treatments as above described. Water bottles were removed at the moment of first injection for all groups until 10 min before the MWM.

2.2. Spatial learning assessment

The modified Morris water maze (MWM) procedure has been described elsewhere [31]. Briefly, a black circular pool (diameter 156 cm, height 80 cm) filled with 30 cm of water (25 ± 1°C) with distant visual cues, was used for this cognitive test. A circular black escape platform (diameter 12 cm) was submerged 1 cm below the water surface. Rats were habituated to this swimming task (without the presence of the platform) a week before the MWM. On the day of the test, rats were allowed up to 60 s to locate the escape platform. If the allowed time ended and the experimental subjects had not found the platform, they were guided to it. Once on the platform, rats were permitted to stay for 10 s and allowed to observe their location. Each rat underwent 8 sequential trials on the same day, with an inter-trial interval of approximately 5 min. The time required to locate the hidden platform in each trial was recorded.

2.3. Statistical analyses

Quantitative results were expressed as mean ± standard error of the mean (SEM). Groups were tested for differences by performing three and two way mixed models analysis of variance followed by Bonferroni post hoc test using STATA 11. Differences were considered statistically significant at a value of * $p < 0.05$; ** $p < 0.01$; *** $p < 0.001$.

3. Results

The three way mixed model analysis of variance of the MWM test showed a significant effect of treatment ($F_{3,704} = 17.37$ $p < 0.0001$) and trial ($F_{7,704} = 382.15$, $p < 0.0001$), whereas no significant effect is showed of group (AFR and MS), but the three factors and all the two factors interactions are statistically significant ($F_{21,704} = 3.25$ $p = 0.01$, $F_{21,704} = 8.21$ $p < 0.001$, $F_{7,704} = 3.40$ $p = 0.05$, $F_{3,704} = 22.32$ $p = 0.001$), therefore we used two way mixed models analysis of variance for each level of (AFR & MS) and each level of treatment. For the two groups we found that the interaction between treatment and trial is statistically significant whereas for each treatment only in SSR149415 treatment (T3) (Fig. 1C) this interaction is statistically significant (Table 1).

No significant difference in spatial learning performance was observed between the AFR and the MS3h groups when isotonic

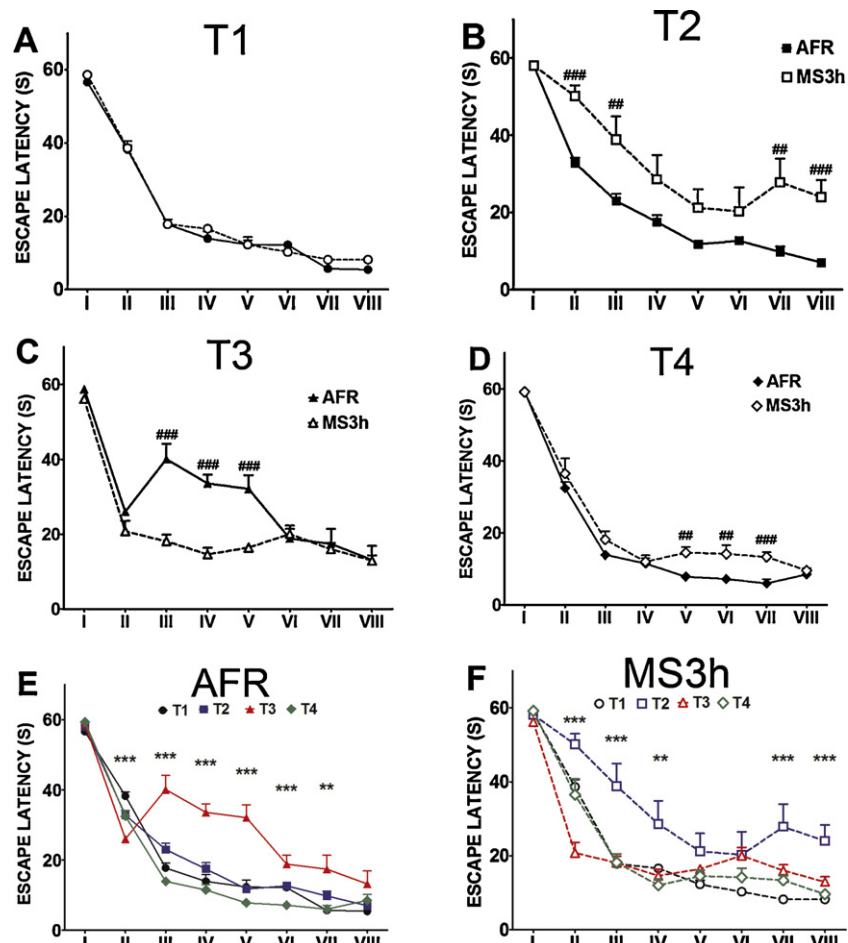


Fig. 1. Spatial learning performance assessed by Morris water maze test (MWM). Tests were performed in adult male rats (postnatal day 90, PND90), from two rearing conditions: animal facility reared (AFR) and neonatal maternal separation (MS3h), after receiving 4 different treatments: (A) isotonic (T1); (B) hypertonic (T2); (C) SSR149415 (T3); (D) hypertonic + SSR149415 (T4). Panel E and F compare the effects of each of the treatments within the AFR (E) and MS3h (F) groups separately. Detailed statistical significance is shown in Table 1. Data show mean \pm SEM ($n=12$) of escape latency across 8 trials. *, **, *** represent 0.05, 0.01 and 0.001 significance differences between treatments for different trials and different groups (MS and AFR). #, ##, ### represent 0.05, 0.01, 0.001 significance differences between rearing groups for different treatments and trials. See Table 1 for details on statistical significance differences.

treatment (T1) was administered (Fig. 1A). In the hypertonic treatment (T2), the MS3h group showed markedly increased escape latencies compared to AFR group at II, III, VII and VIII trials (Fig. 1B). The MS3h hypertonic group also showed significant impairment in spatial learning at the III, VII and VIII trials when compared to the MS3h isotonic group (Fig. 1F, blue line (T2) vs. black line (T1) respectively and Table 1, right panel, intersection of T2 and T1 for trial III, VII and VIII). The hypertonic treatment (T2) had no significant effect on MWM performance in the AFR group (Fig. 1E, blue line (T2) vs. black line (T1) respectively and Table 1, left panel, intersection of T2 and T1 for each trial). In the AFR group (Fig. 1E), the V1b receptor antagonist SSR149415 treatment (T3) produced significant differences on learning performance when compared to isotonic treatment (T1) with significant differences at trials II, III, IV, V, VI and VII (Fig. 1E, red line (T3) vs. black line (T1)), Table 1, left panel, intersection of T3 and T1 for those trial), whereas in MS3h animals, the SSR149415 (T3) produced significant differences on learning performance only at trial II compared to isotonic treatment (T1) (Fig. 1F, red line (T3) vs. black line (T1)). There were also significant differences at trials III, IV and V if the comparison was made between AFR and MS3h groups treated with SSR149415 (T3) (Fig. 1C). Interestingly, an apparent initial improvement (significant shorter escape time latencies) of the water maze performance was observed at the trial II in both AFR and MS3h rats treated with SSR149415 (T3) (Fig. 1 E and F, red lines (T3) vs. black lines

(T1)). When combined treatment (T4) was applied, both hypertonic and SSR149415, deleterious effects on spatial learning performance were effectively cancelled and performance reversed to the isotonic levels compared with the same rearing condition groups (Fig. 1E and 1F, green line (T4) vs. black line (T1)).

4. Discussion

This is the first study in the literature reporting the modulatory effects by up- and down-regulating the vasopressinergic system on spatial learning. Our data showed that the application of an osmotic challenge, which is known to strongly up-regulate the VP system [14], disrupted spatial learning only in the MS3h subjects, whereas a high dose of the V1b receptor-specific antagonist, SSR149415, markedly impaired the water maze performance in AFR subjects, while little effect was observed on the MS3h performance. Both impairments were effectively reversed by a combined treatment of both challenges.

The hippocampus seems to be the site of AVP action on memory processes [3]. Landgraf et al. showed that an hypertonic saline challenge caused a significant rise in plasma VP and an increase in extracellular VP content within the hippocampus, at both 30 and 60 min after intraperitoneal injection [18]. VP metabolite AVP4-9 enhanced learning and memory during a radial maze test and hippocampal lesions blocked this enhancing effect [12]. The

Table 1

Significance values table: Left panel shows statistically significant differences between treatments for different trials in the AFR group. **** represent 0.05, 0.01 and 0.001 significance differences. #, ##, ###, represent 0.05, 0.01, 0.001 significance differences between groups (MS3h and AFR) for different treatments and trials. Right panel shows statistically significant differences between treatments for different trials in the AFR group. T1: isotonic treatment; T2: hypertonic treatment; T3: SSR149415 treatment; T4 hypertonic + SSR149415 treatment. AFR: animal facility reared, MS3h: maternal separation 3 h.

AFR trial1	T1	T2	T3	T4
T1				
T2				
T3				
T4				
AFR trial2	T1	T2	T3	T4
T1				
T2		###		
T3	***	***		
T4	*		*	
AFR trial3	T1	T2	T3	T4
T1				
T2		##		
T3	***	***	###	
T4			***	
AFR trial4	T1	T2	T3	T4
T1				
T2				
T3	***	***	###	
T4			***	
AFR trial5	T1	T2	T3	T4
T1				
T2				
T3	***	***	###	
T4			***	##
AFR trial6	T1	T2	T3	T4
T1				
T2				
T3	*	*		
T4			***	##
AFR trial7	T1	T2	T3	T4
T1				
T2		##		
T3	**			
T4			**	###
AFR trial8	T1	T2	T3	T4
T1				
T2		###		
T3				
T4				
MS3h trial1	T1	T2	T3	T4
T1				
T2				
T3				
T4				
MS3h trial2	T1	T2	T3	T4
T1				
T2				
T3	**	***		
T4		*	**	
MS3h trial3	T1	T2	T3	T4
T1				
T2	***			
T3		***		
T4		***		
MS3h trial4	T1	T2	T3	T4
T1				
T2				
T3		*		
T4		**		
MS3h trial5	T1	T2	T3	T4
T1				
T2				
T3				
T4				
MS3h trial6	T1	T2	T3	T4
T1				
T2				
T3				
T4				

Table 1 (Continued)

MS3h trial7	T1	T2	T3	T4
T1				
T2	***			
T3				
T4		**		
MS3h trial8	T1	T2	T3	T4
T1				
T2	***			
T3		**		
T4		***		

intracerebrovascular administration of vasopressin enhanced LTP in dentate gyrus [13] and long-lasting enhancement of synaptic excitability of CA1/subiculum neurons of the rat ventral hippocampus by vasopressin was demonstrated with *in vitro* preparation [9]. Moreover, Engelmann et al. showed that vasopressin administration via microdialysis into the septum, interfered with the spatial learning and memory during the Morris water maze task (MWM) [16]. Our data obtained under situations where vasopressinergic neurotransmission was up-regulated by osmotic stressor or down-regulated by V1bR antagonist blockage suggested that VP involvement in spatial learning depends on the individual intrinsic ligand-receptor functional state and are in concordance with the previous data.

Several previous studies have shown that MS produces long-lasting up-regulation of the vasopressin system [21] but little is known about the effects of MS on spatial memory in rats. Our results showed that MS exerted no effect on spatial learning under basal conditions (T1). However, when rats were subjected to an osmotic challenge, impairment in the acquisition of spatial learning was displayed. This leads to speculate that the enhanced vasopressinergic system of MS offspring under basal conditions is well regulated by homeostatic mechanisms during water maze task, but not when the osmotic stressor is present – the further increase of VP content in the hippocampus would disrupt this cognitive task. In this study we show that this rearing-generated differences in AVP system anatomy-physiology can be exploited as an instrument to uncover the subtle role of VP played in spatial learning processes.

There are few and controversial studies assessing whether or not the V1b receptor has influence in hippocampal dependent learning. For instance, Egashira et al. found that KO mice for V1b receptor displayed preserved spatial learning in an 8-arm radial maze test [15], while Murgatroyd et al. [21] showed that mice that underwent MS3h, presented impairment in the hippocampus dependent step-down avoidance learning test and treatment with V1b receptor antagonist, SSR149415, partially reversed the learning impairment. The obtained results of this study using SSR149415 support the idea that in rats, V1b receptor is involved in the modulation of spatial learning.

Acknowledgements

This work was supported by grants PAPIIT-IN218111, DGAPA-UNAM and 79641, 127777 from CONACyT-Mexico. VSH was supported by CONACyT PhD scholarship. We thank M. P. Medina and E. Pinzón for technical assistance.

References

- [1] M.A. Abramova, A. Calas, M. Ugrumov, Vasopressinergic neurons of the supraoptic nucleus in perinatal rats: reaction to osmotic stimulation and its regulation, *Brain Structure and Function* 215 (2011) 195–207.
- [2] B. Alescio-Lautier, V. Paban, B. Soumireu-Mourat, Neuromodulation of memory in the hippocampus by vasopressin, *European Journal of Pharmacology* 405 (2000) 63–72.
- [3] B. Alescio-Lautier, B. Soumireu-Mourat, Role of vasopressin in learning and memory in the hippocampus, *Progress in Brain Research* 119 (1998) 501–521.

- [4] C. Barberis, E. Tribollet, Vasopressin and oxytocin receptors in the central nervous system, *Critical Reviews in Neurobiology* 10 (1996) 119–154.
- [5] I.F. Bielsky, S.B. Hu, X. Ren, E.F. Terwilliger, L.J. Young, The V1a vasopressin receptor is necessary and sufficient for normal social recognition: a gene replacement study, *Neuron* 47 (2005) 503–513.
- [6] R.M. Buijs, Intra- and extrahypothalamic vasopressin and oxytocin pathways in the rat. Pathways to the limbic system, medulla oblongata and spinal cord, *Cell and Tissue Research* 192 (1978) 423–435.
- [7] H.K. Caldwell, H.-J. Lee, A.H. Macbeth, W.S. Young, Vasopressin: behavioral roles of an original neuropeptide, *Progress in Neurobiology* 84 (2008) 1–24.
- [8] C. Chen, R.D. Diaz Brinton, T.J. Shors, R.F. Thompson, Vasopressin induction of long-lasting potentiation of synaptic transmission in the dentate gyrus, *Hippocampus* 3 (1993) 193–203.
- [9] A.N. Chepkova, P. French, D. De Wied, A.H. Ontskul, G.M. Ramakers, V.G. Skrebitski, W.H. Gispen, I.J. Urban, Long-lasting enhancement of synaptic excitability of CA1/subiculum neurons of the rat ventral hippocampus by vasopressin and vasopressin(4–8), *Brain Research* 701 (1995) 255–266.
- [10] D. de Wied, J.M. van Ree, Neuropeptides, mental performance and aging, *Life Sciences* 31 (1982) 709–719.
- [11] D. de Wied, T.B. Van Wimersma Greidanus, B. Bohus, The rat supraoptic-neurohypophyseal system and behavior: role of vasopressin in memory processes, *Problemes Actuels d'Endocrinologie et de Nutrition Series* 18 (1974) 323–328.
- [12] A. Dietrich, J.D. Allen, Vasopressin and memory. I. Lesions to the hippocampus block the memory enhancing effects of AVP 4–9 in the radial maze, *Behavioural Brain Research* 87 (1997) 201–208.
- [13] B. Dubrovsky, A. Tatarinov, K. Gijbbers, J. Harris, A. Tsiodras, Effects of arginine-vasopressin (AVP) on long-term potentiation in intact anesthetized rats, *Brain Research Bulletin* 59 (2003) 467–472.
- [14] F.L. Dunn, T.J. Brennan, A.E. Nelson, G.L. Robertson, The role of blood osmolality and volume in regulating vasopressin secretion in the rat, *Journal of Clinical Investigation* 52 (1973) 3212–3219.
- [15] N. Egashira, K. Mishima, K. Iwasaki, R. Oishi, M. Fujiwara, New topics in vasopressin receptors and approach to novel drugs: role of the vasopressin receptor in psychological and cognitive functions, *Journal of Pharmacological Sciences* 109 (2009) 44–49.
- [16] M. Engelmann, J. Bures, R. Landgraf, Vasopressin administration via microdialysis into the septum interferes with the acquisition of spatial memory in rats, *Neuroscience Letters* 142 (1992) 69–72.
- [17] F. Hernandez, O. Schoots, S.J. Lolait, J.P. Burbach, Immunohistochemical localization of the vasopressin V1b receptor in the rat brain and pituitary gland: anatomical support for its involvement in the central effects of vasopressin, *Endocrinology* 142 (2001) 1659–1668.
- [18] R. Landgraf, I. Neumann, H. Schwarzberg, Central and peripheral release of vasopressin and oxytocin in the conscious rat after osmotic stimulation, *Brain Research* 457 (1988) 219–225.
- [19] J. Laycock, Laycock, introduction to vasopressin, in: J. Laycock (Ed.), *Perspectives on Vasopressin*, Imperial College Press, 2010, pp. 1–20.
- [20] S.J. Lolait, A.M. O'Carroll, L.C. Mahan, C.C. Felder, D.C. Button, W.S. Young 3rd, E. Mezey, M.J. Brownstein, Extrahypothalamic expression of the rat V1b vasopressin receptor gene, *Proceedings of the National Academy of Sciences of the United States of America* 92 (1995) 6783–6787.
- [21] C. Murgatroyd, A.V. Patchev, Y. Wu, V. Micale, Y. Bockmühl, D. Fischer, F. Holsboer, C.T. Wotjak, O.F.X. Almeida, D. Spengler, Dynamic DNA methylation programs persistent adverse effects of early-life stress, *Nature Neuroscience* 12 (2009) 1559–1566.
- [22] M. Raggenbass, Vasopressin–oxytocin-induced activity in the central nervous system: electrophysiological studies using in vitro systems, *Progress in Neurobiology* 64 (2001) 307–326.
- [23] B.D. Rood, G.J. De Vries, Vasopressin innervation of the mouse (*Mus musculus*) brain and spinal cord, *Journal of Comparative Neurology* 519 (2011) 2434–2474.
- [24] C. Serradeil-Le Gal, J. Wagnon, J. Simiand, G. Griebel, C. Lacour, G. Guillon, C. Barberis, G. Brossard, P. Soubrié, D. Nisato, M. Pascal, R. Pruss, B. Scatton, J.-P. Maffrand, G. Le Fur, Characterization of (2S,4R)-1-[5-chloro-1-[(2,4-dimethoxyphenyl)sulfonyl]-3-(2-methoxy-phenyl)-2-oxo-2,3-dihydro-1H-indol-3-yl]-4-hydroxy-N,N-dimethyl-2-pyrrolidine carboxamide (SSR149415), a selective and orally active vasopressin V1b receptor antagonist, *The Journal of Pharmacology and Experimental Therapeutics* 300 (2002) 1122–1130.
- [25] J. Stemmelin, L. Lukovic, N. Salome, G. Griebel, Evidence that the lateral septum is involved in the antidepressant-like effects of the vasopressin V1b receptor antagonist, SSR149415, *Neuropsychopharmacology* 30 (2005) 35–42.
- [26] P. Szot, T.L. Bale, D.M. Dorsa, Distribution of messenger RNA for the vasopressin V1a receptor in the CNS of male and female rats, *Brain Research. Molecular Brain Research* 24 (1994) 1–10.
- [27] I.J. Urban, Effects of vasopressin and related peptides on neurons of the rat lateral septum and ventral hippocampus, *Progress in Brain Research* 119 (1998) 285–310.
- [28] A.H. Veenema, A. Blume, D. Niederle, B. Buwalda, I.D. Neumann, Effects of early life stress on adult male aggression and hypothalamic vasopressin and serotonin, *The European Journal of Neuroscience* 24 (2006) 1711–1720.
- [29] W.S. Young, J. Li, S.R. Wersinger, M. Palkovits, The vasopressin 1b receptor is prominent in the hippocampal area CA2 where it is unaffected by restraint stress or adrenalectomy, *Neuroscience* 143 (2006) 1031–1039.
- [30] L. Zhang, V.S. Hernandez, B. Liu, M.P. Medina, A.T. Nava-Kopp, C. Irlles, M. Morales, Hypothalamic vasopressin system regulation by maternal separation: its impact on anxiety in rats, *Neuroscience* 215 (2012) 135–148.
- [31] L. Zhang, V.S. Hernandez, M. Medina-Pizarro, P. Valle-Leija, A. Vega-Gonzalez, T. Morales, Maternal hyperthyroidism in rats impairs stress coping of adult offspring, *Journal of Neuroscience Research* 86 (2008) 1306–1315.

Hypothalamic vasopressin system regulation by maternal separation: its impact on anxiety in rats

Zhang L., Hernández V. S., Liu B., Medina M. P.,
Nava-Kopp A. T., Irles C, Morales M

Neuroscience. 2012, 215: 135-48.

My contributions in:

- Conception of the study: ++
- Performance of the experiments:
 - o Maternal separation protocol: ++
 - o Immunohistochemistry: +++
 - o *In-situ* hybridization: -
 - o Measurement of PVN and SON volumes: +++
 - o 3D-Plot of vasopressinergic neurons in hypothalamic nuclei: ++
 - o Behavioral assessment for anxiety: +++
 - o Measurement of AVP plasma concentrations: +++
 - o Spatial learning assessment: +++
- Statistical analysis: +
- Discussion of the results: +++
- Preparation of the paper: ++

(-): No contribution; (+): Average contribution; (++): Important contribution; (+++); Main contribution

HYPOTHALAMIC VASOPRESSIN SYSTEM REGULATION BY MATERNAL SEPARATION: ITS IMPACT ON ANXIETY IN RATS

L. ZHANG,^{a,*†} V. S. HERNÁNDEZ,^{a†} B. LIU,^b
M. P. MEDINA,^a A. T. NAVA-KOPP,^a C. IRLES^a AND
M. MORALES^{b,*}

^aDepartamento de Fisiología, Facultad de Medicina, Universidad Nacional Autónoma de México, Mexico City 04510, Mexico

^bIntramural Research Program, Neuronal Network Section, National Institute on Drug Abuse, Biomedical Research Center, Baltimore, MD 21224, USA

Abstract—Maternal separation (MS) has been used to model the causal relationship between early life stress and the later stress-over-reactivity and affective disorders. Arginine vasopressin (AVP) is among several factors reported to be abnormal. The role of AVP on anxiety is still unclear. In order to further investigate this causal relationship and its possible role in anxiogenesis, male rat pups were separated from their dams for 3 h daily (3hMS) from post-natal day (PND) 2 to PND15. Fos expression in AVP+ neurons in the hypothalamic paraventricular (PVN) and supraoptic nuclei (SON) triggered by 3hMS, and AVP-mRNA expression, were examined at PND10 and PND21 respectively, whereas AVP-mRNA expression, PVN and SON volumes and plasma AVP concentration were assessed in adulthood. Elevated plus maze test (EPM) and Vogel conflict test (VCT) were also performed to evaluate unconditioned and conditioned anxious states at PND70–75. At PND10, a single 3hMS event increased Fos expression in AVP+ neurons fourfold in PVN and six to twelvefold in SON. AVP-mRNA was over-expressed in whole hypothalamus, PVN and SON between 122% and 147% at PND21 and PND63. Volumes of AVP-PVN and AVP-SON measured at PND75 had marked increases as well as AVP plasma concentration at 12 h of water deprivation (WD). MS rats demonstrated a high conditioned anxious state under VCT paradigm whereas no difference was found under EPM. These data demonstrate direct relationships between enhanced AVP neuronal activation and a potentiated vasopressin system, and this latter one with high conditioned anxiety in MS male rats. © 2012 IBRO. Published by Elsevier Ltd. All rights reserved.

Key words: maternal separation, arginine vasopressin, paraventricular nucleus, supraoptic nucleus, Vogel conflict test, elevated plus maze.

INTRODUCTION

Seymour Levine's group first reported the effects of early life experience on emotionality and stress-responsiveness in adult rats half a century ago (Levine, 1957; Levine et al., 1957). Following this discovery, rodent maternal separation (MS) models have been widely used to investigate the effects of early postnatal adversity at adulthood. Plotsky, Meaney and others had developed a relatively standardized handling/MS model for manipulating early postnatal interaction between mother rats and their pups (Plotsky and Meaney, 1993; Wigger and Neumann, 1999; Lehmann and Feldon, 2000; Cirulli et al., 2003). The most widely studied paradigm consists of periods of daily separation (usually 3 h) performed from post-natal day (PND) 2 to PND14 (Fumagalli et al., 2007). While it is a generally accepted idea that MS permanently changes the offspring's neuroendocrine and behavioral stress reactivity, the factors that promote the sustained effects of early-life stress have not yet been fully elucidated (Wigger and Neumann, 1999; Lehmann and Feldon, 2000; Cirulli et al., 2003).

It has been shown that protracted periods (3 h or more) of separation from the dam may increase the hypothalamus–pituitary–adrenal axis (HPA) activity in pups, and may also increase the stress reactivity during adulthood (Anisman et al., 1998). Our classical understanding of the HPA axis comprises that the release of corticotropin-releasing factor (CRF) and vasopressin (VP) from the paraventricular nucleus (PVN) of the hypothalamus elicits pituitary adrenocorticotropin hormone (ACTH) secretion, which in turn, provokes release of the adrenal glucocorticoids. In addition to a considerable amount of reports describing CRF-ACTH-glucocorticoids secretion and their receptor abnormalities observed in the MS rodent model (Kuhn and Schanberg, 1998; Kalinichev et al., 2002; Fumagalli et al., 2007; Korosi and Baram, 2009), VP system has been reported to undergo developmental changes from the perinatal period through adulthood and MS was shown to disrupt this age-dependent changes. It is interesting to observe that there is a controversy about levels of AVP in MS rodent models, which were found either increased (Murgatroyd et al., 2009; Veenema and Neumann, 2009), decreased (Desbonnet et al., 2008) or unchanged (Oreland et al., 2010) in the hypothalamus, whereas no information about the possible

*Corresponding authors. Address: Departamento de Fisiología, Facultad de Medicina, UNAM, Av. Universidad 3000, Col. Universidad Nacional Autónoma de México, México 04510, D.F., Mexico. Tel/fax: +52-55-56232348 (L. Zhang), tel: +1-443-740-2717; fax: +1-443-740-2817 (M. Morales).
E-mail addresses: limei@unam.mx (L. Zhang), MMORALES@intra.nida.nih.gov (M. Morales).

† Authors contributed equally to this study.
Abbreviations: 3hMS, procedure of maternal separation for 3 h; AFR, animal facility-reared pups; AVP, arginine vasopressin; DEPC, diethyl pyrocarbonate; ELISA, Enzyme linked ImmunoSorbent Assay; EPM, elevated plus maze test; ISH, *in situ* hybridization; mRNA, messenger ribonucleic acid; MS, maternal separation; MS3h, experimental group of maternal separation 3 h (PND2–PND14); PND, post-natal day; PVN, paraventricular nucleus; SON, supraoptic nucleus; VCT, Vogel conflict test; VP, vasopressin; WD, water deprivation.

physiological mechanism(s) underlying this abnormality, regulated by neonatal recurrent MS, is available.

Vasopressin (VP, also widely known as antidiuretic hormone, ADH) is nonapeptide synthesized mainly in magnocellular neurons in the supraoptic nucleus (SON) and PVN of the hypothalamus. Its foremost physiological functions are the regulation of water-electrolyte metabolism, hepatic glucose metabolism, and cardiovascular function in adults (Hatton, 1990). However, together with another nonapeptide, oxytocin, VP is an important generator of behavioral diversity (Goodson, 2008) and provides an integrational neural substrate for the dynamic modulation of behaviors by endocrine and sensory stimuli (Goodson and Bass, 2001).

During ontogenesis, VP contributes to the regulation of proliferation and morphogenesis of the target cells and organs (brain, pituitary, kidney and liver) (Boer, 1987). VP system is known to be activated around birth when VP contributes to the establishment of a new equilibrium in the body fluids and the adaptation of the fetuses to the stress of the labor (Oosterbaan et al., 1985). Following birth, VP induces a redistribution of the blood flow via the cardiovascular system in order to increase blood volume in the vital organs and those responsible for stress reaction (brain, pituitary gland, heart, adrenals), while reducing the blood flow in other peripheral organs (Pohjavuori and Fyhrquist, 1980). Afterward, the physiological role of VP extends to the regulation of the cardiovascular system, water re-absorption in kidney (Dlouha et al., 1982; Siga and Horster, 1991) and glucogenolysis in liver (Ostrowski et al., 1993). Although the physiological mechanism(s) underlying the observed modification of vasopressin system by MS is currently unknown, a recent surprising report from Makara's group demonstrated that AVP was the predominant secretagogue during the perinatal period in a maternal deprivation model using VP producing (AVP +/–) and deficient (AVP –/–) Brattleboro rat pups. Both maternal deprivation and ether inhalation induced remarkable ACTH elevation only in AVP +/– pups, supporting the role of VP in HPA axis regulation. However, corticosterone (CORT) elevations were even more pronounced in AVP –/– pups, suggesting the possibility of an ACTH-independent CORT-secretion regulation (Makara et al., 2008).

AVP's promoting role on angiogenesis is also not widely accepted yet, although there have been several reports in the literature suggesting that AVP system is critically involved in angiogenesis (Landgraf and Wigger, 2002; Zhang et al., 2010). On the other hand, the role of MS on angiogenesis is currently a matter of debate. Several studies have shown that MS promotes an increase in anxiety-like behavior in different anxiety tests (Huot et al., 2002; Wigger et al., 2004; Aisa et al., 2007) while others have found no differences (de Jongh et al., 2005; Sloten et al., 2006; Hulshof et al., 2011; Lajud et al., 2011).

Therefore, the specific aims of the present study were, in the first place, to investigate whether the 3hMS paradigm was capable to modify the neuronal activation of the magnocellular AVP system using the immediate early gene product Fos as a marker of AVP neuron activation

and plasticity (Pirnik and Kiss, 2005) and, in the second place, to evaluate both short- and long-term effects of MS on AVP messenger RNA (mRNA) expression by using *in situ* hybridization (ISH) with AVP riboprobe and quantitative analysis at PND21 and PND63. It is worth mentioning that due to a discrepancy in the literature regarding the AVP-mRNA expression evaluated in adulthood of MS offspring (Desbonnet et al., 2008; Murgatroyd et al., 2009; Veenema and Neumann, 2009; Oreland et al., 2010), and the lack of evidences in the neonatal periods, we used AVP-riboprobe-ISH method, which allows observing much stronger hybridization signals due to its greater sensitivity and better signal-to-noise ratios (Herman et al., 1991; Marks et al., 1992; Grino and Zamora, 1998; Young et al., 2006). Moreover, riboprobes form more stable hybrids than oligo-probes. Further, the volumes of the magnocellular regions expressing vasopressin (AVP-SON and AVP-PVN) were morphometrically and quantitatively characterized at PND75. Finally, the hypothesis that the persistent enhancement of hypothalamic magnocellular vasopressin system should generate in rats a high anxious state, when the AVP system was selectively up-regulated, was assessed using the Vogel conflict test (VCT) for conditioned anxiety and comparing with elevated plus maze (EPM) test for unconditioned anxiety. Plasma AVP concentration during water deprivation (WD) was also measured.

EXPERIMENTAL PROCEDURES

Animals and MS procedure

Wistar rats reared from the local animal facility were used in this study. All animal procedures were approved by the local bioethical and research committees, with the approval ID 138-2009, in accordance with the principles exposed in the National Institute of Health Guide for the Care and Use of Laboratory Animals (NIH Publications No. 80-23) revised 1996.

MS (3 h daily, 3hMS) procedure was performed according to Veenema et al. previously described (Veenema et al., 2006). Briefly, female and male adult rats were mated for 2 days. During the last week of the gestation, female rats were single-housed in standard rat Plexiglas cages and maintained under standard laboratory conditions with 12:12 light–dark cycle (light on 0700), temperature maintained at $22 \pm 2^\circ\text{C}$, food and water *ad libitum*. On the day after parturition, PND2, each litter was culled to 7–8 pups, in which 5–6 were males. During the period from PND2–PND15, the pups were separated daily between 900 h and 1200 h from their dams. Pups were removed and transferred by hands previously coated with fine bedding-powder from the same cage of each litter. They were moved to an adjacent room and placed individually into a small box filled with bedding, and then put into a humid incubator with temperature maintained at $29 \pm 1^\circ\text{C}$. After the 3 h separation period, the pups were returned to the home-cage followed by reunion with their respective dam. Non-separated litters (animal facility-reared pups, AFR) were left undisturbed except for changes of the bedding twice a week and served as control groups for this study.

Experimental design

Four experiments were performed in 2 postnatal stages, neonatal and young adulthood. Experiment 1 evaluated the immediate

early gene product Fos expression in the PVN and the SON at PND10, 90 min after MS for 3 h (3hMS). Experiment 2 assessed the effects of MS on AVP messenger RNA expression in the hypothalamus at both PND21 and PND63 under basal conditions. In experiment 3, hypothalamic AVP nuclei volumes at PND75, under basal conditions, were quantitatively assessed. In experiment 4, long-term effects of MS on young adult rat unconditioned and conditioned anxious states were investigated using elevated plus maze test (EPM) and VCT, respectively. Due to the physiological up-regulation of the vasopressinergic system by the osmotic stressor in VCT (48 h of WD), plasma AVP concentration changing patterns, during the WD, were evaluated.

A total of 162 male rats were used in this study. For experiment 1, 20 PND10 rats were taken from five AFR and five MS litters. For experiment 2, 14 male rats were taken from four AFR and four MS3h litters, ($n = 3$ for PND21 ISH and $n = 4$ for PND63 ISH). For experiment 3, eight male rats were chosen from four AFR and four MS3h litters. Finally, for experiment 4, 120 rats from 20 litters (10 AFR and 10 MS3h) were used ($n = 10$ /group for behavioral tests and $n = 10$ /group for each time-point of plasma AVP concentration measurement). No siblings were used in the same experiment or same time-point for plasma AVP measurement.

Experiment 1 Evaluation of the immediate early gene product Fos expression in the hypothalamic PVN and the SON at PND10, 90 min after acute 3hMS: Fos/AVP double labeling and total Fos+ nuclei quantification

In order to test whether a single 3hMS procedure affects neuronal activation in the hypothalamic magnocellular regions containing vasopressinergic neurons, rats from both AFR and MS3h were perfused at PND10. Two treatments were applied: (1) no 3hMS procedure before perfusion-fixation and (2) 3hMS applied 90 min before perfusion-fixation. Twenty pups from ten litters (five AFR and five MS3h) were used in this experiment. Rats were deeply anaesthetized with an overdose of sodium pentobarbital (63 mg/kg, Sedalparma, México) and then perfused with 10 ml of 0.9% saline followed by 20 ml of cold fixative containing 4% of paraformaldehyde in 0.1 M sodium phosphate buffer (PB, pH 7.4) plus 15% v/v of saturated picric acid and 0.05% of glutaraldehyde for 15 min. AVP/Fos immunofluorescence reaction was performed with guinea pig anti-AVP (T-5048, 1:2000, Peninsula Laboratories) and rabbit anti-Fos (SC52, 1:1000, Santa Cruz Biotechnology, Santa Cruz, CA) as primary antibodies, incubated overnight at 4 °C with gentle shaking. After several washings, sections were further incubated with Alexa Fluor 488 donkey anti-rabbit IgG (1:1000, Molecular Probes Inc. Eugene, OR) and Cy3 conjugated donkey anti-guinea pig IgG (1:1000, Jackson ImmunoResearch Laboratories, Inc., Baltimore, PA) as secondary antibodies, in TBST plus 1% of normal horse serum (NHS), at 4 °C overnight. At the end of the immunofluorescence reaction, sections were rinsed and mounted with Vectashield (Vector Laboratories, Inc., Burlingame, CA) and analyzed by epi-fluorescence microscopy using a Nikon 50i with a N-2B long-pass emission filter. Fields in the PVN and SON regions were randomly chosen with 40 \times objective, corresponding areas of 0.22 mm² and photomicrographs were taken using a digital camera. Total number of AVP+ neurons and the number of Fos+/AVP+ neurons from the PVN and SON (3 matched sections per rat, $n = 15$) were counted. Percentages of double-labeled neurons in total AVP+ neurons were calculated.

Experiment 2: Assessment of MS effects on AVP messenger RNA expression in the hypothalamus in both postnatal stages under basal conditions

Experiment 2 comprises two sets of rats taken from eight litters (four AFR and four MS3h): set 1, six PND21 male rats and set 2, eight PND63 male rats.

Rats were deeply anesthetized with sodium pentobarbital (Sedalparma, México, 63 mg/kg b. w., i. p.) and perfused via ascending aorta with 0.9% saline followed by cold fixative containing 4% of paraformaldehyde in 0.1 M phosphate buffer (PB), pH 7.4. Brains were post-fixed with 1% paraformaldehyde in PB and kept at 4 °C until use. All solutions used had been diethyl pyrocarbonate (DEPC)-treated (0.1% v/v with gentle stir for at least 4 h at room temperature) to inactivate any residual RNase and then autoclaved to inactivate the traces of DEPC.

Two days before the start of sectioning, the brains were moved to 18% sucrose in RNase free PB + NaN₃. Another change was done one day before the sectioning and a third change with fresh sucrose solution was done 1 h before the sectioning.

Serial coronal cryosectioning (12 μ m) of whole hypothalamus (from anterior commissure to the level where ventral hippocampus appears in the rostrocaudal dimension) was made using a Leica CM1950 cryostat (Leica Microsystem, Wetzlar, 35578, Germany). Sections were collected on Leica glass insert and then transferred to a 24-well tissue culture plate with PB.

ISH was performed in 1 in 6 coronal sections as previously described (Morales and Bloom, 1997) using ³⁵S- and ³³P-UTP-labeled ribonucleotide probes. The pT7T3D-Pacl plasmid (accession number: AI072073, clone ID: 1786383 Thermo Scientific) containing rat arginine vasopressin (AVP) cDNA (602 bp, Accession number: NM_016992) was linearized with EcoRI and then transcribed *in vitro* with T3 RNA polymerase to yield antisense complementary RNA probe. The construct was verified by sequencing. The radioactivity was adjusted to 10⁷ cpm per ml hybridization buffer. Sections were mounted on coated slides, air-dried. Slides were first exposed to autoradiography film and analyzed on a phosphorimager (Fuji BAS5000, Tokyo, Japan) and then dipped in nuclear track emulsion (Eastman Kodak, Rochester, NY), and exposed for 4 weeks prior to development. Slides were counterstained with Methylene Blue for histological examination.

Data analysis. The relative abundance of AVP mRNA was measured in two fashions: (A) for whole hypothalamus AVP mRNA expression, all 1 in 6 serial sections from each rat were measured by densitometric quantification on phosphorimager digital images of autoradiograms. (B) For PVN, SON and SCN relative AVP mRNA abundances, 3–4 sections which were matched in the antero-posterior coordinates and containing each of the above-mentioned regions were digitally photographed from the counterstained slides and the silver grain precipitation areas in the studied regions were digitally measured. Fovea Pro 4.0 (Reindeer Graphics, Asheville, NC, USA) plug-in for Adobe Photoshop was used for both measurements. Data in the figures are presented as mean \pm SEM values and expressed as % of the controls.

Experiment 3: Hypothalamic AVP nuclei volume quantitative assessment at PND75 under basal conditions

Perfusion-fixation and immunohistochemistry. Eight male rats at PND75 taken from eight litters (four AFR and four MS3h) were deeply anaesthetized with sodium pentobarbital (Sedalparma México, Mexico, 63 mg/kg b. w., i. p.) and perfused via the ascending aorta with 0.9% saline followed by cold fixative containing 4% of paraformaldehyde in 0.1 M sodium phosphate buffer (PB, pH 7.4) plus 15% v/v of saturated picric acid for 15 min. Brains were removed, blocked with the help of an acrylic adult rat brain matrix (Prod No. 15062, Ted Pella, Inc, CA, USA), then thoroughly rinsed with PB. Vibratome coronal sections of 70 μ m of hypothalamus (spanning from Bregma –0.24 mm to –2.64 mm, (Paxinos and Watson, 2007)) were made immediately after perfusion to enhance the

immunoreaction (in a free floating manner). Alternative sections were then blocked with Tris buffered saline Triton X100 0.3% (TBST), plus 20% normal swine serum (NSS) for 1 h at room temperature and then incubated with rabbit anti-AVP (T-4563, 1:2000, Peninsula Laboratories, San Carlos CA, 94070) in TBST + 1% NSS at 4 °C over two nights. Finishing this lapse, sections were rinsed and proceeded for secondary antibody incubation with swine anti-rabbit IgG with horseradish peroxidase conjugated (P021702, 1:100, Dako, Denmark) in TBST + 1% NSS over night at 4 °C. This immunoreaction was developed using 3,3'-diaminobenzidine (DAB, Electron Microscopy Sciences, Hatfield, PA 19440) at 0.5% and hydrogen peroxide (H₂O₂, 0.01%) as substrates. Sections were mounted in gelatin-coated slides and allowed to dry for one day. Then were further dehydrated by passing through 100% ethanol for 5 min, then rinsed with xylene and mounted with Permount mounting medium (Fisher Scientific).

Hypothalamic vasopressinergic nuclei volume measurement. Sequenced AVP immunoreacted sections were viewed, analyzed and digitally photographed in bright-field using a Nikon Eclipse 50i microscope with a 4× objective lens and a Nikon DS digital camera. AVP positive nuclei in the hypothalamic region were grouped according to Paxinos and Watson (2007) in the PVN and SON nuclei. The cluster AVP+ neuron area inside each group was delimited using Adobe Photoshop and the area in square millimeters (mm²) was calculated with the Fovea Pro 4.0 (Reindeer Graphics, Asheville, NC, USA) plug-in for Photoshop. Volumes of each nucleus/region were determined by integrating all areas inside one group, then multiplying by 0.07 mm (the thickness of the section), times 2 (only the alternative sections were AVP-immunoreacted and measured) and times linear shrinkage constant (*K*). Linear shrinkage after the histochemical procedure was determined measuring the fresh brain diameters at optic chiasm immediately after perfusion (*L_f*) and the dehydrated coronal section widths at the same coordinates after the permanent mounting (*L_d*). Hence, $K = L_f/L_d$.

Representative 3-dimensional reconstruction of PVN. In order to visualize the directionality of the enlargement of PVN, a representative 3D digital reconstruction of PVN was made based on anatomical coordinates determined on digital photomicrographs. Briefly, one pair of AVP immunoreacted serial sections was chosen for 3D reconstruction of PVN. AVP+ neurons inside the PVN were labeled using ImageJ (NIH, MD, USA) on sequential digital photomicrographs. Magnocellular and parvocellular neurons were justified according to their long axes (magnocells were assigned to those with long axes more than 20 μm, (Armstrong, 2004)). For each of the marked neurons, coordinates (*x*, *y*) corresponding the 2D location (obtained from ImageJ, NIH, MD, USA) and *z* coordinate corresponding to the slide sequential position were obtained. Three-D plot was drawn using a computing program written in python (Python Software Foundation).

Experiment 4: MS effects on unconditioned and conditioned anxious states and neuroendocrine reactivity

Anxiety-related behavior could be measured with a variety of tests. For the purpose of this study, which was to assess the behavioral influence of the vasopressinergic system reorganization, elevated plus maze (EPM) and VCT were chosen due to their particular characteristics.

EPM. EPM is based on the conflict between the rodent nature of exploration to new environments vs. the fear of being on open and elevated alleys (Pellow and File, 1986). Hence, it was used at PND65 to assess the unconditioned acute anxious state as

described previously (Zhang et al., 2010). Briefly, the maze was made of wood, consisting of a plus-shaped platform elevated 50 cm above the floor with two closed arms (50 cm × 10 cm × 40cm) and two open arms (50 cm × 10 cm) surrounded by an upward-protruding edge of 0.5 cm connecting to the central square of 10 cm × 10 cm. This latter measure prevents the rat from falling accidentally, without jeopardizing the elemental features of the setting, hence enhances the efficacy of the test. The EPM was lit with dim red light and monitored by CCTV. The maze was cleaned with water containing a neutral detergent and dried before each trial.

Prior to the EPM test, 10 MS3h and 10 AFR randomly chosen rats, one per litter were exposed to a standard open-field box for 5 min during three consecutive days before and immediately previous to the EPM test. This procedure was made to increase the likelihood of entering the open arms of the maze, thus increasing the sensitivity of the test (Walf and Frye, 2007; Zhang et al., 2010). Rats from each experimental group underwent the EPM test during their early activity period. The test starts by placing the rat in the center of the maze heading to an open arm and then left for free exploratory activity for 5 min. The time spent on the open arms, as percentage of total time (300 s) was analyzed as a measure of unconditioned acute anxious state (exploration vs. avoidance).

VCT. VCT (Vogel et al., 1971; File et al., 2004) involves two main steps: WD for 48 h and food deprivation for the latter 24 h, and the conflict test proper. WD as long as 72 h, is well tolerated by rats with weight loss in an acceptable range (approximately 11%) and no apparent loss of physical vigor (Rowland, 2007). Completing the WD period, thirsty rats were exposed to a mild and intermittent electrical shock via a water bottle. This procedure incorporates an element of conflict whereby the subject experiences opposing and concomitant tendencies of desire of drinking for reward and of fear of a potentially aversive stimulus. An indicator of a high conditioned anxious state is when fear prevails in this conflict, where no genuine risk is present (Millan and Brocco, 2003). Hence, VCT was used to assess the conditioned acute anxious state as described previously (Zhang et al., 2010). In contrast to the EPM where the basal physiological parameters are mainly unaltered, in VCT, the vasopressinergic system is known to be up-regulated due to the WD. Hence, VCT provided an interesting paradigm to evaluate the role of a putatively altered AVP system on anxiety.

One day after the EPM test, the same experimental subjects were habituated by staying in the conflict chamber described below, without current application for 30 min each day per 4 consecutive days (started at PND70). The conflict chamber consisted in a clear Plexiglas cage (20 cm × 30 cm × 20 cm) with a metal floor and lattice lid, a water bottle with stainless steel drinking spout, a constant current shock generator with an indicator for counting the number of shocks and a video camera. During the test, a 10% dextrose-water solution (hypertonic solution) was used. The shocker leads were attached between the metal drinking spout and the grid floor. The drinking spout was isolated to avoid contact with the lid of the cage. Different shock levels (0.1–0.3 mA in steps of 0.02 mA) were assessed previously to determine the appropriate current to be used during the test (unpublished data). This was done with a different set of Wistar rats. A current of 0.22 mA was found to be optimal (i.e. it allowed animals to drink the solution with minimal discomfort).

Concluding the 48 h of WD period, the test started in a separate room and a video camera sensitive to low illumination was used for monitoring and recording the test. The test was performed during the dark period and the test-room was illuminated solely with a dim red light. At the beginning of the test, each animal was put in the test chamber and was allowed to drink for 25 s without electrical current applied. After this period, a current of 0.22 mA with a 50% duty cycle of 5 s was applied between the metal drinking spout and the floor alternately during 5 min. The number of shocks received was recorded. Ten rats of each group undertook this test.

Plasma AVP concentration measurement during WD. A hundred male rats at PND75 taken from 20 litters (10 AFR and 10 MS3h) contributed to the blood sampling. In order to characterize the plasma AVP concentration during the WD, blood samples were obtained from rat tail-tips at five time-points: before WD as basal point (Basal), after 6 h of WD (6 h WD), after 12 h of WD (12 h WD), after 24 h of WD (24 h WD) and after 48 h of WD (48 h WD). Each litter provided one and only one sample at each time-point. During the blood sampling, experimental subjects were immobilized using a restraint tube. In order to minimize the stressful effect exerted by this procedure, rats were placed in the same restraint tube (standard for rats) for 30 min during the 3 previous days of the test. At the corresponding time-point, 500 μ l of blood samples from each of the respective intact rats was collected into chilled microtubes containing 0.5 mg of EDTA on the wall (50 μ l of EDTA solution of 10 mg/ml was added to each tube, agitated and then dried inside a fridge). Samples were immediately centrifuged at 1600 \times g for 15 min at 4 °C. Plasma supernatant (200 μ l per tube) was transferred to a new tube and stored at –70 °C until the ELISA test was performed. The Arg8-Vasopressin EIA Kit (Cat. 900-017, Assay Designs, Inc., Ann Arbor, Michigan 48108, USA) was used. The experimental procedure was the one recommended by the manufacturer of the ELISA vasopressin estimation kit. Each sample was analyzed in duplicate.

Statistical analysis

Quantitative results were expressed as mean \pm SEM. The software package Prism (GraphPad Software, San Diego, CA, USA) was used. AVP mRNA expression was analyzed between AFR and MS for each brain region with an unpaired Student's *t*-test. Group normality was validated using D'Agostino & Pearson omnibus normality test. Groups were tested for differences by analysis of variance (ANOVA) followed by the Bonferroni test. Significance was accepted at $p < 0.05$. (* $p < 0.05$, ** $p < 0.01$, and *** $p < 0.001$, vs. the control group).

RESULTS

Experiment 1: Fos expression in vasopressinergic magnocellular nuclei PVN and SON after 3hMS compared with basal conditions

An acute 3hMS significantly increased the expression of the immediate early gene product Fos (a generic marker of neuronal activation) in both SON ($F_{(3, 36)} = 154.3$, $p < 0.0001$) and PVN ($F_{(3, 36)} = 179.6$, $p < 0.0001$) in AFR and MS3h at the PND10, 90 min after the 3hMS. As expected, there were few Fos+ nuclei in the AVP+ populations in PVN and SON under basal conditions (Table 1, treatment 1, and Fig. 1A, B). However, after the 3hMS (Table 1, treatment 2) the majority of this neuronal population was expressing Fos (Table 1 and Fig. 1A', B'). However, one way ANOVA failed to reveal any differences between AFR and MS3h groups under both experimental conditions.

Experiment 2: Effects of MS on AVP mRNA expression in hypothalamic regions in both postnatal stages

By using AVP antisense riboprobes and compared to AFR group at PND21, MS3h group showed a marked increase in the relative AVP mRNA abundance in the whole hypothalamus (Fig. 2A and A'). Densitometric quantification of phosphorimager digital images of the 1/6 serial, 12 μ m-thickness-coronal-section's autoradiograph

revealed an increase to $147 \pm 7.6\%$ compared to AFR ($100 \pm 1.1\%$), ($t = 12.75$, $df = 4$, $p = 0.0002$) (Fig. 2D). The relative abundance of AVP-mRNA in the PVN and SON of MS3h was significantly increased: $139.8 \pm 13.5\%$ ($t = 3.63$, $df = 22$, $p = 0.0013$) and $122.6 \pm 9.6\%$ ($t = 2.356$, $df = 22$, $p = 0.0274$) compared to AFR ($100 \pm 3.5\%$ and $100 \pm 4.7\%$) respectively (Fig. 2B, B' and D). SCN had $109 \pm 10\%$ (MS3h) vs. $100 \pm 8.4\%$ (AFR) (Fig. 2C, C' and D). Statistic analysis with Student's *t*-test failed to reveal a significant difference for SCN ($t = 0.6718$, $df = 22$, $p = 0.5084$).

At PND63, the relative expression level of AVP mRNA in the whole hypothalamus was significantly increased: $136.3 \pm 5.9\%$ compared to AFR ($100 \pm 4.8\%$); $t = 8.108$, $df = 6$, $p = 0.0002$, (Fig. 3A, A' and D). The relative abundance of AVP mRNA in the PVN and SON of MS3h was $142.8 \pm 7.3\%$ ($t = 3.813$, $df = 22$, $p = 0.001$) and $124.5 \pm 4.4\%$ ($t = 3.109$, $df = 22$, $p = 0.0051$) compared to AFR ($100 \pm 8.2\%$ and $100 \pm 6.5\%$) respectively (Fig. 3B, B' and D). SCN had $114.2 \pm 7.4\%$ (MS3h) vs. $100 \pm 3.8\%$ (AFR) (Fig. 3C, C' and D). Statistic analysis with Student's *t*-test revealed no significant differences for this latter one ($t = 1.685$, $df = 22$, $p = 0.10$).

Experiment 3: Volume analysis of AVP+ PVN, SON and SCN at PND75

MS significantly increased the volume of AVP-SON and AVP-PVN nuclei evaluated at PND75 (Fig. 4). The mean volume of AVP-SON MS3h was $0.2086 \text{ mm}^3 \pm 0.0064 \text{ mm}^3$ vs. $0.1671 \text{ mm}^3 \pm 0.0055 \text{ mm}^3$ of AFR group ($t = 4.883$, $df = 14$, $p < 0.001$). In AVP-PVN the MS3h had a volume of $0.0853 \text{ mm}^3 \pm 0.0062 \text{ mm}^3$ vs. $0.0588 \text{ mm}^3 \pm 0.0038 \text{ mm}^3$ in AFR group (Fig. 4D; $t = 4.75$, $df = 14$, $p < 0.001$).

In MS3h rats an increase was observed in the number of neurons expressing AVP in the medial portion of the PVN (data not shown). There was also an increase in the extension of the nucleus in the rostro-caudal and medio-lateral dimensions. (Fig. 4B, B' and C, C').

Experiment 4: Anxiety-like behavioral effects of MS measured at PND75

Unconditioned and conditioned anxious states were assessed using two well-validated behavioral tests, the EPM test and the VCT. EPM tests the exploration vs. avoidance state placing the rat in an unconditioned environment with the closed arm representing safety and the open-elevated arm denoting novelty, though risky. Diminished time spent in the open arms and reduced number of entries imply a higher unconditioned anxious state. The MS3h rats spent similar time lapses in the open arms ($86.2 \text{ s} \pm 6.96 \text{ s}$) as compared to AFR rats ($80.7 \text{ s} \pm 5.50 \text{ s}$) ($t = 0.6198$, $df = 18$, $p = 0.5432$) (Fig. 5A). Subsequently, rats were subjected to WD, as an osmotic stressor, for 48 h. Afterward, thirsty rats underwent the conflict test in which they had to decide between drinking water (reward) and possibly receiving a mild electrical shock (punishment) or rather stay apart from the waterspout (avoidance). MS3h rats showed a

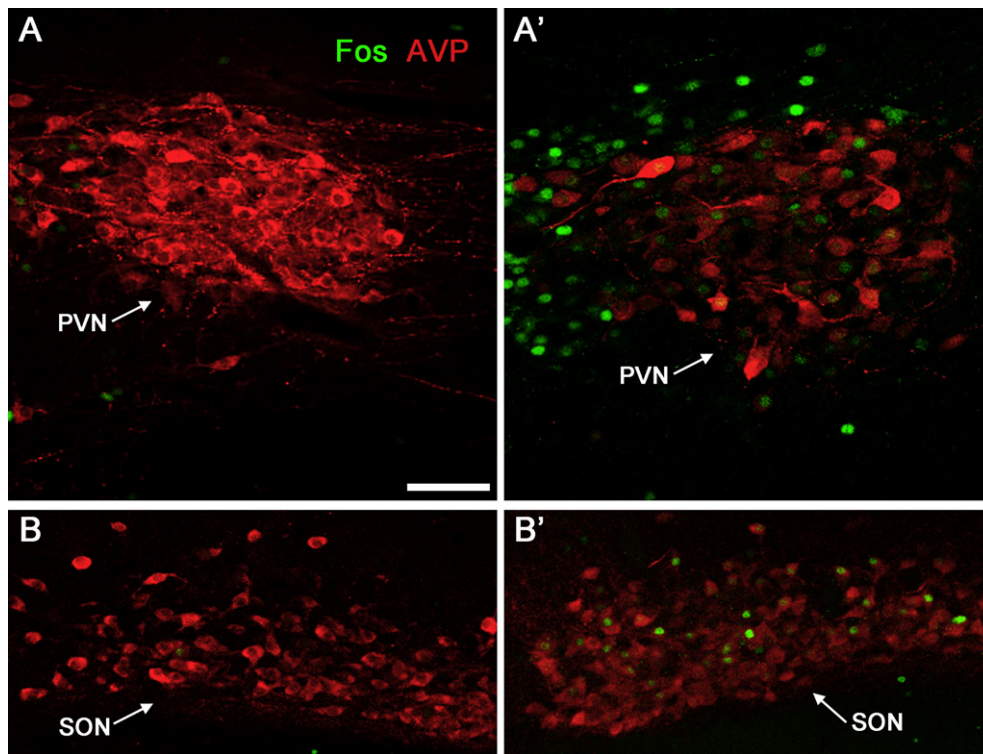


Fig. 1. Fos expression (green) in AVP containing neurons (red) of PVN and SON observed after a single acute 3hMS procedure at PND10. Panel A and B: photomicrographs of PVN and SON under basal conditions. Panels A' and B': same regions 90 min after an acute 3hMS. Scale bar = 100 μ m.

significant reduction in the number of shocks received during the 5 min of the test (11.60 ± 2.56) compared to AFR (91.4 ± 7.58) ($t = 10.04$, $df = 18$, $p < 0.0001$) (Fig. 5B), which indicates a higher anxious state triggered by this osmotic challenge. Values are expressed as mean \pm SEM.

Experiment 4: Altered plasma AVP concentration dynamics during WD

The plasma AVP concentration of MS3h group at 12 h WD had a significant increase (16.14 ± 1.15 pg/ml) compared to AFR group (12.23 ± 1.12 pg/ml) ($p < 0.05$). Two-way ANOVA indicated significant effects for time ($F_{4, 72} = 46.7$, $p < 0.0001$) and treatment ($F_{1, 72} = 14.35$, $p = 0.0013$) (Fig. 6).

DISCUSSION

The results of the present study can be summarized as follows: first, at PND10, a single 3hMS event increased Fos expression in AVP+ neurons, fourfold in PVN and 6- to 12-fold in SON, regardless of the previous 3hMS exposure. Second, AVP mRNA, revealed by an ISH method using a vasopressin riboprobe, was over-expressed in whole hypothalamus, PVN and SON at both rat neonatal stage and adulthood, which indicate that the MS produces an immediate up-regulation of the vasopressin system and a persistent re-organization of this system. The enlarged volumes of PVN and SON measured at PND75 were coherent with the ISH data. Third,

we provide evidence for a functional relationship between MS/AVP abnormalities and the shift toward a high anxious state when the potentiated AVP magnocellular system was up-regulated by WD, demonstrated also by plasma AVP values.

Fos activation triggered by a single 3hMS event and its relationship with AVP mRNA and volume analysis

The PVN and SON of the hypothalamus are major integrative sites for autonomic function by maintaining

Table 1. Fos+/AVP+ neuron percentage in total AVP+ neurons in hypothalamic paraventricular nucleus (PVN) and supraoptic nucleus (SON) at PND10

Region	Group	Treatment 1 (%)	Treatment 2 (%)	
PVN	AFR	12.6 ± 0.40	56.83 ± 2.46	$p < 0.001$
	MS3h	15.49 ± 1.28	63.7 ± 2.87	$p < 0.001$
		ns	ns	
SON	AFR	9.87 ± 2.27	58.08 ± 2.85	$p < 0.001$
	MS3h	5.02 ± 0.89	63.71 ± 2.87	$p < 0.001$
		ns	ns	

ns: not statistically significant, one-way ANOVA.

AFR: animal facility-reared rat group.

MS3h: maternal separation 3 h daily group.

Treatment 1: no maternal separation was performed before perfusion/fixation for Fos/AVP immunoreaction.

Treatment 2: Maternal separation 3 h applied in both groups, 90 min before the perfusion/fixation.

Values represent mean \pm SEM of percentages of Fos+/AVP+ in total AVP neurons in the PVN and SON.

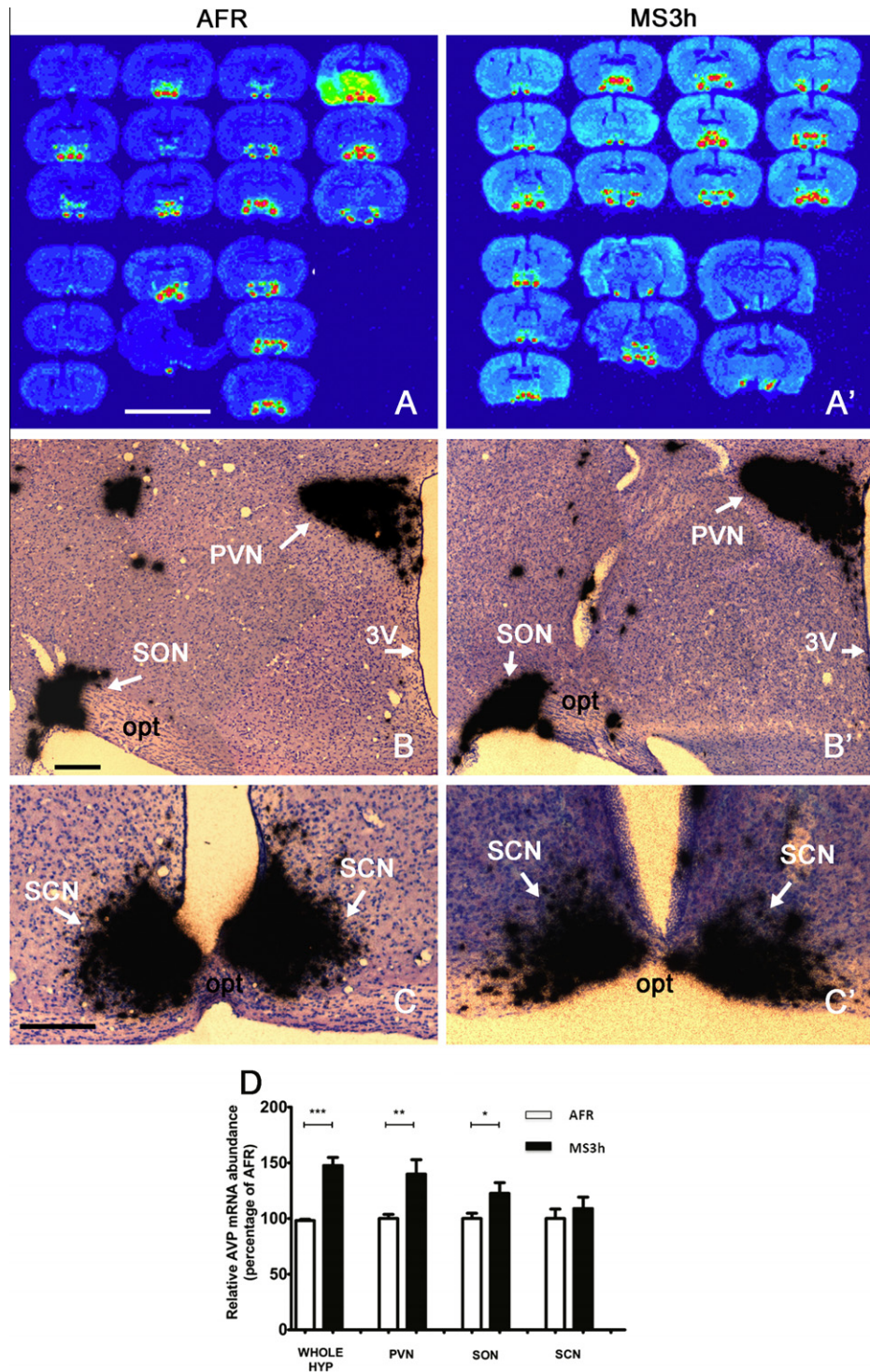


Fig. 2. Effects of maternal separation on AVP mRNA expression in hypothalamus at PND21. Panels A and A': representative (1/6) coronal section series of whole hypothalamus from animal facility-reared (AFR) and maternal separation 3h (MS3h) groups respectively. Sections were hybridized with antisense radioactive AVP riboprobe. Autoradiographs with overnight-exposure were read by phosphorimager. Note that in MS3h group there was an evident increase of section numbers that contained AVP mRNA, which indicated a rostro-caudal enlargement of the expressing regions. Panels B, B', C and C': representative bright-field photomicrographs of sections from Ilford K.5 nuclear tract emulsion dipped slides exposed in the dark at 4 °C for 4 weeks showing, B and B', increased areas in hypothalamic paraventricular nucleus (PVN) and supraoptic nucleus (SON). C and C', suprachiasmatic nucleus (SCN) had no significant difference compared to AFR. Sections were counterstained with Methylene Blue. 3V: third ventricle; opt: optic tract. Scale bars for A, and A' = 10 mm, and for B, B', C and C' = 200 μ m. Panel D: the relative abundance of AVP mRNA in selective areas. "WHOLE HYP" (whole hypothalamus), optical density of the autoradiographs of whole series of coronal sections, was related to the AVP mRNA abundance in three dimensions. PVN, SON and SCN data were obtained by 2-dimension measurement of representative coronal sections. Data are as mean \pm SEM, as % of averaged AFR. *** p < 0.001, ** p < 0.01, * p < 0.05.

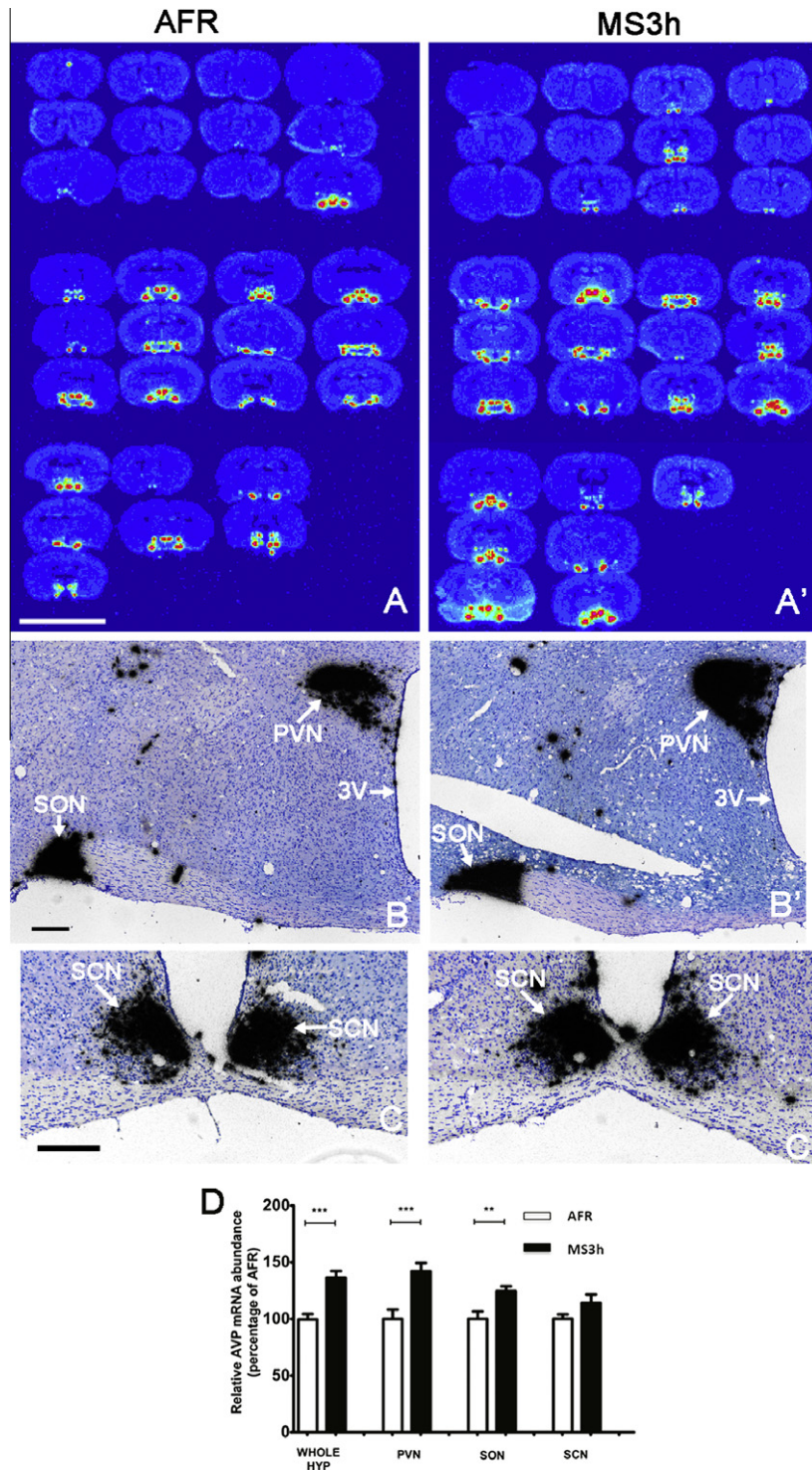


Fig. 3. Effects of MS3h on AVP mRNA expression in hypothalamus at PND63. Panels A and A': representative (1/6) coronal section series of whole hypothalamus from animal facility-reared (AFR) and maternal separation 3 h (MS3h) groups respectively. Sections were hybridized with antisense radioactive AVP riboprobe. Overnight-exposure autoradiographs were read by phosphorimager. Note that in MS3h group there was an evident increase of section numbers that contained AVP mRNA, which indicated a rostro-caudal enlargement of the expressing regions. Panels B, B', C and C': representative bright-field photomicrographs sections from Ilford K.5 nuclear tract emulsion dipped slides exposed in the dark at 4 °C for 4 weeks showing, B and B', increased areas in hypothalamic paraventricular nucleus (PVN) and supraoptic nucleus (SON). C and C', suprachiasmatic nucleus (SCN) had no significant difference compared to AFR. Sections were counterstained with Methylene Blue. 3V: third ventricle; opt: optic tract. Scale bars for A, and A' = 10 mm, and for B, B', C and C' = 200 μ m. Panel D: the relative abundance of AVP mRNA in selective areas. "WHOLE HYP" (whole hypothalamus), optical density of the autoradiographs of whole series of coronal sections, was related to the AVP mRNA abundance in three dimensions. PVN, SON and SCN data were obtained by 2-dimension measurement of representative coronal sections. Data are as mean \pm SEM, as % of averaged AFR. *** p < 0.001, ** p < 0.01.

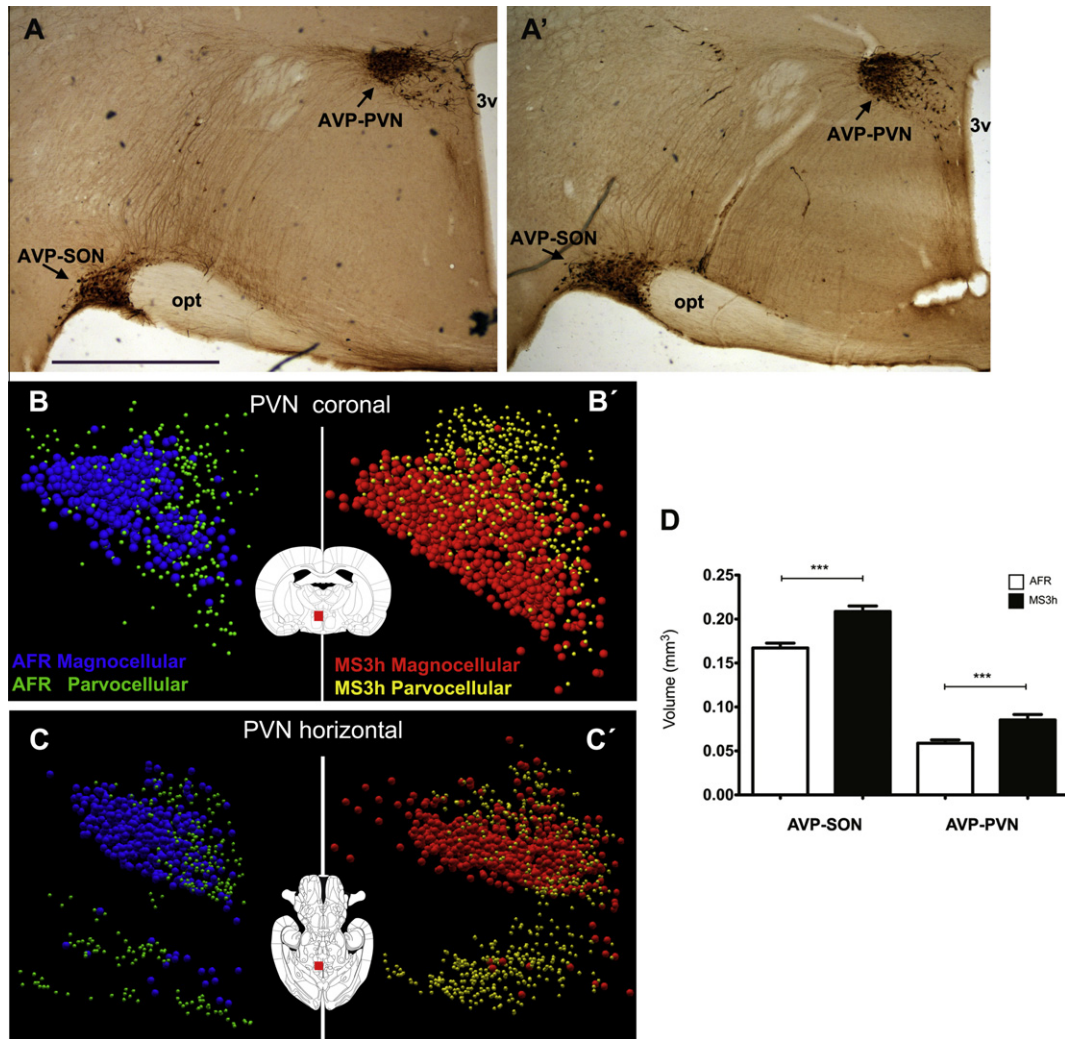


Fig. 4. Effects of MS3h on the extension of AVP+ neurons inside the PVN and SON at PND75. A and A': representative photomicrographs showing immunohistochemical staining for vasopressin on hypothalamic coronal sections showing the enlarged areas occupied by vasopressin neurons in paraventricular (PVN) and supraoptic (SON) nuclei of MS3h (A') compared to AFR (A). B, B', C, C': showing the coronal (B and B') and horizontal (C and C') views of the 3D computer reconstruction of PVN: AVP+ magnocellular neurons are in blue for AFR and in red for MS3h and parvocellular neurons are in green for AFR and in yellow for MS3h. D. Histogram shows the mean \pm SEM of the AVP+ volume extension measurements in SON and PVN regions. 3v, third ventricle, opt, optic tract. *** $p < 0.001$. Scale bar = 1 mm.

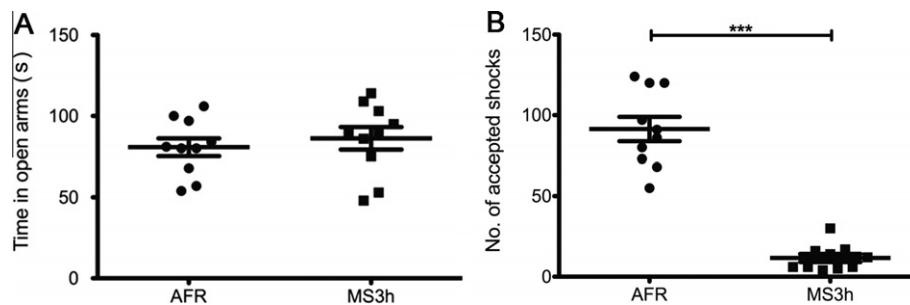


Fig. 5. MS3h subjects showed differential anxious states compared to AFR under unconditioned and conditioned behavioral tests for anxiety assessment. Panel A: Elevated plus maze test performed before water deprivation to evaluate the unconditioned anxiety related behavior revealed by the time spent in the open arms (total test time was 300 s). During this test, the experimental subjects showed similar behavior compared to control subjects. Panel B: Vogel conflict test (VCT). This test assessed conditioned anxious state posterior to a lapse of 48 h of water deprivation. During the test, a 0.22-mA current with a 50% duty cycle (5 s) was applied to the VCT apparatus during 300 s. The operational parameter we tested was the number of shocks the rats received. *** $p < 0.001$.

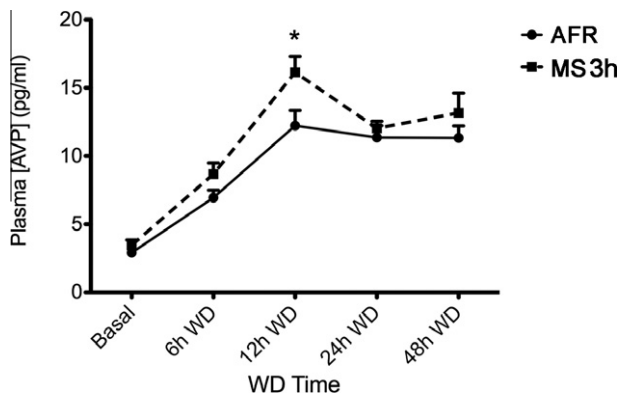


Fig. 6. Time evolution curve of the plasma AVP concentration (mean \pm SEM) in function of water deprivation (WD) progression. * $p < 0.05$.

homeostasis. Neuroanatomic and electrophysiologic evidences indicate that SON and magnocellular division of PVN are reciprocally connected to areas of the central nervous systems (CNS), besides their massive projections to neurolobe of the pituitary gland (Inyushkin et al., 2009; Kc and Dick, 2010). Using Fos mapping for AVP neuronal activation we revealed significant increases in Fos response to a single 3hMS event in both AFR and MS3h at PND10 (Table 1 and Fig. 1). No significant difference was observed between the two experimental groups in terms of percentage of activation of AVP neurons in PVN and SON. This no-difference was also observed under basal conditions (Table 1). These data indicated that the activation was mainly due to the 3hMS procedure and not due to the individual past MS experience. Although it is impossible to rule out a slight variation of plasma osmolarity during the 3hMS in newborn rats, this massive activation in magnocellular AVP containing regions suggested a broader physiological role of AVP during the early-life. It is known that AVP on its own is able to induce ACTH secretion from rat pituitary cells but only in large, supra-physiological concentrations (Antoni, 1993). Therefore, in adult rats it is accepted that CRF is the main secretagogue, while AVP modifies its effects. This seemed not the case during early-life. In two markedly different early-life stress models (maternal deprivation 24 h and repeated ether inhalation), Makara and collaborators reported strong evidence for a dominant regulating role of AVP on HPA axis during neonatal period. In the absence of AVP (AVP $^{-/-}$ Brattleboro rats) there was no measurable ACTH elevation in 10-day-old rat pups. However, both procedures provoked CORT elevations significantly superior to AVP $^{+/+}$ Brattleboro rats, which suggested an ACTH-independent CORT-secretion regulation during neonatal stage, probably related to AVP (Makara et al., 2008). In a recent study, Lajud and collaborators found a dual phenomenon regarding CORT elevation as a consequence of 3hMS using the same MS rat model. At the PND3, the MS group's elevation was significantly higher than the one from AFR, but surprisingly this phenomenon was reversed at PND12 (which correlated to PND13 of this study where the day of birth was assigned as PND1 instead of PND0 as in Lajud's study) (Lajud

et al., 2011), i.e. the MS group's elevation was significantly lower than the one from AFR. It is thus tempting to speculate that the hyper-activation of AVP system during the MS in early postnatal stage represents a homeostatic mechanism to balance the hyper-activated HPA axis and may contribute to the so called "stress hyporesponsive period or SHRP" (Sapolsky and Meaney, 1986; Lajud et al., 2011).

Enhanced Fos expression in AVP containing magnocellular neurons during MS periods implicated an abnormally higher neuronal activity during early post-natal development. During development, neurons establish specific synaptic connections to produce highly organized functional neuronal networks. While the general map of neuronal connections is encoded by genes, spontaneous and sensory-driven activities are thought to be equally important for CNS development (Khazipov and Buzsáky, 2010). Considerable evidence indicates that early electrical activity controls a number of developmental processes including neuronal differentiation, migration, synaptogenesis and synaptic plasticity (for a review see (Ben-Ari, 2001). Moreover, during normal development of the nervous system of most species, large numbers of immature neuronal and glial cells are lost by a process of programmed cell death (PCD). For rats, the postnatal massive process of PCD occurs from PND1 to PND14 (White and Barone, 2001), the period that overlaps with MS. It is well known that neuronal activity plays an important role in modulating neuronal survival (Oppenheim et al., 2010). Hence, our data regarding an immediate and persistent over-expression of AVP mRNA in whole hypothalamus and in particular, in the PVN and SON, and enlarged PVN and SON observed in adulthood are in accordance with the Fos results.

Several transcription factors and intracellular signaling pathways modulate AVP gene regulation. The role of the Fos/Jun proteins in AVP gene regulation is still unclear. However, the rat AVP promoter contains a functional activation protein 1 (AP1) transcription element that consists of hetero- or homodimers of Fos proteins, including c-Fos, and Jun proteins that bind to AP1 (Yoshida et al., 2006). Several studies have shown that Fos/Jun proteins are rapidly expressed in AVP-positive neurons in response to multiple stimuli, such as hypertonic saline challenge, coordinating with the activation of AVP gene expression (Sharp et al., 1991; Shiromani et al., 1995). Our data showed a rapid expression of c-Fos protein in AVP neurons in response to an acute 3hMS. These evidences, together with our results suggest that the expression of Fos/Jun proteins may be one of the possible mechanisms mediating the rapid transcriptional induction of AVP gene.

Recently, the increased expression of AVP mRNA, and protein, in PVN of MS mice was shown to be accompanied by hypomethylation of an AVP key regulatory region (Murgatroyd et al., 2009). One of the proteins responsible for regulating DNA methylation is methyl CpG-binding protein 2 (MeCP2), its binding represses DNA transcription. In a hypothalamic cell line, neuronal depolarization by K $^{+}$ was shown to trigger Ca $^{2+}$ -dependent phosphorylation of MeCP2 by Ca $^{2+}$ -calmodulin kinase II (CAMKII), causing dissociation of MeCP2 from the AVP

promoter and an increase in AVP transcription. Furthermore, MeCP2 and CAMKII phosphorylation levels were found increased in AVP-positive neurons from PND10 MS mice. The authors put forward that MeCP2 phosphorylation, via CAMKII activity, is critical for the repressive role of MeCP2 at the AVP enhancer of MS mice (Murgatroyd et al., 2009).

Methodological considerations

It is worth pointing out that we provided, for the first time, quantitative and morphometric assessments of AVP mRNA in PVN and SON at both neonatal stage and young adulthood. Our data are in discrepancy with some data found in the literature where observations of no-differences under basal condition in SON and PVN were reported (Veenema et al., 2006; Veenema and Neumann, 2009). In our study, we used an AVP riboprobe for ISH for whole hypothalamus, PVN and SON, analyzed through both densitometric and morphological measurements of silver grain precipitation areas on histological slides with Methylene Blue counterstaining. This method allowed observing much more anatomical details with much stronger hybridization signals due to its greater sensitivity and better signal-to-noise ratios. Moreover, riboprobes form more stable hybrids than oligo-probes. Hence we could analyze the histological slide under bright-field microscope and digitally measure the hybridized areas in the respective regions (PVN, SON and SCN). Veenema and collaborator's data were obtained using oligonucleotide probe-ISH (Veenema et al., 2006; Veenema and Neumann, 2009) with lower sensitivity compared with this riboprobe-ISH method.

Regarding the volume assessment of the AVP containing neurons inside PVN and SON (AVP-PVN and AVP-SON), we found a remarkable increase in the volumes of both magnocellular nuclei at rat young adult stage (PND75). This observation is in accordance with data from Veenema and Neumann (2009) but in discrepancy with results from another study in which a decreased AVP+ cell density in the PVN was found in MS adult rats (Desbonnet et al., 2008). We consider that this could be due to methodological discrepancies. Our experience indicates that AVP immunoreaction depends strongly on the histological procedures. A series of factors increases the AVP immunoreaction, such as a relatively short perfusion/fixation period (15 min approximately) with fixative containing 4% paraformaldehyde fixative and 15% v/v picric acid, followed by same day slicing of freshly fixed brain block by vibratome and thorough rinsing of the sections to remove the fixative. These actions enhanced AVP immunoreaction while post-fixation and freeze-thaw procedures dampen the AVP immunoreaction (data not shown).

Functional considerations

We assessed anxiety-like behavior in this MS3h animal model in rat young adulthood. We used two well-validated behavioral models. The EPM assesses internal conflict between voluntary approach and withdrawal tendencies

that is related to unconditioned anxiety. We did not observe any significant difference regarding the unconditioned anxious state between MS3h and AFR rats. This observation supports data published by Lajud et al. (2011). The Vogel thirsty rat conflict test (VCT) assesses conditioned anxiety-behavior under WD conditions (Millan and Brocco, 2003), which involve intrinsically the activation of AVP magnocellular system due to the WD procedure which represents an osmotic stressor. Following the WD, AVP is greatly released in the blood circulation, which was found significantly increased in the MS3h at 12 h. During the last step of the VCT, MS3h rats exhibited a significantly higher anxiety-related behavior than AFR rats. Although the intra-cerebral AVP release under VCT experimental conditions was not measured in this study, this parameter is likely to be increased, according to previous evidence such as intra-PVN release of AVP during stress coping (Engelmann et al., 2004; Leng and Ludwig, 2008). The possible release mechanisms include dendritic release by exocytosis in the PVN and lateral hypothalamus, as previously demonstrated by Pow and Morris at electron microscopy level (Pow and Morris, 1989). Since the high anxious behavior was only detected with VCT, once osmotic stressor was applied and not with the EPM test, it is rational to consider that the main cause of the expressed high anxious state was due to the major physiological mechanism to cope with this stressor, i.e. vasopressinergic system activation. Experimental evidences have shown that intra-PVN administration of an AVP V1 receptor antagonist resulted in a decrease of anxiety-related behavior of the high anxiety bred rats (Engelmann et al., 2004) and increased AVP release within PVN, measured by microdialysis, was observed during anxious situations (Wotjak et al., 1996). These data support the assumption that higher contents of released AVP within PVN serve as a physiological substrate for anxiogenesis, which is in concordance with the results from this study. It is worth mentioning that the pain sensitivity was assessed using a warm water tail withdrawal test in a separate study and the observations indicated that under basal condition this parameter remained unchanged compared to AFR subjects (unpublished data).

There has been broad literature exploring the physiological and anatomical substrates underlying the fear response observed during the VCT (conditioned anxiety-like behavior, (Millan and Brocco, 2003)). It is well known that the amygdala plays an important role in anxiety and fear behavior, integrating emotionally relevant sensory information and encoding the aversive affect of fearful stimuli. Subsystems of the amygdalar complex are known to mediate different aspects of anxiety-related behaviors, as observed in the elevated plus-maze or in the VCT (Graeff et al., 1993; Killcross et al., 1997).

Previous evidence has shown that VCT triggers the expression of c-fos specifically within the central nucleus of the amygdala (Moller et al., 1994). In addition, lesions only to the central nucleus (CeA), but not to the basolateral nucleus (BLA), extraordinarily increased the punished component of the VCT (Moller et al., 1997). Also, lesions to the CeA were observed to produce anxiolytic effects only during the VCT, but not in other anxiety tests

(Kopchia et al., 1992). In this line, CeA has been reported to be mainly involved in the encoding of the anxiety-like behavior when subjects are confronted with an aversive stimulus, i.e. punished drinking (Pesold and Treit, 1995), while BLA has clearly shown a role in unconditioned or basal innate fear as measured by EPM (Green and Vale, 1992; Pesold and Treit, 1995). In this study, behavioral experiments clearly demonstrate a marked divergence between unconditioned (EPM) and conditioned (VCT) anxiety-like behaviors induced by MS, as a significant increase was only observed in the MS3h rats after an aversive stimulus was applied. Based on this divergence, CeA is probably playing a crucial role in the increased anxiety-like behavior observed during the VCT in the MS3h subjects.

AVP is a key component in the regulation of stress response and complex behaviors, such as anxiety, social cognition and fear conditioning (Meyer-Lindenberg et al., 2011). Hypothalamus, specifically PVN and SON nuclei, has been recognized as the principal source of extra- and intra-cerebral AVP projections (Buijs, 1978). Moreover, AVP receptors are distributed throughout the central nervous system, finding a significant expression of V1b subtype in the adenohypophysis and within limbic structures (Lolait et al., 1995). In addition, the anxiogenic effect of AVP has been demonstrated in broad different studies (Landgraf and Neumann, 2004; Zhang et al., 2010; Mak et al., 2011). Likewise, a recent report has found that the systemic administration of a non-peptide V1b antagonist (SSR149415) is able to produce anxiolytic effects in classical (EPM, VCT) and atypical rat models of anxiety, suggesting a crucial role of AVP V1b receptor in the production of anxiogenic states (Griebel et al., 2002).

A number of previous studies have suggested that the amygdala is an important target of AVP to exert its stress-responsive and anxiogenic action. Amygdaloid nuclei present extensive AVP innervation with fibers coming from hypothalamic sources (Buijs, 1978; Sofroniew, 1980), and recent immunohistochemical studies have demonstrated the presence of V1b receptors throughout the entire amygdalar complex: central, medial and basolateral divisions (Hernando et al., 2001; Stemmelin et al., 2005). Activation of amygdalar AVP receptors has been shown to enhance fear and anxiety-like behaviors, as well as aggressiveness, stress levels and the consolidation of fear memory (Bielsky and Young, 2004) (Landgraf and Wigger, 2002). At the cellular level, it has been demonstrated that AVP increases the probability of provoking postsynaptic action potentials in specific populations of neurons within the CeA. This latter finding suggests that the endogenous balance between the activation of the vasopressinergic system and the expression of AVP receptors, paralleled with oxytocin system, may set and tune the levels for the activation of the fear response and anxiety behavior (Huber et al., 2005). In this context, it has been reported that AVP levels within the extracellular fluid of the amygdala increase after WD (Epstein et al., 1983), and during stressful behavioral situations (i.e. FST, (Ebner et al., 2002)). In our study, higher concentration of plasmatic AVP after WD and potentiation of the vasopressinergic system is

demonstrated. This hyper-active AVP system observed in the MS animals could be releasing higher levels of AVP within CeA, increasing the excitability of the network after the application of the osmotic stress in the VCT, thus tuning the endogenous balance of the network toward activation of fear and anxiety responses, with the secondary functional effect of reduced avoidance latency at the conflict test.

CONCLUSION

In the present study, we could demonstrate for the first time a direct relationship between a potentiated vasopressin system induced by MS, evidenced by the enlarged AVP-SON and AVP-PVN volumes and abnormal high level of AVP-mRNA expression and significant increase of AVP release under WD, and the high conditioned anxiety revealed by VCT. The present data not only extended the previous knowledge that MS potentiates the vasopressin systems in adulthood, but they also clearly showed that a single 3hMS event was capable of activating the majority of the AVP neurons inside the SON and PVN, showed by Fos expression analysis. Hence, the data provided a physiological substrate for the observed AVP up-regulation by MS.

DECLARATION FOR AUTHOR'S CONTRIBUTIONS

Conceived and designed the experiments: L.Z., V.S.H. Performed the experiments: L.Z., V.S.H., B.L., M.P.M., A.N.K., C.I. Analyzed the data: L.Z., V.S.H., M.P.M., A.N.K., C.I., M.M. Contributed reagents/materials/analysis tools: L.Z., M.M. Wrote the paper: L.Z., V.S.H., C.I., M.P.M. Revised the manuscript critically for important intellectual content: all authors.

Acknowledgements—This study was supported by Grants: CONACYT: 79641, 127777 and PAPIIT-DGAPA-UNAM IN218111 and the Intramural Research Program of the National Institute on Drug Abuse. V.S.H. was supported by a CONACYT-PhD-scholarship. A.T.N.K. was supported by a research assistantship through Grant IN218111. We greatly thank Tsuyoshi Yamaguchi, Enrique Pinzón, Itzel Nissen, María-José Gómora, Miguel Tapia, Patricia Espinosa, and Elfego Ruiz for their professional technical assistance during the development of this study.

REFERENCES

- Aisa B, Tordera R, Lasheras B, Del Rio J, Ramirez MJ (2007) Cognitive impairment associated to HPA axis hyperactivity after maternal separation in rats. *Psychoneuroendocrinology* 32:256–266.
- Anisman H, Zaharia MD, Meaney MJ, Merali Z (1998) Do early-life events permanently alter behavioral and hormonal responses to stressors? *Int J Dev Neurosci* 16:149–164.
- Antoni FA (1993) Vasopressinergic control of pituitary adrenocorticotropin secretion comes of age. *Front Neuroendocrinol* 14:76–122.
- Armstrong W (2004) Hypothalamic supraoptic and paraventricular nuclei. In: Paxinos G, editor. *The rat nervous system*. Elsevier. p. 369–387.

- Ben-Ari Y (2001) Developing networks play a similar melody. *Trends Neurosci* 24:353–360.
- Bielsky IF, Young LJ (2004) Oxytocin, vasopressin, and social recognition in mammals. *Peptides* 25:1565–1574.
- Boer GJ (1987) Development of vasopressin system and their functions. In: Gash DM, Boer GJ, editors. *Vasopressin: principles and properties*. New York: Plenum Press. p. 117–174.
- Buijs RM (1978) Intra- and extrahypothalamic vasopressin and oxytocin pathways in the rat. *Pathways to the limbic system, medulla oblongata and spinal cord*. *Cell Tissue Res* 192:423–435.
- Cirulli F, Berry A, Alleva E (2003) Early disruption of the mother-infant relationship: effects on brain plasticity and implications for psychopathology. *Neurosci Biobehav Rev* 27:73–82.
- de Jongh R, Geyer MA, Olivier B, Groenink L (2005) The effects of sex and neonatal maternal separation on fear-potentiated and light-enhanced startle. *Behav Brain Res* 161:190–196.
- Desbonnet L, Garrett L, Daly E, McDermott KW, Dinan TG (2008) Sexually dimorphic effects of maternal separation stress on corticotrophin-releasing factor and vasopressin systems in the adult rat brain. *Int J Dev Neurosci* 26:259–268.
- Dlouha H, Kreczek J, Zicha J (1982) Postnatal development and diabetes insipidus in Brattleboro rats. *Ann N Y Acad Sci* 394:10–20.
- Ebner K, Wotjak CT, Landgraf R, Engelmann M (2002) Forced swimming triggers vasopressin release within the amygdala to modulate stress-coping strategies in rats. *Eur J Neurosci* 15:384–388.
- Engelmann M, Landgraf R, Wotjak CT (2004) The hypothalamic-neurohypophysial system regulates the hypothalamic-pituitary-adrenal axis under stress: an old concept revisited. *Front Neuroendocrinol* 25:132–149.
- Epstein Y, Castel M, Glick SM, Sivan N, Ravid R (1983) Changes in hypothalamic and extra-hypothalamic vasopressin content of water-deprived rats. *Cell Tissue Res* 233:99–111.
- File SE, Lippa AS, Beer B, Lippa MT (2004) Animal tests of anxiety. In: Crawley JN, et al., editors. *Current protocols in neuroscience* (editorial board) (Chapter 8:Unit 8.3).
- Fumagalli F, Molteni R, Racagni G, Riva MA (2007) Stress during development: impact on neuroplasticity and relevance to psychopathology. *Prog Neurobiol* 81:197–217.
- Goodson JL (2008) Nonapeptides and the evolutionary patterning of sociality. *Prog Brain Res* 170:3–15.
- Goodson JL, Bass AH (2001) Social behavior functions and related anatomical characteristics of vasotocin/vasopressin systems in vertebrates. *Brain Res Brain Res Rev* 35:246–265.
- Graeff FG, Silveira MC, Nogueira RL, Audi EA, Oliveira RM (1993) Role of the amygdala and periaqueductal gray in anxiety and panic. *Behav Brain Res* 58:123–131.
- Green S, Vale AL (1992) Role of amygdaloid nuclei in the anxiolytic effects of benzodiazepines in rats. *Behav Pharmacol* 3:261–264.
- Griebel G, Simiand J, Serradell-Le Gal C, Wagnon J, Pascal M, Scatton B, Maffrand JP, Soubrie P (2002) Anxiolytic- and antidepressant-like effects of the non-peptide vasopressin V1b receptor antagonist, SSR149415, suggest an innovative approach for the treatment of stress-related disorders. *Proc Natl Acad Sci U S A* 99:6370–6375.
- Grino M, Zamora AJ (1998) An *in situ* hybridization histochemistry technique allowing simultaneous visualization by the use of confocal microscopy of three cellular mRNA species in individual neurons. *J Histochem Cytochem* 46:753–759.
- Hatton GI (1990) Emerging concepts of structure-function dynamics in adult brain: the hypothalamo-neurohypophysial system. *Prog Neurobiol* 34:437–504.
- Herman JP, Schafer MK, Watson SJ, Sherman TG (1991) *In situ* hybridization analysis of arginine vasopressin gene transcription using intron-specific probes. *Mol Endocrinol* 5:1447–1456.
- Hernando F, Schoots O, Lolait SJ, Burbach JP (2001) Immunohistochemical localization of the vasopressin V1b receptor in the rat brain and pituitary gland: anatomical support for its involvement in the central effects of vasopressin. *Endocrinology* 142:1659–1668.
- Huber D, Veinante P, Stoop R (2005) Vasopressin and oxytocin excite distinct neuronal populations in the central amygdala. *Science* 308:245–248.
- Hulshof HJ, Novati A, Sgoifo A, Luiten PG, den Boer JA, Meerlo P (2011) Maternal separation decreases adult hippocampal cell proliferation and impairs cognitive performance but has little effect on stress sensitivity and anxiety in adult Wistar rats. *Behav Brain Res* 216:552–560.
- Huot RL, Plotsky PM, Lenox RH, McNamara RK (2002) Neonatal maternal separation reduces hippocampal mossy fiber density in adult Long Evans rats. *Brain Res* 950:52–63.
- Inyushkin AN, Orlans HO, Dyball RE (2009) Secretory cells of the supraoptic nucleus have central as well as neurohypophysial projections. *J Anat* 215:425–434.
- Kalinichev M, Easterling KW, Plotsky PM, Holtzman SG (2002) Long-lasting changes in stress-induced corticosterone response and anxiety-like behaviors as a consequence of neonatal maternal separation in Long-Evans rats. *Pharmacol Biochem Behav* 73:131–140.
- Kc P, Dick TE (2010) Modulation of cardiorespiratory function mediated by the paraventricular nucleus. *Respir Physiol Neurobiol* 174:55–64.
- Khazipov R, Buzsáky G (2010) Early patterns of electrical activity in the developing cortex. In: Blumberg MS, Freeman JH, Robinson SR, editors. *Oxford handbook of developmental behavioral neuroscience*. Oxford: Oxford University Press. p. 161–180.
- Killcross S, Robbins TW, Everitt BJ (1997) Different types of fear-conditioned behaviour mediated by separate nuclei within amygdala. *Nature* 388:377–380.
- Kopchia KL, Altman HJ, Commissaris RL (1992) Effects of lesions of the central nucleus of the amygdala on anxiety-like behaviors in the rat. *Pharmacol Biochem Behav* 43:453–461.
- Korosi A, Baram TZ (2009) The pathways from mother's love to baby's future. *Front Behav Neurosci* 3:27.
- Kuhn CM, Schanberg SM (1998) Responses to maternal separation: mechanisms and mediators. *Int J Dev Neurosci* 16:261–270.
- Lajud N, Roque A, Cajero M, Gutierrez-Ospina G, Torner L (2011) Periodic maternal separation decreases hippocampal neurogenesis without affecting basal corticosterone during the stress hyporesponsive period, but alters HPA axis and coping behavior in adulthood. *Psychoneuroendocrinology*.
- Landgraf R, Neumann ID (2004) Vasopressin and oxytocin release within the brain: a dynamic concept of multiple and variable modes of neuropeptide communication. *Front Neuroendocrinol* 25:150–176.
- Landgraf R, Wigger A (2002) High vs low anxiety-related behavior rats: an animal model of extremes in trait anxiety. *Behav Genet* 32:301–314.
- Lehmann J, Feldon J (2000) Long-term biobehavioral effects of maternal separation in the rat: consistent or confusing? *Rev Neurosci* 11:383–408.
- Leng G, Ludwig M (2008) Neurotransmitters and peptides: whispered secrets and public announcements. *J Physiol* 586:5625–5632.
- Levine S (1957) Infantile experience and resistance to physiological stress. *Science* 126:405.
- Levine S, Alpert M, Lewis GW (1957) Infantile experience and the maturation of the pituitary adrenal axis. *Science* 126:1347.
- Lolait SJ, O'Carroll AM, Brownstein MJ (1995) Molecular biology of vasopressin receptors. *Ann N Y Acad Sci* 771:273–292.
- Mak P, Broussard C, Vacy K, Broadbear JH (2011) Modulation of anxiety behavior in the elevated plus maze using peptidic oxytocin and vasopressin receptor ligands in the rat. *J Psychopharmacol*.
- Makara GB, Domokos A, Mergl Z, Csabai K, Barna I, Zelena D (2008) Gender-specific regulation of the hypothalamo-pituitary-adrenal axis and the role of vasopressin during the neonatal period. *Ann N Y Acad Sci* 1148:439–445.
- Marks DL, Wiemann JN, Burton KA, Lent KL, Clifton DK, Steiner RA (1992) Simultaneous visualization of two cellular mRNA species in individual neurons by use of a new double *in situ* hybridization method. *Mol Cell Neurosci* 3:395–405.

- Meyer-Lindenberg A, Domes G, Kirsch P, Heinrichs M (2011) Oxytocin and vasopressin in the human brain: social neuropeptides for translational medicine. *Nat Rev Neurosci* 12:524–538.
- Millan MJ, Brocco M (2003) The Vogel conflict test: procedural aspects, gamma-aminobutyric acid, glutamate and monoamines. *Eur J Pharmacol* 463:67–96.
- Moller C, Bing O, Heilig M (1994) c-fos expression in the amygdala: in vivo antisense modulation and role in anxiety. *Cell Mol Neurobiol* 14:415–423.
- Moller C, Wiklund L, Sommer W, Thorsell A, Heilig M (1997) Decreased experimental anxiety and voluntary ethanol consumption in rats following central but not basolateral amygdala lesions. *Brain Res* 760:94–101.
- Morales M, Bloom FE (1997) The 5-HT₃ receptor is present in different subpopulations of GABAergic neurons in the rat telencephalon. *J Neurosci* 17:3157–3167.
- Murgatroyd C, Patchev AV, Wu Y, Micale V, Bockmuhl Y, Fischer D, Holsboer F, Wotjak CT, Almeida OF, Spengler D (2009) Dynamic DNA methylation programs persistent adverse effects of early-life stress. *Nat Neurosci* 12:1559–1566.
- Oosterbaan HP, Swaab DF, Boer GJ (1985) Oxytocin and vasopressin in the rat do not readily pass from the mother to the amniotic fluid in late pregnancy. *J Dev Physiol* 7:55–62.
- Oppenheim RW, Milligan C, Sun W (2010) Programmed cell death during nervous system development: mechanisms, regulation, function, and implications for neurobehavioral ontogeny. In: Blumberg MS, Freeman JH, Robinson SR, editors. *Oxford handbook of developmental behavioral neuroscience*. Oxford: Oxford University Press. p. 76–180.
- Oreland S, Gustafsson-Ericson L, Nylander I (2010) Short- and long-term consequences of different early environmental conditions on central immunoreactive oxytocin and arginine vasopressin levels in male rats. *Neuropeptides* 44:391–398.
- Ostrowski NL, Young 3rd WS, Knepper MA, Lolait SJ (1993) Expression of vasopressin V1a and V2 receptor messenger ribonucleic acid in the liver and kidney of embryonic, developing, and adult rats. *Endocrinology* 133:1849–1859.
- Paxinos G, Watson C (2007) *The rat brain in stereotaxic coordinates*. San Diego, California, USA: Academic Press.
- Pellow S, File SE (1986) Anxiolytic and anxiogenic drug effects on exploratory activity in an elevated plus-maze: a novel test of anxiety in the rat. *Pharmacol Biochem Behav* 24:525–529.
- Pesold C, Treit D (1995) The central and basolateral amygdala differentially mediate the anxiolytic effects of benzodiazepines. *Brain Res* 671:213–221.
- Pirnik Z, Kiss A (2005) Fos expression variances in mouse hypothalamus upon physical and osmotic stimuli: co-staining with vasopressin, oxytocin, and tyrosine hydroxylase. *Brain Res Bull* 65:423–431.
- Plotsky PM, Meaney MJ (1993) Early, postnatal experience alters hypothalamic corticotropin-releasing factor (CRF) mRNA, median eminence CRF content and stress-induced release in adult rats. *Brain Res Mol Brain Res* 18:195–200.
- Pohjavuori M, Fyhrquist F (1980) Hemodynamic significance of vasopressin in the newborn infant. *J Pediatr* 97:462–465.
- Pow DV, Morris JF (1989) Dendrites of hypothalamic magnocellular neurons release neurohypophysial peptides by exocytosis. *Neuroscience* 32:435–439.
- Rowland NE (2007) Food or fluid restriction in common laboratory animals: balancing welfare considerations with scientific inquiry. *Comp Med* 57:149–160.
- Sapolsky RM, Meaney MJ (1986) Maturation of the adrenocortical stress response: neuroendocrine control mechanisms and the stress hyporesponsive period. *Brain Res* 396:64–76.
- Sharp FR, Sagar SM, Hicks K, Lowenstein D, Hisanaga K (1991) c-fos mRNA, Fos, and Fos-related antigen induction by hypertonic saline and stress. *J Neurosci* 11:2321–2331.
- Shiromani PJ, Magner M, Winston S, Charness ME (1995) Time course of phosphorylated CREB and Fos-like immunoreactivity in the hypothalamic supraoptic nucleus after salt loading. *Brain Res Mol Brain Res* 29:163–171.
- Siga E, Horster MF (1991) Regulation of osmotic water permeability during differentiation of inner medullary collecting duct. *Am J Physiol* 260:F710–F716.
- Slotten HA, Kalinichev M, Hagan JJ, Marsden CA, Fone KC (2006) Long-lasting changes in behavioural and neuroendocrine indices in the rat following neonatal maternal separation: gender-dependent effects. *Brain Res* 1097:123–132.
- Sofroniew MV (1980) Projections from vasopressin, oxytocin, and neurophysin neurons to neural targets in the rat and human. *J Histochem Cytochem* 28:475–478.
- Stemmelin J, Lukovic L, Salome N, Griebel G (2005) Evidence that the lateral septum is involved in the antidepressant-like effects of the vasopressin V1b receptor antagonist, SSR149415. *Neuropsychopharmacology* 30:35–42.
- Veenema AH, Blume A, Niederle D, Buwalda B, Neumann ID (2006) Effects of early life stress on adult male aggression and hypothalamic vasopressin and serotonin. *Eur J Neurosci* 24:1711–1720.
- Veenema AH, Neumann ID (2009) Maternal separation enhances offensive play-fighting, basal corticosterone and hypothalamic vasopressin mRNA expression in juvenile male rats. *Psychoneuroendocrinology* 34:463–467.
- Vogel JR, Beer B, Clody DE (1971) A simple and reliable conflict procedure for testing anti-anxiety agents. *Psychopharmacologia* 21:1–7.
- Walf AA, Frye CA (2007) The use of the elevated plus maze as an assay of anxiety-related behavior in rodents. *Nat Protoc* 2:322–328.
- White LD, Barone Jr S (2001) Qualitative and quantitative estimates of apoptosis from birth to senescence in the rat brain. *Cell Death Differ* 8:345–356.
- Wigger A, Neumann ID (1999) Periodic maternal deprivation induces gender-dependent alterations in behavioral and neuroendocrine responses to emotional stress in adult rats. *Physiol Behav* 66:293–302.
- Wigger A, Sanchez MM, Mathys KC, Ebner K, Frank E, Liu D, Kresse A, Neumann ID, Holsboer F, Plotsky PM, Landgraf R (2004) Alterations in central neuropeptide expression, release, and receptor binding in rats bred for high anxiety: critical role of vasopressin. *Neuropsychopharmacology* 29:1–14.
- Wotjak CT, Kubota M, Liebsch G, Montkowski A, Holsboer F, Neumann I, Landgraf R (1996) Release of vasopressin within the rat paraventricular nucleus in response to emotional stress: a novel mechanism of regulating adrenocorticotrophic hormone secretion? *J Neurosci* 16:7725–7732.
- Yoshida M, Iwasaki Y, Asai M, Takayasu S, Taguchi T, Itoi K, Hashimoto K, Oiso Y (2006) Identification of a functional AP1 element in the rat vasopressin gene promoter. *Endocrinology* 147:2850–2863.
- Young WS, Li J, Wersinger SR, Palkovits M (2006) The vasopressin 1b receptor is prominent in the hippocampal area CA2 where it is unaffected by restraint stress or adrenalectomy. *Neuroscience* 143:1031–1039.
- Zhang L, Medina MP, Hernandez VS, Estrada FS, Vega-Gonzalez A (2010) Vasopressinergic network abnormalities potentiate conditioned anxious state of rats subjected to maternal hyperthyroidism. *Neuroscience* 168:416–428.

Vasopressinergic network abnormalities potentiate
conditioned anxious state of rats subjected to maternal
hyperthyroidism

Zhang L., Medina M. P., **Hernández V. S.**, Estrada F. S.,
Vega-González A.

Neuroscience. 2010, 168: 416-28

My contributions in:

- Conception of the study: ++
- Performance of the experiments:
 - o Surgery for T4 pumps in dams: +++
 - o Behavioural assessment for anxiety: +++
 - o Measurement of AVP plasma concentrations: +++
 - o Immunohistochemical procedures and analysis: +++
 - o Electron microscopy procedures: -
- Statistical analysis: ++
- Discussion of the results: +++
- Preparation of the paper: ++

(-): No contribution;; (++): Important contribution; (+++); Main contribution

VASOPRESSINERGIC NETWORK ABNORMALITIES POTENTIATE CONDITIONED ANXIOUS STATE OF RATS SUBJECTED TO MATERNAL HYPERTHYROIDISM

L. ZHANG,* M. P. MEDINA, V. S. HERNÁNDEZ,
F. S. ESTRADA AND A. VEGA-GONZÁLEZ

Departamento de Fisiología, Facultad de Medicina, Universidad Nacional Autónoma de México, México 04510, D. F., Mexico

Abstract—We have previously reported that a mild maternal hyperthyroidism in rats impairs stress coping of adult offspring. To assess anxiogenesis in this rat model of stress over-reactivity, we used two behavioural tests for unconditional and conditional anxious states: elevated plus maze test (EPM) and Vogel conflict test (VCT). In the latter one, arginine vasopressin (AVP) release was enhanced due to osmotic stress. With the EPM test no differences were observed between maternal hyperthyroid rats (MH) and controls. However, with the VCT, the MH showed increased anxiety-like behaviour. This behavioural difference was abolished by diazepam. Plasma AVP concentration curve as a function of water deprivation (WD) time showed a marked increase, reaching its maximal levels within half the time of controls and another significant difference after VCT. A general increase in Fos expression in hypothalamic supraoptic and paraventricular nuclei (PVN) was observed during WD and after VCT. There was also a significant increase of AVP immunoreactivity in anterior hypothalamic area. A large number of Herring bodies were observed in the AVP containing fibres of MH hypothalamic-neurohypophysial system. Numerous reciprocal synaptic connections between AVP and corticotropin releasing factor containing neurons in MH ventromedial PVN were observed by electron microscopy. These results suggest that a mild maternal hyperthyroidism could induce an aberrant organization in offspring's hypothalamic stress related regions which could mediate the enhanced anxiety seen in this animal model. © 2010 IBRO. Published by Elsevier Ltd. All rights reserved.

Key words: anxiety, Vogel conflict test, arginine vasopressin, corticotropin releasing factor, electron microscopy, synapse.

Thyroid hormones (TH) play an important role in the development of the fetal brain. TH cross the placenta reaching the fetus and it is vital up to the first trimester of pregnancy during which time the fetal thyroid gland is not functional (Vulsma et al., 1989). Deficiency of maternal thyroid function at the beginning of fetal neocortico-genesis

alters neuronal migration (Auso et al., 2004) and mild maternal hyperthyroidism in rats leads to an increased dendritic arborization of hippocampus CA3 pyramidal neurons (Zhang et al., 2008). Maternal hyperthyroid rat models have shown that the expression of cytoskeletal proteins is affected, indicating an accelerated neuronal differentiation (Evans et al., 2002).

Wistar rat male offspring of mild hyperthyroid females bred in our laboratory were similar to control animals in a number of physiological parameters when tested in non-stressful conditions. However, their responses to mild acute and sub-chronic stressors were markedly enhanced, leading to an impaired cognitive function and depression-like behaviours (Zhang et al., 2008). However, anxiety-like behaviour measured as unconditioned explorative behaviour showed no difference to controls (Hernandez et al., 2007).

On the other hand, the arginine vasopressin (AVP), also referred as antidiuretic hormone, acts both as a hormone and as a neurochemical. AVP is largely synthesized by hypothalamic magnocellular neurons localized in paraventricular (PVN) and supraoptic (SON) nuclei. Through the hypothalamic–neurohypophysial system (HNS) AVP is transported to the neurolobe of the pituitary gland and further released upon osmoreceptor/baroreceptor activation. Peripherally circulating AVP is responsible for the classic endocrine functions ascribed to this neurohormone (e.g. vasoconstriction, antidiuresis) (Ring, 2005). The central vasopressinergic system includes the sites of AVP synthesis and release, where AVP acts as a neuromodulator/neurotransmitter regulating a variety of CNS-mediated functions (e.g. learning and memory, neuroendocrine reactivity, social behaviours, circadian rhythmicity, thermoregulation, and autonomic function) (Ring, 2005; Caldwell et al., 2008; Frank and Landgraf, 2008). AVP is also critically involved in stress-related anxiogenesis (Millan, 2003; Landgraf, 2005).

Early studies considered AVP originating from magnocellular neurons of the HNS as a major modulator of the hypothalamic–pituitary–adrenal (HPA) axis (Antoni, 1993). However, it is now generally accepted that the parvocellular neurons of the PVN trigger corticotropin (ACTH) secretion via the release of corticotropin-releasing factor (CRF) and AVP. As a consequence, less attention was paid to the contribution of the HNS to the HPA axis regulation (Engelmann et al., 2004). The involvement of vasopressinergic magnocellular neurons in the control of the ACTH secretion has been a much-debated issue. This study was designed and carried out with this issue in mind.

*Corresponding author. Tel: +52-55-56232348; fax: +52-55-56232348. E-mail address: limei@unam.mx (L. Zhang).

Abbreviations: AHA, anterior hypothalamic area; AT, axon terminal; AVP, arginine vasopressin; CRF, corticotropin releasing factor; DAB, 3,3'-diaminobenzidine; EPM, elevated plus maze test; HNS, hypothalamic–neurohypophysial system; HPA, hypothalamic–pituitary–adrenal axis; MH, maternal hyperthyroid rats; PVCT, post Vogel conflict test; PVN, paraventricular nucleus; PVNlm, PVN lateral magnocellular part; PVNmpd, PVN medial parvocellular part, dorsal zone; SON, supraoptic nucleus; VCT, Vogel conflict test; WD, water deprivation.

Using an osmotic stressor we aimed to assess the angiogenesis in maternal hyperthyroid offspring. We combined behavioural characterizations with analysis of plasma AVP variations and the protein product of the immediate early gene *c-fos* (Fos) expression in PVN and SON during the 48 h of water deprivation (WD) and after the conflict test used in this study. Furthermore, AVP immunoreactivity, morphology and synaptic connectivity of AVP containing fibres in PVN and HNS were analyzed under light and electron microscopy.

EXPERIMENTAL PROCEDURES

Animals

Wistar rats were used in this study. All animal procedures were approved by the local bioethical and biosecurity committees in accordance with the principles exposed in the Handbook for the Use of Animals in Neuroscience Research (Society for Neuroscience, Washington, D.C. 1991). Animals were housed on a 12-h light schedule in a room with temperature between 20 and 24 °C with adequate ventilation and given access to standard rat chow and water *ad libitum*, unless otherwise specified.

The breeding of the maternal hyperthyroid rats offspring has been described elsewhere (Zhang et al., 2008). Briefly, 32 female rats of postnatal 90 days (P90) were implanted, under general anaesthesia (pentobarbital, Barbital, Holland de Mexico, S. A. de C. V., 50 mg/kg i.p.), with s.c. Alzet osmotic pumps (Model 2ML4, pumping rate 2.5 μ l/h for 28 days, DURECT Corporation, Cupertino, CA, USA) infusing either L-thyroxine or vehicle ($n=16$). L-thyroxine (T4, Sigma-Aldrich Inc. T2501, St. Louis, MO, USA) dose was 1.5 μ g/100 g/d of pre-mating body weight. With this dose, the female rat serum free T4 concentration was about 2.26 \pm 0.14 ng/dl ($n=4$) whereas the control females was about 1.34 \pm 0.11 ng/dl ($n=4$), which represents a mild hyperthyroid experimental condition (Varas et al., 2001; Evans et al., 2002). This measurement was made through blood samples obtained from sacrificed rats under general anaesthesia at day 10 of gestation and determined with chemiluminescent microparticle immunoassay (CMIA, ARCHITECT[®], Abbott Laboratories, Abbott Park, IL, USA).

After 2 days of recovery from the implantation, female rats were mated with normal males for three consecutive days. The females were then singly housed during the gestational period. The dams gave birth between 19 and 21 days after the 3 day-long mating period and the litter sizes were 11.8 \pm 0.82 (mean \pm SEM) in maternal hyperthyroid rats (MH) group versus 11.6 \pm 0.66 for controls. The dams were then housed with their own litter during the lactation period with minimum disturbances. Osmotic pumps were surgically removed from the females on offspring postnatal day 1 (P1) under local anaesthesia (0.2 ml of 1% lidocaine). After the extraction was completed, skin was surgically sutured and dams were returned to their home cages. The sutures were removed after 4 days. All these procedures lasted at most 20 min. We did not observe any abnormalities regarding maternal care.

On P30, 96 offspring male rats were chosen from both maternal hyperthyroid and control litters ($n=12$) to form MH experimental group and control. Four male offspring from each litter were separated from their dam and housed together in one standard rat Plexiglas cage. Each sibling was designated to a different experiment except for plasma AVP concentration measurement. In this latter one, two siblings were chosen to form the group of 24 rats but they were allocated in different time points. Spontaneous locomotor activity, body weight, glycaemia and serum T4 level were tested on P90, as previously described (Zhang et al., 2008) and showed no significant differences between MH and controls.

Experimental design

Experimental procedures were performed on male offspring rats in young adult stage (starting on P100, body weight 350 \pm 10 g). Two sets of experiments were carried out separately. (1) Behavioural tests to assess the angiogenesis threshold, plasma AVP levels and Fos expression during WD and Vogel conflict test (VCT) proper of MH compared to control. (2) Immunohistochemical and morphological characterizations of AVP labelled fibres in the anterior hypothalamus from MH and control rats under basal conditions by light and electron microscopy.

For the first set of experiments, we used the elevated plus maze test to assess the natural (unconditioned) exploratory behaviour of MH, compared to control subjects, to set a baseline for anxious state, and the VCT as both an osmotic stressor and a measure of trained (conditioned) anxious state (Vogel et al., 1971; Millan, 2003; Millan and Brocco, 2003).

Elevated plus maze test (EPM)

We used EPM to assess first the unconditioned acute anxious state. This experimental procedure was done 1 week before the VCT. The maze was made of wood, consisted of a plus-shaped platform elevated 50 cm above the floor with two closed arms (50 \times 10 \times 40 cm³) and two open arms (50 \times 10 cm²) surrounded by an upwards-protruding edge of 0.5 cm connecting the central square of 10 \times 10 cm². This latter measure prevents the rat falling accidentally without jeopardizing the elemental features of the setting, hence enhances the efficacy of the test. The EPM was lit with dim red light and monitored by CCTV. The maze was cleaned with water containing a detergent and dried before each trial.

Prior to the EPM test, rats were exposed to a standard open-field box (40 \times 40 \times 40 cm³ made of wood (Pierce and Kalivas, 2007)) during 5 min for three consecutive days before and immediately previous to the EPM test. This procedure was made to increase the likelihood of entering the open arm of the maze, thus increasing the sensitivity of the test (Walf and Frye, 2007). Rats from each experimental group underwent the EPM test during their early activity period. The test started by placing the rat in the centre of the maze heading to an open arm and then left for free exploratory activity for 5 min. The percentages of both time spent on the open arms and the number of entries to the open arm in relation to the total number of entries (closed arms plus open arms) were analyzed as a measure of unconditioned acute anxious state (exploration vs. avoidance).

Vogel conflict test (VCT)

We used VCT (File et al., 2004) to assess the conditioned acute anxious state. VCT involves two main steps: WD for 48 h and food deprivation for the latter 24 h, and the conflict test proper. WD as long as 72 h, is well tolerated by rats with weight loss in an acceptable range (approximately 11%) and no apparent loss of physical vigour (Rowland, 2007). Completing the WD period, thirsty rats were exposed to a mild and intermittent electrical shock via a water bottle. This procedure incorporates an element of conflict, whereby the subject experiences opposing and concomitant tendencies of desire (drinking behaviour for reward) and of fear (avoidance of a potentially aversive stimulus). An indicator of a conditioned anxious state is when fear prevails in this conflict, where no genuine risk is present (Millan and Brocco, 2003). We chose the number of shocks received as our operational parameter for anxious state assessment, according to File et al. (2004).

Before the VCT, the experimental subjects were habituated by staying in the conflict-chamber described below, without current application for 30 min each day during four consecutive days. The conflict chamber consisted in a clear Plexiglas cage (20 \times 30 \times 20 cm³) with a metal floor and lattice lid, a water bottle with stainless steel drinking spout, a constant current shock gen-

erator with an indicator for counting the number of shocks and a video camera. During the test, a 10% dextrose–water solution was used. The shocker leads were attached between the metal drinking spout and the grid floor. The drinking spout was isolated to avoid contact with the lid of the cage. Different shock levels (0.1–0.3 mA in steps of 0.05 mA) were assessed previously to determine the appropriate current to be used during the test (unpublished data). This was done with a different set of Wistar rats. A current of 0.15 mA was found to be optimal (i.e. it allowed animals to drink the solution with minimal discomfort).

Concluding the 48 h of water deprivation period, the test started in a separate room and a video camera sensitive to low illumination was used for monitoring and recording the test. The test was performed during the dark period of the artificial light—dark cycle and the test-room was illuminated solely with a dim red light. At the beginning of the test, each animal was put in the test chamber and was allowed to drink for 25 s without electrical current applied. After this period, a 0.15 mA current with a 50% duty cycle of 5 s was applied between the metal drinking spout and the floor during 5 min. Rats received shocks only when the spout licking coincided with the current applied intervals. The number of shocks received was recorded. Eight rats of each group undertook this test without any anxiolytic treatment and another eight rats per each group received a dose of 1,4 benzodiazepine (Diazepam Valium® Roche Syntex, Mexico City, Mexico, 2.5 mg/kg b.w, i.p.) 30 min before the test, aiming at evaluating the reversibility of this high anxiety-related behaviour, if any, by this classical anxiolytic. The procedure carried out after the test was denoted as post-VCT time point (PVCT).

Plasma AVP concentration measurement during water deprivation and after the VCT

In order to characterize the plasma AVP concentration during the 48 h of WD and PVCT, blood samples were obtained from rat tail-tips at six time points: before WD as the basal point, 6 h of WD (WD6h), 12 h of WD (WD12h), 24 h of WD (WD24h), 48 h of WD (WD48h) and immediately after VCT (PVCT). During the blood sampling, experimental subjects were immobilized using a restraint tube. In order to minimize the stressful effect exerted by this procedure, rats were placed in the same restraint tube (standard for rats, (Heinrichs and Koob, 2006)) during 30 min each day during the three previous days to the test. Four rats per each group were tested at each time point ($n=4$) (two male offspring per each litter for this test completing each group with 24 rats). Each rat provided only one blood sample. This criterion was implemented aiming to isolate the stimulus for AVP release, being only the osmotic stressor, not the possible additional AVP release secondary to the stress produced by previous sampling procedures. Especial attention was paid in not putting the subjects from the same litter at the same time point.

At the corresponding time-point, 500 μ l of blood samples from each of the four respective intact rats were collected into chilled microtubes containing 0.5 mg EDTA on the wall (50 μ l of EDTA solution of 10 mg/mL was added to each tube, agitated and then dried inside a fridge). Tubes with samples were immediately centrifuged at 1600 \times g for 15 min at 4 °C. Plasma supernatant (200 μ l per tube) was transferred to a new tube and stored at –70 °C until the ELISA test was performed. The Arg8–Vasopressin EIA Kit (Cat. 900-017, Assay Designs, Inc., Ann Arbor, MI 48108, USA) was used. The experimental procedure was the one recommended by the manufacturer of the ELISA vasopressin estimation kit. Each sample was analyzed in duplicate. The coefficients of variation (CV: standard deviation/mean) for the intra and inter assay variability were 11.28% and 9.9% respectively. This latter parameter was obtained calculating the CV of three standard curves done to the three kits used.

Perfusion-fixation and immunohistochemistry for Fos and AVP double labelling

Subjects ($n=6$) for this experiment were perfused 90 min posterior to time points WD6h and PVCT (i.e. 7.5 h of water deprivation and 90 min after the conflict test respectively). Briefly, rats were deeply anesthetized with an overdose of pentobarbital and perfused transcardially with 0.9% saline followed by cold fixative containing 4% of paraformaldehyde in 0.1 M sodium phosphate buffer (PB, pH 7.4) plus 15% v/v of saturated picric acid and 0.05% of glutaraldehyde for 15 min. Brains were removed, blocked, then thoroughly rinsed with PB. Vibratome coronal sections of 70 μ m of hypothalamus (spanning from Bregma –0.96 to –2.20 mm) were collected.

Immunofluorescence double-labelling method was used. Briefly, two alternated sections between Bregma –1.60 and –1.80 mm, (Paxinos and Watson, 2007) from each rat were chosen. These sections contain the main PVN lateral magnocellular part (PVNlm) which can be easily identified as a grey circular region with higher transparency under a low power stereoscopic microscope, as well as the medial parvocellular part, dorsal zone of the PVN (PVNm), main region of CRF mRNA expression, (Viau and Sawchenko, 2002), and the SON. This criterion was applied to select data for a valid comparison. Sections were blocked with 20% normal horse serum in Tris–buffered (TB, 0.05 M, pH 7.4) saline (0.9%) plus 0.3% of Triton X-100 (Tris buffered saline) for 1 h at room temperature and then immunoreacted with the following primary antibodies: rabbit anti-AVP (courtesy of RM Buijs, 1:1000) and Guinea pig anti-CRF (T-5007, 1:2000, Peninsula Laboratories, Torrance, CA, USA) for AVP/CRF double immunohistochemistry for region references and rabbit anti-Fos (SC52, 1:1000, Santa Cruz Biotechnology, Santa Cruz, CA, USA) and guinea pig anti-AVP (T-5048, 1:2000, Peninsula Laboratories). Sections were incubated overnight at 4 °C with gentle shaking. After corresponding washings, sections were further incubated with Alexa Fluor 488 donkey anti-rabbit IgG (1:1000, Molecular Probes Inc. Eugene, OR, USA) and Cy3 conjugated donkey anti-guinea pig IgG (1:1000, Jackson ImmunoResearch Laboratories, Inc., Baltimore, PA, USA) as secondary antibodies, in Tris buffered saline plus 1% of horse serum, at 4 °C overnight. At the end of the immunofluorescence reaction, sections were rinsed and mounted with Vectashield (Vector Laboratories, Inc., Burlingame, CA, USA) and analyzed by epi-fluorescence microscopy.

For Fos/AVP double labelling and total Fos+ nuclei quantification, total number of AVP+ neurons and the number of Fos+/AVP+ neurons from the PVNlm, and SON per each section were counted. Percents of double-labelled neurons in total AVP+ neurons were calculated. For quantification of total Fos activation, all of Fos+ nuclei inside the AVP immunoreactive magnocellular nuclei (SON and PVNlm) were counted. For PVNm, the counting was made with the help of a drawing tube: a drawn square of 0.04 mm² was placed on the visual field of the drawing tube coinciding with the PVNm zone so that Fos+ nuclei inside the square can be clearly identified and counted.

The second set of experiments was aimed at evaluating AVP content in the HNS before osmotic stressor application. Four rats per each group under basal conditions were processed for AVP immunofluorescence reaction using guinea pig anti-AVP (T-5048, 1:2000, Peninsula Laboratories) as the primary antibody and Alexa Fluor 488 donkey anti-guinea pig IgG (1:1000, Molecular Probes) as the secondary antibody. Optical density of immunoreactivity mainly related to hypothalamic–neurohypophysial tract (HNT) was measured in the anterior hypothalamic area (AHA, dorsal and ventral zones) of each group from antero–posterior-paired coronal sections ($n=10$) collected from the anterior hypothalamus (Bregma –1.08 mm to Bregma –1.86 mm). Fields in the regions (dorsal and ventral zone corresponding to the hypotha-

lamic–neurohypophysial tract) were chosen with 40× objective corresponding areas of 0.22 mm² and photomicrographs were taken using a digital camera with fixed sensibility. Digital pictures were analyzed using Fovea Pro 4.0 (Reindeer Graphics, Asheville, NC, USA). Herring bodies (axonal swellings in the hypothalamic–neurohypophysial tracts) in the fields were quantified. It has been suggested that Herring bodies function as a buffer for the massive vasopressin production, formed by the intermittent synthesis of this neuropeptide (Yukitake et al., 1977).

Double immunoperoxidase labelling of AVP and CRF for electron microscopy

Coronal sections of anterior hypothalamus containing PVN were cryoprotected with 10% sucrose for 10 min and 20% sucrose for 4 h at room temperature with gentle shaking and then underwent quick freeze-thaw procedure using liquid nitrogen and room temperature phosphate buffer (PB 0.1 M). Sections were then blocked with tris buffered saline without Triton X100, plus 20% normal swine serum for 1 h and incubated with rabbit anti-AVP and guinea pig anti-CRF antisera (T-4563 and T-5007, respectively, 1:2000 for both antibodies, Peninsula Laboratories) in Tris buffered saline plus 1% swine serum over two nights at 4 °C with gentle shaking. (Some of the sections underwent firstly incubation with fluorescent secondary antibodies: Alexa 488 conjugated donkey anti-rabbit and Cy3 anti-guinea pig to evaluate the efficacy of the immunoreaction before proceeding to the next step). For immunoperoxidase reaction, sections were rinsed and proceeded for the first secondary antibody incubation with swine anti-rabbit IgG with horseradish peroxidase conjugated (P021702, 1:100, Dako, Denmark) in Tris buffered saline+1% swine serum overnight at 4 °C. This immunoreaction was developed using 3,3'-diaminobenzidine (DAB, 0.5%, Electron Microscopy Sciences, Fort Washington, PA, USA) and hydrogen peroxide (H₂O₂, 0.01%) as substrates and intensified with nickel (400 μl 0.05 M nickel ammonium sulfate and 400 μl of ammonium chloride 0.4% in 20 ml TB) (black reaction product) ((Freund et al., 1990) for method reference). Due to the magnetic field of nickel, this product has a more efficient electron shielding. Hence, the labelling seen at electron microscopy is blacker, more homogeneous compared with the sole DAB labelling. For the second immunoreaction, sections were further incubated with goat anti-guinea pig IgG biotinylated antibody (Vector BA9500, 1:100) overnight at 4 °C followed by the incubation for 2 h at room temperature with avidin–biotin–peroxidase (ABC, 1:100 in TB; ABC Elite Kit, Vector Labs.). The immunolabelling was developed with DAB (0.05%) and 0.01% H₂O₂ in tris buffer (brown reaction product). Peroxidase reaction was stopped by rinsing the sections in TB.

Transmission electron microscopy

Selected coronal sections containing PVN_{IM} and parvocellular medial part (Bregma −1.56 to −1.72 mm) were fixed with 1% osmium tetroxide in 0.1 M PB for 1 h and dehydrated through a series of graded alcohols (including 45 min of incubation of 1% uranyl acetate in 70% ethanol), then rinsed with propylene oxide. Sections were flat embedded in Durcupan ACM epoxy resin (Electron Microscopy Sciences) following a period of resin penetration for more than 4 h at room temperature. Embedded sections on slide were polymerized at 60 °C for 2 days. Fragments of sections containing labelled Herring bodies in HNT and medial PVN were re-embedded in capsules and undertook further polymerization for 24 h. Ultrathin sections (70 nm) were cut with an ultramicrotome using a diamond knife. Sections were collected onto Pioloform-coated single slot grids. Sections were examined with a Philips CM100 transmission electron microscope. Digital electron micrographs were obtained with a digital micrograph 3.4 camera (Gatan, Inc., Pleasanton, CA, USA) and scaled with ImageJ (Image

Processing and analysis in Java, NIH, USA) and Adobe Photoshop.

Statistical analysis

Quantitative results were expressed as mean±standard error of mean (SEM). Groups were tested for differences by analysis of variance followed by the Bonferroni test, using Prism (GraphPad Software, San Diego, CA, USA). Differences were considered statistically significant at $P < 0.05$ (* $P < 0.05$, ** $P < 0.01$, and *** $P < 0.001$, vs. the control group).

RESULTS

Significantly potentiated anxious state in MH occurred only after water deprivation

Unconditioned and conditioned anxious states were assessed using two well-validated behavioural tests, the EPM and the VCT. EPM evaluates the exploration versus avoidance state placing the rat in an unconditioned environment with the closed arm representing safety and the open-elevated arm denoting novelty, though risky. Diminished time spent in the open arm and reduced number of entries implies higher unconditioned anxious state. The MH showed no significant differences in these two measured parameters (Fig. 1A). Subsequently, rats were subjected to WD, as an osmotic stressor, for 48 h. Then, thirsty rats underwent the conflict test in which they had to decide between drinking and possibly receiving a mild electrical shock or rather staying apart from the drinking spout. MH showed a significant reduction in the number of shocks received during the 5 min of the test (11.20 ± 1.68 , mean±SEM) compared to controls (37.50 ± 1.5) (Fig. 1B). Diazepam administration 30 min before the test effectively increased the punishing shocks received by both MH (240.6 ± 47.17) and control (258.2 ± 48.6) rats, resulting in no-significant difference between them.

Altered plasma AVP concentration dynamics during water deprivation and enhanced neuronal activation in PVN and SON of MH

Both plasma osmolarity or plasma AVP content generally reach their maximal levels between 12 and 16 h of WD and then both physiological parameters remain stable for a relatively long period (Rowland, 2007). As illustrated in Fig. 2, WD during this experiment effectively increased plasma AVP concentration, as analyzed with a commercially available Vasopressin ELISA kit (Assay Designs, Inc., Ann Arbor, MI, USA). The time course of this variation had a non-linear pattern. In both groups the baseline AVP plasmatic concentrations were around 4.8 pg/mL (control: 4.94 ± 0.26 pg/mL; MH: 4.74 ± 0.27 pg/mL). The value from control at WD6h was little changed compared to the basal level (5.55 ± 0.19 pg/mL). It reached its maximal levels at WD12h (17.18 ± 1.53 pg/mL), then slightly decreased at WD24h (13.73 ± 2.70 pg/mL) and remained substantially unchanged after VCT. In contrast, MH AVP plasma concentration had a steep increase already at WD6h approaching its maximal level (14.79 ± 0.71 pg/mL). From WD12h, the AVP levels in MH remained comparable to

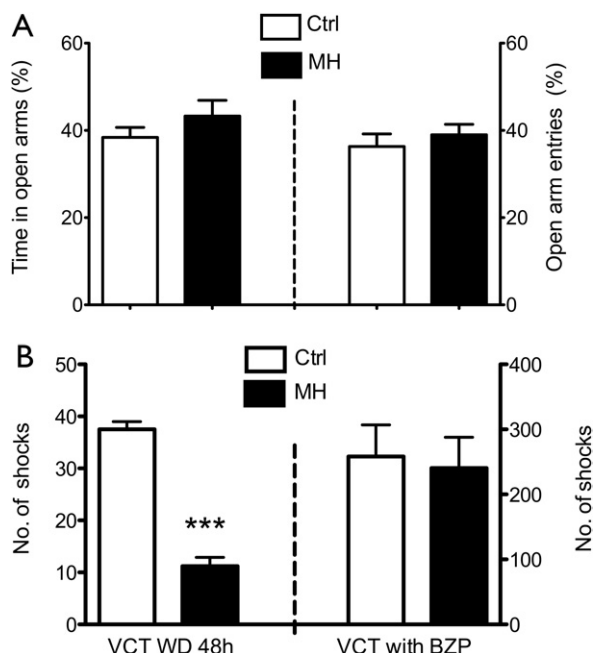


Fig. 1. MH offspring showed differential anxious states compared to control under unconditioned and conditioned behavioural tests for anxiety assessment. (A) Elevated plus maze test performed before water deprivation (WD) to evaluate unconditioned anxiety-related behaviour revealed by the percentages of both, left panel, time spent in the open arms related to the 5 min lapse and right panel, the entries to the open arms in the total entries to both open and closed arms. There are no-significant differences between control and MH groups regarding both metrics. ($n=16$); (B) Vogel conflict test (VCT) with 48 h of WD to assess conditioned anxious state which is reflected in the number of shocks received during the given time lapse (5 min) under the condition specified in the method section. Left panel: without any anxiolytic administration, MH rats showed a significant decrease in the number of shocks received during the test. ($n=8$). Right panel: with administration of benzodiazepine (BZP) (Diazepam, 2.5 mg/kg b.w, i.p) 30 min before the test, the shocks received by both MH and control subjects were greatly increased and the intergroup-difference observed without BZP disappeared. ($n=8$), mean \pm SEM, *** $P<0.001$.

those of the control until WD48h. Immediately after VCT, AVP plasma concentration in MH further increased as compared to controls (Fig. 2 PVCT time point).

In order to make a quantitative assessment of Fos induction in SON, PVNIm and PVNmPd and specifically the induction in AVP containing neurons, experimental subjects were perfused at 90 min posterior to the time points where plasma AVP concentrations showed significant differences. A significant increase in Fos/AVP double labelled neuron numbers was observed in MH at all experimental conditions (Fig. 3F). In all the three anatomical regions, a larger difference was revealed at PVCT, when experimental subjects underwent the conflict test and exhibited high anxious behaviours. Regarding the densities of the total Fos+ nuclei per regions, significant increases were observed except in PVNIm at WD6h. This phenomenon was heightened at the PVCT time point, when MH exhibited higher anxiety behaviour, that is larger difference was observed in the magnocellular nuclei, with $P<0.001$ for SON and $P<0.01$ for PVNIm, compared to $P<0.05$ for PVNmPd (Fig. 3G).

Abnormal AVP storage and some unusual features revealed by morphological analysis were observed in MH under basal condition

An increased AVP content in the AHA corresponding to hypothalamic–neurohypophysial tracts was observed by immunofluorescence (reflected as increased optical densities). Both ventral and dorsal parts of anterior hypothalamic areas (Fig. 4F) revealed increased immunoreactivity to AVP in MH subjects (dorsal AHA: MH 18.84 ± 0.67 , vs. control 16.57 ± 0.49 ; ventral AHA MH 14.34 ± 0.61 , vs. control 11.72 ± 0.87 , arbitrary units), which implied either increased number of vasopressinergic axons passing through the region or an increase in AVP content inside the fibres, or both (Fig. 4).

The number of Herring bodies throughout hypothalamic–neurohypophysial tracts was significantly higher in MH group than in control under basal condition (MH 7.2 ± 0.73 , vs. control 1.2 ± 0.20 , per 0.22 mm^2). In the electron microscope, the AVP-immunoperoxidase labelled Herring bodies were seen as un-myelinated large varicosities with diameters mainly ranging from 1 to $4\ \mu\text{m}$. Herring bodies contain highly compacted labelled dense core vesicles (Fig. 5).

MH AVP+ axon terminals make synapses on soma and dendrites of both CRF immunopositive and immunonegative neurons inside the PVN

We also addressed the ultrastructural features of the neuroendocrine fibres inside the PVN region and the possibility of reciprocal synaptic connections between AVP and CRF containing neurons. Tissue from the ventromedial part of the PVN (Fig. 6A) was re-embedded and examined under electron microscopy. AVP and CRF immunoreactivities (Nickel-DAB “black” and DAB “brown” reactions respectively) were found in both axon terminals and dendritic segments. Concerning the AVP labelled (AVP+) axons and axon terminals (AT), the labelled structures contained small clear as well as dense-core vesicles at highly vari-

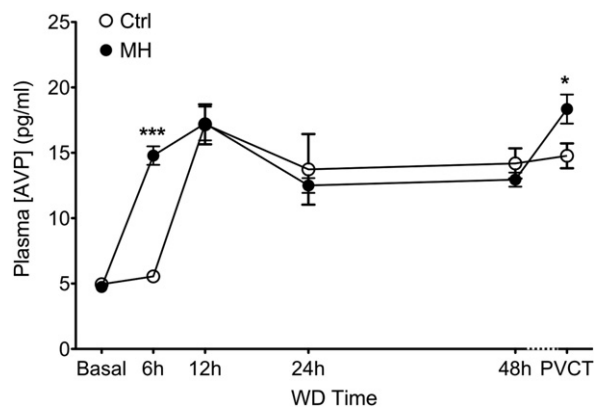


Fig. 2. MH had altered dynamics in plasma vasopressin concentration during water deprivation and post-Vogel conflict test (PVCT). MH time evolution curve of the plasma AVP concentration (mean \pm SEM) in function of WD progression showed an abnormal shape separating from the control at 6 h of WD and PVCT ($n=4$ for each time point). *** $P<0.001$, * $P<0.05$.

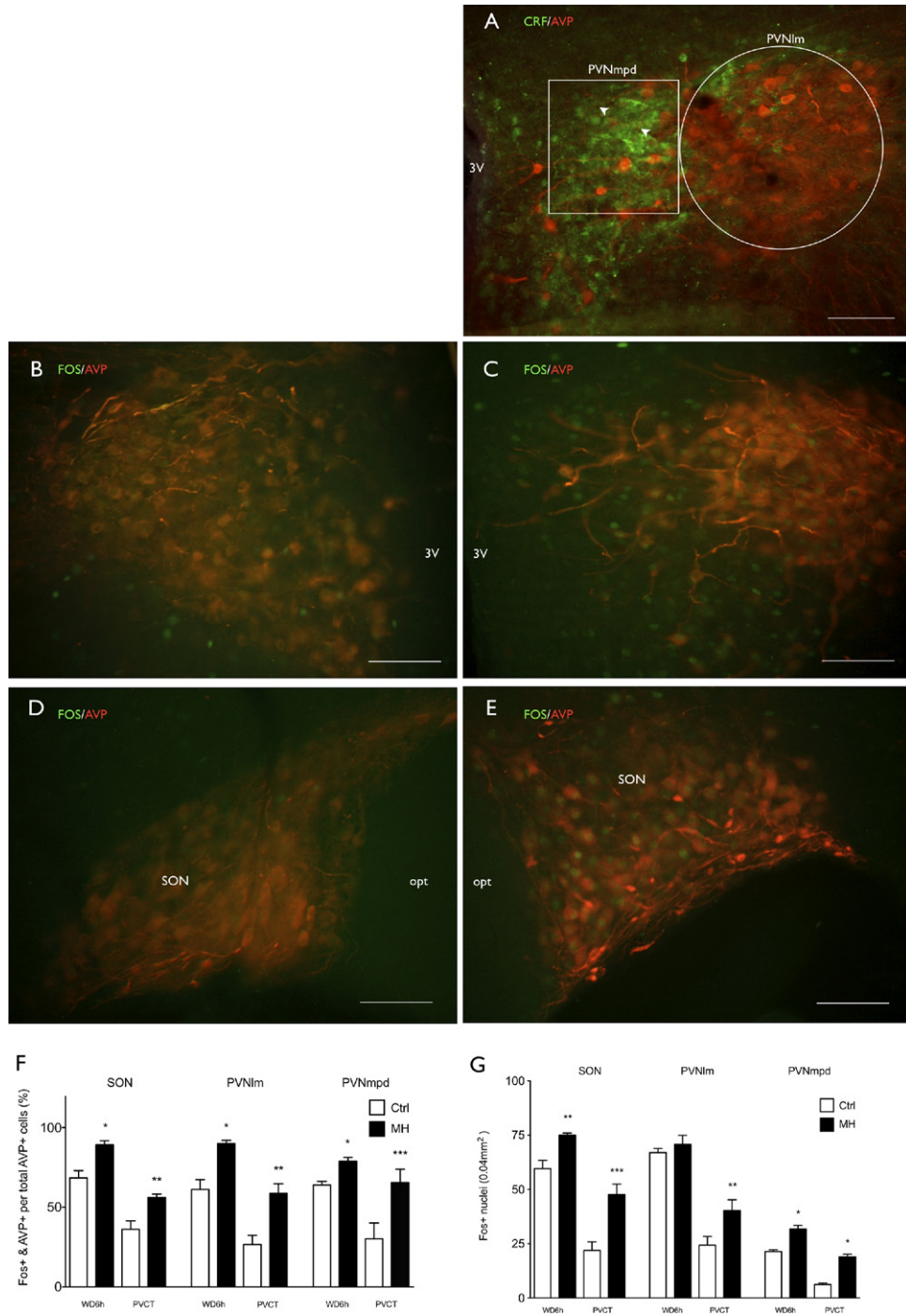


Fig. 3. Changes of Fos expression in paraventricular nucleus, lateral magnocellular part (PVNlm), medial parvocellular part, dorsal zone (PVNmpd) and supraoptic nuclei (SON) at 90 min posterior to the time points WD6h (6 h of water deprivation) and PVCT (Post Vogel conflict test, PVCT). Microphotographs illustrate the increased Fos expression at PVCT. (A) Microphotograph showing CRF/AVP immunoreactivity in PVN which corresponds to the sites where Fos+ nuclei were counted. Circle: PVNlm; square: PVNmpd. Arrowheads indicate AVP containing axons in the PVNmpd. (B, C) correspond to PVN of control and MH respectively; (D, E) SON of control and MH respectively. (F) Percentages of AVP+/Fos+ cells in relation to all AVP+ cells. (G) Densities of all Fos+ nuclei in the three anatomical regions at each experimental time point. 3V, third ventricle; Opt, optic tract. Scale bars=100 μ m. ($n=6$), mean \pm SEM, * $P<0.05$, ** $P<0.01$, *** $P<0.001$. For interpretation of the references to color in this figure legend, the reader is referred to the Web version of this article.

able ratios. AVP+ AT in MH were observed making synaptic contacts with CRF+ neuronal somata (Fig. 6E) and medium-sized dendrites (Fig. 6F–J). Five out of eight syn-

apses (62.5%) between AVP+ AT and PVN neuron dendrites are Gray's type I (asymmetric, characteristic of glutamatergic excitatory synapses, Fig. 6F–I). These AT ex-

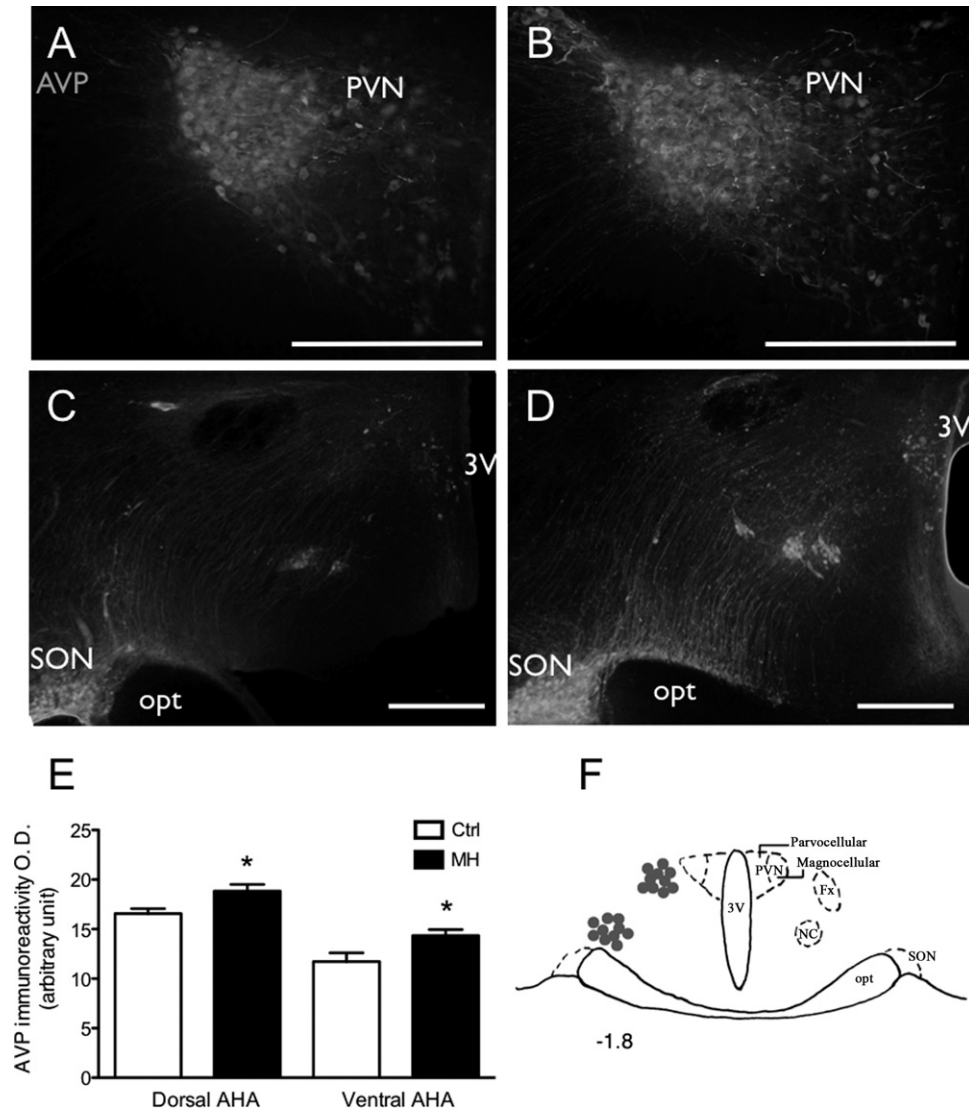


Fig. 4. Increased AVP immunoreactivity in hypothalamic–neurohypophysial tract under basal conditions. Photomicrographs show the AVP immunofluorescence labelling in PVN, (A) and (B), and the hypothalamic–neurohypophysial tracts in the anterior hypothalamic area (AHA), (C) and (D), from control and MH rats respectively. (An increase of AVP+ soma and dendritic area in MH rats compared to control was observed in PVN magnocellular division (for example see A and B)). (E) Histogram shows the optical density (OD) analysis of AVP immunoreactivity, mean \pm SEM, in which MH group showed a significant increase in both ventral and dorsal AHA. (F) Schematic representation of AHA (Bregma -1.08 to -1.86 mm according to Paxinos and Watson, 2007) where the measurement was performed ($n=10$ sections from four rats per group). 3V, third ventricle; PVN, paraventricular nucleus; Opt, optic tract; SON, supraoptic nucleus; Fx, fornix; NC, nucleus circularis. -1.8 : 1.80 mm posterior to Bregma. Scale bars=200 μ m. * $P<0.05$.

hibited a high content of small clear vesicles. On the other hand, AT which were more homogenously labelled by AVP-DAB-Nickel were observed to establish Gray's type II, (symmetric) synapses on CRF+ dendrites (Fig 6J). Two CRF+ AT having high content of small clear vesicles formed Gray's type I, asymmetric, synapses onto AVP+ dendritic segments (Fig 6K, L). We could not observe this type of synaptic connectivity in the same region of control subjects. Reciprocal synaptic connectivity between AVP and CRF containing neurons in PVN has not been previously described, to the best of our knowledge. However, a detailed quantitative assessment and a characterization of the precise origins (magnocellular vs. parvocellular and also suprachiasmatic nucleus or bed nucleus of the stria

terminalis) of the AT making synapses onto CRF soma/dendrites remains to be carried out.

DISCUSSION

Maternal hyperthyroidism due to Grave's disease and gestational transient thyrotoxicosis is a common endocrine condition during human pregnancy. Besides, inadequate doses for hormone replacement and insufficient monitoring could also put the fetal development under an iatrogenic hyperthyroid environment. In consonance with our previous study reporting that maternal hyperthyroid offspring possess a more reactive neuroendocrinological stress-coping system (Zhang et al., 2008), the results from this

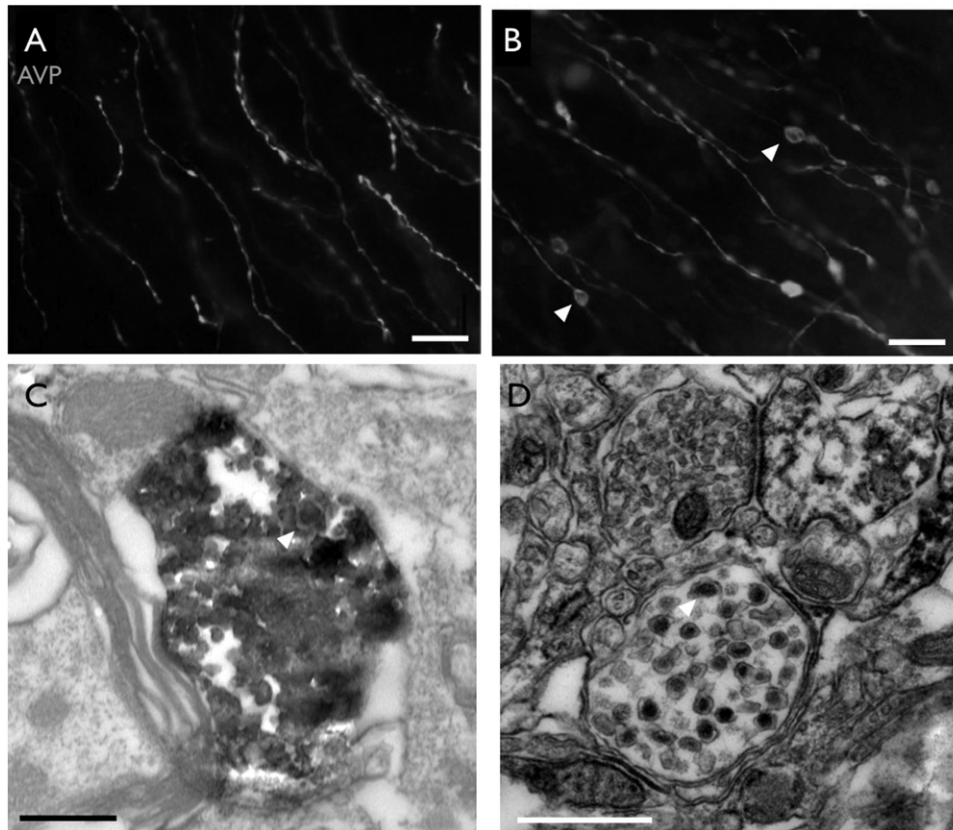


Fig. 5. Abundant Herring bodies throughout hypothalamo-neurohypophysial tract (HNT) were observed in MH anterior hypothalamus. (A, B) Photomicrographs of HNT from control and MH subjects, respectively. Arrowheads indicate Herring bodies. Scale bar: 20 μm . (C) AVP-immunoperoxidase-Nickel labelled Herring body seen by electron microscopy (EM). (D) EM photomicrograph to show a Herring body from a non-immunolabelled but lead citrate counterstained axon in order to better visualize the dense core vesicles (arrowheads, about 80–100 nm of diameter). Scale bar: 0.5 μm .

study clearly indicate that these subjects possess an altered hypothalamic vasopressinergic system resulting in expression of high anxious behaviour under a stressful condition.

Our previous work showed that maternal hyperthyroid adult offspring rats exhibited normal physiological and behavioural parameters unless they were exposed to a sub-chronic mild stressful condition, which triggered cognitive impairment and depression related behaviours. Enhanced serum corticosterone levels after an acute restraint test indicated an over-activated HPA axis (Zhang et al., 2008). In the present work, we tested whether this HPA over-activation could be triggered by an over-activated HNS.

Under basal conditions, an enhanced AVP immunoreactivity in the anterior hypothalamic area and a large amount of Herring bodies in the hypothalamo-neurohypophysial tracts in MH were observed. Herring bodies have been described as axonal swellings, containing neurosecretory and synaptic-like vesicles, and other subcellular components. It has been suggested that Herring bodies function as a buffer for the massive vasopressin production (Yukitake et al., 1977). Under water deprivation, MH plasma concentration of AVP increased dramatically already at WD6h which is consistent with a greater amount of AVP stored under basal condition readily to be released

upon stimuli arrival. At PVCT time point, another significant increase of plasma AVP concentration was observed. These observations clearly indicate that these individuals possess an altered AVP system, not only due to a greater storage but also inferred a more reactive system for a more active synthesis and/or an easier release. It is worth mentioning that in both groups the baseline AVP plasmatic concentrations were around 4.8 pg/mL (control: 4.94 ± 0.26 ; MH: 4.74 ± 0.27), which is slightly higher than reported in the literature using the same kit (Haley and Flynn, 2006). This phenomenon could be due to the sampling procedure—samples were obtained from the tails of restraint-tube immobilized rats. In spite of previous habituation described in the method section, this procedure could still induce a slight increase of plasma AVP concentration due to the immobilization, as can be observed in previous reports in the literature (Hashimoto et al., 1989; Aguilera and Kiss, 1993). Data obtained from naturally AVP-deficient Brattleboro rats showed a significant deficiency of increase of plasma adrenal corticotrophin during restraint stress (Zelena et al., 2009), which suggest a critical role of AVP in this stress coping processes, hence, indirectly support this explanation.

At the same time points where plasma AVP concentration showed significant differences, Fos expression in

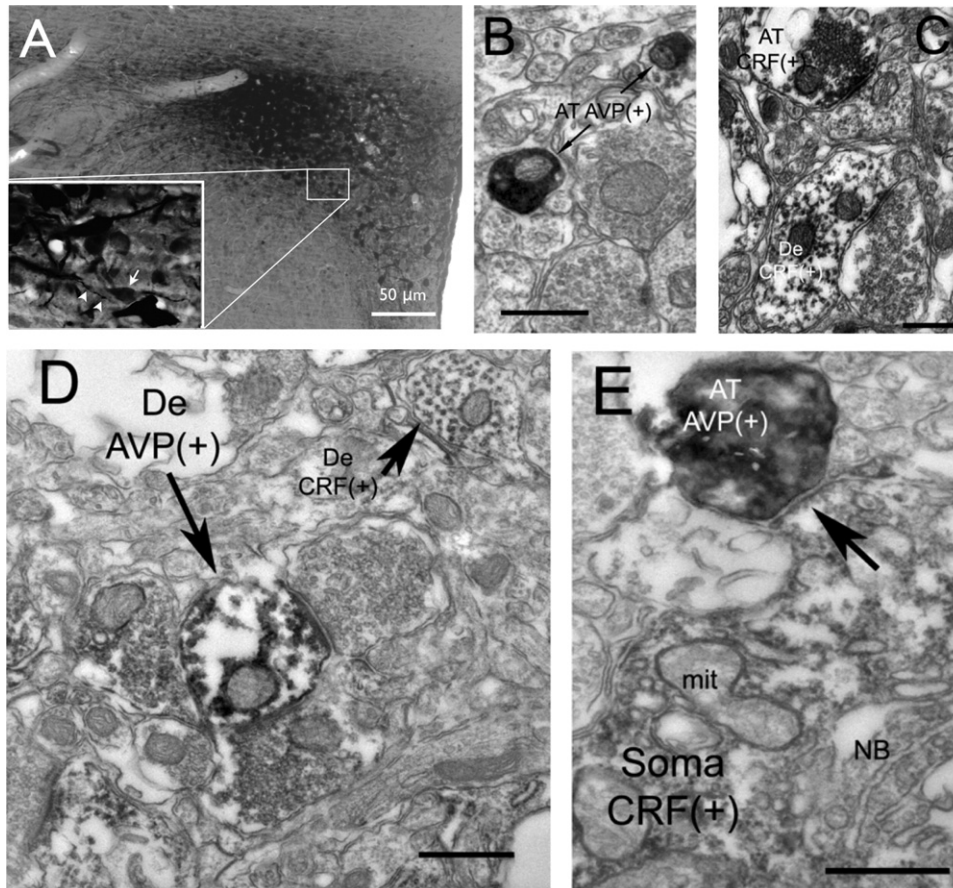


Fig. 6. Reciprocal synaptic connections between AVP and CRF neurons in the ventromedial part of the PVN. (A) A representative photomicrograph of a dual-immunoperoxidase reaction of a MH PVN (Bregma -1.80 mm) to illustrate the whole region of PVN and the sub-region (ventromedial division of PVN, indicated by a square) where tissue was taken for EM examination. DAB only (brown): CRF containing neurons, mainly located in the medial parvocellular part of the PVN; DAB-Nickel (black): AVP containing neurons mainly located in lateral magnocellular part of the PVN. The insert shows a representative light microscopy image of the region with dual-immunoperoxidase reaction prepared for EM examination. Arrowheads indicate AVP(+) black nickel DAB immunoreaction (ir) and arrows indicate CRF(+) brown-DAB-ir. (B, C) Aimed to show the different aspects of DAB-Nickel (AVP+, B) and sole DAB (CRF+, C) axonal labelling. AT, axon terminals. The DAB-Nickel labelling exhibits more homogenous and darker features because of the magnetic shield of Nickel, which deviates electrons more efficiently. De, dendrite. (D) Shows the different aspects of labelling in dendritic segments. (E) An AVP(+) AT making asymmetric synapse (black arrow) to a CRF(+) neuron somata. NB, Nissl bodies; mit, mitochondrion.

AVP containing neurons in the SON, PVNlm and PVNmpd showed a significant increase in the counts of double labelled cells indicating an enhanced activation of vasopressinergic system. Concerning the total Fos activation in the three regions, it is interesting to observe that in the PVNmpd, where the main cellular population of CRF containing neurons is located (see Fig. 3A and also (Viau and Sawchenko, 2002)), the difference of expression is already evident at WD6h. It remains possible that PVNlm Fos/AVP hyperactivation is passively fed forward from PVNmpd. However, this seems unlikely given that there were not other external stimuli for the activation of the HPA axis (PVNmpd) except the osmotic stressor at WD6h. Hence, it is rational to consider that there is a greater influence from the PVN lateral magnocellular part to the medial parvocellular part, dorsal zone, without excluding possible reciprocal influences between these two PVN divisions. Moreover, at the PVCT time point when the MH showed a higher anxiety behaviour, a larger difference of Fos counts was observed in the magnocellular nuclei ($P < 0.001$ for

SON and $P < 0.01$ for PVNlm, compared to $P < 0.05$ for PVNmpd, main location of CRF neurons). This finding further confirmed our hypothesis that the main influence of this activation of PVNmpd comes from PVNlm AVP neurons. In the PVNlm no significant difference was found for total number of Fos+ nuclei density, at WD6h time point although the Fos/AVP double labelled cell count of MH was significantly enhanced. This phenomenon could be attributed to the Fos activation of other cell populations in the region.

In our MH model, unconditioned anxiety measurement showed no significant difference with control groups. We have tested anxiety-like behaviour with the EPM test in both basal condition (from this study) and under sub-chronic mild stress (Hernandez et al., 2007). In both cases we did not observe an increased unconditioned anxious state compared with control. The Vogel thirsty rat conflict test (VCT) assesses conditioned anxiety-behaviour under WD condition (Millan, 2003; Millan and Brocco, 2003), which involved intrinsically the activation of HNS and an

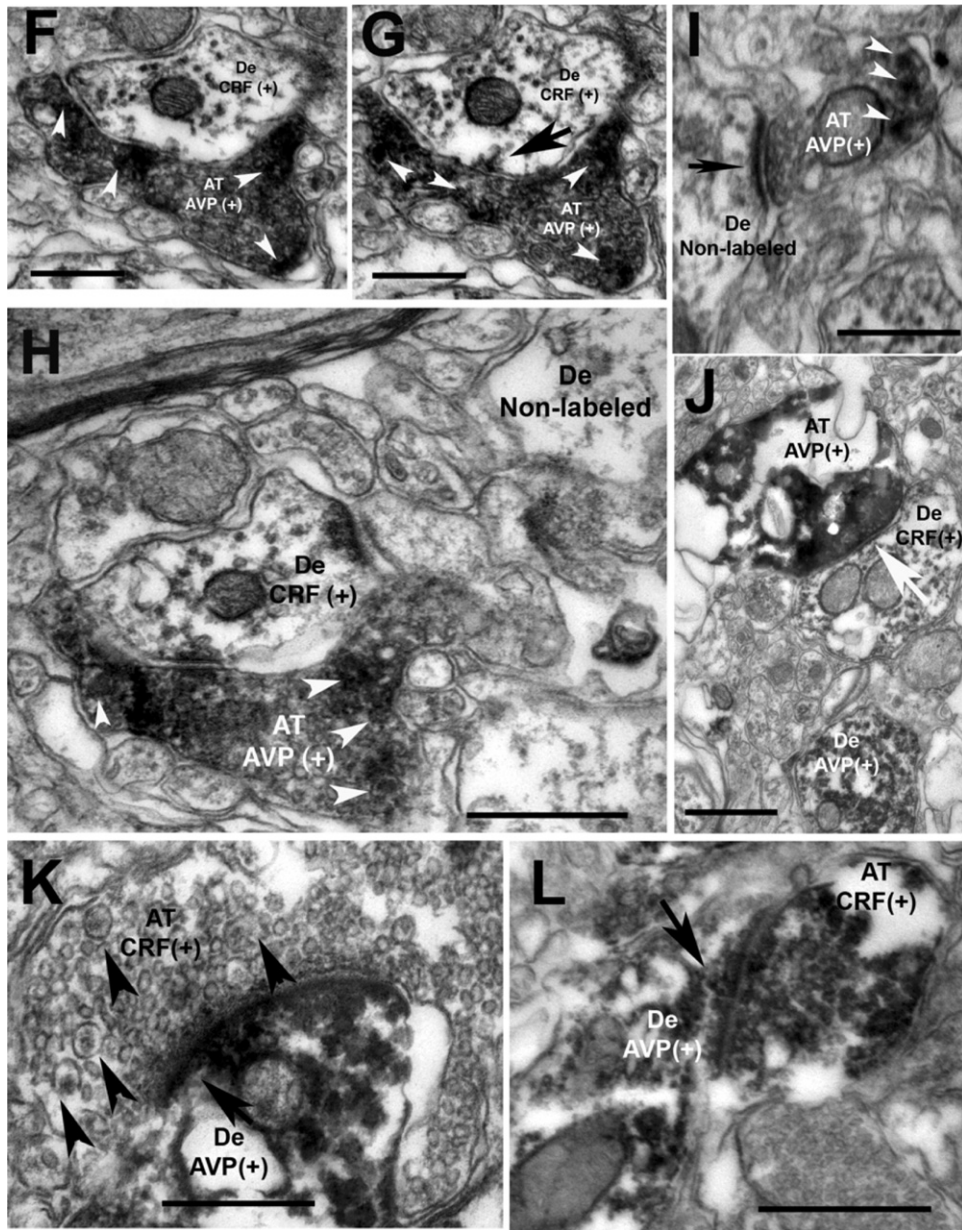


Fig. 6. (Continued.) (F–H) Serial photomicrographs from three adjacent sections (ultramicrotome setting for 70 nm) of an AVP(+) AT with abundant small clear vesicles establishing a type I synapse (black arrow) with a CRF(+) dendrite. A non-labelled dendrite is marked for comparison purposes. White arrowheads indicate dense core vesicle (dcv) containing AVP. (I) Another AVP(+) AT making type I synapse (black arrow) onto a non-labelled dendrite. White arrowheads: dcv-containing AVP. (J) A strongly labelled AVP(+) AT making a type II, symmetrical, synapse (white arrow) onto a CRF(+) dendrite. An AVP(+) dendrite was also marked for comparison purpose. This synapse was followed by three more sections, which showed similar features. Hence they are not showed here. (K) A weakly labelled CRF(+) axon containing abundant small clear vesicles and large dcv containing CRF (indicated by black arrowheads) making an asymmetric synapse on to an AVP(+) dendrite (black arrow). (L) Another example of the later phenomenon. Scale bar: 0.5 μm .

increase in the plasma concentration of AVP. During the last step of the VCT, MH rats exhibited a significantly higher anxiety-related behaviour than control rats. These high anxiety behaviours showed by MH coincided with another significant increase of AVP plasma concentration (PVCT time point), indicating that the MH HNS is responsive to this mild stressor capable to further increase their plasmatic release of AVP. This observation was consistent with the significant increase of Fos expression in the three

regions above mentioned. Although the intracerebral AVP release under VCT experimental condition was not measured in this study, this parameter is likely to be increased, according to previous evidence found in the literature. For instance, with microdialysis Ludwig et al. (Ludwig et al., 1994) found increased intra-SON AVP release upon a local hyperosmotic NaCl infusion, which indicates that the osmotic receptor activation of the vasopressinergic magnocellular nucleus indeed elicits the central release, in

parallel to the peripheral release. In this sense, intra-PVN AVP release is likely increased in this animal model. Evidence from *in vitro* extracellular recordings following bath application of 10^{-7} M of AVP showed that the majority of recorded cells located in the medial PVN present excitatory responses (Inenaga and Yamashita, 1986). Since the high anxious behaviour was only detected with VCT, once osmotic stressor was applied and not with the EPM, it is rational to consider that the main cause of the expressed high anxious state was due to the major physiological mechanism to cope with this stressor, that is vasopressinergic system activation. This evidence is in concordance with our finding of significant augment of Fos⁺ neurons in the medial parvocellular dorsal zone of PVN region, at 90 min post-VCT, suggesting that the hypothalamic part of HPA axis is more activated in correlation with the enhanced activation of HNS. The medial parvocellular division of the PVN is the key neural part of the HPA axis. It is a target region for benzodiazepines as anxiolytic agents (Cullinan, 2000). The fact that this phenomenon was effectively reversed by benzodiazepine administration supports this explanation.

There is extensive evidence about intra-PVN release of AVP during stress coping (Engelmann et al., 2004; Leng and Ludwig, 2008). The possible release mechanisms include dendritic release by exocytosis in the PVN and lateral hypothalamus, as previously demonstrated elegantly by Pow and Morris at electron microscopy (EM) level (Pow and Morris, 1989). Experimental evidences have shown that intra-PVN administration of an AVP V1 receptor antagonist resulted in a decrease of anxiety-related behaviour of the high anxiety bred rats (Engelmann et al., 2004) and increased AVP release within PVN, measured by microdialysis, was observed during anxious situations (Wotjak et al., 1996). These data support the assumption that higher contents of released AVP within PVN serve as a physiological substrate for anxiogenesis, which is in concordance with the results from this study.

AVP over-expression in hypothalamus and potentiated activation and release of AVP observed in the present study could be generated due to an increased number of neurons or extensive wiring due to the maternal hyperthyroidism. Data obtained from cell culture of cerebellar granule cells showed that thyroid hormone promoted Bcl-2 expression, preventing apoptosis of newly formed and early differentiated neurons in a dose-dependent manner (Muller et al., 1995). But, could synaptic connections between AVP and CRF containing neurons play a role in high anxiety MH rats?

The most relevant finding of this study is the identification of the reciprocal synaptic connections between AVP and CRF neurons in ventromedial PVN in MH. The majority of the synapses found are Gray's type I (asymmetric, characteristic of glutamatergic excitatory synapses) with colocalization of small clear and dense-core vesicles, being the latter ones localized mainly in the perisynaptic regions. This observation is in concordance with other studies in the literature reporting short axon collaterals (Sofroniew and Glasmann, 1981) or second axon branched from soma

or proximal dendrite of magnocellular neurosecretory neurons which project intracerebrally. Previous reports have shown that glutamatergic neurons formed prominent cell populations in several hypothalamic nuclei including various parvocellular and magnocellular subdivisions of the PVN (Ziegler et al., 2002; Hrabovszky et al., 2007) and AVP receptors are localized preferentially in perisynaptic regions (Landgraf and Neumann, 2004). AVP release is reported to influence the activation of intracellular Ca^{2+} storage and modify the input synaptic strength as well as to alter the interaction between transcription factors and gene promoters (Landgraf and Neumann, 2004). Moreover, it has been found that among the AVP metabolite, the pentapeptidic fragment AVP(4–8), which did not possess classical endocrine effects, has high effectiveness on behaviour response since its potencies in CNS were hundreds fold higher than those of AVP itself (Burbach et al., 1983). G-protein-coupled receptors for AVP(4–8) were identified on rat hippocampal synaptosomal membrane (Yan and Du, 1998) and its binding resulted in the accumulation of the second messenger IP3 (Yan et al., 2002). Other neurotrophic and branching promoting effects of this AVP metabolite have also been reported (Zhou et al., 1997; Yan et al., 2002). Although, the meaning of the frequent observation of reciprocal synaptic contacts between AVP and CRF containing neurons inside PVN of MH rats remains yet unclear, it suggested the existence of abnormal synaptogenesis which produces short-circuit-like aberrant reciprocal synaptic connections in this neuro-hormonal stress-coping related brain region that could serve as a pathophysiological substrate for the exhibited stress over-reactivity and high anxiety behaviours.

CONCLUSION

In conclusion, the initial EM observation of the reciprocal synaptic connections between AVP and CRF containing neurons in the hypothalamic paraventricular region from this study suggests the existence of synaptic pathways between these two main stress-coping related neuropeptidergic systems in stress over-reactive MH. Hence, our findings open a potential research area for the investigation of the anatomo-functional substrates underlying stress related emotional disturbances in MH offspring. Furthermore, this study demonstrated that hyperthyroidism in an early window of development leads to persistent changes in structure and function of the rat brain, which result in a reduced ability of coping with certain stressful conditions. Due to the possible relevance of this disorder to public health, further detailed studies should be encouraged to be pursued.

Acknowledgments—This study was supported by grants: UNAM IN210406, IN224407; CONACYT: 49704, 79641. LZ was on sabbatical leave at MRC Anatomical Neuropharmacology Unit, Oxford University—hospitality from Peter Somogyi and fellowships from DGAPA-UNAM and CONACYT Mexico are greatly acknowledged. MPM, VSH and FSE were supported by DGAPA-UNAM undergraduate scholarships. We would like to thank Paul Bolam

(Oxford), Francesco Ferraguti (Innsbruck) and Teresa Morales (INB, UNAM), for critical reading of the manuscript, to Ruud M Buijs for rabbit anti-AVP antibody donation, Raul Aguilar for providing some facilities for behavioural tests and Patricia Espinosa for technical assistance for ELISA.

REFERENCES

- Aguilera G, Kiss A (1993) Activation of magnocellular vasopressin responses to non-osmotic stress after chronic adrenal demedullation in rats. *J Neuroendocrinol* 5:501–507.
- Antoni FA (1993) Vasopressinergic control of pituitary adrenocorticotropin secretion comes of age. *Front Neuroendocrinol* 14:76–122.
- Auso E, Lavado-Autric R, Cuevas E, Del Rey FE, Morreale De Escobar G, Berbel P (2004) A moderate and transient deficiency of maternal thyroid function at the beginning of fetal neocortico-genesis alters neuronal migration. *Endocrinology* 145:4037–4047.
- Burbach JP, Kovacs GL, de Wied D, van Nispen JW, Greven HM (1983) A major metabolite of arginine vasopressin in the brain is a highly potent neuropeptide. *Science* 221:1310–1312.
- Caldwell HK, Lee HJ, Macbeth AH, Young WS 3rd (2008) Vasopressin: behavioral roles of an “original” neuropeptide. *Prog Neurobiol* 84:1–24.
- Cullinan WE (2000) GABA(A) receptor subunit expression within hypophysiotropic CRH neurons: a dual hybridization histochemical study. *J Comp Neurol* 419:344–351.
- Engelmann M, Landgraf R, Wotjak CT (2004) The hypothalamic-neurohypophysial system regulates the hypothalamic-pituitary-adrenal axis under stress: an old concept revisited. *Front Neuroendocrinol* 25:132–149.
- Evans IM, Pickard MR, Sinha AK, Leonard AJ, Sampson DC, Ekins RP (2002) Influence of maternal hyperthyroidism in the rat on the expression of neuronal and astrocytic cytoskeletal proteins in fetal brain. *J Endocrinol* 175:597–604.
- File SE, Lippa AS, Beer B, Lippa MT (2004) Animal tests of anxiety. *Curr Protoc Neurosci* Chapter 8: Unit 8.3.
- Frank E, Landgraf R (2008) The vasopressin system—from antidiuresis to psychopathology. *Eur J Pharmacol* 583:226–242.
- Freund TF, Gulyas AI, Acsady L, Gorcs T, Toth K (1990) Serotonergic control of the hippocampus via local inhibitory interneurons. *Proc Natl Acad Sci U S A* 87:8501–8505.
- Haley GE, Flynn FW (2006) Agonist and hypertonic saline-induced trafficking of the NK3-receptors on vasopressin neurons within the paraventricular nucleus of the hypothalamus. *Am J Physiol Regul Integr Comp Physiol* 290:R1242–R1250.
- Hashimoto K, Murakami K, Takao T, Makino S, Sugawara M, Ota Z (1989) Effect of acute ether or restraint stress on plasma corticotropin-releasing hormone, vasopressin and oxytocin levels in the rat. *Acta Med Okayama* 43:161–167.
- Heinrichs SC, Koob GF (2006) Application of experimental stressors in laboratory rodents. *Curr Protoc Neurosci* Chapter 8: Unit 8.4.
- Hernandez VS, Medina MP, Valle-Leija P, Vega-Gonzalez A, Morales T, Zhang L (2007) Enhanced basal exploratory activity, anti-nociceptive behaviour and increased TH and CRF immunoreactivity in amygdala of adult rats subjected to maternal hyperthyroidism. In: *IBRO World Congress of Neuroscience*, p. 287, Melbourne, Australia.
- Hrabovszky E, Deli L, Turi GF, Kallo I, Liposits Z (2007) Glutamatergic innervation of the hypothalamic median eminence and posterior pituitary of the rat. *Neuroscience* 144:1383–1392.
- Inenaga K, Yamashita H (1986) Excitation of neurones in the rat paraventricular nucleus in vitro by vasopressin and oxytocin. *J Physiol* 370:165–180.
- Landgraf R (2005) Neuropeptides in anxiety modulation. *Handb Exp Pharmacol* 169:335–369.
- Landgraf R, Neumann ID (2004) Vasopressin and oxytocin release within the brain: a dynamic concept of multiple and variable modes of neuropeptide communication. *Front Neuroendocrinol* 25:150–176.
- Leng G, Ludwig M (2008) Neurotransmitters and peptides: whispered secrets and public announcements. *J Physiol* 586:5625–5632.
- Ludwig M, Horn T, Callahan MF, Grosche A, Morris M, Landgraf R (1994) Osmotic stimulation of the supraoptic nucleus: central and peripheral vasopressin release and blood pressure. *Am J Physiol* 266:E351–E356.
- Millan MJ (2003) The neurobiology and control of anxious states. *Prog Neurobiol* 70:83–244.
- Millan MJ, Brocco M (2003) The Vogel conflict test: procedural aspects, gamma-aminobutyric acid, glutamate and monoamines. *Eur J Pharmacol* 463:67–96.
- Muller Y, Rocchi E, Lazaro JB, Clos J (1995) Thyroid hormone promotes BCL-2 expression and prevents apoptosis of early differentiating cerebellar granule neurons. *Int J Dev Neurosci* 13:871–885.
- Paxinos G, Watson C (2007) *The rat brain in stereotaxic coordinates*, 6th ed. San Diego, CA: Academic Press.
- Pierce RC, Kalivas PW (2007) Chapter 8: Locomotor behavior. *Curr Protoc Neurosci* Unit 8.1.
- Pow DV, Morris JF (1989) Dendrites of hypothalamic magnocellular neurons release neurohypophysial peptides by exocytosis. *Neuroscience* 32:435–439.
- Ring RH (2005) The central vasopressinergic system: examining the opportunities for psychiatric drug development. *Curr Pharm Des* 11:205–225.
- Rowland NE (2007) Food or fluid restriction in common laboratory animals: balancing welfare considerations with scientific inquiry. *Comp Med* 57:149–160.
- Sofroniew MV, Glasmann W (1981) Golgi-like immunoperoxidase staining of hypothalamic magnocellular neurons that contain vasopressin, oxytocin or neurophysin in the rat. *Neuroscience* 6:619–643.
- Varas SM, Jahn GA, Gimenez MS (2001) Hyperthyroidism affects lipid metabolism in lactating and suckling rats. *Lipids* 36:801–806.
- Viau V, Sawchenko PE (2002) Hypophysiotropic neurons of the paraventricular nucleus respond in spatially, temporally, and phenotypically differentiated manners to acute vs. repeated restraint stress: rapid publication. *J Comp Neurol* 445:293–307.
- Vogel JR, Beer B, Clody DE (1971) A simple and reliable conflict procedure for testing anti-anxiety agents. *Psychopharmacologia* 21:1–7.
- Vulsma T, Gons MH, de Vijlder JJ (1989) Maternal-fetal transfer of thyroxine in congenital hypothyroidism due to a total organification defect or thyroid agenesis. *N Engl J Med* 321:13–16.
- Walf AA, Frye CA (2007) The use of the elevated plus maze as an assay of anxiety-related behavior in rodents. *Nat Protoc* 2:322–328.
- Wotjak CT, Kubota M, Liebsch G, Montkowski A, Holsboer F, Neumann I, Landgraf R (1996) Release of vasopressin within the rat paraventricular nucleus in response to emotional stress: a novel mechanism of regulating adrenocorticotrophic hormone secretion? *J Neurosci* 16:7725–7732.
- Yan QW, Du YC (1998) AVP (4–8) may stimulate a G protein-coupled receptor in rat hippocampal synaptosomal membranes. *Sheng Wu Hua Xue Yu Sheng Wu Wu Li Xue Bao (Shanghai)* 30:505–509.
- Yan QW, Qiao LY, Du YC (2002) AVP (4–8)-induced branching signaling pathway was mediated by a putative GPCR in rat brain. In: *Peptide science—present and future* (Shimonishi Y, ed), pp 174–178. New York: Kluwer Academic Publishers.
- Yukitake Y, Taniguchi Y, Kurosumi K (1977) Ultrastructural studies on the secretory cycle of the neurosecretory cells and the formation of Herring bodies in the paraventricular nucleus of the rat. *Cell Tissue Res* 177:1–8.

Zelena D, Domokos A, Jain SK, Jankord R, Filaretova L (2009) The stimuli-specific role of vasopressin in the hypothalamus-pituitary-adrenal axis response to stress. *J Endocrinol* 202:263–278.

Zhang L, Hernandez VS, Medina-Pizarro M, Valle-Leija P, Vega-Gonzalez A, Morales T (2008) Maternal hyperthyroidism in rats impairs stress coping of adult offspring. *J Neurosci Res* 86:1306–1315.

Zhou AW, Li WX, Guo J, Du YC (1997) Facilitation of AVP(4–8) on gene expression of BDNF and NGF in rat brain. *Peptides* 18: 1179–1187.

Ziegler DR, Cullinan WE, Herman JP (2002) Distribution of vesicular glutamate transporter mRNA in rat hypothalamus. *J Comp Neurol* 448:217–229.

(Accepted 27 March 2010)
(Available online 3 April 2010)

Maternal hyperthyroidism in rats impairs stress coping of adult offspring

Zhang L., **Hernández V. S.**, Medina-Pizarro M., Valle-Leija P., Vega-González A., Morales T.

J. Neurosci. Res, 2008, 86: 1306 – 1315

My contributions in:

- Conception of the study: +
- Performance of the experiments:
 - o Surgery for T4 pumps in dams: +++
 - o Design and application of the chronic mild stress protocol +++
 - o Behavioral assessment of spatial memory +++
 - o Behavioral assessment for “depressive behavior” +++
 - o Measurement of corticosterone concentrations +++
 - o Immunohistochemical reactions and analysis +++
 - o Golgi-Cox impregnation -
- Statistical analysis: +
- Discussion of the results: ++
- Preparation of the paper: +

(-): No contribution; (+): Average contribution; (++): Important contribution; (+++); Main contribution

Maternal Hyperthyroidism in Rats Impairs Stress Coping of Adult Offspring

Limei Zhang,^{1*} Vito S. Hernández,¹ Mauricio Medina-Pizarro,¹ Pablo Valle-Leija,¹ Arturo Vega-González,¹ and Teresa Morales²

¹Departamento de Fisiología, Facultad de Medicina, Universidad Nacional Autónoma de México, México DF, México

²Departamento de Neurobiología Celular y Molecular, Instituto de Neurobiología, Universidad Nacional Autónoma de México, Querétaro, México

Given the evidence that maternal hyperthyroidism (MH) compromises expression of neuronal cytoskeletal proteins in the late fetal brain by accelerated neuronal differentiation, we investigated possible consequences of MH for the emotional and cognitive functions of adult offspring during acute and subchronic stress coping. Experimental groups consisted of male rat offspring from mothers implanted with osmotic minipumps infusing either thyroxine (MH) or vehicle (Ctrl) during pregnancy. Body weight and T4 level were monitored during the first 3 postnatal months, and no differences were found with the controls. We analyzed hippocampal CA3 pyramidal neurons and dentate granular cell morphology during several postnatal stages and found increased dendritic arborization. On postnatal day 90 a modified subchronic mild stress (SCMS) protocol was applied to experimental subjects for 10 days. The Morris water maze was used before, during, and after application of the SCMS protocol to measure spatial learning. The tail suspension test (TST) and forced-swimming test (FST) were used to evaluate behavioral despair. The MH rats displayed normal locomotor activity and spatial memory prior to SCMS, but impaired spatial learning after acute and chronic stress. In both the FST and TST we found that MH rats spent significantly more time immobile than did controls. Serum corticosterone level was found to increase after 30 min of restraint stress, and corticotropin-releasing factor immunoreactivity was found to be increased in the central nucleus of the amygdala. Our results suggest that MH in rats leads to the offspring being more vulnerable to stress in adulthood. © 2007 Wiley-Liss, Inc.

Key words: depression; spatial learning; corticotropin releasing factor; corticosterone

Hormones markedly affect neuronal structure and function in various ways throughout life. During pregnancy, maternal thyroid hormones [triiodothyronine (T3) and thyroxine (T4)] cross the placenta in rat (Obregon et al., 1984; Morreale de Escobar et al., 1988) and human (Vulsma et al., 1989) and are postulated to regulate fetal brain development. The relatively inactive

T4 is converted to the more active form, T3, in brain tissue by the action of the enzyme deiodinase type II (Tanaka et al., 1981; Courtin et al., 1988). Thyroid hormone (TH) appears to regulate those processes associated with terminal brain differentiation such as dendritic and axonal growth, synaptogenesis, neural migration, and myelination (for a review, see Oppenheimer and Schwartz, 1997). TH also plays a significant role in the proliferation and survival of brain cells. A deficiency of TH alters the expression of several members of the Bcl-2 family, down-regulating proapoptotic genes and up-regulating antiapoptotic ones (Singh et al., 2003), and increases pro-nerve growth factor and p75 neurotrophin receptor levels associated with enhanced apoptosis (Kumar et al., 2006) in developing rat cerebellum and cerebral cortex, respectively.

Most studies of prenatal thyroid disorders, both in humans and in rats, have centered on hypofunction because of the high incidence of hypothyroidism and the severe consequences it has for offspring. Nevertheless, maternal hyperthyroidism (MH) is a significant endocrinologic disorder in pregnancy. The prevalence of thyrotoxicosis, predominantly Graves' disease, has been reported to be 0.05–0.2%, with an additional 3% of mothers exhibiting gestational transient thyrotoxicosis (Burrow, 1993; Glinioer, 1997; Polak et al., 2006). However, according to clinical reports, only 1% of children born to women with Graves' disease are described as having hyperthyroidism, and overt neonatal hyperthyroidism is rare and concerns only 1 of 50,000 neonates (Polak, 1998). On the other hand, studies in an animal model of MH have shown that this condition

Contract grant sponsor: CONACYT; Contract grant number: 46141-M (to L.Z.); Contract grant sponsor: DGAPA-UNAM; Contract grant numbers: IN210406 (to L.Z.), IN224407 (to A.V.G.), IN205706 (to T.M.).

*Correspondence to: Limei Zhang, MD/PhD, Department of Physiology, Faculty of Medicine, UNAM, México City 04510, México D. F. E-mail: limei@servidor.unam.mx

Received 3 May 2007; Revised 4 July 2007 and 24 August 2007; Accepted 16 September 2007

Published online 11 December 2007 in Wiley InterScience (www.interscience.wiley.com). DOI: 10.1002/jnr.21580

compromises expression of neuronal and astrocytic cytoskeletal proteins in the late fetal brain, suggesting accelerated neuronal differentiation (Evans et al., 2002). This aberrant timing of the central nervous system (CNS) development might lead to subtle but irreversible changes in its synaptic wiring, which could exert crucial influences on neural plasticity in adulthood, although the individual might be seen as normal in an unaltered situation. Despite numerous studies on the molecular and neurochemical effects of hyperthyroidism in the prenatal period, little is known about the long-term consequences of such postulated early-developmental acceleration of the CNS in the adulthood of offspring.

Any physical or psychological stressor that threatens the homeostasis of an organism can initiate a set of behavioral and neuroendocrine responses intended to help the organism to adapt to the altered situation. In conducting this neuroendocrine response, the limbic-hypothalamo-pituitary-adrenal axis and the sympathoadrenal axis are two major pathways mediating the major components of the stress response (Gulpinar and Yegen, 2004). Recent opinions on stress emphasize that there are individual differences and several response patterns in coping with these challenges (McEwen and Sapolsky, 1995). The role of stress in induction, maintenance, and relapse of psychiatric dysfunction is well established, and there is good evidence that changes in glutamatergic and dopaminergic neurotransmission in the prefrontal cortex and hippocampus may be responsible for behavioral abnormalities seen in emotional disturbances (Moghaddam, 2002). A recent hypothesis on the pathophysiology of depressive disorders involves adaptive plasticity of the neural system. As proposed by Duman et al. (1999), depression could result from an inability to make the appropriate responses to stress, as a consequence of a dysfunction of the normal mechanisms underlying neural plasticity.

The goal of the present study was to investigate whether MH produces anatomocytochemical relatively stable lifelong changes during development that could influence or alter the adulthood behaviors of offspring, especially their vulnerability to stress. We used the well-validated chronic mild stress protocol to produce mild and unpredictable daily stressful situations for the rats. This protocol is regarded as closely modeling the human situation, consisting more of daily hassles than traumatic events (for reviews, see Willner, 1997, 2005).

MATERIALS AND METHODS

Animals

Wistar rats from the animal house of our Faculty of Medicine were used in this study. All animal procedures were performed in accordance with the principles presented in the "Guidelines for the Care and Use of Mammals in Neuroscience and Behavioral Research" by the National Research Council. Ten postnatal day 90 (P90) female rats were implanted subcutaneously with Alzet osmotic pumps (Model 2ML4, pumping rate 2.5 μ L/hr for 28 days) infusing either

thyroxine (to progenitors of MH subjects) or vehicle [to progenitors of control (Ctrl) subjects]. The dose of thyroxine (T4; T2501, Sigma-Aldrich Inc.) was 1.5 μ g/100 g of pre-mating body weight per day (for detailed chemical preparation procedures, see Evans et al., 2002). With this dose, the female rat serum T4 concentration was about 2.26 ± 0.14 ng/dL ($n = 4$), whereas that of the control females was about 1.34 ± 0.11 ng/dL ($n = 4$). This measurement was made with the chemiluminescent microparticle immunoassay (CMIA, ARCHITECT[®], Abbott Laboratories, Abbott Park, IL). After a 2-day recovery period, females were mated with normal males. Osmotic pumps were removed from the females on offspring postnatal day 1 (P1). At the end of lactation (offspring P30), four male offspring rats per progenitor were randomly chosen to form either the MH group ($n = 20$) or the Ctrl group ($n = 20$). Further selection for experimental manipulations was performed randomly. All animals were maintained in an artificial 12-hr light:12-hr dark cycle (lights on at 16:00) in a room at 22°C with food and water ad libitum, except when the subchronic mild stress protocol required deprivation. Body weight was monitored, and plasma T4 level was measured with the CMIA microparticle immunoassay as above mentioned.

Experimental Design and Stress Procedure

Experimental procedures were performed when rats were in the young adult stage (starting at P90, body weight 350 ± 10 g) except for morphological analysis, in which brain samples were collected at P7, P30, and P75 and processed with the Golgi-Cox impregnation method (see detailed description below). A modified subchronic mild stress protocol (SCMS) lasting 10 days was used in this study (Table I). The regimen consisted of the application of a variety of unpredictable stressors, one per day, which included: 30 min of restraint stress (confinement into a cylinder 20 cm long and 7.5 cm in diameter), habitat changing with increased light and noise, one light cycle of sleep deprivation (four rats housed in cages $39 \times 75 \times 34$ cm with a 3-cm water level and four islands made of cylinders 8 cm in height and 7.5 cm in diameter), 1 day of food and water deprivation, one 10-min period of electric foot-shock stressor (0.2 mA, 0.5-sec pulse, 2 per min over 10 min for a total of 20 shocks; Heinrichs and Koob, 2005). The behavioral and cognitive tests specified below also served as unpredictable stressors during the 10-day protocol. A summary of the experimental design is shown in Table I.

Morris Water Maze

The Morris water maze (MWM; Morris, 1984) assesses spatial learning and memory retention. A black circular pool (diameter 156 cm, height 80 cm) filled with 30 cm of water ($25^\circ\text{C} \pm 1^\circ\text{C}$) with visual cues was used for this cognitive test. A circular black escape platform (diameter 12 cm) was submerged 1 cm below the water surface. Rats were allowed up to 120 sec to locate the escape platform. If the allowed time was finished and the experimental subjects had not found the platform, they were guided to the platform. Once on the platform, rats were permitted to stay for 5 sec to allow them

TABLE I. General experimental design

Postnatal Stage	Experimental day	Experimental procedures	Parameters measured
P60		Forced swimming test (n = 9).	Immobility counts (Baseline)
P90	1 st of SCMS	Morris water maze (MWM) (n = 9).	Escape latency
P91	2 nd	Restraint stress (30 min) (n = 14), followed by cardiac blood sample collection (n = 5) ^a .	Serum Corticosterone, T4 levels.
P92	3 rd	Habitat changing with increased light and noise for 2 hrs prior to MWM. MWM (n = 9 for all remaining procedures).	Escape latency.
P93	4 th	Sleep deprivation during light cycle.	
P94	5 th	Food and water deprivation for 24 hrs.	
P95	6 th	Electric footshock stressor.	
P96	7 th	Repeated forced swimming stress (RFSS) day 1, for 15 min.	Immobility counts
P97	8 th	RFSS day 2, 6 min × 4 trials. Time between trials: 12–15 min	Immobility counts
P98	9 th	Tail suspension test (TST)	Immobility time
P99	10 th	MWM	Escape latency.
P100	11 th	MWM Perfusion for immunocytochemistry	Swimming time on platform area

^aMWM at day 1 was not applied to these animals.

to observe place and location. To assess cognitive function in stress-naïve experimental subjects and any possible difference in response to this mild swimming stress, rats were not pre-trained for the first cognitive test (nonstress situation) on day 1 of the SCMS protocol. The second MWM test was performed on day 3 of the SCMS protocol, when the rats had undergone an immobilization stressor on day 2 and habitat changing stress with increased light and noise for 2 hr prior to the cognitive test during the endogenous activity period. This was defined as an acute stress situation. A third MWM test was performed on day 10 of the SCMS protocol and designated as a subchronic stress situation. The memory retention test of the MWM was performed on day 11, when the platform was removed, and the time spent on the platform quadrant was recorded. The starting position was in the quadrant opposite (IV) the platform quadrant (II) and was unchanged for the four tests.

Repeated Forced-Swimming Stress

Animals from the MH and Ctrl groups were assessed for depression-like behavior using a modified version of the forced-swimming test (FST; Porsolt et al., 1978; Wellman et al., 2007), in which experimental subjects were exposed repeatedly to the swimming stressor during the dark period of the artificial light–dark cycle. The repeated FST allowed us to evaluate depression-like behavior after both acute and repeated exposure to the test while acting as a stressor and helped to rule out the possibility of any motor impairment. The test consisted of exposure to a vertical Plexiglas cylinder 45 cm in height and 30 cm in diameter containing water to a height of 25 cm kept at 25°C ± 1°C. On P60, the rats underwent the first FST for 6 min to assess this behavioral parameter prior to the SCMS protocol. We designated this as the baseline test. On P96, day 1 of the test, rats received a single 15-min FST. On day 2 of the test, the rats received four consecutive 6-min exposures with a 12- to 15-min interval between trials. Passive immobility (cessation of spatial displacement with or without minor involuntary movements of the hind limbs) during min

2–6 was analyzed off-line. The observer scored the rats as either “swimming” or “immobile” every 5 sec (sampling frequency criterion described by Detke et al., 1995), and the percentage of immobility episodes was calculated as immobility episodes observed/total number of observations × 100. Immobility counts in the FST are regarded as a measure of behavioral despair.

Tail Suspension Test

In the tail suspension test (TST; Chermat et al., 1986), rats are suspended by the tail for 6 min during which they show periods of agitation and immobility. Duration of immobility is measured as an indicator of behavioral despair as an additional test to confirm the depression-like behavior displayed in the FST. The tail suspension apparatus consisted of a wooden cubicle with inside dimensions of 25 × 25 × 55 cm. A cylinder (5 cm in diameter, 25 cm in length) was fixed inside the cubicle (5 cm from the top) as a tail hanger. Rats were suspended from the cylinder using adhesive tape placed at about half the total tail length. Compared with the traditional design, in which a hook is used as a tail hanger, the TST apparatus used in this study avoided possible harm to the rats' tails. The entire test was video-recorded, and total immobility time was analyzed off-line.

Corticosterone Measurement

Pre- and postrestraint stress (30 min) serum corticosterone (CORT) level during the rats' late activity period was determined. Rats from the MH and Ctrl groups were anesthetized with an overdose of sodium pentobarbital and cardiac blood samples were collected and allowed to coagulate at room temperature for 3 hr. Samples were subsequently centrifuged at 2,000g for 15 min. Serum was removed and stored at –20°C until analysis. Serum CORT concentration was determined by a commercially available ELISA kit according to the manufacturer's instructions (Assay Designs Inc., Ann Arbor,

MI). Serum dilution was 1:10. Each sample and standard was measured in duplicate.

Histological Procedures for Corticotropin-Releasing Factor Immunoreaction

After the MWM memory retention test, rats were treated with an overdose of sodium pentobarbital and perfused transcardially with 0.9% saline followed by cold fixative containing 4% paraformaldehyde in 0.1M sodium phosphate buffer (PB; pH 7.4) plus 15% (v/v) saturated picric acid for 15 min. Brains were removed, blocked, and then thoroughly rinsed with PB. Coronal sections (50 μ m) of amygdala and hypothalamus were obtained using a vibratome (Leica VT 1000, Heidelberg, Germany). Free-floating sections were quenched by incubating brain sections in 3% hydrogen peroxide in PB for 10 min. All the sections for immunoreaction were then incubated with PBST: PB + 0.9% NaCl + 0.3% Triton X-100 (T-7878, Sigma-Aldrich, Inc.) and 20% normal goat serum (NGS; 005-000-121, Jackson ImmunoResearch Laboratories, Inc.) for 1 hr at room temperature (RT). Rabbit antiserum anti-corticotropin-releasing factor (CRF; AP1760, Chemicon International Inc., CA) was used as primary antibody diluted 1:1,000 in PBST + 1% NGS and incubated overnight in a cold room. Afterwards, sections were rinsed for 10 min three times with PBST and then incubated for 4 hr at RT with biotinylated goat antirabbit secondary antibodies (1:200; Vector Labs, Burlingame, CA). Finally, sections were incubated in avidin-biotin-peroxidase complex (Elite ABC kit, Vector Labs) for 1 hr at RT. Peroxidase was detected using diaminobenzidine (DAB) as chromogen. Sections were developed using a Liquid DAB-Plus Substrate Kit (00-2020; Zymed Laboratories, San Francisco, CA). For indirect immunofluorescence Alexa Fluor 488 goat antirabbit IgG was used as a secondary antibody (A11008, Molecular Probes, Eugene, OR).

Image Analysis

The central nucleus of the amygdala (CeA) and paraventricular nuclei (PVN) were analyzed in regions spanning bregma -1.60 and -3.30 mm and -1.80 and -2.12 mm, respectively, according to the Paxinos and Watson brain atlas (Paxinos and Watson, 1998). Immunoreactive (IR) cell counting was performed using a Nikon Eclipse 50i microscope with a 40 \times objective lens. The IR-positive cells were projected and marked into a defined area (being circles 50 μ m in diameter for CeA and 100 μ m in diameter for PVN) through a drawing tube (Nikon Y-IDT) at $\times 8$ magnification. Counting was performed manually, and data were then normalized.

Golgi-Cox Impregnation

For the Golgi-Cox impregnation procedures, on P7, P30, and P75 two rats from each group received an overdose of anesthesia and were decapitated. Brains were removed from the skulls quickly, and their central thirds (along the antero-posterior axis) were cut with a sharp blade into blocks approximately 5 mm thick. Tissues were briefly rinsed with 0.1M PB (pH 7.4) and then immersed in sequenced impregnation solutions (FD Rapid GolgiStain kit, FD Neuro Technologies,

Ellicott City, MD) for 2 weeks in the dark. Sections (100 μ m) were sliced using a vibratome and were dried naturally at RT in the dark and then stained with a solution provided with the stain kit. Dendritic patterns of dentate granule cells and CA3 pyramidal neurons were reconstructed using a drawing tube at $\times 400$ magnification. Dendritic arborization areas in two dimensions were estimated using Adobe Photoshop (Adobe Systems Inc.) and Fovea Pro (an image tool kit from Reindeer Graphics, Asheville, NC).

Statistical Analyses

Quantitative results were expressed as mean \pm standard error of mean (SEM). Groups were tested for differences by analysis of variance followed by the Student-Newman-Keuls test, using InStat (GraphPad Software, San Diego, CA). Differences were considered statistically significant at $P < 0.05$ ($*P < 0.05$, $**P < 0.01$, and $***P < 0.001$, versus the control group).

RESULTS

Spontaneous Locomotor Activity, Body Weight, and T4 Serum Level Are Unaffected in MH Rats

MH rats displayed normal locomotor activity during the manipulations and different tests. Their body weight was similar to that of the Ctrl rats and on P90 was 350 ± 10 g. The measured mean serum T4 concentration was 1.26 ± 0.14 ng/dL, which was not significantly different from that of the control (1.17 ± 0.06 ng/dL).

Altered Serum CORT Level in MH Rats after Acute Stress

To monitor the HPA axis response to an acute restraint stress, serum CORT levels were assessed by comparing MH animals with controls. First, we measured serum CORT level in the rats' late-activity period before any stressor was applied. The mean serum CORT concentrations without restraint stress of the control and MH groups— 3.303 ± 0.416 and 3.029 ± 0.617 μ g/dL ($n = 4$), respectively—did not differ significantly. Rats were subjected to acute restraint stress (30 min) in their late activity period, when the intrinsic circadian amplitude of CORT was expected to reach its minimum (Fig. 1). The average CORT level of MH rats was 18.3 ± 0.7 μ g/dL, whereas that of the controls was 9.4 ± 3.0 μ g/dL. This increase was consistent with previously reported levels in response to such a stressor (Viau and Sawchenko, 2002).

Increased Depressive-Like Behavior during SCMS Application

The speed of development of behavioral despair under the SCMS paradigm was assessed using two well-validated behavioral tests, the FST and the TST. Both tests are based on rats having an immobility response to an inescapable adverse situation. Duration of immobility, reflected as frequency of immobility episodes of total observations in the FST, is understood to be a measure

of behavioral despair with a direct relationship to it. A month before application of the SCMS protocol, rats were subjected to the first FST for 6 min in order to have a baseline reference for immobility (Fig. 2A, baseline). The MH rats had fewer immobility episodes than did the rats from the Ctrl group. On day 7 of the SCMS protocol animals underwent 2 consecutive days of the forced-swimming stress test (FSST; Wellman et al., 2007). Rats from both experimental groups were observed to have a greater number of immobility epi-

sodes during this repeated forced-swimming test. The immobility count of the MH rats was much more pronounced (Fig. 2A, days 1 and 2). However, immobility counts of the MH and Ctrl rats did not differ significantly during the last exposure to the FST on the second day. This lack of difference may suggest that both the control and MH rats were approaching their physical effort limits. On the ninth day of the SCMS, the rats were exposed to the TST for 6 min (Fig. 2B). Again, the mean duration of immobility of the MH animals was longer (205.2 ± 13.79 sec) than that of the Ctrl rats (128.6 ± 37.10 sec).

Impaired Rat Spatial Learning and Memory Retention during SCMS Application

The effects of the SCMS on spatial learning and memory retention of the MH rats were tested using the hidden-platform water maze (Morris water maze, MWM). As shown in Figure 3A–C, the latency to escape to the platform of the Ctrl group decreased while advancing the trials. The slopes of the time sequences of the first three trials were relatively steep, approaching the shortest latency at the third trial, regardless of the duration of application of the SCMS protocol. In contrast, MH rats displayed progressively impaired spatial learning while continuing the SCMS protocol. Figure 3A shows the performance of naive MH rats in stress and swimming. The time sequence of the first four trials revealed a steep slope matching that of the control, suggesting normal spatial learning ability. However, the escape latency in the fifth and sixth trials peaked in the sequence and decreased again in the seventh and eighth trials. This may be related to an overreaction of the

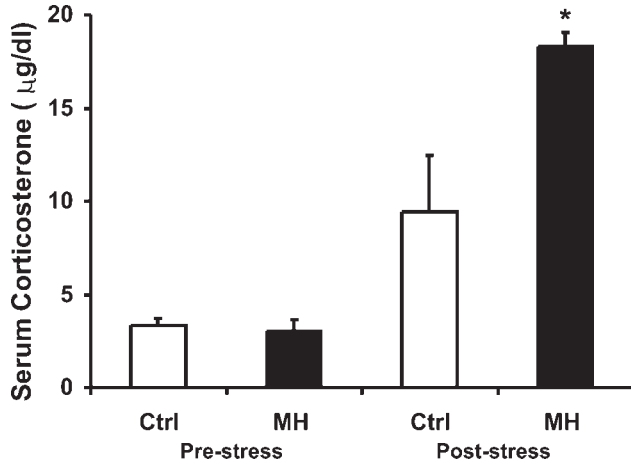


Fig. 1. Serum corticosterone (CORT) levels determined to assess the magnitude of the stress reaction. Serum CORT level increases during stressful events and is mainly regulated by HPA axis. Samples were taken during the rats' late-dark period before (prestress) and after (poststress) restraint stress (for 30 min). Data are given as mean \pm SEM for $n = 5$ (* $P < 0.05$).

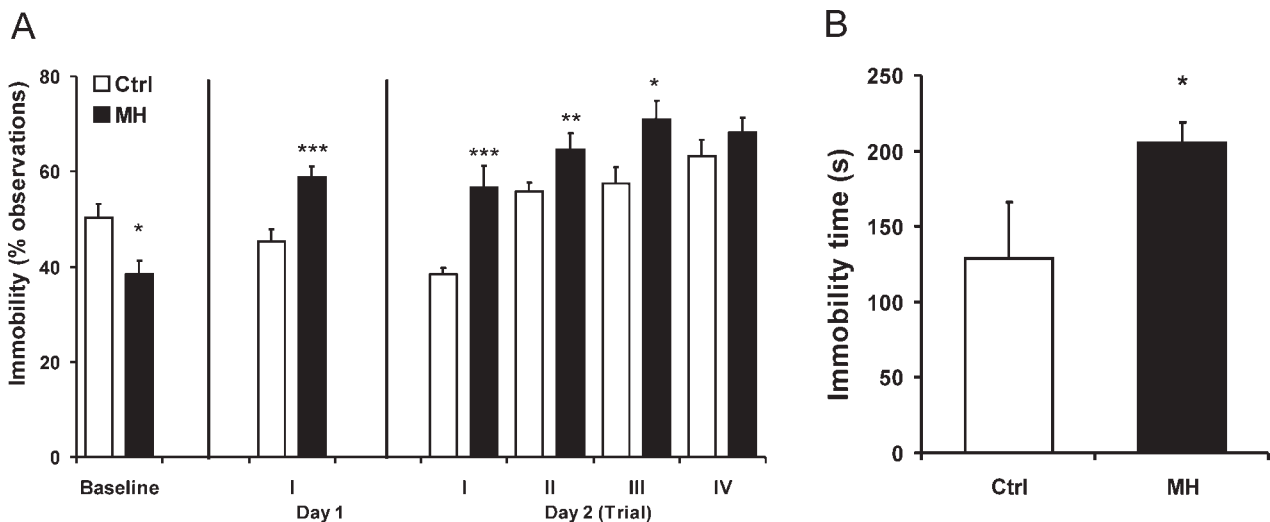


Fig. 2. Repeated forced-swimming stress test (FSST, **A**) and tail suspension test (TST, **B**) used to assess depressive-like behaviors. **A:** Baseline test (6 min) was done at P60 ($n = 9$); the 2-consecutive-day forced-swimming stress test (day 1 and day 2 tests) was done on days 7 and 8 of the SCMS protocol with a duration of 15 min for the first day, and 6 min for each trial on the second day with 12–15 min

between each trial ($n = 9$). The percentage of episodes of immobility of the total number of episodes observed is shown. In all cases, only the swimming behavior from the second to the sixth minutes was analyzed off-line. **B:** Total immobile time during the 6-min TST was recorded ($n = 9$). Mean \pm SEM (** $P < 0.001$, ** $P < 0.01$, * $P < 0.05$).

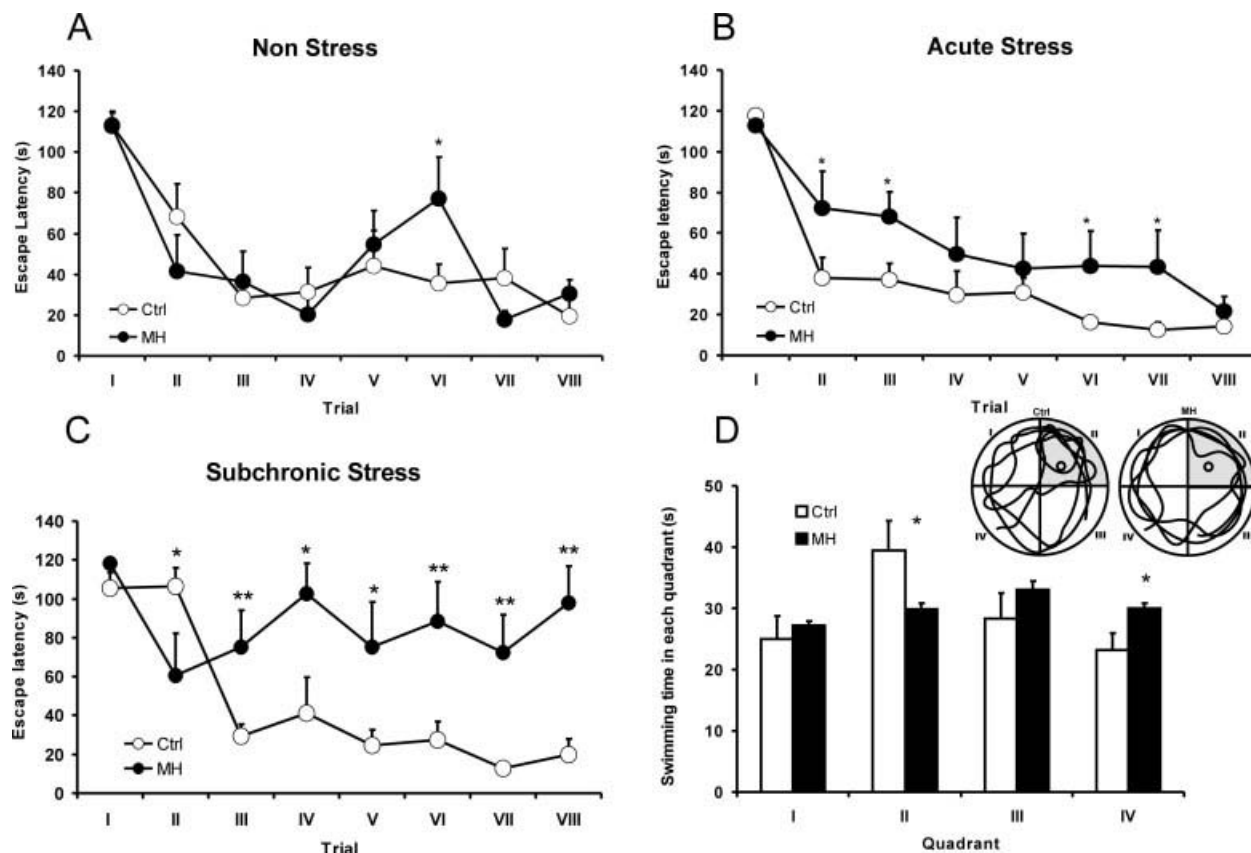


Fig. 3. Morris water maze (MWM) used to assess spatial memory. Tests were performed with rats for different SCMS periods. **A:** Stress-naïve rats on the first day of SCMS protocol. **B:** Rats underwent acute stress. **C:** Rats underwent 10 days of SCMS. **D:** Quadrant preference test for memory retention performed on the 11th day

of SCMS. The platform was in quadrant II. Inserts show paths taken by representative rats with quadrant number indicated. Means \pm SEMs ($n = 9$) of escape latency across 8 trials represented in time sequences (** $P < 0.01$, * $P < 0.05$).

HPA axis to the novelty of swimming and handling generated in the first trial of MH rats, although this novelty did not seem to be a significant stressor for Ctrl rats. Figure 3B shows the performance of rats in an acute mild stress situation, which included habitat changing and increased noise and light 2 hr prior to the MWM. The slope of the MH rats was much smoother than that of the control rats, and clear differences between the MH and Ctrl groups were observed. After the 10 days of the SCMS protocol, the MH rats showed a MWM time sequence with a totally different form than that of the naïve and acute stress MH groups, with several peaks and almost no reduction in latency at the end of the test (Fig. 3C). Latency reduction in the Ctrl group was delayed in comparison with that in the naïve and acute stress Ctrl rats but reached a similar level after the third trial. In the quadrant preference test for memory retention (Fig. 3D), the MH rats showed no preference for the quadrant where the platform was. During the experimental periods, no rats showed any apparent sign of discomfort or locomotor disability.

Increased Number of CRF-IR Neurons in CeA

Immunocytochemical detection for CRF revealed an increased number of CRF-IR cells in the CeA of MH rats subjected to the SCMS scheme (Fig. 4A–C). Positive labeling for CRF was detected in neurons in the dorsal and ventral subdivisions of the medial parvocellular part of the caudal PVN. Also, a few cells were observed in the dorsal and lateral subdivisions of the magnocellular part (PaLM; Fig. 4D–F). These locations correspond with the typical areas of the PVN in which CRF neurons have been described (Swanson and Sawchenko, 1983). We found no significant differences in the number of CRF-IR cells in these hypothalamic regions (Fig. 4F), although the expression pattern in MH rats seemed to be more scattered toward lateral hypothalamic regions (Fig. 4E,F). It is worth noting that this staining was performed in tissue from animals without previous treatment with colchicine, which is known to exert an axonal transport blocking effect and helps the detection of CRF or any other peptide by accumulation of antigens in the cell body.

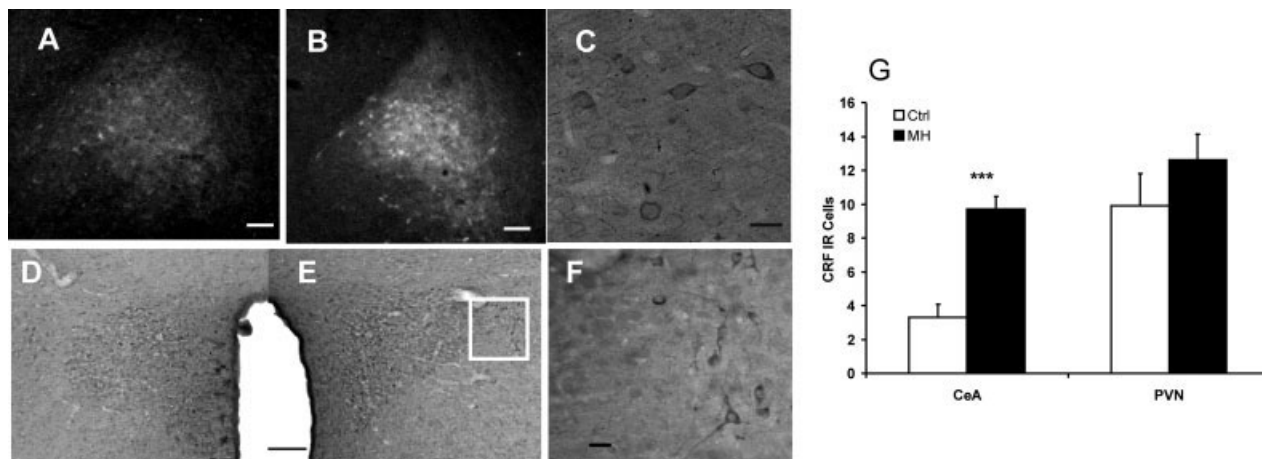


Fig. 4. CRF-IR in the central nucleus of the amygdala (CeA) and the paraventricular nuclei (PVN). **A:** Representative immunofluorescence photomicrograph of CeA from Ctrl rats. Scale bar = 50 μ m. **B:** Representative immunofluorescence photomicrograph of CeA from MH rats. Scale bar = 50 μ m. **C:** Examples of CRF-IR neurons

visualized with the peroxidase method. Scale bar = 20 μ m. **D:** CRF-IR in PVN from Ctrl rats. Scale bar = 100 μ m. **E:** CRF-IR in PVN from MH rats. Scale bar = 100 μ m. **F:** Insert magnification of E. Scale bar = 20 μ m. **G:** Histogram showing the number of CRF-IR cells in CeA and PVN ($n = 5$).

Increased Dendritic Receptive Field in Hippocampal Projection Neurons during Development and Adulthood

To elucidate the possible mechanisms underlying the behavioral changes, hippocampal CA3 pyramidal neurons and dentate gyrus (DG) granule cell dendritic arborization were analyzed through reconstruction of Golgi-Cox-impregnated neurons on postnatal days P7, P30, and P75. A general observation is that the dendritic receptive fields (2-D projection of 3-D arborization) were larger in the MH rats in all three stages, as shown by representative morphology of these neurons in Figure 5. Using Adobe Photoshop and FoveaPro, we estimated the 2-D dendritic receptive fields, finding that at P75 the value of the MH rats of $92.73 \pm 3.56 \mu\text{m}^2$ was significantly different from that of the Ctrl rats of $48.9 \pm 2.66 \mu\text{m}^2$ in CA3 pyramidal neuron apical receptive fields. Regarding DG granule cell dendritic receptive fields, no significant differences were found. However, thicker dendrite shafts were observed in samples from the MH rats. The inserts in Figure 5-P7 illustrate examples of primary and secondary dendrite ramifications.

DISCUSSION

It is well established that thyroid hormone (TH) action early in life plays a key role in determining the normal timing of neural development. An abundant number of studies focusing on excessive or insufficient TH during early development have revealed that this endocrine imbalance leads to abnormalities in brain structure. For instance, neonatal transient elevation of TH, from postnatal day 1 to postnatal day 4 in rats causes hypertrophic development of CA3 pyramidal neurons in the hippocampus and of astroglial cells in the hippocam-

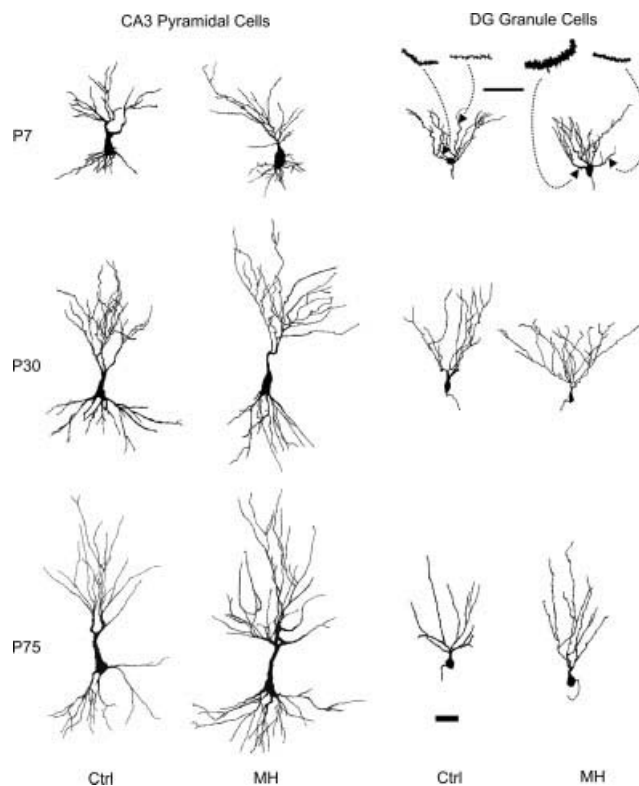


Fig. 5. Reconstruction of representative hippocampal CA3 pyramidal neurons and dentate gyrus granule cells impregnated by the Golgi-Cox method on postnatal day 7 (P7), postnatal day 30 (P30), and postnatal day 75 (P75). Scale bar = 50 μ m for main picture and 10 μ m for inserts.

pus and basal forebrain (Gould et al., 1990a, 1990b). Our data describing an increase in the dendrite receptive fields in hippocampal CA3 pyramidal neurons at three postnatal ages, P7, P30, and P75, are analogous to those

seen in the rodent neonatal hyperthyroidism model and extend existing observations.

The present data are the first to describe the emotional and cognitive consequences of mild maternal hyperthyroidism in adult rat offspring under subchronic mild stress. Earlier studies concerning neonatal hyperthyroidism have suggested that thyroxin accelerates the maturation of the pituitary-adrenal response to electric shock (Schapiro and Norman, 1967) and the onset of physiological and behavioral bioenvironmental interaction in general (Schapiro, 1968). It has also been reported that neonatal thyroxin stimulation of albino rats disrupts hippocampal LTP, and despite hypertrophied hippocampal CA3 pyramidal neurons and elevated density of cholinergic neurons in the basal forebrain, they are actually less efficient in learning a spatial maze (Pavlidis et al., 1991). The present finding of cognitive impairment in the MH rats, shown by their greater number of mistakes and increased latency in the Morris water maze, is compatible with previous observations in neonatal hyperthyroid rats. Moreover, our data make an important addition to previous observations in several areas. The relatively mild degree of maternal hyperthyroidism used in this experimental design apparently did not produce alterations in the adulthood of the offspring under normal conditions, as we reported in the results. However, when the subchronic mild stress scheme was applied, their spatial learning capacity was progressively impaired along the protocol. Furthermore, the display of depression-like behaviors by the MH adult offspring was accelerated, as results of both the forced-swimming stress test (FSST) and the tail suspension test (TST) showed. It is worth mentioning that depression-like behaviors have multiple dimensions and that analysis of such behaviors in an animal model is always difficult to sort out. Normally, a battery of tests is recommended to assess such behaviors. The forced-swimming test (FST) is probably the most widely and frequently used protocol. In the present experimental design, we used a modified version of the Porsolt test (Porsolt et al., 1978), mainly because repeated exposure to the test in a short time is a stressor for rats. Hence, the depression-like behavior could be more quickly observed. On the other hand, the FSST demands a major physical effort by the animal under study. A motor-impaired rat could be easily distinguished during this repeated swim test. Both the FST and TST have immobility as a parameter to be measured. However, the actual parameter being measured is the response of the animal to the specific condition of each test, that is, the adoption of floating behavior in the FST or of stationary behavior in the TST. It has been suggested that the observed behaviors might be produced by different biological substrates, and different hypotheses have been proposed to explain the observed immobility in FST and TST (Cryan et al., 2005). To summarize these observations, our data suggest that maternal hyperthyroidism, however moderate or without apparent alteration in the adult offspring under normal

conditions, could bring about severe consequences because of the enhanced stress response.

A stressful event, either physical or psychological, activates neural circuits involved in emotional responses, cognition, and homeostatic regulation. The hippocampal formation and the amygdala form the central axis of the limbic system and are highly responsible for cognitive and emotional responses to a stressful situation. The hippocampal formation receives major input from the entorhinal cortex through the perforant pathway, where highly processed sensory information from associational, perirhinal, and parahippocampal cortices as well as the prefrontal cortex is transmitted. The proximal segments of the apical dendrites of CA3 pyramidal neurons are covered with complex spines or excrescences that receive mossy fiber input from granule neurons of the dentate gyrus (Blackstad and Kjaerheim, 1961). The dentate gyrus-CA3 pathway provides the major excitatory afferent to the hippocampal regio inferior, and each CA3 neuron excites multiple pyramidal neurons (Ishizuka et al., 1990). Our finding of augmentation of CA3 pyramidal neuron dendrite receptive fields most likely indicates that these excitatory pathways to the hippocampus could be strengthened at the beginning of a stressful situation, which amplifies sensory inputs from the entorhinal cortex. Therefore, the stressors could have a more profound effect on hippocampal function. Ultrastructural studies showed that chronic stress alters the synaptic terminal structure in the hippocampus, especially the mossy fiber synapses boutons en passant from granule neurons to the proximal segments of apical dendrites of CA3 pyramidal neurons (Magariños et al., 1997), indicating a possible reorganization driven by hyperactivation of this pathway. Chronic exposure to higher levels of CORT can cause irreversible hippocampal dysfunction and increase depression-like behavior in rats in a dose-dependent manner and disrupt normal HPA axis function (Johnson et al., 2006). Moreover, clinical evidence has shown that medically healthy patients with recurrent major depression can show decreased hippocampal volume and impaired cognition (Sheline et al., 1999). Using the subchronic mild stress paradigm, we observed faster development of depressive-like behaviors as well as impairment of cognitive functioning in MH rats under mildly stressful conditions.

The neurohormone CRF activates both hormonal and behavioral responses to a variety of stressors. Stress leads to CRF release from the hypothalamic PVN, resulting in increased plasma corticotrophin (ACTH) and adrenal steroid concentration. CRF-containing cells constitute a significant neuronal population in the central nucleus of the amygdala (CeA). The CeA has been shown to be a key regulator of the stress response mediated by CRF release from the PVN (for a review, see Gray and Bingaman 1996). Discrete lesions of the CeA exacerbate the acute stress response (Carter et al., 2004). Our observation of an increased population of CRF-IR cells in the CeA but not in the PVN after being sub-

jected to chronic mild stress might indicate a stronger attempt to limit the stress overreaction in MH animals.

The observations from this study raise the question of the underlying mechanism by which mild maternal hyperthyroidism produces enhanced vulnerability to stress in adulthood. According to the current hypothesis of neural plasticity in some areas of the neural system, once neuronal connections are established during this critical period of brain development, the networks tend to be relatively stable ("rigid" synaptic connections), whereas other types of synaptic connections ("flexible" synaptic connections) undergo lifelong self-optimization processes, so-called use-dependent neural plasticity. The cognitive, behavioral, and emotional reactivity of an individual derived from this kind of connection is stepwise remodeled to meet environmental demands. Although the presence of rigid synaptic connections ensures stability of the principal characteristics of function, variable configuration of flexible synaptic connections determines the unique, nonrepeatable character of an experienced mental act (Arendt, 2001; Gulpinar and Yegen, 2004). There are many possible causes of aberrant synaptic connections. One possible cause is hyper- or hypotrophied neuronal dendritic arborization. In addition, neuronal migration aberrations can, in fact, alter physiological synaptic connections, resulting in loss of neural plasticity and consequently of adaptive capacity. Ausó et al. (2004) recently reported that a moderate and transient deficiency in maternal thyroid function at the beginning of fetal neocortico-genesis alters neuronal migration. The opposite could also alter neuronal migration, although experimental data are required to confirm this hypothesis.

In conclusion, the results from this animal model analyzing the consequences of maternal hyperthyroidism in the adulthood of offspring suggest that this delicate prenatal endocrine modification could alter the neuronal structure of specific brain areas and influence the cognition and emotionality of offspring in adulthood. These modifications were demonstrated, letting the experimental subjects undergo subchronic mild stressful situations. Suffice it to say, the morphological and immunocytochemical changes we have reported represent only a part of the numerous and complex anatomical and physiological abnormalities in adulthood as a result of maternal hyperthyroidism. However, this kind of animal models allow us to gain insight into normal development and to evaluate integrative aspects of the long-term influences of neuroendocrine disorders during development.

ACKNOWLEDGMENTS

We thank Pablo G. Hofmann and Prof. Rafael Barrio for critical reading and insightful comments and Leyla Guadarrama, Guillermo Luna, Manuel Hernandez, and Fernando Carbajal for technical assistance.

REFERENCES

Arendt T. 2001. Alzheimer's disease as a disorder of mechanisms underlying structural brain self-organization. *Neurosci* 102:723–765.

- Ausó E, Lavado-Autric R, Cuevas E, Del Rey FE, Morreale De Escobar G, Berbel P. 2004. A moderate and transient deficiency of maternal thyroid function at the beginning of fetal neocortico-genesis alters neuronal migration. *Endocrinology* 145:4037–4047.
- Blackstad TW, Kjaerheim A. 1961. Special axo-dendritic synapses in the hippocampal cortex: electron and light microscopic studies on the layer of mossy fibers. *J Comp Neurol* 117:133–159.
- Burrow GN. 1993. Thyroid function and hyperfunction during gestation. *Endocr Rev* 14:194–202.
- Carter RN, Pinnock SB, Herbert J. 2004. Does the amygdala modulate adaptation to repeated stress? *Neuroscience* 126:9–19.
- Cherbat R, Thierry B, Mico JA, Steru L, Simon P. 1986. Adaptation of the tail suspension test to the rat. *J Pharmacol* 17:348–350.
- Courtin F, Chantoux F, Francon J. 1988. Thyroid hormone metabolism in neuron-enriched primary cultures of fetal rat brain cells. *Mol Cell Endocrinol* 58:73–84.
- Cryan JF, Mombereau C, Vassout A. 2005. The tail suspension test as a model for assessing antidepressant activity: review of pharmacological and genetic studies in mice. *Neurosci Biobehav Rev* 29:571–625.
- Detke MJ, Rickels M, Lucki I. 1995. Active behaviours in the rat forced swimming test differentially produced by serotonergic and noradrenergic antidepressants. *Psychopharmacology* 121:66–72.
- Duman RS, Malberg J, Thome J. 1999. Neural plasticity to stress and antidepressant treatment. *Biol Psychiatry* 46:1181–1191.
- Evans IM, Pickard MR, Sinha AK, Leonard AJ, Sampson DC, Ekins RP. 2002. Influence of maternal hyperthyroidism in the rat on the expression of neuronal and astrocytic cytoskeletal proteins in fetal brain. *J Endocrinol* 175:597–604.
- Glinoe D. 1997. The regulation of thyroid function in pregnancy: pathways of endocrine adaptation from physiology to pathology. *Endocr Rev* 18:404–433.
- Gray TS, Bingaman EW. 1996. The amygdala: corticotropin-releasing factor, steroids, and stress. *Crit Rev Neurobiol* 10:155–168.
- Gould E, Westlind-Danielsson A, Frankfurt M, McEwen BS. 1990a. Sex differences and thyroid hormone sensitivity of hippocampal pyramidal cells. *J Neurosci* 10:996–1003.
- Gould E, Frankfurt M, Westlind-Danielsson A, McEwen BS. 1990b. Developing forebrain astrocytes are sensitive to thyroid hormone. *Glia* 3:283–292.
- Gulpinar MA, Yegen BC. 2004. The physiology of learning and memory: role of peptides and stress. *Curr Protein Pept Sci* 5:457–473.
- Heinrichs SC, Koob GF. 2005. Electrical footshock stressor. Application of experimental stressors in laboratory rodents. In: *Current Protocols in Neuroscience*. Unit 8.4.4. John Wiley & Sons.
- Ishizuka N, Weber J, Amaral DG. 1990. Organization of intrahippocampal projections originating from CA3 pyramidal cells in the rat. *J Comp Neurol* 295:580–623.
- Johnson SA, Fournier NM, Kalynchuk LE. 2006. Effect of different doses of corticosterone on depression-like behavior and HPA axis responses to a novel stressor. *Behav Brain Res* 168:280–288.
- Kumar A, Sinha RA, Tiwari M, Pal L, Shrivastava A, Singh R, Kumar K, Kumar Gupta S, Godbole MM. 2006. Increased pro-nerve growth factor and p75 neurotrophin receptor levels in developing hypothyroid rat cerebral cortex are associated with enhanced apoptosis. *Endocrinology* 147:4893–4903.
- McEwen BS, Sapolsky RM. 1995. Stress and cognitive function. *Curr Opin Neurobiol* 5:205–216.
- Magariños AM, Verdugo JM, McEwen BS. 1997. Chronic stress alters synaptic terminal structure in hippocampus. *Proc Natl Acad Sci U S A* 94:4002–4008.
- Morris R. 1984. Developments of a water-maze procedure for studying spatial learning in the rat. *J Neurosci Meth* 11:47–60.

- Moghaddam B. 2002. Stress activation of glutamate neurotransmission in the prefrontal cortex: implications for dopamine-associated psychiatric disorders. *Biol Psychiatry* 51:775–787.
- Morreale de Escobar G, Obregón MJ, Ruiz de Ona C, Escobar del Rey F. 1988. Transfer of thyroxine from the mother to the rat fetus near term: effects on brain 3,5,3'-triiodothyronine deficiency. *Endocrinology* 122:1521–1531.
- Obregon MJ, Mallor J, Pastor R, Morreale de Escobar G, Escobar del Rey F. 1984. L-thyroxine and 3,5,3'-triiodo-L-thyronine in rat embryos before onset of fetal thyroid function. *Endocrinology* 114:305–307.
- Oppenheimer JH, Schwartz HL. 1997. Molecular basis of thyroid hormone-dependent brain development. *Endocr Rev* 18:462–475.
- Paxinos G, Watson C. 1998. *The Rat Brain in Stereotaxic Coordinates*. New York: Academic Press.
- Pavlidis D, Westlind-Danielsson AI, Nyborg H, McEwen BS. 1991. Neonatal hyperthyroidism disrupts hippocampal LTP and spatial learning. *Exp Brain Res* 85:559–564.
- Polak M. 1998. Hyperthyroidism in early infancy: pathogenesis, clinical features and diagnosis with a focus on neonatal hyperthyroidism. *Thyroid* 8:1171–1177.
- Polak M, Legac I, Vuillard E, Guibourdenche J, Castanet M, Luton D. 2006. Congenital Hyperthyroidism: the fetus as a patient. *Horm Res* 65:235–242.
- Porsolt RD, Anton G, Blavet N, Jalfre M. 1978. Behavioral despair in rats: a new model sensitive to antidepressant treatments. *Eur J Pharmacol* 47:379–391.
- Schapiro S. 1968. Some physiological, biochemical, and behavioral consequences of neonatal hormone administration: cortisol and thyroxine. *Gen Comp Endocrinol* 10:214–228.
- Schapiro S, Norman RJ. 1967. Thyroxine: Effects of neonatal administration on maturation, development, and behavior science. *155:1279–1281*.
- Sheline YI, Shanghavi M, Mintum MA, Gado MH. 1999. Depression duration but not age predicts hippocampal volume loss in medically healthy women with recurrent major depression. *J Neurosci* 19:5034–5043.
- Singh S, Upadhyay G, Kumar S, Kapoor A, Kumar A, Tiwari M, Godbole MM. 2003. Hypothyroidism alters the expression of Bcl-2 family genes to induce enhanced apoptosis in the developing cerebellum. *J Endocrinol* 176:39–46.
- Swanson LW, Sawchenko PE. 1983. Hypothalamic integration: organization of the paraventricular and supraoptic nuclei. *Annu Rev Neurosci* 6:269–324.
- Tanaka K, Inada M, Ishii H, Naito K, Nishikawa M, Mashio Y, Imura H. 1981. Inner ring monodeiodination of thyroxine and 3,5,3'-triiodothyronine in rat brain. *Endocrinology* 109:1619–1624.
- Viau V, Sawchenko PE. 2002. Hypophysiotropic neurons of the paraventricular nucleus respond in spatially, temporally, and phenotypically differentiated manners to acute vs. repeated restraint stress: rapid publication. *J Comp Neurol* 445:293–307.
- Vulsma T, Gons MH, de Vijlder JJ. 1989. Maternal-fetal transfer of thyroxine in congenital hypothyroidism due to a total organification defect or thyroid agenesis. *N Engl J Med* 321:13–16.
- Wellman CL, Izquierdo A, Garrett JE, Martin KP, Carroll J, Millstein R, Lesch KP, Murphy DL, Holmes A. 2007. Impaired stress-coping and fear extinction and abnormal corticolimbic morphology in serotonin transporter knock-out mice. *J Neurosci* 27:684–691.
- Willner P. 1997. Validity, reliability and utility of the chronic mild stress model of depression: a 10-year review and evaluation. *Psychopharmacology (Berl)* 134:319–329.
- Willner P. 2005. Chronic mild stress (CMS) revisited: consistency and behavioural-neurobiological concordance in the effects of CMS. *Neuropsychobiology* 52:90–110.

11.2 Otras publicaciones científicas durante mis estudios doctorales

Dopamine receptor dysregulation in hippocampus of aged rats underlies chronic pulsatile L-Dopa treatment induced cognitive and emotional alterations

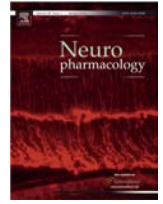
Hernández V. S., Luquín S., Jáuregui-Huerta F.,
Corona-Morales A. A., Medina M. P., Ruíz-Velasco S.,
Zhang L.

Neuropharmacology 2014, 82: 88-100

My contributions in:

- Conception of the study: +++
- Performance of the experiments:
 - o Chronic L-Dopa Treatment +++
 - o Behavioral assessment for “depressive behavior” +++
 - o Behavioral assessment for spatial learning +++
 - o Immunohistochemical procedures and analysis ++
- Statistical analysis: +
- Discussion of the results: +++
- Preparation of the paper: +++

(+): Average contribution; (++): Important contribution; (+++); Main contribution



Dopamine receptor dysregulation in hippocampus of aged rats underlies chronic pulsatile L-Dopa treatment induced cognitive and emotional alterations[☆]



Vito S. Hernández^a, Sonia Luquín^b, Fernando Jáuregui-Huerta^b,
Alejandra Corona-Morales^{a,c}, Mauricio P. Medina^a, Silvia Ruíz-Velasco^d, Limei Zhang^{a,*}

^aDepartamento de Fisiología, Facultad de Medicina, Universidad Nacional Autónoma de México, México 04510, D. F. México

^bDepartamento de Neurociencias, Centro Universitario de Ciencias de la Salud, Universidad de Guadalajara, Guadalajara, México

^cFacultad de Nutrición, Universidad Veracruzana, Xalapa, México

^dInstituto de Investigaciones en Matemáticas Aplicadas y de Sistemas, Universidad Nacional Autónoma de México, México 04510, D. F. México

ARTICLE INFO

Article history:

Received 3 May 2013

Received in revised form

11 November 2013

Accepted 19 November 2013

Available online 1 December 2013

Keywords:

Anhedonia

Depression

Learning and memory

Palliative care in Parkinson's disease

D5r

D3r

D2r

ABSTRACT

L-Dopa is the major symptomatic therapy for Parkinson's disease, which commonly occurs in elderly patients. However, the effects of chronic use on mood and cognition in old subjects remain elusive. In order to compare the effects of a chronic pulsatile L-Dopa treatment on emotional and cognitive functions in young (3 months) and old (18 months) intact rats, an L-Dopa/carbidopa treatment was administered every 12 h over 4 weeks. Rats were assessed for behavioural despair (repeated forced swimming test, RFST), anhedonia (sucrose preference test, SPT) and spatial learning (Morris water maze, MWM) in the late phase of treatment (T). Neuronal expression of Fos in the hippocampus at the early and late phases of T, as well as after MWM was studied. The density and ratio of dopamine D5r, D3r and D2r receptors were also evaluated in the hippocampus using immunohistochemistry and confocal microscopy. Young rats showed similar patterns during behavioural tests, whereas aged treated rats showed increased immobility counts in RFST, diminished sucrose liquid intake in SPT, and spatial learning impairment during MWM. Fos expression was significantly blunted in the aged treated group after MWM. The density of D5r, D3r and D2r was increased in both aged groups. The treatment reduced the ratio of D5r/D3r and D5r/D2r in both groups. Moreover, aged treated subjects had significant lower values of D5r/D3r and higher values of D5r/D2r when compared with young treated subjects. These results indicate that chronic L-Dopa treatment in itself could trigger emotional and cognitive dysfunctions in elderly subjects through dopamine receptor dysregulation.

© 2014 The Authors. Published by Elsevier Ltd. All rights reserved.

1. Introduction

L-3,4-dihydroxyphenylalanine (L-Dopa or levodopa) is the direct precursor of dopamine (DA) (Elsworth and Roth, 1997; Nutt, 1987) and has been suggested to have direct effects on DA receptors (Goshima, 1993). It is widely used in the therapy of Parkinson's disease (PD) (National Collaborating Centre for Chronic Conditions (UK), 2006) and has also been used, although to a minor extent, to treat some neurological and psychiatric disorders such as Alzheimer's disease (Martorana et al., 2008) and schizophrenia (Jaski

and Popli, 2004). It has been implicated as a potential substance for drug abuse (Limotai et al., 2012; Spigset and von Scheele, 1997; Witjas et al., 2012).

Whether the use of L-Dopa can induce DA system dysregulation in treated subjects is controversial (Macdonald and Monchi, 2011). Although there are several studies showing that L-Dopa is toxic *in vitro* (Corona-Morales et al., 2003, 2000; Mytilineou et al., 2003), there is little convincing evidence suggesting that L-Dopa, at its therapeutic dose, exerts dysregulatory effects on the *in vivo* dopaminergic system (Evans and Lees, 2004; Olanow et al., 2009). The plasmatic half-life of the widely used L-Dopa/carbidopa is about 2 h (Chana et al., 2003). Hence, a twice-daily L-Dopa/carbidopa therapeutic scheme produces pulsatile intracerebral L-Dopa concentration (Schapira, 2003). Furthermore, the erratic absorption of

[☆] This is an open access article under the CC BY-NC-ND license (<http://creativecommons.org/licenses/by-nc-nd/3.0/>).

* Corresponding author. Tel./fax: +52 55 56232348.

E-mail address: limei@unam.mx (L. Zhang).

l-Dopa makes the pulsatility unpredictable (Nutt, 1987). Most neurotransmitter-receptor systems compensate for over- or under-stimulation with a reduction in responsiveness or desensitization, or an enhanced responsiveness or supersensitivity, respectively. In general, results from *in vivo* and *in vitro* studies of DA receptor regulation fit within this scheme (Creese et al., 1981; Sibley and Neve, 1997). However, the functional limits of this resilience mechanism can be surpassed by external or internal factors, such as drug dose, pulsatility, ageing, etc. It is commonly accepted that DA D1r-class of receptors (D1r and D5r) activates the $G_{\alpha s/olf}$ family of G proteins to stimulate cAMP production by adenylyl cyclase (AC). These are found exclusively postsynaptically on dopamine-receptive cells. D5r is highly expressed in the hippocampus (Ciliax et al., 2000; Jay, 2003; Marsdan, 2006; Meador-Woodruff et al., 1992; Sunahara et al., 1991). The DA D2r-class of receptors (D2r, D3r, and D4r) couples to the $G_{\alpha i/o}$ family of G proteins and thus induces inhibition of AC. In contrast to the D1-class of DA receptors, D2r and D3r DA receptors are expressed both postsynaptically and presynaptically (Beaulieu and Gainetdinov, 2011; Sokoloff et al., 2006) and are highly expressed in the hippocampal region (Khan et al., 1998). D2r and D3r have been reported to be modified prominently during the l-Dopa treatment (Joyce, 2001; Joyce et al., 2004).

DA critically contributes to cellular consolidation of hippocampal-dependent memories by modifying synaptic plasticity in hippocampal neurons (Frey et al., 1991; O'Carroll et al., 2006), and is particularly sensitive to ageing (Amenta et al., 2001). Hippocampal dopaminergic innervation arises mainly from the midbrain, and is part of the mesolimbic dopaminergic pathway (Scatton et al., 1980; Swanson, 1982). It has been shown that activation of the ventral tegmental area (VTA) leads to DA release in the hippocampus (Jay, 2003). Recent studies (Bolam and Pissadaki, 2012; Pissadaki and Bolam, 2013) have suggested that the unique cellular architecture of both the *nigro-striatal* and mesolimbic dopaminergic pathways makes them differentially susceptible in PD. *Substantia nigra pars compacta* (SNc) DA neurons possess large, complex axonal arborizations, which put them under a tight energy budget that makes them particularly susceptible to factors that contribute to cell death. However, this seems not to be the case for mesolimbic VTA DA neurons (Bolam and Pissadaki, 2012). Hence, the effects of a systemically increased l-Dopa availability can have differential impacts on the *nigro-striatal* and mesolimbic dopaminergic pathways, and the latter modulates emotionality and cognitive function (Nieoullon and Coquerel, 2003).

In view of the above findings, it becomes important to ask what the impact(s) of the systemic increase of l-Dopa availability are on the mesolimbic dopaminergic pathway. One strategy to dissect them is to expose young and old rats to chronic and pulsatile l-Dopa treatment and subsequently examine them for possible mood and cognition impairments with well-validated tests. Hence, we hypothesize that a global increase in the dopaminergic tone, due to l-Dopa administration, can impair cognitive and emotional functions in old subjects possibly through modification of dopaminergic receptors. We have evaluated this hypothesis using a hippocampus-dependent spatial learning task and the consequences of l-Dopa treatment on the activation of the hippocampus by assessing the expression of the immediate early gene Fos as well as the dopaminergic receptor densities and their ratios.

2. Material and methods

2.1. Animals and treatment

Sixty-eight male Wistar rats from the local animal facility were used in this study. All animal procedures were approved by the local bioethical and research committees in accordance with the principles exposed in the National Institute of Health Guide for the Care and Use of Laboratory Animals (NIH Publications No. 80-

23) revised 1996. Rats were housed two per cage, maintained on an inverted 12-h light schedule in a room with controlled temperature between 20 °C and 24 °C with adequate ventilation, and given access to standard rat chow and water *ad libitum*.

Rats were separated into two groups. The "Young" group comprised of 34 three-month old male rats (250 g \pm 15 g b. w.): 17 "Control Young" and 17 L-Dopa-treated "l-Dopa Young". The "old" group comprised of 34 eighteen-month old male rats (600 g \pm 25 g, b. w.): 17 "Control Old" and 17 L-Dopa-treated "l-Dopa Old". The experimental young and old groups were treated with oral l-Dopa/carbidopa dose 25mg/2.5 mg per kg, (Sinemet® 250/25 mg, l-Dopa/carbidopa, Merck & Co., Inc.) twice daily (period $T = 12$ h). The tablet was grinded and the corresponding amounts were mixed with soft cheese pellets (approximately 1 g of wet weight per pellet). Experimental subjects were previously habituated with the soft-cheese pellets for about 3 days until the rats ate the pellets readily. The experimenter watched over the drug/cheese intake process until each subject ate the corresponding pellet in its entirety. This administration was continued for four weeks in a twice-daily schedule (at the beginning of the light- and dark- periods). The control groups received the soft-cheese pellets only, in the same schedule.

The reason for which we used this unconventional drug administration method is because we aimed to examine mood and cognition functions in young and old rats under a chronic and pulsatile treatment of l-dopa – our experimental-treatment variable. It was important to avoid any treatment-related stressful events, such as oral gavage or intraperitoneal injection. Based on this reasoning, we established this low-stress drug/soft-cheese co-administration method. Both cheese (in pellets of 1 g) and drug (corresponding dosage per subject) were weighed using an analytical balance before being mixed. After a 3-day training period in which we gave only cheese pellets directly to the rats, the pellets were completely eaten as soon as they were introduced to the cage, on small weighing boats (generally in less than 30 s). In this way, we were able to administer the precise dosage of drug without introducing significant stress, an important condition for the behavioural tests.

2.2. Behavioural assessments

All behavioural assessments were carried out at the late phase of the T , i.e. after more than 10 h of the last l-Dopa dose.

2.2.1. Repeated forced swimming test (RFST)

After 4 weeks of l-Dopa treatment, young and old rats ($n = 7$) were assessed for depression-like behaviour using a modified version of forced swimming test in which experimental subjects were repeatedly exposed to the swimming stressor. Briefly, the modified Porsolt forced swim test paradigm used (Porsolt et al., 1977a; Zhang et al., 2008) (McLaughlin et al., 2003) was a 2-day procedure in which rats swam without the opportunity to escape. In all trials, rats were placed in a Plexiglas cylinder (45 cm tall \times 30 cm in diameter) containing 30 cm of water, kept at 24 °C. After the trial, rats were removed, dried with towels, and returned to their home cages for at least 10 min before further testing. On day 1, animals were placed in water to swim for a single trial of 15 min. The time spent immobile in the last 5 min of the trial was recorded. On day 2, animals were again placed in water to swim but in a series of four trials, each 6 min long. Trials were separated by a 12–15 min return to a home cage. Swimming behaviour was recorded with a video camera, and immobility during minutes 2–6 was analysed off-line according to criteria described elsewhere (Detke et al., 1995; Zhang et al., 2008). Briefly, the observer gave a score of either "swimming" or "immobile" every 5 s. A rat was judged to be immobile when it remained floating, making only minimum necessary movements to keep its head over the surface without horizontal displacement. Percentages of immobility counts out of total counts (60) were calculated.

2.2.2. Sucrose preference test (SPT)

After the forced swimming test, the same rats were singly housed and presented to a sucrose solution drop dispenser (3% sucrose in H₂O) and a plain water drop dispenser side by side during 24 h in order to let the rats habituate to the sweet liquid. Concluding this period, the dispensers were removed and the rats underwent water deprivation for 6 h. Subsequently, the drop dispensers with a previously quantified liquid volume were placed in the same locations for the next 24 h allowing the rats to drink *ad libitum* and undisturbed. Completing this period, the liquid consumption was measured and the sucrose liquid drinking volume, as a percentage of the total liquid consumption, was calculated. This test has been used for anhedonia assessment and was first described by Willner et al. (Willner et al., 1987).

2.2.3. Morris water maze (MWM)

After 4 weeks of l-Dopa treatment, spatial learning was evaluated with a separate set of rats ($n = 10$) during the beginning of the dark period, using a modified version of MWM described elsewhere (Hernandez et al., 2012; Nissen et al., 2012). Rats were exposed to the swimming pool without the platform for 2 min one day before, aiming to habituate them to this experimental procedure and reduce the stress caused by novelty. The test consisted of eight consecutive trials with 5 min rest intervals and was video-recorded. Off-line blind analysis was made.

In order to ensure that this ι -Dopa treatment scheme did not produce locomotor alterations, the swimming speed in the first trial was measured as follows: the swimming paths were manually traced using an acetate projection sheet placed on a monitor and traced with a marker while playing the experimental recording. Swimming velocity was measured only when rats were swimming and floating movements were eliminated. The tracings were then digitalized and the swimming distance per minute was measured with the “NeuroJ” plugin for ImageJ (Meijering et al., 2004). Path lengths were divided by latencies and velocity was obtained (expressed as cm/s).

2.3. Immunohistochemistry (IHC)

For perfusion-fixation, rats were deeply anesthetized with an overdose of pentobarbital (63 mg/kg) and perfused for 15 min transcardially with 0.9% saline followed by cold ice fixative containing paraformaldehyde 4% in 0.1M sodium phosphate buffer (PB, pH 7.4) plus 15% v/v of saturated picric acid. After perfusion, the brains were removed from the skull, thoroughly rinsed with PB and brain vibratome sections of 70 μ m were collected.

2.3.1. IHC against Fos

To evaluate the neuronal activity the protein product of the proto-oncogene fos was used (Kovacs, 1998). Fos is best detected in the interval between 60 and 120 min after a neuron is activated (Kovacs, 1998). Hence, we chose the following time-points after the last ι -Dopa administration: a) early phase of T: 3 h after last ι -Dopa administration (Basal 3 h, $n = 4$); b) late phase of T: 12 h after last ι -Dopa administration (Basal 12 h, $n = 4$); c) sixty minutes after MWM test (MWM, $n = 4$). It is worth mentioning that ι -Dopa plasmatic concentration peaks around 2 h after administration and drops to a negligible level at 10–11 h after administration (Chana et al., 2003; Khor and Hsu, 2007). Hence, the late phase of T represented a virtual abstinence phase.

For IHC, every third section spanning from Bregma – 3.6 mm to Bregma – 4.3 mm, according to the Paxinos and Watson brain atlas (Paxinos G, 1998), were blocked with 20% normal goat serum (NGS) in Tris-buffered (0.05M, pH 7.4) saline (0.9%) plus 0.3% of Triton X-100 (TBST) for 1 h at room temperature (RT) and then immunoreacted overnight with rabbit anti-Fos primary antibody (SC52, 1:1000, Santa Cruz Biotechnology, Santa Cruz, CA) in TBST +1% NGS at 4 °C with gentle shaking. Afterwards, sections were rinsed three times for 10 min with TBST and then incubated for 2 h at RT with biotinylated goat anti-rabbit secondary antibody (1:200; Vector Labs, Burlingame, CA). Finally, sections were incubated in avidin-biotin-peroxidase complex (Elite ABC kit, Vector Labs) for 1 h at RT. Peroxidase was detected using diaminobenzidine 0.05% as chromogen. Sections were rinsed and permanently mounted with Permount mounting medium (Electron Microscopy Sciences, Hatfield, PA). Fos immunoreactive nuclei per 540 μ m of length of cell body layers were counted using a Nikon Eclipse 50i microscope and a drawing tube.

2.3.2. IHC against dopamine receptors

Four rats per group were perfused as previously described (Section 2.3). One sagittal section per subject, containing dorsal and ventral hippocampus (lateral 3.9 mm according to the Paxinos and Watson brain atlas (Paxinos G, 1998), was selected for IHC against the DA receptors. It is worth noting that the fixation, cutting and IHC procedures were strictly controlled to be uniform for all rats and all the freely floating brain sections were labelled with different cuts and underwent the IHC reaction inside the same vial. Sections were blocked with 20% normal donkey serum (NDS) in Tris-buffered (0.05M, pH 7.4) saline (0.9%) plus 0.3% of Triton X-100 (TBST) for 1 h at RT and then immunoreacted overnight with the following primary antibodies: guinea pig against D2r (1:1000, Frontier Institute, Af500); rabbit against D3r (1:1000, Chemicon, AB1786p); mouse against D5r (1:1000, Chemicon, MAB5292). After the incubation, the slices were washed three times with TBST and incubated for 2 h with the following secondary antibodies: CY5 donkey against guinea pig (AP1935, Millipore); Alexa 594 donkey against rabbit (A-21207, Molecular probes); Alexa 488 donkey against mouse (A-21202, Molecular probes). Sections were rinsed and mounted with Vectashield mounting medium. Analysis of signal intensity was done in photographs taken at 20 \times with a confocal Leica microscope at 1.5 μ m of thickness. For image acquisition and initial observation, Leica LASAF software was used, while the Fiji version of ImageJ (Schindelin et al., 2012), was used to calculate the signal intensity, in 50 μ m \times 50 μ m areas inside the cell body layer for each reading of the corresponding receptor at CA1, CA2, CA3 and dentate gyrus regions.

2.4. Data analyses

Quantitative results were expressed as mean \pm SEM. Multiple pair-comparisons were performed using Bonferroni *post hoc* test after ordinary one-way, two-way or three way analysis of variance (ANOVA), specified in the “result section” for each experiment. For RFST, second day analysis, and MWM, repeated measures analysis of variance (RM-ANOVA) followed by Bonferroni *post hoc* test were used, where ‘trials’ was the within-subject factor and ‘treatment’ was the between-subject factor. *Post hoc* differences were considered statistically significant at a value $p < 0.05$ ($^*p < 0.05$, $^{**}p < 0.01$, $^{***}p < 0.001$).

In order to better understand each population’s dynamic behaviour during the MWM spatial learning task, probability of escape was analysed. The escape latency of the individuals was treated as a different data point and then its frequency was collected using bins of five seconds for each of the four groups (Age – Treatment). The frequency count was used to construct the cumulative frequency distribution. The normalization of the cumulative frequency to the total of data points in each population defines the cumulative probability function of escape latency (CPFEL). Then a cumulative Weibull distribution function was fitted to the CPFEL using Matlab R2012a (MathWorks Inc., Natick, MA). The cumulative Weibull distribution function $f(x) = 1 - e^{-(t/\lambda)^\kappa}$, where κ is the shape parameter and λ is the scale parameter, was chosen and is commonly used in survival analysis. The cumulative distribution function obtained in this way provided additional information about the groups analysed because it better fits the naturally random aspects of rat behaviour, and because it is a direct measure of the probability of escape. It also allows us to determine the half-time of escape and the spread of the escape latency distribution. In order to test for statistical differences between the models, we compare the resulting parameters from the non-linear fit with an F statistic. As it will be shown below, this analytical model has the advantage that it naturally follows the logic of the experiment and it is able to reveal new characteristics in the interpretation of the MWM spatial learning behaviour.

3. Results

3.1. Behavioural despair measured with RFST was only observed in the old-treated group

The repeated forced swimming test (RFST) allows for the assessment of depression-like behaviour, on both acute (first day of the test) and repeated exposure (second day of the test) and helps to rule out the possibility of motor impairments. Seven rats per experimental group were exposed to the RFST. For the first day data, one-way ANOVA was applied. The analysis showed that the percentage of immobility differed significantly between age groups, ($p < 0.01$, $F_{(3,27)} = 6.816$), but not between treatments within the same age group.

For the second day data, repeated measure-two-way ANOVA was used. Analysis showed that in both age groups, the effect of the factor *trial* was significant ($p < 0.001$, $F_{(3,36)} = 35.31$ for young and $F_{(3,36)} = 40.66$ for old subjects). *Treatment* had no significant effect on young rats ($p = 0.427$, $F_{(1,36)} = 0.675$), however a significant effect was shown on old rats ($p < 0.01$, $F_{(1,36)} = 11.09$). No interaction between *treatment* and *trial* was found in either group. Young control and L-Dopa-treated rats showed similar immobility patterns along the entire course of the test (Fig. 1A). In contrast, old animals treated with ι -Dopa showed a significant increase in immobility in trials II ($p < 0.01$), III ($p < 0.05$) and IV ($p < 0.05$) of the second day of the test when compared to the corresponding control group (Fig. 1B).

3.2. Sucrose intake test revealed anhedonia in ι -Dopa treated old rats

Anhedonia, a behavioural expression of hyposensitivity to reward, is interpreted as a symptom of depression and is commonly tested in rats as a decreased consumption of a sweet palatable solution. After 4 weeks of pulsatile ι -Dopa administration, anhedonia was assessed by means of the sucrose (3% sucrose solution) intake test in a 24hr period. One-way ANOVA showed that the percentage of sucrose intake in old rats treated with ι -Dopa was significantly reduced compared with all other groups ($p < 0.001$, $F_{(3,27)} = 42.94$) (Fig. 2).

3.3. Chronic pulsatile ι -Dopa treatment effectively impaired spatial learning in old rats

The effect of the long-term pulsatile administration of ι -Dopa on spatial learning was tested using the MWM test. Data was analysed using a mixed model analysis of variance (ANOVA) of the MWM

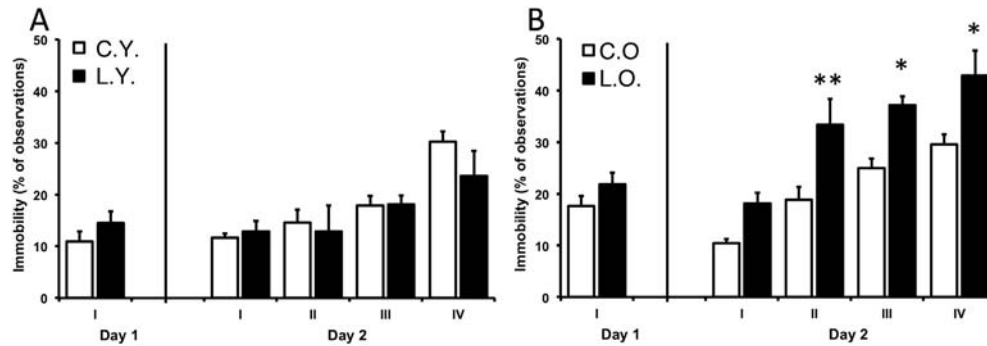


Fig. 1. Behavioural despair assessed by repeated forced swimming test (RFST). Histograms show the percentage of immobility episodes that occurred in the young (A) and old (B) groups. Day 1: the last 5 min of a 15 min trial were assessed; day 2: the last 5 min in each of four 6 min trials were assessed. Values represent mean \pm SEM, * $P < 0.05$, ** $P < 0.01$, $n = 7$. C.Y.: control young; L.Y.: L-dopa young; C.O.: control old; L.O.: L-Dopa old.

latency time of escape, with factors *age* (young, old), *treatment* (cheese pellets with or without L-Dopa) and *trial* with repeated measures (I, II, III, IV, V, VI, VII, VIII). The non-sphericity of the data was significant, as reported from the Mauchly test. To correct for the non-sphericity, we used the Huynh - Feldt correction. Using this correction, three factor interaction was significant, $F_{(4,193)} = 2.815$, $p = 0.023$. Then, in order to search for the interactions we restricted our analysis to a mixed model ANOVA leaving the *age* factor fixed, again assigning the factor *trial* as the repeated measures.

In the young rat group, the interaction between *trial* and *treatment* was not significant, $F_{(7, 154)} = 0.821$, $p = 0.571$. The main effect *trial* was significant, ($F_{(7,154)} = 47.245$, $p < 0.001$). These results indicate that the spatial learning process increases with repetition (Fig. 3A), but there was no effect of the treatment in the young group. In the case of the old group, both the interaction and the main effect were significant: $F_{(7,154)} = 5.101$, $p < 0.001$ and $F_{(7,154)} = 34.6$, $p < 0.001$. Then again, the learning process was different along between the trials but a significant difference due to the treatment is shown (Fig. 3B). The Bonferroni *post hoc* test showed that both the young and old control rats found the platform in significant less time compared to the L-Dopa treated aged rats in trials III, V and VII. Fig. 3C combined the panels A and B. In this panel, a subtle difference between the control groups (young vs. old) can be seen (see insert of panel D, where we analyse the curve “shape” parameter kappa (one can easily observe the similitude inside and the difference between the age groups). Fig. 3D shows the cumulative probability of the escape latency (CPFEL) for the different groups. The symbols represent the experimental data and the segmented lines the corresponding non - linear fit. A clear difference in the CPFEL was observed for the L-Dopa old group in

which half of the population reached the platform with times lower than 22.5 s. The insert in Fig. 3D shows the estimators for the shape (κ) and the scale (λ) parameters (open symbols) with their 95% CI (error bar). The estimators are showed in segmented lines in the inset. It can also be seen that the halftime of escape is greater only for the old treated group (Fig. 3D, right insert), while the halftime of escape for the three other groups is statistically the same. Nonetheless, the data distribution for the control old group, reflected by the curve shape estimator (κ), was different compared to the young groups (Fig. 3D, left insert). With this representation, the individual variation became part of the population behaviour and the differences between the groups could be clearly visualized.

3.4. The L-Dopa treatment did not produce locomotor alterations as revealed by swimming speed analysis

The swimming speed measured for the first trial of the MWM test is showed in Table 1. No differences were found between control and L-Dopa treated groups, whereas significant differences were detected between age groups (Table 1).

3.5. “Spontaneous” Fos expression in hippocampus at “basal 12 h” in the treated groups and dampened Fos induction by MWM in the old treated group

The expression of Fos was evaluated in the hippocampus (CA1, CA3 and DG) after 4 weeks of pulsatile L-Dopa administration at three different time-points: 3 h and 12 h after the last L-Dopa administration, and 1 h after MWM using immunohistochemical method (see Fig. 4, panels A, B, C and inserts as examples of these immunoreactions). Using a three-way ANOVA analysis (factors: *age*, *treatment*, *time*), we observed that for CA3, the *time*, *age*, *treatment* and all second order and third order interactions had a significant effect (*time*: $F_{(2,372)} = 814.99$, $p < 0.001$; *treatment*: $F_{(1,372)} = 4.91$, $p < 0.02$; *age*: $F_{(1,372)} = 26.51$, $p < 0.001$; *time.treatment*: $F_{(2,372)} = 17.49$, $p < 0.001$; *treatment.age*: $F_{(1,372)} = 4.91$, $p = 0.027$; *time.age*: $F_{(2,372)} = 14.18$, $p < 0.001$; *treatment.age.time*: $F_{(2,372)} = 4.72$, $p = 0.009$). For CA1 the main effect of *time* and *treatment* as well as its interaction, the interaction of *time* and *age* and the three order interaction had a significant effect (*time*: $F_{(2,372)} = 961.7$, $p < 0.001$; *treatment*: $F_{(1,372)} = 14.15$, $p < 0.001$; *time.group*: $F_{(2,372)} = 4.0$, $p = 0.019$; *treatment.age*: $F_{(1,372)} = 5.74$, $p = 0.071$; *treatment.age.time*: $F_{(2,372)} = 5.82$, $p = 0.003$). For DG the third order interaction and the second order interaction *treatment.age* were not significant, therefore we fitted a simple model without these terms (*time*: $F_{(2,375)} = 445.43$, $p < 0.001$; *treatment*: $F_{(1,375)} = 25.51$, $p < 0.001$; *age*: $F_{(1,375)} = 20.58$, $p < 0.001$,

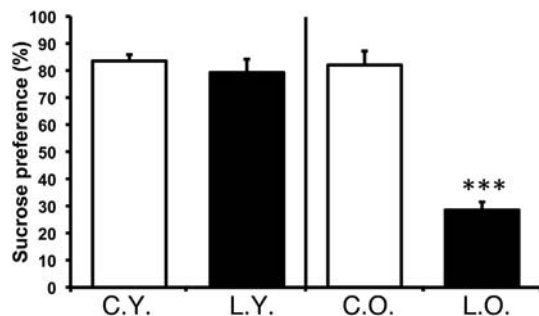


Fig. 2. Anhedonic behaviour measured by the sucrose preference test (SPT). Histograms show the percentage of sucrose intake related to the total volume of liquid consumption (plain water + water with 3% of sucrose). Values represent mean \pm SEM. *** $p < 0.001$, $n = 7$. C.Y.: control young; L.Y.: L-Dopa young; C.O.: control old; L.O.: L-Dopa old.

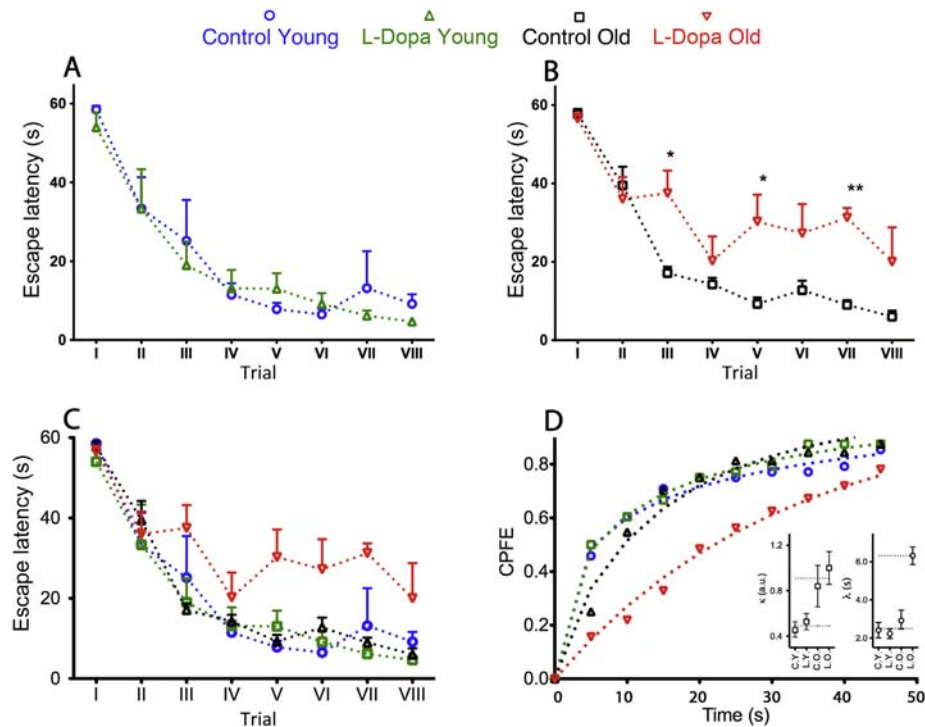


Fig. 3. Mean latency of escape from the Morris Water Maze test comparing control and ι -Dopa treated groups in young (A) and old subjects (B) and comparison of the performance of the 4 groups (C) ($n = 10$; * $p < 0.05$; ** $p < 0.01$). (D) Cumulative probability of escape latency (CPFE) from the Morris Water Maze test. Note that the cumulative probability of escape was lower for the ι -Dopa treated old group (L.O.) than for any other group at any time. The probability of escape of 50% of the population, other than the L.O., presented a latency time lower than 10 s (less than half of the time for the L.O.). The insert shows the comparison of the parameters κ and λ from the non-linear fit of the Weibull distribution function. It can be noticed that the values for κ groups/cluster seem to draw together in young and old groups, but the difference is significant between them. On the other side, the λ parameter is different only for the L.O. (For details see discussion in the text). C.Y.: control young; L.Y.: ι -Dopa young; C.O.: control old; L.O.: ι -Dopa old.

time.treatment: $F_{(2,375)} = 17.19$, $p < 0.001$; *time.age*: $F_{(2,375)} = 24.83$, $p < 0.001$). *Post hoc* Bonferroni test was used to compare the data from different *time* but within the same group and same hippocampal subfield. The results are reported in the table at the end of Fig. 4.

Minimum Fos expression levels were found in all groups at 3 h after the last administration of ι -Dopa, (Fig. 4, panel A and blue bars of panels D, E, F). However, at the 12 h point, young and old treated animals showed a significant increase ($p < 0.001$) in the neuronal activation in the CA3 and DG hippocampal subfields (Fig. 4, panel B and green bars of panels D, E, F). The spatial learning test induced a further significant increase of Fos expression in all groups when compared with the basal 12 h condition ($p < 0.001$) (Fig. 4, panel C and red bars of histograms D, E and F). However, the relative Fos elevation induced by the MWM was blunted in the old treated group, especially in the DG (Fig. 4, panel F, C.O vs L.O., shade segments).

3.6. The density of D5r, D3r and D2r was increased in the old groups and the treatment differentially modified the ratios D5r/D3r and D5r/D2r, between the age groups

Using IHC and confocal microscopy, D5r, D2r and D3r optical density measurements were performed in the CA1, CA2, CA3 and

Table 1
First trial speed analysis.

	Young (cm/s)	Old (cm/s)	
Control	20.8 ± 2.9	14.2 ± 1.8	$p < 0.01$
ι -Dopa	22.1 ± 1.8	14.6 ± 2.1	$p < 0.01$
	ns	ns	

ns: not significant.

DG hippocampal subfields, the results of a two-way ANOVA analysis (*treatment + age pooled as group*), showed significant effects of: *group* ($p < 0.001$; CA1: $F_{(3,138)} = 777.9$; CA2: $F_{(3,108)} = 469.5$; CA3: $F_{(3,180)} = 359.9$; DG: $F_{(3,138)} = 334$), receptor subtype ($p < 0.001$; CA1: $F_{(2,138)} = 135.8$; CA2: $F_{(2,108)} = 248.5$; CA3: $F_{(2,180)} = 234.4$; DG: $F_{(2,138)} = 251.5$), and interaction ($p < 0.001$; CA1: $F_{(6,138)} = 45.26$; CA2: $F_{(6,108)} = 44.39$; CA3: $F_{(6,180)} = 23.09$; DG: $F_{(6,138)} = 16.61$). The results for the receptor density ratios showed also significant effects of *group* ($p < 0.001$; CA1: $F_{(3,92)} = 305.3$; CA2: $F_{(3,72)} = 226$; CA3: $F_{(3,120)} = 102.8$; DG: $F_{(3,92)} = 8.67$), receptor density ratio ($p < 0.001$; CA1: $F_{(1,92)} = 323.5$; CA2: $F_{(1,72)} = 611.3$; CA3: $F_{(1,120)} = 585.4$; DG: $F_{(1,92)} = 65.3$) and interaction ($p < 0.001$; CA1: $F_{(3,92)} = 22.42$; $p < 0.001$, CA2: $F_{(3,72)} = 70.16$; $p < 0.001$, CA3: $F_{(3,120)} = 44.9$, $p < 0.05$, DG: $F_{(3,92)} = 3.85$). A Bonferroni *post-hoc* test to compare receptor densities or receptor density ratios between groups within each region was performed.

By performing confocal microscopic observation, we found that D5r, D3r and D2r were mainly localized at the somata and the proximal segments of the main dendrites (Fig. 5, panels A' and B' and Fig. 6). The distribution of immunoreactivity for the three studied receptors was not homogeneous through the hippocampus subfields but displayed a CA2/3, CA1 and DG gradient. A significantly increased density of the D5r, D3r and D2r was found in the aged control group as compared with the young control rats (Fig. 5, A panels compared to B panels, and histogram of 5C). ι -Dopa treatment had no effect on D5r expression in young subjects, except in DG where a reduction was observed. In contrast, the treatment enhanced the D5r expression in aged rats in all hippocampal regions evaluated. Conversely, the treatment enhanced globally the D3r and D2r expression in both young and aged rats, except in CA3 and DG of young subjects where no significant differences were detected (Fig. 6, panels As and Bs, C, D, E, F),

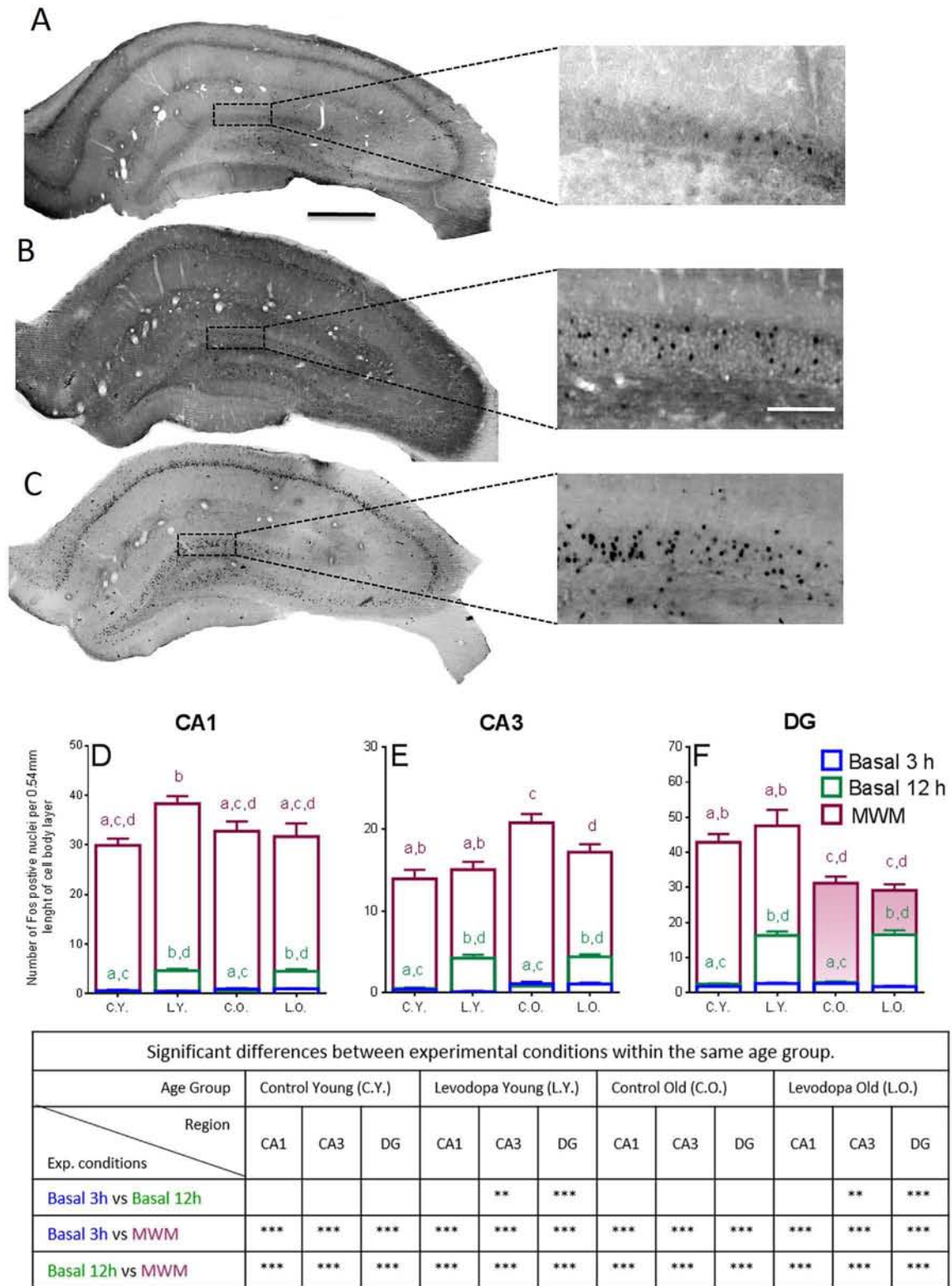


Fig. 4. Hippocampal Fos expression observed at time-points “Basal 3 h”, “Basal 12 h” and 1 h post MWM conditions. Panels A, B, and C, photomicrographs of typical Fos expression patterns in aged hippocampus under the three conditions above mentioned. Scale bars: 1 mm for A, B and C; 200 μ m for inserts. Histograms show the number of Fos positive nuclei in CA1 (D), CA3 (E) and dentate gyrus (F) under the three experimental conditions: “Basal 3 h”: blue bars, “Basal 12 h”: green bars and “MWM”: red bars. Bars with unequal lettering are statistically different at $p < 0.05$. Table underneath histograms reports statistic results between experimental conditions within the same age/treatment group. C.Y.: control young; L.Y.: L-dopa young; C.O.: control old; L.O.: L-Dopa old. (For interpretation of the references to colour in this figure legend, the reader is referred to the web version of this article.)

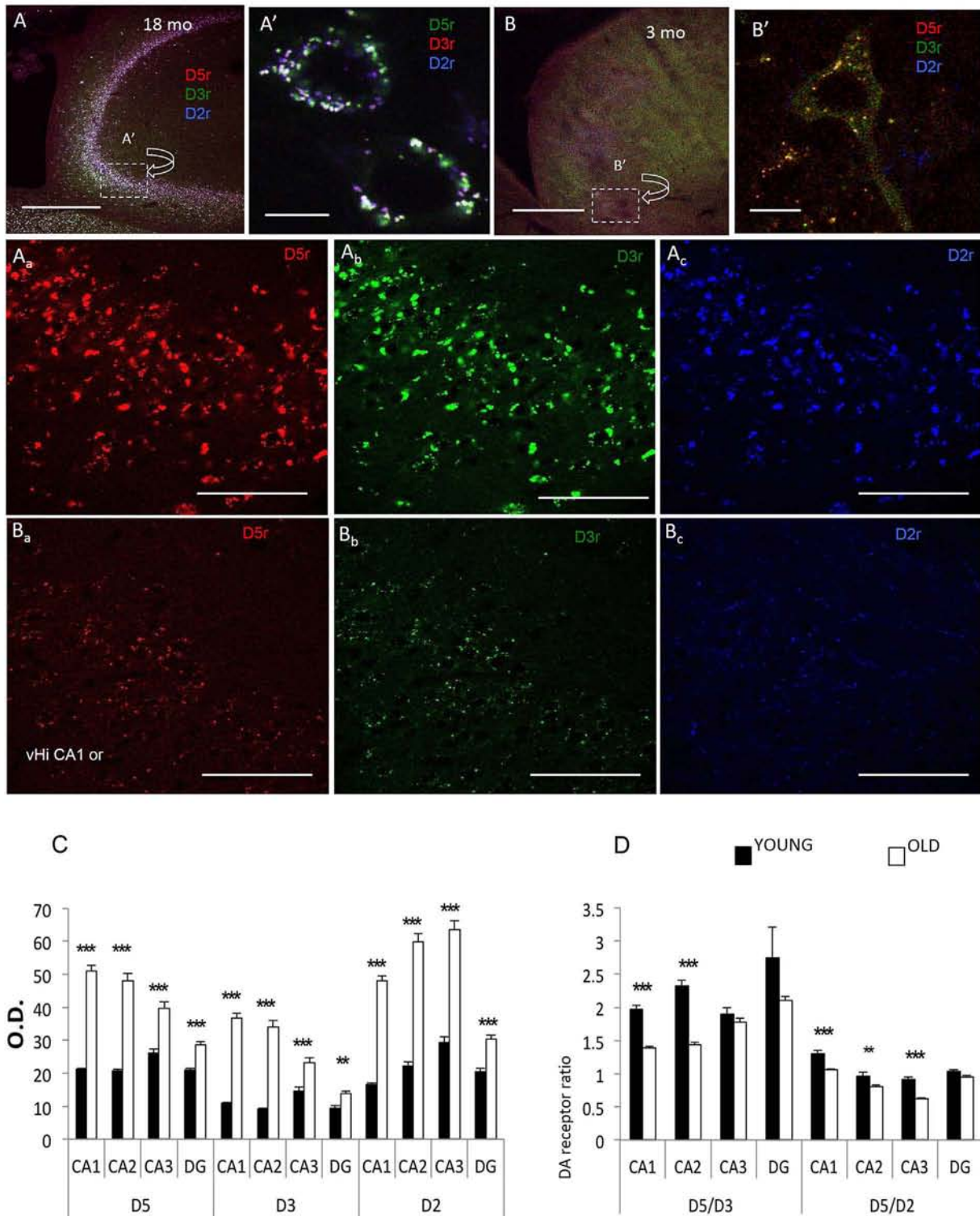


Fig. 5. Hippocampal dopamine receptor expression in control rats. A and A' and As: low and high magnification of immunofluorescence photomicrographs of ventral hippocampus of old rat. D5r (red), D3r (green) and D2r (blue); B and B' and Bs: the same region of a young rat processed with the same immunohistochemical conditions. Scale bars: A, B: 500 μ m; As and Bs: 50 μ m; A' and B': 10 μ m. G. C and D: Histograms showing the immunofluorescence optical density differences of D5r, D3r, D2r in dorsal (dHi) and ventral (vHi) hippocampal cell body layers between old and young control subjects (C) and the ratio between D5r/D3r, D5r/D2r in the above regions. *** p < 0.001, ** p < 0.01. (For interpretation of the references to colour in this figure legend, the reader is referred to the web version of this article.)

We next examined the modification of D5r/D3r and D5r/D2r ratios as consequences of ageing and L-Dopa treatment. Because binding of D5r and D2r/D3r produces opposing influences on adenylyl cyclase signalling cascades, as previously mentioned in the "Introduction", and the experimental data mentioned above

indicated that the three DA receptors studied here were mostly co-expressed in the same cellular compartments, the ratio of D5r/D3r and D5r/D2r become important factors for dopaminergic neurotransmission homeostasis (Neve, 2005; Thompson et al., 2010). The assessment of these indicators after chronic L-Dopa treatment

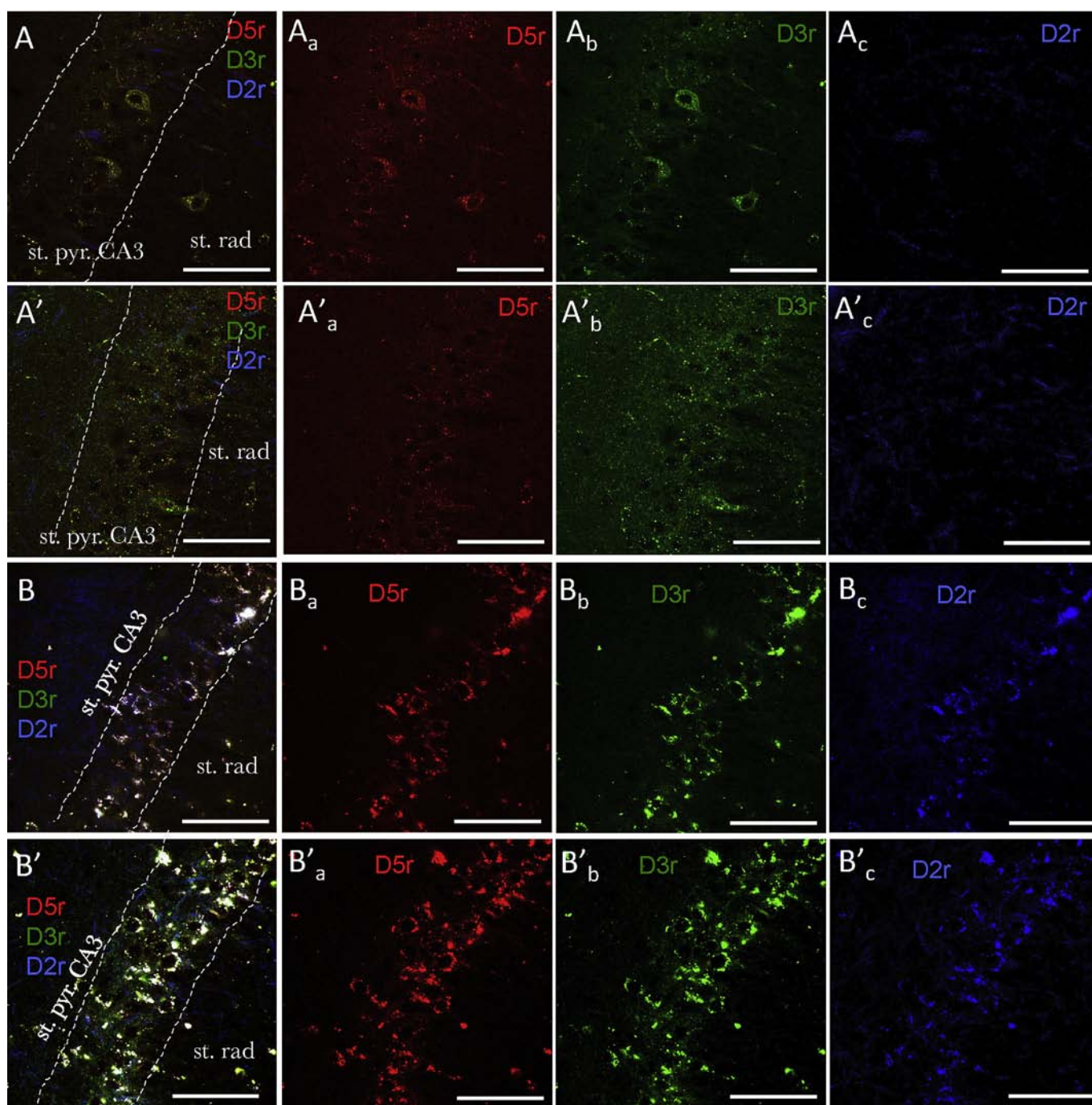


Fig. 6. Hippocampal cell body layer co-expression of D5r, D3r and D2r of young and old, control and *l*-Dopa treated rats. As and A's showing the expression patterns of young control and young treated subjects, respectively, and Bs and B's are from the old counterparts/cohorts. Scale bars: 500 μ m. Panels C, D, E, F: histograms showing the immunofluorescence optical density of D5r, D3r and D2r in the dorsal hippocampus CA1, CA2, CA3 and DG respectively, of the four experimental groups. C', D', E' and F' show the D5r/D3r and D5r/D2r ratios analysis of the respective subfields and experimental groups. Bars with unequal lettering are statistically different at $p < 0.05$.

provides a functional measurement of the dopaminergic system regulation in different treatment/age groups.

Ageing *per se* produced reduction in the ratio of D5r/D3r in CA1 and CA2 regions, and D5r/D2r in CA 1–3 in control rats (old rats vs. young rats) (Fig 5D). Treatment further globally reduced these ratios (Fig. 6, C'–F'). Moreover, aged treated subjects had significantly lower values of D5r/D3r and higher values of D5r/D2r when compared with young treated subjects in most of the regions evaluated (Fig. 6, C', D', E', F').

4. Discussion

The results from this series of experiments provide the first evidence that chronic treatment with a therapeutic dose of *l*-Dopa could exert an *age-dependent effect* regarding the genesis of depression-like behaviour, anhedonia and cognitive dysfunction. A blunted Fos induction after performing a spatial learning task in the old treated group, compared both with its age-control group and treatment-reference from young rats, indicates that the age-related

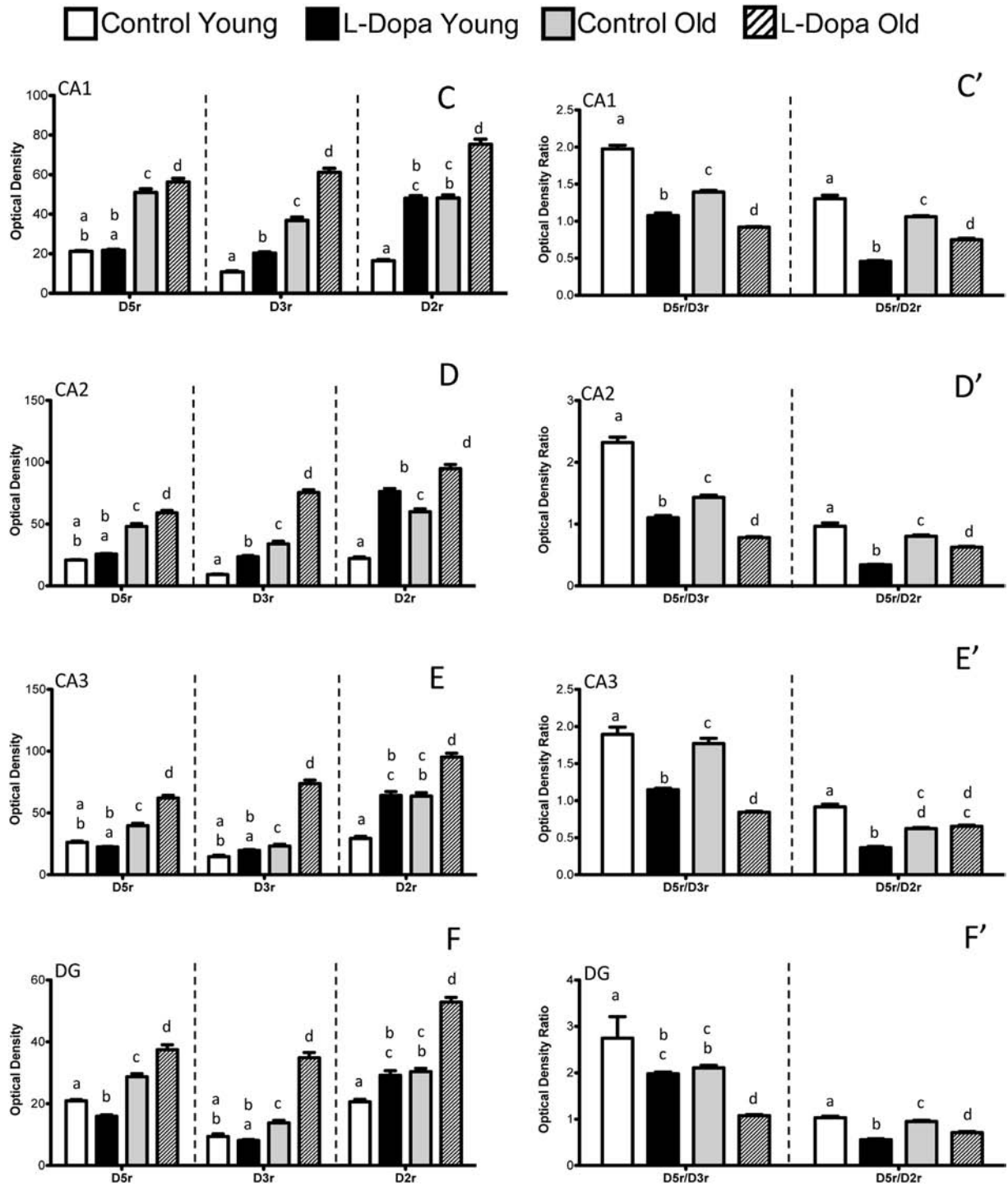


Fig. 6. (continued).

decline of neuroplasticity can make this group particularly susceptible to a centrally acting drug, such as L-Dopa. We also observed a significant reduction in the ratios between D5r/D3r and D5r/D2r in both treated groups compared with their respective controls, which is consistent with previously reported data (Beaulieu and Gainetdinov, 2011; Creese et al., 1981; Sibley and Houslay, 1994). Surprisingly, however, we found differential reductions in D5r/D3r and D5r/D2r by the treatment between the age groups: significant lower values for D5r/D3r and higher values for D5r/D2r were observed when comparing old vs. young treated subjects. A functional interpretation of this finding is currently lacking.

Nevertheless, our data suggests that ageing plays a crucial role on DA receptor dysregulation in L-Dopa treated subjects.

4.1. The effects of a long-term pulsatile L-Dopa treatment on hippocampus dependent spatial learning in aged subjects

Previous reports have found that after long-term administration of L-Dopa, normal monkeys developed L-Dopa-induced dyskinesia (Pearce et al., 2001; Togasaki et al., 2001). However, young rats treated with one daily dose of L-Dopa for five days showed an improvement in learning and memory tests (Reinholz et al., 2009).

It is worth noting that these authors evaluated learning 30 min after the last ι -Dopa administration, but studies on other time-points during the pulsatile drug administration cycle were missing. Moreover, there is an absence of well-controlled studies on the effect of ι -Dopa on cognition and emotionality in old subjects in spite of it being a therapeutic agent commonly used in elderly people with PD. DA modulatory effect for cognitive functions is a complex phenomenon and subtly controlled by the temporal variation of the levels of ligand/receptors and the presence of growth factors (for instance, brain derived neurotrophic factor regulate D3r expression in a development-dependent manner (Guillin et al., 2001)).

There are few studies assessing the effects of chronic ι -Dopa treatment in an intact dopaminergic system ((Hagenah et al., 1999) for instance). Some studies in humans have shown cognition improvement in subjects given ι -Dopa after stroke, brain trauma or hypoxic-ischemic episodes (Knecht et al., 2004). However, young subjects were always used in those reports (Mytilineou et al., 2003) (Reinholz et al., 2009). It has been reported that most of the biophysical properties of hippocampal neurons in aged subjects remain constant over the life span (Burke and Barnes, 2006). These include resting membrane potential, membrane time constant, input resistance, threshold to reach an action potential, and the width and amplitude of Na^+ dependent action potential (for a review, see (Burke and Barnes, 2006)). However, subtle changes in Ca^{2+} conductance in aged neurons have been reported. CA1 pyramidal neurons in the aged hippocampus have an increased density of L-type Ca^{2+} channels (Thibault and Landfield, 1996) that might lead to disruptions in Ca^{2+} homeostasis (Toescu et al., 2004), contributing to the plasticity deficits that occur with ageing. DA innervation in hippocampus, arisen mainly from the midbrain dopaminergic pathways, plays an important modulatory role for hippocampal function (Wittmann et al., 2005). Long-term potentiation in the hippocampus can be enhanced and prolonged by dopaminergic inputs from midbrain structures (Morris et al., 2003).

On the other hand, it has been reported since the late 80's that after ι -Dopa loading, DA, DOPAC and HVA are increased in striatum, hypothalamus, hippocampus and cerebellum, with the largest increases in those tissues with less dopaminergic activity (el Gemayel et al., 1986). This study suggested alternative sources of DA release in those regions. Recent studies have demonstrated that serotonergic innervations to hippocampus serve as an important source of DA release induced by ι -DOPA treatment (Navailles et al., 2010, 2013).

DA D1 and D5 receptors are involved in the persistence of LTP (Frey et al., 1991; Swanson-Park et al., 1999). On the other hand, Otmakhova and Lisman showed that DA strongly inhibits the response to perforant pathway (pp) stimulation (IC50; 3 mM), but not the response to Schaffer collateral stimulation (Otmakhova and Lisman, 1999). DA reduces both the NMDA and AMPA components of transmission at the pp (Otmakhova and Lisman, 1999). The data from this study showed that there is a natural increase of the D5r, D3r and D2r densities in the normal ageing rat hippocampus. This observation is in concordance with other data in the literature showing that old subjects' dopaminergic systems undergo changes in DA receptor density in the hippocampus (Amenta et al., 2001; Hemby et al., 2003; Xing et al., 2010). DA D3 receptor regulates cAMP-response element binding protein (CREB) signalling, which is one of the cellular molecules that has been strongly implicated in synaptic plasticity (Xing et al., 2010). Alterations in the DA D3r signalling were reported in age-related memory and cognitive impairment (Xing et al., 2010). Furthermore, a reduced concentration of DA in the dorsal hippocampus of aged rats (Stemmelin et al., 2000) could render them less able to compensate for the fluctuating concentrations of DA resulting from pulsatile ι -Dopa treatment, as observed in this study.

We have extended the previous observations on the constitutive Fos expression in the rat hippocampus (Desjardins et al., 1997) by measuring two time points between two ι -Dopa administrations. Interestingly, we have observed a spontaneously increased Fos induction during the late phase of the inter-administration period in the hippocampus. In fact, the observed cognitive impairment was temporally mirrored by a blunted MWM-induced activation of Fos expression in the hippocampus (Fos counts after MWM vs. Fos counts at Basal 12 h, Fig. 4, panel F, shade areas). As we mentioned before, there was a significant global reduction of the ratio D5r/D3r comparing the old treated subjects with the young ones, which implicated a pronounced, up-regulated expression of the D3r in the old rat's hippocampus. D3r's function is of particular interest because evidence suggests its effects are primarily inhibitory (Flores et al., 1996).

4.2. Differential effect of chronic ι -Dopa treatment on mood and cognition in young and aged intact rats

As early as 1971, Persson and Walinder reported non-Parkinsonian human cases in which ι -Dopa treatment caused short-term alleviating but long-term exacerbating effects on depressive symptoms – just one month of treatment already prompted patients with worsening of original depressive symptoms (Persson and Walinder, 1971). In the present study, we set out to test the effect of a pulsatile chronic administration scheme of ι -Dopa on mood and cognition in an intact rat model, emphasizing a comparison at two different ages. We chose a common clinical used dose and application format. With RFST, an established and predictive animal model for the study of depression in which antidepressants typically reduce the duration of the immobility exhibited (Lucki et al., 2001; Porsolt et al., 1977b), we observed that in the first day of the test all the experimental groups had similar performance, discarding any possible locomotor impairment by chronic ι -Dopa treatment. In the second day of RFST, aged-treated rats showed increased immobility compared to controls. This finding is in accordance with a recent study that used longer and higher doses of ι -Dopa in intact young rats, and showed increased immobility in a forced swimming test correlated with impaired DA and serotonin metabolism in some brain areas (Borah and Mohanakumar, 2007).

The sucrose intake test assesses another aspect of depression-like behaviour in rats. A reduction of the sucrose liquid intake provides an indirect measure of desensitization of the brain reward mechanisms. Aged treated subjects had a marked reduction of sucrose intake, indicating anhedonia which defined as a lowered ability to experience pleasure, an important component of depression. The putative neural substrate of anhedonia is represented by the dysfunction of a dopaminergic mesolimbic reward circuit involving the ventral striatum (nucleus accumbens), the prefrontal cortex and the entorhinal and amygdaloid complexes (Berke and Hyman, 2000; Kondo, 2008; Tanti and Belzung, 2010). These structures, and particularly the dopaminergic receptors in the nucleus accumbens, are considered to mediate the euphorising effects of psychostimulants, antiparkinsonian drugs and gustatory reward (Cantello et al., 1989; Norgren et al., 2006) or, as elsewhere suggested, mediate behavioural activation and effort-related processes (Salamone et al., 2007). Our observation suggests an alteration in DA responsiveness in the above regions.

The DA α expression patterns we observed in young control rats (Fig. 6, panels As) are in concordance with those reported in literature on the subject (Ciliax et al., 2000). The elevation of D3r in ι -Dopa treated subjects has also been reported (Joyce et al., 2004). Conversely, we have observed significant increases of D2r, D3r and D5r expression the cell body layer in CA1, CA2, CA3 and DG in aged

rats (Fig. 6, panel C, D, E, F respectively) which is in discrepancy with a study in humans using positron emission tomography (PET) in which a 10% of loss of D2r/D3r in the hippocampus was reported (Kaasinen et al., 2000). One possible explanation of this discrepancy is that the resolution of a PET image study is much lower than immunohistochemistry combined with confocal microscopy as we used in our study. The altered hippocampal D5r/D3r and D5r/D2r ratios in the old treated group matched with lower sucrose consumption and increased immobility in RFST. Given that the hippocampus is involved in the feedback regulation of the HPA axis function, structural and functional changes in hippocampus are related to mood disorders, including depression, which could result from an inability to appropriately respond to stress (Duman et al., 1999). DA receptors are also implicated in the underlying mechanisms in mood modulation; for example, antidepressants based on adenosine receptor antagonists probably involve interaction with D2 receptors (Crema et al., 2013).

4.3. Technical consideration for the usage of cumulative probability of escape latency (CPFEL) for the Morris Water Maze test analysis

Regarding the MWM performance analysis, It is worth mentioning that the significant interaction between “age”, “treatment” and “trial” factors made the differences observed difficult to interpret using ANOVA and the Bonferroni *post hoc* test. This is a common problem for the experiments on spatial learning such as the MWM test: the individual differences and the not-fully predictable nature of rat behaviour increase the variation for a given trial, and the lack of independence between the different trials. The trial correlation is clearly observed in the experiment, and it is an expected result for a learning-type curve, at least for the control group. On the other hand, the variability of the response of the rat in a *specific trial* could be, even less probable, a *temporal* behaviour that does not necessarily reflect its intrinsic *learning process*. Evidently, this problem can be solved increasing the *n*, but by using the *cumulative probability of escape latency (CPFEL)*, as proposed in this study, in addition to the repeated measure ANOVA analysis, this problem can be better solved with smaller *n*. Moreover, using this probabilistic approach can reveal additional characteristics of the rat behaviour. Firstly, the usual analysis could only report the mean latency time of escape with its variability at a definite trial and could not answer the question: at which time does the population learn the task? As an example, see Fig. 3C. We could interpret that the experimental old group learn to escape in the trial IV and on trial V the group unlearned it. Therefore, did the group learn to escape on trial IV or did they not? In our analysis it is possible to extract this information because we answer that half of the experimental old population was able to learn to escape on trial VI with a time lower than 22.5 s. This information provides useful aspects complementing those reported in the traditional analysis. Secondly, the usual way to report the variation is to report the standard error for each trial, because the variation of all of the trials does not have any sense. However, with our analysis we could report the variability of the behaviour of the population, and as can be seen, this variability increases with the age group, as the common sense would indicate, but now in a quantitative way of testing it. However, we have to be aware that the span of time chosen could affect the estimators or λ and κ .

4.4. Conclusion remark and implications for palliative care in Parkinson's disease

Receptor up- and down-regulation has long been implicated in adaptive responses to continued pharmacological stimuli. Our results indicate that a chronic pulsatile L-Dopa treatment within the

therapeutic range could produce depression-like behaviour and spatial learning impairment in intact rats, with aged subjects being more vulnerable. Dopaminergic receptor dysregulation is implicated as the underlying mechanism for the demonstrated emotional and cognitive dysfunctions.

In the past, the non-motor symptoms of PD patients have received little attention, particularly in the clinical settings (Bunting-Perry, 2006). Patients with this disorder often develop depression and cognitive decline culminating in dementia (Cummings, 1992; Leverenz et al., 2009; Svenningsson et al., 2012). The results of this study could have important implications for elderly patients who are treated with L-Dopa for Parkinsonism and who often develop cognitive impairment and emotional disturbances. Hence, this study calls attention to the need for heightened monitoring of emotional and cognitive functions, as well as accentuated palliative care for elderly Parkinson's patients treated with L-Dopa.

Acknowledgement

This study was supported by grants: CONACYT: 127777, 179616 and PAPIIT-DGAPA-UNAM: IN210406, IN218111. We are thankful to Javier González-Damian for proposing the cumulative probability function of escape latency (CPFEL) analytical model and for performing the analysis on an early version of this paper, to Francesco Ferraguti (Innsbruck, Austria) and Rafael Lujan (Albacete, Spain) for a careful reading of an early version of the manuscript and for giving helpful comments; to Maria José Gómora and Enrique Pinzon for technical assistance; to Marisela Morales (Baltimore, USA) for generous gifts of antibodies for DA receptors and to Freya Chay (Alaska, USA) for language editing.

References

- Amenta, F., Mignini, F., Ricci, A., Sabbatini, M., Tomassoni, D., Tayebati, S.K., 2001. Age-related changes of dopamine receptors in the rat hippocampus: a light microscope autoradiography study. *Mech. Ageing Dev.* 122, 2071–2083.
- Beaulieu, J.M., Gainetdinov, R.R., 2011. The physiology, signaling, and pharmacology of dopamine receptors. *Pharmacol. Rev.* 63, 182–217.
- Berke, J.D., Hyman, S.E., 2000. Addiction, dopamine, and the molecular mechanisms of memory. *Neuron* 25, 515–532.
- Bolam, J.P., Pissadaki, E.K., 2012. Living on the edge with too many mouths to feed: why dopamine neurons die. *Mov. Disord.* 27, 1478–1483.
- Borah, A., Mohanakumar, K.P., 2007. Long-term L-DOPA treatment causes indiscriminate increase in dopamine levels at the cost of serotonin synthesis in discrete brain regions of rats. *Cell Mol. Neurobiol.* 27, 985–996.
- Bunting-Perry, L.K., 2006. Palliative care in Parkinson's disease: implications for neuroscience nursing. *J. Neurosci. Nurs.* 38, 106–113.
- Burke, S.N., Barnes, C.A., 2006. Neural plasticity in the ageing brain. *Nat. Rev. Neurosci.* 7, 30–40.
- Cantello, R., Aguggia, M., Gilli, M., Delsedime, M., Chiardo Cutin, I., Riccio, A., Mutani, R., 1989. Major depression in Parkinson's disease and the mood response to intravenous methylphenidate: possible role of the “hedonic” dopamine synapse. *J. Neurol. Neurosurg. Psychiatry* 52, 724–731.
- Chana, P., Fierro, A., Reyes-Parada, M., Saez-Briones, P., 2003. Pharmacokinetic comparison of Sinemet and Grifoparkin (levodopa/carbidopa 250/25 mg) in Parkinson's disease: a single dose study. *Rev. Med. Chil.* 131, 623–631.
- Ciliax, B.J., Nash, N., Heilman, C., Sunahara, R., Hartney, A., Tiberi, M., Rye, D.B., Caron, M.G., Niznik, H.B., Levey, A.I., 2000. Dopamine D(5) receptor immunolocalization in rat and monkey brain. *Synapse* 37, 125–145.
- Corona-Morales, A.A., Castell, A., Zhang, L., 2000. L-DOPA-induced neurotoxic and apoptotic changes on cultured chromaffin cells. *Neuroreport* 11, 503–506.
- Corona-Morales, A.A., Castell, A., Escobar, A., Drucker-Colin, R., Zhang, L., 2003. Fullerene C60 and ascorbic acid protect cultured chromaffin cells against levodopa toxicity. *J. Neurosci. Res.* 71, 121–126.
- Creese, I., Sibley, D.R., Leff, S., Hamblin, M., 1981. Dopamine receptors: subtypes, localization and regulation. *Fed. Proc.* 40, 147–152.
- Crema, L.M., Petteuzzo, L.F., Schlabit, M., Diehl, L., Hoppe, J., Mestriner, R., Laureano, D., Salbego, C., Dalmaz, C., Vendite, D., 2013. The effect of unpredictable chronic mild stress on depressive-like behavior and on hippocampal A1 and striatal A2A adenosine receptors. *Physiol. Behav.* 109, 1–7.
- Cummings, J.L., 1992. Depression and Parkinson's disease: a review. *Am. J. Psychiatry* 149, 443–454.

- Desjardins, S., Mayo, W., Vallee, M., Hancock, D., Le Moal, M., Simon, H., Abrous, D.N., 1997. Effect of aging on the basal expression of c-Fos, c-Jun, and Egr-1 proteins in the hippocampus. *Neurobiol. Aging* 18, 37–44.
- Detke, M.J., Rickels, M., Lucki, I., 1995. Active behaviors in the rat forced swimming test differentially produced by serotonergic and noradrenergic antidepressants. *Psychopharmacology (Berl)* 121, 66–72.
- Duman, R.S., Malberg, J., Thome, J., 1999. Neural plasticity to stress and antidepressant treatment. *Biol. Psychiatry* 46, 1181–1191.
- Elsworth, J.D., Roth, R.H., 1997. Dopamine synthesis, uptake, metabolism, and receptors: relevance to gene therapy of Parkinson's disease. *Exp. Neurol.* 144, 4–9.
- Evans, A.H., Lees, A.J., 2004. Dopamine dysregulation syndrome in Parkinson's disease. *Curr. Opin. Neurol.* 17, 393–398.
- Flores, G., Barbeau, D., Quirion, R., Srivastava, L.K., 1996. Decreased binding of dopamine D3 receptors in limbic subregions after neonatal bilateral lesion of rat hippocampus. *J. Neurosci.* 16, 2020–2026.
- Frey, U., Matthies, H., Reymann, K.G., 1991. The effect of dopaminergic D1 receptor blockade during tetanization on the expression of long-term potentiation in the rat CA1 region in vitro. *Neurosci. Lett.* 129, 111–114.
- el Gemayel, G., Trouvin, J.H., Prioux-Guyonneau, M., Jacquot, C., Cohen, 1986. Dopaminergic metabolism in various rat brain areas after L-dopa loading. *J. Pharm. Pharmacol.* 38, 691–694.
- Goshima, Y., 1993. Transmitter-like release and pharmacological activities of levodopa. *Nihon Yakurigaku Zasshi* 102, 11–21.
- Guillin, O., Diaz, J., Carroll, P., Griffon, N., Schwartz, J.C., Sokoloff, P., 2001. BDNF controls dopamine D3 receptor expression and triggers behavioural sensitization. *Nature* 411, 86–89.
- Hagenah, J., Klein, C., Sieberer, M., Vieregge, P., 1999. Exogenous levodopa is not toxic to elderly subjects with non-parkinsonian movement disorders: further clinical evidence. *J. Neural. Transm.* 106, 301–307.
- Hemby, S.E., Trojanowski, J.Q., Ginsberg, S.D., 2003. Neuron-specific age-related decreases in dopamine receptor subtype mRNAs. *J. Comp. Neurol.* 456, 176–183.
- Hernandez, V.S., Ruiz-Velazco, S., Zhang, L., 2012. Differential effects of osmotic and SSR149415 challenges in maternally separated and control rats: the role of vasopressin on spatial learning. *Neurosci. Lett.* 528, 143–147.
- Jaskiw, G.E., Popli, A.P., 2004. A meta-analysis of the response to chronic L-dopa in patients with schizophrenia: therapeutic and heuristic implications. *Psychopharmacology (Berl)* 171, 365–374.
- Jay, T.M., 2003. Dopamine: a potential substrate for synaptic plasticity and memory mechanisms. *Prog. Neurobiol.* 69, 375–390.
- Joyce, J.N., 2001. Dopamine D3 receptor as a therapeutic target for antipsychotic and antiparkinsonian drugs. *Pharmacol. Ther.* 90, 231–259.
- Joyce, J.N., Der, T.C., Renish, L., Osredkar, T., Hagner, D., Reploge, M., Sakakibara, S., Ueda, S., 2004. Loss of D3 receptors in the zitter mutant rat is not reversed by L-dopa treatment. *Exp. Neurol.* 187, 178–189.
- Kaasinen, V., Vilkmann, H., Hietala, J., Nagren, K., Helenius, H., Olsson, H., Farde, L., Rinne, J., 2000. Age-related dopamine D2/D3 receptor loss in extrastriatal regions of the human brain. *Neurobiol. Aging* 21, 683–688.
- Khan, Z.U., Gutierrez, A., Martin, R., Penafiel, A., Rivera, A., De La Calle, A., 1998. Differential regional and cellular distribution of dopamine D2-like receptors: an immunocytochemical study of subtype-specific antibodies in rat and human brain. *J. Comp. Neurol.* 402, 353–371.
- Khor, S.P., Hsu, A., 2007. The pharmacokinetics and pharmacodynamics of levodopa in the treatment of Parkinson's disease. *Curr. Clin. Pharmacol.* 2, 234–243.
- Knecht, S., Breitenstein, C., Bushuven, S., Wailke, S., Kamping, S., Floel, A., Zwitserlood, P., Ringelstein, E.B., 2004. Levodopa: faster and better word learning in normal humans. *Ann. Neurol.* 56, 20–26.
- Kondo, T., 2008. Dopamine dysregulation syndrome. Hypothetical application of reward system stimulation for the treatment of anhedonia in Parkinson's disease patients. *J. Neurol.* 255 (Suppl. 4), 14–18.
- Kovacs, K.J., 1998. c-Fos as a transcription factor: a stressful (re)view from a functional map. *Neurochem. Int.* 33, 287–297.
- Leverenz, J.B., Quinn, J.F., Zabetian, C., Zhang, J., Montine, K.S., Montine, T.J., 2009. Cognitive impairment and dementia in patients with Parkinson disease. *Curr. Top Med. Chem.* 9, 903–912.
- Limotai, N., Oyama, G., Go, C., Bernal, O., Ong, T., Moum, S.J., Bhidayasiri, R., Foote, K.D., Bowers, D., Ward, H., Okun, M.S., 2012. Addiction-like manifestations and Parkinson's disease: a large single center 9-year experience. *Int. J. Neurosci.* 122, 145–153.
- Lucki, I., Dalvi, A., Mayorga, A.J., 2001. Sensitivity to the effects of pharmacologically selective antidepressants in different strains of mice. *Psychopharmacology (Berl)* 155, 315–322.
- Macdonald, P.A., Monchi, O., 2011. Differential effects of dopaminergic therapies on dorsal and ventral striatum in Parkinson's disease: implications for cognitive function. *Parkinsons Dis.* 2011, 572743.
- Marsdan, C.A., 2006. Dopamine: the rewarding years. *Br. J. Pharmacol.* 147, S136–S144.
- Martorana, A., Stefani, A., Palmieri, M.G., Esposito, Z., Bernardi, G., Sancesario, G., Pierantozzi, M., 2008. L-dopa modulates motor cortex excitability in Alzheimer's disease patients. *J. Neural Transm.* 115, 1313–1319.
- McLaughlin, J.P., Marton-Popovici, M., Chavkin, C., 2003. Kappa opioid receptor antagonism and prodynorphin gene disruption block stress-induced behavioral responses. *J. Neurosci.* 23, 5674–5683.
- Meador-Woodruff, J.H., Mansour, A., Grandy, D.K., Damask, S.P., Civelli, O., Watson Jr., S.J., 1992. Distribution of D5 dopamine receptor mRNA in rat brain. *Neurosci. Lett.* 145, 209–212.
- Meijering, E., Jacob, M., Sarría, J.C., Steiner, P., Hirling, H., Unser, M., 2004. Design and validation of a tool for neurite tracing and analysis in fluorescence microscopy images. *Cytometry A* 58, 167–176.
- Morris, R.G., Moser, E.I., Riedel, G., Martin, S.J., Sandin, J., Day, M., O'Carroll, C., 2003. Elements of a neurobiological theory of the hippocampus: the role of activity-dependent synaptic plasticity in memory. *Philos. Trans. R. Soc. Lond. B Biol. Sci.* 358, 773–786.
- Mytilineou, C., Walker, R.H., JnoBaptiste, R., Olanow, C.W., 2003. Levodopa is toxic to dopamine neurons in an in vitro but not an in vivo model of oxidative stress. *J. Pharmacol. Exp. Ther.* 304, 792–800.
- National Collaborating Centre for Chronic Conditions (UK), 2006. Parkinson's Disease: National Clinical Guideline for Diagnosis and Management in Primary and Secondary Care. Royal College of Physicians (UK), London (NICE Clinical Guidelines, No. 35). Available from: <http://www.ncbi.nlm.nih.gov/books/NBK48513/>.
- Navailles, S., Bioulac, B., Gross, C., De Deurwaerdere, P., 2010. Serotonergic neurons mediate ectopic release of dopamine induced by L-DOPA in a rat model of Parkinson's disease. *Neurobiol. Dis.* 38, 136–143.
- Navailles, S., Lagièrre, M., Contini, A., De Deurwaerdere, P., 2013. Multisite intracerebral microdialysis to study the mechanism of L-DOPA induced dopamine and serotonin release in the parkinsonian brain. *ACS Chem. Neurosci.* 4 (5), 680–692. <http://dx.doi.org/10.1021/cn400046e>.
- Neve, K.A., 2005. Dopamine receptors. In: Schmidt, W. a. R., Maarten, E.A. (Eds.), *Dopamine and Glutamate in Psychiatric Disorders*. Humana Press, Totowa, New Jersey, pp. 3–43.
- Nieoullon, A., Coquerel, A., 2003. Dopamine: a key regulator to adapt action, emotion, motivation and cognition. *Curr. Opin. Neurobiol.* 16 (Suppl. 2), S3–S9.
- Nissen, I., Estrada, F.S., Nava-Kopp, A.T., Irlès, C., de-la-Pena-Diaz, A., Fernandez, G.J., Govezensky, T., Zhang, L., 2012. Prolame ameliorates anxiety and spatial learning and memory impairment induced by ovariectomy in rats. *Physiol. Behav.* 106, 278–284.
- Norgren, R., Hajnal, A., Mungarndee, S.S., 2006. Gustatory reward and the nucleus accumbens. *Physiol. Behav.* 89, 531–535.
- Nutt, J.G., 1987. On-off phenomenon: relation to levodopa pharmacokinetics and pharmacodynamics. *Ann. Neurol.* 22, 535–540.
- O'Carroll, C.M., Martin, S.J., Sandin, J., Frenguelli, B., Morris, R.G., 2006. Dopaminergic modulation of the persistence of one-trial hippocampus-dependent memory. *Learn. Mem.* 13, 760–769.
- Olanow, C.W., Stern, M.B., Sethi, K., 2009. The scientific and clinical basis for the treatment of Parkinson disease (2009). *Neurology* 72, S1–S136.
- Otmakhova, N.A., Lisman, J.E., 1999. Dopamine selectively inhibits the direct cortical pathway to the CA1 hippocampal region. *J. Neurosci.* 19, 1437–1445.
- Paxinos, G., W.C., 1998. *The Rat Brain in Stereotaxic Coordinates*. Academic Press, San Diego, California, USA.
- Pearce, R.K., Heikkilä, M., Linden, I.B., Jenner, P., 2001. L-dopa induces dyskinesia in normal monkeys: behavioural and pharmacokinetic observations. *Psychopharmacology (Berl)* 156, 402–409.
- Persson, T., Walinder, J., 1971. L-DOPA in the treatment of depressive symptoms. *Br. J. Psychiatry* 119, 277–278.
- Pissadaki, E.K., Bolam, J.P., 2013. The energy cost of action potential propagation in dopamine neurons: clues to susceptibility in Parkinson's disease. *Front. Comput. Neurosci.* 7, 13.
- Porsolt, R.D., Bertin, A., Jalbre, M., 1977a. Behavioral despair in mice: a primary screening test for antidepressants. *Arch. Int. Pharmacodyn. Ther.* 229, 327–336.
- Porsolt, R.D., Le Pichon, M., Jalbre, M., 1977b. Depression: a new animal model sensitive to antidepressant treatments. *Nature* 266, 730–732.
- Reinholz, J., Skopp, O., Breitenstein, C., Winterhoff, H., Knecht, S., 2009. Better than normal: improved formation of long-term spatial memory in healthy rats treated with levodopa. *Exp. Brain Res.* 192, 745–749.
- Salamone, J.D., Correa, M., Farrar, A., Mingote, S.M., 2007. Effort-related functions of nucleus accumbens dopamine and associated forebrain circuits. *Psychopharmacology (Berl)* 191, 461–482.
- Scatton, B., Simon, H., Le Moal, M., Bischoff, S., 1980. Origin of dopaminergic innervation of the rat hippocampal formation. *Neurosci. Lett.* 18, 125–131.
- Schapira, A.H., 2003. Disease-modifying strategies and challenges in PD: interactive breakout sessions. *Neurology* 61, S56–S63.
- Schindelin, J., Arganda-Carreras, I., Frise, E., Kaynig, V., Longair, M., Pietzsch, T., Preibisch, S., Rueden, C., Saalfeld, S., Schmid, B., Tinevez, J.Y., White, D.J., Hartenstein, V., Eliceiri, K., Tomancak, P., Cardona, A., 2012. Fiji: an open-source platform for biological-image analysis. *Nat. Methods* 9, 676–682.
- Sibley, D., Houslay, M., 1994. *Molecular Pharmacology of Cell Regulation*. Wiley, Chichester.
- Sibley, D.R., Neve, K.A., 1997. Regulation of dopamine receptor function and expression. In: Neve, K.A., Neve, R.L. (Eds.), *The Dopamine Receptors*. Humana Press, Totowa, NJ, pp. 383–424.
- Sokoloff, P., Diaz, J., Le Foll, B., Guillin, O., Leriche, L., Bezard, E., Gross, C., 2006. The dopamine D3 receptor: a therapeutic target for the treatment of neuropsychiatric disorders. *CNS Neurol. Disord. Drug Targets* 5, 25–43.
- Spigset, O., von Scheele, C., 1997. Levodopa dependence and abuse in Parkinson's disease. *Pharmacotherapy* 17, 1027–1030.
- Stemmelin, J., Lazarus, C., Cassel, S., Kelche, C., Cassel, J.C., 2000. Immunohistochemical and neurochemical correlates of learning deficits in aged rats. *Neuroscience* 96, 275–289.
- Sunahara, R.K., Guan, H.C., O'Dowd, B.F., Seeman, P., Laurier, L.G., Ng, G., George, S.R., Torchia, J., Van Tol, H.H., Niznik, H.B., 1991. Cloning of the gene for a human

- dopamine D5 receptor with higher affinity for dopamine than D1. *Nature* 350, 614–619.
- Svenningsson, P., Westman, E., Ballard, C., Aarsland, D., 2012. Cognitive impairment in patients with Parkinson's disease: diagnosis, biomarkers, and treatment. *Lancet Neurol.* 11, 697–707.
- Swanson, L.W., 1982. The projections of the ventral tegmental area and adjacent regions: a combined fluorescent retrograde tracer and immunofluorescence study in the rat. *Brain Res. Bull.* 9, 321–353.
- Swanson-Park, J.L., Coussens, C.M., Mason-Parker, S.E., Raymond, C.R., Hargreaves, E.L., Dragunow, M., Cohen, A.S., Abraham, W.C., 1999. A double dissociation within the hippocampus of dopamine D1/D5 receptor and beta-adrenergic receptor contributions to the persistence of long-term potentiation. *Neuroscience* 92, 485–497.
- Tanti, A., Belzung, C., 2010. Open questions in current models of antidepressant action. *Br. J. Pharmacol.* 159, 1187–1200.
- Thibault, O., Landfield, P.W., 1996. Increase in single L-type calcium channels in hippocampal neurons during aging. *Science* 272, 1017–1020.
- Thompson, D., Martini, L., Whistler, J.L., 2010. Altered ratio of D1 and D2 dopamine receptors in mouse striatum is associated with behavioral sensitization to cocaine. *PLoS One* 5, e11038.
- Toescu, E.C., Verkhatsky, A., Landfield, P.W., 2004. Ca^{2+} regulation and gene expression in normal brain aging. *Trends Neurosci.* 27, 614–620.
- Togasaki, D.M., Tan, L., Protell, P., Di Monte, D.A., Quik, M., Langston, J.W., 2001. Levodopa induces dyskinesias in normal squirrel monkeys. *Ann. Neurol.* 50, 254–257.
- Willner, P., Towell, A., Sampson, D., Sophokleous, S., Muscat, R., 1987. Reduction of sucrose preference by chronic unpredictable mild stress, and its restoration by a tricyclic antidepressant. *Psychopharmacology (Berl)* 93, 358–364.
- Witjas, T., Eusebio, A., Fluchere, F., Azulay, J.P., 2012. Addictive behaviors and Parkinson's disease. *Rev. Neurol. (Paris)* 168, 624–633.
- Wittmann, B.C., Schott, B.H., Guderian, S., Frey, J.U., Heinze, H.J., Düzel, E., 2005. Reward-related FMRI activation of dopaminergic midbrain is associated with enhanced hippocampus-dependent long-term memory formation. *Neuron* 45, 459–467.
- Xing, B., Meng, X., Wei, S., Li, S., 2010. Influence of dopamine D3 receptor knockout on age-related decline of spatial memory. *Neurosci. Lett.* 481, 149–153.
- Zhang, L., Hernandez, V.S., Medina-Pizarro, M., Valle-Leija, P., Vega-Gonzalez, A., Morales, T., 2008. Maternal hyperthyroidism in rats impairs stress coping of adult offspring. *J. Neurosci. Res.* 86, 1306–1315.

Hippocampal CA field neurogenesis after pilocarpine insult: The hippocampal fissure as a neurogenic niche

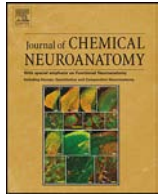
Zhang L., Hernández V. S., Estrada F. S. , Luján R.

J Chem Neuroanat. 2014, 56: 45-57

My contributions in:

- Conception of the study: ++
- Performance of the experiments:
 - o Pilocarpine treatment to model temporal lobe epilepsy +++
 - o Immunohistochemistry for neurogenesis markers +++
 - o Quantification of neurogenesis at different time points ++
- Statistical analysis: ++
- Discussion of the results: +++
- Preparation of the paper: +

(-): No contribution; (+): Average contribution; (++) : Important contribution; (+++); Main contribution



Hippocampal CA field neurogenesis after pilocarpine insult: The hippocampal fissure as a neurogenic niche



Limei Zhang^{a,*}, Vito S. Hernández^a, Felipe S. Estrada^a, Rafael Luján^{b,**}

^a Departamento de Fisiología, Facultad de Medicina, Universidad Nacional Autónoma de México, Mexico City 04510, Mexico

^b Instituto de Investigación en Discapacidades Neurológicas, Departamento de Ciencias Médicas, Facultad de Medicina, Universidad Castilla-La Mancha, 02006 Albacete, Spain

ARTICLE INFO

Article history:

Received 7 November 2013

Received in revised form 26 February 2014

Accepted 26 February 2014

Available online 6 March 2014

Keywords:

Ipratropium bromide

Nestin

Glial fibrillary acidic protein (GFAP), doublecortin (DCX)

Neuronal specific nuclear protein (NeuN)

5-Bromo-2'-deoxyuridine (BrdU)

ABSTRACT

Pilocarpine model for temporal lobe epilepsy has shown aberrant neurogenesis, but mainly restricted to the dentate gyrus (DG). Herein, by using a modified protocol, combining pilocarpine with ipratropium bromide, we unexpectedly observed a heretofore-unrecognized distinct cellular population expressing the neuroprogenitor marker doublecortin (DCX) on post insult days (PID) 10, 14 and 18, mainly located in the temporal segment of the hippocampal fissure (hf). Some of these DCX+ cells possessed high morphological complexity and seemed to disperse toward the CA fields. Next, we injected bromodeoxyuridine (BrdU) in early (PID 2–4) and delayed (PID 5–7) fashions and killed the rats 7–35 days later for immunohistochemical and anatomical analysis. Massive increase of BrdU labeling was found in the delayed group and the neural stem cell-specific marker nestin was highly expressed in the same narrow band on PID7, so was glial fibrillary acidic protein (GFAP). Using double labeling with BrdU and a mature neuron marker NeuN, we found discrete but clear BrdU+/NeuN+ double labeled cells in the *Cornu Ammonis* (CA) pyramidal cell layer on PID35. Based on immunohistochemical and anatomical observations, as well as time-course analysis of BrdU, nestin, GFAP, DCX and NeuN expressions in this population of cells located in/near hf, we wish to suggest that this structure harbors neurogenic niches, in addition of the possible dispersion of neuroprogenitors from subgranular niches to CA fields also revealed by this study. Our results support the few previous reports demonstrating hippocampal CA field neurogenesis in adult rats. Mechanistic basis of the phenomenon is discussed.

© 2014 Elsevier B.V. All rights reserved.

1. Introduction

Rodent hippocampus is well documented as a structure of high degree of plasticity. The dentate gyrus (DG) subgranular zone (SGZ) of the hippocampal formation is widely recognized as holding neurogenic niches, which continuously produce new neurons under physiological conditions (Altman and Das, 1965; Bayer et al., 1982; Kempermann, 2002; Kempermann and Gage, 1999; Kuhn et al., 1996). There have been some reports showing neurogenesis

in the hippocampal Ammon's horn (*Cornu Ammonis*, CA) fields in rats (Nakatomi et al., 2002; Rietze et al., 2000) and gerbils (Salazar-Colocho et al., 2008; Schmidt and Reymann, 2002). However, this phenomenon remains controversial due to the difficulties in replicating those observations. Moreover, using the pilocarpine rat model, researchers have shown that cells generated from neural stem cells located in the caudal subventricular zone (cSVZ) and the *corpus callosum*, migrate to the CA fields and were mostly not neurons but oligodendrocytes (Parent et al., 2006).

Pilocarpine is a systemic chemoconvulsant widely used to model experimental epilepsy in rodents (Curia et al., 2008; Turski et al., 1983). The ability of pilocarpine to induce a *status epilepticus* (SE) is likely to depend on activation of the muscarinic acetylcholine mAChR1 (M1) receptor subtype (Hamilton et al., 1997). However, this potent parasympathomimetic alkaloid produces strong cholinergic side effects (Clifford et al., 1987; Curia et al., 2008). To minimize pilocarpine peripheral actions, peripheral

* Corresponding author at: Department of Physiology, Faculty of Medicine, National University of Mexico, Mexico. Tel.: +52 55 56232348; fax: +52 55 56232348.

** Corresponding author at: Departamento de Ciencias Médicas, Facultad de Medicina, Universidad de Castilla-La Mancha (UCLM), Campus Biosanitario, Spain. Tel.: +34 967 599200x2196/2197.

E-mail addresses: limei@unam.mx (L. Zhang), Rafael.Lujan@uclm.es (R. Luján).

mAChR antagonists are used. Atropine methylbromide and alpha-methylscopolamine are widely used antagonists for pre-treatment in this model (Curia et al., 2008), although no apparent contraindications, nor characterizations, on the usage of other broad-spectrum peripheral mAChR antagonists have been documented in the literature for this animal model.

In a previous study in which we sought to quantitatively characterize astrogliosis and microgliosis after pilocarpine insult in relation to the installation of spontaneous seizures (Estrada et al., 2012), the atropine methylbromide used as peripheral mAChR antagonist for our study became temporally unavailable and ipratropium bromide, a broad-spectrum peripheral mAChR antagonist, was used in one set of rats. This drug is characterized by a longer duration of action (Gross and Skorodin, 1984; Stoyanov et al., 1984; Trieb et al., 1979) and can be safely administered intravenously and intraperitoneally (Urso et al., 1991). Unexpectedly, using the neuroprogenitor marker doublecortin (DCX) (Brown et al., 2003; Kuhn and Peterson, 2008; Rao and Shetty, 2004), we observed a heretofore unrecognized distinct population of cells expressing DCX, mainly located in the temporal segment of the hippocampal fissure (hf), forming dense clusters. Hence, we used anatomical and immunohistochemical techniques against the neural stem cell-specific marker nestin (Lendahl et al., 1990; Zimmerman et al., 1994), in combination with glial fibrillary acidic protein (GFAP) to label the neurogenic region and neural stem cells (Kuhn and Peterson, 2008), doublecortin (DCX) to label neuroblasts, neuronal specific nuclear protein (NeuN) to label mature neurons (Mullen et al., 1992) and 5-bromo-2'-deoxyuridine (BrdU) to evaluate cell proliferation (Gratzner, 1982) during the first 5 weeks after pilocarpine insult.

2. Material and methods

2.1. Animals and treatments

Seventy-six juvenile male Wistar rats (weighing 200 g ± 20 g, post natal day 45–49) were used in this study. All animal procedures were approved by the local bioethical committee (*approval ID CIEFM-UNAM-101-2009-mod.2011*). Animals were housed on a 12-h light schedule in a room with temperature between 20 °C and 24 °C with adequate ventilation and given access to standard rat chow and water *ad libitum*.

At the beginning of this study, we injected *i.p.* ipratropium bromide/sodium chloride solution (dose 1 mg/kg, 1 mg/1 ml 0.9% saline, Nephron Pharmaceuticals Corporation, Orlando, USA) in order to minimize pilocarpine peripheral effects. Thirty minutes later, we injected pilocarpine hydrochloride *i. p.* (380 mg/kg) (Sigma, St. Louis, MO) dissolved in 0.9% saline. The beginning of *status epilepticus* (SE) was considered when the animal suffered a class 4 motor seizure in Racine's scale of limbic seizures (Racine, 1972), characterized by forelimb clonus followed by sustained tonic-clonic seizures. Diazepam (5 mg/kg) was administered 1 h after the induction of SE to stop seizures and as a measure to standardize the duration of seizure activity. Additional injections of this drug were administered as needed in order to prevent further seizures. Five rats received saline and diazepam injections only and another three rats received ipratropium bromide/saline and diazepam injections as controls.

During the first 48 h post-insult, rats received *i.p.* injections of 0.9% saline (2.5 ml every 12 h and alternating with glucose solution 5% 2.5 ml every 12 h) as fluid replacement therapy. All rats were fed with pap made from rat chow for the first week.

Fifty percent of the pilocarpine injected rats survived the insult until post insult day (PID) 7. Twenty-two of the rats received 5-bromo-2'-deoxyuridine injections (BrdU, Sigma, 50 mg/kg/12 h) in two schemes: early injection on PID 2, 3 and 4 ("PID2–4 inj")

(*n* = 13) and delayed injection on PID 5, 6 and 7 ("PID5–7 inj") (*n* = 9).

2.2. Antibodies

An affinity-purified polyclonal antibody against BrdU (Accurate Scientific, NY, USA, Cat. No. OBT0030, Clone BU1/75 (ICR1), 0.5 mg/ml in stock solution) was raised in rats and characterized. An affinity-purified polyclonal antibody against DCX (C-18, Santa Cruz Biotechnology, CA, USA, Cat. No. SC-8066, 0.2 mg/ml in stock solution) was raised in goats and characterized previously (Ekdahl et al., 2003). The monoclonal antibody against NeuN, obtained from Chemicon Millipore (Temecula, CA; Cat. No. MAB377, 1 mg/ml stock solution) was raised in mice. The monoclonal antibody against nestin, obtained from Chemicon Millipore (Temecula, CA; Cat. No. MAB353, 0.54 mg/ml stock solution), was raised in mice, and the polyclonal antibody against glial fibrillary acidic protein (GFAP), obtained from Biocare Medical (Concord, CA, Control Number: 901-040-031511) was raised in rabbits, and characterized previously (McLendon and Bigner, 1994). Polyclonal antibody anti vesicular glutamate transporter 2 (vGluT2), obtained from Synaptic Systems (Goettingen, Germany, Cat. No. 135 404), was raised in guinea pigs, and previously characterized (Ziegler et al., 2005). Secondary antibodies conjugated with different fluorophores (Alexa Fluor 488 goat anti-rat IgG, Alexa Fluor 594 donkey-anti-goat IgG, Alexa Fluor 488 donkey anti-mouse IgG and Alexa Fluor 594 donkey anti-mouse IgG) were obtained from Molecular Probes (Eugene, Oregon, USA). For DCX and BrdU diaminobenzidine (DAB) immunoreaction, we used biotinylated donkey-anti-goat and donkey-anti-rat antibodies (Jackson ImmunoResearch Laboratories Inc., Pennsylvania, USA, 1:500).

2.3. Tissue processing and immunohistochemistry

On PID 7, 10, 14, 18, and 35, rats were deeply anesthetized with an overdose of pentobarbital and transcardially perfused with 0.9% saline followed by cold fixative containing 4% of paraformaldehyde and 15% v/v of saturated picric acid in 0.1 M sodium phosphate buffer (PB, pH 7.4) for 15 min. Brains were removed, blocked, then thoroughly rinsed with PB. Coronal sections of 70 μm-thickness from whole hippocampus were obtained.

Immunohistochemical reactions (IR) were performed using the immunoperoxidase (for single labeling) and immunofluorescence (for double labeling) methods. Sets of one out of every six sections containing hippocampus were blocked incubating them with 0.3% Triton X-100 (Sigma, T-7878) and 20% normal horse serum (NHS, Vector) in Trizma buffer 0.05 M + 0.9% NaCl (TBS), for 1 h at room temperature. Next, sections were incubated with the following primary antibodies (dilutions are referred to the stock solutions specified in Section 2.2): rat anti-BrdU (1:1000), goat anti-DCX (1:2000) or mouse anti-nestin (1:1000), rabbit anti-GFAP (1:1000) diluted in TBS containing 1% NHS over night in at 4 °C with gentle shaking. BrdU immunoreaction pretreatment was described elsewhere (Zhang et al., 2006). Sections were then washed and incubated with the corresponding secondary antibodies at room temperature for 2 h. Some of the sections were used for immunoperoxidase detection of DCX and vGluT2. In these cases, sections were incubated in biotinylated secondary antibodies, followed by incubation in avidin-biotin-peroxidase complex (Elite ABC kit: Vector Laboratories, Peterborough, UK) for 1 h at room temperature. Bound peroxidase enzyme activity was revealed using 3, 3'-diaminobenzidine tetrahydrochloride (DAB; 0.05% in TB, pH 7.4) as the chromogen and 0.01% H₂O₂ as the substrate. For morphological and double immunolabeling analysis, a Nikon Eclipse 50i light microscope and Leica TCS-SP5 confocal microscope were used.

2.4. Quantification and statistical analysis

For BrdU labeling quantification in saline-treated, and pilocarpine treated rats of two injection schemes (“PID 2–4 inj” and “PID 5–7 inj”), immunoperoxidase-DAB processed and permanently mounted coronal sections containing hippocampus were subjected to blinded counting under light microscope. BrdU+ nuclei per 540 μm (diameter of the observation field under 40 \times objective) length of cell body layer or hf region on all focal planes were sketched on paper with the help of a drawing tube. Quantitative results were expressed as mean \pm standard error of mean (SEM); groups were tested for differences by performing one-way-ANOVA followed by Bonferroni test comparing all pairs of columns, using GraphPad Prism (La Jolla, CA). Differences were considered statistically significant at a value $p < 0.05$.

3. Results

3.1. General behavioral observations

Following injection of pilocarpine, rats remained motionless and exhibited diverse signs of cholinergic stimulation, such as diarrhea and piloerection for about 10 min, until gustatory and olfactory automatisms began. These automatisms (mouth movement, mild salivation, scratching, eye-blinking, tremor, chromodacryorrhea and vibrissae twitching) persisted for 15–25 min. Immediately after this phenomenon, animals developed motor seizures, which were accompanied by intense salivation, rearing and falling and built up progressively into a SE (which was pharmacologically limited after 60 min, as a measure to standardize the magnitude of the insult in this study).

3.2. DCX expression under control conditions

DCX expression in control conditions in the whole hippocampal formation is shown in Fig. 1. The SGZ neurogenic niche can be clearly seen (panel A and D). Numerous immunopositive fibers for DCX can be observed in the cSVZ/alveus (Table 1 and Fig. 1, inset a) and alveus/external capsule (Fig. 1B) with sparse somatic labeling (Fig. 1B, arrowhead). Moderate DCX-expressing fibers were present in the *stratum lucidum* of CA3 (SL), mainly parallel to the pyramidal layer at basal (saline) condition (Fig. 1C, black hollow arrows). It is worth mentioning that “ipratropium” control group, consisting of rats receiving only the cholinergic antagonist, did not exhibit significant changes of DCX labeling pattern in the SGZ (data not shown).

3.3. Extent of DCX expression at early time-points after SE

At time-points PID 7 (Fig. 2) and PID 10 (Fig. 3), the DG neurogenesis, revealed by immunolabelling for DCX, showed a dramatic increase in the production of neuroblasts in the SGZ (Fig. 2, panels A and B and Fig. 3, panel A) and aberrant presence of DCX-expressing basal dendrites of newborn granular cells in the hilar region (Fig. 2A and B, arrows and Table 1). Aberrant migration of DCX-expressing clusters seemingly dispersed from the SGZ toward the molecular layer (Fig. 2, panel B). DCX-expressing “tube-like” migration chains, consisting of spiral profiles, were observed on PID 7 and 10 (Figs. 2, panels B and C; Fig. 3, panels B and C, double arrowheads). Several large cells in the pyramidal cell layer of CA1 (Fig. 2, panel D, arrowhead) lightly expressed DCX on PID7. Only somatic expression could be clearly seen, no dendrites connecting to soma were labeled. However, some dendrite and

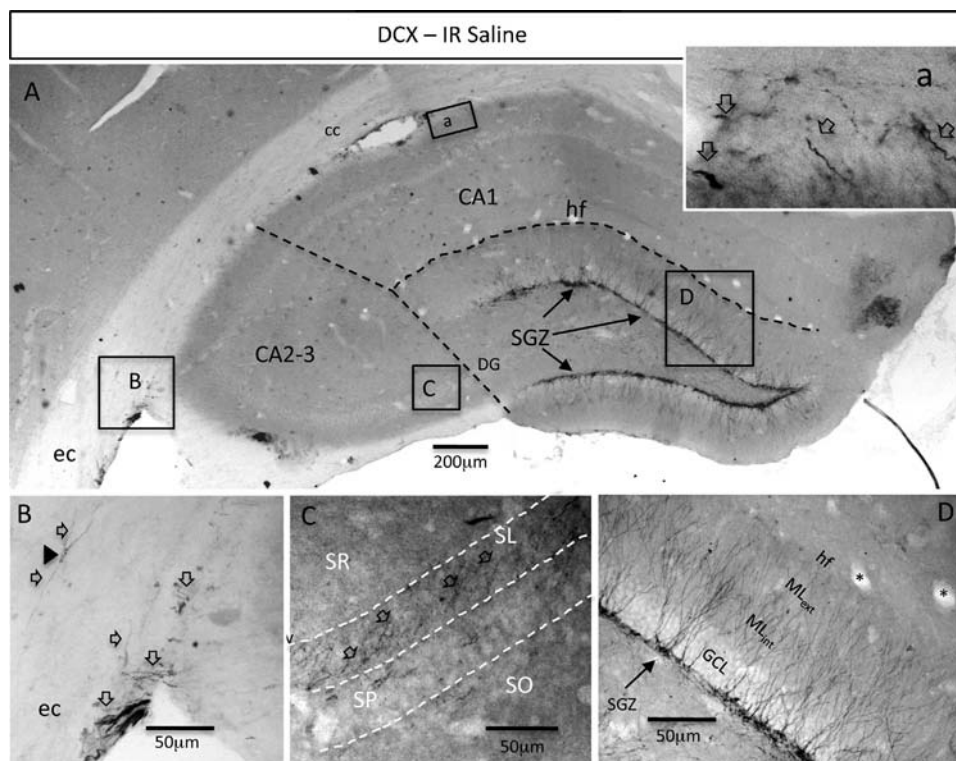


Fig. 1. Immature neuronal marker DCX expression under control conditions. (A) A low magnification of whole hippocampal view of DCX expression in a saline injected rat. The SGZ neurogenic niche is indicated by solid arrows. Inset (a) and panel (B) show the moderate immunolabeling of DCX+ cells and fibers in the infrallosal/caudal subventricular zone (cSVZ) and alveus. (C) The presence of DCX+ fibers in the SL of the CA3, demonstrates that the newly born granular neuroblasts extended their axons to join the mossy fibers. (D) the well-established SGZ neurogenic niche in higher magnification. Hollow arrows indicate DCX-expressing fibers. Arrowheads indicate DCX-expressing somata. Asterisks (*) indicate medium size blood vessels in the hf region. Note that there is no presence of DCX-expressing fibers in the hf. DCX: doublecortin; SGZ: subgranule zone; hf: hippocampal fissure; CA: *cornu ammonis*; hf: hippocampal fissure; DG: dentate gyrus; SP: *stratum pyramidale*; SR: *stratum radiatum*; SL: *stratum lucidum*; SO: *stratum oriens*; GCL: granule cell layer. ML_{int} and ML_{ext}: internal and external molecular layer respectively; SGZ: subgranular zone; cc: *corpus callosum*; ec: external capsule.

Table 1

	SGZ	ML _{int}	ML _{ext}	hf	hilus	CA3	CA1	Alveus	Notes
Ctrl (Saline)	s: + f: +	s: – f: ++	s: – f: +	s: – f: –	s: – f: –	s: – f: + (SL)	s: – f: –	s: – f: +	n = 5, 10 hi _{sep} sections Served as reference for comparison
PID 7	s: +++ f: +++	s: + f: ++	s: – f: +	s: – f: –	s: + f: ++	s: – f: –	s: + f: +	s: + f: ++	n = 2, 16 hi _{sep} sections
PID 10	s: +++ f: ++++	s: ++ f: +++	s: ++ f: ++	s: ++ f: ++	s: ++ f: ++	s: – f: –	s: – f: +	s: + f: +	n = 2, 14 hi _{sep} sections 1 hi _{temp} section
PID 14	s: +++ f: +++	s: ++ f: +++	s: ++ f: ++	s: ++++ f: ++++	s: ++ f: ++	s: + f: +++ (SL)	s: + f: ++	s: + f: ++	n = 5, 62 hi _{sep} sections, 46.7% w/fissure niche 15 hi _{temp} sections 60% w/fissure niche
PID 18	s: + f: ++	s: – f: ++	s: – f: +	s: – f: –	s: + f: +	s: – f: +	s: + f: +	s: +++ f: ++	n = 4, 39 hi _{sep} sections, 10.2% w/fissure niche 18 hi _{temp} sections 5.5% w/fissure niche

Morphological evaluation under light microscopy of the extent of DCX expression in the hippocampal formation at diverse time-points after SE. hi_{sep}: septal hippocampus; hi_{temp}: temporal hippocampus; PID: post-insult day; SGZ: subgranular zone; ML_{int}: internal molecular layer; ML_{ext}: external molecular layer; hf: hippocampal fissure. “s”: Dcx+soma; “f”: Dcx+fibers; “–”: not observed; “+”: sparse presence; “+++”: moderate presence. Control (saline group, bold) served as reference. Percentages indicate the number of hippocampal fissures containing neurogenic niches in total hippocampal fissures evaluated.

axon-like processes were immunopositive to DCX, without clear connection to the immunopositive soma (Fig. 2, panel D, hollow arrows). It seems that there was a short-term post insult re-expression of DCX in mature neurons for hippocampal network repair, as suggested by (Kremer et al., 2013). DCX labeling in the *stratum lucidum* (SL) of the CA3, observed under basal conditions, had disappeared mostly by PID 7 (Fig. 2, panel A) and PID10 (Fig. 3, panel D). The DCX+ fibers reappeared in the SL with increased intensity on PID 14 (Fig. 4A, black hollow arrows) and PID 18 (Fig. 5, panel A).

3.4. Massive DCX+ cell clusters appeared in the hippocampal fissure region in apposition to blood vessels on PID14, across the septotemporal axis

On PID10, clear clusters of DCX-expressing cells appeared in the hf proximal to the fusion zone, most of them surrounding the internal transversal arteries (Table 1 and Fig. 3, panels A and B, asterisks). These clusters peaked in number and size on PID 14 (Fig. 4 panels A, C, D and E) and many neuron-like cells dispersed toward CA1 *stratum lacunosum-moleculare* (SLM) and *stratum radiatum* (SR) (Fig. 4, panels C–F). Only a few DCX-expressing cells were found within the pyramidal cell layer (*stratum pyramidale*, SP, Fig. 4, panel B). The cells within the CA field showed high complexity regarding their morphology, possessing several dendrite-like processes and axon-like neurites, which suggest the possibility of functional integration. Several pyramidal-shaped cells were found in the CA1 field (Fig. 4, panel D, double arrowheads). Other DCX-expressing neuroglial-form-shaped cells were found aligned with the border between SLM and SR of CA1 in the temporal hippocampus (Fig. 4, panel F, arrowheads). This phenomenon greatly diminished on PID18 (Fig. 5 and Table 1), although dispersed DCX-expressing cells in hilus can be clearly seen (Fig. 5, panel D). The DCX-expressing cells aligned to the border between SLM and SR in the CA1 region can also be seen (Fig. 5, panel B). Furthermore, abundant DCX-expressing cells with smaller soma and glial shape, were observed in the CA2-3 SO/SP (Fig. 5, panels C and E) confirming previously described evidence by other research group (Parent et al., 2006).

Fig. 6 shows one double-labeled cluster in the hf in close relation with a medium size blood vessel, with nuclear expression of BrdU and somatic expression of DCX (Fig. 6).

The presence of DCX-expressing cell clusters in the hf was observed across the entire septotemporal axis of the hippocampal formation. Fig. 7 depicts this phenomenon by charting under light microscope observation, examined on PID14 (Fig. 7). It is worth noting that massive DCX-expressing clusters in close proximity to the internal transversal arteries were observed across the whole septotemporal axis (indicated by asterisks in Fig. 7).

3.5. Pilocarpine-ipratropium bromide protocol induced a delayed increase of cell proliferation in the SGZ, hf and pyramidal layer of CA1

To examine the potential effects of this pilocarpine-ipratropium bromide protocol on cell proliferation in the hippocampus, we first injected BrdU during PID2–4. In this first subset of rats, in spite of having observed massive increase of DCX expression on PID14 in the hf and CA subfields as mentioned before, the double labeled cells with BrdU+/DCX+ or BrdU+/NeuN+ were rare observances. For the second subset of rats, we chose two BrdU injection schemes, i.e. the early, “PID 2–4 inj” and the delayed, “PID 5–7 inj” and quantitatively evaluated on PID 14. Consistent with previous reports (Parent et al., 1997), a small number of clustered nuclei located in the SGZ in control rats, as well as few BrdU+ nuclei in the lateral segment of the hf and in the CA1 pyramidal layer, were observed in control groups (Fig. 8, panels A). In the “PID 2–4 inj” group, numerous BrdU+ nuclei, dispersed from the SGZ to the hilar region, were found (Fig. 8, panels B, arrows and arrowhead). However, no quantitative differences in BrdU immunostaining were noted in the three evaluated regions when compared to control (Fig. 8, panels D–F). In contrast, quantitative analysis of sections from group “PID 4–7” revealed significant increases in BrdU immunostaining in the SGZ/GCL, the hf and in the pyramidal layer of CA1 (Fig. 8, panels C and D–F and Fig. 9: immunofluorescence for hf proliferative activity).

3.6. Stem cell marker nestin expression in the hf was markedly increased in a well-limited band, together with GFAP and BrdU (delayed group) observed on PID7

Nestin is the most widely used marker for neural stem cells, although it can also be detected in vascular structures (Lendahl et al., 1990). However, the combination of GFAP and nestin appears to label multi-potent cells in neurogenic regions (Kuhn and

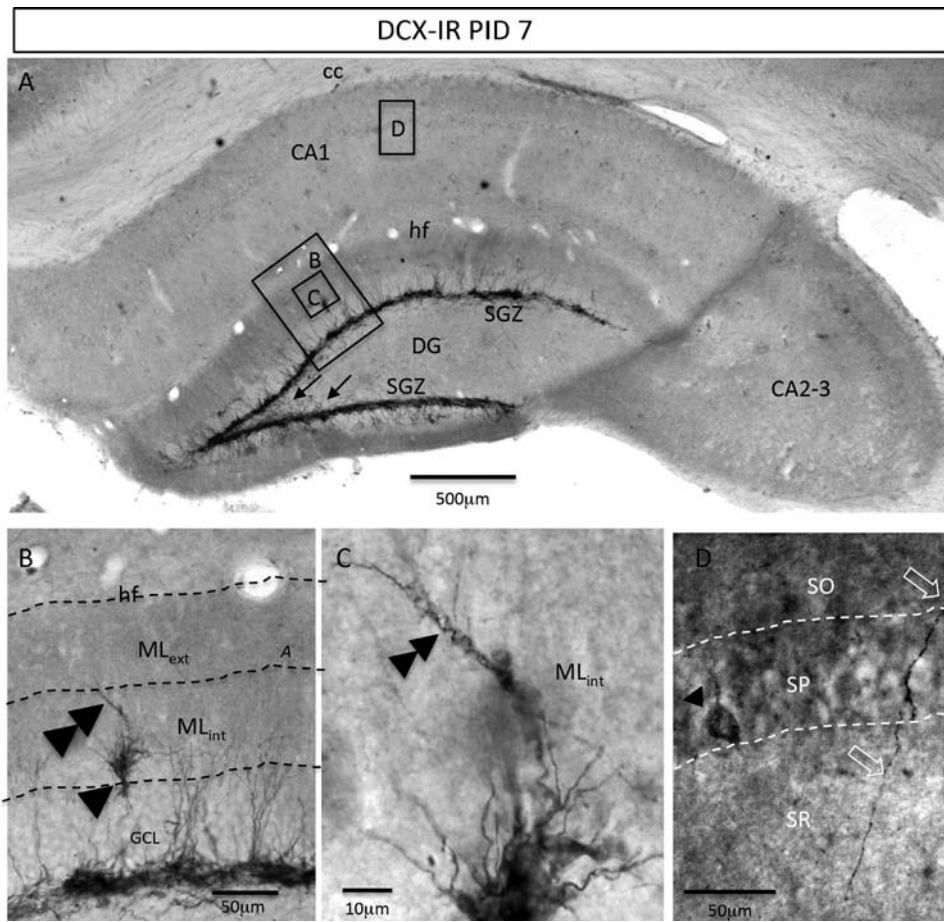


Fig. 2. (A) Low magnification of whole hippocampal view of DCX expression on pilocarpine PID 7. In SGZ, DCX expression was massively increased (compare the thickness of the SGZ). The newly born SGZ DCX-expressing neuroblasts extended horizontal and basal neurites in the hilus (solid arrows). (B) and (C) DCX-expressing cellular clusters (arrowhead) seem to migrate toward the hf. A “tube-like” structure, consisting of several spiral-shaped DCX-expressing fibers (double-arrowheads), precedes the large cell cluster. (D) Light somatic DCX-expression in some large somata of the SP (arrowhead), as well as in some fibers (hollow arrows); however, no clearly labeled dendrites connecting the soma were observed. PID: post-insult day; DCX: double cortin; SGZ: subgranule zone; hf: hippocampal fissure; CA: *cornu ammonis*; hf: hippocampal fissure; DG: dentate gyrus; SP: *stratum pyramidale*; SR: *stratum radiatum*. SL: *stratum lucidum*. SO: *stratum oriens*. GCL: granule cell layer. ML_{int} and ML_{ext}: internal and external molecular layer respectively; SGZ: subgranular zone; cc: *corpus callosum*; ec: external capsule; ML_{int} and ML_{ext}: internal and external molecular layer, respectively; SGZ: subgranular zone.

Peterson, 2008). In the rat hf, no specific staining of nestin was detected in saline injected control sections, while GFAP positive astrocytes showed thin glial processes (data not shown). Nevertheless, nestin expression was markedly increased on PID 7 in all examined experimental rats ($n = 8$). In the septal hippocampus (Fig. 9, panels A), in addition to their expression in the SGZ and GCL (Fig. 9, panel A, hollow arrows) and in the CA1 pyramidal layer (Fig. 9, panel B_a), clusters of nestin/GFAP expressing processes surrounding the medium arteries (Fig. 9, panel A, asterisks) were clearly seen (Fig. 9, panels A). It is worth noting that this location corresponds to DCX+ neuroprogenitor clusters seen on PID14 (for example, see panel (C) of Fig. 7). In the temporal hippocampus (Fig. 9, panels B–E), a region in/around the hf with massive expression of nestin, GFAP and BrdU labeling (in the delayed group) was found. The extension of this region was well correlated with the one determined by DCX immunostaining, as shown in Fig. 7 panels F and H. It is interesting to observe that this region was well overlapped with a marked glutamatergic input, containing vesicular glutamate transporter 2 (vGLUT2, Fig. 9, A_c, B_c and E_c).

3.7. Discrete generation of new neurons in the CA fields as revealed by BrdU/NeuN double labeling on PID35

We further investigated whether those post-insult newborn neuroblasts had become mature neurons by immunofluorescent

staining for BrdU and mature neuron marker NeuN. The study clearly revealed that on PID35, numerous BrdU+/NeuN+ neurons were inserted in the *stratum radiatum* (Fig. 10, panels A) and in the CA1 (Fig. 10, panels B) and CA3 (Fig. 10, panels C) pyramidal layer.

4. Discussion

In the present study we provide a detailed spatial-temporal description in relation to cell proliferation and neurogenesis along the hippocampal septotemporal axis in a pilocarpine rat model of experimental epilepsy. The two key findings of this study are (1) the experimental protocol used here triggered neurogenesis in the hippocampal fissure and in the CA fields, seen from PID 7 to PID 35, based on the observations that the DCX expressing neuron-shaped cells were widely distributed across the septotemporal axis and NeuN+/BrdU+ cells were found in the pyramidal layers and in the stratum radiatum at PID35; (2) hippocampal fissure was identified as a neurogenic niche under this experimental condition, as there was an increased mitotic activity in the “PID 5–7 inj” group in a well-limited band in/surrounding hippocampal fissure, which overlapped with increased expression of nestin and GFAP observed at PID7 and DCX expressing clusters, which peaked at PID14. The complex neuron-like morphology suggests that endogenous neural stem cells contribute to the self-repair of the hippocampal CA fields after the insult. The intriguing overlap of this dense BrdU

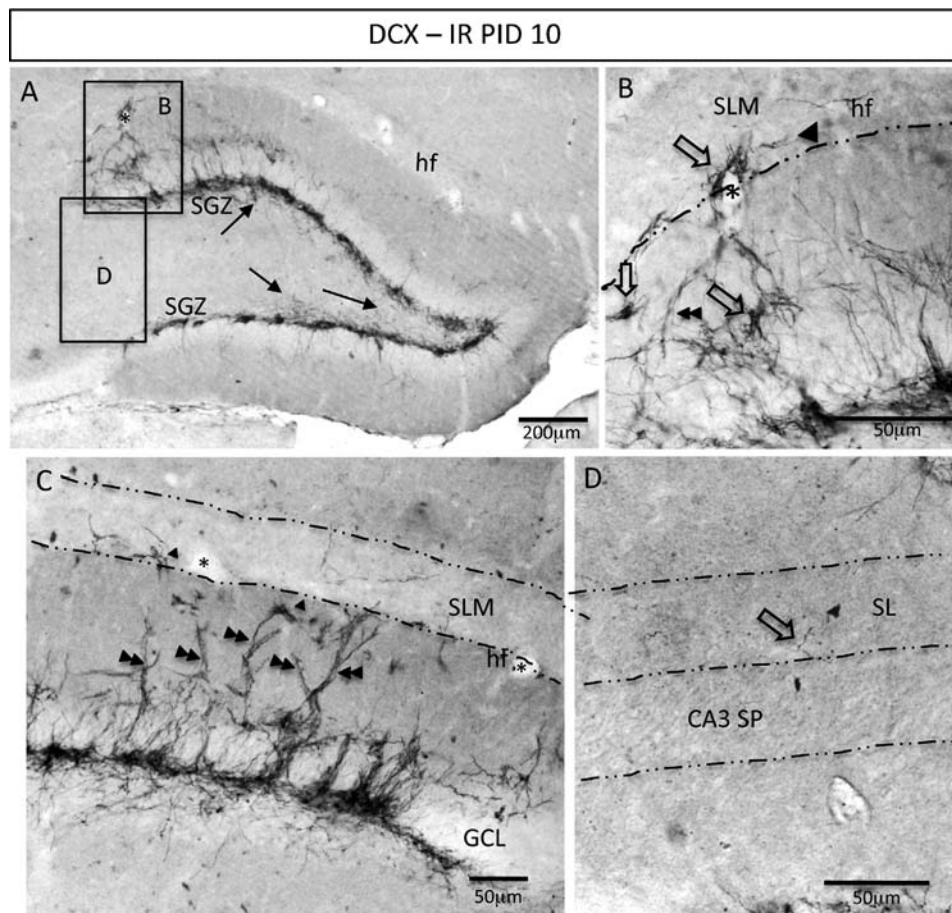


Fig. 3. (A) A low magnification of DG and hf at PID 10. Significant presence of DCX-expressing cell bodies (arrowheads) and fibers were found in the hf (panel B), in close relationship to the medium size blood vessels (*). Numerous migration chain-like structures were found in the ML (C, double arrowheads). However, the presence of DCX-expressing fibers (arrowhead) in the SL is greatly reduced (panel D). PID: post-insult day; DCX: double cortin; hf: hippocampal fissure; CA: cornu ammonis; DG: dentate gyrus; SP: stratum pyramidale; SL: stratum lucidum. SLM: stratum lacunosum moleculare. GCL: granule cell layer. ML_{int} and ML_{ext}: internal and external molecular layer respectively; SGZ: subgranular zone.

labeling and high nestin expressing with the dense extra-hippocampal glutamatergic input containing vGluT2, in a narrow band, suggests possible extra-hippocampal mechanisms for hippocampal CA field neurogenesis control.

4.1. Experimental proofs of the hippocampal fissure harboring neurogenic niches as implied by anatomical basis and recent discoveries

Based on the data of this study, hippocampal fissure (hf) is identified as a region that harbors neurogenic niches. This conclusion is already implied by anatomical knowledge and recent discoveries. Hippocampal fissure is formed at an early embryonic stage as a telencephalic external surface indentation (covered by leptomeninges) between the primordial dentate gyrus (DG) and the cornu ammonis (CA) due to the uneven thickening of the two structures (Humphrey, 1967). The fissure deepens, becomes more sharply defined and is orientated toward the CA after the DG begins to develop its granular layer. As the DG increases in size, it grows toward the CA, in part as a result of cell migration into it. This growth, added to that of the CA, causes the triangular zone of scattered cells between the molecular layer of the DG and that of the CA to be compressed into a narrow band (compression zone). Fusion of this zone occurs quickly afterwards to form a total fissure, entrapping blood vessels and leptomeninges (Decimo et al., 2012; Humphrey, 1967). During this developmental stage, the region

around the hippocampal fissure contains central radial glial scaffolding (Zhao et al., 2006). It has been reported that leptomeningeal-derived DCX+ cells participate in post-stroke neocortex repair (Decimo et al., 2012; Nakagomi et al., 2012). Furthermore, stem cell niches are closely associated with blood vessels, namely, a vascular stem cell niche (Palmer et al., 2000). Endothelial cells produce factors that promote self-renewal and expansion of the neural stem/progenitor cell population (Shen et al., 2004).

On the other hand, it has been reported that pilocarpine induced experimental SE dilates to 125% the diameter of internal transversal arteries, located in the fissure region (Ndode-Ekane et al., 2010). The hf is a richly vascularized region harboring the internal transversal arteries and veins (Coyle, 1978). Accurate anatomical evaluations revealed that meninges penetrate the central nervous system (CNS) by projecting between structures (as in the case of the hippocampus proper and the DG (Humphrey, 1967)) to form the perivascular (Virchow–Robin) space of every parenchymal vessel (Decimo et al., 2012; Zhang et al., 1990). Brain ischemia, derived from inadequate hemodynamic changes, produces extravasation of inflammatory factors to the CNS (Iadecola and Alexander, 2001; Lipton, 1999). This is more pronounced in the Virchow–Robin space of the hippocampal fissure region (Decimo et al., 2012; Zhang et al., 1990). Data from our previous research has shown a dense band of microglial activation in the hf region, supporting this notion (Estrada et al., 2012).

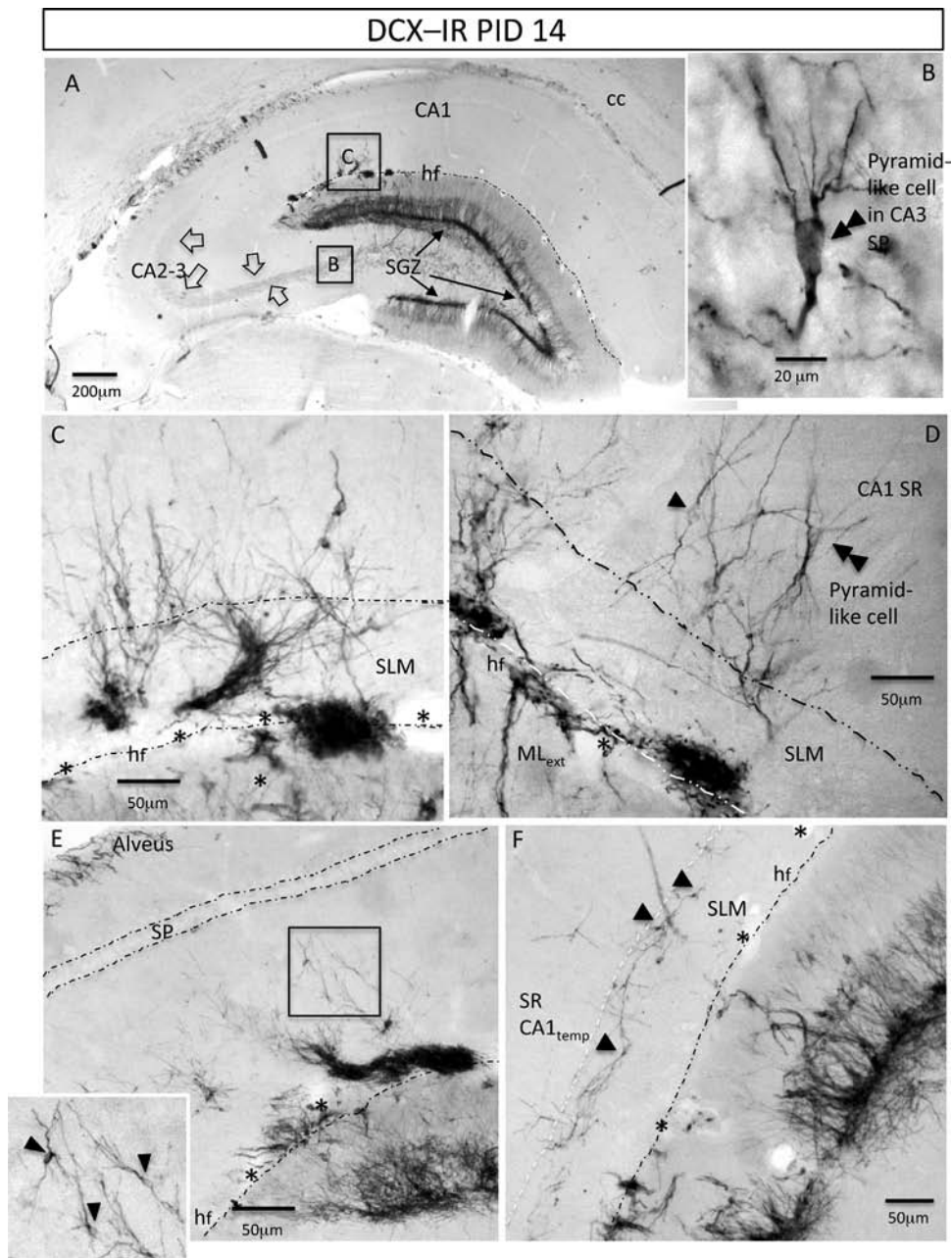


Fig. 4. (A) A low magnification view of the exuberant DCX expression on PID 14 in the whole hippocampus. The DCX expression in SGZ was massively increased. The newly born SGZ neuroblasts also extended horizontal and basal neurites in the hilus (solid arrows) and DCX-expressing mossy fiber sprouting was observed (hollow arrows). (B) A pyramidal shaped cell, with strong DCX expression both in soma and numerous dendrites, was found inside the SP of CA3. (C)–(E) Some striking examples of the massive presence of DCX-expressing cell clusters in the hf perivascular regions in juxtaposition with medium size blood vessels (*). Individual neuron-shaped cells (e.g. pyramidal, double-arrowheads, and bipolar and stellate shaped, arrowheads) seemed to disperse from these clusters toward the CA1. F: temporal (temp) hippocampus, in which DCX-expressing neurogliaform-like cells were found aligned between the CA1 SLM and SR. PID: post-insult day; DCX: doublecortin; SGZ: subgranular zone; hf: hippocampal fissure; CA: *cornu ammonis*; hf: hippocampal fissure; DG: dentate gyrus; SP: *stratum pyramidale*; SR: *stratum radiatum*. SL: *stratum lucidum*. SO: *stratum oriens*. GCL: granule cell layer. ML_{int} and ML_{ext}: internal and external molecular layer respectively; SGZ: subgranular zone; cc: *corpus callosum*; ec: external capsule; ML: molecular layer, respectively; SGZ: subgranular zone.

4.2. Possible mechanisms of this pilocarpine-insult-triggered activation of the dormant neurogenic niches in hf

Our data on increased BrdU labeling is in consistency with previous results, which demonstrate that pilocarpine-induced *status epilepticus* leads to increased dentate granule cell neurogenesis (Parent et al., 1997; Shapiro and Ribak, 2006; Shapiro et al., 2007). However, the time-course reported (Parent et al., 1997) was not phase-coherent with the present data (Parent and cols reported a sharp increase of BrdU labeling from PID 3 onwards, whereas we found a similar phenomenon between PID 5–7, see Fig. 8, panel E),

nor were the increased mitotic/neurogenic activities in hf reported. The chronological discrepancy here reported, suggests that intrinsic mechanisms triggering increased DG neurogenesis in these two pilocarpine protocols are not the same. So, what are the functional differences of the present rat pilocarpine model from other similar models? Due to the limitation of this study, which was mainly a time course analysis of the anatomical and immunohistochemical expression of a few classical neurochemical markers for the study of neurogenesis, the following discussion is based mainly on correlative data in relation to previous results published in the literature.

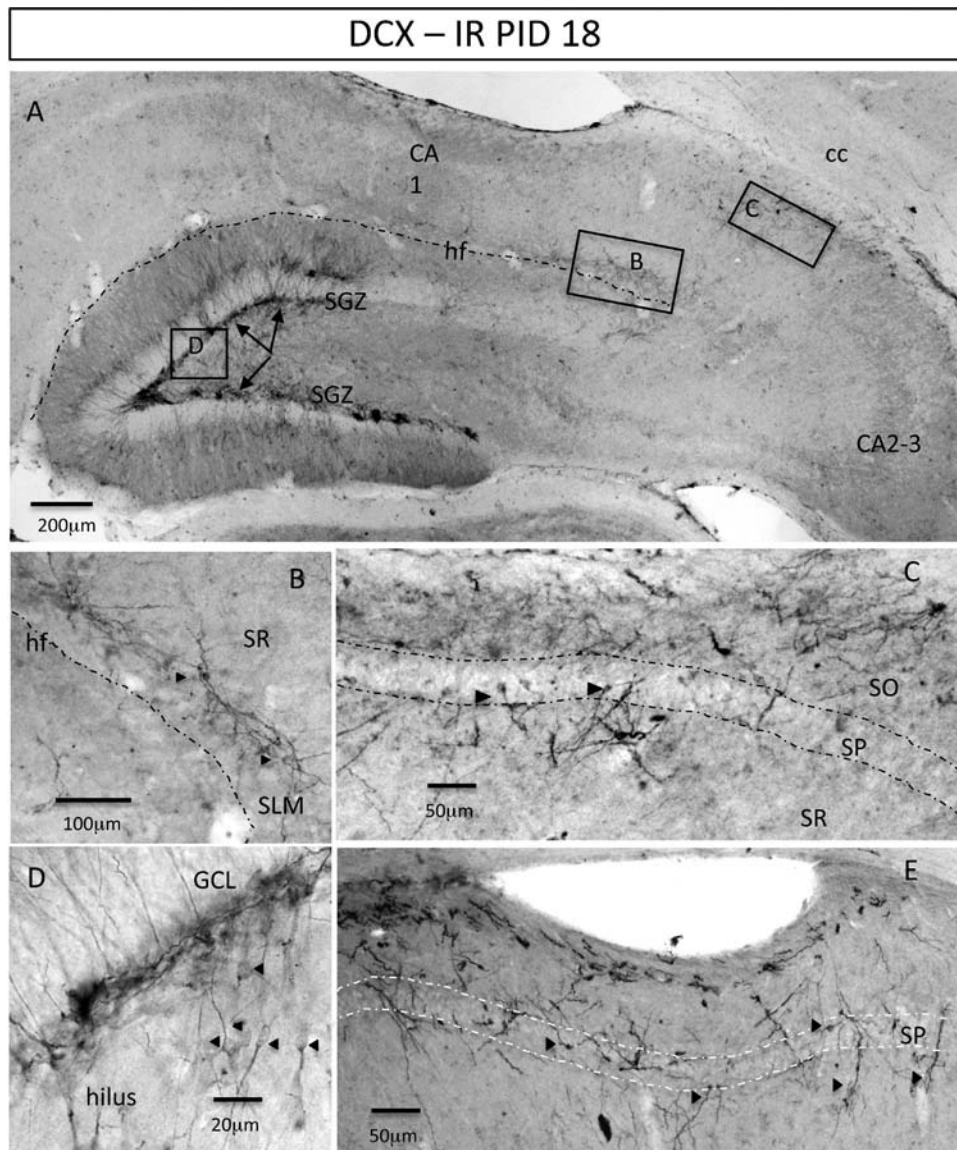


Fig. 5. (A) A low magnification whole hippocampal view of DCX expression in pilocarpine PID 18, showing persistent increased SGZ neurogenesis that exhibits a more heterogenous pattern (solid arrows) and abundant DCX-expressing cells dispersed in the hilus (panel D, arrowheads). Individual DCX-expressing cells could still be observed in the SLM but no DCX-expressing clusters were present in the hf (panel B, arrowheads). DCX-expressing cells were observed in the transition between SLM and SR in CA1 (panel C, arrowheads). Abundant DCX-expressing cells, which had a smaller soma and were glial shaped, were observed in the CA2-3 SO/SP (panel E, arrowheads). PID: post-insult day; DCX: double cortin; SGZ: subgranule zone; hf: hippocampal fissure; CA: cornu ammonis; hf: hippocampal fissure; DG: dentate gyrus; SP: stratum pyramidale; SR: stratum radiatum. SL: stratum lucidum. SO: stratum oriens. GCL: granule cell layer. ML_{int} and ML_{ext}: internal and external molecular layer respectively; SGZ: subgranular zone; cc: corpus callosum; ec: external capsule; ML_{int} and ML_{ext}: internal and external molecular layer, respectively; SGZ: subgranular zone.

Pilocarpine is a systemic chemoconvulsant which produces widespread neuronal injury and seizure activity, in addition to various systemic alterations (Cavalheiro, 1995). The present pilocarpine insult protocol was designed using ipratropium

bromide as a peripheral mAChR antagonist. During the first hour after pilocarpine administration, we observed pronounced peripheral cholinergic signs (as described in the “Results” section), indicating that our drug combination had an over-

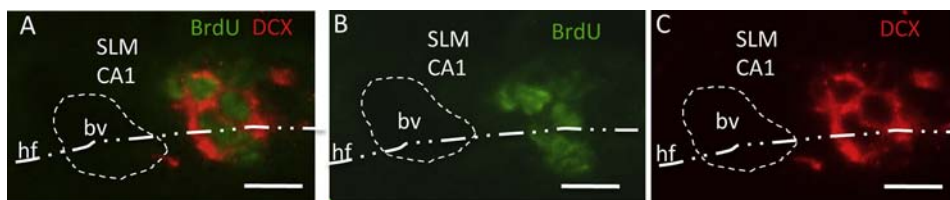


Fig. 6. Cellular co-localization of doublecortin (DCX) and 5-bromo-2'-deoxyuridine (BrdU) immunoreactivity in hippocampal fissure (hf), analyzed by confocal microscopy. (A) Co-localization of BrdU (green) with DCX (red) in the fissure, in close relation to a medium size blood vessel (bv: delineated with a dashed line). (B) and (C) Single channel for BrdU and DCX, respectively. Scale bar: 10 µm. CA: cornu ammonis; SLM: stratum lacunosum-moleculare. Scale bar: 20 µm. (For interpretation of the references to color in this figure legend, the reader is referred to the web version of this article.)

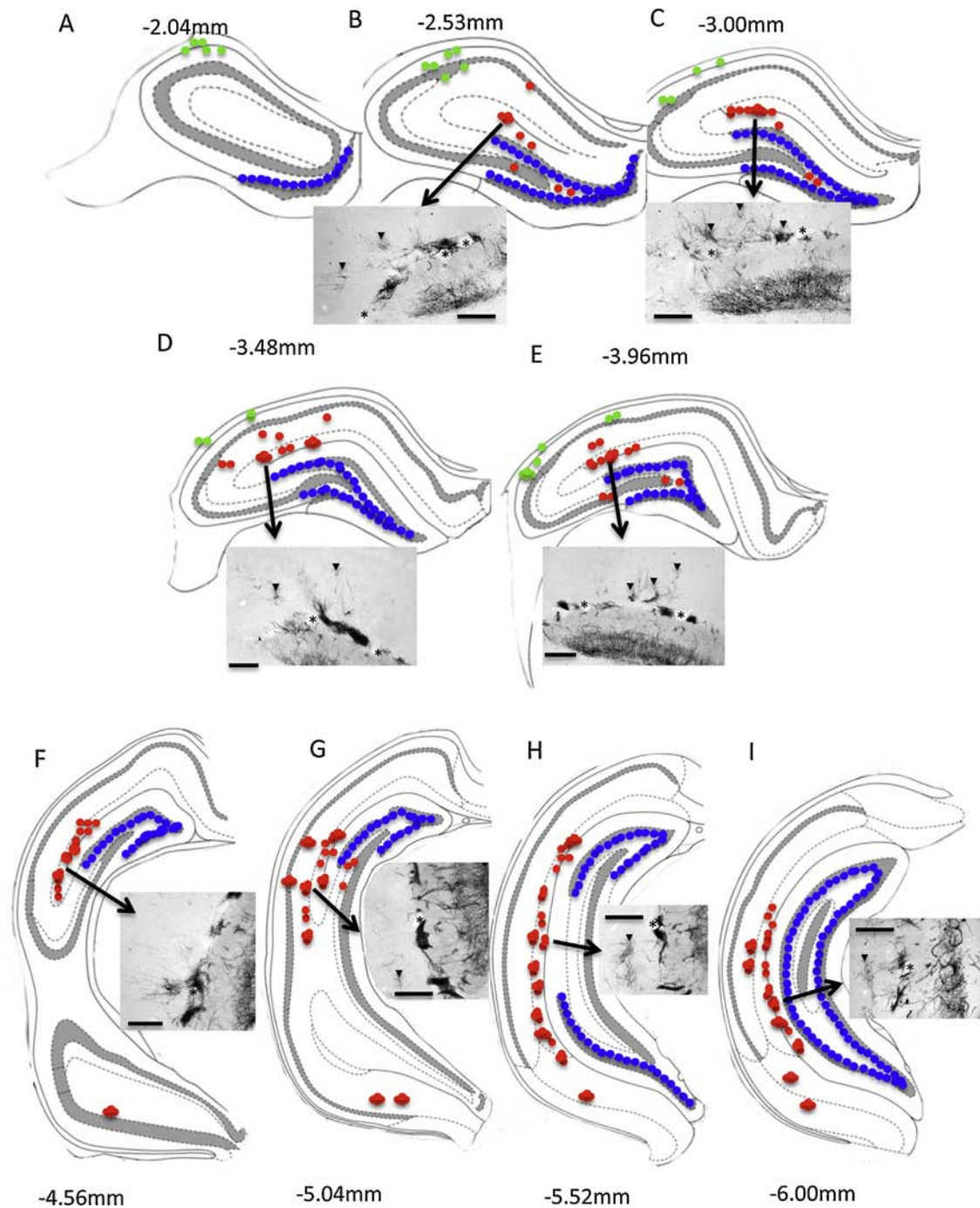


Fig. 7. Charting of the septotemporal position of DCX positive cells revealed by anatomical analysis using the immunoperoxidase method on PID 14. Blue dots symbolize the well-established subgranular zone neurogenic niches. Green dots symbolize the resurgence of DCX-expressing cells and fibers in the infracallosal/caudal-SVZ and alveus dispersed to the CA2–3 SO and SP. Red dots symbolize the appearance of neurogenic niches in the hf and the possible dispersion of newborn neuroblasts from these niches toward CA fields. Photomicrograph insets show the most striking features of this phenomenon observed in the corresponding coronal sections. Observe the massive DCX-expressing clusters in close proximity to the internal transversal arteries, indicated by asterisks. Dispersed DCX-expressing cells in the SLM/SR of the CA1 region (insets B–E) and neurogliaform-like DCX-expressing cells (insets G–I) are indicated by arrowheads. PID: post-insult day; DCX: double cortin; SGZ: subgranular zone; hf: hippocampal fissure; CA: *cornu ammonis*; hf: hippocampal fissure; DG: dentate gyrus; SP: *stratum pyramidale*; SR: *stratum radiatum*. SL: *stratum lucidum*. SO: *stratum oriens*. GCL: granule cell layer. ML_{int} and ML_{ext}: internal and external molecular layer, respectively; SGZ: subgranular zone; cc: *corpus callosum*; ec: external capsule; ML_{int} and ML_{ext}: internal and external molecular layer respectively; SGZ: subgranular zone. Scale bars in insets: 100 μ m. (For interpretation of the references to color in this figure legend, the reader is referred to the web version of this article.)

weighed parasympathomimetic peripheral action. It was evident that the insufficient antagonism exerted by this ipratropium bromide dose, in comparison to the potent agonistic actions of pilocarpine, resulted in a transient global hypoxia/ischemia state, as pilocarpine causes short-term hypotension and bradycardia

and long-lasting compensatory hypertension and tachycardia effects (Takakura et al., 2011). It is also known that pilocarpine application activates the hypothalamic supraoptic and paraventricular magnocellular nuclei (Takakura et al., 2011) and that vasopressin released from these nuclei has been shown to

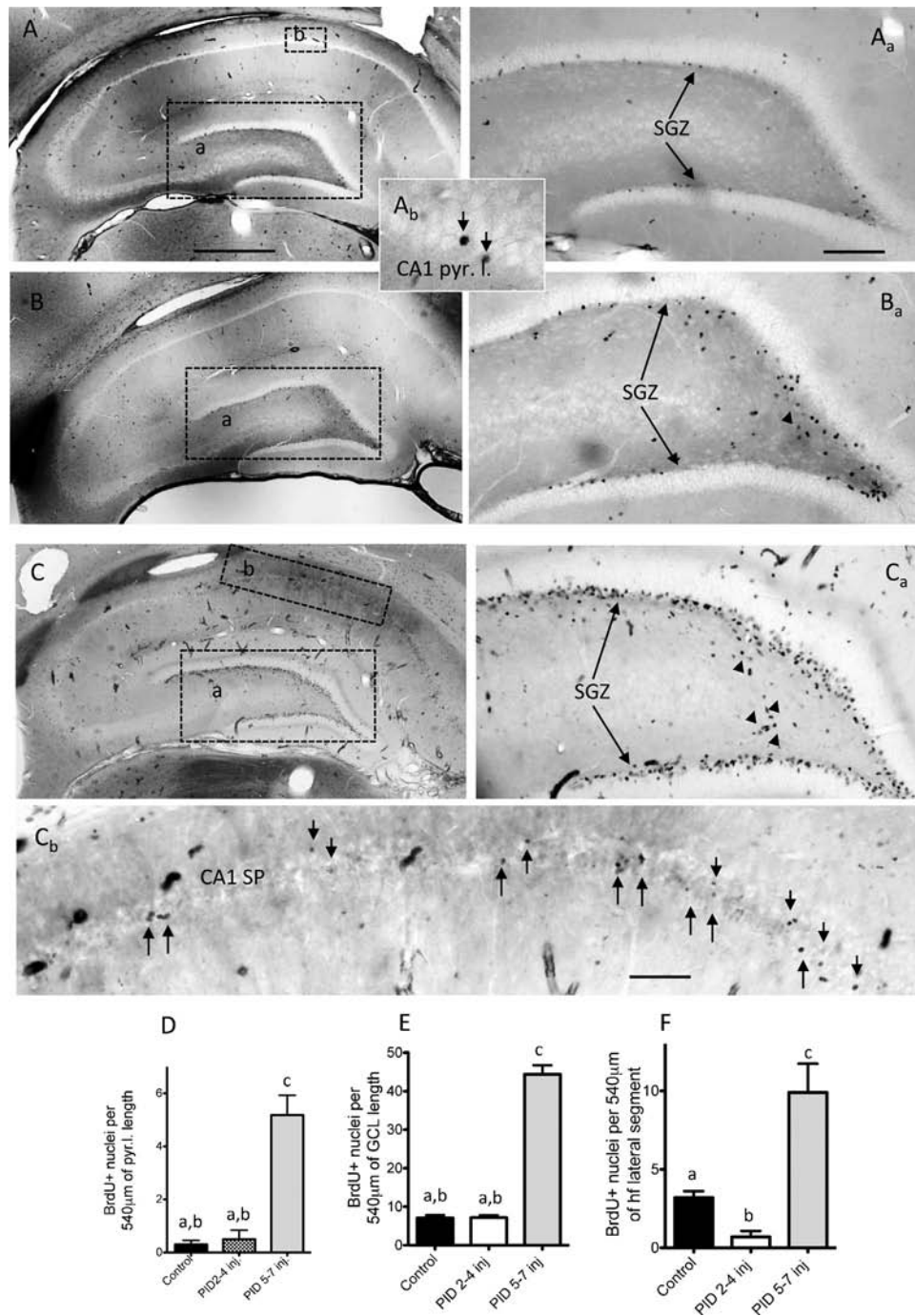


Fig. 8. Delayed up-regulation of cell proliferation in the adult rat hippocampus after the application of pilocarpine-ipratropium bromide protocol evaluated on PID-14. Panel (A): baseline mitotic activity of saline treated control rat identified by BrdU labeling and immunohistochemistry. Note that few BrdU+ nuclei could be seen in the CA1 pyramidal layer (pyr. l.) (inset A_b). Panel (B): mitotic activity of experimental group with BrdU injection during the early post-insult stage (PID 2–4, “PID 2–4 inj”). Note that numerous BrdU+ nuclei, dispersed from SGZ to the hilar region, were found (arrowheads). Panel (C): proliferative activity in SGZ and CA1 was significantly increased, as identified with delayed BrdU injection during the post-insult days 5, 6, 7 (“PID 5–7 inj”). (D)–(F) Quantitative analysis (mean ± SEM) of proliferative activity in the 3 groups from the region CA1 pyramidal layer (pyr. l. in D), subgranular zone/granule cell layer (GCL in E) and lateral segment of hippocampal fissure (hf in F). BrdU: bromodeoxyuridine. Different lettering in (D)–(F) denote statistically significant differences ($p < 0.05$; ANOVA with Bonferroni *post hoc* multiple comparisons). Scale bars (A)–(C) 500 μm and the rest 100 μm.

constrict hippocampal blood vessels (Smock et al., 1987). Vascular endothelial growth factor (VEGF) is part of a system which restores oxygen supply to hypoperfused tissues when blood circulation is inadequate (Holmes et al., 2007) and has been demonstrated to promote perivascular niche neurogenesis (Palmer et al., 2000). Hence, the first important mechanism for the activation of the hf neurogenic niches could be the systemic factors, triggered by the aforementioned mechanisms, which

reached the fissure region through the internal transversal arteries. This deduction is consistent with the data showing that the nestin+/GFAP+ cells and processes were found in high-density in apposition to blood vessels (Fig. 9, panels A and panels D) at the early post-insult stage (PID 7), so was the BrdU labeling (Fig. 9, panels E). Additionally, it was revealed that the DCX clusters in the hf were in juxtaposition with the internal transversal arteries on PID 14.

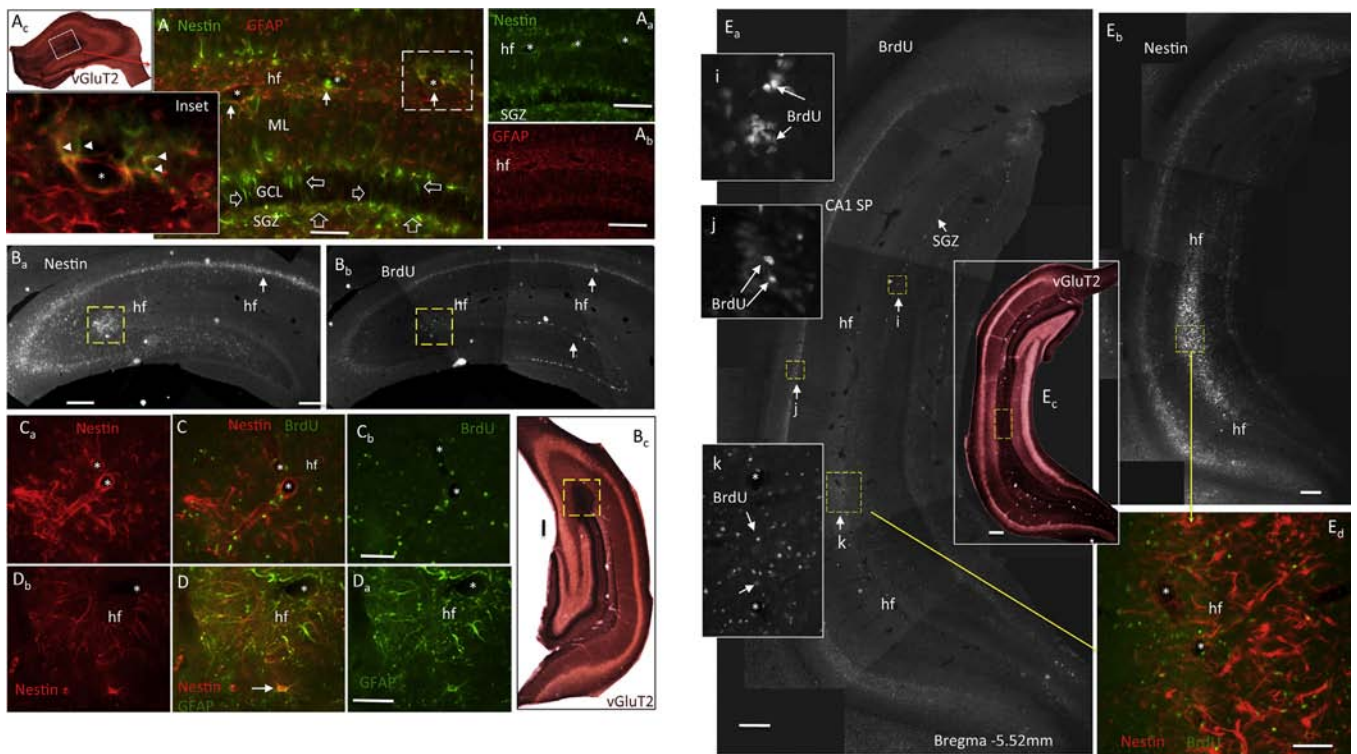


Fig. 9. Increased nestin immunoreactivity in hf region, in correlation with BrdU, GFAP and vGluT2 immunostaining on PID7. (A) Representative examples of double immunofluorescence labeling of nestin and GFAP in septal hippocampus (corresponding to the DCX-IR of panel (C) of Fig. 7), showing neural stem cells/processes in the SGZ and GCL (hollow arrows). In the hf, increased but heterogeneous expression of nestin was found in close relationship to blood vessels (asterisks) (A and A_a), while GFAP immunostaining labeled enlarged and thicker astrocytic processes (A_b). Note that the nestin/GFAP double-positive cells/processes surround a medium size artery (A inset, arrowheads). A_c shows the whole septal hippocampus, corresponding to the same coordinates as vGluT2 immunostaining. The region corresponding to panel (A) is highlighted with a rectangle. Panels (B): coronal sections of hippocampus (around Bregma –4.56 mm, corresponding to the DCX-IR of panel (F) of Fig. 7) with nestin (B_a), BrdU (B_b) and vGluT2 (B_c) immunostaining. Squared regions correspond to high magnifications of panel (C), double immunostaining of nestin/BrdU and panel (D), double immunostaining nestin/GFAP. The arrow in (D) indicates an example of nestin/GFAP co-expressing neuroprogenitor cell located in the hf. Panel (E): coronal sections of temporal hippocampus around Bregma –5.52 mm (corresponding to the DCX-IR of panel (H) of Fig. 7) with BrdU (E_a), nestin (E_b) and vGluT2 (E_c) immunostaining. Note that a well-limited band with massive BrdU incorporation from the delayed group situated in and surrounding the temporal hf, correspond with high expression of nestin (E_d). Inset “i” illustrates the BrdU+ clusters in the SGZ in high magnification. Inset “j” illustrates the BrdU+ nuclei in CA1 SP. Note that due to the DNA denature procedure for BrdU immunostaining, the immunofluorescence reaction had high background in the SP. Inset k: high magnification of hf BrdU labeling. PID: post-insult day; DCX: doublecortin; GFAP: glial fibrillary acidic protein; vGluT2: vesicular glutamate transporter isoform 2; BrdU: bromodeoxyuridine; SGZ: subgranular zone; hf: hippocampal fissure; hf: hippocampal fissure; SP: stratum pyramidale. Scale Bars (A) 50 μm; (A_a), (A_b) (D_s) and (G): 100 μm; (B) and (C) and panel (E): 500 μm; SP: stratum pyramidale; hf: hippocampal fissure; ML: molecular layer.

We have here reported that as a result of using this pilocarpine insult protocol, the increase of mitotic activity, both in the SGZ and in the hf, as well as in the CA pyramidal layer was delayed. The significant increases were observed in the “PID 5–7” group but not in the “PID 2–4” group (Fig. 8). Adding this chronological data to the interesting observation concerning the anatomical concurrence of increased BrdU labeling and enhanced nestin expression together with the immunostaining of the vesicular glutamatergic transporter isoform 2 (vGluT2) in a well-limited narrow band along the hf (Fig. 9), we wish to suggest that the activation of the hf neurogenic niches depends, at least in part, on a slowly reorganizing homeostatic mechanism of the up-stream region(s), rather than on hippocampal local factors. This suggestion is based on the observation and reasoning that the glutamatergic pathway revealed by vGluT2 intense labeling (Fig. 9, panels A_c, B_c, E_c), overlapped almost perfectly with the hf neurogenic band (labeled by high BrdU+/nestin+ expression, Fig. 9). It has been shown that the mRNA for vGluT2 is absent inside hippocampus (Freneau et al., 2004; Ziegler et al., 2002) indicating the extra-hippocampal origin of these vGluT2 containing fibers. Hypothalamus is a highly probable site because of the fact that it is the main brain center for homeostatic regulation and that the main isoform for vesicular transporters of the glutamatergic neurons is vGluT2 (Ziegler et al., 2002, 2005). Several hypothalamic nuclei have been shown to

project to hippocampus. Hippocampal fissure region, the *stratum lacunosum moleculare* (SLM) and the hippocampal CA2 subfield receive rich excitatory innervations from the hypothalamus (Cui et al., 2013; Haglund et al., 1984; Zhang and Hernandez, 2013). Interestingly, in this report, those regions also had high presence of DCX+ neuroblasts (Figs. 4–6) and Nestin/BrdU co-expressing cells were found in SR near this region at PID35 (Fig. 10). In a recent study, the neurodevelopmental role for vGluT2 in pyramidal neurons was unveiled using recombinant vGluT2 knockout mice (He et al., 2012). Based on this analysis, an interesting possibility becomes evident: the hf dormant neurogenic niche could be regulated by hypothalamic glutamatergic input to the hippocampus. In support of this hypothesis of extra-hippocampal glutamatergic transmission regulating hf dormant neurogenic niches, Parent and cols. reported an appealing finding in 1997, which showed that neurogenesis in the SGZ is significantly increased 6 days after a 6 h electrical stimulation to the perforant path, in absence of prolonged motor seizure, widespread injury or convulsant drug effects (Parent et al., 1997).

An additional, but not less important finding from this study, is that in the time-course anatomical analysis of DCX expression and location, we frequently observed “tube-like” structures (Fig. 2 panels B and C; Fig. 3, panels B and C; Fig. 4, panel F; Fig. 7, panel G), with several spiral-shaped DCX-expressing processes,

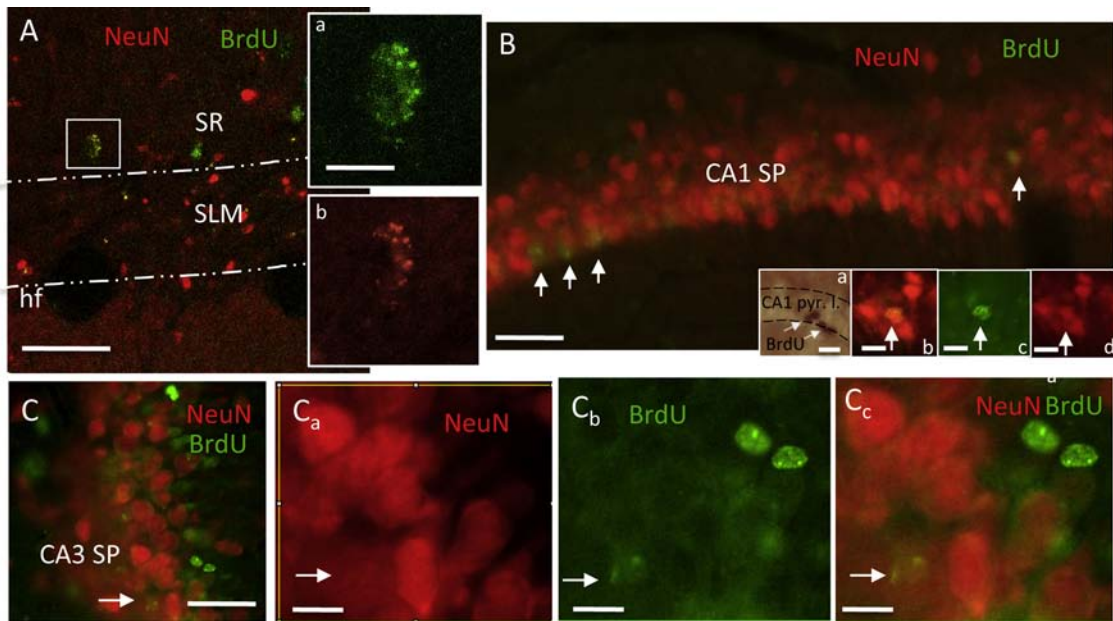


Fig. 10. Generation of new neurons in the CA fields. (A) Co-localization of nuclear neuronal marker (NeuN, red) with BrdU (green) in the *stratum radiatum* (SR) close to the *stratum lacunosum-moleculare* (SLM) border of the CA1. (B) Low magnification photomicrograph of CA1 SP with numerous NeuN+/BrdU+ cells labeled. Inset B_a shows an example of immunoperoxidase-DAB BrdU reaction in the SP; B_{b–d} shows a double-labeled neuron in higher magnification. (C) Co-localization (arrows) of NeuN+/BrdU+ in CA3 SP. BrdU: bromodeoxyuridine; NeuN: neuronal nuclear specific protein; SP: stratum pyramidale; SR: stratum radiatum; SLM: stratum lacunosum moleculare; hf: hippocampal fissure. Scale bars for (A)–(C): 100 μ m; rest: 10 μ m. (For interpretation of the references to color in this figure legend, the reader is referred to the web version of this article.)

which seemingly served as migration-chains connecting the neuroprogenitors generated in the SGZ to the fissure through the interior and exterior molecular layers. While this finding does not contradict our main conclusion, it clearly indicates the existence of attracting factors in the fissure region and suggests that at least portions of these progenitor clusters found in the hippocampal fissure arose from the SGZ. These cells could have either arrived as neuroblasts or as neural stem/progenitor cells, which underwent further proliferation/differentiation in peri-vascular niche-like regions rich in neurogenic promoting factors, as discussed above, in addition to the ones brought from the blood torrent as previously suggested (Palmer et al., 2000). Interestingly, a “switching-effect” of the fibroblast growth factor 2 (FGF-2) on neural progenitor proliferation/differentiation has been demonstrated: a low concentration determines neurite outgrowth direction and a high concentration promotes progenitor proliferation (Irasena et al., 2004; Kelly et al., 2003). It seems that this hypothesis of FGF-2 “concentration-dependent switching effect” could apply to the phenomenon observed in this study.

5. Author contributions

VSH, LZ and FSE designed research; FSE, VSH and LZ performed research; LZ, FSE, VSH and RL analyzed data; LZ and RL wrote the paper; LZ, FSE, VSH and RL revised the manuscript.

Acknowledgements

This study was supported by grants: CONACYT: 127777, 179616 and PAPIIT-DGAPA-UNAM: IN216214. We are thankful to Mauricio P. Medina for his contribution in the experimental design of this study, to Maria José Gómora and Enrique Pinzón for technical assistance, to Alfredo Quiñones-Hinojosa (Baltimore) for

reading of an early version of the manuscript and for encouragement and to Barbara Ann Ailstock for language editing.

References

- Altman, J., Das, G.D., 1965. Autoradiographic and histological evidence of postnatal hippocampal neurogenesis in rats. *J. Comp. Neurol.* 124, 319–335.
- Bayer, S.A., Yackel, J.W., Puri, P.S., 1982. Neurons in the rat dentate gyrus granular layer substantially increase during juvenile and adult life. *Science* 216, 890–892.
- Brown, J.P., Couillard-Despres, S., Cooper-Kuhn, C.M., Winkler, J., Aigner, L., Kuhn, H.G., 2003. Transient expression of doublecortin during adult neurogenesis. *J. Comp. Neurol.* 467, 1–10.
- Cavalheiro, E.A., 1995. The pilocarpine model of epilepsy. *Ital. J. Neurol. Sci.* 16, 33–37.
- Clifford, D.B., Olney, J.W., Maniotis, A., Collins, R.C., Zorumski, C.F., 1987. The functional anatomy and pathology of lithium-pilocarpine and high-dose pilocarpine seizures. *Neuroscience* 23, 953–968.
- Coyle, P., 1978. Spatial features of the rat hippocampal vascular system. *Exp. Neurol.* 58, 549–561.
- Cui, Z., Gerfen, C.R., Young 3rd, W.S., 2013. Hypothalamic and other connections with dorsal CA2 area of the mouse hippocampus. *J. Comp. Neurol.* 521, 1844–1866.
- Curia, G., Longo, D., Biagini, G., Jones, R.S., Avoli, M., 2008. The pilocarpine model of temporal lobe epilepsy. *J. Neurosci. Methods* 172, 143–157.
- Decimo, I., Fumagalli, G., Berton, V., Krampera, M., Bifari, F., 2012. Meninges: from protective membrane to stem cell niche. *Am. J. Stem Cells* 1, 92–105.
- Ekdahl, C.T., Claassen, J.H., Bonde, S., Kokaia, Z., Lindvall, O., 2003. Inflammation is detrimental for neurogenesis in adult brain. *Proc. Natl. Acad. Sci. USA* 100, 13632–13637.
- Estrada, F.S., Hernandez, V.S., Lopez-Hernandez, E., Corona-Morales, A.A., Solis, H., Escobar, A., Zhang, L., 2012. Glial activation in a pilocarpine rat model for epileptogenesis: a morphometric and quantitative analysis. *Neurosci. Lett.* 514, 51–56.
- Freneau Jr., R.T., Voglmaier, S., Seal, R.P., Edwards, R.H., 2004. VGLUTs define subsets of excitatory neurons and suggest novel roles for glutamate. *Trends Neurosci.* 27, 98–103.
- Gratzner, H.G., 1982. Monoclonal antibody to 5-bromo- and 5-iododeoxyuridine: a new reagent for detection of DNA replication. *Science* 218, 474–475.
- Gross, N.J., Skorodin, M.S., 1984. Anticholinergic, antimuscarinic bronchodilators. *Am. Rev. Respir. Dis.* 129, 856–870.
- Kuhn, H.G., Peterson, D.A., 2008. Detection and phenotypic characterization of adult neurogenesis. In: Gage, F.H., Kempermann, G., Song, H. (Eds.), *Adult Neurogenesis*. Cold Spring Harbor Laboratory Press, New York, pp. 25–48.

- Haglund, L., Swanson, L.W., Kohler, C., 1984. The projection of the supramammillary nucleus to the hippocampal formation: an immunohistochemical and anterograde transport study with the lectin PHA-L in the rat. *J. Comp. Neurol.* 229, 171–185.
- Hamilton, S.E., Loose, M.D., Qi, M., Levey, A.I., Hille, B., McKnight, G.S., Idzerda, R.L., Nathanson, N.M., 1997. Disruption of the m1 receptor gene ablates muscarinic receptor-dependent M current regulation and seizure activity in mice. *Proc. Natl. Acad. Sci. USA* 94, 13311–13316.
- He, H., Mahnke, A.H., Doyle, S., Fan, N., Wang, C.C., Hall, B.J., Tang, Y.P., Inglis, F.M., Chen, C., Erickson, J.D., 2012. Neurodevelopmental role for VGLUT2 in pyramidal neuron plasticity, dendritic refinement, and in spatial learning. *J. Neurosci.* 32, 15886–15901.
- Holmes, K., Roberts, O.L., Thomas, A.M., Cross, M.J., 2007. Vascular endothelial growth factor receptor-2: structure, function, intracellular signalling and therapeutic inhibition. *Cell. Signal.* 19, 2003–2012.
- Humphrey, T., 1967. The development of the human hippocampal fissure. *J. Anat.* 101, 655–676.
- Iadecola, C., Alexander, M., 2001. Cerebral ischemia and inflammation. *Curr. Opin. Neurol.* 14, 89–94.
- Israsena, N., Hu, M., Fu, W., Kan, L., Kessler, J.A., 2004. The presence of FGF2 signaling determines whether beta-catenin exerts effects on proliferation or neuronal differentiation of neural stem cells. *Dev. Biol.* 268, 220–231.
- Kelly, C.M., Zietlow, R., Dunnett, S.B., Rosser, A.E., 2003. The effects of various concentrations of FGF-2 on the proliferation and neuronal yield of murine embryonic neural precursor cells in vitro. *Cell Transplant.* 12, 215–223.
- Kempermann, G., 2002. Why new neurons? Possible functions for adult hippocampal neurogenesis. *J. Neurosci.* 22, 635–638.
- Kempermann, G., Gage, F.H., 1999. Experience-dependent regulation of adult hippocampal neurogenesis: effects of long-term stimulation and stimulus withdrawal. *Hippocampus* 9, 321–332.
- Kremer, T., Jagasia, R., Herrmann, A., Matile, H., Borroni, E., Francis, F., Kuhn, H.G., Czech, C., 2013. Analysis of adult neurogenesis: evidence for a prominent “non-neurogenic” DCX-protein pool in rodent brain. *PLoS ONE* 8, e59269.
- Kuhn, H.G., Dickinson-Anson, H., Gage, F.H., 1996. Neurogenesis in the dentate gyrus of the adult rat: age-related decrease of neuronal progenitor proliferation. *J. Neurosci.* 16, 2027–2033.
- Lendahl, U., Zimmermann, L.B., McKay, R.D., 1990. CNS stem cells express a new class of intermediate filament protein. *Cell* 60, 585–595.
- Lipton, P., 1999. Ischemic cell death in brain neurons. *Physiol. Rev.* 79, 1431–1568.
- McLendon, R.E., Bigner, D.D., 1994. Immunohistochemistry of the glial fibrillary acidic protein: basic and applied considerations. *Brain Pathol.* 4, 221–228.
- Mullen, R.J., Buck, C.R., Smith, A.M., 1992. NeuN, a neuronal specific nuclear protein in vertebrates. *Development* 116, 201–211.
- Nakagomi, T., Molnar, Z., Taguchi, A., Nakano-Doi, A., Lu, S., Kasahara, Y., Nakagomi, N., Matsuyama, T., 2012. Leptomeningeal-derived doublecortin-expressing cells in poststroke brain. *Stem Cells Dev.* 21, 2350–2354.
- Nakatomi, H., Kuriu, T., Okabe, S., Yamamoto, S., Hatano, O., Kawahara, N., Tamura, A., Kirino, T., Nakafuku, M., 2002. Regeneration of hippocampal pyramidal neurons after ischemic brain injury by recruitment of endogenous neural progenitors. *Cell* 110, 429–441.
- Ndode-Ekane, X.E., Hayward, N., Grohn, O., Pitkanen, A., 2010. Vascular changes in epilepsy: functional consequences and association with network plasticity in pilocarpine-induced experimental epilepsy. *Neuroscience* 166, 312–332.
- Palmer, T.D., Willhoite, A.R., Gage, F.H., 2000. Vascular niche for adult hippocampal neurogenesis. *J. Comp. Neurol.* 425, 479–494.
- Parent, J.M., von dem Bussche, N., Lowenstein, D.H., 2006. Prolonged seizures recruit caudal subventricular zone glial progenitors into the injured hippocampus. *Hippocampus* 16, 321–328.
- Parent, J.M., Yu, T.W., Leibowitz, R.T., Geschwind, D.H., Sloviter, R.S., Lowenstein, D.H., 1997. Dentate granule cell neurogenesis is increased by seizures and contributes to aberrant network reorganization in the adult rat hippocampus. *J. Neurosci.* 17, 3727–3738.
- Racine, R.J., 1972. Modification of seizure activity by electrical stimulation II. Motor seizure. *Electroencephalogr. Clin. Neurophysiol.* 32, 281–294.
- Rao, M.S., Shetty, A.K., 2004. Efficacy of doublecortin as a marker to analyse the absolute number and dendritic growth of newly generated neurons in the adult dentate gyrus. *Eur. J. Neurosci.* 19, 234–246.
- Rietze, R., Poulin, P., Weiss, S., 2000. Mitotically active cells that generate neurons and astrocytes are present in multiple basal regions of the adult mouse hippocampus. *J. Comp. Neurol.* 424, 397–408.
- Salazar-Colocho, P., Lanciego, J.L., Del Rio, J., Frechilla, D., 2008. Ischemia induces cell proliferation and neurogenesis in the gerbil hippocampus in response to neuronal death. *Neurosci. Res.* 61, 27–37.
- Schmidt, W., Reymann, K.G., 2002. Proliferating cells differentiate into neurons in the hippocampal CA1 region of gerbils after global cerebral ischemia. *Neurosci. Lett.* 334, 153–156.
- Shapiro, L.A., Ribak, C.E., 2006. Newly born dentate granule neurons after pilocarpine-induced epilepsy have hilar basal dendrites with immature synapses. *Epilepsy Res.* 69, 53–66.
- Shapiro, L.A., Wang, L., Upadhyaya, P., Ribak, C.E., 2007. Seizure-induced increased neurogenesis occurs in the dentate gyrus of aged Sprague-Dawley rats. *Aging Dis.* 2, 286–293.
- Shen, Q., Goderie, S.K., Jin, L., Karanth, N., Sun, Y., Abramova, N., Vincent, P., Pumiglia, K., Temple, S., 2004. Endothelial cells stimulate self-renewal and expand neurogenesis of neural stem cells. *Science* 304, 1338–1340.
- Smock, T., Cach, R., Topple, A., 1987. Action of vasopressin on neurons and microvessels in the rat hippocampal slice. *Exp. Brain Res.* 66, 401–408.
- Stoyanov, M., Muller, H., Lobisch, M., Hempelmann, G., 1984. [Hemodynamic effects in antagonism of neuromuscular blockage: atropine-pyridostigmine versus ipratropium bromide-pyridostigmine]. *Anaesthesist* 33, 499–503.
- Takakura, A.C., Moreira, T.S., Borella, T.L., Paulin, R.F., Colombari, D.S., De Luca Jr., L.A., Colombari, E., Menani, J.V., 2011. Central mechanisms involved in pilocarpine-induced pressor response. *Auton. Neurosci.* 164, 34–42.
- Trieb, G., Mertens, H.M., Bistreau, I., Mannebach, H., Gleichmann, U., 1979. [Long-term treatment of bradycardia by means of an atropine ester (SCH 1000). Electrophysiological and clinical results] *Z Kardiol.* 68, 700–704.
- Turski, W.A., Cavalheiro, E.A., Schwarz, M., Czuczwar, S.J., Kleinrok, Z., Turski, L., 1983. Limbic seizures produced by pilocarpine in rats: behavioural, electroencephalographic and neuropathological study. *Behav. Brain Res.* 9, 315–335.
- Urso, R., Segre, G., Bianchi, E., Bruni, G., Dal Pra, P., Fiaschi, A.I., 1991. Plasma kinetics of atropine and ipratropium in rats after different routes of administration evaluated by a radioreceptor assay. *Eur. J. Drug Metab. Pharmacokinet.* 3, 111–115.
- Zhang, E.T., Inman, C.B., Weller, R.O., 1990. Interrelationships of the pia mater and the perivascular (Virchow–Robin) spaces in the human cerebrum. *J. Anat.* 170, 111–123.
- Zhang, L., Guadarrama, L., Corona-Morales, A.A., Vega-Gonzalez, A., Rocha, L., Escobar, A., 2006. Rats subjected to extended L-tryptophan restriction during early postnatal stage exhibit anxious-depressive features and structural changes. *J. Neuropathol. Exp. Neurol.* 65, 562–570.
- Zhang, L., Hernandez, V.S., 2013. Synaptic innervation to rat hippocampus by vasopressin-immuno-positive fibres from the hypothalamic supraoptic and paraventricular nuclei. *Neuroscience* 228, 139–162.
- Zhao, T., Kraemer, N., Oldekamp, J., Cankaya, M., Szabo, N., Conrad, S., Skutella, T., Alvarez-Bolado, G., 2006. Emx2 in the developing hippocampal fissure region. *Eur. J. Neurosci.* 23, 2895–2907.
- Ziegler, D.R., Cullinan, W.E., Herman, J.P., 2002. Distribution of vesicular glutamate transporter mRNA in rat hypothalamus. *J. Comp. Neurol.* 448, 217–229.
- Ziegler, D.R., Cullinan, W.E., Herman, J.P., 2005. Organization and regulation of paraventricular nucleus glutamate signaling systems: N-methyl-D-aspartate receptors. *J. Comp. Neurol.* 484, 43–56.
- Zimmerman, L., Parr, B., Lendahl, U., Cunningham, M., McKay, R., Gavin, B., Mann, J., Vassileva, G., McMahon, A., 1994. Independent regulatory elements in the nestin gene direct transgene expression to neural stem cells or muscle precursors. *Neuron* 12, 11–24.

Glial activation in a pilocarpine rat model for epileptogenesis: A morphometric and quantitative analysis

Estrada F. S., Hernández V. S., López-Hernández E.,
Corona-Morales A. A., Solís H, Escobar A., Zhang L.

Neurosci Lett. 2012, 514: 51-56

My contributions in:

- Conception of the study:
- Performance of the experiments:
 - o Pilocarpine treatment to model temporal lobe epilepsy ++
 - o Immunohistochemistry ++
 - o Assessment of astrocytes/microglia density and morphology ++
- Statistical analysis: +
- Discussion of the results: ++
- Preparation of the paper: -

(-): No contribution; (+): Average contribution; (++): Important contribution.



Glial activation in a pilocarpine rat model for epileptogenesis: A morphometric and quantitative analysis

Felipe S. Estrada^a, Vito S. Hernández^a, Estela López-Hernández^b, Aleph A. Corona-Morales^d, Hugo Solís^{a,b}, Alfonso Escobar^c, Limei Zhang^{a,*}

^a Departamento de Fisiología, Facultad de Medicina, Universidad Nacional Autónoma de México, Mexico City, Mexico

^b Departamento de Anatomía, Facultad de Medicina, Universidad Nacional Autónoma de México, Mexico City, Mexico

^c Departamento de Fisiología y Biología Celular, Instituto de Investigaciones Biomédicas, Universidad Nacional Autónoma de México, Mexico City, Mexico

^d Dirección General de Investigaciones, Universidad Veracruzana, Xalapa, Mexico

ARTICLE INFO

Article history:

Received 26 October 2011

Received in revised form 15 February 2012

Accepted 17 February 2012

Keywords:

Astrocyte

GFAP

CD11b

Microglia

Morphometric analysis

ABSTRACT

In this work we examined the correlation between long-term glial resilience and slow epileptogenesis using the pilocarpine-insult rat model. We assessed, quantitatively and morphometrically, glial fibrillary acidic protein (GFAP) expression and cell densities in hippocampus in a dose–response manner 2, 4 and 8 weeks after the pilocarpine insult. GFAP changes were correlated with observations on microglial activation. We used a commonly applied epileptogenic pilocarpine dose (380 mg/kg) and its fractions of 1/10, 1/4 and 1/2. GFAP expression evaluated at 2 weeks revealed dose-dependent cytoskeletal hypertrophy and loss of GFAP+ cell densities in hippocampus. At 4-week timepoint, recoveries of the above mentioned parameters were observed in all groups, except for the full dose group in which the astrocytic hypertrophy reached the highest level, while its density dropped to the lowest level. Strong and localized microgliosis revealed by CD11b immunoreactivity was observed in hilus in the full dose group at 2- and 4-, persisting at 8-week timepoints. Through changing pattern analysis, we conclude that the loss of astroglial resilience is likely to be a determining factor for spontaneous recurrent seizure onset.

© 2012 Elsevier Ireland Ltd. All rights reserved.

1. Introduction

The excitotoxic insult triggered by pilocarpine induces short-term status epilepticus (SE) in rats, when the applied dose is about 380 ± 20 mg/kg [11,18,34]. This procedure leads to delayed epileptogenesis, characterized by spontaneous recurrent seizures (SRSs), which occur after a relatively long “silent” period, characterized by an apparently normalized EEG and behavior [3,27]. The ability of pilocarpine to induce SE seems to depend on activation of the M1 muscarinic receptor subtype [9]. However, the factors contributing to the development of SRSs after the silent lapse are not well understood.

Hippocampus is the brain structure most commonly involved in temporal lobe and limbic epilepsy both in human and in rodent models, which have been extensively studied [27]. Currently, there is a controversy about the role of neuronal reorganization on SRSs generation. The “recurrent–excitation–hypothesis” proposes that after epileptogenic insults, the granule cell axons (mossy

fibers) reorganize and establish an abnormal recurrent excitatory circuit that generates SRSs throughout positive feedback loops between granule cells [32]. In contrast, the “recurrent-inhibition–hypothesis” proposes that the sprouted mossy fibers preferentially synapse with inhibitory interneurons rather than with granule cells [7]. Hence, neuronal reorganization may be a homeostatic mechanism to control hyperexcitability produced by epileptogenic insults. Recent observations using focally infused or systemically applied rapamycin, which suppresses mossy fiber sprouting but not seizure frequency, in a mouse model of temporal lobe epilepsy [1] suggested that mossy fiber sprouting is neither pro- nor anti-convulsant. Therefore, the main mechanism(s) contributing to delayed epileptogenesis remain(s) unclear.

There has been a growing interest in the role of glial activation and brain inflammation in epileptogenesis [11,14,13,28,35]. It is well known that neuroglia plays a pivotal role for brain metabolism, extracellular ion homeostasis, intactness of blood–brain-barrier, immune function, maintenance of extracellular space, exerting key influences on neuronal functions [12]. Enlargement of astrocytes and increased expression of glial fibrillary acidic protein (GFAP) are indicators of reactive astrogliosis. Reactive astrocytes over-expressing GFAP may exert a protective function in the injured nervous system by participating in diverse biological processes [20,23]. Recent studies have shown that astrocytes and microglia

* Corresponding author at: Departamento de Fisiología, Facultad de Medicina, Universidad Nacional Autónoma de México, Ciudad Universitaria, México D.F. 04510, Mexico. Tel.: +52 55 56232348; fax: +52 55 56232348.

E-mail addresses: limei@unam.mx, limei.zhangdebarrio@gmail.com (L. Zhang).

are rapidly activated after pilocarpine insult [29] and that the activation of microglia drives to astrocytic death [11] suggesting that glial responses after SE may contribute to epileptogenesis.

Given the controversy and evidences above mentioned, we hypothesized that there is a functional limit for neuronal network activation “imposed” by glial homeostatic regulation. Once this limit is surpassed, the neuronal network hyperactivates itself, driving the system to instability. In this case, glial dysregulation caused by the progression of abnormal astrocytic morphology synergized by the loss of astrocytic density makes the glial controlled homeostasis weakened enough to reach the threshold for neural network hyperactivation. To examine this hypothesis, we made medium and long-term quantitative morphometric assessments on individual astroglial cytoskeletal hypertrophy and population density loss in the rat hippocampus after pilocarpine insult, in a dose–response manner. Through the analysis of differential responses to distinct pilocarpine doses and their temporal changing patterns, we conclude that the massive astrocytic enlargement and dramatic increase of GFAP expression in individual astrocytes, together with the lowest level of astrocytic density detected in hippocampus, is likely linked to the SRSs installation.

2. Materials and methods

Sixty-seven male Wistar rats weighing 220 ± 20 g were used in this study. All animal procedures were approved by the local research and ethics committees (Comisiones de Investigación y Ética de la Facultad de Medicina, Universidad Nacional Autónoma de México), with the approval IDs 063–2011, in accordance with the principles exposed in the Handbook for the Use of Animals in Neuroscience Research (Society for Neuroscience, Washington, DC 1991).

A commonly used epileptogenic dose of pilocarpine (380 mg/kg) and its fractions of 1/10, 1/4 and 1/2 were used for this study. The experimental subjects were distributed in 10 groups ($n=6$), namely, control, “38 mg/kg”, “95 mg/kg”, “190 mg/kg” groups at 2- and 4-week timepoints and “380 mg/kg” at 2-, 4-, and 8-week timepoints (2W, 4W, 8W).

At the beginning of this study, we first injected i.p. atropine methylbromide (5 mg/kg, Sigma, St. Louis, MO) in order to minimize pilocarpine peripheral effects. Twenty minutes later, we injected i.p. pilocarpine hydrochloride (Sigma, St. Louis, MO) dissolved in 0.9% saline with the corresponding doses to each experimental group. The dose of 380 mg/kg was injected to 25 rats and 18 survived the insult, yielding a survival rate of 72%, and were subdivided in 2-, 4- and 8-week groups (2W, 4W and 8W respectively). The beginning of status epilepticus (SE) was considered when the animal suffered a class-4 motor seizure in Racine’s scale of limbic seizures [24]. Diazepam (5 mg/kg) was administered 1 h after the induction of SE and then with 30 min intervals (2.5 mg/kg) for the following 2 h. It is worth mentioning that with this treatment scheme, the interval between SE and the onset of spontaneous recurrent seizures (SRSs) is around 4 weeks (unpublished data) which is comparable with data from literature [4,15,17], although we did not properly monitor this parameter in this study. Taking into account these data and the extensive studies published in the literature regarding astrogliosis and microgliosis during the first few days after the pilocarpine insult, we considered that the best evaluation time-points for this study were 2W, 4W and 8W.

For tissue processing, rats were deeply anesthetized with an overdose of pentobarbital and transcardially perfused at the corresponding time-points with 0.9% saline followed by cold fixative containing 4% of paraformaldehyde in 0.1 M sodium phosphate buffer (PB, pH 7.4) and 15% (v/v) of saturated picric acid for 15 min. Brains were removed, blocked, then thoroughly rinsed

with PB. Coronal sections of 70 μm of dorsal hippocampi were obtained, using Leica vibratome VT 1000 (Heidelberg, Germany). For immunostaining, sets of one out of every six sections from Bregma -3.2 to -3.8 mm were incubated with Tris buffer (pH 7.4 at 20 °C) plus 0.9% of NaCl (TBS) and 0.3% Triton X-100 (Sigma, T-7878) and 20% normal horse serum (Vector Laboratories, Burlingame, CA) in PB for 1 h at room temperature. Afterwards, conventional immunoreactions were carried out using the following primary antibodies: mouse anti-GFAP (Chemicon MAB360, Temecula, CA, 1:2000), mouse anti-CD11b (OX-42) (Serotec MCA275G, Oxford, UK, 1:2000) and secondary antibodies Alexa 488 donkey-anti-mouse IgG (Invitrogen, Carlsbad, CA, 1:1000) and biotinylated goat-anti-mouse IgG (Vector Laboratories, Burlingame CA, 1:1000). For this latter one, sections were then incubated in avidin–biotin–peroxidase complex (Elite ABC kit, Vector Laboratories) for 1 h at room temperature. Peroxidase was detected using DAB (0.05%) as chromogen and hydrogen peroxide (H_2O_2 , 0.01%, v/v) as substrate.

For morphometric assessments, 2 matching sections from the hippocampi of each of the 6 rats per group were analyzed using a Nikon Eclipse 50i light microscope and a drawing tube. Astrocyte density and morphological changes in stratum radiatum (str. rad.) from CA1 and CA3 and hilus of the dentate gyrus (DG) were examined. For density assessment, astrocyte somata were drawn at 10 \times , digitalized and analyzed by counting the number of cell bodies per unit of area using ImageJ (National Institutes of Health, USA). To assess the 3D cytoplasmic GFAP arrangement, 4 astrocytes were randomly chosen in str. rad. (CA1 and CA3) and hilus. Drawings were elaborated at 100 \times and 10 \times for the drawing tube, varying the focal planes. A total of 720 cells, i.e. 24 cells per hippocampal sub-field per group were reconstructed and analyzed. This criterion was set considering that astrocytes are a relatively homogeneous population at the anatomical level we are studying [2,16,33]. To compare the relative size of the astrocyte cytoskeletal hypertrophy, filament thickness was quantified using digitalized drawings. Summation of the intersection lengths within the concentric spheres of Sholl [31] were analyzed as previously described [36]. Briefly, the stereological graticule consists of seven concentric circles representing 5 μm of actual distance between each circle (under the above optical settings). The astrocyte somata, identified as having the nuclear hollow, were placed on the center of the graticule. Thickness of each intersection was measured with ImageJ and the sum of the total length of intersections per each astrocyte was analyzed.

Quantitative results were expressed as mean \pm standard error of mean (SEM); groups were tested for differences by performing a two-way ANOVA (factors: time-points vs doses of pilocarpine) followed by Bonferroni tests, using Graph Pad Prism (La Jolla, CA). Differences were considered statistically significant at a value $P < 0.05$ (* $P < 0.05$, ** $P < 0.01$, *** $P < 0.001$).

3. Results

Alterations produced by the systemic administration of pilocarpine were dose-dependent. In the groups of pilocarpine dose of 38 mg/kg, 95 mg/kg and 190 mg/kg, animals exhibited mild signs of cholinergic stimulation. At pilocarpine dose of 380 mg/kg, rats developed motor limbic seizures approximately 15–20 min after the injection, which built up progressively into a SE.

Using GFAP labeling and Sholl-ring analysis on intersection lengths as an operational parameter for astrocytic cytoskeleton hypertrophy, we observed dose-dependent dynamics of morphological changes in CA1, CA3 and DG. Systemic administration of pilocarpine induced short-term GFAP cytoskeletal hypertrophy with doses of 95 mg/kg and higher evaluated at 2W (Fig. 1G–I, red bars). However, this phenomenon was reverted when evaluated

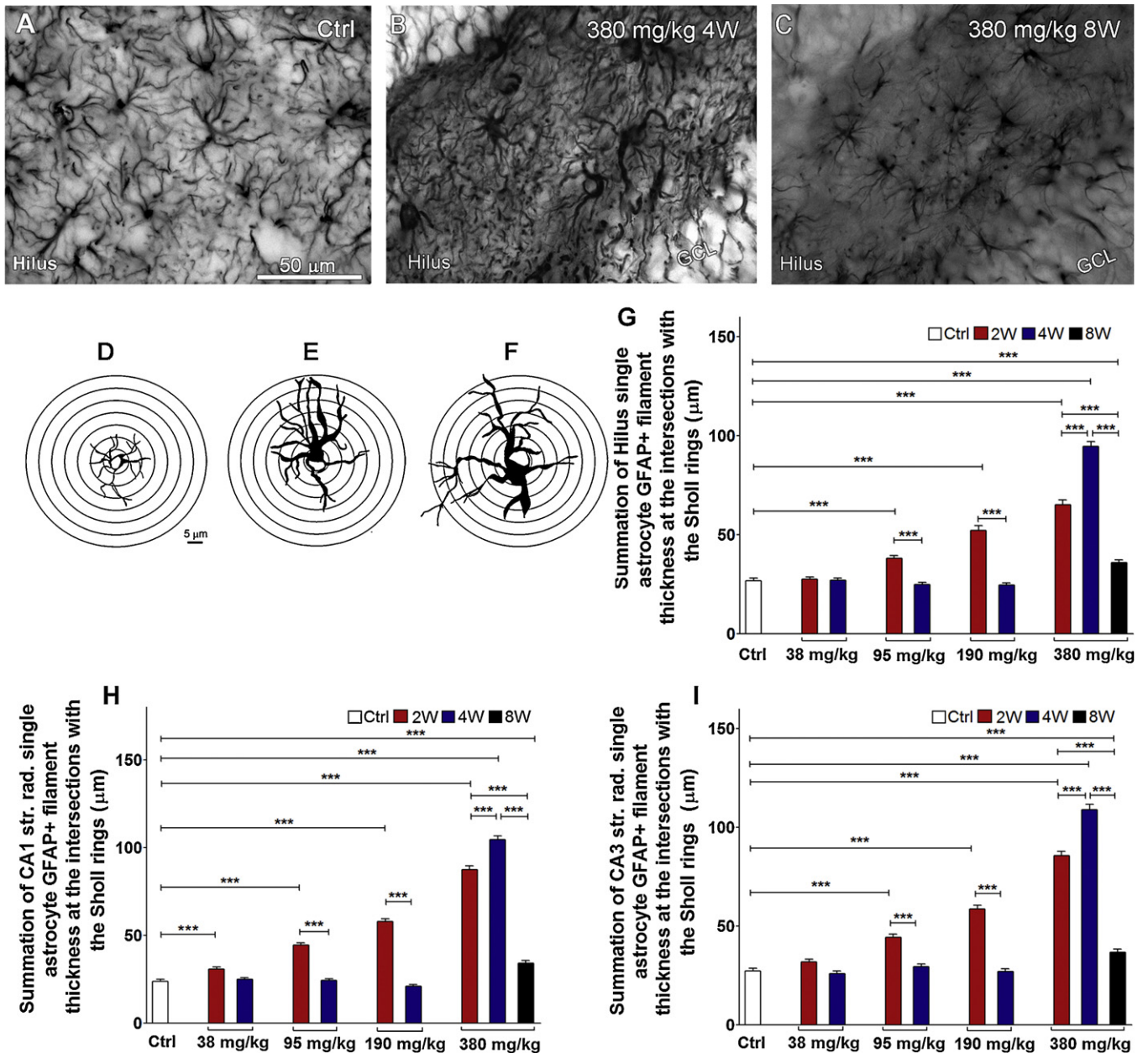


Fig. 1. Morphometric analysis of GFAP expression in the astrocytic populations. Morphometric analysis of GFAP expression in the astrocytic populations within stratum radiatum (str. rad.) of CA1 and CA3 and hilus of the dentate gyrus. A, B, C, are photomicrographs of GFAP immunoreaction in the hilus of control (Ctrl), 380 mg/kg group at 4-week timepoint (4W) and at 8-week timepoint (8W), respectively. D, E and F are examples of the 2D projections of 3D hilar astrocyte cytoskeletal reconstructions using a drawing tube corresponding to Ctrl (D), 2W (E) and 4W (F) of the 380 mg/kg groups respectively. G, H and I show the Sholl-ring analysis on summed intersection lengths, which we used as an operational parameter for astrocytic cytoskeletal hypertrophy in the hilus of the dentate gyrus (DG, G), str. rad. of CA1 (H) and CA3 (I). $n = 24$. Values are shown as mean \pm SEM. *** $P < 0.001$. (For interpretation of the references to color in the text, the reader is referred to the web version of the article.)

at 4W in the groups which did not develop SRSs (Fig. 1G–I, blue bars of 38 mg/kg, 95 mg/kg and 190 mg/kg groups). In contrast, in the 380 mg/kg group this phenomenon, evaluated at 4W, was further exacerbated and still showing significant difference compared to control at 8W (Fig. 1G–I, blue and black bars). Abundant astrocytes with cellular and nuclear edema (for morphology reference see [13]) were observed in the full dose groups at 2W and 4W (Fig. 1E and F).

GFAP+ cell density in hilus suffered a medium-term loss, starting at 95 mg/kg group, observed at 2W (Fig. 2G, red bars). However, recoveries were observed at 4W in the 95 mg/kg and 190 mg/kg groups, which did not develop SRSs before 4W (Fig. 2G, blue bars of 95 mg/kg). In the 190 mg/kg group complete recovery was not observed at 4W ($P < 0.001$ vs. control). However, a significant

difference respect to the 2W timepoint of this same group was observed ($P < 0.001$). Recovery was not observed in the 380 mg/kg group, which should have developed SRSs around 4W (Fig. 2G, 380 mg/kg group, red and blue bars) neither at 8W (Fig. 2G, black bars).

In order to compare microglial activation with astrocytic morphometric and density changes in this dose-temporality study of the pilocarpine model, we performed an immunoreaction against CD11b (OX42), a marker for microglia [26], at the same timepoints studied for astroglial hypertrophy and density changes. Many of the CD11b labeled cells of 380 mg/kg groups in hilus at 2W, 4W and 8W were pleomorphic, with thickened processes and increased branching points, indicative of activated microglial cells. The activated microglial cells were intensely immunolabeled and displayed

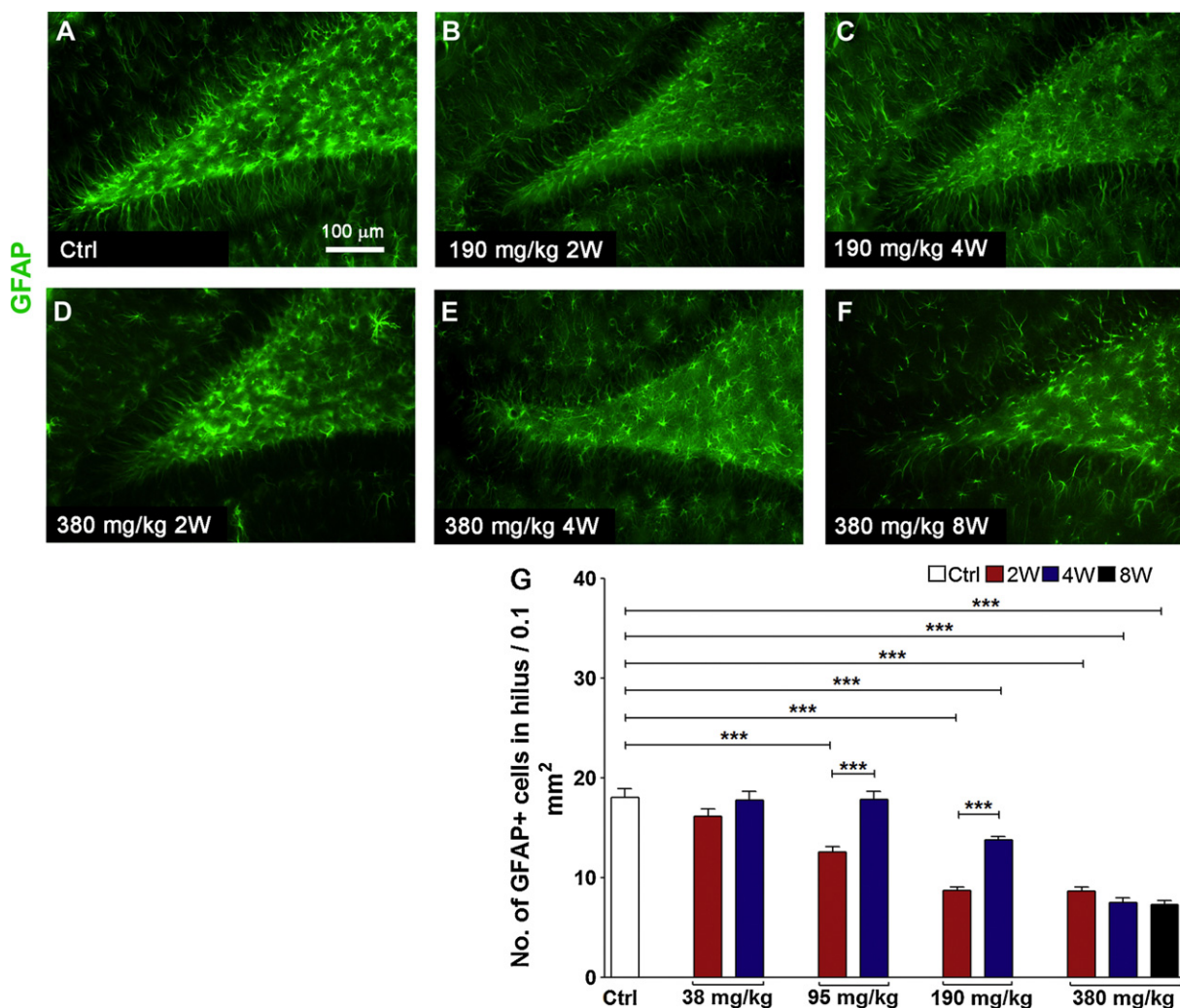


Fig. 2. Density analysis of hilar astrocytes. (A–F) Sample photomicrographs of hilar GFAP immunoreactions, showing the reversible loss of astrocytic density in the 190 mg/kg group (B, C) and long term loss in the 380 mg/kg group (D, E, F). (G) Histogram showing astrocytic densities in hilus. *** $P < 0.001$. (For interpretation of the references to color in the text, the reader is referred to the web version of the article.)

bushy/ramified branching patterns (Fig. 3F, L and M, for instance), being the most notorious at 2 W (Fig. 3J). This population of activated microglial cells was not observed in the control rats (Fig. 3A and E). Fig. 3 shows clearly that the microglial activation is mainly located in the hippocampus, thalamus and amygdalo/entorhinal cortex in the group with 380 mg/kg dose (Fig. 3J and K). This activation had its peak at 2 W (Fig. 3J and K). It was followed by a slow recovery observed at 8 W, though partial microglial activation could still be detected (Fig. 3N and M).

4. Discussion

Recent studies have shown that astrocytes and microglia are rapidly activated after pilocarpine insult [29]. However, there is a lack of information on this phenomenon assessed at medium- and long-terms, and the effects of minor doses of this chemoconvulsant on glial populations. The present study provides the first dose–time–course quantitative evidences of medium and long-term astrocyte and microglia morphometric and density changes on the pilocarpine model and its possible relation with the onset of SRSs. We found that with the epileptogenic dose, hippocampus had long-term significant GFAP intermediate filament network alterations and astrocyte density loss. The peak value of astrocyte cytoskeletal hypertrophy and the trough value of astrocyte density coincided with the time-point (4 W) at which

installation of SRSs for this pilocarpine/atropine methylbromide treatment was observed. In contrast, groups treated with fractions of the epileptogenic dose (190 mg/kg and 95 mg/kg) suffered initial astrocytic alterations and cell loss at 2 W, but they were able to restore the measured parameters towards control levels at the 4 W.

It has been shown that chronic microglial reactivity can produce astrocytic dysfunction, including astrocytic cell death, retraction of astrocytic foot processes, loss of aquaporin-4 and connexins [5,13,30], which are crucial for regulation of neuronal oscillations [21,25]. In the 380 mg/kg group, microglial activation peak was observed at 2 W and 4 W and was followed by a slow recovery at 8 W. This is consistent with the astrocyte density loss observed in the 380 mg/kg group at all time-points.

Aberrant GFAP intermediate filament networks and loss of astrocyte density modify the glial regulatory capacity for brain hydroelectrolytic and excitatory amino acid metabolism and the extracellular space [10]. It seemed that under the observed parameters, the limit of glial metabolic regulation capacity was surpassed serving as the triggering factor for the delayed SRSs generation. In an early electron microscopy study, Norenberg and Chu examined rat cerebral cortex in the preictal state following the intraperitoneal injection of aminophylline and observed morphological changes only in astrocytes. These changes consisted chiefly in nuclear and cytoplasmic hydropic alterations, nuclear

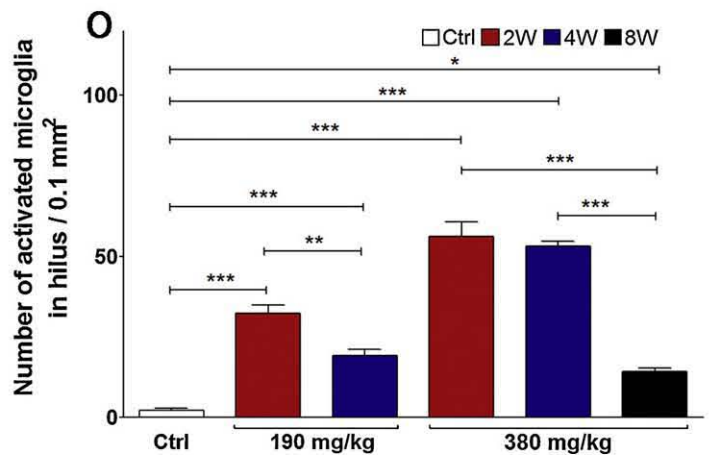
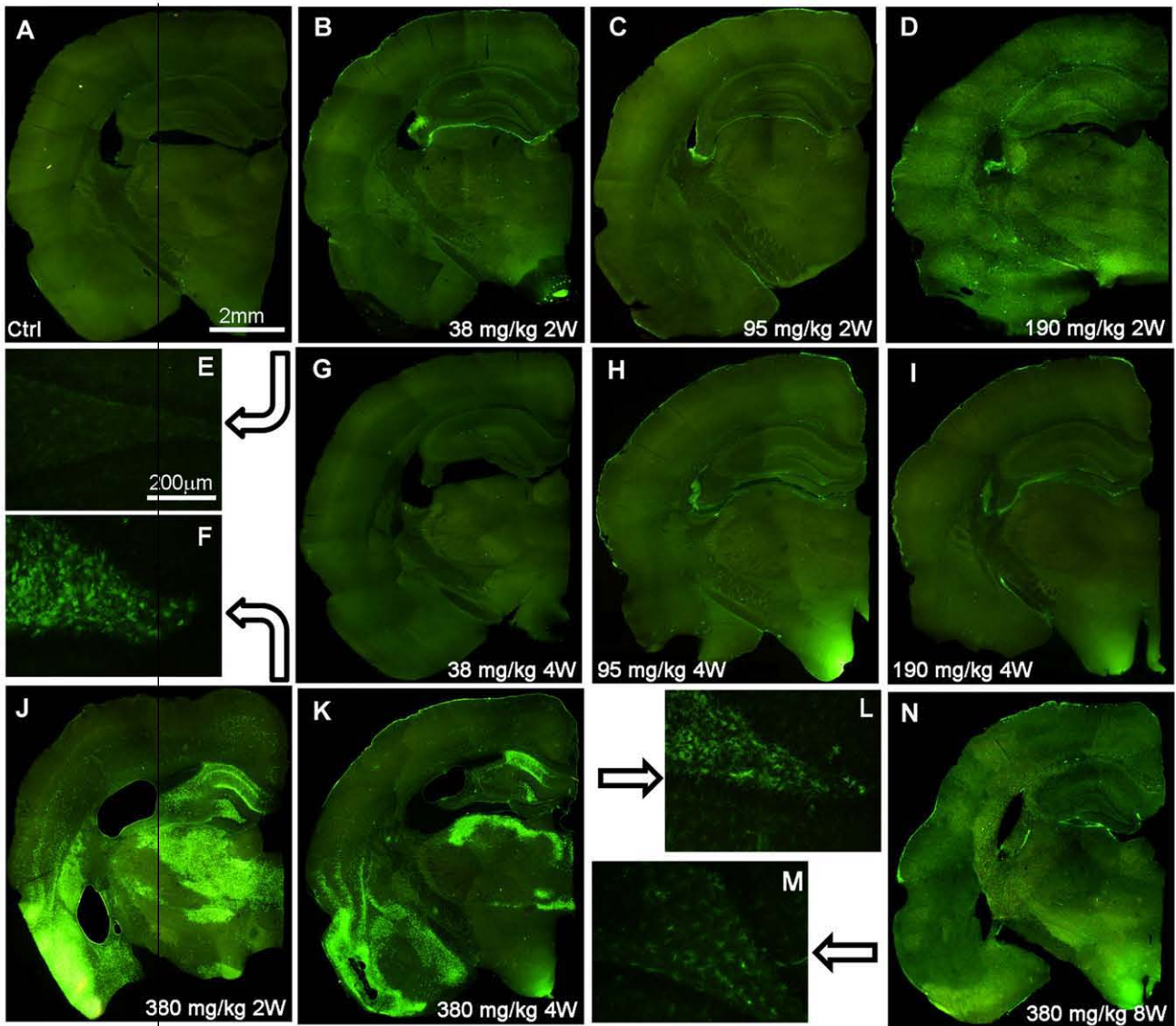


Fig. 3. Dose-dependent temporal evolution of microglial activation. Low-power composed photomicrographs showing the patterns of microglial activation in different dose-groups, except for E, F, L, M, which are 20× photomicrographs of corresponding hila. Timepoints of 2-, 4-, and 8-week were denoted as 2W, 4W and 8W respectively. (O) Quantification of activated microglial cells intensely labelled with CD11b which display bushy/ramified branching patterns in the hilus. * $P < 0.01$, ** $P < 0.01$, *** $P < 0.001$.

chromatin clumping, and a slight increase in cytoplasmic glycogen [22], supporting the observation from this study of massive astrocyte swelling before the expected occurrence of SRSs (Fig. 1E and J). Moreover, Guo et al. [8] measured the regional normalized

cerebral metabolic rate for glucose with (18)F-fluorodeoxyglucose using small positron emission tomography (PET) in animals receiving systemic pilocarpine administration in day 2 (early), day 7 (latent) and day 42 (chronic phase) after the initial SE,

finding specific spatiotemporal changes in glucose utilization in rats during the course of epileptogenesis. Interestingly, they found that in the early phase, limbic structures underwent the largest decrease in glucose utilization. Most brain structures were still hypometabolic in the latent phase and recovered in the chronic phase. However, the hippocampus and thalamus presented persistent hypometabolism during epileptogenesis. Although there is only fragmentary knowledge concerning the relationship between specific cell type activation and the cerebral metabolic rate seen through PET and functional imaging data is commonly interpreted in terms of the underlying neuronal activity, glial cells vastly outnumber neurons. Besides, a number of recent studies imply that astrocytes are likely to play a key role in regulating cerebral blood delivery. Therefore, by mediating neurometabolic and neurovascular processes throughout the CNS, astrocytes could provide a common physiological basis for neuroimaging signals [6]. Hence, the results from Guo and cols. [8] support our data, showing a marked loss of astroglia in the dentate gyrus of the group treated with the epileptogenic dose of pilocarpine.

Brain blood flow and oxygen metabolism provide the basis for normal brain function. Some recent studies associate CNS inflammation with breakdown of the blood brain barrier (BBB), inducing seizures and contributing to its progression [19]. Our data regarding astrocyte density loss and aberrant morphology are coherent with a possible BBB breakdown, which could be contributing to the installation of the SRSs.

Concluding, in this study we have provided evidence showing that a long-term gradual loss of glial resilience is present in the group treated with the epileptogenic dose of pilocarpine. The temporal and spatial coexistence of astrocyte pathology, i.e. massive astrocytic enlargement and a dramatic increase in GFAP expression of individual astrocytes and the lowest astrocytic density detected in hippocampus occurring around the time of SRSs installation raises the possibility of a causal relationship between these two phenomena.

Author contributions

Conceived and designed the experiments: FSE, LZ. Performed the experiments: FSE, VSH, ELH. Analyzed the data: FSE, VSH, AACM, AE, LZ. Contributed reagents/materials/analysis tools: LZ, HS. Wrote the paper: LZ, FSE, AACM. Revised the manuscript critically for important intellectual content: all authors.

Acknowledgement

This study was supported by grants: CONACYT: 79641, 127777. FSE, VSH were supported by CONACYT PhD scholarships. We thank Tzipe Govezensky, Mauricio Medina and María José Gómora Herrera for their technical assistance.

References

- [1] P.S. Buckmaster, F.H. Lew, Rapamycin suppresses mossy fiber sprouting but not seizure frequency in a mouse model of temporal lobe epilepsy, *J. Neurosci.* 31 (2011) 2337–2347.
- [2] J. Casullo, K. Krnjevic, Glial potentials in hippocampus, *Can. J. Physiol. Pharmacol.* 65 (1987) 847–855.
- [3] G. Curia, D. Longo, G. Biagini, R.S. Jones, M. Avoli, The pilocarpine model of temporal lobe epilepsy, *J. Neurosci. Methods* 172 (2008) 143–157.
- [4] M. Esclapez, J.C. Hirsch, Y. Ben-Ari, C. Bernard, Newly formed excitatory pathways provide a substrate for hyperexcitability in experimental temporal lobe epilepsy, *J. Comp. Neurol.* 408 (1999) 449–460.
- [5] P.M. Faustmann, C.G. Haase, S. Romberg, D. Hinkerohe, D. Szlachta, D. Smikalla, D. Krause, R. Dermietzel, Microglia activation influences dye coupling and Cx43 expression of the astrocytic network, *Glia* 42 (2003) 101–108.
- [6] C.R. Figley, P.W. Stroman, The role(s) of astrocytes and astrocyte activity in neurometabolism, neurovascular coupling, and the production of functional neuroimaging signals, *Eur. J. Neurosci.* 33 (2011) 577–588.
- [7] M. Frotscher, P. Jonas, R.S. Sloviter, Synapses formed by normal and abnormal hippocampal mossy fibers, *Cell Tissue Res.* 326 (2006) 361–367.
- [8] Y. Guo, F. Gao, S. Wang, Y. Ding, H. Zhang, J. Wang, M.P. Ding, In vivo mapping of temporospatial changes in glucose utilization in rat brain during epileptogenesis: an 18F-fluorodeoxyglucose-small animal positron emission tomography study, *Neuroscience* 162 (2009) 972–979.
- [9] S.E. Hamilton, M.D. Loose, M. Qi, A.I. Levey, B. Hille, G.S. McKnight, R.L. Idzarda, N.M. Nathanson, Disruption of the m1 receptor gene ablates muscarinic receptor-dependent M current regulation and seizure activity in mice, *Proc. Natl. Acad. Sci. U.S.A.* 94 (1997) 13311–13316.
- [10] G.I. Hatton, *Glial Neuronal Signaling*, Kluwer Academic Publishers, 2004, 26 pp.
- [11] T.C. Kang, D.S. Kim, S.E. Kwak, J.E. Kim, M.H. Won, D.W. Kim, S.Y. Choi, O.S. Kwon, Epileptogenic roles of astroglial death and regeneration in the dentate gyrus of experimental temporal lobe epilepsy, *Glia* 54 (2006) 258–271.
- [12] H. Kettenmann, B.R. Ransom, *Neuroglia*, Oxford University Press, Oxford, 2005, xix, 601 pp.
- [13] J.E. Kim, S.I. Yeo, H.J. Ryu, M.J. Kim, D.S. Kim, S.M. Jo, T.C. Kang, Astroglial loss and edema formation in the rat piriform cortex and hippocampus following pilocarpine-induced status epilepticus, *J. Comp. Neurol.* 518 (2010) 4612–4628.
- [14] D.S. Kim, J.E. Kim, S.E. Kwak, K.C. Choi, D.W. Kim, O.S. Kwon, S.Y. Choi, T.C. Kang, Spatiotemporal characteristics of astroglial death in the rat hippocampal–entorhinal complex following pilocarpine-induced status epilepticus, *J. Comp. Neurol.* 511 (2008) 581–598.
- [15] M. Kobayashi, P.S. Buckmaster, Reduced inhibition of dentate granule cells in a model of temporal lobe epilepsy, *J. Neurosci.* 23 (2003) 2440–2452.
- [16] S.W. Kuffler, J.G. Nicholls, R.K. Orkand, Physiological properties of glial cells in the central nervous system of amphibia, *J. Neurophysiol.* 29 (1966) 768–787.
- [17] S.E. Kwak, J.E. Kim, D.S. Kim, M.H. Won, H.J. Lee, S.Y. Choi, O.S. Kwon, J.S. Kim, T.C. Kang, Differential paired-pulse responses between the CA1 region and the dentate gyrus are related to altered CLC-2 immunoreactivity in the pilocarpine-induced rat epilepsy model, *Brain Res.* 1115 (2006) 162–168.
- [18] Z. Liu, T. Nagao, G.C. Desjardins, P. Gloor, M. Avoli, Quantitative evaluation of neuronal loss in the dorsal hippocampus in rats with long-term pilocarpine seizures, *Epilepsy Res.* 17 (1994) 237–247.
- [19] N. Marchi, E. Oby, A. Batra, L. Uva, M. De Curtis, N. Hernandez, A. Van Boxel-Dezaire, I. Najm, D. Janigro, In vivo and in vitro effects of pilocarpine: relevance to ictogenesis, *Epilepsia* 48 (2007) 1934–1946.
- [20] J. Middeldorp, E.M. Hol, GFAP in health and disease, *Prog. Neurobiol.* 93 (2011) 421–443.
- [21] M. Nedergaard, B. Ransom, S.A. Goldman, New roles for astrocytes: redefining the functional architecture of the brain, *Trends Neurosci.* 26 (2003) 523–530.
- [22] M.D. Norenberg, N.S. Chu, Aminophylline-induced preictal alterations in cortical astrocytes, *Exp. Neurol.* 54 (1977) 340–351.
- [23] N. Otani, H. Nawashiro, S. Fukui, H. Ooigawa, A. Ohsumi, T. Toyooka, K. Shima, H. Gomi, M. Brenner, Enhanced hippocampal neurodegeneration after traumatic or kainate excitotoxicity in GFAP-null mice, *J. Clin. Neurosci.* 13 (2006) 934–938.
- [24] R.J. Racine, Modification of seizure activity by electrical stimulation. II. Motor seizure, *Electroencephalogr. Clin. Neurophysiol.* 32 (1972) 281–294.
- [25] B. Ransom, T. Behar, M. Nedergaard, New roles for astrocytes (stars at last), *Trends Neurosci.* 26 (2003) 520–522.
- [26] A.P. Robinson, T.M. White, D.W. Mason, Macrophage heterogeneity in the rat as delineated by two monoclonal antibodies MRC OX-41 and MRC OX-42, the latter recognizing complement receptor type 3, *Immunology* 57 (1986) 239–247.
- [27] F.A. Scorza, R.M. Arida, G. Naffah-Mazzacoratti Mda, D.A. Scerni, L. Calderazzo, E.A. Cavalheiro, The pilocarpine model of epilepsy: what have we learned? *An. Acad. Bras. Cienc.* 81 (2009) 345–365.
- [28] G. Seifert, G. Carmignoto, C. Steinhilber, Astrocyte dysfunction in epilepsy, *Brain Res. Rev.* 63 (2010) 212–221.
- [29] L.A. Shapiro, L. Wang, C.E. Ribak, Rapid astrocyte and microglial activation following pilocarpine-induced seizures in rats, *Epilepsia* 49 (Suppl. 2) (2008) 33–41.
- [30] R. Sharma, M.T. Fischer, J. Bauer, P.A. Felts, K.J. Smith, T. Misu, K. Fujihara, M. Bradl, H. Lassmann, Inflammation induced by innate immunity in the central nervous system leads to primary astrocyte dysfunction followed by demyelination, *Acta Neuropathol.* 120 (2010) 223–236.
- [31] D.A. Sholl, Dendritic organization in the neurons of the visual and motor cortices of the cat, *J. Anat.* 87 (1953) 387–406.
- [32] D.L. Tauck, J.V. Nadler, Evidence of functional mossy fiber sprouting in hippocampal formation of kainic acid-treated rats, *J. Neurosci.* 5 (1985) 1016–1022.
- [33] B.R.R.S.B. Tekkok, The glial-neuronal interaction and signaling: an introduction, in: V.P.G. Hatton (Ed.), *Glial-neuronal Signaling*, Kluwer Academic Publishers, Boston, 2004, pp. 1–20.
- [34] W.A. Turski, E.A. Cavalheiro, M. Schwarz, S.J. Czuczwar, Z. Kleinrok, L. Turski, Limbic seizures produced by pilocarpine in rats: behavioural, electroencephalographic and neuropathological study, *Behav. Brain Res.* 9 (1983) 315–335.
- [35] F. Yang, Z.R. Liu, J. Chen, S.J. Zhang, Q.Y. Quan, Y.G. Huang, W. Jiang, Roles of astrocytes and microglia in seizure-induced aberrant neurogenesis in the hippocampus of adult rats, *J. Neurosci. Res.* 88 (2010) 519–529.
- [36] L. Zhang, A.A. Corona-Morales, A. Vega-Gonzalez, J. Garcia-Estrada, A. Escobar, Dietary tryptophan restriction in rats triggers astrocyte cytoskeletal hypertrophy in hippocampus and amygdala, *Neurosci. Lett.* 450 (2009) 242–245.

Astrogliosis is temporally correlated with enhanced neurogenesis in adult rat hippocampus following a glucoprivic insult

Estrada F. S. , **Hernández V. S.**, Medina M. P.,
Corona-Morales A. A., Gonzalez-Perez O.,
Vega-Gonzalez A., Zhang L.

.Neurosci Lett, 2009, 459: 109-14

My contributions in:

- Conception of the study: -
- Performance of the experiments:
 - o Glucoprivic insult +
 - o Immunohistochemistry for neuro- glio- genesis markers ++
 - o Image analysis and quantification ++
- Statistical analysis: +
- Discussion of the results: ++
- Preparation of the paper: -

(-): No contribution; (+): Average contribution; (++): Important contribution;



Astroglialosis is temporally correlated with enhanced neurogenesis in adult rat hippocampus following a glucoprivic insult

Felipe S. Estrada^a, Vito S. Hernandez^a, Mauricio P. Medina^a, Aleph A. Corona-Morales^{a,b}, Oscar Gonzalez-Perez^c, Arturo Vega-Gonzalez^a, Limei Zhang^{a,*}

^a Departamento de Fisiología, Facultad de Medicina, Universidad Nacional Autónoma de México, Av. Universidad 3000, México D. F., 04510, Mexico

^b Dirección General de Investigaciones, Universidad Veracruzana, Xalapa, Mexico

^c Lab. Neurociencias, Facultad de Psicología, Universidad de Colima, Colima, Mexico

ARTICLE INFO

Article history:

Received 17 March 2009

Received in revised form 23 April 2009

Accepted 6 May 2009

Keywords:

2-Deoxy-D-glucose

BrdU

GFAP

NeuN

DCX

ABSTRACT

2-Deoxy-D-glucose (2-DG) administration causes transient depletion of glucose derivatives and ATP. Hence, it can be used in a model system to study the effects of a mild glucoprivic brain insult mimicking transient hypoglycemia, which often occurs when insulin or oral hypoglycemic agents are administered for diabetes control. In the present study, the effect of a single 2-DG application (500 mg/kg, a clinically applicable dose) on glial reactivity and neurogenesis in adult rat hippocampus was examined, as well as a possible temporal correlation between these two phenomena. Post-insult (PI) glial reactivity time course was assessed by immunoreaction against glial-fibrillary acidic protein (GFAP) during the following 5 consecutive days. A clear increase of GFAP immunoreactivity in hilus was observed from 48 to 96 h PI. Moreover, enhanced labeling of long radial processes in the granule cell layer adjacent to hilus was evidenced. On the other hand, a transient increase of progenitor cell proliferation was detected in the subgranular zone, prominently at 48 h PI, coinciding with the temporal peak of glial activation. This increase resulted in an augment of neuroblasts double labeled with 5-bromo-deoxyuridine (BrdU) and with double cortin (DCX) at day 7 PI. Around half of these cells survived 28 days showing matured neuronal phenotype double labeled by BrdU and a neuronal specific nuclear protein marker (NeuN). These findings suggest that a transient neuroglycoprivic state exerts a short-term effect on glial activation that possibly triggers a long-term effect on neurogenesis in hippocampus.

© 2009 Elsevier Ireland Ltd. All rights reserved.

Transient hypoglycemia occurs frequently when insulin or oral hypoglycemic agents are administered for diabetes control; depending on the severity of this metabolic disorder, temporal and long lasting autonomic, neuro-endocrine and behavioral responses could be induced [22]. Glucose is the most important source of energy for brain metabolism. Reduction of cellular glucose utilization (glucoprivation) increases aspartate and glutamate levels during and after the glycopenic insult inducing a sustained activation of glutamate receptors that results in an excitotoxic neuropathology in which certain neurons are selectively killed [1,2]. Hypoglycemia-induced neuronal death occurs predominantly in the hippocampal formation, superficial layers of the cortex, and striatum [2], probably contributing to neurological sequelae such as cognitive decline. Clinical studies have reported that significant learning and memory deficits correlate with the frequency of hypoglycemia not only in patients with type 1 diabetes but also in the younger group among the population with type 2 diabetes

[6]. Despite the high incidence of this common complication for diabetes control, the specific pathophysiological changes derived from glucoprivic brain insult and the mechanisms that contribute to brain repair are still not well defined.

Glial cells have been demonstrated as participating in a vast number of brain transactions, both normal and pathological. They exert a particular prominent role in the repairing processes responding to all forms of central nervous system insults [19]. The astroglial cells become reactive (astroglialosis) after a particular insult by increasing the synthesis of glial-fibrillary acidic protein (GFAP), the main cytoskeletal protein for astrocytes, resulting in hypertrophied somata, thickened and prolonged processes under GFAP immunohistochemical assessment [19,25,26]. There exists substantial information concerning molecules able to induce reactive astrocytosis or about changes in molecular expression during glial activation. Nevertheless, the time course of this process after injury and the specific functions exerted by it are not well defined.

On the other hand, adult neurogenesis has been implicated in processes that lead to neural regeneration following central nervous system disease and injuries. In a rat model of hypoglycemia induced by insulin, Suh et al. [20] reported a transient increase in

* Corresponding author. Tel.: +52 55 56232348; fax: +52 55 56232348.

E-mail address: limei@unam.mx (L. Zhang).

progenitor cell proliferation in the dentate gyrus (DG) subsequent to an extensive neuronal loss, suggesting a remarkable role for ameliorating brain injury by boosting endogenous neural regeneration.

The present experiments aimed to determine several aspects of short- and long-term consequences of a single glucoprivic insult. The first goal was to determine the time courses and the interrelationship of reactive astrogliosis and cell proliferation in the DG of hippocampus subsequent to a mild neuroglucoprivic insult. The second goal was to investigate whether the altered cell proliferation has an impact on neuroblast and mature neuron generation. To establish a neuroglucoprivic model system that could induce specifically a glycopenic brain insult restricting both the adrenal medullary release of epinephrine and the cortical release of glucocorticoids as physiological responses to systemic hypoglycemia, we used the antimetabolic glucose analog 2-deoxy-D-glucose (2-DG). 2-DG has the 2-hydroxyl group replaced by hydrogen. Hence, it cannot undergo further glycolysis. Briefly, 2-DG is taken up into the cell through the glucose transporters [16] and it is phosphorylated by glucose hexokinase to produce 2-deoxy-D-glucose-6-phosphate. The fact that this molecule cannot be metabolized via the glycolytic pathway causes its gradual accumulation within the cell, followed by the inhibition of glucose-6-phosphate isomerase and the subsequent blockade of the conversion from glucose-6-phosphate to fructose-6-phosphate, a crucial step in this metabolic pathway [11]. This intrinsic property of 2-DG has been applied in clinical pharmacology for the treatment of two common diseases, cancer and epilepsy, in which elevated metabolic demands are required by the pathophysiological states. Moreover, 2-DG crosses the blood–brain barrier so it can be used experimentally to induce neuroglucoprivation.

Ninety-two young Wistar male rats of 300 ± 10 g were used in this study. All animal procedures were approved by the local Bioethical and Biosecurity committees. Animals were housed on an artificial light/dark cycle (light on at 18:00 and light off at 6:00) with temperatures between 20 and 24 °C, adequate ventilation, food and water *ad libitum* unless specified differently. Fig. 1 depicts the general experimental design of the three experiments.

For glucoprivation induction (GI), experimental subjects were injected (i.p.) a single dose (500 mg/kg) of 2-deoxy-D-glucose (2-DG, Sigma–Aldrich) dissolved in 0.9% saline; control groups were injected with saline. Injection was performed at 10:00, denoted as time 0 (Fig. 1, indicated by an arrow), with 4 h of food restriction before and after the injection.

To characterize the time course of reactive astrogliosis, rats were sacrificed at the following time points post-GI: T (T denotes a period of 24 h), $2T$, $3T$, $4T$ and $5T$, $n=6$ for each group (Fig. 1, green group) through transcardial perfusion with 0.9% saline and 4% paraformaldehyde in PB 0.1 M fixative posterior to sodium pentobarbital anesthesia. Coronal sections (50 μ m) of dorsal hippocampus were obtained. For immunostaining, sets of one out every six sections from Bregma -3.2 to -3.8 mm were processed. Mouse anti-GFAP (1:1000, Chemicon) and chicken anti-mouse Alexa fluor 594 (1:1000, Molecular Probes) were used as primary and secondary antibodies, respectively through conventional immunohistochemical procedures. Hilus of DG was photographed and optical density was determined for each group using Fovea Pro 4.0 (Reindeer Graphics).

To characterize the time course of cell proliferation due to the GI in the subgranular zone (SGZ), 5-bromo-2-deoxyuridine (BrdU, Sigma, 50 mg/kg/12 h divided in three injections) was prepared, injected and immunoreacted as described elsewhere [27]. In order to get a relatively precise rate of proliferation near the time point, BrdU injections covered only the immediate 12 h before the perfusions at T , $2T$, $3T$, $4T$, $5T$, $7T$ and $14T$ time points (Fig. 1, orange group). Sections were selected with the same criteria of experiment 1. Rat anti-BrdU (1:1000, Accurate Scientific) and goat anti-rat IgG (Alexa

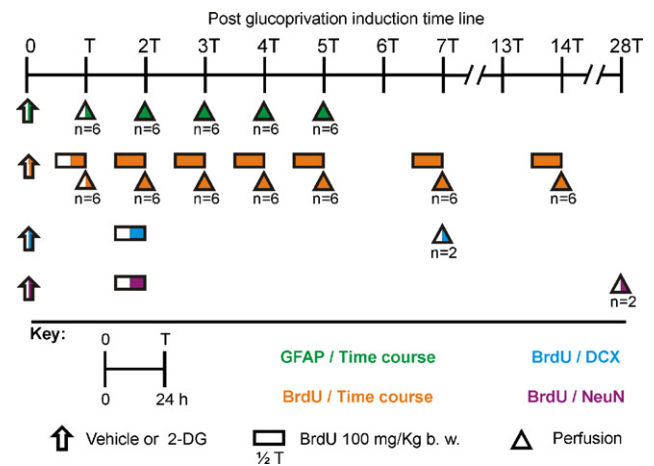


Fig. 1. General experimental design. The time line correlates the experiments performed post-glucoprivation induction (GI). Each interval of time (T) represents a period of 24 h. Glucoprivation was induced by an injection of 2-deoxy-D-glucose at time 0, indicated by an open arrow (saline 0.9% for control group). Semi-filled symbols indicate time points where data from control subjects were obtained. Green color indicates the characterization of time course of reactive astrogliosis reflected in GFAP immunoreactivity; orange color indicates the characterization of time course of altered progenitor cell proliferation by GI in SGZ. Blue and purple colors indicate the evaluations of neurogenesis rates reflected in double labeled neuroblast (BrdU/DCX) and matured neuron (BrdU/NeuN) counting, respectively. Triangles indicate perfusion time points and rectangles denote BrdU exposure time (12 h). A total of 92 Wistar male rats were used, the number of animals per group included in each time point is indicated below the point of perfusion. SGZ: subgranular zone; GFAP: glial-fibrillary acidic protein; BrdU: 5-bromo-deoxyuridine (BrdU); DCX: double cortin; NeuN: neuronal specific nuclear protein.

Fluor 488, 1:1000, Invitrogen) were used as primary and secondary antibodies, respectively. Immunolabeled nuclei across the section in the SGZ-hilus were counted.

To assess the post-GI neurogenesis rate in the time point where highest cell proliferation was observed, rats from experimental and control conditions ($n=4$) were injected with BrdU 12 h previous to $2T$. Half of each group was perfused at $7T$ for BrdU labeled neuroblast detection, using double cortin (DCX) immunolabeling (Fig. 1, blue group), and the other half was perfused at $28T$ for BrdU labeled matured neuron detection, using neuronal specific nuclear protein (NeuN) labeling (Fig. 1, purple group). Perfusion, cutting and section selection were done as described above. Following primary antibodies were used for the corresponding immunoreactions: rat anti-BrdU (1:1000, Accurate Scientific), goat anti-DCX (1:1000, Santa Cruz Biotechnology) and mouse anti-NeuN (1:1000, Chemicon); secondary antibodies: Alexa 488 donkey anti-rat IgG, Alexa 594 rabbit anti-goat IgG and donkey anti-mouse IgG (Molecular Probes). Blind cell counting was performed by two experimentalists directly under fluorescent microscope in the SGZ adjacent to hilus (this region was chosen to set a consistent criterion for all sections). By quickly changing the filters for Alexa 488 and Alexa 594, one can unambiguously identify the double-labeled cell, either BrdU/DCX or BrdU/NeuN.

To evaluate the morphological aspects of the radial glial cell-like processes, we used a modified version of Sholl rings [26]. Briefly, the stereological graticule consists of concentric circles with 10 μ m of distance between each. The cellular somata with their visible branches were placed on the center of the graticule and the number of intersections (NoI) of radial glial cell-like processes projections within the graticule was counted.

Quantitative results were expressed as mean \pm standard error of mean (SEM). Groups were tested for differences by performing one-way ANOVA followed, when appropriate, by the Dunnett's post hoc test using Prism (GraphPad Software Inc., La Jolla, CA, USA). Differences were considered statistically significant at a value $P < 0.05$.

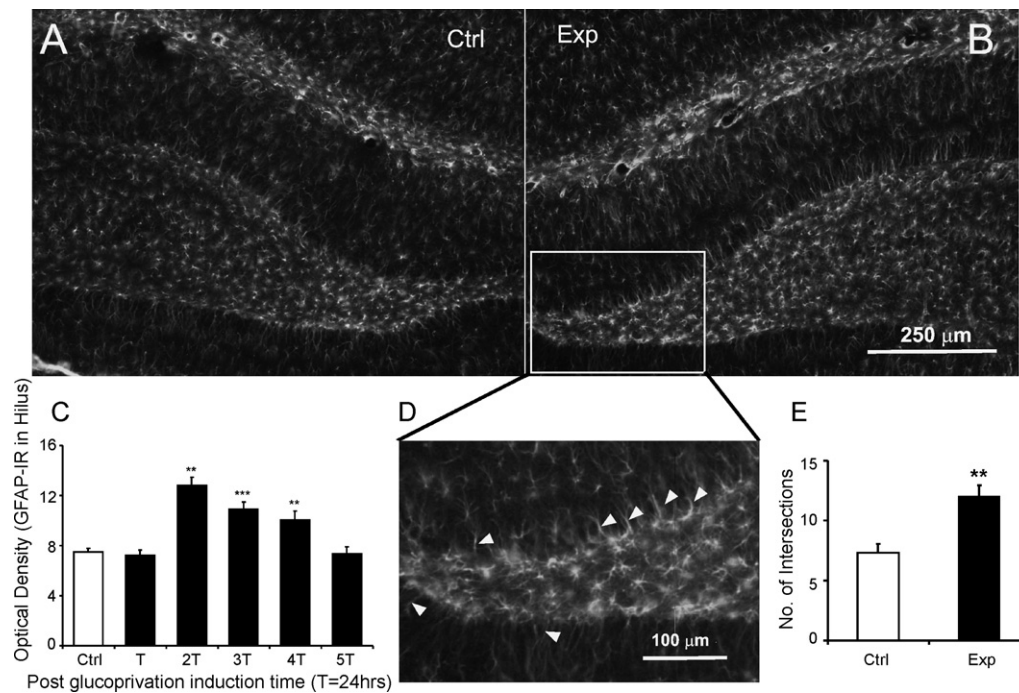


Fig. 2. Representative photomicrographs of GFAP immunohistochemistry in the DG from control (A) and experimental (B) subjects perfused 48 h post-glucoprivation induction (PGI) are shown. Insert (D) shows the hilar region adjacent to the merge region of dorsal and ventral granule cell layers (GCL) with higher magnification. Some radial-like GFAP-IR processes extending into the GCL are indicated by arrowheads. (C) Histogram showing time course of astrocytic reactivity measured by optical density analysis in the hippocampus PGI. $T=24$ h. (E) Quantification of the number of intersections of radial glial cell-like cytoskeletal processes with the modified Sholl rings at 2T. $**P < 0.01$, $***P < 0.001$.

Reactive astrogliosis after a single glucoprivic induction peaked at 48 h post-insult (PI) and remained significantly different to control for 3 days: 1 day after the 2-DG administration, astroglial cells appeared normal under general observation; measurements performed at hilus of hippocampus revealed no difference compared with control. However, optical density at 2T showed a sheer augment of GFAP-IR of almost twofolds, it remained elevated in the following 2 days and decreased to the control level at 5T (Fig. 2C, optical density at Ctrl = 7.50 ± 0.28 ; T = 7.24 ± 0.40 ; 2T = 12.78 ± 0.71 ; 3T = 10.89 ± 0.59 ; 4T = 10.07 ± 0.69 ; 5T = 7.34 ± 0.57). During morphological analysis at 2T, an increase of length (larger number of intersections) of radial glial cell-like processes was observed. These processes arise from GFAP-IR somata located on the border between hilus and granule cell layer (GCL) and extend into GCL more distally than control (Fig. 2E).

A single glucoprivic insult induced by 2-DG altered SGZ progenitor cell proliferation in a time dependent manner with its peak value observed at 48 h PI: immunolabeling revealed an elevation of BrdU+ nuclei at 2T (26.7 ± 3.5), 3T (19.2 ± 0.8) and 4T (21.9 ± 1.9) with the highest value at 2T PI, coinciding with the peak of GFAP-IR. From 5T to 14T, no significant difference of BrdU+ counts between experimental and control (15.5 ± 1.7) was observed (Fig. 3).

Long-term modification on neurogenesis rate was revealed by higher counts of newly formed cells becoming neuroblasts at 7T and matured neurons at 28T in 2-DG rats: the number of BrdU+/DCX+ cells was significantly higher in the 2-DG-injected group (13.63 ± 1.4) than in the control (5.5 ± 1.1 ; Fig. 4). These cells were commonly observed in clusters along the SGZ. To study whether this increased rate of neuroblast formation reaches its final differentiation and become mature neurons, perfusion of animals at 28T PI and immunostained sections with BrdU and NeuN was performed (Fig. 1, purple group). A twofold increase in the number of BrdU+/NeuN+ nuclei was observed in the 2-DG group, compared to the control (5.0 ± 0.5 vs 2.5 ± 0.2 , respectively; Fig. 4).

Hypoglycemia is a major risk factor of insulin and oral hypoglycemic agent therapy for diabetes. Clinical studies revealed that diabetes patients have a greater rate of decline in cognitive function [5]. The mechanisms behind this dysfunction are not well known.

In the present work, experimental rats were treated with the synthetic non-metabolizable glucose analog 2-DG, a molecule used extensively as an inhibitor of glycolysis from bacteria to humans. Experimental rats received a single dose of 500 mg/kg of 2-DG. This single pharmacological dose used in our study specifically blocks brain glucose metabolism in a transient fashion, without producing behavioral effects, coma or convulsions [3]. The brain, in contrast to other tissues, is particularly vulnerable to hypoglycemia due to its critical dependence on glucose for adequate performance. It has

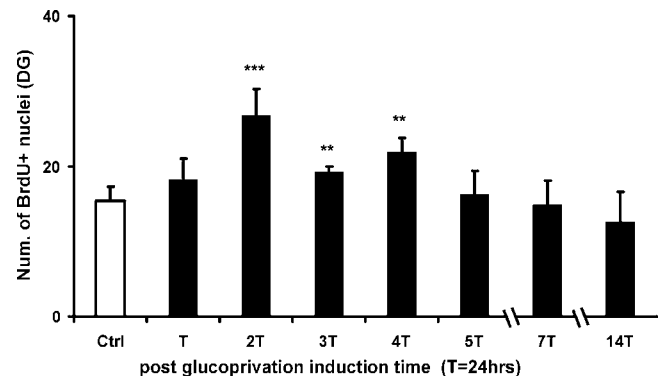


Fig. 3. Histogram showing time course of cell proliferation in the DG post-glucoprivation induction. The temporal effect of a single dose of 2-DG (500 mg/kg) on the number of BrdU nuclei was observed during the first 5 days. Note that the peak in BrdU nuclei temporally coincides with the peak in GFAP expression in the hilus at 2T (Fig. 2), $T=24$ h. $**P < 0.01$, $***P < 0.001$. Counts were obtained from the total numbers of BrdU+ nuclei per section's hilar subgranular zone.

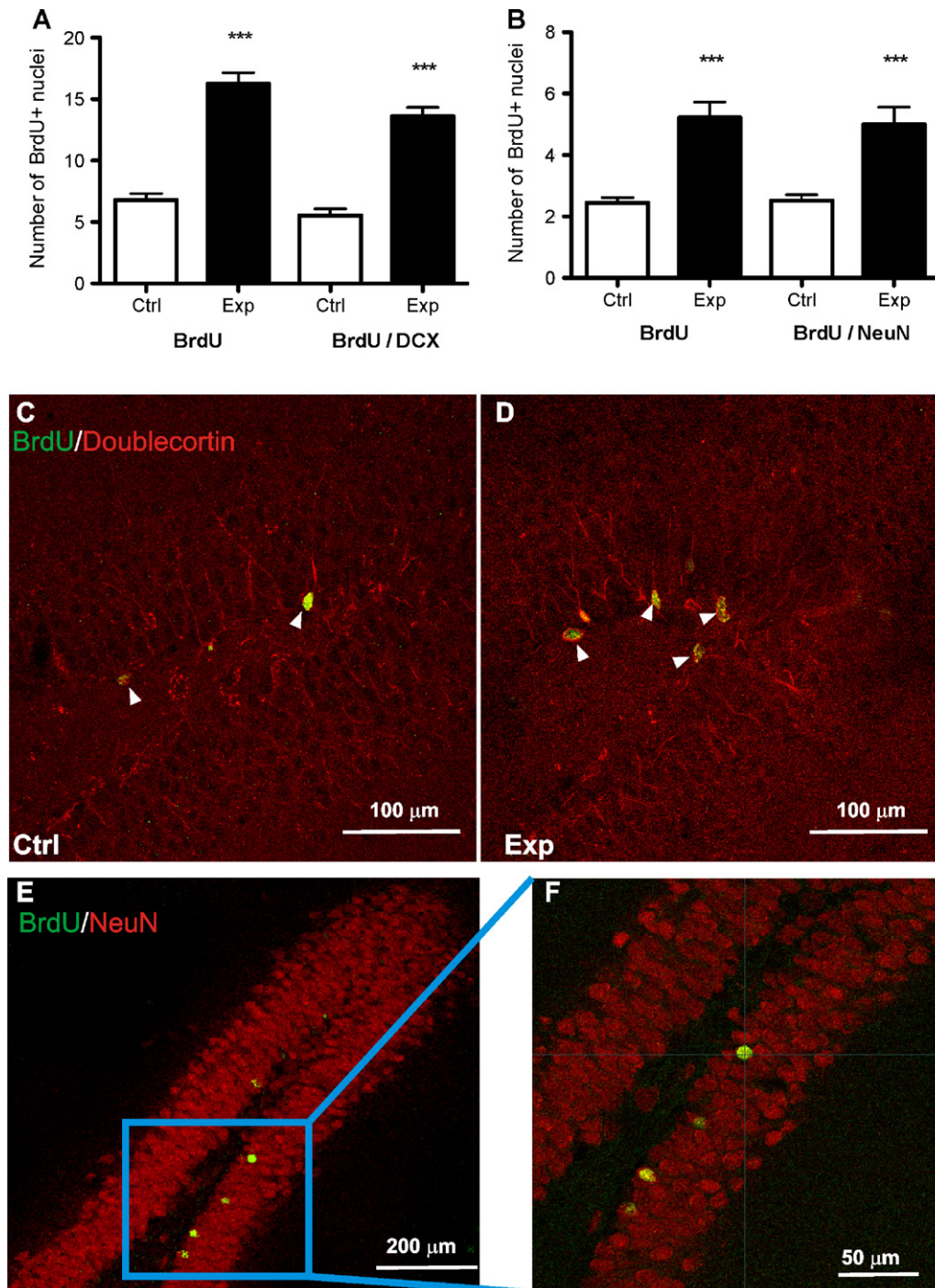


Fig. 4. Effect of transient glucoprivation on neurogenesis in hilar granule cell layer. (A) Histogram showing the number of BrdU+ nuclei and the number of cells BrdU+/DCX+ in control (Ctrl) and experimental (Exp) subjects. (B) Histogram showing the number of BrdU+ nuclei and the number of cells BrdU+/NeuN+ in control (Ctrl) and experimental (Exp) subjects. To analyze the nature of the newly formed neurons induced by 2-DG, BrdU was injected 2 days after the 2-DG dose, taking into account the temporal peak of cell proliferation showed in Fig. 3. (C and D) Representative photomicrographs of double immunohistochemistry for BrdU/DCX (arrowheads) from control (left) and experimental (right) groups. (E) Representative photomicrograph of double immunohistochemistry for BrdU/NeuN. (F) Insert of E. *** $P < 0.001$. Counts were obtained from the total number of double-labeled cells (A) and nuclei (B) per section's hilar subgranular zone.

been shown that neuronal damage and cell death may occur when insulin or other hypoglycemic drugs are administered [4,28]. Studies in human cases and animal models of hypoglycemic brain injury revealed that the dentate gyrus of the hippocampus is preferentially damaged, whereas glial cells are generally spared [1]. Evidence suggests that neuronal death stimulated by hypoglycemia involves a process of excitotoxicity. Hypoglycemia induces neuronal depolarization and therefore raises extracellular glutamate and aspartate

concentrations, leading to sustained activation of glutamatergic receptors. Consequently, there is an increase of Ca^{2+} influx that generates mitochondrial calcium deregulation and excessive production of free radicals, inducing mitochondrial dysfunction and DNA damage, finally conducting to cell death [9,15]. The increase in cell proliferation after 2-DG injection observed in the present study is in accordance with other reports, showing that diverse brain injuries stimulate cell proliferation in the SVZ of the DG [12,23],

probably contributing to the replacement and repair of damaged tissue.

Astrocytes are involved in normal brain functioning through intense interactions with neurons. Astroglial cells also play a pivotal role in brain homeostasis regulation and repairing process after brain injury. The assessment of reactive astrogliosis in the neurogenic regions is of great importance for understanding the mechanisms underlying the integrative response to brain injury. The observed glial reactivity early after 2-DG treatment suggests a change in astrocyte-neuron dynamics, which may include modifications on blood–brain barrier, extrasynaptic space diffusion, neurotrophic factors secretion, neurotransmitter removal [21]. Although the consequences of astrocytic reactivity are a controversial issue [7], there is strong evidence suggesting that altered neuron–glia interactions may be beneficial [8]. Astrocytes have been implicated in reducing neuronal vulnerability to excitotoxicity, since they exert a key role for glutamate uptake within the CNS [18]. Furthermore, due to their high-energy demands and restricted energy stores, neurons are acutely and critically dependent on a stretched regulation of energy metabolism and supply. This metabolic energy regulation is mainly sustained in the brain by astrocytes, as they directly participate in matching glucose supply to neuronal demands [24]. There exists evidence suggesting a core glucose-sensing role in the CNS to the glucose transporter type 2, which is expressed in glial cells, implicating astrocytes as hypoglycemic sensors [13]. Experimental evidence suggests that glucose could be first metabolized by astrocytes, generating extracellular lactate, which is shuttled to the neurons as a substrate for neuronal pyruvate synthesis [17]. Other molecules, like fatty acids and ketone bodies, may also be used as energy sources in the brain under certain circumstances. Astrocytes are the only identified cell type to perform β -oxidation of fatty acids in the brain and they also use fatty acids as precursors for synthesis of ketone bodies that are exchanged with neurons [10].

We have observed a phase-matching relationship between the time courses of both astrogliosis in the hilus of DG, where resides the SGZ – the germinal layer for adult hippocampal neurogenesis – and the cell proliferation rate variation of the same layer post-insult. This observation suggests an intrinsic interrelationship between the two phenomena. Besides, cytoskeletal hypertrophy of radial-glia-like astrocytes towards the deep level of granule cell layer (GCL) was clearly observed. The phenotype, biological properties and the fate of the glial-fibrillary acidic protein-expressing cells in the SGZ are currently of great interest, regarding both normal function and the capacity for ameliorating brain injury. Do all of these GFAP-expressing astrocytes in the SGZ have multipotent neurogenic potential? To answer this question satisfactorily, more detailed knowledge is needed. However, several feasible explanations can be given for this phase-matching condition above mentioned. For instance, it is well documented that astrocytes participate importantly in the creation of the microenvironment—or “niche” that stimulates neurogenesis [29]. In the 2-DG rat SGZ, there were consistent increases of both GFAP immunoreactivity and BrdU+/DCX+ cell counting in the niche-like region where the dorsal and ventral GCL merged (Figs. 2 and 4 photomicrographs). This phenomenon suggests that astrogliosis in this region has an active role in neurogenesis. On the other hand, Muller et al. [14] showed that ciliary neurotrophic factor (CNTF) is necessary for regulating the extent of newly formed neurons in the adult SGZ. In unlesioned brain, CNTF is expressed by astrocytes at low concentrations, whereas its expression increases after a lesion. Thus, the injury-induced neurogenesis can be promoted by a transient increase in CNTF levels by astrocytes. Our finding of similar temporalities of both GFAP immunoreactivity and DG cell proliferation supports this hypothesis.

Acknowledgements

This work was supported by grants IN210406, IN224407 from DGAPA-UNAM and 46141-M, 49740-R, 61344, 79641 from CONACYT-Mexico. FSE, VSH, MPM were recipients of undergraduate scholarship from DGAPA-UNAM through participating in a scientific research program. LZ was on sabbatical leave in MRC Anatomical Neuropharmacology Unit, Oxford University supported by fellowships from DGAPA-UNAM and CONACYT-Mexico.

References

- [1] R.N. Auer, Hypoglycemic brain damage, *Forensic Sci. Int.* 146 (2004) 105–110.
- [2] R.N. Auer, B.K. Siesjö, Hypoglycaemia: brain neurochemistry and neuropathology, *Baillière's Clin. Endocrinol. Metab.* 7 (1993) 611–625.
- [3] A. Breier, A.M. Crane, C. Kennedy, L. Sokoloff, The effects of pharmacologic doses of 2-deoxy-D-glucose on local cerebral blood flow in the awake, unrestrained rat, *Brain Res.* 618 (1993) 277–282.
- [4] P.E. Cryer, Hypoglycemia, functional brain failure, and brain death, *J. Clin. Invest.* 117 (2007) 868–870.
- [5] G.H. Cukierman, J.D. Williamson, Cognitive decline and dementia—systematic overview of prospective observational studies, *Diabetologia* (2005) 2460–2469.
- [6] J. Dey, A. Misra, N.G. Desai, A.K. Mahapatra, M.V. Padma, Cognitive function in younger type II diabetes, *Diabetes Care* 20 (1997) 32–35.
- [7] C. Escartin, K. Pierre, A. Colin, E. Brouillet, T. Delzescaux, M. Guillemier, M. Dhenain, N. Deglon, P. Hantraye, L. Pellerin, G. Bonvento, Activation of astrocytes by CNTF induces metabolic plasticity and increases resistance to metabolic insults, *J. Neurosci.* 27 (2007) 7094–7104.
- [8] J.R. Faulkner, J.E. Herrmann, M.J. Woo, K.E. Tansey, N.B. Doan, M.V. Sofroniew, Reactive astrocytes protect tissue and preserve function after spinal cord injury, *J. Neurosci.* 24 (2004) 2143–2155.
- [9] H. Friberg, T. Wieloch, R.F. Castilho, Mitochondrial oxidative stress after global brain ischemia in rats, *Neurosci. Lett.* 334 (2002) 111–114.
- [10] M. Guzman, C. Blazquez, Is there an astrocyte-neuron ketone body shuttle? *Trends Endocrinol. Metab.* 12 (2001) 169–173.
- [11] R.W. Horton, B.S. Meldrum, H.S. Bachelard, Enzymic and cerebral metabolic effects of 2-deoxy-D-glucose, *J. Neurochem.* 21 (1973) 507–520.
- [12] S.D. Kadam, J.D. Mulholland, J.W. McDonald, A.M. Comi, Neurogenesis and neuronal commitment following ischemia in a new mouse model for neonatal stroke, *Brain Res.* 1208 (2008) 35–45.
- [13] N. Marty, M. Dallaporta, M. Foretz, M. Emery, D. Tarussio, I. Bady, C. Binnert, F. Beermann, B. Thorens, Regulation of glucagon secretion by glucose transporter type 2 (glut2) and astrocyte-dependent glucose sensors, *J. Clin. Invest.* 115 (2005) 3545–3553.
- [14] S. Muller, B.P. Chakrapani, H. Schwegler, H.D. Hofmann, M. Kirsch, Neurogenesis in the dentate gyrus depends on CNTF and STAT3 signaling, *Stem Cells* (2008).
- [15] B. Nelgard, T. Wieloch, Cerebral protection by AMPA- and NMDA-receptor antagonists administered after severe insulin-induced hypoglycemia, *Exp. Brain Res.* 92 (1992) 259–266.
- [16] H. Pelicano, D.S. Martin, R.H. Xu, P. Huang, Glycolysis inhibition for anticancer treatment, *Oncogene* 25 (2006) 4633–4646.
- [17] L. Pellerin, G. Pellegrini, P.G. Bittar, Y. Charnay, C. Bouras, J.L. Martin, N. Stella, P.J. Magistretti, Evidence supporting the existence of an activity-dependent astrocyte–neuron lactate shuttle, *Dev. Neurosci.* 20 (1998) 291–299.
- [18] J.D. Rothstein, M. Dykes-Hoberg, C.A. Pardo, L.A. Bristol, L. Jin, R.W. Kuncl, Y. Kanai, M.A. Hediger, Y. Wang, J.P. Schielke, D.F. Welty, Knockout of glutamate transporters reveals a major role for astroglial transport in excitotoxicity and clearance of glutamate, *Neuron* 16 (1996) 675–686.
- [19] M.V. Sofroniew, Reactive astrocytes in neural repair and protection, *Neuroscientist* 11 (2005) 400–407.
- [20] S.W. Suh, Y. Fan, S.M. Hong, Z. Liu, Y. Matsumori, P.R. Weinstein, R.A. Swanson, J. Liu, Hypoglycemia induces transient neurogenesis and subsequent progenitor cell loss in the rat hippocampus, *Diabetes* 54 (2005) 500–509.
- [21] E. Sykova, Glia and volume transmission during physiological and pathological states, *J. Neural. Transm.* 112 (2005) 137–147.
- [22] C. The Diabetes, G. Complications Trial Research, The effect of intensive treatment of diabetes on the development and progression of long-term complications in insulin-dependent diabetes mellitus, *N. Engl. J. Med.* 329 (1993) 977–986.
- [23] A.B. Tonchev, T. Yamashima, “Transcribing” postischemic neurogenesis: a tale revealing hopes of adult brain repair, *J. Mol. Med.* 85 (2007) 539–542.
- [24] B. Voutsinos-Porche, G. Bonvento, K. Tanaka, P. Steiner, E. Welker, J.Y. Chatton, P.J. Magistretti, L. Pellerin, Glial glutamate transporters mediate a functional metabolic crosstalk between neurons and astrocytes in the mouse developing cortex, *Neuron* 37 (2003) 275–286.
- [25] U. Wilhelmsson, E.A. Bushong, D.L. Price, B.L. Smarr, V. Phung, M. Terada, M.H. Ellisman, M. Pekny, Redefining the concept of reactive astrocytes as cells that remain within their unique domains upon reaction to injury, *Proc. Natl. Acad. Sci. U.S.A.* 103 (2006) 17513–17518.
- [26] L. Zhang, A.A. Corona-Morales, A. Vega-Gonzalez, J. Garcia-Estrada, A. Escobar, Dietary tryptophan restriction in rats triggers astrocyte cytoskeletal hypertrophy in hippocampus and amygdala, *Neurosci. Lett.* 450 (2009) 242–245.

- [27] L. Zhang, L. Guadarrama, A.A. Corona-Morales, A. Vega-Gonzalez, L. Rocha, A. Escobar, Rats subjected to extended L-tryptophan restriction during early postnatal stage exhibit anxious-depressive features and structural changes, *J. Neuropathol. Exp. Neurol.* 65 (2006) 562–570.
- [28] D. Zhou, J. Qian, C.X. Liu, H. Chang, R.P. Sun, Repetitive and profound insulin-induced hypoglycemia results in brain damage in newborn rats: an approach to establish an animal model of brain injury induced by neonatal hypoglycemia, *Eur. J. Pediatr.* 167 (2008) 1169–1174.
- [29] H. Zhu, A. Dahlstrom, Glial fibrillary acidic protein-expressing cells in the neurogenic regions in normal and injured adult brains, *J. Neurosci. Res.* 85 (2007) 2783–2792.

11.3 Presentaciones en congresos nacionales e internacionales

Sponsors

Neurobiology of Stress Workshop

University of Cincinnati

June 17-20, 2014

Cincinnati, OH

Support graciously provided by the following organizations:



- Department of Psychiatry and Behavioral Neuroscience
- Neuroscience Graduate Program
- UC Neuroscience Institute
- Network for Neuroscience Discovery
- The Epilepsy Center



Poster Abstracts

POSTER # 41

ANATOMICAL AND ELECTROPHYSIOLOGICAL CHARACTERIZATION OF VASOPRESSINERGIC INNERVATION IN RAT LATERAL HABENULA

Hernandez, Vito; Vazquez-Juarez, Erika; Chay, Freya; Zhang, Limei, Faculty of Medicine, UNAM, Mexico City, D.F., Mexico

Converging evidence suggest that lateral habenula is an important node in the dorsal diencephalic conduction system, controlling the flux of information between forebrain and midbrain structures including the ventral tegmental area, substantia nigra and raphe nuclei. The synaptic innervation of axons containing the nonapeptide vasopressin to the lateral habenula was first reported by R. M Buijs in the late 70s suggesting that this neuromodulator potentially influences the activity of mesencephalic nuclei through regulating the activity of lateral habenular neurons. However it remains unknown what are the regional and cellular targets of the vasopressinergic fibers in habenula, and how vasopressin modulates the activity of habenular cells. In order to identify the vasopressinergic fiber's distribution and targets in the habenula, we performed immunohistochemistry against vasopressin, and characterized its innervation pattern. We found dense vasopressinergic innervation restricted to the medial part of lateral habenula. At electron microscopy level, we found that AVP containing fibers establish asymmetric synapses with lateral habenular neurons. By using acute slice patch clamp recording and bath application of vasopressin (10 nM), we found that AVP increased the firing rate (FR) (50%, some of them were identified to be vGAT+), or decrease in FR (30%) or had no effects (20%) of lateral habenular recorded neurons. Our results suggest that the neuropeptide vasopressin, by altering the firing characteristics of lateral habenular neurons, modulate the intra-habenular processing of information.

POSTER # 42

A GENOME-WIDE TARGETED CAPTURE INVESTIGATION OF DNA METHYLATION CHANGES IN CHRONIC SOCIAL DEFEAT STRESS

Hing, Benjamin; Bair, Tom; Dubravka, Jancic Potash, Jame; McKaine, Melissa; Braun, Patricia, University of Iowa, Iowa City, Iowa; Tamashiro, Kellie; Cordner, Zachary, The Johns Hopkins University School of Medicine, Baltimore, MD

Stress is a significant risk factor for mood and anxiety disorders. This could be mediated through epigenetic factors, such as DNA methylation, which can influence gene expression. Although previous studies have identified individual loci where changes in DNA methylation can contribute to anxiety and depression-like behavior, genome-wide assessment has not been done. Using a state-of-the-art genome-wide assay called Methyl-Seq, the current study investigates genome-wide DNA methylation from dentate gyrus of mice exposed to an animal model of stress called social defeat stress. The Methyl-Seq approach involves capturing ~100MB of CpG islands and shores, promoters, and regulatory regions across the mouse genome with the Agilent SureSelect kit. DNA was sequenced with the Illumina HiSeq, and the data was analyzed with the Bismark and GeneSpring programs. Mice exposed to a 14 day protocol of chronic social stress displayed anxiety-like behavior as assessed by elevated plus maze and open field test. Using Methyl-Seq, ~50 million reads per genome were uniquely aligned to the mouse genome giving an average depth of coverage of ~40X. Of ~86 million CpGs analyzed, ~35% (~30 million) were observed to be methylated. From these, 0.02% was differentially methylated (~5,000 CpGs). The majority of these were detected outside of CpG islands. Differentially methylated regions were identified in genes or upstream of genes involved in diverse cellular and molecular processes such as the Wnt signaling pathway (Wnt7a and Dact3), apoptosis (Aatk), and micro-RNA processing (Drosha). Future studies aim to validate these findings in a separate cohort of chronic stressed mice.

Poster Abstracts

POSTER # 97

MULTI-AXONAL FEATURE OF HYPOTHALAMIC PVN MAGNOCELLULAR VASOPRESSINERGIC NEURONS REVEALED BY IN VIVO JUXTACELLULAR RECORDING: ITS RHYTHMIC CHANGES UNDER OSMOTIC STRESS AND IMPLICATIONS ON PREDATOR FEAR PROCESSING

Vazquez-Juarez, Erika; Hernandez, Vito; Zhang, Limei, Faculty of Medicine, UNAM, Mexico City, D.F., Mexico

Conventional neuroanatomical and immunohistochemical methods may fail to detect the presence of axons of VP magnocellular neurons. The difficulties include the high cell density in the PVN and SON, the changing chemical nature from preprovasopressin to vasopressin during the intra-axonal transport and the uneven axonal distribution of the dense core vesicles. Previous studies using Golgi staining and antidromic activation have suggested the presence of double axonal projections from neurons of hypothalamo-neurohypophysial system (HNS). Here, by using in vivo juxtacellular recording, labelling and post hoc analysis, we show that some PVN vasopressin containing magnocellular neurons possessed multi-axonal projections or axons branching very near the soma projecting to preoptical and anterior hypothalamic area, SCN, thalamus and entering the stria medularis fibre-system probably innervating lateral habenula (LHb). Frequency analysis of LFP showed clear theta rhythms (7-9 Hz) in the region and the osmotic stressor increased the theta power and shifted the frequency band to 8-10 Hz. To evaluate the functional consequence of those intracerebral projections of the HNS, we used predator (cat) fear behavioural test and c-Fos expression to assess the neural processing under osmotic stress. Our data showed a four-fold increase of freezing behaviour and modified Fos expression patterns in hypothalamus, amygdala, LC and LHb. These findings clearly indicate a regulatory role of HNS in stress coping.

POSTER # 98

ROLE OF A CRF RECEPTOR-REGULATED DOPAMINERGIC PROJECTION FROM THE VTA TO THE PRELIMBIC CORTEX IN STRESS-INDUCED RELAPSE

Vranjkovic, Oliver; Blacktop, Jordan; Resch, Jon; Gerndt, Clayton; Baker, David; Mantsch, John, Marquette University Biomedical Science, Milwaukee, WI

The ventral bed nucleus of the stria terminalis (vBNST) has been implicated in stress-induced cocaine use. Here we demonstrate that corticotropin releasing factor (CRF) is expressed in vBNST neurons that innervate the ventral tegmental area (VTA), a site where the CRF receptor antagonist antalarmin prevents reinstatement of cocaine seeking by a stressor, footshock (EFS), following self-administration in rats. Stress-induced reinstatement involves VTA dopamine neurons projecting into the prelimbic cortex (PLC). The objective of this study is to examine whether CRF-mediated activation of mesocortical DA projections to the PLC is also necessary for stress-induced cocaine seeking. To assess the activation of downstream VTA targets associated with stress-induced relapse, we used immunohistochemistry to examine Fos expression in the PLC and other prefrontal subregions in rats that had undergone cocaine self-administration and extinction and were tested for reinstatement in response to EFS or under EFS-free control conditions. Preliminary data show increased Fos immunoreactivity in the PLC is associated with stress-induced reinstatement. The role of VTA CRF receptor-mediated activation of DA projections to the PLC in stress-induced reinstatement was examined using a disconnection approach involving unilateral intra-VTA delivery of the CRFR antagonist, antalarmin (250ng) and contralateral intra-PLC administration of the D1 receptor antagonist, SCH 23390 (200ng). Disconnection of the PLC-VTA pathway blocked stress-induced reinstatement. Examination of the effects of ipsilateral antagonist delivery into the VTA/PLC is in progress. These preliminary findings suggest that CRF receptor activation in the VTA induces relapse to cocaine use by activating DA cells that project to the PLC.

Login to view your options.



July 5-9, 2014
Milan | Italy

[Forum Information](#) [Programme](#) [Industry](#) [My FENS](#) [Help](#) [Advanced Search](#)

All

[Home](#) > [Speakers and Authors](#) > [H](#) > [Person](#) > [Abstract](#)

ABSTRACT

Poster Instructions

Title	ORIGIN, DISTRIBUTION, SYNAPTIC TARGETS AND ELECTROPHYSIOLOGICAL ACTIONS OF VASOPRESSIN INNERVATION IN RAT LATERAL HABENULA: ITS ROLE IN BEHAVIOURAL DESPAIR Room: Poster Area - Session: E05 - Abstract Number: FENS-2595 - Poster Board Number: E008
Poster No:	E008
Presenter:	V. Hernandez
Author(s):	V. Hernandez(1), F. Chay(1), E. Vazquez-Juarez(1), L. Zhang(1)
Affiliation(s):	(1)Fisiología Facultad de Medicina, Universidad Nacional Autónoma de México, Distrito Federal, Mexico
Session:	E05: Poster Session - Stress and the brain - Stress modulated pathways Poster boards: E001-017
Date:	Monday - July 07, 2014 12:15 - 13:15
Location:	Poster Area
Subtopic:	E.6.e Stress modulated pathways
Topic:	E.6 Stress and the brain
Theme:	E. Homeostatic and neuroendocrine systems

The lateral habenula (LHb) is a highly evolutionarily conserved region that connects telencephalic structures with brainstem structures and has been implicated in the selection of behavioral stress coping strategies. In congenitally helpless rats, fluoxetine treatment has been shown to decrease metabolic activity in the habenula and reduce immobility time in the forced swimming test (FST). LHb expresses mainly arginine vasopressin (AVP) V1a receptor, though the presence of V1b receptor is not discarded. However, the role of AVP innervation to LHb in selecting a stress coping strategy is unclear. Here, by using fluorogold retrograde tracing and single cell juxtacellular labelling from hypothalamic paraventricular nucleus (PVN), we demonstrated a direct projection from PVN magnocellular AVP neurons to LHb. We characterized the AVP innervation using immunohistochemistry, finding that the medial division of the LHb is the main target region for AVP innervation. Using electron microscopy, we found that AVP containing fibres establish Gray type I (asymmetric) synapses (N=10) into lateral habenula neurons. Using in-vitro acute slice preparations, we showed that 75% of LHb neurons responded to AVP 0.1nM with hyperpolarization and reduction of their firing rate, while 25% increased their firing rate. A hyperosmotic challenge that potently up-regulates the hypothalamic vasopressin system was capable to increase the c-Fos expression in a specific neuronal population of LHb, correlating with high behavioural despair in FST. The results of this study revealed that the PVN could modulate the activity of LHb, via direct vasopressinergic connections, influencing the selection of stress coping strategies in the rat.

[Home](#) [Forum Information](#) [Programme](#) [Industry](#) [My FENS](#) [Help](#) [Advanced Search](#)

For all queries, please write directly to support@meetingxpert.net.
Support is available from Monday-Friday 08:00-16:00 (GMT).
We currently support Chrome, Firefox, Internet Explorer 9 or newer.

[Print this Page](#)

Presentation Abstract

Program#/Poster#: 642.16/QQ13

Presentation Title: Vasopressin modulates lateral habenula network activity via both V1a and V1b receptors: Dual electrophysiological mechanisms revealed by *in vitro* whole-cell patch clamp recording

Location: WCC Hall A-C

Presentation time: Tuesday, Nov 18, 2014, 1:00 PM - 5:00 PM

Presenter at
Poster: Tue, Nov. 18, 2014, 4:00 PM - 5:00 PM

Topic: ++E.03.e. Hormones and cognition

Authors: ***V. S. HERNANDEZ**, F. CHAY, C. IRLES, L. ZHANG;
Dept. of Physiology, Fac. of Medicine, Natl. Autonomous Univ. of Mexico,
Mexico City, Mexico

Abstract: The lateral habenula (LHb) is an important epithalamic structure within the dorsal diencephalic conduction system, which controls the exchange of information between forebrain and midbrain structures. Its involvement is implicated in a variety of biological functions, including a strikingly powerful role in the regulation of midbrain monoamine release. Glutamatergic projections from the lateral hypothalamus targeting VTA-projecting neurons in the lateral habenula have recently been reported (Poller WC et al, 2013). We have also recently reported (Hernandez and Zhang, SfN, 2013) that vasopressin (VP) containing fibers from the hypothalamic paraventricular nucleus, specifically the medial magnocellular division (PVNmmd), strongly project to the medial division of the LHb. However, little is known about the vasopressin (VP) signaling pathway or the electrophysiological response in the LHb. Using whole cell patch clamp recording in an acute slice preparation of the rat LHb, we demonstrate that the application of VP (10nM) to the recording chamber induces a differential electrophysiological respons. 50% of

recorded neurons increased their firing rate [post-hoc identification revealed some of these neurons to contain vesicular GABA transporter (vGAT)], 30% decreased their firing rate, and 20% had no evident response. Western blot analysis on fresh microdissected habenula revealed a remarkable expression of V1a protein (protein bands: ≈ 47 KDa as well as ≈ 70 KDa, Alomone Avr-010) and the presence of V1b protein as well (protein bands: ≈ 47 KDa as well as ≈ 70 KDa Enzo ADI-905-750), although the latter one was near the limit of detection. The ≈ 70 KDa protein band has been attributed to the glycosylation of the receptors these receptors. These data support the previously reported presence of vasopressin receptors V1a and V1b mRNA in the habenula by in situ hybridization. Moreover, at the electron microscopic level, we found AVP containing fibers establishing asymmetric synapses with lateral habenular neurons (synapse n=10, 100% type I). Our data strongly suggests that the PVN VP population is an upstream element for a function of the LHb that mainly plays an activation role implicated in the promotion of negative rewards

Disclosures: **V.S. Hernandez:** None. **F. Chay:** None. **C. Irlles:** None. **L. Zhang:** None.

Keyword (s): HABENULA

VASOPRESSIN

EPITHALAMUS

Support: CONACyT: 127777

CONACyT: 179616

PAPIIT-DGAPA-UNAM IN216214

PAPIIT-DGAPA-UNAM IA202314

PAPIIT-DGAPA-UNAM IN218111

[Print this Page](#)

Presentation Abstract

Program#/Poster#: 642.09/QQ6

Presentation Title: Límbic-Region projections of vasopressin containing mangocellular neurosecretory neurons revealed by *in vivo* juxtacellular recording and anatomical analysis: its rhythmic changes under osmotic stress and implications on predator fear processing

Location: WCC Hall A-C

Presentation time: Tuesday, Nov 18, 2014, 1:00 PM - 5:00 PM

Presenter at
Poster: Tue, Nov. 18, 2014, 1:00 PM - 2:00 PM

Topic: ++E.03.e. Hormones and cognition

Authors: ***L. ZHANG**, E. VAZQUEZ-JUAREZ, V. S. HERNÁNDEZ;
Facultad de Medicina, Physiology, Medicine, Natl. Autonomous Univ. of Mexico, Mexico City, Mexico

Abstract: Hypothalamic vasopressinergic mangocellular neurosecretory neurons (VP-MNNs) are well known to release their peptidergic contents from neurohypophyseal axonal terminals into the circulation as well as to release VP locally from their dendrites serving as powerful autocrine and paracrine signals to their neighboring neuronal populations. However, the possible crosstalk between these MNNs population and distant neuronal populations has not yet been explored. In order to assess whether this subcortical neuropeptidergic system also exerts fast/precise influence to the limbic regions, we used a combination of electrophysiological approaches, including *in vivo* juxtacellular recording, labeling and frequency analysis, *in vitro* acute slices patch-clamp recording and pharmacological tools, fluorogold retrograde tracing, immunohistochemistry, confocal imaging, electron microscopy and behavioral tests as our study strategy. We show an *in vivo* labelled PVN VP-MNN possessing multiple axons and other axons branching very near the

soma. Beside of the neurohypophyseal axon, neurobiotin labelled axon segments/terminals were found in the preoptical area, anterior hypothalamic area (AHA), suprachiasmatic nucleus, in the thalamus and the lateral habenula (LHb). Frequency analysis of LFP recorded in the PVN showed clear theta rhythms (7-9 HZ) in the region and the osmotic stressor increased the theta power and shifted the frequency band to 8-10 Hz. To evaluate the functional consequence of those intracerebral projections of the MNNs, we used predator fear behavioural test and c-Fos expression to assess the neural circuits involved in fear processing under osmotic stress. Our data showed a four-fold increase of freezing behaviour and modified Fos expression patterns in lateral septum, AHA, ventromedial hypothalamus, amygdala (MeApd, CeC and BLA), locus coeruleus and LHb. These findings clearly indicate a regulatory role of VP-MNNs in stress coping.

Disclosures: **L. Zhang:** None. **E. Vazquez-Juarez:** None. **V.S. Hernández:** None.

Keyword (s): VASOPRESSIN
HYPOTHALAMUS
FEAR

Support: CONACYT grant 127777
CONACYT grant 179616
PAPIIT-DGAPA-UNAM IN216214

[Print this Page](#)

Presentation Abstract

Program#/Poster#: 642.06/QQ3

Presentation Title: Hypertonicity increases arousal and anxiety following predator exposure: The direct and indirect modulation of hypothalamic vasopressin containing magnocellular neurosecretory neurons on Fos expression in limbic regions in rat

Location: WCC Hall A-C

Presentation time: Tuesday, Nov 18, 2014, 1:00 PM - 5:00 PM

Presenter at
Poster: Tue, Nov. 18, 2014, 2:00 PM - 3:00 PM

Topic: ++E.03.e. Hormones and cognition

Authors: ***E. VAZQUEZ-JUAREZ**¹, F. JÁUREGUI-HUERTA², V. S. HERNÁNDEZ¹, L. ZHANG¹;

¹Fac. of Medicine, Physiol., Univ. Nacional Autonoma De Mexico, Mexico City, Mexico; ²Dept. de Neurociencias, Ctr. Universitario de Ciencias de la Salud, Univ. de Guadalajara, Guadalajara, Mexico

Abstract: Hypothalamic vasopressin containing magnocellular neurosecretory neurons (VP-MNNs) are potently upregulated by hypertonicity. Traditionally, it has been considered that this population of neurons almost exclusively projects to the posterior pituitary. However, recent results from our group, together with other few groups, have challenged this notion. We have found by *in vivo* juxtacellular labeling, retrograde tracing and anatomical analysis that a subpopulation of MNNs possess important axonal branches from/near MNN-somata projecting intracerebrally, especially to the limbic regions, such as ventral hippocampus (1), amygdala (2), locus coeruleus (3) and lateral habenula (4). However, the functional implications of these intracerebral projections remain elusive. In order to assess whether a potent upregulation of

this VP-MNN population modulates predator-fear processing and the neuronal activation weights in different nodes of the so called "survival circuit", we used a live-predator (cat) exposure test in rats to assess the changes in behavior and the neuronal activation weights in hypothalamus, amygdala, locus coeruleus, hippocampus, striatum and thalamus, under two conditions: basal and hypertonicity, i.e. 900mM saline, 2% b.w., injected under sevoflurane-inhalation as transient anesthesia, 30min before the behavioral test. Ethological analysis showed significant behavioral modifications in "hypertonicity" group, including a four-fold increase of freezing behaviour. Immunohistochemical assessment of C-Fos expression showed generally sharpened patterns in amygdala, thalamus and hypothalamus. The Fos expression in the basolateral (BLA) and corticomедial (CoMA) nuclei of the amygdala were significantly attenuated, while the expression of central and medial nucleus (the postero-dorsal division (MeApd)) were increased. Remarkable increase of Fos+ nucleus counts was also observed in the locus coeruleus (LC). Immunohistochemical analysis with light and electronic microscopy has showed increased VP immunopositive fibers in MeApd, CeA and LC, where VP containing type I synapse were found. Our data, together with recent findings reported in the literature, suggest that the up-regulation of the VP-MNNs exert strong modulatory effects on fear processing. 1. Zhang L. & Hernandez VS. Neuroscience (2013)228:139-62. 2. Hernandez VS & Zhang L. SfN 2012, abstract. 3. Zhang L. SfN 2008, abstract. 4. Zhang L., Vazquez-Juarez E., Hernandez V. S. SfN 2014, abstract.

Disclosures: **E. Vazquez-Juarez:** None. **F. Jáuregui-Huerta:** None. **V.S. Hernández:** None. **L. Zhang:** None.

Keyword (s): FOS
ELECTRON MICROSCOPY
FEAR

Support: CONACyT Grant 127777
CONACyT Grant 179716
PAPIIT DGAPA-UNAM IN128111
PAPIIT DGAPA-UNAM IN216214

[Print this Page](#)

Presentation Abstract

Program#/Poster#: 382.28/KKK20

Presentation Title: Role of vasopressinergic innervation of habenula in the selection of stress coping strategies in rat

Location: Halls B-H

Presentation time: Monday, Nov 11, 2013, 11:00 AM -12:00 PM

Topic: ++E.05.e. Stress-modulated pathways: Hypothalamus, amygdala, and bed nucleus

Authors: ***V. S. HERNANDEZ**, L. ZHANG;
Dept. of Physiology, Fac. of Medicine, Natl. Autonomous Univ. of Mexico,
Mexico City, Mexico

Abstract: The habenula is an evolutionarily highly conserved region that connects telencephalic structures with brainstem structures and has been implicated in selecting among stress coping behavioural strategies, in particular through the modulation of the dopaminergic and serotonergic systems. In congenitally helpless rats, fluoxetine treatment has been shown to decrease metabolic activity in the habenula and reduce immobility time in the forced swimming test (FST).

Habenula possesses a dense vasopressinergic innervation from hypothalamus, both magno- and parvocellular regions (data unpublished) and express mainly V1a receptor through the presence of V1b receptor is not discarded. Synaptic innervation (Gray type I, glutamatergic mainly) was first demonstrated by Buijs and Swaab (Buijs RM, Swaab DF. Immun-electron microscopical demonstration of vasopressin and oxytocin synapses in the limbic system of the rat. *Cell Tissue Res.* 1979; 204(3): 355-65). However the role of vasopressin innervation to habenula in selecting a stress coping strategy is unclear.

In this study we aim to characterize the effect of up-regulating the vasopressinergic system, on the FST-induced habenular neuronal-activation and the display of learned helplessness behaviour. For this purpose an osmotic challenge was applied to experimental rats by injecting a hypertonic saline solution, 2h before the FST and allowing the rats to drink water ad-libitum for

30 min before the FST, the percentage of immobility episodes was evaluated as a measure of learned helplessness. Fos expression was evaluated in the habenula, as a marker of neuronal activity induced by the FST. Our results show that FST induced an alteration in the pattern of activation of habenular neurons and this is correlated with an increase in immobility in the FST.

Disclosures: **V.S. Hernandez:** None. **L. Zhang:** None.

Keyword(s): VASOPRESSIN

DEPRESSION

habenula

Support: CONACyT 127777

CONACyT 179616

PAPIIT IN218111



8th
FENS
 FORUM OF
 NEUROSCIENCE

July 14–18, 2012
 Barcelona | Spain
 International Convention Center (CCIB)

General Info Programme Login Help Site Map

All

Session Type Posters Daily Authors Presenters Timetable

Home > Welcome > Search > Abstract

ABSTRACT

Poster Instructions

Title: (P116.22) The Vasopressinergic V1b Receptor Antagonist Ssr-149415 Exerts A Differential Effect On Spatial Learning In Normal And Maternally Separated Rats
 Room: Poster Area - Session: P116 - Abstract Number: 271 - Poster Board Number: F107
 Ref.: FENS Abstr., vol 7, p116.22, 2012

Speaker: Vito S.V.S. Hernandez

Author: Hernandez V.S. & Zhang L.

Affiliation: Department of Physiology, Faculty of Medicine, National Autonomous University of Mexico, Mexico City, Mexico

Session: P116: Poster Session - Learning and Memory III
 Poster boards: F86-117

Date: Tuesday - July 17, 2012 11:15 - 13:15 (attendance: 7/17/2012 11:15:00 AM)

Location: Poster Area

Subtopic: F.2.h Learning and memory: pharmacology

Topic: F.2 Animal cognition and behaviour

Theme: F. Cognition and behaviour

The maternal separation model has been shown to affect the normal development of the vasopressinergic system. Previous results from our group showed that adult rats that were subjected to maternal separation during the first two weeks of postnatal life, when exposed to water deprivation, show a steeper rise in the plasmatic concentrations of vasopressin as well as a higher level of anxiety behavior compared with animal facility reared (AFR) animals.

On the other hand it has been demonstrated a significant vasopressinergic innervation to hippocampus, a structure with a key influence on spatial learning and memory. Besides, it has been reported the expression of vasopressin V1b receptors, in dorsal hippocampus, mainly in the CA2 region, but the role of these receptors on spatial learning and memory is still controversial.

The aim of this study is to evaluate the spatial learning and memory processes, in maternally separated and AFR rats, under basal conditions and after modulating the vasopressinergic neurotransmission with the selective V1b receptor antagonist SSR-149415 or with an hyperosmotic NaCl solution.

Home General Info Programme Login Help Site Map

For all queries, please write directly to support@meetingxpert.net.
 Support is available from Monday–Friday 08:00-16:00 (GMT).



8th
FENS
 FORUM OF
 NEUROSCIENCE

July 14–18, 2012
 Barcelona | Spain
 International Convention Center (CCIB)

[General Info](#) [Programme](#) [Login](#) [Help](#) [Site Map](#)

All

[Home](#) > [Welcome](#) > [Search](#) > [Abstract](#) > [Abstract](#)

ABSTRACT

Poster Instructions

Title: (P118.24) Maternal Separation Upregulates Hypothalamic Vasopressin Expression In Rat Early Postnatal And Young Adult Stages: Impacts On Conditioned Anxious State
 Room: Poster Area - Session: P118 - Abstract Number: 268 - Poster Board Number: A24
 Ref.: FENS Abstr., vol 7, p118.24, 2012

Speaker: Limei L. Zhang

Author: Zhang L., Hernández V.S., Nava-Kopp A.T. & Irlés C.

Affiliation: Department of Physiology - Medicine, National Autonomous University of Mexico, Mexico City, Mexico

Session: P118: Poster Session - Epigenetic Factors
 Poster boards: A1-24

Date: Tuesday - July 17, 2012 13:30 - 15:30 (attendance: 7/17/2012 1:30:00 PM)

Location: Poster Area

Subtopic: A.8 Epigenetic factors (hormones, nutrition, experience)

Topic: A.8 Epigenetic factors (hormones, nutrition, experience)

Theme: A. Development

Maternal separation (MS) has been used to model the causal relationship between early life stress and the later stress-over-reactivity and affective disorders. Arginine vasopressin (AVP) is among several factors reported to be abnormal. The role of AVP on anxiety is still unclear. In order to further investigate this causal relationship and its possible role in anxiogenesis, male rat pups were separated from their dams for 3 hours daily (3hMS) from post-natal day (PND) 2 to 15. Fos expression in AVP containing hypothalamic paraventricular (PVN) and the supraoptic nuclei (SON) triggered by 3hMS and AVP-mRNA expression were examined at PND10 and PND21 whereas AVP-mRNA expression, PVN and SON volumes and plasma AVP concentration were assessed in young adulthood. Elevated plus maze test (EPM) and Vogel conflict Test (VCT) were also performed to evaluate unconditioned and conditioned anxious states at PND70-75. At PND10, a single 3hMS event increased the Fos expression in AVP+ neurons four-fold in PVN and six- to twelvefold in SON. AVP-mRNA was over-expressed in whole hypothalamus, PVN and SON, as high as 142%, observed at PND21 and PND62. Volumes of PVN and SON measured at PND75 had marked increases so as for AVP plasma concentration at 12 hr of water deprivation. MS rats demonstrated high conditioned anxious state under VCT paradigm whereas no difference was found under EPM. These data describe significant AVP-related molecular, anatomical and behavioral abnormalities in MS rat model and indicate a casual relationship between high conditioned anxiety and potentiated AVP system in MS male rats.

[Home](#) [General Info](#) [Programme](#) [Login](#) [Help](#) [Site Map](#)

For all queries, please write directly to support@meetingxpert.net.
 Support is available from Monday–Friday 08:00-16:00 (GMT).

[Print this Page](#)**NEUROSCIENCE 2012**

Presentation Abstract

Program#/Poster#: 737.06/B12

Presentation Title: [Vasopressin containing fibers distribution and synaptic innervation in the medial and central amygdala: an immunohistochemical study using light and electron microscopy](#)

Location: Hall F-J

Presentation time: Wednesday, Oct 17, 2012, 9:00 AM -10:00 AM

Authors: ***V. S. HERNANDEZ**, L. ZHANG;
Dept. of Physiology, Fac. of Medicine, Natl. Autonomous Univ. of Mexico,
Mexico City, Mexico

Abstract: Arginine-vasopressin (AVP) is an important neuropeptide modulating a wide range of central nervous system (CNS) functions. Synapses containing AVP immunoreactivity have been only reported in the lateral septum, medial amygdala and thalamic lateral habenular nucleus (Buijs and Swaab, 1979) and paraventricular nucleus of the hypothalamus (Zhang et al, 2010) of the rat and suprachiasmatic nuclei of mouse (Castel et al., 1990) and the information about the co-localization with other neurotransmitters remained unclear. In this study, we made a detailed anatomical study on the AVP immunopositive fiber distribution across the central, medial and lateral amygdala through 3D NeuroLucida mapping and density analysis using NeuronJ for ImageJ. The neurotransmitter-colocalization and ultra-structure of the synapses were investigated. The results from our study demonstrated that: 1) the medial amygdala is the most densely innervated region by vasopressinergic fibres; 2) thick and thin axons can be observed in the region; 3) thick axons in medial amygdala colocalize with vesicular glutamate transporter 2 (vGlut2); 4) At electron microscopy level, both types, the thick axons (type A) with high ratio between dense-core vesicles and small clear vesicles and the thin axons (type B) with low ratio of previous parameter were able to establish conventional synaptic connections. 5) Both Gray type I and Gray type II synapses were found containing AVP immunoreactivity.

Disclosures: **V.S. Hernandez:** None. **L. Zhang:** None.

Keyword(s): VASOPRESSIN

AMYGDALA

ELECTRON MICROSCOPY

Support:

CONACyT 79641

CONACyT 127777

PAPIIT UNAM IN218111

[Authors]. [Abstract Title]. Program No. XXX.XX. 2012 Neuroscience Meeting Planner. New Orleans, LA: Society for Neuroscience, 2012. Online.

2012 Copyright by the Society for Neuroscience all rights reserved.

Permission to republish any abstract or part of any abstract in any form must be obtained in writing by SfN office prior to publication.

I Congreso FALAN

55 Congreso Nacional de Ciencias Fisiológicas
Neurociencias y Neurobiología de México

Cancún 2012
November 4 to 9

Federación de Asociaciones Latinoamericanas y del Caribe de Neurociencias

Date: 06/19/2012

Corresponding author

Name:	Vito Hernandez		
Email:	no.vito.no@gmail.com		
Country:	Mexico	Phone (work)	52 5556232348
Institutional affiliation	Universidad Nacional Autónoma de México, Facultad de Medicina, Departamento de Fisiología		

Authors

	Name	Institutional affiliation	Country
1	Hernandez Vito S	Universidad Nacional Autónoma de México, Facultad de Medicina, Departamento de Fisiología	Mexico
2	Zhang Limei	Universidad Nacional Autónoma de México, Facultad de Medicina, Departamento de Fisiología	Mexico
3			
4			
5			
6			
7			
8			
9			
10			
11			
12			

Abstract

keywords:	Toxicology,Cognitive function,Learning and memory,Receptors,Dopamine, Levodopa		
Type of presentation	Poster		
Authors:	Hernandez VS(1), Zhang Limei(1) (1) Universidad Nacional Autónoma de México, Facultad de Medicina, Departamento de Fisiología		

Effects of chronic levodopa treatment on hippocampal dopamine receptors and spatial learning: a comparative study in young and aged intact rats

Levodopa is the direct precursor of dopamine and is widely used for the treatment of Parkinson's disease. It is known that chronic pulsatile levodopa treatment can induce damage to the dopaminergic system demonstrated in vitro or in damaged-dopaminergic animal models. However, the age susceptibility for this treatment has not been properly evaluated. In order to evaluate the effects of a chronic pulsatile treatment of levodopa on hippocampal dependent spatial learning, comparing aged and young male intact wistar rats, 12.5mg of levodopa plus 1.25 mg of carbidopa per kg were administered twice daily during 4 weeks. Dopamine receptors D2r and D5r expression in the dentate gyrus (DG) and CA 1-3 were evaluated immunohistochemically using confocal microscope. Spatial learning during the late phase of the interval between levodopa administrations was assessed using Morris Water Maze (MWM) paradigm and the consequent neuronal activation revealed by Fos expression was evaluated. Our results showed impaired spatial learning in the MWM only in the treated aged rats compared to their controls. Fos expression analysis in hippocampal subfields showed that the short-term abstinence of levodopa induced an increase in basal Fos expression, evaluated 12h after the last dose. Furthermore, aged rats displayed a dampened Fos activation induced by the MWM in the DG and CA3. Dopamine receptors expression analysis showed that the chronic pulsatile levodopa treatment induced a significant increase on the D5r/D2r ratio in the granule cell layer only in the treated aged rats. Our results indicate that a chronic pulsatile levodopa treatment with a therapeutic dose could modify the ratios of the diverse types of dopamine receptors and produce spatial learning impairment in intact rats, being the aged subjects the more vulnerable ones. In this sense, an accentuated monitoring on old subjects under levodopa therapy and an improved supporting strategy should be strengthened.

LIV Congreso Nacional de Ciencias Fisiológicas

**LIV CONGRESO NACIONAL
DE
CIENCIAS FISIOLÓGICAS**

**10 – 14 de septiembre de 2011
León, Guanajuato, México.**

LIV Congreso Nacional de Ciencias Fisiológicas

APRENDIZAJE Y MEMORIA 2

Lunes 12 de septiembre 16:00 – 18:00 horas

- | | | |
|-------|--|---|
| C-107 | PARTICIPACIÓN DE LA CORTEZA FRONTAL DORSOLATERAL EN LOS EFECTOS COMO ESTIMULO DISCRIMINATIVO DE LA ESCOPOLAMINA | Aguayo A, Velázquez-Martínez DN, Sánchez-Castillo H, Del Río-Portilla Y, Casasola C |
| C-108 | EFFECTO DE LA ADMINISTRACIÓN DE CORTICOSTERONA E INDUCCIÓN DE ESTRÉS POR RESTRICCIÓN EN UNA PRUEBA DE LET, SOBRE LA CONSOLIDACIÓN Y RECUPERACIÓN DE LA MEMORIA | Barrera Flores DY, Favila García P, García Saldivar V, Gómez Romero NL, Cruz JG, Morales SE |
| C-109 | EVALUACIÓN DE LA MEMORIA ESPACIAL EN RATAS PREVIAMENTE ESTRESADAS Y TRATADAS CON DOS FÁRMACOS 5-HT6 | Campos-Contreras A, Ossio R, Prado-Alcalá RA, Briones-Aranda A, Quirarte GL |
| C-110 | PARTICIPACIÓN DE LOS RECEPTORES MUSCARÍNICOS EN EL APRENDIZAJE AVERSIVO AL OLOR | Esquivelzeta JF, Tovar-Díaz J, Roldán G |
| C-111 | EFFECTOS DEL CONSUMO CRÓNICO DE SABORES DULCES CON DIFERENTE CONTENIDO CALÓRICO SOBRE LA PREFERENCIA DE SABOR Y EL RE-APRENDIZAJE AVERSIVO | Fregoso-Urrutia DJ, Miranda MI |
| C-112 | EFFECTO DUAL DEL ANTAGONISTA VASOPRESINERGICO V1B SSR-149415 SOBRE EL APRENDIZAJE ESPACIAL EN RATAS NORMALES Y CON SEPARACIÓN MATERNA, EN CONDICIONES BASALES Y ANTE UN ESTRÉS OSMÓTICO AGUDO | Hernández VA, Zhang L |
| C-113 | LA FRACCIÓN A β 25-35 INCREMENTA LAS PROTEÍNAS DE CHOQUE TÉRMICO EN EL HIPOCAMPO Y DISMINUYE LA MEMORIA ESPACIAL EN UN MODELO DE RATA | Ortega HL, Rubio OM, Aguilar AP, Guevara FJ, Garcia MI, Limon ID |
| C-114 | CARACTERIZACIÓN DEL EFFECTO INDUCIDO POR EL NADO FORZADO SOBRE LA ADQUISICIÓN Y CONSOLIDACIÓN DE LA MEMORIA EN LA TAREA DE RECONOCIMIENTO DEL NUEVO OBJETO | Ossio R, Prado-Alcalá RA, Briones-Aranda A, Quirarte GL |

LIV Congreso Nacional de Ciencias Fisiológicas

- C-153 LA PARTICIPACIÓN DEL NERVI VAGO EN LA REGULACIÓN DE LA OVULACIÓN ES ASIMÉTRICA Y VARÍA DURANTE EL DÍA DEL PROESTRO Zárata-Pérez A, Santiago-Chiñas ML, González-Espinosa LE, Silva-Méndez CC, Everardo-Arévalo PM, Cruz-Beltrán ME, Flores-Ramírez A, Domínguez-Casalá R
- C-154 **INNERVACION VASOPRESINERGICA AL HIPOCAMPO DE RATAS NORMALES Y SOMETIDAS A SEPARACIÓN MATERNA NEONATAL: ORIGEN, DISTRIBUCION Y BLANCOS SINAPTICOS.** Zhang L, Hernández VS

FARMACOLOGIA 2

Lunes 12 de septiembre 16:00 – 18:00 horas

- C-155 EFECTO ANTIALODÍNICO DE INHIBIDORES DE CICLOOXIGENASAS Y UN ANTAGONISTA DE CCK EN NEUROPATÍA DIABÉTICA Bermúdez-Ocaña DY, Tovilla-Zárata CA, Ramón-Frías T, Granados-Soto V, Juárez-Rojop I.
- C-156 EFECTO DE LA ADMINISTRACIÓN CRÓNICA DE NICOTINA EN LA EXPRESIÓN DE C-FOS EN LOS GANGLIOS BASALES DEL MODELO ROEDOR DE LA ENFERMEDAD DE PARKINSON Boronat-García A, Equihua-Benítez AC, García-Montes JR, Millán-Aldaco DA, Palomero-Rivero M, Drucker-Colín RR, Guerra-Crespo M
- C-157 PARTICIPACIÓN DE LA VÍA ON/GMPc EN EL EFECTO ANTINOCICEPTIVO Y ANTIINFLAMATORIO DEL BIOFLAVONOIDE ACACETINA EN EL MODELO DE FORMALINA EN ROEDORES Carballo Villalobos AI, López Muñoz FJ, González Trujano ME
- C-158 REQUERIMIENTOS DE ANESTESICOS DE PACIENTES EN PROTOCOLO DE TRANSPLANTE RENAL MONITORIZADOS CON ENTROPIA Castellanos-Alvarado EA , Perez Vega MI, Zepeda-González A, González-Hernández I, Miranda Beltrán ML, Soria Fregozo C, Neri-Alonso R, Morgan-Villela G, Balderas Peña LM, Monteón-Ramos F
- C-159 ACTIVIDAD ANTINOCICEPTIVA DE EXTRACTOS ORGÁNICOS DE AGASTACHE MEXICANA (TORONJIL) EN UN MODELO DE NOCICEPCIÓN VISCERAL EN RATONES González Ramírez AE, López Muñoz FJ, González Trujano ME

EFFECTO DUAL DEL ANTAGONISTA VASOPRESINERGICO V1B SSR-149415 SOBRE EL APRENDIZAJE ESPACIAL EN RATAS NORMALES Y CON SEPARACIÓN MATERNA, EN CONDICIONES BASALES Y ANTE UN ESTRÉS OSMÓTICO AGUDO

V. S. HERNANDEZ, I. NISSEN, L. ZHANG

Se ha demostrado recientemente que el estrés perinatal por separación materna interfiere con el desarrollo normal del sistema vasopresinergico en el cerebro de ratas (Lukas et al 2010, Hernández et al 2010). Así mismo, en nuestro laboratorio hemos observado que ratas adultas sometidas a separación materna (SM) durante el periodo perinatal muestran una potenciación en la dinámica y magnitud de liberación de AVP hacia la circulación periférica tras ser sometidas a un estrés osmótico. También se observa una mayor conducta de ansiedad condicionada en la prueba de conflicto de Vogel.

Por otro lado, antagonistas no selectivos de vasopresina han mostrado efectos deletéreos sobre el aprendizaje espacial, sin embargo el papel que juegan los receptores V1b aun es controversial. En el presente trabajo evaluamos el efecto de bloquear los receptores V1b por medio del antagonista selectivo V1b, SSR-149415, sobre el aprendizaje espacial en ratas normales y SM, tanto en condiciones basales como después de un estrés osmótico agudo.

Ratas macho de la cepa Wistar, fueron separadas por 3 horas diarias desde el día 3 hasta el día 17 postnatal, y a los 90 días fue evaluado su desempeño en la prueba de aprendizaje espacial, (laberinto acuático de Morris). Bajo condiciones basales, no existen diferencias en el desempeño de la prueba entre animales controles y SM. Tras la administración aguda de una solución hipertónica de NaCl, ambos grupos mostraron un empobrecimiento en su desempeño, siendo mas pronunciado en los animales MS. SSR-149415 ejerce un efecto deletéreo sobre el aprendizaje espacial en condiciones basales, con mayor influencia sobre los sujetos controles. SSR-149415 revierte el efecto deletéreo sobre el aprendizaje espacial generado por la administración de solución hipertónica de NaCl. Estos resultados sugieren que una potenciación de la señalización de vasopresina a través del receptor V1b esta implicada en el deterioro cognitivo observado en ratas sometidas a un estrés osmótico agudo.

DGAPA-UNAM IN218111
CONACYT 79641
CONACYT 127777

INNERVACION VASOPRESINERGICA AL HIPOCAMPO DE RATAS NORMALES Y SOMETIDAS A SEPARACIÓN MATERNA NEONATAL: ORIGEN, DISTRIBUCION Y BLANCOS SINAPTICOS

L. ZHANG, V. S. HERNANDEZ

DEPARTAMENTO DE FISIOLÓGÍA, FACULTAD DE MEDICINA, UNIVERSIDAD NACIONAL AUTÓNOMA DE MEXICO, MEXICO D. F. 04510

La arginina vasopresina (AVP), cuando se libera en el hipocampo, tiene una fuerte influencia sobre el aprendizaje espacial y otros comportamientos complejos tales como la ansiedad y conducta social. Sin embargo, el origen, la distribución y sus blancos sinápticos de la vasopresina en el hipocampo aun no están muy claros. Para abordar esta pregunta, realizamos un estudio anatómico sistemático usando métodos de marcaje retrógrado con *fluorogold (FG)*, técnicas de inmunohistoquímica (*IHC*) y de microscopia electrónica (*EM*) en ratas normales y las que fueron sometidas a separación materna neonatal, las cuales hemos demostrado previamente que sufren una reorganización del sistema vasopresinérgico debido a esta manipulación experimental. Las neuronas y los axones vasopresinérgicos se marcaron con tres anticuerpos a AVP. Los blancos tanto regionales como celulares fueron identificados con la ayuda del atlas cerebro de la rata y el uso de los siguientes anticuerpos: calbindina, parvalbúmina, NK1R, mGluR1 alfa, M2R. Nuestros datos preliminares muestran que existen tres fuentes principales de fibras de entrar en la formación del hipocampo. La primera, la más novedosa, es la que proviene de las neuronas magnocelulares del hipotálamo (núcleos *PVN*, *SON* y accesorios) a través de la vía *forix - fimbria*, demostrado por marcaje de FG desde varias regiones del hipocampo siguiente análisis anatómica con IHC. Estas proyecciones viajan a través de la materia blanca entrando al hipocampo a través de la parte más medio-dorso-rostral. La mayoría de las fibras de este vía de descender a través de la porción rostral del fimbria al hipocampo ventral y ampliamente inervan la parte ventral de las regiones CA3 y CA2, siendo los estratos oriens, radiatum las regiones más inervado. Estas fibras descendentes son especialmente finos y largos que llegan hasta mas de 10 mm de longitud desde su origen hipotalámico). Una parte pequeña pero significativa de estas fibras viajan a través del alveus dorsal e inervan CA2/CA3 del hipocampo dorso rostral principalmente. La segunda vía vasopresinérgica se origina en el *bed nucleus stria (BNST)*, inerva al hipocampo via *septum y fimbria*. La tercera vía provien de las neuronas vasopresinérgicas en los núcleos del amigdala, sobre todo la parte dorso medial y el núcleo intercalar. En el nivel de EM, hay aparentemente dos tipos de axones vasopresinérgicas en hipocampo: los que están llenos de grandes vesículas de núcleo denso (DCV), que rara vez hacen sinapsis en el segmento celular del hipocampo, y los que contienen DCV co-localizadas con pequeñas vesículas sinápticas y hacen sinápsis tanto Gray de tipo I (28%) y gris tipo II (72%) sinapsis con interneuronas y las neuronas piramidales en hipocampo.

[Print this Page](#)

Presentation Abstract

Program#/Poster#: 598.04/QQ11

Presentation Title: Dual effect of AVP V1b antagonist SSR-149415 on spatial learning in normal and maternal separated rats under basal and mild stress conditions

Location: Hall A-C

Presentation time: Tuesday, Nov 15, 2011, 11:00 AM -12:00 PM

Authors: ***V. S. HERNANDEZ**, I. NISSEN, L. ZHANG;
Dept. of Physiology, Fac. of Medicine, Natl. Autonomous Univ. of Mexico,
Mexico City, Mexico

Abstract: A recent paper showed that neonatal maternal separation (MS) interferes with developmental changes in brain vasopressin and oxytocin receptor binding in male rats (Lukas et al, Neuropharm 2010) and data from our group demonstrated that MS induces vasopressinergic system reorganization which resulted in high plasmatic concentration of this neurohormone under water deprivation (WD) and enhanced anxiety in their adulthood triggered by WD. It is still unclear which are the neurochemical components involved in this impaired stress coping. On the other hand, non-selective vasopressinergic antagonists have shown deleterious effects on spatial working memory. However, there is currently controversy about the effects of the selective V1b antagonist on spatial working memory, SSR149415. In the present study, we investigated the effect of blockade of V1b receptors on spatial learning in normal and maternal separated rats under basal and mild stress conditions. Male Wistar rats underwent neonatal maternal separation (MS; 3 h daily, postnatal days 3-17). Spatial learning test using Morris water maze was carried out at rat young adult stage (3 month-old). Under basal conditions there were no differences in the performance between the groups. However, four days after chronic mild stress (CMS) procedure, the MS subjects showed impaired performance in the MWM. On the other hand, SSR149415 (3mg/kg) exerted a disrupting effect on spatial learning under basal condition, in a greater extent on the performance of the control subjects. Interestingly, SSR149415 reverted the CMS induced working memory impairment observed in MS subjects. These results suggest that a potentiation of AVP signaling through V1b receptor is implicated in the cognitive impairment seen in the adult MS

subjects after CMS.

Disclosures: **V.S. Hernandez:** None. **I. Nissen:** None. **L. Zhang:** None.

Keyword(s): MATERNAL SEPARATION

WORKING MEMORY

WATER MAZE

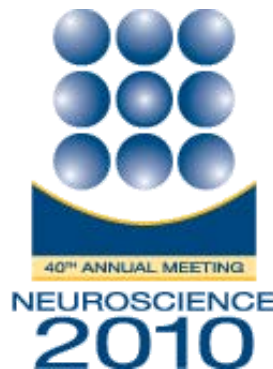
Support: DGAPA-UNAM IN218111

CONACYT 79641

CONACYT 127777

[Authors]. [Abstract Title]. Program No. XXX.XX. 2011 Neuroscience Meeting Planner. Washington, DC: Society for Neuroscience, 2011. Online.

2011 Copyright by the Society for Neuroscience all rights reserved.
Permission to republish any abstract or part of any abstract in any form must be obtained in writing by SfN office prior to publication.

[Print this Page](#)

Presentation Abstract

Program#/Poster#: 736.5/A5

Title: Neonatal maternal separation on developing hypothalamic vasopressinergic system of rats: A quantitative topographic analysis

Location: Halls B-H

Presentation Time: Wednesday, Nov 17, 2010, 8:00 AM - 9:00 AM

Authors: ***V. S. HERNANDEZ**, M. P. MEDINA, I. NISSEN, E. PINZÓN, A. VEGA-GONZALEZ, L. ZHANG;
Dept. of Physiology, Fac. of Medicine, Natl. Autonomous Univ. of Mexico, Mexico City, Mexico

Abstract: Neonatal recurrent maternal separation (MS) during the first 2 weeks of life has been widely used to model the casual relationship between stress in early life and the later development of stress-over-reactivity, anxiety and depression. Among several factors reported to be abnormal, it is interesting to observe that there is a controversy about levels of arginine-vasopressin (AVP), which were found either increased or decreased in the hypothalamus and bed nucleus of stria terminalis. AVP is synthesized largely by hypothalamic magnocellular neurons localized in paraventricular nucleus (PVN) and supraoptic nucleus (SON). Through the hypothalamic - neurohypophysial system AVP is mostly transported to the neurolobe of pituitary gland and further released upon osmoreceptor/baroreceptor activation. AVP is also critically involved in stress coping and anxiogenesis. PVN is mainly characterised by its lateral magnocellular division containing mainly AVP and oxytocin neurons and medial parvocellular division containing mainly corticotropin releasing factor neurons which had local and wide-ranging connections. The function of PVN is partially explained by the topographic distribution and their major connections. To understand whether the recurrent maternal separation (3-6 h daily) during the first 2 postnatal weeks, in which the postnatal neuronal patterning (innervation/synaptogenesis vs programmed cell death) is actively taking place, could exert major influence on

hypothalamic vasopressinergic system organization, we labelled the AVP neurons by immunocytochemistry and analysed their numbers and topographic distribution within the PVN using a stereological method at different postnatal stages. Our preliminary results showed that the spatial extension of AVP neurons in PVN from MS rats at postnatal day 15 (PND15) was increased by 15-20%, compared to control, with a remarked modification of the size and augment of cell number of the medial magnocellular division. These results indicated that the experimental condition of 3 h daily recurrent maternal separation till PND15 is already sufficient to produce a re-organization to the hypothalamic vasopressinergic system in rats.

Disclosures: **V.S. Hernandez**, None; **M.P. Medina**, None; **I. Nissen**, None; **E. Pinzón**, None; **A. Vega-Gonzalez**, None; **L. Zhang**, None.

Keyword(s): AVP

Support: DGAPA-UNAM IN210406

DGAPA-UNAM IN224407

CONACYT-49740

CONACYT-79641

[Authors]. [Abstract Title]. Program No. XXX.XX. 2010 Neuroscience Meeting Planner. San Diego, CA: Society for Neuroscience, 2010. Online.

2010 Copyright by the Society for Neuroscience all rights reserved.
Permission to republish any abstract or part of any abstract in any form must be obtained in writing by SfN office prior to publication.

[Print this Page](#)

Presentation Abstract

Program#/Poster#: 85.15/CC39

Title: Evidences of an altered vasopressinergic system in hypothalamic PVN and SON of maternal hyperthyroid rat offspring

Location: South Hall A

Presentation Time: Saturday, Oct 17, 2009, 3:00 PM - 4:00 PM

Authors: ***V. S. HERNANDEZ**¹, M. P. MEDINA¹, F. S. ESTRADA¹, A. VEGA-GONZALEZ¹, C. MENDEZ², L. ZHANG¹;
¹Dept. of Physiology, Fac. of Medicine, Natl. Autonomous Univ. of Mexico, Mexico City, Mexico; ²Developmental Biol., Fac. of Medicine, Natl. Autonomous Univ. of Mexico, Mexico City, Mexico

Abstract: Thyroid hormones are key modulators of brain development. Previous studies have shown that variations in normal concentrations of these hormones during pregnancy can induce subtle but persistent changes in the adult brain. We have recently reported that high anxious states were exhibited in maternal hyperthyroid offspring in their adulthood under 48 h of water deprivation (Vogel conflict test, VCT, for conditioned anxiety), whereas exploratory behavior showed no differences compared to control (elevated plus maze, EPM, for unconditioned anxious state). To understand this dual-anxious-state-behavior, we assessed hypothalamic paraventricular nuclei (PVN) and supraoptic nuclei (SON) arginine vasopressin (AVP) systems during water deprivation. We monitored plasmatic AVP levels at different intervals of water deprivation (6h, 12h, 24h, 48h and postVCT) and with RT-PCR we assessed the level of preproAVP in PVN and SON at different time points. Immediate early gene Fos expression in PVN and SON was also measured. In 6h and postVCT, we found a steeper rise in plasmatic AVP levels and increased Fos expression. These preliminary results suggest an important role for embryonic thyroxine levels in the regulation of neurodevelopment of vasopressinergic networks and provide new insights of the functional role of vasopressin on conditioned anxiety.

Disclosures: **V.S. Hernandez**, None; **M.P. Medina**, None; **F.S. Estrada**, None; **A. Vega-Gonzalez**, None; **C. Mendez**, None; **L. Zhang**, None.

Keyword(s): Thyroxine

Vasopressin

Hypothalamus

Support: CONACYT Grant 46141

CONACYT Grant 49740

CONACYT Grant 79641

DGAPA-UNAM-PAPIIT Grant IN210406

DGAPA-UNAM-PAPIIT Grant IN224407

[Authors]. [Abstract Title]. Program No. XXX.XX. 2009 Neuroscience Meeting Planner. Chicago, IL: Society for Neuroscience, 2009. Online.

2009 Copyright by the Society for Neuroscience all rights reserved.

Permission to republish any abstract or part of any abstract in any form must be obtained in writing by SfN office prior to publication.

[Print this Page](#)

Presentation Abstract

Program#/Poster#: 191.6/EE69

Title: Anxiogenesis and impaired spatial memory induced by ovariectomy are reverted by a 17beta-aminoestrogen (prolame): A behavioral study in young female rats

Location: South Hall A

Presentation Time: Sunday, Oct 18, 2009, 9:00 AM -10:00 AM

Authors: ***F. S. ESTRADA**¹, H. S. GONZALEZ¹, V. S. HERNANDEZ¹, A. VEGA-GONZALEZ¹, A. DE LA PEÑA², J. M. FERNANDEZ-G³, L. ZHANG¹;
¹Dept. of Physiology, Fac. of Medicine, Natl. Autonomous Univ. of, Mexico City, Mexico; ²Pharmacol., Fac. of Medicine, Natl. Autonomous Univ. of Mexico, Mexico City, Mexico; ³Inst. Chem., Natl. Autonomous Univ. of Mexico, Mexico City, Mexico

Abstract: Estrogens exert diverse actions in the central nervous system and its deficiency produces cognitive and emotional impairment. Hormone replacement therapy (HRT) has been widely used to treat symptoms caused by natural or surgical menopause. However, possible side effects of HRT, such as an increased risk of thromboembolic events and breast cancer have risen the need for alternative therapeutical strategies. In this study, we used N-(3-hydroxy-1,3,5(10)estratrien-17 beta-yl)-3-hydroxypropylamine (prolame), a synthetic amino-estrogen with prolonged anticoagulant and brief estrogenic effects, to examine its influence on the effects elicited by ovariectomy on spatial memory and anxiety in young adult female rats. 90-day-old female Wistar rats were assigned to one of the following groups: wild type (WT), ovariectomized (Ovx), ovariectomized plus estradiol treatment (OvxET) and ovariectomized plus prolame treatment (OvxPT). At day 28 post surgery, OvxET and OvxPT rats started receiving a daily subcutaneous injection (50 µg/kg) of estradiol cyclopentyl propionate and prolame respectively, whereas WT and Ovx groups were injected with vehicle only. After 2 months of treatment, rats were subjected to Morris Water Maze (MWM) and Elevated

Plus Maze (EPM) testing. Treatment with prolame effectively prevented the increase in latency to find the platform in the MWM task, as well as the anxiety-like behavior exhibited in the Ovx group during EPM examination. These results suggest that prolame could represent an improved option of HRT ameliorating cognitive and emotional impairments produced by estrogen deficiency.

Disclosures: **F.S. Estrada**, None; **H.S. Gonzalez**, None; **V.S. Hernandez**, None; **A. Vega-Gonzalez**, None; **A. De la Peña**, None; **J.M. Fernandez-G**, None; **L. Zhang**, None.

Keyword(s): Estradiol
Working memory
Anxiety

Support: CONACYT Grant 46141
CONACYT Grant 49740
CONACYT Grant 79641
DGAPA-UNAM-PAPIIT Grant IN210406
DGAPA-UNAM-PAPIIT Grant IN224407

[Authors]. [Abstract Title]. Program No. XXX.XX. 2009 Neuroscience Meeting Planner. Chicago, IL: Society for Neuroscience, 2009. Online.

2009 Copyright by the Society for Neuroscience all rights reserved.
Permission to republish any abstract or part of any abstract in any form must be obtained in writing by SfN office prior to publication.

[Print this Page](#)

Presentation Abstract

Program#/Poster#: 820.3/B30

Title: Immunohistochemical characterization of catecholaminergic innervation during development in amygdala and hippocampus of maternal hyperthyroid rat offspring

Location: Hall A-C

Presentation Time: Wednesday, Nov 19, 2008, 3:00 PM - 4:00 PM

Authors: ***V. S. HERNANDEZ**, F. S. ESTRADA, A. VEGA-GONZÁLEZ, L. ZHANG;
Dept. of Physiol. Fac. of Med., Natl. Univ. of Mexico, Mexico City, Mexico

Abstract: There exist several reports regarding the effect of maternal hyperthyroidism on neurodevelopment. Particular interest was laid on the accelerated neuronal differentiation probably produced by abnormal level of thyroxin during fetal brain development.. We have previously reported that adult rat offspring subjected to maternal hyperthyroidism showed increased susceptibility to mild stressful situations, displaying depression-like behavior and impaired cognitive functions. Due to the involvement of amygdala and hippocampus in cognitive and emotional functions, we have undertaken the characterization of the expression of the catecholaminergic system in these regions at different postnatal stages (P7, P14, P21, P28, P50, and P100) using indirect fluorescent immunocytochemistry against tyrosine hydroxylase and image analysis. Our results showed a significant increase in optical density in the central and basolateral regions of amygdala, and in hilus of hippocampus at all examined stages, which could suggest an aberrant development of this neurotransmission system.

Disclosures: **V.S. Hernandez**, None; **F.S. Estrada**, None; **A. Vega-González**, None; L. Zhang , None.

Support: CONACYT Grant 46141
CONACYT Grant 49740

DGAPA-PAPIIT IN210406

DGAPA-PAPIIT IN224407

DGAPA-UNAM and CONACYT research fellowships and hospitality of MRC-ANU Oxford to LZ for her sabbatical stay are fully acknowledged.

[Authors]. [Abstract Title]. Program No. XXX.XX. 2008 Neuroscience Meeting Planner. Washington, DC: Society for Neuroscience, 2008. Online.

2008 Copyright by the Society for Neuroscience all rights reserved.
Permission to republish any abstract or part of any abstract in any form must be obtained in writing by SfN office prior to publication.

[Print this Page](#)

Presentation Abstract

Program#/Poster#: 839.8/V8

Title: A temporal correlation between cell proliferation and astrocytic reactivity in the adult rat hippocampus induced by a single 2-Deoxy-D-glucose application

Location: Hall A-C

Presentation Time: Wednesday, Nov 19, 2008, 4:00 PM - 5:00 PM

Authors: ***F. S. ESTRADA**¹, A. CORONA-MORALES^{1,2}, V. HERNÁNDEZ¹, M. P. MEDINA¹, A. VEGA-GONZÁLEZ¹, L. ZHANG¹;
¹Dept. of Physiol. Fac. of Med., Natl. Univ. of Mexico, Mexico City, Mexico;
²Univ. Veracruzana, Xalapa, Mexico

Abstract: 2-Deoxy-D-glucose (2-DG) is a non-metabolizable glucose analogue able to inhibit glycolysis and protein glycosylation, therefore causing depletion of ATP and glucose derivatives. 2-DG has been widely studied in biomedicine, as a possible therapeutic molecule for anticancer and antiviral strategies, as well as a calorie restriction mimetic. It is well known that glucose deprivation may cause brain function impairment and neuronal damage, including cell death, probably through excitotoxicity. Hippocampus seems to be an area particularly vulnerable to brain challenges. Astroglialosis has been observed to be a brain response to diverse brain injuries. Consequently, in the present study, we focused in the effect of a sole dose of 2-DG (500 mg/kg i.p.) on astrocytosis (using glial fibrillar acidic protein (GFAP) expression as an indicator) and on cell proliferation in the subgranular zone of the dentate gyrus of the hippocampus. Adult male Wistar rats were injected with 2-DG or saline solution at experimental day 0 (D0) and then divided in the following groups: for astroglialosis, rats were sacrificed at D1, D2, D3, D4 or D5; for cell proliferation, animals were treated with 5-bromo-2-deoxyuridine (BrdU) (300 mg/kg, divided by two doses) and sacrificed 8 hours later at D2. Brains were cut and processed for GFAP or BrdU immunofluorescence. Results show a significant increase in GFAP optical density in 2-DG rats from D2 to D4. In the same experimental group, nearly a 100% increase in the number of BrdU

nuclei was found also at D2. Our findings suggest that a single 2-DG administration induces functional alterations in the hippocampus, showing a temporal correlation between cell proliferation and astrogliosis after such brain insult.

Disclosures: **F.S. Estrada**, None; **A. Corona-Morales**, None; **V. Hernández**, None; **M.P. Medina**, None; **A. Vega-González**, None; **L. Zhang**, None.

Support: CONACYT Grant 46141

CONACYT Grant 49740

CONACYT Grant 61344

DGAPA-UNAM-PAPIIT Grant IN210406 and IN224407

Fellowships from CONACYT and DGAPA and hospitality of MRC-ANU Oxford to LZ for her sabbatical stay are fully acknowledged

[Authors]. [Abstract Title]. Program No. XXX.XX. 2008 Neuroscience Meeting Planner. Washington, DC: Society for Neuroscience, 2008. Online.

2008 Copyright by the Society for Neuroscience all rights reserved.
Permission to republish any abstract or part of any abstract in any form must be obtained in writing by SfN office prior to publication.



First author Zhang, Limei (poster)

Poster board F11 - Tue 15/07/2008, 12:15 - Hall 1
Session 159 - Neuroendocrine 2
Abstract n° 159.11
Publication ref.: *FENS Abstr.*, vol.4, 159.11, 2008

Authors Zhang L. *, Medina-Pizarro M., Hernandez V. S. & Vega-Gonzalez A.

Address Dept. Physiology, Medicine, UNAM, Mexico City, Mexico

Title Vasopressinergic innervations to locus coeruleus in normal and maternal hyperthyroid rats: its role in triggering anxiety-like behaviour during stress coping.

Text The pontine nucleus locus coeruleus (LC) is a key system involved in arousal and plays a secondary yet important role in HPA activation. Disrupted noradrenergic transmission is associated with depression and anxiety. Arginine vasopressin (Avp) is secreted primarily under circumstances of dehydration. Hypothalamic Avp synthesizing nuclei (PVN and SON) send vasopressin-containing projections to several neural target areas thought to be involved mainly in cardiovascular regulation. Post-mortem study of suicide subjects reported an increased Avp-ir in LC, amongst other brain regions relevant to emotionality. Yet the role of Avp in stress, anxiety and depressive states remains elusive. To address the question whether Avp plays a regulator role in LC during stress coping, we used the Vogel thirsty conflict test (VTCT) and rats subjected to maternal hyperthyroidism (MHT), which have showed an increased vulnerability to mild stressors producing cognitive impairment, but not anxiety-like behaviour. Young adult rats from control and MHT groups (n=10) were deprived of water for 48 hours before they underwent VTCT. Two parameters were registered: number of punished responses (electrical shocks punishing attempts to drink) and time latency to the start of water intake. The MHT rats showed anxiety-like behaviour expressed as a decreased number of shocks received (6/5min vs. 43/5min control) and increased time latency (132s vs. 28s). Immunoreaction of Avp showed Avp-ir fibres innervating preferentially TH-ir dendrites in the rat pericoerulear regions, with few fibres observed in the "core" of LC in control rats. In MHT rat LC, there are an increased number of Avp-ir fibres with boutons passing in proximity to TH-ir cell bodies. Functional contacts and receptor types remained to be investigated. The preliminary results suggest that MHT could induce reorganisation of Avp innervations to LC.
*On sabbatical leave in MRC-ANU Oxford UK supported by CONACYT & UNAM-DGAPA fellowships.

Theme E - Homeostatic and neuroendocrine systems
Neuroendocrine - Neuroendocrine regulation: thirst, water balance and other

 [Print this Page for Your Records](#)[Close Window](#)

Program#/Poster#: 730.9/PP19

Title: Maternal hyperthyroidism enhances basal exploratory activity and increases TH immunoreactivity in the amygdala of adult rat offspring

Location: San Diego Convention Center: Halls B-H

Presentation Start/End Time: Tuesday, Nov 06, 2007, 1:00 PM - 2:00 PM

Authors: ***V. S. HERNANDEZ**¹, A. VEGA-GONZALEZ², L. ZHANG²;
¹UNAM, Mexico City, Mexico; ²Dept. Physiology, Fac. Med. UNAM, Mexico City, Mexico

It is well known that thyroid hormones play a key role in early neurodevelopment, studies in rats have showed that there are anatomical modifications in some brain regions when subjected to transient maternal hyperthyroidism. In order to further investigate the consequences of fetal exposure to increased concentrations of thyroid hormones in adult life, we used the male offspring of female rats implanted with osmotic pumps, either containing thyroxine (T4) (1.5 µg/100 g pre-mating body weight/day) or saline (control).

We monitored weight, seric thyroid hormones and glucose levels of the offspring, founding no differences between control and experimental groups. Then at postnatal day 60, we evaluated the basal exploratory behavior applying the Elevated Plus Maze (EPM), and afterwards we performed an immunohistochemistry against TH, in amygdala, a central region of the limbic system involved in emotion and stress coping.


Our results showed an increased basal exploratory behavior in experimental subjects, expressed as more time spent in the open arms of the maze and an intensification of the TH-ir in the central nucleus of the amygdala (CeA). These results suggest that exposure to abnormal high levels of thyroid hormones during early brain development, might modify catecholamine neurotransmission.

Disclosures: **V.S. Hernandez** , None; **A. Vega-Gonzalez**, None; **L. Zhang**, None.

Support: DGAPA-UNAM IN210406
 CONACYT 46141-M

[Authors]. [Abstract Title]. Program No. XXX.XX. 2007 Neuroscience Meeting Planner. San Diego, CA: Society for Neuroscience, 2007. Online.

2007 Copyright by the Society for Neuroscience all rights reserved. Permission to republish any abstract or part of any abstract in any form must be obtained in writing by SfN office prior to publication.

 [Print this Page for Your Records](#) [Close Window](#)

Program#/Poster#: 96.1/UU30

Title: Chronic pulsatile L-DOPA application alters emotionality and cognitive functions: a study in intact aged rat

Location: San Diego Convention Center: Halls B-H

Presentation Start/End Time: Saturday, Nov 03, 2007, 1:00 PM - 2:00 PM

Authors: ***L. ZHANG**¹, V. S. HERNANDEZ¹, A. VEGA-GONZALEZ¹, A. A. CORONA-MORALES²;
¹Physiology, Fac Med., Univ. Nacional Autonoma de Mexico (UNAM), Mexico, Mexico;
²Dirección Gen. de Investigaciones, Univ. Veracruzana, Jalapa, Mexico

Dopamine (DA) is involved in a variety of behaviors such as locomotor activity, stereotyped behaviors, learning, motivation, food intake, reward and pathological conditions like Parkinson's disease (PD), schizophrenia and attention deficit hyperactivity disorder. DA acts as a powerful regulator of different aspects of cognitive brain functions. In this respect, normalizing DA transmission will contribute to improve the cognitive deficits not only related to neurologic or psychiatric diseases, but also in normal aging. L-3,4 dihydroxyphenylalanine (L-DOPA) is the chemical precursor of dopamine and acts also as a non-specific catecholamine agonist. L-DOPA has been the gold standard treatment of Parkinson's disease. Nevertheless, chronic treatment with L-DOPA brings several collateral damages as dyskinesia and neuropsychiatric problems. There were significant but contrasting effects of L-DOPA therapy on PD patients on cognition and affective functions. L-DOPA treatment to intact rats is reportedly decreasing D1 receptor stimulated adenylate cyclase activity. However, the effects of L-DOPA administration on other DA receptors and consequently on behavior and cognition are less understood. This study was aimed to assess whether L-DOPA application *per se* could produce mood alterations and cognition changes in old intact rats. Twenty male adult Wistar rats of 14 months were separated in 4 experimental groups: Ctrl1, Exp1, Ctrl2, Exp2. Animals were maintained in light-dark cycle 12:12 with food and water *ad libitum*. L-DOPA 25mg/kg/12hr with carbidopa were given to the groups Exp1 and Exp2 for 4 weeks. Open field test (OFT) was used to assess locomotor activity 45min to 60min after drug application and tail suspension test (TST) to assess helplessness to groups Ctrl1, Exp1 during abstinence (6hrs after drug application). Morris Water Maze (MWM) complex was used to measure spatial learning and memory (groups Ctrl2, Exp2) after 1hr of drug application. OFT showed a decreased motor activity during the post drug application period. TST showed a significant increase on immobility accounts. MWM showed learning and memory deficit in Exp2: smaller slope in spatial learning test but memory retention tests kept unaffected. C-fos expression was decreased in dorsolateral prefrontal cortex (Pfc) but not in medial Pfc. The results suggest that intermittent administration of L-DOPA and consequently the pulsatile elevation of L-DOPA and dopamine contents in the brain in intact aged rats *per se*: 1) may be directly relevant to depression observed in Parkinson's disease patients; 2) produce modification of motor pattern during OFT; 3) impair spatial learning showed by MWM.

Disclosures: **L. Zhang** , None; **V.S. Hernandez**, None; **A. Vega-Gonzalez**, None; **A.A. Corona-Morales**, None.

Support: PAPIIT-UNAM IN210406
 CONACYT 46141-M

[Authors]. [Abstract Title]. Program No. XXX.XX. 2007 Neuroscience Meeting Planner. San Diego, CA: Society for Neuroscience, 2007. Online.

2007 Copyright by the Society for Neuroscience all rights reserved. Permission to republish any abstract or part of any abstract in any form must be obtained in writing by SfN office prior to publication.

 [Print this Page for Your Records](#)[Close Window](#)

Program#/Poster#: 475.24/P14

Title: Effects of chronic application of beta-1 adrenergic antagonist metoprolol on spatial learning and c-Fos expression

Location: San Diego Convention Center: Halls B-H

Presentation Start/End Time: Monday, Nov 05, 2007, 4:00 PM - 5:00 PM

Authors: ***F. S. ESTRADA**, V. S. HERNANDEZ, A. VEGA-GONZALEZ, L. ZHANG;
Fac Medicina, Dep. Fisiologia, Univ. Nacional Autonoma Mexico, Mexico City, Mexico

Norepinephrine (NE) plays an important role in modulating a large variety of processes implied in general brain function. It is well known that in cortical structures such as the hippocampus, NE is capable to enhance cognitive processes of memory and attention via activation of $\beta 1$ adrenergic receptor ($\beta 1AR$). Metoprolol is a selective $\beta 1AR$ blocking agent that, due to its chemical structure, is capable of crossing the blood-brain barrier. It's widely used as a treatment for hypertension and some other cardiovascular diseases, such as acute myocardial infarction. Considering the clinical relevance of this drug, we designed the current study in order to assess the extent to which chronic administration of metoprolol might alter cognition and neural activity. Experimental rats started to receive subcutaneous injections of metoprolol (4 mg/kg b.w./day dissolved in 0.9% saline) and control rats were injected using only 0.9% saline vehicle at postnatal day 60. After two weeks treatment, both groups underwent the Radial Arm Water Maze task. Animals were perfused 90 minutes after the first trial and brain slices were processed for c-Fos immunoreaction. Our results showed a slight impairment in spatial learning of experimental subjects correlating with a significant difference in c-Fos positive nucleus density counting on the dentate gyrus. These preliminary data suggest that blockade induced by $\beta 1AR$ antagonist metoprolol may cause cognitive impairment in rats subjected to a chronic treatment.

Disclosures: **F.S. Estrada** , None; **V.S. Hernandez**, None; **A. Vega-Gonzalez**, None; **L. Zhang**, None.

Support: PAPIIT-UNAM IN210406
PAPIIT-UNAM IN224407
CONACYT 46141-M

[Authors]. [Abstract Title]. Program No. XXX.XX. 2007 Neuroscience Meeting Planner. San Diego, CA: Society for Neuroscience, 2007. Online.

2007 Copyright by the Society for Neuroscience all rights reserved. Permission to republish any abstract or part of any abstract in any form must be obtained in writing by SfN office prior to publication.



IBRO 2007 ONLINE ABSTRACT

Form Submission Successful

Thank you, your details have been processed, and may be viewed below. Please check your abstract text carefully if you cut and pasted it from a word processor, as certain symbols (particularly quotes and apostrophes) may not have transferred correctly.

If you would like to change your abstract, please [return to the IBRO 2007 Online Abstract form](#).

To complete the IBRO 2007 Online Abstract you will need click the **continue** button at the bottom of this page.

Abstract:

ENHANCED BASAL EXPLORATORY ACTIVITY, ANTI-NOCICEPTIVE BEHAVIOUR AND INCREASED TH AND CRF IMMUNOREACTIVITY IN AMYGDALA OF ADULT RATS SUBJECTED TO MATERNAL HYPERTHYROIDISM

Hernandez V.S.¹, Medina M.P.¹, Valle-Leija P.¹, **Vega-Gonzalez A.¹**, Morales T.² and Zhang L.²

¹Department of Physiology, Faculty of Medicine. ²Institute of Neurobiology, National Autonomous University of Mexico.

Thyroid hormone (T4) has a central role in early brain development. It has been suggested that hyperthyroidism during prenatal stages induces long-term anatomical changes. In order to investigate the effects of gestational exposure to maternal hyperthyroidism (MH) in adulthood, we studied male rat offspring from mothers implanted with alzet osmotic pumps, either containing T4 (1.5 µg/100 g pre-mating body weight/day) or saline (control). At P90, thirsty rat conflict (TRC) and elevated plus maze (EPM) experimental protocols were used to evaluate antinociceptive and exploratory behaviours. Seric corticosterone level was measured with ELISA posterior to TRC. Tyrosine hydroxylase (TH) and corticotropin releasing factor (CRF) immunoreactivity was also analysed in amygdala as a key region of the corticolimbic system involved in stress coping and cognition. The results showed a significant enhancement of basal exploratory behaviour in MH subjects with EPM. TRC test showed a higher degree of antinociceptive behaviour, regarded as an increased number of electric shocks received in the MH subjects compared to control. Seric corticosterone level was significantly higher in MH

subjects. Immunoreactivity for TH and CRF in amygdala was markedly increased in MH subjects. These observations suggest a modified stress coping system in adult rats exposed to maternal hyperthyroidism.

Details:

Name of presenting author: A. Vega-Gonzalez

Email address for notification: artvega@servidor.unam.mx

Presentation Category: Free communication - poster presentation

Special oral presentation: No

Ethics Declaration: I accept the declaration

Result Declaration: I accept the declaration

Student Poster: No

Abstract Classification:

Congress Theme 1: H - Neuroendocrinology

Congress Theme 2: B - Development

Congress Theme 3: N - Behaviour and cognition

To continue:

[Back](#)

Return to IBRO 2007 Online Abstract form and continue editing

[Continue](#)

Complete online abstract submission. Click the **Continue** button ONCE ONLY.

[Cancel](#)

Cancel online abstract submission and return to the IBRO 2007 Webpage.
Click the **cancel** button ONCE ONLY.



IBRO 2007 ONLINE ABSTRACT

Form Submission Successful

Thank you, your details have been processed, and may be viewed below. Please check your abstract text carefully if you cut and pasted it from a word processor, as certain symbols (particularly quotes and apostrophes) may not have transferred correctly.

If you would like to change your abstract, please [return to the IBRO 2007 Online Abstract form](#).

To complete the IBRO 2007 Online Abstract you will need click the **continue** button at the bottom of this page.

Abstract:

MATERNAL HYPERTHYROIDISM IN RATS IMPAIRS STRESS COPING OF ADULT OFFSPRING

Zhang L.¹, Hernandez V.S.¹, Medina M.P.¹, Valle-Leija P.¹, Hofmann P.G.¹, Vega-Gonzalez A.¹ and Morales T.²

¹Department of Physiology, Faculty of Medicine. ²Institute of Neurobiology, National Autonomous University of Mexico (UNAM).

Given the evidence that maternal hyperthyroidism (MH) compromises the expression of neuronal cytoskeletal proteins in the late foetal brain, which is suggestive of a pattern of accelerated neuronal differentiation, we investigated its possible consequence on adult offspring emotional and cognitive functions during acute and sub-chronic stress coping. Study groups consisted of male adult rat offspring from mothers implanted with osmotic mini-pumps infusing thyroxine (T4 1.5 µg/100 g pre-mating body weight/day) or vehicle (control) during pregnancy. Body weight, blood glucose and plasma T4 levels were measured at different postnatal stages, and found no significant differences between study groups. At P90, forced swimming stress (FSS) and a modified chronic mild stress (CMS) paradigm for 10 days were applied to experimental subjects. Morris water maze was used before, during and after CMS application to measure spatial learning and memory. Both tail suspension test (TST) and forced swimming test (FST) were used to evaluate depression-like behaviour. The MH rats displayed normal spontaneous locomotor activity and normal spatial memory prior to stressor application, but impaired spatial learning and memory retention after acute and chronic stress. FST during FSS showed a significant increase in the immobility episodes. This behavioural abnormality was confirmed with TST at the end of CMS.

These results suggest that adult rats who were subjected to maternal hyperthyroidism are more susceptible to mild stressful situations compared to control, displaying depressive-like behaviour and impaired cognitive functions, though their motor and cognitive functions seem to be normal without stress.

Details:

Name of presenting author: L. Zhang

Email address for notification: limei@servidor.unam.mx

Presentation Category: Free communication - poster presentation

Special oral presentation: No

Ethics Declaration: I accept the declaration

Result Declaration: I accept the declaration

Student Poster: No

Abstract Classification:

Congress Theme 1: H - Neuroendocrinology

Congress Theme 2: B - Development

Congress Theme 3: N - Behaviour and cognition

To continue:



Return to IBRO 2007 Online Abstract form and continue editing



Complete online abstract submission. Click the **Continue** button ONCE ONLY.



Cancel online abstract submission and return to the IBRO 2007 Webpage.
Click the **cancel** button ONCE ONLY.



IBRO 2007 ONLINE ABSTRACT

Form Submission Successful

Thank you, your details have been processed, and may be viewed below. Please check your abstract text carefully if you cut and pasted it from a word processor, as certain symbols (particularly quotes and apostrophes) may not have transferred correctly.

If you would like to change your abstract, please [return to the IBRO 2007 Abstract form](#).

To complete the IBRO 2007 Online Abstract you will need click the [continue](#) button at the bottom of this page.

Abstract:

MORPHOLOGICAL ANALYSIS OF HIPPOCAMPAL PROJECTIONS OF NEURONS IN DIFFERENT POSTNATAL STAGES OF RATS SUBJECTED TO MATERNAL HYPERTHYROIDISM

Medina M.P., Hernandez V.S., Valle-Leija P., Vega-Gonzalez A. and Zhang L.
Dept of Physiology, Faculty of Medicine, National Autonomous University of Mexico.

Thyroid hormones play an important role on central nervous system development, affecting proliferation, migration and growth. Previous studies in our group showed that adult rats were subjected to maternal hyperthyroidism are more susceptible to mild stressful situations, displaying depressive-like behaviour and impaired cognitive functions. Hippocampal formation (HF), together with the amygdala, form the central axis of the limbic system, which is a major component of stress circuitry.

has major input from the entorhinal cortex through the perforant path where highly processed information is transmitted. Due to these reasons, we analysed the hippocampal CA3 pyramidal and dentate granular cell morphology during postnatal development. Male Wistar rat offspring mothers implanted with an infusing thyroxin pump (T4 1.5 µg/100 g pre-mating body weight/saline (control) were used. Brain samples were collected at P7, P30 and P75 and were processed by the Golgi-Cox impregnation method. Increased dendritic arborisation of hippocampal CA3 pyramidal neurons and dentate gyrus granular cells was observed in rats subjected to MH, compared to controls at all developmental stages studied. These results suggest that hippocampal projection hypertrophy could be a possible anatomical substrate for the observed stress vulnerability in this subject.

Details:

Name of presenting author: M.P. Medina

Email address for notification: mmedinapizarro@gmail.com

Presentation Category: Free communication - poster presentation

Special oral presentation: No

Ethics Declaration: I accept the declaration

Result Declaration: I accept the declaration

Student Poster: No

Abstract Classification:

Congress Theme 1: H - Neuroendocrinology

Congress Theme 2: B - Development

Congress Theme 3: N - Behaviour and cognition


To continue:

[Back](#)

Return to IBRO 2007 Online Abstract form and continue editing

[Continue](#)

Complete online abstract submission. Click the **Continue** button ONCE ONLY

 [Print this Page for Your Records](#) [Close Window](#)

Program#/Poster#: 832.23/II2

Title: Adult anxiety-like behavior, cognitive deficiency, and neocortical pyramidal cell structural changes in rats subjected to transient neonatal hyperthyroidism

Location: Georgia World Congress Center: Halls B3-B5

Presentation Start/End Time: Wednesday, Oct 18, 2006, 3:00 PM - 4:00 PM

Authors: **V. S. HERNÁNDEZ**¹, M. P. MEDINA¹, L. GUADARRAMA¹, C. A. GALINDO¹, A. VEGA-GONZÁLEZ¹, M. S. LUQUIN-DE-ANDA², J. S. GARCÍA-ESTRADA², *L. ZHANG¹;
¹Dept Physiology, Fac Medicine, Univ Nacional Autonoma de Mexico (UNAM), Mexico, MEXICO, ²Neuroscience, Univ Guadalajara, Guadalajara, MEXICO.

Neonatal hyperthyroidism (NH) occurs between 0.2 to 1% of human neonates. The most common cause of this condition has been reported to be due to abnormal TSH receptor activity in infants born to Graves' disease mothers. Since the half-life of the TSH receptor is only a few weeks, NH usually resolves completely within 1-3 months after birth. However, thyroid hormone action early in life has a key role in determining the normal timing of neural development. It has been suggested that transient NH induces permanent changes in some neuronal structures. Nevertheless, there have been fewer experiments examining affective and/or cognitive changes in adulthood in relation to morphological changes, as a consequence of NH. To have a better understanding of this, an animal model of NH was established, in which the male pups were fed during P1 to P28 by lactating females implanted with osmotic pumps infusing either vehicle (control) or supraphysiological dose of T4 (1.5µg/100g b.w). At P60, NH and control groups were evaluated with the classical elevated plus maze (EPM) and Morris water maze (MWM) paradigms to assess anxiety and working memory. Neuron structural changes were examined with Golgi-Cox impregnation. Preliminary results of this study showed that (1) NH animals had an enhanced anxiety level at young adulthood; (2) NH animals had impaired spatial learning abilities; (3) Neocortical (S1BF) pyramidal neuron dendrite arborisation exhibited a marked atrophy and there was a loss of spine densities. These findings suggest that the anatomical abnormalities may underlie the emotional and cognitive changes.

Disclosures: **V.S. Hernández**, None; **M.P. Medina**, None; **L. Guadarrama**, None; **C.A. Galindo**, None; **A. Vega-González**, None; **M.S. Luquin-de-Anda**, None; **J.S. García-Estrada**, None; **L. Zhang**, None.

Support: CONACYT 41694-M
 CONACYT 40615-F
 CONACYT 46141-M
 DGAPA UNAM IN210406

[Authors]. [Abstract Title]. Program No. XXX.XX. 2006 Neuroscience Meeting Planner. Atlanta, GA: Society for Neuroscience, 2006. Online.

2006 Copyright by the Society for Neuroscience all rights reserved. Permission to republish any abstract or part of any abstract in any form must be obtained in writing by SfN office prior to publication.

 [Print this Page for Your Records](#) [Close Window](#)

Program#/Poster#: 832.11/HH16

Title: Stress differentially affects transcription factor c-Fos expression and SGZ neurogenesis in adult rats subjected to transient neonatal hyperthyroidism

Location: Georgia World Congress Center: Halls B3-B5

Presentation Start/End Time: Wednesday, Oct 18, 2006, 3:00 PM - 4:00 PM

Authors: ***M. P. MEDINA**, V. S. HERNANDEZ, L. GUADARRAMA, C. A. GALINDO, A. VEGA-GONZALEZ, H. SOLIS, L. ZHANG;
Dept. Physiology, Fac. Med., UNAM, Mexico City, MEXICO.

Neonatal hyperthyroidism (NH) which has an incidence of about 0.2% of human neonates, has been reportedly associated with hypertrophy of both CA3 pyramidal neurons and basal forebrain glial cells which have been suggested to be permanent changes through adulthood. It is well known that hippocampus plays an important role in stress response. The transcription factor c-Fos is activated in the hippocampus following a number of stressors, including restraint stress and forced swimming test (FST). On the other hand, granule cell neurogenesis occurs in the subgranular zone (SGZ) of dentate gyrus (DG) of the mammalian hippocampus throughout adult life, and incorporation of bromodeoxyuridine (BrdU) into DNA can serve as a marker of cell division associated with such neurogenesis. The purpose of this study is to analyze the relationship between the expression patterns of such immediate early gene and SGZ neurogenesis after restraint and FST stressor applications of adult rats subjected to NH. Wistar male rats were used in this study and were separated in three groups: pups fed during P1 to P28 by lactating females implanted with osmotic pumps infusing either vehicle (NH-/S+) or supraphysiological dose of T4 (1.5 µg/100g b.w., NH+/S+). At P60, NH-/S+ and NH+/S+ rats were subjected to restraint stress for 3 weeks. A separate group with same age/b.w. but restraint-stress-naive (NH-/S-) was also prepared. At P80, all experimental subjects underwent to FST for 7 min. Half of the subjects were perfused 2hrs after FST and the other half received BrdU injections for the next 48 hrs before perfusion. Immunoreaction against c-Fos and BrdU were carried out. Our results showed that Fos+ neurons counts in DG were significantly increased in NH+/S+ and decreased in NH-/S+ compared with NH-/S-, whereas BrdU+ nuclei in SGZ are both decreased compared with NH-/S-. However, counts from NH+/S+ are significantly higher than NH-/S+. These findings suggest that there might be a higher rate of cell turnover/apoptosis in the NH animals due to excitotoxicity generated from an abnormal hippocampal neural network activity more sensitive to stress.

Disclosures: **M.P. Medina**, None; **V.S. Hernandez**, None; **L. Guadarrama**, None; **C.A. Galindo**, None; **A. Vega-Gonzalez**, None; **H. Solis**, None; **L. Zhang**, None.

Support: CONACYT 41694-M
CONACYT 40615-F
DGAPA UNAM IN210406
CONACYT 46141-M

[Authors]. [Abstract Title]. Program No. XXX.XX. 2006 Neuroscience Meeting Planner. Atlanta, GA: Society for Neuroscience, 2006. Online.

2006 Copyright by the Society for Neuroscience all rights reserved. Permission to republish any abstract or part of any abstract in any form must be obtained in writing by SfN office prior to publication.